**UNIWERSYTET MARII CURIE-SKŁODOWSKIEJ
W LUBLINIE**

Wydział Chemii

Instytut Nauk Chemicznych

mgr Edyta Rekiel

BADANIE WŁAŚCIWOŚCI ADSORPCYJNYCH, AGREGACYJNYCH I ZWILŻAJĄCYCH MIESZANIN ZAWIERAJĄCYCH BIOSURFAKTANT, SURFAKTANT NIEJONOWY I ETANOL

Rozprawa doktorska

wykonana w Katedrze Zjawisk Międzyfazowych

pod kierunkiem prof. dr hab. Anny Zdziennickiej

Lublin 2023

„Nadajemy światu znaczenia przez odwagę naszych pytań
i głębię naszych odpowiedzi."

„Nauka prowadzi nas do zrozumienia tego, jaki jest świat,
a nie tego, jaki chcielibyśmy, by był."

Carl Sagan

Składam serdeczne podziękowania

Pani Promotor Prof. dr hab. Annie Zdziennickiej

za merytoryczną pomoc w przygotowaniu rozprawy doktorskiej,

wyrozumiałość, cenne uwagi, wskazówki, komentarze,

a także poświęcony czas, wsparcie i ogromną życzliwość.

SPIS TREŚCI

1. STRESZCZENIE

Przedstawiona rozprawa doktorska zatytułowana *„Badanie właściwości adsorpcyjnych, agregacyjnych i zwilżających mieszanin zawierających biosurfaktant, surfaktant niejonowy i etanol"* stanowi cykl sześciu oryginalnych artykułów naukowych powiązanych spójnie tematycznie i opublikowanych w specjalistycznych czasopismach naukowych z listy Ministerstwa Edukacji i Nauki (MEiN) [**D1-D6**].

Tematyka cyklu prac będących podstawą rozprawy doktorskiej dotyczy badania właściwości adsorpcyjnych, agregacyjnych i zwilżających wodnych roztworów mieszanin biosurfaktantu (mono–ramnolipidu (RL) lub surfaktyny (SF)) z surfaktantem niejonowym (Tritonem X–165 (TX165)) lub alkoholem krótkołańcuchowym (etanolem (ET)). Zastosowane w badaniach RL i SF wybrano ze względu na ich dużą aktywność powierzchniową, która warunkuje różnorodne zastosowanie tych biosurfaktantów w wielu gałęziach przemysłowych, ochronie środowiska oraz medycynie. Mimo to głównym problemem w powszechnym zastosowaniu RL i SF są wciąż wysokie koszty ich produkcji na masową skalę. Rozwiązaniem tej sytuacji może być zastosowanie RL i SF w mieszaninach z innymi klasycznymi surfaktantami, bądź dodatkami organicznymi, co ma nie tylko aspekt ekonomiczny, ale pozwoli również ograniczyć ilość stosowanych surfaktantów syntetycznych.

Niestety, w literaturze brak jest prac dotyczących kompleksowej analizy właściwości różnego typu mieszanin w oparciu o właściwości fizykochemiczne poszczególnych składników, a szczególnie możliwości przewidywania tych właściwości. Z tego powodu uzasadnione było podjęcie badań dotyczących wzajemnego wpływu ramnolipidu i surfaktyny, niejonowego Tritonu X–165 oraz etanolu na ich adsorpcję i micelizację. Badania te oparto na pomiarach napięcia powierzchniowego przeprowadzonych w temperaturze 293 K w szerokim zakresie stężenia biosurfaktantów, TX–165 i ET tak, aby występowały one w postaci monomerycznej i zagregowanej oraz kąta zwilżania na powierzchni modelowych ciał stałych: politetrafluoroetylenu (PTFE), poli(metakrylanu metylu) (PMMA) i kwarcu (Q).

Analizę uzyskanych wyników przeprowadzono w oparciu o termodynamikę roztworów i zjawisk międzyfazowych. Stwierdzono między innymi, że izotermy napięcia powierzchniowego wodnych roztworów badanych mieszanin można opisać równaniem funkcji ekspotencjalnej drugiego rzędu nawet w przypadku, gdy występują na nich maksima. Również za pomocą funkcji ekspotencjalnych o podobnych stałych można

opisać izotermy kąta zwilżania. Możliwe jest także przewidywanie tych izoterm w oparciu o wartości kąta zwilżania dla poszczególnych składników mieszaniny.

Na podstawie izoterm napięcia powierzchniowego wyznaczono stężenie powierzchniowe składników mieszaniny w warstwie powierzchniowej stosując równanie izotermy adsorpcji Gibbsa oraz zmodyfikowane równanie Frumkina. Wykorzystując izotermy napięcia powierzchniowego składników mieszaniny wyznaczono skład tej warstwy, a w oparciu o nie możliwe było również przewidywanie napięcia powierzchniowego wodnych roztworów badanych mieszanin. Przeprowadzona termodynamiczna analiza procesów micelizacji i adsorpcji pozwoliła na zaproponowanie równania pozwalającego na wyznaczenie standardowej swobodnej energii adsorpcji Gibbsa biosurfaktantów i ET na podstawie ich krytycznego stężenia micelizacji i agregacji oraz redukcji napięcia powierzchniowego wody. Z kolei w oparciu o wartości kątów zwilżania określono kryteria jakie powinny być spełnione, aby uzyskać całkowite rozpływanie się mieszanin po powierzchni apolarnych, monopolarnych i bipolarnych ciał stałych. Otrzymane wyniki i płynące z nich wnioski mają nie tylko znaczenie poznawcze, ale również aplikacyjne, gdyż mogą być pomocne przy dobieraniu składu mieszanin, który pozwoli na otrzymanie optymalnych warunków w danym procesie.

2. STRESZCZENIE W JĘZYKU ANGIELSKIM

The presented doctoral thesis entitled *"Studies on the adsorption, aggregation, and wetting properties of mixtures containing the biosurfactant, non-ionic surfactant, and ethanol"* is a cycle of six original and closely thematically interrelated scientific papers published in the specialistic journals included in the Ministry of Education and Science (MEiN) list [**D1–D6**].

The subject of the papers being the basis of the doctoral thesis is related to the studies on adsorption, aggregation, and wetting properties of aqueous solution mixtures of the biosurfactant (mono–rhamnolipid (RL) or surfactin (SF) with the non–ionic surfactant (Triton X– 165 (TX165)) or short–chain alcohol (ethanol (ET)). RL and SF used in the studies were selected due to their significant surface and biological activities, which determine their various uses in many industries, environmental protection, and medicine. The major problem in the common use of RL and SF is their still high mass production cost. The solution to this problem may consist in the use of RL and SF in the mixtures with other classical surfactants or organic additives. This has not only an economical advantage – but it allows to reduce the amount of already used synthetic surfactants.

Unfortunately, the literature does not report about a comprehensive analysis of the properties of various types of mixtures based on the physicochemical properties of individual components, and especially on the possibility of their prediction. For this reason, the research carried out on the mutual influence of RL and SF, non–ionic TX165 and ET on their adsorption and micellization was justified. The studies were based on the surface tension measurements at 293 K in a wide range of concentrations of the biosurfactants, TX165, and ET, so that they could occur in monomeric and aggregated forms. Moreover, this was based on the contact angle measurements of the obtained mixtures on the surface of the three model solids: polytetrafluoroethylene (PTFE), poly(methacrylate methyl), and quartz (Q). The analysis of the obtained results was based on the solution thermodynamics and interfacial phenomena. It was found that the surface tension isotherms of aqueous solutions of the tested mixtures can be described by the exponential function of the second order even when the maxima are present. The contact angle isotherms could be described by the exponential functions of similar constants. It is also possible to predict those isotherms on the basis of the contact angle values for the individual mixture components.

Based on the surface tension isotherms, the surface concentration of mixture components in the surface layer was determined using the Gibbs adsorption isotherm equation and the modified Frumkin equation. Applying the surface tension isotherms of the mixture components, it was possible to determine the composition of this layer. On the other hand, it was possible to use the mixture component surface tensions to predict the surface tension of the aqueous solutions of the studied mixtures. The thermodynamic analysis of the micellization and adsorption processes allowed to propose an equation that can be used to determine the standard Gibbs free energy of adsorption of biosurfactants and ET on the basis of their critical micelle and aggregation concentration as well as the reduction of water surface tension value. In turn, on the basis of the contact angle values, the criteria that have to be met to achieve complete spreading of the mixture solution over the apolar, monopolar and bipolar solid surfaces were determined. The obtained results and conclusions drawn from them have not only cognitive but also application significance. They can be a helpful factor in selecting the mixture composition, allowing to obtain optimal conditions for a given process.

3. WYKAZ PRAC

Podstawą niniejszej rozprawy doktorskiej jest cykl tematycznie powiązanych **sześciu** publikacji naukowych opublikowanych w latach **2020 – 2022** na łamach czasopism znajdujących się na liście Ministerstwa Edukacji i Nauki sporządzonej zgodnie z art. 267 ust. 3 ustawy z dnia 20 lipca 2018 r. – Prawo o szkolnictwie wyższym i nauce (Dz. U. z 2020 r. poz. 85, z późn. zm.). Wszystkie z nich charakteryzują się współczynnikiem wpływu (IF, ang. *impact factor*).

Publikacje te oznaczono w rozprawie doktorskiej numerami **D1**, **D2**, **D3**, **D4**, **D5**, **D6**, natomiast numerem **SD5** oznaczono materiał uzupełniający (ang. *Supplementary Material*) do artykułu **D5**. Do każdej publikacji dołączona została informacja na temat punktacji wg. Ministerstwa Edukacji i Nauki (MEiN), wartości wskaźnika wpływu zgodnie z rokiem publikacji (IF$_{rok}$), a także wskaźnika wpływu na przestrzeni ostatnich pięciu lat (IF$_{5-letni}$).

[D1] E. Rekiel, A. Zdziennicka*, K. Szymczyk, B. Jańczuk, *Thermodynamic Analysis of the Adsorption and Micellization Activity of the Mixtures of Rhamnolipid and Surfactin with Triton X-165*. ***Molecules***, 2022, 27, 3600.

Mój udział w powstaniu wyżej wymienionej pracy polegał na przygotowaniu koncepcji badań i dobraniu odpowiedniej metodologii, wykonaniu wszystkich badań eksperymentalnych, interpretacji otrzymanych wyników, przygotowaniu rysunków, gromadzeniu literatury przedmiotu, weryfikacji procesu pisania pracy oraz przeprowadzonych badań, analizie formalnej, edycji manuskryptu, redagowaniu manuskryptu oraz współredagowaniu i edycji odpowiedzi na recenzje pracy.

*Mój udział oceniam na **50%**.*

MEiN$_{2022}$ / MEiN$_{2023}$: 140 pkt. / 140 pkt.

IF$_{2022}$ / IF$_{5-letni}$: 4,148 / 4,189

[D2] E. Rekiel, A. Zdziennicka, K. Szymczyk, B. Jańczuk*, *Wetting Properties of Rhamnolipid and Surfactin Mixtures with Triton X-165*. **Molecules**, 2022, 27, 4706.

Mój udział w powstaniu wyżej wymienionej pracy polegał na przygotowaniu koncepcji badań i dobraniu odpowiedniej metodologii, przeprowadzeniu wszystkich badań eksperymentalnych, interpretacji otrzymanych wyników, gromadzeniu literatury przedmiotu, analizie formalnej, wizualizacji wyników, redagowaniu i edycji manuskryptu oraz współredagowaniu i edycji odpowiedzi na recenzje pracy,
*Mój udział oceniam na **55 %**.*

MEiN$_{2022}$ / MEiN$_{2023}$: 140 pkt. / 140 pkt.
IF$_{2022}$ / IF$_{5-letni}$: 4,148 / 4,189

[D3] E. Rekiel, A. Zdziennicka*, B. Jańczuk, *Adsorption properties of rhamnolipid and ethanol at water/ethanol solution-air interface.* **Journal of Molecular Liquids**, 2020, 308, 113080.

Mój udział w powstaniu wyżej wymienionej pracy polegał wykonaniu wszystkich badań eksperymentalnych, analizie formalnej otrzymanych wyników, ich interpretacji i wizualizacji, gromadzeniu literatury przedmiotu, a także na pisaniu oryginalnej wersji manuskryptu, jej edycji oraz współredagowaniu i edycji odpowiedzi na recenzje pracy.
*Mój udział oceniam na **55%**.*

MEiN$_{2020}$ / MEiN$_{2023}$: 100 pkt. / 100 pkt.
IF$_{2020}$ / IF$_{5-letni}$: 6,165 / 6,132

[D4] E. Rekiel, A. Zdziennicka*, B. Jańczuk, *Adsorption of surfactin at water with ethanol mixture-air interface*. **Journal of Molecular Liquids**, 2020, 300, 112240.

Mój udział w powstaniu wyżej wymienionej pracy polegał na zaplanowaniu i przeprowadzeniu wszystkich badań, interpretacji i analizie wyników, ich wizualizacji, gromadzeniu literatury przedmiotu, a także na pisaniu i edycji oryginalnej wersji manuskryptu oraz współredagowaniu i edycji odpowiedzi na recenzje pracy.
*Mój udział oceniam na **55%**.*

MEiN$_{2020}$ / MEiN$_{2023}$: 100 pkt. / 100 pkt.
IF$_{2020}$ / IF$_{5-letni}$: 6,165 / 6,132

[D5] E. Rekiel, A. Zdziennicka*, B. Jańczuk, *Mutual influence of ethanol and surfactin on their wetting and adhesion properties*, **Colloids and Surfaces A: Physicochemical and Engineering Aspects**, 2021, 627, 127161.

Mój udział w powstaniu wyżej wymienionej pracy polegał na zaplanowaniu i przeprowadzeniu wszystkich badań eksperymentalnych, interpretacji i wizualizacji otrzymanych wyników, gromadzeniu literatury przedmiotu, a także na pisaniu i edycji oryginalnej wersji manuskryptu oraz współredagowaniu i edycji odpowiedzi na recenzje pracy.

Mój udział oceniam na **60%**.

MEiN_{2021} / MEIN_{2023}: 70 pkt. / 70 pkt.

IF_{2021} / $\text{IF}_{\text{5-letni}}$: 5,518 / 4,746

[D6] E. Rekiel, A. Zdziennicka*, B. Jańczuk, *Effect of ethanol on wetting and adhesion properties of rhamnolipid*. **International Journal of Adhesion and Adhesives**, 2021, 110, 102955.

Mój udział w powstaniu wyżej wymienionej pracy polegał na zaplanowaniu i przeprowadzeniu wszystkich badań eksperymentalnych, wizualizacji oraz interpretacji otrzymanych wyników, gromadzeniu literatury przedmiotu, pisaniu i edycji oryginalnej wersji manuskryptu, współredagowaniu i edycji manuskryptu, a także współredagowaniu i edycji odpowiedzi na recenzje pracy.

Mój udział oceniam na **60%**.

MEiN_{2021} / MEiN_{2023}: 100 pkt. / 100 pkt.

IF_{2021} / $\text{IF}_{\text{5-letni}}$: 3,848 / 3,751

- Sumaryczna liczba punktów przypisanych czasopismom według list MEiN / MEiN_{2023}: **650 pkt. / 650 pkt.**
- Sumaryczna wartość wskaźnika IF / $\text{IF}_{\text{5-letni}}$: **30,064 / 29,139**
- Średni udział: **56%**

4. KOMENTARZ DO ROZPRAWY DOKTORSKIEJ

4.1. LISTA SYMBOLI

RL – mono–ramnolipid

SF – surfaktyna

TX165 – Triton X–165

ET – etanol

PTFE – politetrafluoroetylen

PMMA – poli(metakrylan metylu)

Q – kwarc

CMC – krytyczne stężenie micelizacji

CAC – krytyczne stężenie agregacji

AB – składowa kwasowo–zasadowa

LW – składowa Lifshitza–van der Waalsa

$\boldsymbol{\gamma}$ – napięcie powierzchniowe

$\boldsymbol{\gamma_W}$ – napięcie powierzchniowe wody

$\boldsymbol{\gamma_{LV}}$ – napięcie powierzchniowe ciecz–powietrze

$\boldsymbol{\gamma_{LV}^{min}}$ – minimalne napięcie powierzchniowe cieczy

$\boldsymbol{\gamma_{SV}}$ – napięcie powierzchniowe ciało stałe – powietrze

$\boldsymbol{\gamma_{SL}}$ – napięcie międzyfazowe ciało stałe – ciecz

γ^{LW} – składowa napięcia powierzchniowego wynikająca z oddziaływań międzycząsteczkowych Lifshitza–van der Waalsa

γ_{LV}^{LW} – składowa napięcia powierzchniowego cieczy wynikająca z oddziaływań międzycząsteczkowych Lifshitza–van der Waalsa

γ_{SV}^{LW} – składowa napięcia powierzchniowego ciała stałego wynikająca z oddziaływań międzycząsteczkowych Lifshitza–van der Waalsa

γ^{AB} – składowa napięcia powierzchniowego wynikająca z kwasowo–zasadowych oddziaływań międzycząsteczkowych w ujęciu Lewisa

γ^+ – parametr elektrono–akceptorowy składowej kwasowo-zasadowej napięcia powierzchniowego

γ_{LV}^+ – parametr elektrono-akceptorowy składowej kwasowo-zasadowej napięcia powierzchniowego cieczy

γ_{SV}^+ – parametr elektrono-akceptorowy składowej kwasowo-zasadowej napięcia powierzchniowego ciała stałego

γ^- – parametr elektrono–donorowy składowej kwasowo-zasadowej napięcia powierzchniowego

γ_{LV}^- – parametr elektrono–donorowy składowej kwasowo-zasadowej napięcia powierzchniowego cieczy

γ_{SV}^- – parametr elektrono–donorowy składowej kwasowo-zasadowej napięcia powierzchniowego ciała stałego

$\gamma_{LV} \cos\theta$ – napięcie adhezyjne

γ_c – krytyczne napięcie powierzchniowe zwilżania ciała stałego

Γ – nadmiarowe stężenie powierzchniowe Gibbsa

Γ_{LV} – nadmiarowe stężenie powierzchniowe na granicy faz ciecz–powietrze

Γ_{SV} – nadmiarowe stężenie powierzchniowe na granicy faz ciało stałe–powietrze

Γ_{SL} – nadmiarowe stężenie powierzchniowe na granicy faz ciało stałe–ciecz

Γ_{ET} – nadmiarowe stężenie powierzchniowe Gibbsa dla etanolu

Γ_{RL} – nadmiarowe stężenie powierzchniowe Gibbsa dla ramnolipidu

Γ^{max} – maksymalne nadmiarowe stężenie powierzchniowe Gibbsa

Γ_1^{max} – maksymalne nadmiarowe stężenie powierzchniowe Gibbsa składnika 1

Γ_2^{max} – maksymalne nadmiarowe stężenie powierzchniowe Gibbsa składnika 2

Γ_{12} – maksymalne nadmiarowe stężenie powierzchniowe Gibbsa mieszaniny składników 1 i 2

Γ^∞ – graniczne stężenie powierzchniowe Gibbsa

Γ_1^∞ – graniczne stężenie składnika 1 mieszaniny

Γ_2^∞ – graniczne stężenie składnika 2 mieszaniny

$\mathbf{\Gamma}_{12}^{\infty}$ – graniczne stężenie obu składników mieszaniny

$\Delta \mathbf{G}_{ads}^{0}$ – standardowa swobodna energia adsorpcji Gibbsa

$\Delta \mathbf{G}_{mic}^{0}$ – standardowa swobodna energia micelizacji Gibbsa

$\Delta \mathbf{H}_{ads}^{0}$ – standardowa entalpia adsorpcji Gibbsa

$\Delta \mathbf{S}_{ads}^{0}$ – standardowa entropia adsorpcji Gibbsa

$\mathbf{C}_{min}^{sat}$ – minimalne stężenie odpowiadające tworzeniu się nasyconej monowarstwy adsorpcyjnej na granicy faz woda–powietrze

$\mathbf{C}_{unsat}$ – stężenie odpowiadające nienasyconej monowarstwie adsorpcyjnej na granicy faz woda–powietrze

$\boldsymbol{\pi}$ – ciśnienie warstwy

$\boldsymbol{\theta}$ – kąt zwilżania

$\boldsymbol{\theta}^{min}$ – minimalny kąt zwilżania

$\mathbf{A}^{0}$ – graniczna powierzchnia zajmowana przez jedną cząsteczkę

$\mathbf{A}^{min}$ – minimalna powierzchnia zajmowana przez jedną cząsteczkę

$\mathbf{W}_{a}$ – praca adhezji cieczy do powierzchni ciała stałego

$\mathbf{W}_{c}$ – praca kohezji cieczy

$\mathbf{S}_{L/S}$ – współczynnik rozpływania cieczy po powierzchni ciała stałego

$\boldsymbol{\omega}$ – powierzchnia zajmowana przez 1 mol każdego składnika lub mieszaniny

$\mathbf{x}^{S}$ – ułamek molowy w warstwie powierzchniowej

$\mathbf{x}_{1}^{S}$ // $\mathbf{X}_{1}$ – ułamek molowy surfaktantu 1 w warstwie powierzchniowej

$\mathbf{x}_{2}^{S}$ // $\mathbf{X}_{2}$ – ułamek molowy surfaktantu 2 w warstwie powierzchniowej

$\boldsymbol{\beta}^{\sigma}$ – parametr oddziaływań międzycząsteczkowych w mieszanej monowarstwie adsorpcyjnej

$\boldsymbol{\beta}^{M}$ – parametr oddziaływań międzycząsteczkowych w mieszanej miceli

$\mathbf{f}^{M}$ – współczynnik aktywności surfaktantów w mieszanej miceli

$\boldsymbol{\varphi}$ – parametr oddziaływań międzyfazowych

4.2. WSTĘP

Biosurfaktanty to amfifilowe związki powierzchniowo czynne pochodzenia naturalnego. Ich niepolarny, hydrofobowy ogon stanowią reszty węglowodorowe, które mogą mieć różne długości oraz być w różnym stopniu rozgałęzione. Polarna hydrofilowa głowa składa się z peptydów, węglowodanów, aminokwasów, alkoholu lub kwasu karboksyfosforowego [1]. Budowa i struktura cząsteczek biosurfaktantów decyduje o ich podziale na różne grupy. Biosurfaktanty klasyfikuje się także ze względu na typ szczepu bakteryjnego, masę cząsteczkową oraz sposób działania. Należy pamiętać, że biosurfaktanty choć wytwarzane przez mikroorganizmy, np. bakterie, drożdże czy grzyby nitkowate, wydzielane są również przez niektóre wielokomórkowe organizmy eukariotyczne takie jak rośliny i zwierzęta [2,3] (Rys. 1).

Rys. 1. *Źródła biosurfaktantów (opracowanie własne)*

Biosurfaktanty pochodzące od mikroorganizmów produkowane są jako metabolity wtórne, które przylegają do powierzchni komórki lub są wydzielane poza nią. Część z nich może być też otrzymywana w wyniku procesów enzymatycznych

z wykorzystaniem enzymów hydrolitycznych [3]. Sanchez i Demain [4] określają wtórne produkty przemiany materii jako niskocząsteczkowe związki wytwarzane zazwyczaj w fazie równowagi, czyli późnej fazie wzrostu mikroorganizmów. Aby jak najbardziej zoptymalizować proces otrzymywania biosurfaktantów przez mikroorganizmy należy wziąć pod uwagę takie czynniki jak źródła azotu oraz węgla, stężenie substratu lipofilowego, dostępność mikroelementów, wielkość inokulum (populacji mikroorganizmów lub komórek, która zostaje wprowadzona do fermentacyjnej lub każdej innej, odpowiedniej pożywki [5]), temperaturę, pH, stopień napowietrzania i szybkość mieszania [2].

Jednym z kryteriów podziału biosurfaktantów jest ich masa cząsteczkowa. Średnia masa cząsteczkowa biosurfaktantu wynosi od 500 do 1500 Da [2]. Związki o niskiej masie cząsteczkowej (LMW, ang. *low–molecular weight*) mieszczącej się w zakresie od 500 do 1000 kDa wykazują większą skuteczność w obniżaniu napięcia powierzchniowego na granicach faz woda–powietrze czy woda–olej [2,3,6]. Przykładami takich związków mogą być: glikolipidy (ramnolipidy, soforolipidy ksylolipidy, lipidy celobiozowe, trehalozowe), lipopeptydy (surfaktyna, ituryna) lub fosfolipidy [2,3,6,7]. Niska masa cząsteczkowa pozwala na ich wykorzystanie, m.in. w bioremediacji zanieczyszczeń [7]. Biosurfaktanty, których masa cząsteczkowa wynosi zazwyczaj powyżej 1000 kDa [7] należą do związków wielkocząsteczkowych (HMW, ang. *high–molecular weight*). Związki te są bardziej skuteczne w stabilizowaniu emulsji oleju w wodzie i mogą silnie przylegać do różnych powierzchni, zachowując się jak bioemulgatory [2,3]. Przykładami tego typu biosurfaktantów mogą być lipoproteiny i lipopolisacharydy, kwasy tłuszczowe (nasycone i nienasycone) oraz surfaktanty polimerowe, np. liposan, alasan i emulsan [2,3,6,7]. W praktyce jednak częściej wykorzystywane są LMW ze względu na ich wysoki potencjał obniżania napięcia powierzchniowego i międzyfazowego [8].

Podobnie jak w przypadku klasycznych surfaktantów przy stężeniu zwanym krytycznym stężeniem micelizacji (CMC, ang. *critical micelle concentration*), monomery biosurfaktantów mogą organizować się w agregaty – micele. W zależności od struktury cząsteczkowej danego biosurfaktantu [1,9] wartości CMC mieszczą się w przedziale od 1 do 2000 mg/L. Biosurfaktanty tworzą micele sferyczne o średnicy równej kilku nanometrom, ale mogą tworzyć również micele mające inne kształty, np. pęcherzykowe, lamellarne, kubiczne czy heksagonalne. Właściwości tych agregatów związane są z równowagą hydrofilowo–lipofilową (HLB, ang. *hydrophilic–lipophilic balance*) [1].

Biosurfaktanty w porównaniu z klasycznymi surfaktantami charakteryzuje wysoka biodegradowalność, większa specyficzność działania nawet w ekstremalnych warunkach otoczenia, niższe napięcie powierzchniowe i międzyfazowe, niższa toksyczność, wysoka biozgodność oraz kompatybilność środowiskowa [7]. Istotne jest również to, że związki te otrzymywane są przy udziale surowców odnawialnych, a do produktów, które mogą być wykorzystywane do przyszłej produkcji biosurfaktantów zalicza się: słomę i wytłoki z trzciny cukrowej, melasę, słomę ryżową, otręby, łuski soi, mąkę z manioku i ścieki rolnicze [1]. Zastosowanie surowców odpadowych do produkcji biosurfaktantów ma nie tylko wymiar ekonomiczny, gdyż pozwala obniżyć wysokie koszty ich produkcji, ale również umożliwia zagospodarowanie odpadów poprodukcyjnych. Tendencja ta jest również związana z jednym z obecnie najważniejszych aspektów ochrony środowiska, tzw. rozwojem zrównoważonym [10], którego celem jest także zastąpienie surfaktantów klasycznych (syntetycznych) substancjami, które będą nietoksyczne dla fauny i flory, i będą też całkowicie biodegradowalne. Z uwagi na ten fakt i właściwości jakimi charakteryzują się biosurfaktanty, związki te cieszą się coraz większym zainteresowaniem w wielu gałęziach przemysłu (Rys. 2).
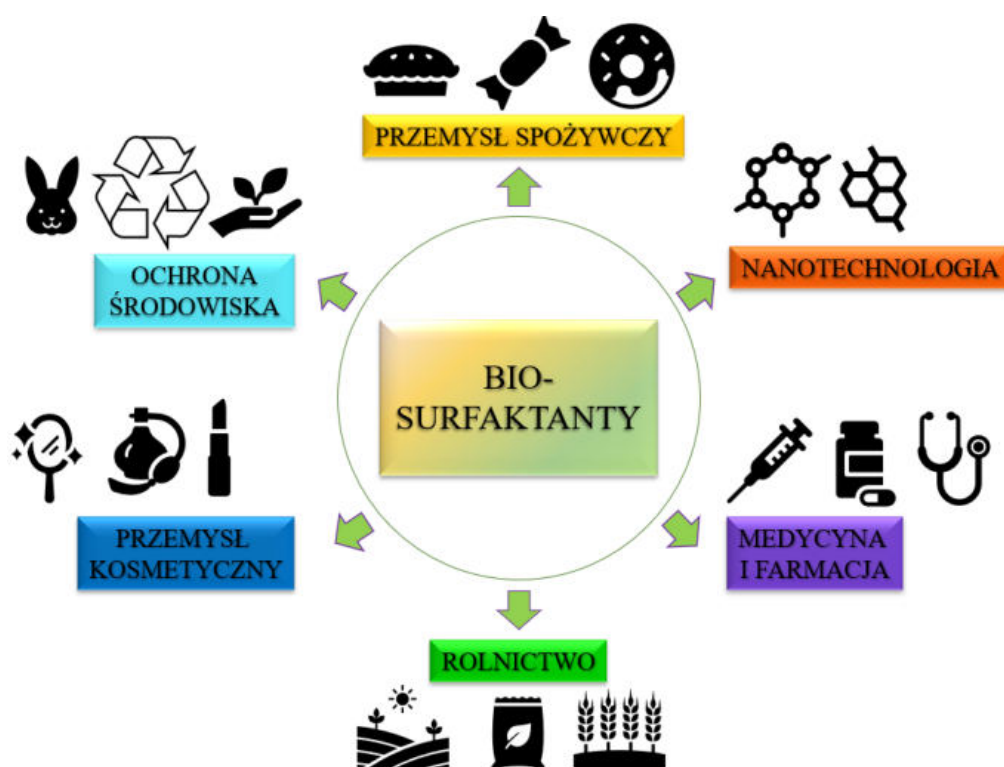
Rys. 2. *Zastosowania biosurfaktantów (opracowanie własne)*

Nie bez znaczenia jest również rosnąca świadomość konsumencka, która ma odbicie w coraz chętniej nabywanych produktach zawierających substancje pochodzenia naturalnego.

Dobre właściwości emulgujące biosurfaktantów powodują, że wchodzą one w skład detergentów, środków czyszczących oraz higieny osobistej. Ich właściwości pieniące, zwilżające, dysulgujące, czy solubilizujące są badane pod kątem wykorzystania w produkcji szamponów, mydeł, kremów do golenia, czy też polepszania pigmentacji lakierów do paznokci lub farb do włosów. Zastosowanie biosurfaktantów wpływa na gęstość oraz teksturę niektórych produktów, a także zmniejsza potencjalny wzrost drobnoustrojów chorobotwórczych poprzez działanie antyoksydacyjne i stabilność w warunkach zmieniającego się pH czy temperatury [2]. W przemyśle spożywczym właściwości antybakteryjne wobec bakteryjnych biofilmów oraz zdolność do emulgowania olejów jadalnych sprawiają, że biosurfaktanty zaczynają cieszyć się szerokim zainteresowaniem nie tylko jako dodatki do żywności, ale również w obszarze jego przetwórstwa i zapobieganiu kontaminacji [11]. Dzięki właściwościom przeciwwirusowym, przeciwnowotworowym oraz zapobiegającym tworzeniu się biofilmów bakteryjnych biosurfaktanty są w coraz większym stopniu wykorzystywane w medycynie i przemyśle farmaceutycznym [12-14]. Zastosowanie biosurfaktantów dotyczy również ich wykorzystania jako środków terapeutycznych, dodatków do szczepionek, czy środków wspomagających działanie układu odpornościowego i wchodzących w układy dostarczania leków. Çelik i wsp. [15] zwracają uwagę na działanie przeciwzapalne i przeciwwirusowe biosurfaktantów porównując je do mechanizmu działania cytokininy i receptorów toll–like. Poza tym biosurfaktanty mają wpływ na procesy hamujące enzymy, wykorzystywane są w nanotechnologii (np. przy syntezie i stabilizacji nanocząstek), rolnictwie (przy poprawie jakości ziemi czy produkcji nowych środków ochrony roślin), a także w przemyśle ropy naftowej, szczególnie w procesie intensyfikacji wydobycia ropy naftowej za pomocą mikroorganizmów (MEOR, ang. *microbial enhanced oil recovery*) oraz procesie bioremediacji wielopierścieniowych węglowodorów aromatycznych (PAHs, ang. *polycyclic aromatic hydrocarbons*) [1–3,6–8,10,16–19].

Wśród biosurfaktantów szczególne miejsce zajmują ramnolipid i surfaktyna, które ze względu na wysoką aktywność powierzchniową, niskie CMC oraz szereg aktywności biologicznych takich jak działanie antywirusowe, antynowotworowe i zapobieganie tworzeniu biofilmów mogą mieć potencjalnie bardzo szerokie zastosowanie [13,20-23].

Ramnolipidy, zaliczane do glikolipidów, w swoich cząsteczkach posiadają polisacharydową hydrofilową głowę i hydrofobowy ogon w postaci alifatycznego lub hydroksyalifatycznego kwasu połączonych ze sobą wiązaniem eterowym lub estrowym [1,3] (Rys. 3). Głównym producentem ramnolipidów jest rodzaj *Pseudomonas*, a przede wszystkim Gram–ujemna bakteria *Pseudomonas aeruginosa*. Ramnolipidy mogą być również syntetyzowane przez inne rodzaje i szczepy bakteryjne, np. *Bacillus sp.*, *Burkholderia sp.*, *Serratia rubidaea*, *Enterobacter sp.* [2,7].
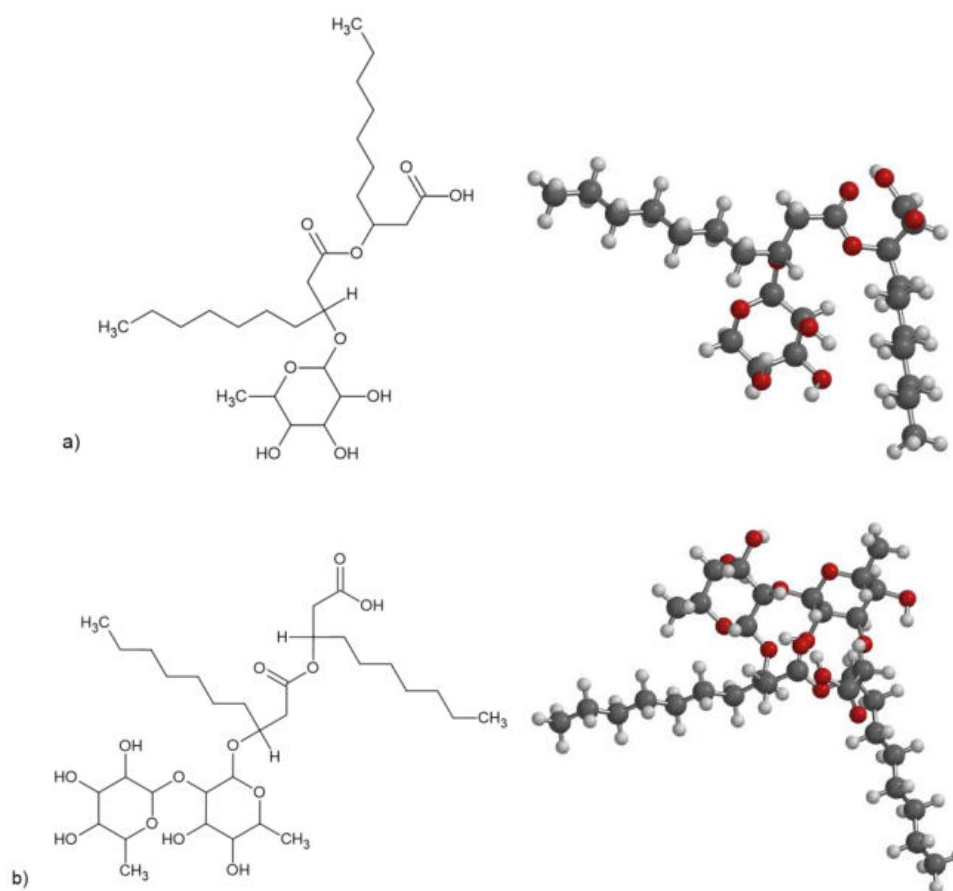
Rys. 3. *Wizualizacja struktur (a) mono– i (b) di–ramnolipidu (opracowanie własne na podstawie https://pubchem.ncbi.nlm.nih.gov/ z wykorzystaniem programu ACD/ChemSketch oraz Spartan 08 V 1.2.0).*

Ramnolipidy mogą występować w formie di–ramnolipidu: α–L–amnopiranozylo–α–L–ramnopiranozylo–β–hydroksydekanoilo–β–hydroksydekanianu   (Rha–Rha–C10–C10) i α–L–ramnopiranozylo–α–L–ramnopiranozylo–β–hydroksydekanianu (Rha–Rha–C10)   (IUPAC: *3-[3-[(2R,3R,4R,5R,6S)-4,5-dihydroksy-6-metylo-3-[(2S,3R,4R,5R,6S)-3,4,5trihydroksykwas-6-metyloksan-2-ylo]oksyoksan-2-ylo]oksydekanoiloksy]*

dekanowy; $C_{32}H_{58}O_{13}$) lub formie mono–ramnolipidu (Rha–C10–C10 i Rha–C10) (IUPAC: *kwas 3-[3-[(2R,3R,4R,5R,6S)-3,4,5-trihydroksy-6-metyloksan-2-ylo]oksydekan –oiloksy]dekanowy*; $C_{26}H_{48}O_9$) [9]. Naturalnie występujące ramnolipidy to najczęściej mieszanina mono–ramnolipidów i di–ramnolipidów [24-26]. Do chwili obecnej zidentyfikowano ponad 20 homologów ramnolipidów różniących się między sobą budową kwasu tłuszczowego [7]. Badania nad ramnolipidami udowodniły, że ich różne struktury odpowiadają za różne właściwości, np. mono–ramnolipidy wykazują większe zdolności hamowania grzybicznych patogenów roślin, a także większą aktywność emulgującą w porównaniu do di–ramnolipidów [27].

Ramnolipidy, które ze względu na budowę zaliczane są do surfaktantów anionowych [1], według niektórych badaczy pozwalają na obniżenie napięcia powierzchniowego na granicy faz woda–powietrze w temperaturze 298 K z 72 mN/m do wartości bliskich 30 mN/m [1,28-32], a na granicy międzyfazowej olej–woda z 43 mN/m do wartości bliskich 1 mN/m [2,9,30,33]. CMC czystych ramnolipidów i ich mieszanin mieści się w przedziale od 1 do 200 mg/L [2,33-38,39], przy czym ich agregacja zależy od zmiany pH roztworu. Ramnolipidy tworzą pęcherzyki o średnicy 50 – 100 nm przy pH 4,3 – 5,8; struktury lamellarne przy pH 6,0 – 6,5; cząstki lipidowe przy pH 6,2 – 6,6 i micele, gdy pH roztworu jest wyższe niż 6,8 [1,40]. Ramnolipidy oprócz dużej aktywności powierzchniowej i niskiego CMC wykazują aktywność przeciwwirusową wobec wirusów opryszczki zwykłej i HSV [41,42]. Wykazują dobre działanie w leczeniu i łagodzeniu łuszczycy, przewlekłych ran, w tym oparzeniowych, a także korzystne działanie przy minimalizowaniu bliznowacenia [43,44]. Ostatnie badania sugerują, że ramnolipidy mogą mieć zastosowanie w onkologii [45-48]. W badaniach z dziedziny nanobiotechnologii można znaleźć prace [49,50] dotyczące ramnolipidów jako stabilizatorów mikroemulsji innych nanocząstek w układach dostarczania leków z nanocząstkami srebra i tlenku niklu. Ponieważ tworzą one liposomy mogą być zastosowane do podawania leków. Ponadto ramnolipidy mogą być stosowane do usuwania zanieczyszczeń olejowych z powierzchni mórz, do degradacji składników ropy naftowej z wód morskich skażonych wyciekami z tankowców oraz wykorzystywane są na szeroką skalę w remediacji i detoksyfikacji gruntów [51-54].

Jak już wspomniano, surfaktyna (IUPAC: kwas 3-[(3S,6R,9S,12S,15R, 18S,21S,25R)-9-(karboksymetylo)-3,6,15,18-tetrakis(2-metylopropylo)-25-(10-metyloundecylo)-2,5,8,11,14,17,20,23-oktaokso-12-propan-2-ylo-1-oksa-4,7,10,13,16,19,22-heptazacyklopentakos-21-yl] propanowy; $C_{53}H_{93}N_7O_{13}$) to drugi

z biosurfaktantów o możliwym szerokim zastosowaniu, uważany jednocześnie za jeden z najlepiej poznanych naturalnych związków powierzchniowo czynnych. Związek ten jest produkowany między innymi przez bakterie z rodzaju *Bacillus* głównie szczep *Bacillus subtilis* [55,56]. Surfaktyna jest lipopeptydem składającym się z cyklicznej struktury heptapeptydu połączonego z β–hydroksykwasem tłuszczowym [55,56] oraz pierścienia składającego się z 7 aminokwasów (L–asparaginy, L–leucyny, kwasu glutaminowego, L–leucyny, L–waliny i dwóch D–leucyn) połączonych ze sobą strukturą laktonu [8] (Rys. 4). Pierścień peptydowy posiada budowę β–harmonijki nazywaną również „budową siodełkową" [57]. Naturalnie występująca surfaktyna najczęściej jest mieszaniną typów A, B, C i D, które są swoimi izoformami o różnych właściwościach fizykochemicznych [55].
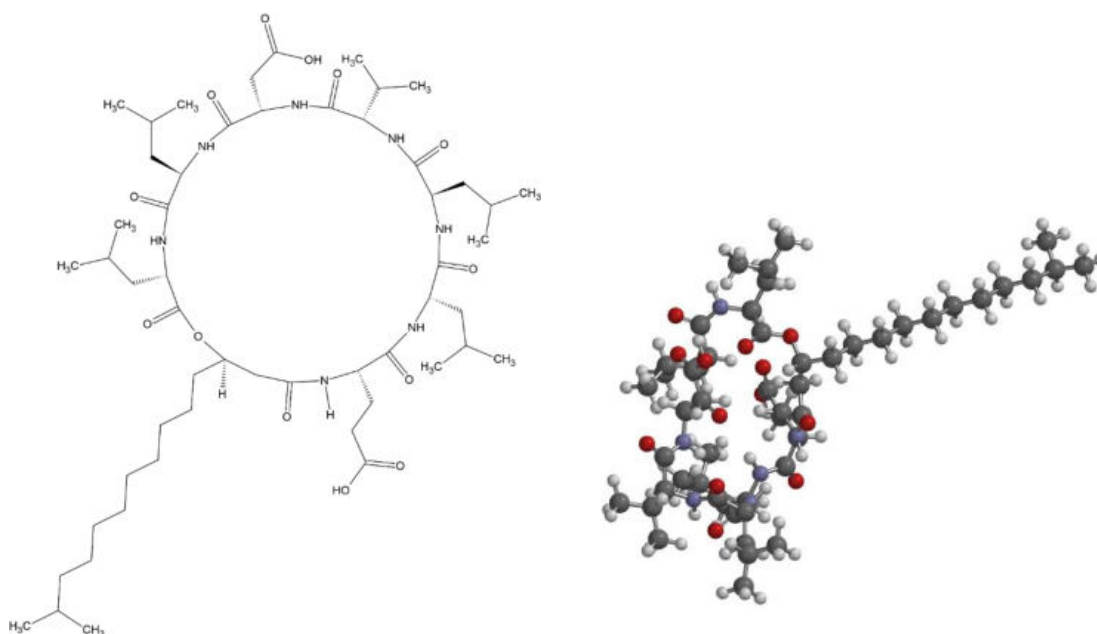
Rys. 4. *Wizualizacja struktury surfaktyny (opracowanie własne [**SD5**] z wykorzystaniem programów ACD/ChemSketch oraz Spartan 08 V 1.2.0)*

Surfaktyna, podobnie jak ramnolipid, dzięki obecności w jej cząsteczce grupy karboksylowej zaliczana jest do surfaktantów anionowych i wykazuje dużą aktywność powierzchniową redukując napięcie powierzchniowe wody do 27 mN/m [8,58-64]. Oprócz aktywności powierzchniowej surfaktyny szczególnie interesująca jest jej aktywność biologiczna: hamuje ona proces krzepnięcia krwi, powoduje lizę erytrocytów i wielu sferoplastów, protoplastów bakteryjnych, wpływa na warstwę lipidową błon komórkowych, hamuje wzrost bakterii należących do rodzaju *Mycobacterium* oraz

formuje kanały jonowe w błonach biologicznych [56,61,65-68]. Związek ten ma również działanie przeciwgrzybiczne oraz przeciwnowotworowe, a wpływając na fosfolipazę A2 zmniejsza stany zapalne [69]. Pochodne surfaktyny hamują wirusa opryszczki, chronią przed wrzodami żołądka oraz wywołują apoptozę w komórkach raka piersi [70-72].

Należy jednak pamiętać, że nawet tak aktywne powierzchniowo związki jak biosurfaktanty nie zapewniają wszystkich optymalnych warunków wymaganych w danym procesie przemysłowym. Stąd zachodzi konieczność stosowania wieloskładnikowych mieszanin różnego typu biosurfaktantów i surfaktantów lub mieszanin biosurfaktantów z dodatkami organicznymi. Do najczęściej stosowanych dodatków organicznych należą alkohole krótkołańcuchowe, które w zależności od stężenia mogą zachowywać się jako ko–surfaktanty lub ko–rozpuszczalniki. Związki te nie tylko modyfikują właściwości surfaktantów poprzez zmianę takich wielkości jak CMC czy stopień hydratacji, ale także wpływają na ich adsorpcję na różnych granicach faz [73-81]. Z chemicznego punktu widzenia alkohole krótkołańcuchowe to związki składające się z grupy alkilowej i hydroksylowej. Szczególne miejsce wśród nich zajmuje etanol (C_2H_6O), który stosowany jest między innymi jako środek odkażający. Zgodnie z wytycznymi WHO z 2015 roku etanol denaturowany o stężeniu 70% klasyfikowany jest jako antyseptyczny, a 80% (v/v) jako środek dezynfekujący do odkażania rąk. Roztwory na bazie alkoholu są trwałe i wytrzymałe, o szerokim spektrum działania przeciwdrobnoustrojowego. Nadają się one do stosowania podczas długich, otwartych operacji z ryzykiem infekcji lub rozlania chirurgicznego, do zabiegów przezskórnych z cewnikami na stałe oraz do implantacji protez, gdy ważne jest zmniejszenie liczby kolonii bakteryjnych na skórze i powstrzymanie możliwej infekcji [82].

Jak już wspomniano w skład mieszanin z biosurfaktantami mogą wchodzić także surfaktanty syntetyczne. Często są to surfaktanty niejonowe, których przedstawicielem jest grupa Tritonów. Związki należące do tej grupy mają podobną budowę chemiczną, ale różnią się długością łańcucha. Ta różnica może wpływać na wielkość i hydratację micel tych związków, a tym samym na dynamikę ich solwatacji i zmiany strukturalne [83]. Surfaktanty zaliczane do Tritonów takie jak TX–114, TX–100 i TX–165 zbudowane są z reszt fenoksypolietoksyetanolu ze średnią ilością 7 – 8 (TX–114), 9 – 10 (TX–100) i 8 – 16 (TX–165) moli tlenku etylenu [84]. Triton X–165 ($C_{14}H_{21}(OC_2H_4)_{x=8-16}OH$) (Rys. 5) podobnie jak pozostałe surfaktanty z tej grupy charakteryzuje się tym, że jest obojętny i nietoksyczny oraz kompatybilny z anionowymi i kationowymi związkami powierzchniowo czynnymi [85]. W porównaniu z surfaktantami jonowymi niejonowa

natura Tritonów jest uznawana za fizjologicznie obojętną i z tego względu oraz ich niskiego CMC [86] są one postrzegane jako bezpieczne związki służące do dostarczania leków niezależnie od rozcieńczenia w ludzkim organizmie. Dlatego też niejonowe Tritony są wykorzystywane jako nośniki leków do rozpuszczania ich hydrofobowych monomerów [87]. Surfaktanty te są także szeroko wykorzystywane w solubilizowaniu enzymów związanych z błonami komórkowymi, wchodzą w skład łagodnych detergentów stosowanych w gospodarstwach domowych i mają zastosowanie jako środki emulgujące i zwilżające [84].

R = C8
x = 8-16
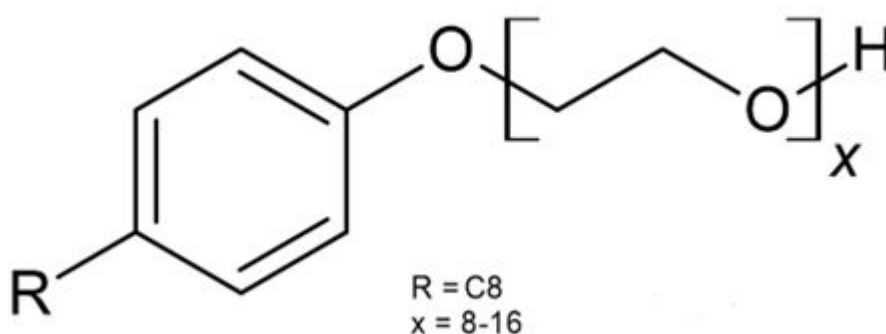
Rys. 5. *Wizualizacja struktury Tritonu X-165 (opracowanie własne na podstawie DOW ® Technical Data Sheet)*

Pomimo rosnącego zainteresowania surfaktyną i ramnolipidem w literaturze przeważają głównie prace dotyczące metod ich otrzymywania, właściwości biologicznych i potencjalnego zastosowania. Przeszkodą w powszechnym zastosowaniu ramnolipidu i surfaktyny są wciąż wysokie koszty ich otrzymywania. Z ekonomicznego punktu widzenia konieczne jest stosowanie tych związków jako dodatków do roztworów klasycznych surfaktantów. Niestety, w literaturze brak jest prac dotyczących kompleksowej analizy właściwości różnego typu mieszanin w oparciu o właściwości fizykochemiczne poszczególnych składników. Dogłębne poznanie tego typu właściwości wydaje się być uzasadnione również tym, że odpowiednio dobrana mieszanina różnego typu surfaktantów może wykazywać działanie synergetyczne, np. w redukcji napięcia powierzchniowego i tworzeniu mieszanych micel. W efekcie, pozwoli to zmniejszyć ilość stosowanych klasycznych, syntetycznych surfaktantów. Drugą alternatywą może być zastosowanie biosurfaktantów w obecności dodatków organicznych takich jak,

np. etanol. Oczywiście stosowanie takich wieloskładnikowych układów wymaga znajomości teoretycznych podstaw wzajemnego wpływu ich składników na właściwości adsorpcyjne, agregacyjne, adhezyjne i zwilżające mieszanin. Należy jednak pamiętać, że zmianie mogą nie tylko ulegać właściwości roztworu w fazie objętościowej, czy skład micel, ale również struktura i skład warstw adsorpcyjnych na granicy faz roztwór–powietrze i ciało stałe–roztwór. To z kolei będzie decydować o wielkości pracy kohezji i adhezji roztworu do powierzchni ciała stałego, których znajomość jest podstawą do przewidywania procesu zwilżania ciał stałych przez dany roztwór. Należy podkreślić, że w literaturze można spotkać tylko nieliczne badania dotyczące tych właściwości fizykochemicznych mieszanin biosurfaktantów z klasycznymi surfaktantami i nie są one oparte na kompleksowej analizie termodynamicznej uwzględniającej właściwości poszczególnych składników mieszanin. Biorąc to pod uwagę, z praktycznego i teoretycznego punktu widzenia, uzasadnione było poznanie wzajemnego wpływu biosurfaktantu: mono-ramnolipidu (RL) i surfaktyny (SF) oraz niejonowego Tritonu X– 165 (TX165) na ich adsorpcję i micelizację. Ze względu na ważne znaczenie praktyczne celowe było również wyjaśnienie pomijanego w literaturze wzajemnego oddziaływania biosurfaktant–alkohol, szczególnie w aspekcie właściwości zwilżających takiej mieszaniny. W związku z tym przeprowadzono badania właściwości adsorpcyjnych, agregacyjnych i zwilżających mieszanin RL(SF)+TX165 oraz RL(SF)+etanol (ET) w szerokim zakresie stężeń RL i SF ($2 \times 10^{-4} - 40$ mg/dm^3) oraz TX165 ($1 \times 10^{-8} - 1 \times 10^{-2}$ M) tak, aby związki te występowały w postaci monomerycznej i zagregowanej. W celu dogłębnego wyjaśnienia wzajemnego wpływu składników mieszaniny biosurfaktant+surfaktant na wymienione właściwości fizykochemiczne przeanalizowano je zarówno w funkcji stężenia mieszaniny przy jej stałym składzie, jak również przy zmiennym składzie i stężeniu mieszaniny. W przypadku etanolu badania prowadzono w zakresie jego stężenia od 7×10^{-2} M do 17,13 M, a więc w zakresie stężenia poniżej i powyżej jego krytycznego stężenia agregacji (CAC, ang. *critical aggregation concentration*).

Badania prowadzono przy stałym stężeniu biosurfaktantu i zmieniającym się stężeniu TX165 lub ET w temperaturze 293 K w oparciu o pomiary napięcia powierzchniowego wodnych roztworów mieszanin oraz ich kąta zwilżania na powierzchni modelowych ciał stałych jakimi są apolarny politetrafluoroetylen (PTFE), monopolarny poli(metakrylan metylu) (PMMA) i bipolarny kwarc (Q). Uzyskane wyniki umożliwiły przeprowadzenie termodynamicznej analizy procesu adsorpcji składników

mieszanin nie tylko na granicy faz woda-powietrze, ale również ciało stałe-woda i ciało stałe-powietrze, ustalenie relacji pomiędzy ich adsorpcją na tych granicach faz oraz określenie składu mieszanych monowarstw adsorpcyjnych. Uzyskane izotermy napięcia powierzchniowego i kąta zwilżania wodnych roztworów badanych mieszanin przeanalizowano w oparciu o te izotermy dla poszczególnych składników mieszanin. Miało to na celu znalezienie zależności, na podstawie której możliwe byłoby przewidywanie izoterm napięcia powierzchniowego i kąta zwilżania mieszanin w oparciu o te izotermy dla składników mieszaniny. Z kolei aby wyjaśnić możliwość wystąpienia efektu synergetycznego w tworzeniu mieszanych micel biosurfaktantu i Tritonu X-165 przeanalizowano zmiany krytycznego stężenia micelizacji mieszaniny biorąc pod uwagę wartości CMC poszczególnych jej składników.

4.3. WŁAŚCIWOŚCI FIZYKOCHEMICZNE RAMNOLIPIDU, SURFAKTYNY, TRITONU X–165 I ETANOLU

Właściwości adsorpcyjne, agregacyjne i zwilżające poszczególnych związków powierzchniowo czynnych zależą od rodzaju i ilości grup chemicznych występujących w częściach hydrofobowych oraz hydrofilowych ich cząsteczek. Właściwości adsorpcyjne surfaktantów na granicy faz woda–powietrze oraz agregacyjne w roztworach wodnych można między innymi określić na podstawie izoterm napięcia powierzchniowego. Adsorpcję na granicach faz ciało stałe–woda i ciało stałe–powietrze można ustalić w oparciu o pomiary kąta zwilżania wodnych roztworów surfaktantów i ich mieszanin na powierzchni różnych ciał stałych. W przypadku mieszanin RL oraz SF z TX165 jak również dla mieszanin biosurfaktantów z ET ich właściwości adsorpcyjne, agregacyjne i zwilżające przeanalizowano w oparciu o właściwości poszczególnych składników mieszanin.

Aktywność powierzchniowa biosurfaktantów i niejonowego TX165 jest różna, czego dowodem mogą być wartości minimalnego napięcia powierzchniowego ich wodnych roztworów (γ_{LV}^{min}) (Tabela 1). Z drugiej strony jeśli założymy, że związki te redukują napięcie powierzchniowe (γ_{LV}) wody do tej samej wartości, np. do 55 mN/m to redukcja ta zachodzi przy stężeniu TX165 około 8,5 razy większym niż RL i 69,8 razy większym niż SF. W przypadku wartości krytycznego stężenia micelizacji stosunek CMC TX165 do CMC RL i SF wynosi 10,4 oraz 56, zaś stosunek CMC RL do CMC SF jest równy 5,4 [**D1**]. Jak wynika z Tabeli 1 tendencja tych surfaktantów do adsorpcji na granicy faz woda–powietrze określona poprzez wartość standardowej swobodnej energii adsorpcji Gibbsa (ΔG_{ads}^0) wyznaczoną na podstawie zmodyfikowanego równania Langmuira jest zbliżona. Może to wskazywać na fakt, że przeniesienie jednej cząsteczki TX165, RL i SF z fazy objętościowej roztworu do warstwy powierzchniowej powoduje podobne zmiany swobodnej energii Gibbsa roztworu. Zmiany te prawdopodobnie związane są ze stopniem hydratacji grupy hydrofobowej i hydrofilowej w cząsteczkach TX165, RL i SF. Liczbę cząsteczek wody będących w bezpośrednim kontakcie z cząsteczkami RL, SF i TX165 można określić na podstawie powierzchni kontaktu wody oraz surfaktantów. Dla wody w temp. 293 K powierzchnia kontaktu jej cząsteczki wynosi 10 Å^2 [88], a dla surfaktantów może być wyznaczona teoretycznie na podstawie długości wiązań chemicznych pomiędzy atomami w cząsteczce, kąta między wiązaniami oraz średniej odległości między cząsteczkami danego związku. Obliczenia teoretyczne

wykazały, że objętość cząsteczki surfaktantu w środowisku wodnym może być wyznaczona w oparciu o model sześcianu, w który ta cząsteczka zostanie wpisana lub sumę sześcianów, które zawierają poszczególne fragmenty surfaktantu. Biorąc więc pod uwagę wielkość powierzchni kontaktu części hydrofobowych TX165, RL, SF oraz wody stwierdzono, że około 36, 30 i 34 cząsteczek wody może bezpośrednio kontaktować się z niepolarną częścią cząsteczek surfaktantów [**D1**].

Tabela 1. Wielkości fizykochemiczne charakteryzujące RL, SF, TX165 oraz ET w temperaturze 293 K [39,64,86,89–91] (W–A odnosi się do granicy faz woda–powietrze).

Wielkość	RL	SF	TX165	ET
CMC [M] CAC [M]	$5,21 \times 10^{-5}$ -	$9,66 \times 10^{-6}$ -	$5,41 \times 10^{-4}$ -	- 7,04
γ_{LV}^{min} [mN/m]	27,89	32,37	39,50	23,2
γ_{LV} ogona [mN/m]	21,80	24,70	22,00	-
γ_{LV} głowy [mN/m]	38,39	42,80	35,84	-
γ^{LW} głowy [mN/m]	35,38	34,25	27,70	-
γ^{AB} głowy [mN/m]	3,01	8,55	8,14	-
γ^{+} głowy [mN/m]	0,04	0,37	0,33	-
γ^{-} głowy [mN/m]	56,74	49,39	50,20	-
C_{min}^{sat} W–A [M]	$1,98 \times 10^{-6}$	$9,65 \times 10^{-8}$	5×10^{-5}	3,75
Γ^{max} W–A [mol/m^2]	$2,01 \times 10^{-6}$	$1,38 \times 10^{-6}$	$2,12 \times 10^{-6}$	$7,91 \times 10^{-6}$
ΔG_{ads}^{0} W–A [kJ/mol]	-43,55	-46,22 -51,23	-44,00	-9,28
ΔG_{mic}^{0} [kJ/mol]	-33,80	-37,90	-28,10	-
θ^{min} PTFE [°]	50,18	62,00	78,15	37,70
θ^{min} PMMA [°]	32,80	51,90	49,40	0,00
θ^{min} Q [°]	28,10	25,20	32,71	0,00

Jeśli przyjmiemy, że główną siłą napędową procesu adsorpcji na granicy faz woda–powietrze jest hydratacja części hydrofobowej cząsteczek surfaktantów to przytoczone liczby cząsteczek wody mogących kontaktować się z tą częścią uzasadniają podobne wartości ΔG_{ads}^{0} RL, SF i TX165. Fakt ten jednak nie tłumaczy różnicy

w redukcji γ_{LV} wody wskutek adsorpcji TX165, RL i SF. Z przeprowadzonych badań γ_{LV} wodnych roztworów biosurfaktantów i TX165 wynika, że ich adsorpcja na granicy faz woda–powietrze redukuje przede wszystkim składową kwasowo–zasadową (AB) napięcia powierzchniowego wody wynikającą z wiązań wodorowych. Prawdopodobnie rozrywanie tych wiązań przez zaadsorbowane cząsteczki biosurfaktantów zachodzi w większym stopniu niż przez cząsteczki TX165 [**D1,D2**].

Etanol traktowany w literaturze jako ko–surfaktant lub ko–rozpuszczalnik podobnie do biosurfaktantów i TX165 adsorbuje się na granicy faz woda–powietrze i redukuje γ_{LV} wody. Cząsteczka ET podobnie jak cząsteczki surfaktantów posiada grupę hydrofobową składającą się grup funkcyjnych –CH$_3$ i –CH$_2$– oraz polarną, którą stanowi grupa –OH. Z drugiej strony właściwości grupy –OH w ET są prawie takie same jak w cząsteczce wody. Etanol miesza się z wodą w całym zakresie stężeń. Wynika to z faktu, że moment dipolowy grupy –OH zarówno w ET jak i w wodzie jest prawie taki sam, a grupa alkilowa ET jest zbyt krótka by ograniczyć jego rozpuszczalność w wodzie.

Etanol miesza się nieograniczenie z wodą i raczej jest to mieszanina wody i ET, a nie roztwór ET w wodzie. Niemniej jednak, wskutek obecności grup hydrofobowych w cząsteczce ET, wykazuje on zarówno właściwości adsorpcyjne jak i agregacyjne. W odróżnieniu jednak od biosurfaktantów i TX165 jego maksymalne nadmiarowe stężenie Gibbsa (Γ^{max}) jest prawie równe stężeniu granicznemu (Γ^{∞}). Agregaty ET tworzące się w wodzie nie są podobne do micel biosurfaktantów oraz TX165. Należy również podkreślić, że potencjał chemiczny ET jest definiowany jako symetryczny w przeciwieństwie do potencjału biosurfaktantów, który jest asymetryczny. Ma to istotne znaczenie przy termodynamicznej interpretacji zarówno procesu adsorpcji jak i agregacji [**D1,D3,D4**].

W procesie adsorpcji biosurfaktantów, TX165 i ET na granicy faz woda–powietrze związanej z redukcją γ_{LV} wody decydującą rolę odgrywa nie tylko rodzaj i wielkość grupy hydrofobowej w ich cząsteczkach, ale również wielkość grupy hydrofilowej. Decydują one o powierzchni granicznej (A^0) zajmowanej przez cząsteczkę biosurfaktantów, TX165 i ET. Wartość A^0 przy prostopadłej orientacji cząsteczek do granicy faz woda–powietrze dla RL wynosi 69,09 Å^2, zaś dla SF w zależności od konfiguracji części hydrofilowej 93,17 lub 120,24 Å^2 [64]. W przypadku TX165 i ET o A^0 decyduje wielkość części hydrofobowej ich cząsteczek i odpowiednio wynosi ona 35,70 Å^2 [92] i 21,00 Å^2 [90]. Biorąc pod uwagę powierzchnię zajmowaną przez

cząsteczkę wody można stwierdzić, że jedna cząsteczka RL zastępuje 7 cząsteczek wody, SF 9 lub 12, TX165 3,5, zaś ET 2 cząsteczki wody. Być może jest to główną przyczyną znacznych różnic w redukcji napięcia powierzchniowego wody poprzez adsorpcję biosurfaktantów, TX165 i ET przy tym samym ich stężeniu [**D1**].

Właściwości zwilżające biosurfaktantów, TX165 i ET ustalono na podstawie pomiarów kąta zwilżania (θ) ich wodnych roztworów na powierzchni apolarnego politetrafluoroetylenu (PTFE), monopolarnego poli(metakrylanu metylu) (PMMA) i bipolarnego kwarcu (Q). Napięcie powierzchniowe PTFE (γ_{SV}) wynika jedynie z oddziaływań międzycząsteczkowych Lifshitza–van der Waalsa (LW), a praktycznie z samych oddziaływań dyspersyjnych. Zatem γ_{SV} PTFE równe jest składowej LW, a składowa kwasowo–zasadowa (AB) tego napięcia oraz parametry elektrono–akceptorowy (γ^+) i elektrono–donorowy (γ^-) są równe 0 (Tabela 2). Wartość γ_{SV} monopolarnego PMMA jest również równa jego składowej LW, ponieważ składowa AB jest równa 0 z powodu zerowej wartości parametru γ^+. W przypadku bipolarnego Q obie składowe γ_{SV} i parametry γ^+ i γ^- są większe od 0 (Tabela 2). Przeprowadzone pomiary wykazały, że zarówno biosurfaktanty, TX165, jak i ET nie posiadają dobrych właściwości zwilżających w przypadku niskoenergetycznych, hydrofobowych ciał stałych. Podobnie jak na PTFE minimalne wartości θ wodnych roztworów biosurfaktantów i TX165 na powierzchni PMMA i Q są większe od 0. Jedynie wodne roztwory ET przy jego stężeniu zbliżonym do CAC całkowicie rozpływają się po powierzchni PMMA i Q.

Zwilżalność ciał stałych przez wodne roztwory surfaktantów związana jest nie tylko z ich adsorpcją na granicy faz woda–powietrze, ale również na granicach faz ciało stałe–woda i ciało stałe–powietrze. W badaniach adsorpcji na granicach faz ciało stałe–woda i ciało stałe–powietrze przyjęto zgodnie z Fowkesem [93] oraz van Ossem i wsp. [94,95], że γ_{SV} ciała stałego poza kroplą osadzoną na jego powierzchni zmienia się pod wpływem adsorpcji substancji o γ_{LV} niższym od γ_{SV} ciała stałego. Ponieważ γ_{LV} ET oraz biosurfaktantów i TX165 przy orientacji częścią hydrofobową w kierunku powietrza jest mniejsze od γ_{SV} PMMA i Q, a większe od napięcia PTFE (Tabela 2) przyjęto, że ich warstwa utworzona na PMMA i Q poza osadzoną kroplą roztworu redukuje napięcie powierzchniowe tych ciał stałych [**D2,D5,D6**].

Tabela 2. Napięcie powierzchniowe (γ) oraz składowa LW i AB, parametry γ^+ i γ^- tego napięcia dla wody, ET, PTFE, PMMA i Q.

Wielkość	Woda	ET	PTFE	PMMA	Q
γ [mN/m]	72,80	23,20	20,24	41,28	47,70
γ^{LW} [mN/m]	26,85	21,40	20,24	41,28	38,07
γ^{AB} [mN/m]	45,95	1,80	0,00	0,00	9,63
γ^+ [mN/m]	22,98	0,09	0,00	0,00	1,61
γ^- [mN/m]	22,98	9,00	0,00	7,28	14,36

Brak całkowitego zwilżania powierzchni ciała stałego przez ciecz można wyjaśnić w oparciu o założenie, że ciecz rozpływa się całkowicie po jego powierzchni jeśli $2\sqrt{\gamma_{LV}^{LW}\gamma_{SV}^{LW}} + 2\sqrt{\gamma_{LV}^+\gamma_{SV}^-} + 2\sqrt{\gamma_{LV}^-\gamma_{SV}^+} = 2\gamma_{LV}$. W przypadku apolarnych ciał stałych wyrażenie to upraszcza się do postaci $2\sqrt{\gamma_{LV}^{LW}\gamma_{SV}^{LW}} = 2\gamma_{LV}$. Aby uzasadnić zachowanie się RL, SF, TX165 w takich układach obliczono pracę adhezji (W_a) dla nich oraz wody do powierzchni PTFE, PMMA i Q bazując na składowych i parametrach ich napięcia powierzchniowego, napięcia powierzchniowego wody oraz wymienionych ciał stałych [**D2**]. Obliczenia W_a wykonane dla ogona i głowy surfaktantów zorientowanych w kierunku ciała stałego wykazały, że w przypadku PTFE wszystkie wartości są mniejsze od wartości pracy kohezji (W_c), a współczynnik rozpływania ($S_{L/S}$) jest mniejszy niż 0. Wyniki te potwierdziły, że niemożliwe jest całkowite zwilżenie PTFE przez wodne roztwory RL, SF i TX165 [**D2**]. W przypadku PMMA przy orientacji cząsteczek biosurfaktantów i TX165 ogonem w kierunku jego powierzchni wartości $S_{L/S}$ są dodatnie, natomiast dla Q są dodatnie przy orientacjach RL, SF i TX165 zarówno głową jak i ogonem do jego powierzchni. Sugeruje to, że w przypadku wodnych roztworów TX165, RL i SF przy odpowiednim stężeniu, powinno nastąpić całkowite rozpływanie tych roztworów na powierzchni PMMA i Q, co jednak nie miało miejsca. Zjawisko to można wytłumaczyć biorąc pod uwagę orientację cząsteczek RL, SF i TX165 na granicach faz ciało stałe–woda i ciało stałe–powietrze. W przypadku prostopadłych orientacji cząsteczek RL, SF i TX165 do granicy faz woda–powietrze zajmują one powierzchnię graniczną, której wielkość jest związaną z wielkością ich cząsteczek. Powierzchnia ta dla TX165 jest mniejsza niż dla RL i SF, a SF większa niż RL. Przy takim upakowaniu cząsteczek biosurfaktantu i TX165 napięcia powierzchniowe wodnych roztworów powinny być takie same jak napięcia powierzchniowe ich ogonów.

Niestety, maksymalne upakowanie (Γ^{max}) TX165, RL i SF odpowiada powierzchni minimalnej (A^{min}) zajętej przez jedną ich cząsteczkę, a ta jest większa niż powierzchnia graniczna (A^0). Co więcej, A^{min} TX165 i SF są większe niż powierzchnie kontaktu ogonów cząsteczek przy ich równoległej orientacji do granicy faz woda–powietrze. W przypadku RL powierzchnie te są porównywalne. Sugeruje to, że ogony biosurfaktantu i TX165 w nasyconej monowarstwie mogą być zorientowane równolegle w kierunku granicy faz woda–powietrze, podczas gdy głowa może być zorientowana prostopadle i/lub pod pewnym kątem do granicy faz [**D2**].

W przypadku TX165 występuje największa różnica pomiędzy A^{min} w nasyconej monowarstwie na granicy faz woda–powietrze i A^0. Odzwierciedleniem tego może być minimalna wartość γ_{LV} wodnego roztworu TX165, która jest znacząco wyższa niż dla roztworów RL i SF mimo niewielkich różnic między wartościami γ_{LV} ich ogonów (Tabela 1). Różnice pomiędzy A^{min} i A^0 zajmowanymi przez biosurfaktanty i TX165 w monowarstwie adsorpcyjnej na granicy faz woda–powietrze wynikają prawdopodobnie z sił przyciągania i odpychania pomiędzy tymi cząsteczkami. Część hydrofilowa cząsteczki TX165 jest w dużej mierze zhydratyzowana w środowisku wodnym i w wyniku tego może nawet uzyskać ładunek dodatni. Z tego powodu w monowarstwie adsorpcyjnej na granicy faz woda–powietrze mogą pojawić się odziaływania odpychające pomiędzy cząsteczkami TX165, których obecność powoduje wzrost powierzchni zajętej przez cząsteczkę TX165. W przypadku biosurfaktantów, które ze względu na specyficzną strukturę głowy mogą być traktowane jako elektrolit typu 1:1, oddziaływania odpychające pomiędzy cząsteczkami w monowarstwie mogą być zobojętnione poprzez tworzenie się między nimi wiązań wodorowych. Cząsteczki biosurfaktantów w nasyconej monowarstwie będą mocniej upakowane niż w przypadku TX165, co ma wpływ na napięcia powierzchniowe ich roztworów [**D2**].

Zachowanie cząsteczek biosurfaktantów i TX165 na granicy faz PTFE–woda jest podobne do tego na granicy faz woda–powietrze. Wniosek taki może być podparty wartościami ich Γ^{max}. Podobieństwo między nadmiarowym stężeniem powierzchniowym Gibbsa na granicach faz ciało stałe–ciecz (Γ_{SL}) i ciecz–powietrze (Γ_{LV}) zostało też potwierdzone na podstawie równania Lucassen–Reynders [96]. Dla PTFE zależności napięcia adhezyjnego ($\gamma_{LV}\cos\theta$) od powierzchniowego (γ_{LV}) dla biosurfaktantów i TX165 mogą być opisane funkcją liniową ze stałą a bliską –1. Zgodnie z równaniem Lucassen–Reynders [96], Γ_{SL} jest bliskie Γ_{LV} jeśli nie zachodzi adsorpcja

surfaktantów wokół kropli roztworu umieszczonej na powierzchni PTFE (nadmiarowe stężenie powierzchniowe na granicy faz ciało stałe–powietrze, $\Gamma_{SV} = 0$). Dla apolarnych ciał stałych takich jak PTFE, których napięcie powierzchniowe wynika jedynie z oddziaływań LW, jeśli stała $a = -1$ wówczas stała b spełniała równanie $b = W_a = \gamma_{LV}(\cos\theta + 1) = 2\sqrt{\gamma_{LV}^{LW}\gamma_{SV}^{LW}}$. Jeśli θ jest równy 0, to z jednej strony $\gamma_{LV} = \frac{b}{2}$, a z drugiej, $\gamma_{LV} = 2\sqrt{\gamma_{LV}^{LW}\gamma_{SV}^{LW}}$. Z liniowej zależności pomiędzy $\gamma_{LV}\cos\theta$ i γ_{LV} dla PTFE dla wodnych roztworów TX165, RL i SF wynika, że stała b jest równa 47,29 mN/m. Ta wartość jest nieznacznie większa niż W_a wody do PTFE (46,62 mJ/m^2). To wskazuje, że TX165 i biosurfaktanty zmniejszają jedynie składową AB γ_{LV} wody, co spowodowane jest adsorpcją ich cząsteczek na granicy faz woda–powietrze. Jeśli θ jest równy 0 nie można zastosować liniowej zależności pomiędzy $\gamma_{LV}\cos\theta$ i γ_{LV}, ponieważ γ_{LV}^{LW} nie może być wyższe niż γ_{LV}. Nie jest też więc możliwe określenie krytycznego napięcia powierzchniowego zwilżania (γ_c) PTFE, które odpowiada θ równemu 0. Kąt zwilżania równy 0 pojawia się tylko jeśli γ_{LV} cieczy jest równe γ_{SV} PTFE i wynika jedynie z oddziaływań LW [**D2**].

Dowodem na podobne zachowanie biosurfaktantów i TX165 na granicach faz PTFE–woda i woda–powietrze mogą być izotermy napięcia powierzchniowego (γ_{LV}) ich wodnych roztworów oraz kąta zwilżania (θ), które mogą być opisane przez równanie Szyszkowskiego [97] o podobnych stałych, które odpowiadają ΔG_{ads}^0. Przy założeniu, że równania termodynamiczne mogą być zastosowane dla wszystkich granic faz, a γ_{SV} ciał stałych nie zależy od stężenia surfaktantów w roztworze, równanie Szyszkowskiego można poddać modyfikacji [**D2**]. Okazuje się, że stosując to równanie możliwe jest uzyskanie prawie takich samych wartości Γ^{max} i stałej a_1 dla TX165, RL i SF co wskazuje, że wartości ΔG_{ads}^0 obliczone z wykorzystaniem stałej a_1 są do siebie podobne. Są one również podobne do wartości otrzymanych z równania Langmuira zmodyfikowanego przez de Boera [97,98]. Należy też wspomnieć, że w obliczeniach Γ^{max} i stałej a_1 zastosowano wartości stężenia odpowiadające występowaniu biosurfaktantów i TX165 w formie monomerycznej.

Izotermy kąta zwilżania wodnych roztworów tych związków na powierzchni PTFE mogą być opisane nie tylko przez równanie Szyszkowskiego, ale również przez funkcję ekspotencjalną drugiego rzędu. Pomimo faktu, że trudno jest znaleźć zależność pomiędzy stałymi tej funkcji i niektórymi właściwościami fizykochemicznymi składowych roztworu, można je jednak skorelować ze składowymi i parametrami γ_{LV}

surfaktantów i wody. Podobna sytuacja miała miejsce przy opisie izoterm γ_{LV} wodnych roztworów surfaktantów.

W przeciwieństwie do PTFE, napięcie powierzchniowe PMMA jest większe niż napięcia głowy i ogona TX165 i RL, a Q wyższe niż głowy i ogona wszystkich analizowanych związków aktywnych powierzchniowo. Co więcej, minimalne γ_{LV} wodnych roztworów biosurfaktantów i TX165 jest mniejsze niż γ_{SV} PMMA i Q (Tabela 1 i 2). Opierając się na modelu van Ossa [94,95] można stwierdzić, że wodne roztwory biosurfaktantów i TX165 przy ich odpowiednim stężeniu powinny rozpływać się całkowicie po powierzchniach PMMA i Q. Niestety, nie ma to miejsca dla wszystkich roztworów, co może wynikać z migracji cząsteczek biosurfaktantów i TX165 na powierzchnię PMMA i Q. Proces ten powoduje powstanie warstwy adsorpcyjnej wokół kropli roztworu umieszczonej na powierzchniach PMMA i Q, która powoduje zmianę ich γ_{SV}. Potwierdzeniem tej hipotezy są dodatnie wartości $S_{L/S}$ biosurfaktantów i TX165. Na możliwość adsorpcji TX165, RL i SF wokół kropli roztworu umieszczonej na powierzchniach PMMA i Q wskazują także krzywe obrazujące zależności $\gamma_{LV}\cos\theta$ od γ_{LV}. Nachylenie krzywych dla wodnych roztworów surfaktantów na Q jest dodatnie oprócz tych dla wodnych roztworów TX165. Natomiast w przypadku PMMA nachylenie zależności $\gamma_{LV}\cos\theta$ od γ_{LV} jest dodatnie dla TX165 w całym zakresie badanych stężeń, natomiast ujemne dla RL i SF przy ich stężeniach większych niż CMC. Przy założeniu, że biosurfaktanty i TX165 nie adsorbują się na PMMA i Q wokół osadzonej kropli to zgodnie z równaniem Lucassen–Reynders [96] powinna mieć miejsce ich ujemna adsorpcja na granicy faz ciało stałe–woda. W praktyce jest to niemożliwe. Prawdopodobnie z powodu obecności warstw adsorpcyjnych RL, SF i TX165 na granicach faz PMMA–powietrze i Q–powietrze, izotermy θ ich wodnych roztworów nie mogą być opisane za pomocą zmodyfikowanego równania Szyszkowskiego [**D2**]. Interesujące jest jednak to, że stosując różnicę pomiędzy kątem zwilżania dla wody i roztworu zamiast ciśnienia warstwy (π) na granicach faz PMMA(Q)-ciecz (różnica pomiędzy napięciem międzyfazowym PMMA(Q)–woda a napięciem międzyfazowym PMMA(Q)–roztwór) możliwe było opisanie izoterm θ dla wodnych roztworów TX165 na PMMA i Q. Wartości ΔG_{ads}^{0} obliczone ze zmodyfikowanego równania Szyszkowskiego w oparciu o wartości stałej a_1 są bliskie ΔG_{ads}^{0} dla TX165 na granicach faz PMMA–woda i Q–woda obliczonych z równania Langmuira zmodyfikowanego przez de Boera [97,98]. Dla wodnych roztworów RL stosując równanie Szyszkowskiego

niemożliwe było opisanie izoterm θ na PMMA i Q, a dla roztworów SF na PMMA. Zgodnie z równaniem Lucassen–Reynders [96] dodatnie nachylenie krzywych otrzymanych z zależności $\gamma_{LV}\cos\theta$ od γ_{LV} wskazuje, że adsorpcja surfaktantu na granicy faz ciało stałe–woda jest mniejsza niż na ciało stałe–powietrze. Może to wynikać z bardzo silnych oddziaływań cząsteczek wody z powierzchnią ciała stałego, co utrudnia adsorpcję surfaktantów i ma odzwierciedlenie w wartościach W_a. Z powodu oddziaływań cząsteczek wody z PMMA i Q ma miejsce zmniejszona adsorpcja TX165, RL i SF na granicach faz PMMA–woda i Q–woda w porównaniu do adsorpcji na granicy faz woda–powietrze. Dodatkowo porównanie A^{min} i A^0 zajmowanych przez cząsteczki TX165, RL i SF na tych granicach faz z powierzchnią ich kontaktu wskazuje na ich równoległą orientację do powierzchni PMMA i Q [**D2**].

Mechanizm adsorpcji ET i zachowanie się jego cząsteczek w warstwach adsorpcyjnych na różnych granicach faz, a zatem i jego właściwości zwilżające, są nieco inne niż RL, SF i TX165. Praca adhezji (W_a) ET do stosowanych w badaniach ciał stałych jest mniejsza od pracy adhezji wody, biosurfaktantów oraz TX165. Również napięcie powierzchniowe (γ_{LV}) ET jest mniejsze od składowej LW γ_{LV} wody. Z tego też powodu dla wodnego roztworu ET prostoliniowa zależność pomiędzy $\gamma_{LV}\cos\theta$ i γ_{LV} dla PTFE istnieje tylko w pewnym zakresie jego stężenia. W układach PMMA(Q)–kropla roztworu ET–powietrze mechanizm adsorpcji na granicy faz PMMA(Q)–woda jest oparty nie tylko na silnych oddziaływaniach hydrofobowych, ale również na tworzeniu wiązań wodorowych. Prawdopodobnie przy niskich stężeniach ET adsorpcja na granicy faz zachodzi nie na „czystej" powierzchni PMMA lub Q, a raczej na powierzchni tych ciał stałych pokrytych monowarstwą wody. Podobny mechanizm adsorpcji może występować na granicy faz PMMA(Q)–powietrze. W przeciwieństwie do biosurfaktantów i TX165, ET tworzy film poza kroplą jego wodnego roztworu osadzonego na PMMA lub Q nie tylko w wyniku penetracji jego cząsteczek z tej kropli, ale również wskutek adsorpcji jego par na tych powierzchniach. Podobnie do RL, SF i TX165 adsorpcja ET na granicach faz PMMA(Q)–powietrze i PMMA(Q)–woda jest mniejsza aniżeli na granicy faz woda–powietrze. Należy jednak pamiętać, że ułamek molowy ET zmieniał się od 0 do 1 i powyższe stwierdzenie nie dotyczy całego zakresu stężenia ET w fazie objętościowej [**D5**,**D6**].

4.4. WŁAŚCIWOŚCI ADSORPCYJNE I AGREGACYJNE MIESZANIN RAMNOLIPID (SURFAKTYNA)+ETANOL I RAMNOLIPID (SURFAKTYNA)+TRITON X–165

4.4.1. Właściwości adsorpcyjne mieszanin ramnolipid+etanol i surfaktyna+etanol

Skład roztworu oraz stężenie występujących w nim składników wpływa na jego napięcie powierzchniowe (γ_{LV}), co potwierdziły izotermy γ_{LV} wodnych roztworów RL+ET oraz SF+ET, z których wynika, że przy stałych stężeniach ET powyżej jego krytycznego stężenia agregacji (CAC) [90] bez względu na stężenie biosurfaktantu w roztworze γ_{LV} badanych roztworów jest zbliżone do γ_{LV} roztworu ET o jego danym stężeniu. Dodatkowo minimalne napięcie powierzchniowe roztworów jest równe γ_{LV} czystego ET [90,**D3**,**D4**]. Napięcie powierzchniowe wody w temperaturze 293 K wynosi 72,8 mN/m i wynika z odziaływań międzycząsteczkowych Lifshitza–van der Waalsa (LW) oraz kwasowo–zasadowych (AB) związanych z tworzeniem wiązań wodorowych (Tabela 2). Van Oss i wsp. [94,95] traktując wodę jako ciecz modelową założyli, że parametry elektrono–akceptorowy (γ^+) i elektrono–donorowy (γ^-) składowej AB jej napięcia powierzchniowego mają taką samą wartość. Napięcie powierzchniowe ET również wynika z oddziaływań międzycząsteczkowych LW oraz AB jednak γ^+ jest mniejszy od γ^-. W przypadku biosurfaktantów, zgodnie z van Ossem i Constanzo [99], ich γ_{LV} zależy od orientacji cząsteczek w kierunku fazy gazowej. Jeśli więc RL zorientowany jest częścią hydrofobową w kierunku powietrza jego γ_{LV} powinno odpowiadać γ_{LV} oktanu [**D3**] i wynosić 21,80 mN/m, natomiast γ_{LV} tak zorientowanej SF odpowiada γ_{LV} 2,2-dimetylodekanu i wynosi 24,70 mN/m [64]. Przy orientacji cząsteczek RL i SF hydrofilową głową w kierunku fazy gazowej ich napięcie powierzchniowe będzie wynikać nie tylko z oddziaływań LW, ale również AB (Tabela 1). W roztworze wodnym cząsteczki ET i SF powinny być zorientowane ogonem hydrofobowym w kierunku powietrza i z uwagi na fakt, że składowe LW dla wody, ET i ogona SF są do siebie zbliżone, wzrost stężenia ET lub SF w roztworze powoduje spadek wartości składowej AB napięcia powierzchniowego wody. Z tego powodu γ_{LV} roztworu zmniejsza się zarówno przy stałym stężeniu SF jak i ET [**D4**].

Przy stałym stężeniu SF napięcie powierzchniowe roztworu SF+ET zmniejsza się od wartości γ_{LV} wodnego roztworu SF przy jej danym stężeniu do γ_{LV} ET. W przypadku roztworów mieszaniny RL i ET przy stałym stężeniu RL napięcie powierzchniowe

również zmienia się od napięcia powierzchniowego wodnego roztworu RL do napięcia powierzchniowego ET. Jednak na izotermach obrazujących te zmiany dla roztworów o stałym stężeniu RL w zakresie odpowiadającym jego nasyconej monowarstwie adsorpcyjnej na granicy faz woda–powietrze występują maksima. Taki przebieg izoterm potwierdziły obliczenia oparte na izotermach γ_{LV} wodnych roztworów RL w nieobecności ET [39] i ET w nieobecności RL [90] przeprowadzone z wykorzystaniem zmodyfikowanego równania Fainermana i Millera [100,101], a nie potwierdziły obliczenia z wykorzystaniem równania Connorsa [102]. Z drugiej strony równanie Connorsa pozwoliło na opisanie zmian γ_{LV} wodnych roztworów SF+ET w funkcji stężenia SF przy zastosowaniu w tym równaniu odpowiednich stałych [**D3,D4**].

Zmiany γ_{LV} wodno–etanolowych roztworów SF i RL zależą od ich adsorpcji na granicy faz roztwór–powietrze [**D3,D4**]. W przypadku biosurfaktantów w zakresie ich badanych stężeń można przyjąć, że zgodnie z asymetryczną definicją potencjału chemicznego ich współczynniki aktywności są bliskie 1, stąd ich nadmiarowe stężenia powierzchniowe Gibbsa (Γ) można było obliczyć stosując stężenia molowe w równaniu izotermy adsorpcji Gibbsa [97]. Należy także zauważyć, że Γ biosurfaktantów można traktować jako praktycznie równe ich całkowitym stężeniom w warstwie powierzchniowej na granicy faz roztwór–powietrze. Jednakże w przypadku ET jego Γ nie jest równe całkowitemu stężeniu w warstwie powierzchniowej i wartości otrzymane w zakresie wysokich stężeń ET nie są prawdziwe. Stąd też aby otrzymać całkowite stężenie ET w warstwie powierzchniowej należało zastosować stężenie powierzchniowe otrzymane z równania Guggenheima–Adama [103], obliczone na podstawie Γ przy założeniu, że powierzchnia międzyfazowa Gibbsa została tak wybrana, że liczba moli ET w układzie rzeczywistym jest porównywalna do tej w układzie odniesienia o takiej samej objętości. Przeprowadzone obliczenia pozwoliły na stwierdzenie, że w zakresie niskich stężeń SF i ET adsorpcja obydwu związków rośnie, jednakże wzrost adsorpcji ET zachodzi w mniejszym stopniu niż SF [**D4**].

Przy stężeniach ET wyższych niż te odpowiadające stężeniu, przy którym występuje jego maksymalne nadmiarowe stężenie powierzchniowe Gibbsa, Γ^{max}, ale niższych od jego CAC, występuje większy spadek adsorpcji ET niż SF. W roztworach, w których stężenie ET jest wyższe od CAC, nie obserwuje się adsorpcji SF. Takie zachowanie się SF i ET być może wynika z faktu, że przy ich niskich stężeniach zastąpienie cząsteczek wody związanych z głową SF przez cząsteczki ET jest bardziej prawdopodobne niż zastąpienie tych związanych z ogonem. Powoduje to zwiększenie

hydrofobowości cząsteczek SF i wzrost ich adsorpcji. Wzrost stężenia ET w roztworze powoduje całkowite zastąpienie cząsteczek wody hydratyzujących głowę i ogon SF, a w wyniku tej dehydratacji ogon SF staje się hydrofilowy zaś głowa hydrofobowa, i w konsekwencji adsorpcja jest hamowana [**D4**].

Uzyskane wartości Γ_{ET} i Γ_{RL} potwierdziły przypuszczenie, że zmiany stopnia hydratacji hydrofilowej głowy i hydrofobowego ogona cząsteczki RL oraz zmiany stałej dielektrycznej roztworu odgrywają znaczącą rolę w adsorpcji RL i ET na granicy faz roztwór–powietrze. Nie stwierdzono natomiast efektu synergetycznego w adsorpcji obydwu związków [**D3**].

Tendencja do adsorpcji poszczególnych składników roztworu na granicy faz roztwór–powietrze może być określona na podstawie standardowej swobodnej energii Gibbsa adsorpcji (ΔG_{ads}^0). Wśród wielu metod pozwalających na wyznaczenie tej energii szczególne miejsce zajmuje równanie Langmuira zmodyfikowane przez de Boera [97,98]. Możliwe jest również wyznaczenie ΔG_{ads}^0 z liniowej postaci izotermy adsorpcji Langmuira [97]. Równania te zostały wykorzystane do wyznaczania ΔG_{ads}^0 RL, SF i ET podobnie jak nowe zaproponowane równanie uwzględniające napięcie powierzchniowe i aktywność ET w jego CAC [**D3,D4**].

W wyniku obliczeń przeprowadzonych dla danego układu otrzymano wartości ΔG_{ads}^0 różniące się w zależności od wybranej metody obliczeniowej oraz rodzaju izotermy nadmiarowego stężenia powierzchniowego. Różnice pomiędzy otrzymanymi wartościami wzrastają wraz ze wzrostem stężenia ET. Należy jednak zauważyć, że dla SF wartości ΔG_{ads}^0 rosną w funkcji stężenia ET. Dodatkowo przy niskich stężeniach ET w roztworze wartości te są porównywalne do ΔG_{ads}^0 SF w nieobecności ET. Interesujące jest również to, że wartości ΔG_{ads}^0 dla SF przy stężeniu ET powyżej jego CAC sugerują, że adsorpcja SF w takich roztworach może zachodzić, ale jej cząsteczki w monowarstwie adsorpcyjnej zorientowane są głowami w kierunku fazy gazowej. W zakresie stężenia SF w roztworze od 2×10^{-4} do 20 mg/dm^3 obserwuje się wzrost wartości ΔG_{ads}^0 ET obliczonych ze zmodyfikowanego równania Langmuira [97,98,**D4**].

Porównując wartości ΔG_{ads}^0 ET do tych otrzymanych z jego wodnego roztworu w nieobecności RL możemy stwierdzić, że te obliczone ze zmodyfikowanego przez de Boera równania Langmuira [97,98] i zaproponowanego równania są podobne. Może to wynikać z faktu, że zmodyfikowane równanie Langmuira zakłada, że współczynnik aktywności substancji adsorbującej się na granicy woda–powietrze jest równy 1.

W przypadku RL, w przeciwieństwie do ET, bezwzględne wartości jego ΔG^0_{ads} na granicy faz roztwór–powietrze maleją wraz ze wzrostem stężenia ET w fazie objętościowej od wartości odpowiadającej ΔG^0_{ads} indywidualnego RL do wartości niższej o około 10 kJ/mol. Ponieważ bezwzględna wartość ΔG^0_{ads} dla RL w nieobecności ET jest w przybliżeniu większa niż ΔG^0_{ads} ET w nieobecności RL, prawdopodobnie przy stałym niskim stężeniu alkoholu ramnolipid wpływa w większym stopniu na adsorpcję etanolu niż odwrotnie. Z kolei wzrost stężenia ET bardziej wpływa na adsorpcję RL niż odwrotnie [**D3**].

Izotermy napięcia powierzchniowego mieszanin RL oraz SF z TX165 [**D1**] przy stałym stężeniu biosurfaktantów niższym niż minimalne stężenie, przy którym tworzy się nasycona monowarstwa adsorpcyjna na granicy faz woda-powietrze są zbliżone do izotermy γ_{LV} wodnego roztworu TX165 [92]. Zaskakujące jest jednak to, że powyżej tego stężenia biosurfaktantów na izotermach występują maksima, które w miarę wzrostu ich stałego stężenia stają się coraz bardziej widoczne. Podobne maksima występują również na izotermach γ_{LV} przy stałym stężeniu TX165, natomiast nie zaobserwowano ich na izotermach dla mieszanin o stałym składzie. Kształt tych izoterm jest zbliżony do kształtu izoterm γ_{LV} wodnych roztworów RL i SF [64], co prawdopodobnie wynika z faktu, że przy porównywalnych stężeniach RL, SF i TX165 biosurfaktanty wykazują większą aktywność powierzchniową i wywierają większy wpływ na kształt izoterm w porównaniu do TX165. Okazało się, że otrzymane izotermy γ_{LV} przy stałym stężeniu jednego składnika bez obecności na nich maksimum można opisać równaniem funkcji ekspotencjalnej drugiego rzędu w całym zakresie zmieniającego się stężenia drugiego składnika mieszaniny bez względu na to czy wzięto pod uwagę zmieniające się stężenie, czy sumę stężeń obydwu składników. Zastosowanie sumarycznego stężenia obydwu składników skutkowało otrzymaniem większych rozbieżności między zmierzonymi, a obliczonymi wartościami γ_{LV}. Jeśli na izotermach γ_{LV} występowały maksima, to wówczas zostały one opisane przez dwie różne funkcje ekspotencjalne drugiego rzędu. W przypadku roztworów mieszaniny TX165 z RL i/lub SF, w których stężenie jednego składnika jest stałe a drugiego zmienne, zmianie ulega nie tylko skład, ale również stężenie. Dlatego też analizę stałych w równaniu funkcji ekspotencjalnej przeprowadzono dla wodnych roztworów mieszanin surfaktantów o stałym składzie i zmiennym stężeniu. Okazało się, że dla takich roztworów wartości stałej y_0 maleją w funkcji ułamka molowego biosurfaktantu w mieszaninie, a dla SF+TX165 zależność ta jest w przybliżeniu prostoliniowa. Należy podkreślić, że wartości tej stałej są skorelowane z wartością składowej LW napięcia powierzchniowego ogona surfaktantu i napięcia międzyfazowego woda–ogon. Dodatkowo oddziaływania LW są bezpośrednio związane z minimalnym napięciem powierzchniowym surfaktantów (Tabela 1) i wodnych roztworów ich mieszanin (γ_{LV}^{min}), co oznacza, że również wartość y_0 jest zbliżona do γ_{LV}^{min} wodnych roztworów mieszanin TX165 z RL lub SF. Na krzywych

obrazujących zmiany pozostałych stałych występujących w równaniu ekspotencjalnym w funkcji składu badanych mieszanin występują maksima i minima, i trudno jest powiązać ich wartości z właściwościami RL, SF i TX165 [**D1**].

W literaturze można spotkać informacje, że izotermy γ_{LV} wodnych roztworów pojedynczych surfaktantów opisuje równanie Szyszkowskiego [97,104]. W wyniku przeprowadzonych obliczeń okazało się, że równanie Szyszkowskiego można również zastosować do opisu izoterm γ_{LV} badanych mieszanin. Najlepszą zgodność pomiędzy zmierzonymi, a obliczonymi z równania Szyszkowskiego wartościami γ_{LV} dla mieszanin o stałym stężeniu jednego składnika a zmiennym drugiego uzyskano jeśli przyjęto w nim za rozpuszczalnik wodny roztwór składnika o stałym stężeniu równym jego stężeniu w mieszaninie. Było to jednak możliwe tylko dla roztworów, dla których stałe stężenie jednego składnika było niższe od stężenia, przy którym zaczyna się tworzyć jego nasycona monowarstwa adsorpcyjna na granicy faz woda–powietrze. Dodatkowo, analizując stałe występujące w równaniu Szyszkowskiego opisującym izotermy napięcia powierzchniowego roztworów o stałym składzie i zmieniającym się stężeniu, stwierdzono że wartości $n\Gamma^{max}$ zmieniają się prawie liniowo wraz ze zmianą składu mieszaniny, natomiast w przypadku stałej a_1 występuje ujemne odchylenie od liniowości. Z obliczeń przeprowadzonych na podstawie równania Szyszkowskiego wynika, że nie tylko opisuje ono izotermy γ_{LV}, ale również pozwala na ich przewidywanie na podstawie danych dla poszczególnych składników mieszaniny jeśli znane są zależności pomiędzy tymi danymi a składem mieszaniny [**D1**].

Jak wynika z danych literaturowych γ_{LV} dla mieszaniny surfaktantów można przewidzieć stosując równanie Fainermana i Millera [100,101] jeśli zostanie dokładnie określona powierzchnia zajmowana przez 1 mol każdego składnika jak i samej mieszaniny (ω). Określenie powierzchni zajmowanej przez 1 mol mieszaniny surfaktantu i biosurfaktantu nie jest łatwe ponieważ występują duże różnice w tzw. powierzchni granicznej (A^0) dla TX165, RL i SF. Z tego względu wydaje się, że graniczne stężenie obu składników (Γ_{12}^{∞}) dla mieszaniny surfaktantów powinno spełniać zależność ($\Gamma_{12}^{\infty} = \Gamma_1^{\infty} x_1^S + \Gamma_2^{\infty} x_2^S$) [**D1**], gdzie ułamek molowy surfaktantu w warstwie powierzchniowej (x^S) został obliczony na podstawie ciśnienia warstwy dla danego indywidualnego surfaktantu. Okazało się, że przy takich założeniach można przewidzieć γ_{LV} dla wodnych roztworów mieszaniny TX165 z RL lub SF jeśli stałe stężenie jednego składnika było niższe od minimalnego stężenia, przy którym tworzy się nasycona

monowarstwa adsorpcyjna w całym zakresie zmieniającego się stężenia drugiego składnika. W przypadku mieszanin TX165 z RL i/lub SF o stałym składzie wartości eksperymentalne γ_{LV} różniły się od tych obliczonych w całym zakresie stężenia mieszaniny [**D1**]. Przyczyną tych rozbieżności mogą być silniejsze oddziaływania między cząsteczkami TX165 i biosurfaktantu w porównaniu do oddziaływań pomiędzy cząsteczkami tego samego związku oraz fakt, że powierzchnia zajmowana przez 1 mol mieszaniny odbiega od tej obliczonej teoretycznie. Przypuszczenie to oparto na tym, że hydrofilowa część TX165 może być związana z jonami H_3O^+ poprzez wiązania wodorowe i niejonowy Triton X–165 może być traktowany jak surfaktant kationowy. W związku z tym pomiędzy cząsteczkami TX165 i anionowego biosurfaktantu będą występowały oddziaływania elektrostatyczne. Możliwe jest również, że ułamek molowy poszczególnych składników mieszaniny w warstwie powierzchniowej na granicy faz woda–powietrze nie różni się znacznie od ułamka obliczonego na podstawie ciśnienia monowarstwy indywidualnych składników. Potwierdzeniem tego przypuszczenia mogą być wartości napięcia powierzchniowego obliczone z wykorzystaniem tych ułamków i γ_{LV} składników mieszaniny. Co więcej, obliczenia te potwierdziły występowanie maksimów na izotermach γ_{LV} [**D1**].

Ponieważ redukcja napięcia powierzchniowego wody związana jest z adsorpcją surfaktantów na granicy faz roztwór–powietrze wyznaczono nadmiarowe stężenie powierzchniowe Gibbsa TX165, RL i SF korzystając z odpowiedniej formy równania izotermy adsorpcji Gibbsa [97]. Oczywiście założono, że Γ surfaktantów jest równe całkowitemu ich stężeniu w warstwie powierzchniowej. Obliczenia te były możliwe tylko tam gdzie zmiany γ_{LV} opisywała jedna funkcja ekspotencjalna w całym zakresie stężenia, a więc tam gdzie nie zaobserwowano występowania maksimów. Izotermy Γ uzyskane z tych obliczeń przy stałym stężeniu RL lub SF mają kształt podobny do izotermy dla indywidualnego TX165, natomiast te przy stałym stężeniu TX165 były podobne do izotermy RL lub SF. Ponieważ trudno było wyznaczyć z równania Gibbsa izotermy dla wszystkich badanych układów analizę tendencji do adsorpcji przeprowadzono wykorzystując równanie Frumkina [97,**D1**]. Aby zastosować to równanie założono, że maksymalne stężenie każdego składnika mieszaniny w warstwie adsorpcyjnej przy danym stężeniu w fazie objętościowej jest w przybliżeniu równe iloczynowi ułamka powierzchni zajmowanej przez ten składnik i jego indywidualnego maksymalnego stężenia. Założono także, że redukcja γ_{LV} wody wynikająca z adsorpcji danego składnika mieszaniny może być wyrażona jako różnica pomiędzy γ_{LV} wody i roztworu pomnożona

przez ułamek molowy tego składnika w warstwie powierzchniowej. Korzystając więc z zaproponowanej formy równania Frumkina [**D1**] obliczono stężenie powierzchniowe składników mieszaniny, nawet gdy na izotermach γ_{LV} występowały maksima. Obliczenia te wykazały, że w przypadku mieszanin RL+TX165 i SF+TX165 występują różnice w wartościach Γ otrzymanych z równania Gibbsa i Frumkina [**D1**]. Powodem tych różnic może być wspomniane już przyłączenie grup H_3O^+ do jednostek oksyetylenowych w hydrofilowej części cząsteczki TX165.

Okazało się również, że obliczone ułamki molowe dla poszczególnych składników w mieszanej monowarstwie są podobne do wartości otrzymanych z równania Hua i Rosena [105]. Korzystając z modelu Hua i Rosena [105] wyznaczono także parametr oddziaływań międzycząsteczkowych w mieszanej monowarstwie adsorpcyjnej (β^σ). Wartości tego parametru wykazały, że efekt synergetyczny w redukcji γ_{LV} wody jest bardziej widoczny w przypadku mieszaniny RL+TX165 niż SF+TX165 [**D1**]. Może to wynikać z faktu, że aktywność adsorpcyjna SF na granicy faz woda–powietrze jest dużo większa niż TX165 i nie może on wpłynąć na adsorpcję SF w takim stopniu, aby występował znaczny efekt synergetyczny w redukcji γ_{LV} wody. Oprócz tworzenia się mieszanej warstwy adsorpcyjnej w układzie SF+TX165 mogą również powstawać mieszane micele. Uzyskane izotermy γ_{LV} pozwoliły na wyznaczenie CMC tylko dla mieszanin o stałym składzie. Wartości CMC wykazywały ujemne odchylenia od liniowości w funkcji ułamka molowego biosurfaktantu w fazie objętościowej roztworu. Otrzymane wartości CMC zostały następnie porównane z tymi obliczonymi z równania dla idealnej mieszaniny oraz równania Bergströma i Erikssona [106]. Dodatkowo z modelu Hua i Rosena [105] wyznaczono parametry oddziaływań międzycząsteczkowych w mieszanej miceli (β^M) oraz współczynniki aktywności surfaktantów w mieszanej miceli (f^M). Współczynniki te następnie zastosowano w obliczaniu CMC dla nieidealnej mieszaniny surfaktantów. Wykonane obliczenia wykazały między innymi, że wartości CMC mieszanin biosurfaktantów z TX165 uzyskane z równania Bergströma i Erikssona [106,**D1**] były zbliżone do tych wyznaczonych z izoterm γ_{LV}. Wartości wyznaczone z równania dla nieidealnej mieszaniny były zbliżone do wartości eksperymentalnych, zarówno dla mieszanin RL+TX165 jak i SF+TX165. Zbieżność wartości CMC wyznaczonych teoretycznie i uzyskanych z izoterm γ_{LV} w funkcji składu mieszaniny nie wskazuje wyraźnie na wystąpienie efektu synergetycznego w tworzeniu mieszanych micel. Efekt ten

potwierdziły jednak ujemne wartości β^M uzyskane dla obydwu rodzajów mieszanin dla wszystkich badanych składów. Natomiast drugi warunek istnienia synergetyzmu w tworzeniu mieszanych micel ($|\beta^M| > |\ln\frac{CMC_2}{CMC_1}|$ [97]) potwierdził jego istnienie tylko dla wybranych ułamków RL i SF w mieszaninie [105,**D1**].

Wydaje się, że brak wiarygodnych dowodów na wystąpienie efektu synergetycznego w procesie micelizacji może wynikać z bardzo dużych różnic wartości CMC poszczególnych składników mieszaniny, a teorie jakie zastosowano do obliczeń zostały zaproponowane dla układów gdzie składniki mieszanin wykazują między sobą mniejsze różnice we właściwościach powierzchniowych i objętościowych [**D1**].

W celu pełniejszego wyjaśnienia procesów adsorpcji i micelizacji jakie zachodzą w badanych układach obliczono standardową swobodną energię Gibbsa adsorpcji (ΔG_{ads}^0) i micelizacji (ΔG_{mic}^0). Do obliczeń ΔG_{ads}^0 wykorzystano stałą a_1, która może być wyznaczona z równania Szyszkowskiego lub liniowej postaci równania izotermy Langmuira [97]. Obliczenia na podstawie stałej a_1 w równaniu Szyszkowskiego [91] były możliwe tylko dla roztworów, gdzie równanie to opisywało izotermy γ_{LV} [**D1**]. Okazało się, że w przypadku roztworów o stałym stężeniu jednego składnika, a zmieniającym się drugiego wartości ΔG_{ads}^0 obliczone dla TX165, RL i SF w ich mieszaninach są zbliżone do wartości tej energii obliczonej dla roztworów indywidualnych związków (Tabela1). Roztwory o stałym składzie wykazywały odchylenie od liniowej zależności ΔG_{ads}^0 od ułamka molowego biosurfaktantu w mieszaninie. Dodatkowo ΔG_{ads}^0 obliczono z równania uwzględniającego swobodną energię mieszania surfaktantów i ułamki molowe poszczególnych składników w fazie objętościowej. Różnice pomiędzy obliczonymi z tego równania wartościami ΔG_{ads}^0 i uzyskanymi ze stałej a_1 dla mieszanin SF+TX165 mogą wynikać z różnic w aktywności adsorpcyjnej TX165 i SF oraz ułamków molowych w nasyconej monowarstwie wyznaczonych z modelu Hua i Rosena [105]. Z kolei wartości ΔG_{mic}^0 obliczono z klasycznego równania [97] oraz równania uwzględniającego ułamki molowe składników mieszaniny w fazie objętościowej oraz mieszanej miceli. Różnice pomiędzy wartościami ΔG_{mic}^0 uzyskanymi z tych dwóch podejść potwierdziły możliwość wystąpienia efektu synergetycznego w procesie micelizacji [**D1**].

4.5. WŁAŚCIWOŚCI ZWILŻAJĄCE MIESZANIN RAMNOLIPID (SURFAKTYNA)+ ETANOL I RAMNOLIPID (SURFAKTYNA)+TRITON X–165

4.5.1. Właściwości zwilżające mieszanin ramnolipid+etanol i surfaktyna+etanol

Napięcie powierzchniowe (γ_{LV}) wodnych roztworów surfaktantów/ biosurfaktantów zmniejsza się w funkcji ich stężenia w zakresie od 0 do CMC, a po przekroczeniu CMC wartości γ_{LV} są praktycznie stałe. Z kolei napięcie powierzchniowe ciała stałego (γ_{SV}) może być stałe lub zmniejszać się w funkcji stężenia surfaktantu lub ich mieszaniny, co zależy od właściwości warstwy utworzonej wokół kropli umieszczonej na powierzchni ciała stałego. Zmiany napięcia międzyfazowego ciało stałe–ciecz (γ_{SL}) w funkcji stężenia są bardziej skomplikowane niż γ_{LV} i γ_{SV}, ponieważ może ono rosnąć, maleć lub nie ulegać zmianie.

Jak wynika z przeprowadzonych badań kąt zwilżania (θ) dla wodnych roztworów RL+ET i SF+ET maleje w funkcji stężenia alkoholu lub biosurfaktantu co powoduje wzrost zwilżalności PTFE przez te roztwory [**D5,D6**]. Mimo to w żadnym przypadku nie wystąpiło całkowite rozpływanie się roztworu po powierzchni PTFE. Jak już wspomniano, napięcie powierzchniowe apolarnego PTFE równe 20,24 mN/m wynika jedynie z oddziaływań Lifshitza–van der Waalsa (LW) i jest niższe od γ_{LV} wody, ET, a także głowy i ogona RL oraz SF (Tabela 1 i 2). Prawdopodobnie z tego powodu nie występuje całkowite zwilżanie PTFE [**D5,D6**]. Należy podkreślić, że podobnie jak w przypadku izoterm γ_{LV} wodnych roztworów RL+ET przy zmiennym stężeniu ET i stałym RL na izotermach θ występują niewielkie maksima, jeśli wartości stałego stężenia RL odpowiadają nasyconej monowarstwie na granicy faz woda–powietrze w nieobecności ET. Można przypuszczać, że maksima te powstały wskutek usuwania cząsteczek RL z monowarstwy adsorpcyjnej na granicach faz roztwór–powietrze i PTFE–roztwór przez cząsteczki ET. Innymi słowy wkład RL i ET w adsorpcję w wyniku, której zmniejsza się napięcie międzyfazowe woda–powietrze i PTFE–woda decyduje o zmianach kąta zwilżania w funkcji składu i stężenia mieszaniny ET i RL [**D6**].

Wielu autorów sugeruje [93,94,107], że jeśli napięcie powierzchniowe cieczy jest większe niż ciała stałego, to adsorpcja takiej cieczy nie powoduje zmniejszenia napięcia powierzchniowego ciała stałego. Zgodnie z tym stwierdzeniem w przeprowadzonych badaniach założono, że γ_{SV} PTFE jest stałe niezależnie od stężenia ET, RL i SF, a zmiana

θ zależy tylko od zmiany napięć międzyfazowych roztwór–powietrze i PTFE–roztwór [**D5,D6**]. W takim przypadku możliwe jest określenie napięcia międzyfazowego PTFE–roztwór bezpośrednio z równania Younga [97]. Obliczenia z równania Younga wykazały, że na krzywych obrazujących zmiany γ_{SL} PTFE–roztwór w funkcji stężenia ET dla roztworów o stałym stężeniu RL odpowiadającym nasyconej monowarstwie na granicy faz roztwór–powietrze w nieobecności ET obecne są maksima, podobnie jak na izotermach θ i γ_{LV} roztworów [**D6**]. W przeciwieństwie do PTFE po powierzchni monopolarnego PMMA i bipolarnego Q występuje całkowite rozpływanie się wodnych roztworów SF+ET przy stężeniu ET odpowiednio równym lub wyższym 11,97 M i 15,40 M niezależnie od stałego stężenia biosurfaktantu w mieszaninie [**D5**]. Roztwory RL+ET również rozpływają się po powierzchni PMMA przy stężeniu ET równym i wyższym od 12,15 M, a w przypadku kwarcu 15,40 M. Należy zauważyć, że na izotermach θ dla PMMA i Q podobnie jak dla PTFE występują maksima dla roztworów RL+ET. Ich obecność wynika z konkurencyjnej adsorpcji ET i RL na granicach faz roztwór–powietrze oraz ciało stałe–roztwór [**D6**]. Takie zachowanie się biosurfaktantu i ET może być również przyczyną występowania maksimum na izotermie θ dla SF+ET na powierzchni kwarcu [**D5**].

Proces rozpływania się kropli cieczy lub roztworu po powierzchni ciał stałych można wyjaśnić poprzez parametr oddziaływań międzyfazowych (φ). Na podstawie równań Younga-Dupré [97] oraz Girifalco i Gooda [108,109] można stwierdzić, że parametr φ równy jest 1 dla zerowego kąta zwilżania cieczy na powierzchni PTFE jeśli jej napięcie powierzchniowe jest równe napięciu powierzchniowemu tego ciała stałego. Jest to warunek konieczny, ale nie wystarczający. Z porównania równań Girifalco i Gooda [108,109] oraz van Ossa i wsp. [94,95] wynika, że aby dana ciecz lub roztwór rozpływały się po powierzchni PTFE nie tylko napięcie powierzchniowe cieczy powinno być równe napięciu powierzchniowemu PTFE, ale musi ono dodatkowo wynikać jedynie z oddziaływań międzycząsteczkowych LW.

Przeprowadzone obliczenia parametru oddziaływań międzyfazowych (φ) dla układu PTFE–wodny roztwór mieszaniny ET z RL(SF) wykazały, że jego wartości są znacznie niższe od 1, co tłumaczy dlaczego nie można osiągnąć całkowitego rozpływania tych roztworów w tym układzie [**D5,D6**]. Okazało się też, że wartości parametru φ obliczone na podstawie równań Younga–Dupré [91] oraz Girifalco i Gooda [108,109] są zbliżone do tych obliczonych na podstawie równań Girifalco i Gooda [108,109] oraz

van Ossa i wsp. [94,95]. Dowodzi to, że w badanych układach PTFE–kropla roztworu–powietrze poszczególne składniki roztworu nie obniżają γ_{SV} PTFE poza kroplą roztworu osadzoną na jego powierzchni [**D5**]. Jest to zgodne ze stwierdzeniami Fowkesa [93], Gooda [109] oraz van Ossa [94] mówiących o tym, że ciecz o napięciu powierzchniowym większym od napięcia powierzchniowego danego ciała stałego tworząc warstwę adsorpcyjną na jego powierzchni nie obniża jego γ_{SV}. Dla badanych układów, w przeciwieństwie do podejścia Neumanna i wsp. [110], nie można za pomocą funkcji liniowej opisać zależności między parametrem φ a napięciem międzyfazowym PTFE–roztwór. Istnieje natomiast prostoliniowa zależność pomiędzy parametrem φ a logarytmem z sumy γ_{LV} wodnego roztworu mieszaniny alkoholu i biosurfaktantu oraz γ_{SL} PTFE–roztwór. Wydaje się logiczne, że zmiany θ wodnych roztworów mieszaniny ET z RL lub SF w funkcji składu i stężenia związane z parametrem φ zależą tylko od γ_{LV} roztworów i γ_{SL} PTFE–roztwór, ponieważ γ_{SV} PTFE jest stałe. Wniosek ten potwierdza również liniowa zależność pomiędzy $\cos\theta$ a $\frac{\varphi}{\sqrt{\gamma_{LV}}}$, która obejmuje wszystkie roztwory zarówno przy stałym stężeniu biosurfaktantu a zmieniającym się stężeniu ET jak i odwrotnie [**D5,D6**].

Zależność pomiędzy parametrem oddziaływań międzyfazowych (φ) a całkowitym rozpływaniem wodnych roztworów RL+ET i SF+ET po powierzchniach PMMA i Q jest bardziej skomplikowana niż dla PTFE. Na podstawie wyżej przytoczonych równań można jedynie stwierdzić, że jeśli warstwa adsorpcyjna składników roztworu poza jego kroplą osadzoną na powierzchni PMMA lub Q nie zmienia ich γ_{SV}, wówczas parametr φ przyjmuje wartość równą 1 dla zerowego θ i dla roztworu o napięciu powierzchniowym równym napięciu powierzchniowemu monopolarnego PMMA lub bipolarnego Q. Oprócz tego warunku ważny jest udział oddziaływań kwasowo–zasadowych (AB) w ujęciu Lewisa w γ_{LV} roztworu. Z obliczeń przeprowadzonych w układach obejmujących PMMA i Q wynika, że wartości parametru φ dla tego samego roztworu różnią się w zależności jaką parę równań zastosowano do ich wyznaczenia. Różnica w wartościach parametru φ świadczy o redukcji γ_{SV} PMMA i Q przez warstwę mieszaniny ET z biosurfaktantami utworzoną poza osadzoną na powierzchni tych ciał stałych kroplą roztworu. Jak wspomniano wyżej, wynika to z faktu, że γ_{LV} ET oraz części hydrofobowych RL i SF jest niższe od γ_{SV} PMMA i Q (Tabela 1 i 2). Różnice między wartościami φ dla tego samego roztworu obliczonymi na podstawie równań Younga–Dupré [97] i Girifalco i Gooda [108,109] oraz równań van Ossa i wsp.

[94,95] i Girifalco i Gooda [108,109] mogą wynikać z tego, że dotyczą one dwóch różnych granic faz. W pierwszym przypadku parametr φ dotyczy granicy faz PMMA(Q)/mieszana warstwa adsorpcyjna alkoholu i biosurfaktantu–roztwór, a w drugim granicy faz PMMA(Q)–roztwór. Za pierwszym przypadkiem przemawia fakt, że γ_{LV} roztworu mieszaniny ET i biosurfaktantu, przy którym obserwuje się całkowite rozpływanie roztworu po powierzchni PMMA lub Q i jednocześnie odpowiadające parametrowi φ równemu 1 jest zbliżone do γ_{SV} PMMA lub Q wyznaczonych z równania Neumanna i wsp. [110,**D5**,**D6**].

Dla PMMA i Q, podobnie jak dla PTFE, prostoliniowa zależność występuje jedynie między parametrem φ a logarytmem z sumy γ_{LV} roztworu i γ_{SL} PMMA(Q)–roztwór. W przypadku Q zależność ta nie obejmuje wszystkich badanych stężeń wodnych roztworów mieszaniny ET z biosurfaktantem [**D5**,**D6**]. Zarówno dla PMMA, jak i Q nie uzyskano liniowej zależności $\cos\theta$ w funkcji $\frac{\varphi}{\sqrt{\gamma_{LV}}}$ jeśli parametr φ został obliczony na podstawie równań Girifalco i Gooda [108,109] oraz van Ossa i wsp. [94,95]. Co więcej, potwierdza to, że w rzeczywistości jest to układ obejmujący PMMA(Q) pokryty warstwą adsorpcyjną mieszaniny ET i biosurfaktantu, a nie sam „czysty" PMMA lub Q.

W przypadku gdy zależność napięcia adhezyjnego ($\gamma_{LV}\cos\theta$) od napięcia powierzchniowego (γ_{LV}) jest liniowa, a stała a w równaniu opisującym tę zależność jest zbliżona do -1, wówczas stała b jest liczbowo równa pracy adhezji (W_a) wodnego roztworu mieszaniny do PTFE, zaś wartość krytycznego napięcia powierzchniowego zwilżania (γ_c) jest równa $\frac{b}{2}$. Z tego wynika, że gdyby W_a wodnych roztworów mieszanin RL+ET i SF+ET do PTFE były stałe niezależnie od stężenia poszczególnych składników mieszanin, to wodne roztwory tych mieszanin o γ_{LV} równym krytycznemu napięciu powierzchniowemu zwilżania (γ_c) powinny się całkowicie rozpływać po powierzchni PTFE. Niestety w zakresie dużego stężenia ET w mieszaninach z biosurfaktantami nie ma liniowej zależności między $\gamma_{LV}\cos\theta$ i γ_{LV} roztworów, a zatem W_a zmienia się wraz ze stężeniem ET. Tym samym wartość γ_c wyznaczona z liniowej zależności między $\gamma_{LV}\cos\theta$ i γ_{LV} roztworu jest wyższa od napięcia powierzchniowego PTFE i nie jest związana z całkowitym zwilżaniem jego powierzchni przez badane roztwory. Wartość γ_c wyznaczona z zależności pomiędzy $\cos\theta$ i γ_{LV} roztworu, chociaż bardziej zbliżona do napięcia powierzchniowego PTFE, nie jest również związana z całkowitym zwilżaniem jego powierzchni [**D5**,**D6**].

Zależność pomiędzy napięciem adhezyjnym ($\gamma_{LV}\cos\theta$) a powierzchniowym (γ_{LV}) dla PMMA i Q jest liniowa, podobnie jak dla PTFE, a wartości γ_c PMMA i Q określone z tej zależności są bliskie tym wyznaczonym z zależności pomiędzy $\cos\theta$ i napięciem powierzchniowym. W przeciwieństwie do PTFE stała b w równaniu liniowym opisującym zależność między $\gamma_{LV}\cos\theta$ i γ_{LV} dla PMMA i Q nie jest równa pracom adhezji (W_a) badanych roztworów do ich powierzchni [**D5**]. Wyznaczone γ_{LV} roztworu mieszaniny SF i ET, przy którym roztwór ten rozpływa się całkowicie po powierzchni PMMA jest nieznacznie mniejsze od 27 mN/m i nie zależy od stężenia SF. Napięcie to może być traktowane jako γ_c PMMA przez badane roztwory, a jego wartość jest niższa od γ_{SV} PMMA. Ten fakt oraz wartości parametru φ i jego składowych potwierdzają wcześniejszy wniosek, że kropla roztworu mieszaniny ET i SF umieszczona na powierzchni PMMA rozpływa się raczej po jego powierzchni pokrytej warstewką mieszaniny ET i SF niż po „czystym" PMMA. Dodatkowo potwierdzają to oddziaływania sił adhezji ET i ogona SF większe niż oddziaływania sił kohezji pomiędzy ich cząsteczkami. Tym samym obecność ET w warstwie poza kroplą roztworu umieszczoną na granicy faz wynika nie tylko z adsorpcji jego par, ale również z penetracji cząsteczek ET z kropli do powierzchni PMMA. Z drugiej strony obecność SF wynika raczej tylko z penetracji jej cząsteczek z kropli do powierzchni poza kroplą. Tę sugestię potwierdza to, że przy stężeniach SF i ET odpowiadających ich indywidualnej nasyconej monowarstwie, stan równowagi układu PMMA–kropla roztworu–powietrze jest osiągany w dłuższym czasie niż dla układu PTFE–kropla roztworu–powietrze. Stąd prawdopodobnie wynika, że nachylenie liniowej zależności pomiędzy $\gamma_{LV}\cos\theta$ i γ_{LV} jest różne od –1 i zależy od stałego stężenia SF. Z kolei zależności między $\gamma_{LV}\cos\theta$ i γ_{LV}, czy też między $\cos\theta$ i γ_{LV}, wynikają z adsorpcji ET i biosurfaktantu na granicach faz woda–powietrze i ciało stałe–woda, a w przypadku PMMA i Q z adsorpcji na granicy faz ciało stałe–powietrze [**D5**].

Zgodnie z Lucassen–Reynders [96] jeśli nachylenie zależności pomiędzy $\gamma_{LV}\cos\theta$ i γ_{LV} jest większe niż –1, ale mniejsze niż 0, nie można wykluczyć adsorpcji ET i SF na granicy faz ciało stałe–powietrze [**D5**]. Dla Q zależność $\gamma_{LV}\cos\theta$ od γ_{LV} jest liniowa dla ET przy stałym stężeniu SF odpowiadającym jej nienasyconej monowarstwie w nieobecności ET z wyjątkiem zakresu niskiego stężenia ET i może być opisana przez tę samą funkcję liniową dla każdej stałej wartości stężenia SF. Jeśli nachylenie tej zależności jest dodatnie, co ma miejsce w przypadku Q, to zgodnie z równaniem

Lucassen–Reynders [96] jeśli γ_{SV} Q nie zależy od stężeń ET i SF, adsorpcja ET na granicy faz Q–woda jest ujemna. Jeśli jednak γ_{SV} Q zmienia się wskutek adsorpcji ET i SF, wtedy adsorpcja ET na granicy faz Q–powietrze jest wyższa niż ta na granicy Q–woda. To potwierdza, że na powierzchni kwarcu ma miejsce tworzenie się mieszanej warstwy adsorpcyjnej poza kroplą roztworu umieszczoną na jego powierzchni [**D5**].

Niestety, na podstawie zależności $\gamma_{LV}\cos\theta$ od γ_{LV} przy stałym stężeniu SF odpowiadającym tworzeniu się nasyconej monowarstwy adsorpcyjnej na granicy faz woda–powietrze trudno jest ocenić adsorpcję ET na granicach faz Q–powietrze i Q–woda. Może to wynikać z faktu, że na powierzchni Q powstaje film wody, w którym jej cząsteczki tworzą silne wiązania wodorowe nie tylko z powierzchnią Q, ale także między sobą. Wskutek tego cząsteczki wody w warstwie powierzchniowej mogą tworzyć z przylegającym medium jedynie słabe wiązania wodorowe, a powierzchnia Q oddziałuje z tym medium przede wszystkim siłami LW. Taka warstwa wody ma właściwości podobne do lodu i w związku z tym w zależności od stężenia ET lub SF, adsorpcja ET może mieć miejsce na granicach faz Q/warstwa wodna–woda i/lub Q–woda [**D5**].

Analiza adsorpcji mieszaniny ET i biosurfaktantów na podstawie zależności między $\gamma_{LV}\cos\theta$ i γ_{LV} roztworu pozwala jedynie stwierdzić jaka jest relacja pomiędzy adsorpcją tej mieszaniny na granicach faz PTFE–roztwór i roztwór–powietrze. Natomiast na jej podstawie trudno jest dokładnie ustalić wzajemny wpływ ET i biosurfaktantów na ich adsorpcję na granicy faz PTFE–roztwór. W przypadku PMMA i Q na podstawie nie można nawet określić stosunku stężenia mieszaniny ET z biosurfaktantem na granicach faz PMMA(Q)–roztwór do tego na granicy faz roztwór–powietrze. Wynika to, jak wykazano wcześniej, z faktu, że adsorpcja mieszaniny ET i biosurfaktantu zachodzi też na granicach faz PMMA(Q)–powietrze, a na podstawie zależności $\gamma_{LV}\cos\theta$ od napięcia powierzchniowego roztworów można jedynie ustalić stosunek różnicy stężeń badanych mieszanin na granicach faz PMMA(Q)–powietrze i PMMA(Q)–roztwór do ich stężeń na granicy faz roztwór–powietrze [**D5**,**D6**].

W celu poznania stężenia i składu warstw adsorpcyjnych mieszaniny ET z RL lub SF na granicach faz PTFE–roztwór, PMMA(Q)–roztwór i PMMA(Q)–powietrze wykorzystano równanie izotermy Gibbsa i Frumkina [97,**D5**,**D6**]. Do obliczeń stężenia ET i biosurfaktantów na wymienionych granicach faz na podstawie tych równań konieczna jest znajomość zmiany γ_{SV} PMMA i Q oraz γ_{SL} PMMA(Q)–roztwór w funkcji stężenia i składu badanych mieszanin. Napięcie wymienionych granic faz określono zarówno przy pomocy równania Younga [97], jak również van Ossa i wsp. [94,95].

Napięcia powierzchniowe PMMA(Q) pokrytych warstwą adsorpcyjną określono na podstawie wartości równej $\frac{\gamma_W - \gamma_{LV}}{2}$ (gdzie γ_{LV} oznacza napięcie powierzchniowe roztworu mieszaniny ET z biosurfaktantami, a γ_W to napięcie powierzchniowe wody). Rozwiązanie równania Gibbsa względem stężenia na danej granicy faz oparto na znajomości odpowiedniej funkcji matematycznej opisującej zmiany γ_{SV} lub γ_{SL} od stężenia ET przy stałych stężeniach RL lub SF oraz zmiennych stężeniach RL i SF a stałym stężeniu ET. Natomiast rozwiązanie równania Frumkina wymagało znajomości udziałów ET i biosurfaktantu w redukcji γ_{SV} PMMA i Q oraz γ_{SL} PMMA(Q)–woda. W tym celu zastosowano odpowiednie izotermy γ_{SV} i γ_{SL} oraz wartości maksymalnego stężenia poszczególnych składników [**D5**,**D6**].

Na podstawie przeprowadzonych obliczeń stwierdzono, że pomimo liniowej zależności pomiędzy $\gamma_{LV}\cos\theta$ i γ_{LV} o nachyleniu zbliżonym do –1 dla wodnych roztworów mieszanin ET z RL lub SF nie ma porównywalnych adsorpcji poszczególnych składników na granicach faz PTFE–roztwór i roztwór–powietrze. Wzajemny wpływ ET i biosurfaktantów na adsorpcję zależy od składu i stężenia mieszaniny w fazie objętościowej. Analizując wzajemny wpływ ET i biosurfaktantów na ich adsorpcję na granicy faz PTFE–roztwór należy zwrócić szczególną uwagę na zakresy stężeń SF i RL w fazie objętościowej odpowiadające ich nienasyconej i nasyconej monowarstwie adsorpcyjnej na granicy faz roztwór–powietrze w nieobecności alkoholu oraz zakresy stężenia ET od 0 do CAC i powyżej CAC [64,90]. W zakresie stężeń ET i biosurfaktantu odpowiadających ich indywidualnym nienasyconym monowarstwom adsorpcyjnym na granicy faz roztwór–powietrze, wzajemny wpływ ET i RL lub SF na adsorpcję na granicy faz PTFE–roztwór jest nieznaczny, a nawet można stwierdzić, że występuje niezależna adsorpcja. Co więcej wpływ ten jest mniejszy niż na granicy faz roztwór–powietrze. W zakresie stężenia jednego lub obu składników badanych mieszanin odpowiadającego ich indywidualnej nasyconej monowarstwie na granicy faz roztwór–powietrze uwidacznia się większy wpływ biosurfaktantu na adsorpcję ET na granicy faz PTFE– roztwór niż odwrotnie. Niemniej jednak powyżej CAC etanolu adsorpcja biosurfaktantów gwałtownie maleje, co sugeruje, że wpływ ET na adsorpcję biosurfaktantu jest większy niż odwrotnie [**D5**,**D6**].

Wzajemny wpływ ET i biosurfaktantów na ich adsorpcję na granicy faz PTFE– roztwór wynika z oddziaływań cząsteczek wody, ET i biosurfaktantu z powierzchnią PTFE oraz ich oddziaływań między sobą. Praca adhezji wody (W_a) do powierzchni PTFE

jest większa niż ET i biosurfaktantów skierowanych częścią hydrofobową do tej powierzchni. Co więcej napięcie międzyfazowe PTFE–woda jest dużo większe niż napięcie międzyfazowe PTFE–ET i PTFE–część hydrofobowa biosurfaktantów. Z kolei biosurfaktanty wykazują największe oddziaływania hydrofobowe z powierzchnią PTFE poprzez fazę wodną. Te oddziaływania oraz minimalne napięcie pomiędzy częścią hydrofobową biosurfaktantu i PTFE decydują o największej tendencji do adsorpcji biosurfaktantów na granicy faz PTFE–woda. Z drugiej strony cząsteczki ET mogą zmniejszać hydratację zarówno części hydrofilowej, jak i hydrofobowej cząsteczek SF i RL. Cząsteczki ET zastępując cząsteczki wody otaczające części hydrofilowe cząsteczek RL lub SF zwiększają ich hydrofobowość, a tym samym tendencje do adsorpcji na granicy faz PTFE–woda. Jednak jeśli cząsteczki ET zastępują cząsteczki wody wokół części hydrofobowych RL i SF zmniejszają ich tendencję do adsorpcji. Przy niskich stężeniach ET i biosurfaktantów proces usuwania cząsteczek wody wokół grup hydrofilowych RL i SF jest dominujący, przez co zwiększają się tendencje do adsorpcji RL i SF na granicy faz PTFE–woda i stąd wpływ ET na adsorpcje RL i SF jest nieco mniejszy niż odwrotnie. W miarę wzrostu stężenia ET jego cząsteczki dehydratyzują zarówno część hydrofilową jak i hydrofobową biosurfaktantów. Maleje też stała dielektryczna roztworu, co powoduje większy wpływ alkoholu na adsorpcje biosurfaktantów niż odwrotnie. Niewykluczone, że powyżej krytycznego stężenia agregacji etanolu występują agregaty cząsteczek RL lub SF z jego cząsteczkami, a sam ten efekt wywołuje większe zmiany energetyczne roztworu niż ich adsorpcja na granicy faz PTFE–woda. Stąd też zmiany θ wodnych roztworów mieszaniny ET i biosurfaktantów na powierzchni PTFE przy stężeniach ET powyżej jego CAC są prawie analogiczne do zmian θ dla roztworów ET w nieobecności biosurfaktantów [**D5**,**D6**].

Przeprowadzona analiza adsorpcji ET i biosurfaktantów z wodnego roztworu ich mieszanin w układzie PMMA–kropla roztworu–powietrze za pomocą równań izoterm adsorpcji Gibbsa i Frumkina [97] potwierdziła sugestię, że ET, RL oraz SF adsorbują się nie tylko na granicy faz PMMA–woda, ale również na granicy faz PMMA–powietrze. Adsorpcja ET na granicach faz PMMA–powietrze i PMMA–woda jest mniejsza od jego adsorpcji na granicy faz woda–powietrze, a ilość ET zaadsorbowana na granicy faz PMMA–powietrze jest mniejsza niż na granicy faz PMMA–woda. Oczywiście, wielkość adsorpcji na wymienionych granicach faz zależy od stężenia i składu mieszanin ET i biosurfaktantu [**D5**,**D6**].

Adsorpcja składników roztworu zależy w pewnym stopniu od oddziaływań sił adhezji i kohezji. Badania dotyczące układu PMMA–roztwór dowiodły, że woda wykazuje największe oddziaływania adhezyjne z powierzchnią PMMA, a ET najmniejsze. Różnica pomiędzy oddziaływaniami adhezji i kohezji jest ujemna dla wody i dodatnia dla ET. Tym samym przy niskich stężeniach ET i RL lub SF, cząsteczki wody mogą tworzyć uporządkowany film na granicy faz PMMA–woda. Chociaż ET i woda mieszają się w fazie objętościowej bez ograniczeń, nie są aż tak dobrze mieszalne w warstwie powierzchniowej. Może to wynikać z tego, że cząsteczki ET są adsorbowane na granicy faz PMMA/warstwa wody–roztwór, a nie na granicy faz PMMA–roztwór. Potwierdza to fakt, że ET może całkowicie rozpływać się po warstwie wody. Adsorpcję ET na granicy faz PMMA–woda przy jego niskim stężeniu i biosurfaktantu można wytłumaczyć w inny sposób. Ze względu na to, że tendencje RL i SF do adsorpcji na granicy faz PMMA–woda są dużo większe niż ET, ich cząsteczki mogą usuwać cząsteczki wody z powierzchni PMMA. Cząsteczki wody związane z grupami hydrofilowymi biosurfaktantów usunięte przez cząsteczki etanolu mogą adsorbować się razem z nimi. Przy wysokich stężeniach ET, RL i SF tworzenie się warstewek wodnych, w których cząsteczki są silnie uporządkowane, jest mniej prawdopodobne. W tym wypadku adsorpcja ET wzrasta. Należy zauważyć, że zachowanie adsorpcyjne RL i SF na granicach faz PMMA–powietrze i PMMA–woda jest różne od ET. Przykładowo w zakresie stężenia surfaktyny od 0 do CMC [64] jej adsorpcja na granicy faz PMMA–powietrze jest wyższa niż na granicy faz PMMA–woda, a powyżej CMC jest odwrotnie. Porównując adsorpcje biosurfaktantów na granicach faz woda–powietrze, PMMA–powietrze oraz PMMA–woda można stwierdzić, że wartości izoterm Γ_{SV} i Γ_{SL} są mniejsze od Γ_{LV}. [**D3**,**D4**,**D5**,**D6**] To oraz obliczenia dotyczące rozmiaru cząsteczek RL i SF sugerują, że cząsteczki biosurfaktantów zarówno na granicy faz PMMA–powietrze jak i PMMA–roztwór są zorientowane równolegle do granicy faz, ale ich część hydrofilowa może być odchylona od tej granicy o pewien kąt. Interesującym jest, że w przypadku roztworów mieszanin ET z RL i SF, dla których istnieje liniowa zależność między $\gamma_{LV}\cos\theta$ i γ_{LV} nachylenie tej zależności było zbliżone do wartości $\frac{\Gamma_{SV}-\Gamma_{SL}}{\Gamma_{LV}}$ [**D5**,**D6**].

W przypadku kwarcu (Q), na podstawie obliczeń dokonanych przy zastosowaniu równań Gibbsa i Frumkina [97], można stwierdzić, że adsorpcja ET na granicach faz Q–powietrze i Q–woda jest mniejsza niż na granicy faz woda–powietrze, oraz że adsorpcja ET na granicy faz Q–powietrze jest większa niż na granicy faz Q–woda.

Udowadnia to sugestię wynikającą z zależności pomiędzy $\gamma_{LV}\cos\theta$ i γ_{LV}. Trzeba zaznaczyć, że obliczona na podstawie izoterm adsorpcji Frumkina wartość $\frac{\Gamma_{SV}-\Gamma_{SL}}{\Gamma_{LV}}$ jest bliska wartości nachylenia zależności $\gamma_{LV}\cos\theta$ od γ_{LV} uzyskanej dla ET przy stałym stężeniu SF odpowiadającym jej nienasyconej indywidualnej monowarstwie adsorpcyjnej. Ze wzrostem stężenia SF obniża się adsorpcja ET. Efekt ten jest bardziej widoczny na granicy faz Q–woda niż woda–powietrze. Należy podkreślić, że na izotermie Frumkina dla ET na granicach faz Q–powietrze i Q–woda można zaobserwować maksima. Można przypuszczać, że od stężenia ET odpowiadającego maksimum na izotermie Frumkina następuje niszczenie warstewki wody na tych granicach faz. Izotermy adsorpcji Gibbsa i Frumkina potwierdzają też sugestię wynikającą z zależności $\gamma_{LV}\cos\theta$ i γ_{LV}, mówiącą o tym, że adsorpcja SF, podobnie jak ET na granicy Q–powietrze, jest większa niż na granicy faz Q–woda. W zakresie stężenia ET od 0 do wartości odpowiadającej maksimum na izotermie Gibbsa dla adsorpcji na granicy faz woda–powietrze, w którym występuje linowa zależność pomiędzy $\gamma_{LV}\cos\theta$ i γ_{LV}, nachylenie tej zależności jest zbliżone do $\frac{\Gamma_{SV}-\Gamma_{SL}}{\Gamma_{LV}}$ [**D5**].

Analizując izotermy adsorpcji oraz wymiary cząsteczki SF w zależności od jej konfiguracji można stwierdzić, że przy niskim stężeniu ET cząsteczki biosurfaktantu są zorientowane równolegle zarówno do granicy faz Q–powietrze jak i Q–woda. Biorąc zaś pod uwagę prace kohezji SF i prace jej adhezji do powierzchni Q należy sądzić, że części hydrofilowe cząsteczek SF w warstwie międzyfazowej są skierowane do powierzchni Q, w przeciwieństwie do ich orientacji na PMMA [**D5**].

Adsorpcja mieszaniny ET i RL na granicach faz Q–powietrze i Q–woda podobnie do mieszaniny ET i SF jest mniejsza niż na granicy faz woda–powietrze [**D3**,**D4**,**D5**,**D6**]. Występują jedynie różnice w wartościach $\frac{\Gamma_{SV}-\Gamma_{SL}}{\Gamma_{LV}}$. Jak już wspomniano, na powierzchni Q tworzy się monowarstwa wody o bardzo sztywnej strukturze wynikającej z oddziaływania wiązań wodorowych. Powoduje to, że właściwości powierzchniowe tak pokrytego kwarcu różnią się znacznie od jego „czystej" powierzchni. Obecność takiej warstwy wody powoduje zmiany mechanizmu adsorpcji ET i RL w zależności od stężenia ET. W przypadku Q przy niskim stężeniu ET może zachodzić adsorpcja na jego powierzchni pokrytej warstwą wody. W miarę wzrostu stężenia etanolu adsorpcje ET i RL mogą zachodzić bezpośrednio na czystej powierzchni Q [**D6**]. Niszczenie warstwy wody może mieć szczególny wpływ na orientacje cząsteczek biosurfaktantów. Nawet

przy równoległej orientacji RL czy SF ważne jest w jakim kierunku oddziałują części hydrofilowe ich cząsteczek, co ma wpływ na wartość θ wodnych roztworów mieszaniny ET z biosurfaktantami [**D5**,**D6**].

Podczas adsorpcji ET i SF na granicach faz w układach ciało stałe–kropla roztworu–powietrze mają miejsce zmiany standardowej energii Gibbsa adsorpcji (ΔG^0_{ads}), entalpii (ΔH^0_{ads}) i entropii (ΔS^0_{ads}). Gdy nie ma adsorpcji chemicznej, zmiany entalpii podczas procesu adsorpcji są związane jedynie ze zmianami stopnia hydratacji składników roztworu. Powstawanie i niszczenie wiązań wodorowych określa wartość entalpii adsorpcji. Podczas procesu adsorpcji surfaktantów na granicach faz ΔH^0_{ads} osiągają niską ujemną lub dodatnią wartość, a z kolei zmiany ΔS^0_{ads} decydują o zmianach wartości ΔG^0_{ads}. Wartości ΔG^0_{ads} obliczone dla stężeń ET i SF mniejszych niż te odpowiadające ich nasyconej monowarstwie są dla nich rzeczywiste. Wartości ΔG^0_{ads} dla ET na granicy faz PTFE–woda są takie same jak na granicy faz woda–powietrze. Podobny wniosek jak dla ET można wyciągnąć z obliczonych wartości ΔG^0_{ads} dla SF [**D5**]. To sugeruje, że w zakresie stężeń SF odpowiadających nienasyconej monowarstwie adsorpcyjnej na granicy faz woda-powietrze w nieobecności ET [64] i ET w nieobecności SF [90] mają miejsce praktycznie niezależne adsorpcje ET i SF na granicy faz PTFE–woda. W przypadku PMMA i Q można obliczyć ΔG^0_{ads} dla ET i SF nie tylko dla granic faz PMMA–woda i Q–woda, ale również PMMA–powietrze i Q–powietrze. Wartości ΔG^0_{ads} dla ET na granicach faz PMMA–powietrze i PMMA–woda są bardzo zbliżone i nie zależą od wartości stałego stężenia SF odpowiadającego jej nienasyconej monowarstwie adsorpcyjnej na granicy faz woda-powietrze w nieobecności ET. Tendencja ET do adsorbowania się na granicach faz PMMA–powietrze i PMMA–woda jest mniejsza niż na granicy faz woda–powietrze. Należy przypuszczać, że powodem są absolutne wartości ΔG^0_{ads} dla ET na granicach faz PMMA–powietrze i PMMA–woda mniejsze niż te na granicy faz woda–powietrze. Jest to prawdopodobnie związane ze zwiększeniem ΔH^0_{ads} wynikającej z niszczenia warstwy powierzchniowej wody. Mogą o tym świadczyć niewielkie zmiany ΔG^0_{ads} dla ET na granicy faz PMMA–woda zachodzące w funkcji stężenia SF. Wartości ΔG^0_{ads} dla SF na granicach faz PMMA–powietrze i PMMA–woda zmieniają się wraz ze wzrostem stężenia ET w większym stopniu niż ET w funkcji stężenia SF, co sugeruje, że SF niszczy warstwę adsorpcyjną wody bardziej niż ET [**D5**]. Warstwa wody na powierzchni Q jest uporządkowana za pomocą silnych wiązań wodorowych pomiędzy cząsteczkami, co może powodować,

że całkowite wartości ΔG_{ads}^0 dla ET na granicy Q–woda są dużo mniejsze niż całkowite wartości ΔG_{ads}^0 ET na granicy faz woda–powietrze. Całkowite wartości ΔG_{ads}^0 ET na granicy Q–powietrze są porównywalne z tymi na granicy faz woda–powietrze. Gdy stężenie SF odpowiada nienasyconej monowarstwie adsorpcyjnej w nieobecności ET [64] praktycznie nie wpływa ono na adsorpcję ET na dwóch branych pod uwagę granicach faz. Oznacza to, że stężenie ET znacząco wpływa na ΔG_{ads}^0 SF. Podobnie jak dla ET całkowite wartości ΔG_{ads}^0 SF na granicy Q–woda są nieznacznie mniejsze niż te na granicy faz woda–powietrze [**D5**].

W przypadku adsorpcji ET i RL na badanych ciałach stałych wzięto pod uwagę wartości ΔG_{ads}^0 obliczone z równania Langmuira zmodyfikowanego przez de Boera [97,98] przy stężeniach ET i RL odpowiadających nienasyconym monowarstwom adsorpcyjnym na granicy faz woda–powietrze. W zakresie tego stężenia RL wartości ΔG_{ads}^0 ET na granicy PTFE–roztwór są niemal stałe i bliskie tym na granicy faz roztwór–powietrze. Jest to spójne z wartościami obliczonymi z izotermy Frumkina na granicach faz PTFE–roztwór i roztwór–powietrze [**D6**]. W przeciwieństwie do ET wartości ΔG_{ads}^0 RL na granicy faz PTFE–roztwór rosną w funkcji stężenia ET. Oznacza to, że tendencja RL do adsorpcji na granicy faz zmniejsza się w funkcji stężenia alkoholu. Z porównania zmian ΔG_{ads}^0 dla ET w funkcji stężenia RL i ΔG_{ads}^0 RL w funkcji stężenia ET wynika, że ET ma silniejszy wpływ na adsorpcję RL na granicy faz PTFE–roztwór niż odwrotnie. Wartości ΔG_{ads}^0 ET na granicach faz PMMA–powietrze i PMMA–roztwór zostały również obliczone ze zmodyfikowanego równania Langmuira [97]. Wartości te są podobne do tych uzyskanych dla PTFE i praktycznie nie zależą od stężenia RL w zakresie jego nienasyconej monowarstwy w nieobecności ET. Wartości ΔG_{ads}^0 dla ET na granicach faz PMMA–powietrze i PMMA–roztwór są podobne do tych otrzymanych dla granicy faz PMMA–woda (w nieobecności RL), a jednocześnie są nieznacznie większe od wartości ΔG_{ads}^0 ET na granicy faz woda–powietrze. Podobnie jak w przypadku PTFE ΔG_{ads}^0 RL rośnie w funkcji stężenia ET. Wartości ΔG_{ads}^0 RL na granicy faz PMMA–rozwór są wyższe niż te na granicy faz roztwór–powietrze [**D6**]. Z porównania wpływu ET na adsorpcję RL i vice versa możliwe jest stwierdzenie, że ET wpływa na adsorpcję RL na granicy faz PMMA–roztwór w większym stopniu niż RL na adsorpcję ET. Wartości ΔG_{ads}^0 ET i RL na granicy faz Q–powietrze są bliskie tym dla granicy faz roztwór–powietrze. Podobnie jak w przypadku PMMA, RL wpływa na ΔG_{ads}^0 ET w mniejszym stopniu niż odwrotnie. W przypadku granicy faz Q–roztwór wartości ΔG_{ads}^0

ET i RL są większe niż te dla granicy faz roztwór–powietrze, a ET wpływa na ΔG_{ads}^0 RL na tej granicy faz w mniejszym stopniu niż na innych. Potwierdza to sugestię, że w zakresie niskich stężeń ET, napięcie powierzchniowe kwarcu pod kroplą roztworu jest inne niż to wokół kropli [D6].

Z przeprowadzonych badań wynika, że żadna z badanych mieszanin RL+TX165 i SF+TX165 nie zwilża całkowicie PTFE, PMMA i Q [**D2**]. Aby wyjaśnić właściwości zwilżające wodnych roztworów mieszanin RL+TX165 i SF+TX165 obliczono kąt zwilżania (θ) hipotetycznej cieczy na powierzchni PTFE, zakładając, że jej napięcie powierzchniowe wynika jedynie z oddziaływań Lifshitza–van der Waalsa i jest równe składowym LW wody i ogona RL, SF i TX165. Otrzymane wartości θ dla wody, RL, SF i TX165 wynoszą odpowiednio 42,6; 22,0; 35,9; 23,3°. Wartości te wskazują, że nie jest możliwe osiągnięcie całkowitego rozpływania wodnych roztworów mieszanin biosurfaktantu i TX165 na powierzchni PTFE. Potwierdziły to też wartości otrzymane eksperymentalnie. Należy jednak pamiętać, że minimalne wartości γ_{LV} wodnych roztworów RL, SF i TX165 są większe niż składowa LW napięcia powierzchniowego wody. Z drugiej strony składowa LW napięcia powierzchniowego wodnego roztworu biosurfaktantu i TX165 nie zależy od stężenia roztworu i jest bliska składowej LW γ_{LV} wody (Tabela 2). To oznacza, że w wyniku adsorpcji biosurfaktantów i TX165 na granicy faz woda–powietrze nie dochodzi do obniżenia wartości składowej LW γ_{LV} wody. Jednocześnie w wyniku tej adsorpcji zmniejszona zostaje składowa AB, chociaż nie do 0. Z drugiej strony minimalne napięcie powierzchniowe wodnych roztworów mieszanin biosurfaktantów i TX165 nie jest mniejsze od γ_{LV} wodnych roztworów indywidualnych składników mieszaniny (Tabela 1). Może to być przyczyną tego, że wartości θ wodnych roztworów badanych mieszanin nie są mniejsze od tych dla indywidualnych roztworów biosurfaktantów i TX165 (Tabela 1).

Ponieważ izotermy θ wodnych roztworów mieszanin biosurfaktantów i TX165 na PTFE [**D2**] są podobne do izoterm γ_{LV} [**D1**], możliwe wydaje się przewidywanie kąta zwilżania mieszaniny w oparciu o wartości θ dla jej poszczególnych składników. Innymi słowy, wartości θ wodnych roztworów mieszanin surfaktantów na powierzchni PTFE powinny być równe sumie iloczynów θ składników mieszaniny przy odpowiednim stężeniu i ich ułamka molowego w mieszanej warstwie adsorpcyjnej na granicy faz PTFE–woda. Ułamki molowe RL, SF i TX165 w mieszanej monowarstwie na granicy faz PTFE–woda wyznaczono na podstawie ciśnienia monowarstwy indywidualnych składników mieszaniny na granicy faz woda–powietrze, zakładając zgodnie z równaniem Lucassen–Reynders [96], że skład mieszanej monowarstwy na tych granicach faz jest

w przybliżeniu taki sam. Dla układów PTFE–kropla roztworu–powietrze, w których stężenie biosurfaktantu i/lub TX165 w fazie objętościowej roztworu odpowiada nienasyconej indywidualnej monowarstwie adsorpcyjnej na granicy faz woda–powietrze (C_{unsat}), obliczone w ten sposób wartości θ dla mieszanin są bliskie wartościom zmierzonym. Niestety przy stężeniu jednego lub dwóch składników mieszaniny biosurfaktant+TX165 większych niż C_{unsat} występuje mniejsza zgodność pomiędzy zmierzonymi i obliczonymi wartościami θ. Tym samym skład mieszanej warstwy adsorpcyjnej na granicy faz PTFE–woda może różnić się nieco od tego na granicy faz woda–powietrze mimo takiego samego całkowitego stężenia mieszaniny surfaktantów na tych granicach faz [**D2**]. Należy podkreślić, że izotermy θ dla wszystkich badanych roztworów na powierzchni PTFE mogą być opisane funkcją ekspotencjalną drugiego rzędu. Przy stężeniu jednego lub dwóch składników w fazie objętościowej wyższym niż C_{unsat}, izotermy θ, na których obserwuje się maksima, mogą być opisane przez dwie funkcje ekspotencjalne: jedną od początkowej wartości θ do wartości maksymalnej i drugą od maksymalnej wartości θ do wartości końcowej. Izotermy θ wodnych roztworów mieszaniny biosurfaktant+TX165 na powierzchni PTFE mogą być opisane przez zmodyfikowane równanie Szyszkowskiego, podobnie jak izotermy γ_{LV} wodnych roztworów RL, SF i TX165 [**D2**]. Niestety, równanie to jest spełnione tylko dla roztworów, w których stałe stężenie jednego ze składników mieszaniny jest równe C_{unsat}. Warto zauważyć, że wartości ΔG^0_{ads} niezależnych składników mieszanin biosurfaktant+TX165, obliczone na podstawie stałych w równaniu Szyszkowskiego [97], są podobne do tych obliczonych ze zmodyfikowanego równania Langmuira [97,98] na granicy faz woda–powietrze. Sugeruje to, że adsorpcja mieszanin biosurfaktantu i TX165 na granicy faz PTFE–woda wpływa jedynie na udział składowej AB napięcia międzyfazowego PTFE–woda. Wniosek ten potwierdza zależność pomiędzy $\gamma_{LV}\cos\theta$ i γ_{LV}, która wskazuje, że nie tylko adsorpcja mieszaniny biosurfaktant+TX165 na granicach faz PTFE–woda i woda–powietrze jest podobna, ale też, że praca adhezji roztworu do powierzchni PTFE nie zależy od składu mieszaniny i jej stężenia. Wartości W_a wodnych roztworów badanych mieszanin do powierzchni PTFE są zbliżone do pracy adhezji wody do PTFE. Zgodnie z sugestią Blake'a [111] w przypadku liniowej zależności pomiędzy $\gamma_{LV}\cos\theta$ i γ_{LV} o nachyleniu równym –1, stała b spełnia warunek: $\frac{b}{2} = \gamma_c$. W przypadku wodnych roztworów mieszanin biosurfaktantu i TX165 otrzymana w ten sposób wartość $\frac{W_a}{2}$ jest równa 23,75 mJ/m^2, co sugeruje, że γ_c jest równe

23,75 mN/m. Potwierdza to, że niemożliwe jest całkowite rozpływanie się badanych mieszanin na powierzchni PTFE [**D2**].

Jak już wspomniano, w przypadku PMMA i Q nie występuje całkowite zwilżanie ich powierzchni przez wodne roztwory RL+TX165 i SF+TX165. Takie zachowanie się badanych mieszanin nie ma jednak uzasadnienia teoretycznego. Jak wiadomo napięcia powierzchniowe ogona surfaktantów są mniejsze niż napięcia powierzchniowe PMMA i Q (Tabela 1 i 2). W przypadku głowy SF wartość jej napięcia powierzchniowego jest nieznacznie większa od napięcia powierzchniowego PMMA. Tym samym z teoretycznego punktu widzenia możliwe jest całkowite rozpływanie się wodnych roztworów mieszanin RL+TX165 i SF+TX165 po powierzchni PMMA i Q. Wartości współczynników rozpływania biosurfaktantów i TX165 na PMMA i Q są dodatnie niezależnie od sposobu zorientowania cząsteczek do powierzchni tych ciał stałych (oprócz układu głowa TX165–PMMA). Tym samym jest możliwe, aby biosurfaktanty i TX165 przechodziły z kropli roztworu umieszczonej na powierzchni Q lub PMMA i zmieniały ich napięcie powierzchniowe wokół kropli. W takim przypadku γ_{SV} PMMA i Q zmienia się w funkcji stężenia i składu mieszanin biosurfaktantów i TX165. Przypuszczenie to potwierdza zależność pomiędzy $\gamma_{LV}cos\theta$ i γ_{LV}. Nachylenia krzywych obrazujących te zależności zmieniają się w funkcji składu i stężenia roztworów badanych mieszanin, a także zależą od rodzaju ciała stałego. Dla PMMA nachylenie wspomnianej zależności zmienia się z ujemnego na dodatnie. Wskazuje to, że nachylenia krzywych reprezentujących zależność $\gamma_{LV}cos\theta$ i γ_{LV} roztworu mieszanin biosurfaktant+TX165 przy tym samym składzie i stężeniu jest inne dla PMMA i Q. Zgodnie z równaniem Lucassen–Reynders [96] zmiany nachylenia tej zależności w funkcji składu i stężenia roztworu mieszanin są skorelowane z tymi pomiędzy adsorpcją mieszanin na granicach faz ciało stałe–powietrze i ciało stałe–ciecz.

Na izotermach kąta zwilżania dla wodnych roztworów RL+TX165 i SF+TX165 na powierzchni PMMA i Q, podobnie jak na PTFE, obecne są maksima. Maksima te występują przy wartościach stałego stężenia jednego lub dwóch składników mieszaniny wyższego niż jego C_{unsat}. Ich obecność wyjaśniono podobnie jak w układzie PTFE-kropla roztworu-powietrze w oparciu o znaczną różnicę między aktywnością adsorpcyjną biosurfaktantu i TX165 na różnych granicach faz oraz na podstawie składu warstw adsorpcyjnych. Wartości kąta zwilżania obliczone z uwzględnieniem składu warstw adsorpcyjnych w większości przypadków są zbliżone do wartości uzyskanych eksperymentalnie nawet wtedy gdy na izotermach kąta zwilżania występują maksima.

Zgodność pomiędzy izotermami kąta zwilżania uzyskanymi eksperymentalnie i teoretycznie sugeruje, że wkłady poszczególnych składników mieszaniny do wartości θ są proporcjonalne do redukcji γ_{LV} wody [**D1,D2**]. Zgodność ta sugeruje również, że skład mieszanych monowarstw adsorpcyjnych na granicach faz woda-powietrze, PMMA(Q)-woda i PMMA(Q)-powietrze jest podobny mimo różnic w stężeniu tych monowarstw. W przypadku braku zgodności między obliczonymi, a zmierzonymi wartościami kąta zwilżania można przypuszczać, że nie tylko stężenia mieszanych warstw adsorpcyjnych, ale również ich składy zależą od typu granicy faz.

Należy wspomnieć, że podobnie jak dla PTFE, wszystkie izotermy kąta zwilżania wodnych roztworów RL+TX165 i SF+TX165 na PMMA i Q mogą być opisane funkcjami ekspotencjalnymi drugiego rzędu. Dla tych ciał stałych izotermy θ roztworów o stałych stężeniach jednego lub dwóch składników mieszaniny wyższych niż C_{unsat} mogą być opisane przez dwie funkcje ekspotencjalne: jedną w zakresie zmieniającego się stężenia składnika mieszaniny od jego wartości początkowej do stężenia, przy którym występuje maksymalna wartość θ i drugą powyżej tego stężenia. W wyniku przeprowadzonych obliczeń okazało się także, że izotermy θ mogą być opisane zmodyfikowanym równaniem Szyszkowskiego [**D2**].

Ponieważ liniowa zależność pomiędzy $\gamma_{LV}\cos\theta$ i γ_{LV} o nachyleniu równym –1 nie udowadnia, że skład mieszanej monowarstwy na granicy woda–powietrze i PTFE–woda jest taki sam pomimo tych samych stężeń mieszaniny biosurfaktantu i TX165, obliczono nadmiarowe stężenie powierzchniowe Gibbsa (Γ). Obliczenia te przeprowadzono stosując równanie izotermy Gibbsa, ale tylko w zakresie stałego stężenia jednego ze składników mieszaniny mniejszego niż jego stężenie, przy którym, tworzy się jego nasycona monowarstwa adsorpcyjna na granicy faz woda–powietrze. Z tego powodu zależność pomiędzy $\gamma_{LV}\cos\theta$ i zmieniającym się stężeniem składnika mieszaniny może być wyrażona funkcją ekspotencjalną drugiego rzędu. W przypadku izoterm, na których występuje maksimum θ, nadmiarowe stężenie powierzchniowe Gibbsa obliczono z równania $\Gamma_1^{max}X_1 + \Gamma_2^{max}X_2 = \Gamma_{12}$ [**D2**]. Można założyć, że wkład danego składnika mieszaniny w jej całkowite stężenie na granicy faz PTFE–woda, podobnie jak dla θ, powinien być proporcjonalny do jego wkładu w redukcję γ_{LV} wody [**D1**]. Z porównania wartości Γ biosurfaktantu i TX165 na granicach faz PTFE–woda i woda–powietrze wynika, że składy mieszanych monowarstw adsorpcyjnych na tych granicach faz są inne. Należy pamiętać, że mechanizmy adsorpcji dla tego samego surfaktantu na granicach faz

PTFE–woda i woda–powietrze są różne. W adsorpcji na granicy faz PTFE–woda ważną rolę odgrywają oddziaływania hydrofobowe pomiędzy PTFE i ogonem surfaktantu, które nie zależą od napięć powierzchniowych na granicach faz PTFE–woda i ogon–woda, i powierzchni kontaktu ogona. Możliwe jest więc pojawienie się różnic w składach mieszanej monowarstwy na granicach faz PTFE–woda i woda–powietrze. Niemniej, wartości ΔG_{ads}^0 biosurfaktantu i TX165 obliczone zarówno z równania Langmuira zmodyfikowanego przez de Boera [97,98] jak i otrzymane w oparciu o zmodyfikowane równanie Szyszkowskiego wskazują, że tendencje biosurfaktantu i TX165 do adsorpcji na granicach faz PTFE–woda i woda–powietrze są podobne [**D2**]. Niestety, w przypadku monopolarnego PMMA i bipolarnego Q na podstawie zależności pomiędzy $\gamma_{LV}\cos\theta$ i γ_{LV} wodnych roztworów mieszanin biosurfaktantu i TX165 nie można określić ilości substancji zaadsorbowanej na granicy faz ciało stałe–woda. Zależność pomiędzy $\gamma_{LV}\cos\theta$ i γ_{LV} nie jest liniowa, a krzywe ją obrazujące mogą przyjmować nachylenia dodatnie, które sugerują ujemną adsorpcję. Wartości W_a otrzymane na podstawie równań van Ossa [94,95] oraz Younga-Dupré [97] dla wszystkich badanych roztworów do PMMA i Q wykazują, że $2\sqrt{\gamma_{LV}^{LW}\gamma_{SV}^{LW}} + 2\sqrt{\gamma_{LV}^+\gamma_{SV}^-} + 2\sqrt{\gamma_{LV}^-\gamma_{SV}^+} > \gamma_{LV}(\cos\theta + 1)$. Sugeruje to, że γ_{SV} PMMA i Q zmieniają się w funkcji składów i stężeń mieszanin biosurfaktantu i TX165. Spełnione jest również równanie $2\sqrt{\gamma_{LV}^{LW}\gamma_{SV}^{LW}} + 2\sqrt{\gamma_{LV}^+\gamma_{SV}^-} + 2\sqrt{\gamma_{LV}^-\gamma_{SV}^+} - \gamma_{LV}(\cos\theta + 1) = \pi$, z którego wynika, że $\pi \approx \frac{\gamma_W - \gamma_{LV}}{2}$. Biorąc to pod uwagę oraz równanie Younga [97] określono napięcie międzyfazowe na granicach faz PMMA(Q)–roztwór i PMMA(Q)–warstwa powierzchniowa, a następnie wyznaczono nadmiarowe stężenie powierzchniowe dla SF, RL i TX165 na tych granicach faz. Otrzymane wyniki wskazują, że wartości Γ_{SV} i Γ_{SL} [**D2**] są znacznie mniejsze od Γ_{LV} [**D1**]. Jak wynika z właściwości warstw pojedynczych surfaktantów na granicach faz PMMA–powietrze, PMMA–woda, Q–powietrze i Q–woda cząsteczki biosurfaktantu i TX165 w mieszanej warstwie adsorpcyjnej są zorientowane równolegle do granicy faz. Wartości Γ TX165 w nasyconych mieszanych monowarstwach na granicach faz PMMA–powietrze, Q–powietrze jak również PMMA–woda i Q–woda są większe niż biosurfaktantów. Może to wynikać z trzech powodów: 1) grupy oksyetylenowe w cząsteczkach TX165 mogą być połączone z atomem wodoru, 2) istnieją aktywne oddziaływania elektrostatyczne pomiędzy grupami oksyetylenowymi i jonami wodoru, 3) mają miejsce oddziaływania naładowanej ujemnie powierzchni Q i/lub grup –CO na

powierzchni PMMA. Z drugiej strony jedna cząsteczka biosurfaktantu może usunąć więcej cząsteczek wody z granicy faz niż jedna cząsteczka TX165 [**D2**].

Zależność pomiędzy wartościami Γ_{SV} i Γ_{SL} wyjaśnia nachylenie krzywych reprezentujących zależność pomiędzy $\gamma_{LV}\cos\theta$ i γ_{LV}. W przypadku Q nachylenie to jest dodatnie dla wszystkich badanych roztworów, ponieważ $\Gamma_{SV} > \Gamma_{SL}$. Może to być spowodowane tym, że głowy cząsteczek biosurfaktantu i TX165 oddziałują silnie z cząsteczkami wody. Oddziaływania cząsteczek biosurfaktantu i TX165 z powierzchniami PMMA i Q przez fazę wodną zależą od oddziaływań ciało stałe–ogon, ciało stało–głowa, jak również woda–ogon i woda–głowa oraz powierzchni kontaktu głowy i ogona, które mogą być związane z napięciem międzyfazowym. Ponieważ napięcia międzyfazowe woda–głowa biosurfaktantu i/lub woda–głowa TX165 są ujemne, zmniejsza się prawdopodobieństwo adsorpcji surfaktantów na granicach faz PMMA–woda i Q–woda w porównaniu z adsorpcją na granicach faz PMMA–powietrze i Q–powietrze. Jest to wyraźniejsze w przypadku układów zawierających Q. Mimo mniejszych adsorpcji mieszaniny biosurfaktantu i TX165 na granicach faz PMMA–powietrze, Q–powietrze, PMMA–woda i Q–woda w porównaniu do adsorpcji na granicy faz woda–powietrze wartości ΔG^0_{ads} obliczone ze zmodyfikowanego równania Langmuira [97,98] są podobne do ΔG^0_{ads} na granicy faz woda–powietrze [**D1, D2**]. Warto wspomnieć, że wartości ΔG^0_{ads} określone z równania Szyszkowskiego są bliskie wartościom uzyskanym z równania Langmuira [97]. Należy też zauważyć, że do obliczenia wartości Γ_{SV} i Γ_{SL} ze zmodyfikowanego równania Szyszkowskiego, zamiast różnicy pomiędzy napięciem międzyfazowym wody i roztworu, zastosowano różnice pomiędzy θ dla wody i roztworu odpowiednio na powierzchniach PMMA i Q [**D2**].

5. WNIOSKI

Do najważniejszych osiągnięć uzyskanych na podstawie wyników z przeprowadzonych badań i ich termodynamicznej analizy [**D1-D6**] można zaliczyć między innymi:

- Zmodyfikowanie równania Fainermana i Millera stosowanego do przewidywania napięcia powierzchniowego wodnych roztworów dwuskładnikowej mieszaniny surfaktantów o stałym składzie do zastosowania go dla wieloskładnikowych mieszanin o zmiennym składzie.

- Zaproponowanie nowej metody określania składu mieszanej monowarstwy adsorpcyjnej na podstawie izoterm napięcia powierzchniowego wodnych roztworów składników mieszaniny.

- Zaproponowanie metody przewidywania wartości kąta zwilżania dla wodnych roztworów mieszaniny substancji powierzchniowo czynnych na podstawie izoterm kąta zwilżania i napięcia powierzchniowego poszczególnych składników mieszaniny.

- Wyjaśnienie możliwości występowania maksimów na izotermie napięcia powierzchniowego i kąta zwilżania dla wodnych roztworów mieszanin biosurfaktantów z surfaktantami lub etanolem.

- Określenie kryteriów, jakie muszą być spełnione przez wodne roztwory mieszanin surfaktantów z dodatkami dla ich całkowitego rozpływania się po powierzchni apolarnych, monopolarnych i bipolarnych ciał stałych.

- Wyjaśnianie mechanizmu adsorpcji wodnych roztworów mieszaniny biosurfaktantów z etanolem na granicach faz PTFE–woda, PMMA–woda i Q–woda.

- Udowodnienie tworzenia się mieszanej warstwy adsorpcyjnej etanolu i biosurfaktantu oraz biosurfaktantu i TX165 na granicach faz PMMA–powietrze i Q–powietrze wokół kropli roztworu osadzonej na powierzchni PMMA lub Q.

- Wykazanie, że dodatnie nachylenie prostoliniowej zależności między napięciem adhezyjnym i powierzchniowym wodnego roztworu mieszanin biosurfaktantów z etanolem lub surfaktantem nie świadczy o ujemnej adsorpcji tych mieszanin na granicach faz PMMA–woda i Q–woda.

- Zaproponowanie mechanizmu adsorpcji mieszanin biosurfaktantu i etanolu na granicach faz PMMA–powietrze, PMMA–woda, Q–powietrze i Q–woda.

- Wyjaśnianie stężenia i składu warstw adsorpcyjnych na granicach faz ciało stałe–powietrze, ciało stałe–woda i woda–powietrze w oparciu o oddziaływania Lifshitza–van der Waalsa, rodzaje grup chemicznych występujących w cząsteczkach biosurfaktantów, TX165 i etanolu oraz rozmiarów tych cząsteczek.
- Zaproponowanie równania pozwalającego na określenie standardowej swobodnej energii Gibbsa adsorpcji etanolu i biosurfaktantów na podstawie ich CAC i CMC.

6. LITERATURA

[D1] E. Rekiel, A. Zdziennicka*, K. Szymczyk, B. Jańczuk, Thermodynamic Analysis of the Adsorption and Micellization Activity of the Mixtures of Rhamnolipid and Surfactin with Triton X-165. Molecules, 2022, 27, 3600.

[D2] E. Rekiel, A. Zdziennicka, K. Szymczyk, B. Jańczuk*, Wetting Properties of Rhamnolipid and Surfactin Mixtures with Triton X-165. Molecules, 2022, 27, 4706.

[D3] E. Rekiel, A. Zdziennicka*, B. Jańczuk, Adsorption properties of rhamnolipid and ethanol at water/ethanol solution-air interface. J. Mol. Liq., 2020, 308, 113080.

[D4] E. Rekiel, A. Zdziennicka*, B. Jańczuk, Adsorption of surfactin at water with ethanol mixture-air interface. J. Mol. Liq., 2020, 300, 112240.

[D5] E. Rekiel, A. Zdziennicka*, B. Jańczuk, Mutual influence of ethanol and surfactin on their wetting and adhesion properties, Colloids Surf. A Physicochem. Eng. Asp., 2021, 627, 127161.

[D6] E. Rekiel, A. Zdziennicka*, B. Jańczuk, Effect of ethanol on wetting and adhesion properties of rhamnolipid. Int. J. Adhes. Adhes., 2021, 110, 102955.

[1] A. Kashif, R. Rehman, A. Fuwad, M.K. Shadid, H.N.P. Dayarathne, A. Jamal. M.N. Aftab, B. Mainali, Y. Choi Current advances in the classification, production, properties and applications of microbial biosurfactants – A critical review. Adv. Colloid Interface Sci., 2022, 306, 102718.

[2] L.A. Sarubbo, MdG.C.S. Silva, I.J.B. Durval, K.G.O. Bezerra, B.G. Ribeiro, I.A.Silva, M.S. Twigg, I.M. Banat, Biosurfactants: Production, properties, applications, trends, and general perspectives. Biochem. Eng. J., 2022, 181, 108377.

[3] R. Jahan, A.M. Bodratti, M. Tsianou, P. Alexandridis, Biosurfactants, natural alternatives to synthetic surfactants: Physicochemical properties and applications. Adv. Colloid Interface Sci., 2020, 275, 102061.

[4] S. Sanchez, A.L. Demain, Secondary Metabolites, M. Moo-Young (Ed.). In: Comprehensive Biotechnology, Vol. 1, 2nd Edition, Pergamon, Elsevier, 2011, 155–67.

[5] S. Sood, R. Singhal, S. Bhat, A. Kumar, Inoculum Preparation, M. Moo-Young (Ed.). In: Comprehensive Biotechnology, Vol. 2, 2nd Edition, Pergamon, Elsevier, 2011, 151–164.

[6] A.A. Jimoh, J. Lin, Biosurfactant: A new frontier for greener technology and environmental sustainability. Ecotoxicol. Environ. Saf., 2019, 184 (2), 109607.

[7] S. Mishra, Z. Lin, S. Pang, Y. Zhang, P. Bhatt, S. Chen, Biosurfactant is a powerful tool for the bioremediation of heavy metals from contaminated soils. J. Hazard. Mater., 2021, 418 (10), 126253.

[8] F. Carolin C, P.S. Kumar, P.T. Ngueagni, A review on new aspects of lipopeptide biosurfactant: Types, production, properties and its application in the bioremediation process. J. Hazard. Mater., 2021, 407 (3), 124827.

[9] D.K.F. Santos, R.D. Rufino, J.M. Luna, V.A. Santos, L.A. Sarubbo, Biosurfactants: multifunctional biomolecules of the 21st century. Int. J. Mol. Sci., 2016, 17(3), 401.

[10] C.E. Drakontis, S. Amin, Biosurfactants: Formulations, properties, and applications. Curr. Opin. Colloid Interface Sci., 2020, 48, 77–90.

[11] D. Sharma, Applications of Biosurfactants w Food. In: Biosurfactants in Food. Springer Briefs in Food, Health, and Nutrition. 1st Edition, Springer Cham, 2016, 43–80.

[12] E.Z. Gomaa, Antimicrobial and anti-adhesive properties of biosurfactant produced by lactobacilli isolates, biofilm formation and aggregation ability. J. Gen. Appl. Microbiol., 2013, 59 (6), 425–36.

[13] S.K. Walvekar, S. Yasaswi, K.Shetty, K.S.Yadav, Applications of surfactin and other biosurfactants in anticancer activity, Inamuddin, C.O. Adetunji, M.I. Ahamed (Eds.). In: Green Sustainable Process for Chemical and Environmental Engineering and Science, Biomedical Application of Biosurfactant in Medical Sector, Academic Press, Elsevier, 2022, 223–234

[14] L. Rodrigues, I.M. Banat, J.Teixeira, R. Oliveira, Biosurfactants: potential applications in medicine. J. Antimicrob. Chemother., 2006, 57 (4), 609–618.

[15] P.A. Çelik, E.B. Manga, A. Çabuk, I.M. Banat, Biosurfactants' Potential Role in Combating COVID-19 and Similar Future Microbial Threats. Appl. Sci., 2021, 11 (1), 334.

[16] A.R. Markande, D. Patel, S. Varjani, A review on biosurfactants: properties, applications and current developments. Bioresour. Technol., 2021, 330 (13), 124963.

[17] E.B. Manga, P.A. Çelik, A. Çabuk, I.M. Banat, Biosurfactants: Opportunities for the development of a sustainable future. Curr. Opin. Colloid Interface Sci., 2021, 56, 101514.

[18] B.G. Ribeiro, J.M.C. Guerra, L.A. Sarubbo, Biosurfactants: Production and application prospects in the food industry. Biotechnol. Prog., 36 (5), 1–16.

[19] C. Nikolova, T. Gutierrez, Biosurfactants and Their Applications in the Oil and Gas Industry: Current State of Knowledge and Future Perspectives. Front. Bioeng. Biotechnol., 2021, 9, 626639.

[20] M. Kracht, G. Rokos, M. Özel, M. Kowall, G. Pauli, J. Vater, Antiviral and Hemolytic Activities of Surfactin Isoforms and Their Methyl Ester Derivatives. J. Antibiot. (Tokyo), 1999, 52 (7), 613–619.

[21] T. Stipcevic, T. Piljac, R.R. Isseroff, Di-rhamnolipid from Pseudomonas aeruginosa displays differential effects on human keratinocyte and fibroblast cultures. J. Dertmatol. Sci., 2005, 40 (2), 141–143.

[22] M. Sodagari, H. Wang, B.Z. Newby, L–K. Ju, Effect of rhamnolipids on initial attachment of bacteria on glass and octadecyltrichlorosilane-modified glass. Colloids Surf. B. Biointerfaces,2013, 103, 121–128.

[23] P. Singh, S.S. Cameotra, Potential applications of microbial surfactants in biomedical sciences. Trends Biotechnol., 2004, 22 (3), 142–146.

[24] S.G.V.A.O. Costa,S. R. de Souza, M. Nitschke, S.M.M. Franchetti, M. Jafelicci Jr, R.B. Lovaglio, J. Contiero, Wettability of Aqueous Rhamnolipids Solutions Produced by Pseudomonas aeruginosa LBI. J. Surfactants Deterg., 2008, 12 (2), 125–130.

[25]   M.M. Müller, J.H. Kügler, M. Henkel, M. Gerlitzki, B. Hörmann, M. Pöhnlein, C. Syldatk, R. Hausmann, Rhamnolipids—Next generation surfactants?. J. Biotechnol., 2012, 162 (4), 366–380.

[26]   H. Chong, Q. Li, Microbial production of rhamnolipids: opportunities, challenges and strategies. Microb. Cell Fact., 2017, 16 (1), 137.

[27]   L. Biktasheva,A. Gordeev, S. Selivanovskaya, P. Galitskaya, Di- and Mono-Rhamnolipids Produced by the Pseudomonas putida PP021 Isolate Significantly Enhance the Degree of Recovery of Heavy Oil from the Romashkino Oil Field (Tatarstan, Russia). Processes, 2022, 10 (4), 779.

[28]   A. N. Mendes, L.A. Filgueiras, J.C. Pinto, M. Nele, Physicochemical Properties of Rhamnolipid Biosurfactant from Pseudomonas aeruginosa PA1 to Applications in Microemulsions. J. Biomater. Nanobiotechnol., 2015, 6 (1), 64–79.

[29]   J.M.D.A. Câmara, M.A.S.B. Sousa, E.L. Barros Neto, M.C.A. Oliveira, Application of rhamnolipid biosurfactant produced by Pseudomonas aeruginosa in microbial-enhanced oil recovery (MEOR). J. Pet. Explor. Prod. Technol., 2019, 9 (3), 2333–2341.

[30]   S. Kong, C. Shen, Y. Li, Q. Meng, Rhamnolipids Sustain Unchanged Surface Activities during Decomposition in Alkaline Solutions. ACS Omega, 2021, 6 (24), 15750–15755.

[31]   B. Hörmann, M.M. Müller, C. Syldatk, R. Hausmann, Rhamnolipid production by Burkholderia plantarii DSM 9509T. Eur. J. Lipid. Sci. Technol., 2010, 112 (6), 674–680.

[32]   H. Amani,M.R. Mehrnia,M.H. Sarrafzdeh, M. Haghighi, M.R. Soudi, Scale up and application of biosurfactant from Bacillus subtilis in enhanced oil recovery. Appl. Biochem. Biotechnol., 2010, 162 (2), 510–523.

[33]   S.G.V.A.O. Costa, M. Nitschke, F. Lépine, E. Déziel, J.Contiero, Structure, properties and applications of rhamnolipids produced by Pseudomonas aeruginosa L2-1 from cassava wastewater. Process Biochem., 2010, 45 (9), 1511–1516.

[34]   J.C. Mata-Sandoval, J. Karns, A. Torrents, High-performance liquid chromatography method for the characterization of rhamnolipid mixtures produced by Pseudomonas aeruginosa UG2 on corn oil. J. Chromatogr. A., 1999, 864 (2), 211–220.

[35]   A. Abalos, A. Pinazo, M.R. Casals, F. García, A. Manresa, Physicochemical and antimicrobial properties of new rhamnolipids produced by Pseudomonas aeruginosa AT10 from soybean oil refinery wastes. Langmuir, 2001, 17 (5), 1367– 1371.

[36]   O. Pornsunthorntwee, S. Chavadej, R. Rujiravanit, Solution properties and vesicle formation of rhamnolipid biosurfactants produced by Pseudomonas aeruginosa SP4. Colloids Surf. B. Biointerfaces, 2009, 72 (1), 6–15.

[37]   M. Benincasa, A. Abalos, I. Oliveira, A. Manresa, Chemical structure, surface properties and biological activities of the biosurfactant Chemical structures and biological activities of rhamnolipids produced by Pseudomonas aeruginosa LBI from soapstock. Antonie van Leeuwenhoek, 2004, 85 (1), 1–8.

[38] Y. Zhang, R.M. Miller, Enhanced octadecane dispersion and biodegradation by a Pseudomonas rhamnolipid surfactant (biosurfactant). Appl. Environ. Microbiol., 1992, 58 (10), 3276–3282.

[39] D. Mańko, A. Zdziennicka, B. Jańczuk, Thermodynamic properties of rhamnolipid micellization and adsorption. Colloids Surf. B: Biointerfaces, 2014, 119, 22–29.

[40] J. Penfold, R.K. Thomas, H–H. Shen, Adsorption and self-assembly of biosurfactants studied by neutron reflectivity and small angle neutron scattering: glycolipids, lipopeptides and proteins. Soft Matter, 2012, 8 (3), 578.

[41] R. Kumar, A.J. Das, Industrial Applications of Rhamnolipid: An Innovative Green Technology for Industry. In: Rhamnolipid Biosurfactant, 1st Edition, Springer Singapore, 2018, 65–77.

[42] L. Jin, W. Black, T. Sawyer, Application of Environment-Friendly Rhamnolipids against Transmission of Enveloped Viruses Like SARS-CoV2. Viruses., 2021, 13 (2), 322.

[43] P. Zhu, S. Zhang, R. Kumar, Z. Zhang, Y. Wang, X. Jiang, K. Lin, G. Kaur, K.K.L. Yung, Rhamnolipids from non-pathogenic *Acinetobacter calcoaceticus*: Bioreactor-scale production, characterization and wound healing potency. N. Biotechnol., 2022, 67,23–31.

[44] S.A. Adu, M.S. Twigg, P.J. Naughton, R. Marchant, I.M. Banat, Characterisation of cytotoxicity and immunomodulatory effects of glycolipid biosurfactants on human keratinocytes. Appl. Microbiol. Biotechnol., 2023, 107 (1), 137–152.

[45] S. Semkova, G. Antov, I. Illiev, I. Tsoneva, P. Lefterov, N. Christova, L. Nacheva, I. Stoineva, L. Kabaivanova, G. Staneva, B. Nikolova, Rhamnolipid Biosurfactants – Possible Natural Anticancer Agents and Autophagy Inhibitors. Separations, 2021, 8 (7), 92.

[46] K. Rahimi, T.B. Loftabad, F. Jabeen, S.M. Ganji, Cytotoxic effects of mono- and di-rhamnolipids from Pseudomonas aeruginosa MR01 on MCF-7 human breast cancer cells. Colloids Surf. B. Biointerfaces., 2019, 181, 943–952.

[47] M.S. Twigg, S.A. Adu, S. Sugiyama, R. Marchant, I.M. Banat, Mono-Rhamnolipid Biosurfactants Synthesized by Pseudomonas aeruginosa Detrimentally Affect Colorectal Cancer Cells. Pharmaceuticals., 2022, 14 (12), 2799.

[48] N. Christova, B. Tuleva, A. Kril, M. Georgieva, S. Konstantinov, I. Terziyski, B. Nikolova, I. Stoineva, Chemical Structure and In Vitro Antitumor Activity of Rhamnolipids from Pseudomonas aeruginosa BN10. Appl. Biochem. Biotechnol., 2013, 170 (3), 676–689.

[49] M. Ohadi, A. Shahravan,N. Dehghannoudeh, T. Eslaminejad, I.M. Banat, G. Dehghannoudeh, Potential Use of Microbial Surfactant in Microemulsion Drug Delivery System: A Systematic Review. Drug Des. Devel. Ther., 2020, 14, 541– 550.

[50] O. Kuntyi, A. Mazur, A. Kytsya, O. Karpenko, L. Bazylyak, I. Mertsalo, T. Pokynbroda, A. Prokopalo, Electrochemical synthesis of silver nanoparticles in solutions of rhamnolipid. Micro Nano Lett., 2020, 15 (12), 802–807.

[51] A. Chebbi, A. Franzetti, F. Formicola, T.G. Ambaye, F.H. Gomez, B. Murena, E. De Marco, T. Beltrani, S. Sbaffoni, M. Vaccari, Insights into rhamnolipid-based

soil remediation technologies by safe microorganisms: A critical review. J. Clean. Prod., 2022, 367 (5), 133088.

[52] G. Liu, H. Zhong, X. Yang, Y. Liu, B. Shao, Z. Liu, Advances in applications of rhamnolipids biosurfactant in environmental remediation: A review. Biotechnol Bioeng., 2018, 115 (4), 796–814.

[53] C.N. Mulligan, S. Wang, Remediation of a heavy metal-contaminated soil by a rhamnolipid foam. Eng. Geol., 2006, 85 (1–2), 75–81.

[54] L. Dobler, H.C. Ferraz, L. V. Araujo de Castilho, L.S. Sangenito, I.P. Pasqualino, A.L.S. dos Santos, B.C. Neves, R.R. Oliveira, D.M.G. Freire, R.V. Almeida, Environmentally friendly rhamnolipid production for petroleum remediation. Chemosphere, 2020, 252, 126349.

[55] N.S. Shaligram, R.S. Singhal RS, Surfactin – A Review on Biosynthesis, Fermentation, Purification and Applications. Food Technol. Biotechnol.,2010, 48 (2), 119–134.

[56] G. Seydlová, J. Svobodová, Review of surfactin chemical properties and the potential biomedical applications. Cent. Eur. J. Med., 2008, 3 (2), 123–133.

[57] V.S.V. Santos, E. Silveira, B.B. Pereira, Toxicity and applications of surfactin for health and environmental biotechnology. J. Toxicol. Environ. Health B. Crit. Rev., 2018, 21 (6–8), 382–399.

[58] S. Lang, Biological amphiphiles (microbial biosurfactants). Curr. Opin. Colloid Interface Sci., 2002, 7 (1–2), 12–20.

[59] E. Rosenberg, E.Z. Ron, High- and low-molecular-mass surfactants. Appl. Microbiol. Biotechnol., 1999, 52 (2), 154–162.

[60] M. Deleu, H. Razafindralambo, Y. Popineau,P. Jacques, P. Thonart, M. Paquot, Interfacial and emulsifying properties of lipopeptides from Bacillus subtilis. Colloids Surf. A Physicochem. Eng. Asp., 1999, 152 (1–2), 3–10.

[61] K. Arima, A. Kakinuma, G. Tamura, Surfactin, a crystalline peptidelipid surfactant produced by Bacillus subtilis: isolation, characterization and its inhibition of fibrin clot formation. Biochem. Biophys. Res. Commun., 1968, 31 (3), 488–494.

[62] D.G. Cooper, C.R. Macdonald, S.J.B. Duff, N. Kosaric, Enhanced production of surfactin from Bacillus subtilis by continuous product removal and metal cation additions. Appl. Environ. Microbiol., 1981, 42 (3), 408–512.

[63] F. Peypoux, J.M. Bonmatin, J. Wallach, Recent trends in the biochemistry of surfactin. Appl. Microbiol. Biotechnol., 1999, 51 (5), 553–563.

[64] A. Zdziennicka, B. Jańczuk, Thermodynamic parameters of some biosurfactants and surfactants adsorption at water-air interface, J. Mol. Liq., 2017, 243, 236–244.

[65] J.D. Sheppard, C. Jumarie, D.G. Cooper, R. Laprade, Ionic channels induced by surfactin in planar lipid bilayer membranes. Biochim. Biophys. Acta, 1991, 1064 (1), 13–23.

[66] J.S. Ferguson, D.R. Voelker, F.X. McCormack, L.S. Schlesinger, Surfactant protein D binds to Mycobacterium tuberculosis bacilli and lipoarabinomannan via carbohydrate-lectin interactions resulting in reduced phagocytosis of the bacteria by macrophages. J. Immunol., 1999, 163 (1), 312–321.

[67] D. Sharma, S.S. Singh, P. Baindara, S. Sharma, N. Khatri, V. Grover, P.B. Patil, S. Korpole, Surfactin Like Broad Spectrum Antimicrobial Lipopeptide Co-produced With Sublancin From *Bacillus subtilis* Strain A52: Dual Reservoir of Bioactives. Front. Microbiol.,2020 11, 1167.

[68] G. Seydlová, R. Čabala, J. Svobodová, Sufactin – novel solutions for global issues, S. Olsztyńska-Janos (Ed.). In: Biomedical Engineering, Trends, Research and Technologies, InTech, 2011, 305-330.

[69] D. Malviya, P.K. Sahu, U.D. Singh, S. Paul, A. Gupta, A.R. Gupta, S. Singh, M. Kumar, D. Paul, J.P. Rai, H.V. Singh, G.P. Brahmaprakash, Lesson from Ecotoxicity: Revisiting the Microbial Lipopeptides for the Management of Emerging Diseases for Crop Protection. Int. J. Environ. Res. Public Health, 2020, 17 (4), 1434.

[70] D. Vollenbroich, M. Özel, J. Vater, R.M. Kamp, G. Pauli, Mechanism of inactivation of enveloped viruses by the biosurfactant surfactin from *Bacillus subtilis*. Biologicals, 1997, 25 (3), 289–297.

[71] K. Kim, S.Y. Jung, D.K. Lee, J.K. Jung, J.K. Park, D.K. Kim, C.H. Lee, Suppression of Inflammatory Responses by Surfactin,1 a Selective Inhibitor of Platelet Cytosolic Phospholipase A2. Biochem Pharmacol., 55 (7), 975–985.

[72] X-h. Cao, A-h. Wang A, C-l. Wang, D-z. Mao, M-f. Lu, Y-q. C, R-z. Jiao, Surfactin induces apoptosis in human breast cancer MCF-7 cells through a ROS/JNK-mediated mitochondrial/caspase pathway. Chem. Biol. Interact., 2010, 183 (3), 357–362.

[73] K. Shirahama, T. Kashiwabara, The CMC-decreasing effects of some added alcohols on the aqueous sodium dodecyl sulfate solutions. J. Colloid Interface Sci.,19714, 36 (1), 65–70.

[74] R. Zana, S. Yiv, C. Strazielle, P. Lianos, Effect of alcohol on the properties of micellar systems: I. Critical micellization concentration, micelle molecular weight and ionization degree, and solubility of alcohols in micellar solutions. J. Colloid Interface Sci., 1981, 80 (1), 208–223.

[75] J-B. Huang, M. Mao, B-Y. Zhu, The surface physico-chemical properties of surfactants in ethanol-water mixtures. Colloids Surf. A Physicochem. Eng. Asp., 1999, 155 (2–3), 339-348.

[76] S. Javadian, H. Gharibi, B. Sohrabi, H. Bijanzadeh, M.A. Safarpour, R. Behjatmanesh-Ardakani, Determination of the physico-chemical parameters and aggregation number of surfactant in micelles in binary alcohol–water mixtures. J. Mol. Liq., 2008, 137 (1–3), 74–79.

[77] B. Sarkar, S. Lam, P. Alexandridis, Micellization of Alkyl-Propoxy-Ethoxylate Surfactants in Water−Polar Organic Solvent Mixtures. Langmuir, 2010, 26 (13), 10532–10540.

[78] S. Mahbub, S. Rana, M.A. Rub, A. Hoque, S. E. Kabir, A.M. Asiri, Influence of Alcohol/Temperature on the Interaction of Sodium Dodecyl Sulfate with Cetyltrimethylammonium Bromide: Experimental and Theoretical Study. J. Chem. Eng. Data, 2019, 64 (10), 4376–4389.

[79] T. Sidim, H. Akbaş H, Thermodynamic and Interfacial Properties of Cationic Gemini Surfactant in the Presence of Alcohols. Tenside Surfactants Deterg., 2018, 54 (4), 287–293.

[80] J. Hossain, N.H. Al-Shaalan, R. Amin, S. Aktar, S. Rana, S.M. Wabaidur, M.A. Rub, A. Hoque, S.E. Kabir, A.M. Asiri, Physicochemical Observation of the Impact of Various Additives on the Clouding Nature of Triton X-100 Solution. J. Chem. Eng. Data, 2020, 65 (2), 841–847.

[81] F.I. El-Dossoki, E.A. Gomaa, O.K. Hamza, Solvation thermodynamic parameters for sodium dodecyl sulfate (SDS) and sodium lauryl ether sulfate (SLES) surfactants in aqueous and alcoholic-aqueous solvents. SN Appl. Sci., 2019, 1, 933.

[82] A. Gopinath, M.P. Karthick, A. Harikumar, A, Anandaraj, Effectiveness of single application alcohol based antiseptic solution in preventing surgical site infection. Int. J. Surg. Sci., 2020, 4 (4), 226–230.

[83] M. Kumbhakar, S. Nath, T. Mukherjee, H. Pal, Solvation dynamics in triton-X-100 and triton-X-165 micelles: Effect of micellar size and hydration. J. Chem. Phys., 2004, 121 (12), 6026.

[84] S. Jaiswal, R. Mondal, D. Paul, S. Mukherjee, Investigating the micellization of the triton-X surfactants: A non-invasive fluorometric and calorimetric approach. Chem. Phys. Lett., 646, 18–24.

[85] A. Zdziennicka, Surface Behavior of Triton X-165 and Short Chain Alcohol Mixtures. Langmuir, 2010, 26 (3), 1860–1869.

[86] A. Zdziennicka, K. Szymczyk, J. Krawczyk, B. Jańczuk, Critical micelle concentration of some surfactants and thermodynamic parameters of their micellization. Fluid Phase Equilib., 2012, 322–323(3), 126–134.

[87] M.A. Rub, N. Azum, D. Kumar, A. Khan, M.N. Arshad, A.M. Asiri, M.M. Alotaibi, Aggregational behaviour of promethazine hydrochloride and TX-45 surfactant mixtures: A multi-techniques approach. J. Mol. Liq.,2021, 342, 117558.

[88] A.J. Groszek, Selective adsorption at graphite/hydrocarbon interfaces. Proc. R. Soc. Lond. A Math. Phys. Sci., 1970, 314, 473–478.

[89] K. Szymczyk, A. Zdziennicka, J. Krawczyk, B. Jańczuk, Wettability, adhesion, adsorption and interface tension in the polymer/surfactant aqueous solution system. I. Critical surface tension of polymer wetting and its surface tension., Colloids Surf. A Physicochem. Eng. Asp., 2012, 402, 132–138.

[90] A. Chodzińska, A. Zdziennicka, B. Jańczuk, Volumetric and Surface Properties of Short Chain Alcohols in Aqueous Solution–Air Systems at 293 K. J. Solution Chem., 2012, 41, 2226–2245.

[91] A. Zdziennicka, B. Jańczuk, Wetting and adhesion properties of rhamnolipid and surfactin. Inter. J. Adhes. Adhes., 2017, 84, 275–282.

[92] A.Zdziennicka, K. Szymczyk, J. Krawczyk, B. Jańczuk, Activity and thermodynamic parameters of some surfactants adsorption at the water–air interface. Fluid Ph. Equilibria, 2012, 318, 25–33.

[93] F.M. Fowkes, Attractive forces at interfaces. Ind. Eng. Chem., 1964, 56, 40–52.

[94] C.J. van Oss, Interfacial Forces in Aqueous Media. 1st Edition. Marcel Dekker, NY, USA, 1994.

[95] C.J. van Oss, M.K. Chaudhury, R.J. Good, Monopolar surfaces. Adv Colloid Interface Sci., 1987, 28, 35–64.

[96] E.H. Lucassen-Reynders, Contact angles and adsorption on solids. J. Phys. Chem., 1963, 67, 969–972.

[97] M.J. Rosen, Surfactants and Interfacial Phenomena. 3rd Edition. Wiley–Interscience, NY, USA, 2004.

[98] J.H. Boer, The Dynamical Character of Adsorption. 1st Edition. Oxford University Press, London, UK, 1953.

[99] C.J. van Oss, P.M. Constanzo, Adhesion of anionic surfactants to polymer surfaces and low-energy materials. J. Adhes. Sci.Technol., 1992, 4, 477–487.

[100] V.B. Fainerman, R. Miller, E.V. Aksenenko, Simple model for prediction of surface tension of mixed surfactant solutions., Adv. Colloid Interface Sci., 2002, 96, 339–359.

[101] V.B. Fainerman, R. Miller, Simple method to estimate surface tension of mixed surfactant solutions. J. Phys. Chem. B, 2001, 105, 11432–11438.

[102] K.A. Connors, K.A. Wright, Dependence of surface tension on composition of binary aqueous-organic solutions, Anal. Chem., 1989, 61 194–198.

[103] E.A. Guggenheim, N.K. Adam, Thermodynamics of adsorption at the surface of solutions. Proc. Roy. Soc. Lond. A, 1933, 139, 218–236.

[104] K. Szymczyk, A. Zdziennicka, B. Jańczuk, Properties of some nonionic fluorocarbon surfactants and their mixtures with hydrocarbon ones. Adv. Colloid Interface Sci., 2021, 292, 102421.

[105] M.J. Rosen, X.Y. Hua, Surface concentrations and molecular interactions in binary mixtures of surfactants. J. Colloid Interface Sci., 1982, 86, 164–172.

[106] M. Bergström, J.C. Eriksson, Theoretical analysis of synergistic effects in mixed surfactant systems. Langmuir, 2000, 16, 7173–7181.

[107] A.W. Adamson, A.P. Gast, Physical Chemistry of Surfaces. 6th Edition, Wiley–Interscience, NY, USA, 1997.

[108] L.A. Girifalco, R.J. Good RJ, A Theory for the Estimation of Surface and Interfacial Energies. I. Derivation and Application to Interfacial Tension. J. Phys. Chem., 1957, 61 (7), 904–909.

[109] R.J. Good, L.A. Girifalco LA, A theory for estimation of surface and interfacial energies. III. Estimation of surface energies of solids from contact angle data. J. Phys. Chem., 1960, 64 (5) 561–565.

[110] A.W. Neumann, R.J. Good, C.J. Hope, An equation-of-state approach to determine surface tensions of low-energy solids from contact angles. J. Colloid Interface Sci., 1974, 49 (2) 291–304.

[111] T. D. Blake, Wetting, T.F. Tadros (Ed.). In: Surfactants, Academic Press, London, UK, 1984.

7. DOROBEK NAUKOWY

7.1. PUBLIKACJE

Oprócz artykułów będących podstawą rozprawy doktorskiej jestem autorką i współautorką **dwóch** artykułów z list indeksowanych, a także **dziesięciu** rozdziałów w monografiach w języku polskim i **jednego** w języku angielskim.

- **E. Rekiel**, W. Smułek, A. Zdziennicka, E. Kaczorek, B. Jańczuk, Wetting properties of Saponaria officinalis saponins. Colloids and Surfaces A: Physicochemical and Engineering Aspects, 2020, 584, 123980.

  IF_{2020} / $IF_{5-letni}$: 4,540 / 4,746
  $MEiN_{2020}$/$MEiN_{2023}$: 70 pkt. / 70 pkt.

- **E. Rekiel**, Adsorption effectiveness and adsorption efficiency of chosen surfactants. Annales UMCS Sectio AA Chemia, 2019, 74 (2), 25-39.

  $MEiN_{2019}$ / $MEiN_{2023}$: 20 pkt. / 20 pkt.

- **E. Rekiel**, Saponiny – roślinne biosurfaktanty. Badania i Rozwój Młodych Naukowców w Polsce, Nauki Przyrodnicze część IV, Edytor: Jędrzej Nyćkowiak, Jacek Leśny, 2019, ISBN: 978-83-66139-81-7, 137-141.
- **E. Rekiel**, Soforolipidy – budowa, właściwości i zastosowanie. Badania i Rozwój Młodych Naukowców w Polsce, Nauki Przyrodnicze część IV, Edytorzy: Jędrzej Nyćkowiak, Jacek Leśny, 2019, ISBN: 978-83-66139-81-7, 142-147.
- **E. Rekiel**, Biosurfaktanty bakteryjne a tworzenie biofilmu. Badania i Rozwój Młodych Naukowców w Polsce, Nauki Przyrodnicze część I, Edytorzy: Jędrzej Nyćkowiak, Jacek Leśny, 2020, 978-83-66392-51-9, 88-92.
- **E. Rekiel**, Biosurfaktanty w medycynie. Badania i Rozwój Młodych Naukowców w Polsce, Nauki Przyrodnicze część I, Edytorzy: Jędrzej Nyćkowiak, Jacek Leśny, 2020, 978-83-66392-51-9, 93-97.
- **E. Rekiel**, Wybrane biosurfaktanty drożdżowe. Badania i Rozwój Młodych Naukowców w Polsce, Nauki Przyrodnicze część II, Edytorzy: Jędrzej Nyćkowiak, Jacek Leśny, 2020, ISBN: 978-83-66392-59-5, 112-116.
- **E. Rekiel**, Biosurfaktanty w zastosowaniach kosmetycznych. Badania i Rozwój Młodych Naukowców w Polsce, Nauki Przyrodnicze część II, Edytorzy: Jędrzej Nyćkowiak, Jacek Leśny, 2020, ISBN: 978-83-66392-59-5, 117-121.
- **E. Rekiel**, Rhamnolipid – budowa, właściwości i zastosowanie. Badania i Rozwój Młodych Naukowców w Polsce, Chemia, Edytorzy: Jędrzej Nyćkowiak, Jacek Leśny, 2021, ISBN: 978-83-66392-91-5, 21-25.
- **E. Rekiel**, Surfaktyna – synteza, właściwości i zastosowanie. Badania i Rozwój Młodych Naukowców w Polsce, Chemia, Edytorzy: Jędrzej Nyćkowiak, Jacek Leśny, 2021, ISBN: 978-83-66392-91-5, 26-30.

- **E. Rekiel**, Biosurfaktanty w przemyśle spożywczym. Badania i Rozwój Młodych Naukowców w Polsce, Nauki Przyrodnicze, Edytorzy: Jędrzej Nyćkowiak, Jacek Leśny, 2021, ISBN: 978-83-66743-20-5, 49-53.
- **E. Rekiel**, Biosurfaktanty lipopeptydowe produkowane przez bakterie – charakterystyka i zastosowanie. Badania i Rozwój Młodych Naukowców w Polsce, Nauki Przyrodnicze, Edytorzy: Jędrzej Nyćkowiak, Jacek Leśny, 2021, ISBN: 978-83-66743-20-5, 54-58.
- **E.Rekiel**, A. Zdziennicka, Biosurfactants in environmental protection, EYEC Monograph 10 th European Young Engineers Conference, 2016, ISBN 978-83-953822-0-8, 45-49.

7.2. KONFERENCJE

W trakcie studiów doktoranckich byłam autorką i zaprezentowałam samodzielnie **jedenaście** wystąpień ustnych, a także byłam autorką i współautorką **siedemnastu** wystąpień posterowych (z czego **trzynaście** zaprezentowałam samodzielnie) na **dziesięciu** konferencjach międzynarodowych i **jedenastu** konferencjach ogólnokrajowych.

<u>WYSTĄPIENIA USTNE</u>

- **E. Rekiel**, A. Zdziennicka, Biosurfaktanty jako naturalne zamienniki surfaktantów, IX Ogólnokrajowa Konferencja Naukowa. Młodzi Naukowcy w Polsce - Badania i Rozwój. 05.04.2019, Lublin.
- **E. Rekiel**, Właściwości zwilżające wybranych surfaktantów naturalnych. Nauka i przemysł – lubelskie spotkania studenckie. 24.06.2019, Lublin.
- **E. Rekiel**, Porównanie właściwości wybranych biosurfaktantów i surfaktantów klasycznych. III Konferencja Doktorantów Nauk Przyrodniczych. 25-28.06.2019, Gdańsk.
- **E. Rekiel**, Rhamnolipid i surfaktyna – lek czy surfaktant?. X Ogólnokrajowa Konferencja Naukowa. Młodzi Naukowcy w Polsce - Badania i Rozwój. 22.11.2019, Lublin.
- J. Krawczyk, **E. Rekiel**, A. Zdziennicka, Polymer materials as substitutes in studies on human skin wettability. 18th Young Researchers' Conference – Materials Science and Engineering. 04-06.12.2019. Belgrad (Serbia).
- **E. Rekiel**, Biosurfaktanty w zastosowaniach medycznych. XII Ogólnokrajowa Konferencja Naukowa. Młodzi Naukowcy w Polsce - Badania i Rozwój. 16.11.2020, Lublin.
- **E. Rekiel**, Zastosowania biosurfaktantów drożdżowych. XIII Ogólnokrajowa Konferencja Naukowa. Młodzi Naukowcy w Polsce - Badania i Rozwój. 22.03.2021, Lublin (on-line).
- **E. Rekiel**, J. Krawczyk, A. Zdziennicka, Comparison of wettability of human skin and its equivalents by aqueous solutions of chosen surfactants. 9th European Young Engineers Conference. 19-21.04.2021, Warszawa (on-line).
- **E. Rekiel**, A. Zdziennicka, B. Jańczuk, Adsorpcja biosurfaktantów z wodno-etanolowych roztworów na granicy faz roztwór-powietrze. Fizykochemia granic faz – metody instrumentalne. 22-26 sierpnia 2021, Lublin.
- **E. Rekiel**, A. Zdziennicka, Biosurfactants as a way to protect the environment. 10th European Young Engineers Conference, 4-6.04.2022, Warszawa.
- **E. Rekiel**, A. Zdziennicka, B. Jańczuk. Adsorption of rhamnolipid and surfactin from mixed water-ethanol solvent. Summer School for PhD Students, 18-20.05.2022, Lublin.

POSTERY NAUKOWE

- **E. Rekiel**, A. Zdziennicka, B. Jańczuk, Biosurfactants and their aggregation properties. 17th European Student Colloids Conference. 18-22.06.2019, Warna (Bułgaria).
- **E. Rekiel**, A. Zdziennicka, B. Jańczuk, Wettability of model solids by chosen biosurfactants. 17th European Student Colloids Conference. 18-22.06.2019, Warna (Bułgaria).
- **E. Rekiel**, Skuteczność i efektywność adsorpcji wybranych surfaktantów na granicy faz ciecz-gaz. 62. Zjazd Naukowy Polskiego Towarzystwa Chemicznego. 2-6.09.2019, Warszawa.
- **E. Rekiel**, Zastosowanie soforolipidów w kosmetykach. XI Ogólnokrajowa Konferencja Naukowa. Młodzi Naukowcy w Polsce - Badania i Rozwój. 03.04.2020, Lublin.
- **E. Rekiel**, Soforolipidy – biosurfaktanty stosowane w kosmetykach. IISympozjum Biomateriały w medycynie i kosmetologii. 28.01.2021, Toruń (on-line).
- **E. Rekiel**, A. Zdziennicka, Adsorption of chosen surfactants at the liquid–gas interface. 9th European Young Engineers Conference. 19-21.04.2021, Warszawa (on-line).
- **E. Rekiel**, A. Zdziennicka, Biosurfaktanty w kosmetykach. Fizykochemia granic faz – metody instrumentalne. 22-26.08.2021, Lublin.
- **E. Rekiel**, A. Zdziennicka, Contact Angle Measurements as Method of Surface Analysis. 23rd International Conference-School Advanced Materials and Technologies. 23-27.08.2021, Połąga (Litwa), (on-line).
- **E. Rekiel**, A. Zdziennicka, B. Jańczuk, Wetting of solids by aqueous solutions of ethanol and rhamnolipid mixture. 35th Conference of the European Colloid & Interface Society. 5-10.09.2021, Ateny (Grecja).
- **E. Rekiel**, Natural ingredients in cosmetics – biosufactants. 10th European Young Engineers Conference, 4-6.04.2022, Warszawa.
- **E. Rekiel**, A. Zdziennicka, B. Jańczuk. Usefulness of contact angle measurements for determination of solid surface tension. Summer School for PhD Students, 18- 20.05.2022, Lublin.
- **E. Rekiel**, A. Zdziennicka, B. Jańczuk, Biosurfactants and wetting of chosen polymers. Polymers 2022 - New Trends in Polymer Science: Health of the Planet, Health of the People. 25-27.05.2022, Turyn (Włochy).
- **E. Rekiel**, A. Zdziennicka, B. Jańczuk, Characterization of solids wetting by aqueous solutions of ethanol and surfactin mixture. 4th International Conference on Materials: Advanced and Emerging Materials. 19-21.10.2022, Barcelona (Hiszpania).
- A. Zdziennicka, **E. Rekiel**, B. Jańczuk, K. Szymczyk. J. Krawczyk, Description and prediction of the contact angle of the TX165+biosurfactant mixtures at different solids. 23rd International Symposium on Surfactants in Solutions, 11-16.09.2022, Lublin.

- A. Zdziennicka, B. Jańczuk, **E. Rekiel**, J. Krawczyk, K. Szymczyk, Surface tension of the nonionic surfactant+biosurfactant mixtures. 23rd International Symposium on Surfactants in Solutions, 11-16.09.2022, Lublin.
- A. Zdziennicka, K. Szymczyk, B. Jańczuk, **E. Rekiel**, Influence of ethanol on the biosurfactants adsorption properties. 64 Zjazd Naukowy Polskiego Towarzystwa Chemicznego, 11-16.09.2022, Lublin.
- A. Zdziennicka, B. Jańczuk, K. Szymczyk, **E. Rekiel**, Adsorption and aggregation properties of the nonionic surfactant and biosurfactants mixtures. 64 Zjazd Naukowy Polskiego Towarzystwa Chemicznego, 11-16.09.2022, Lublin.

7.3. SZKOŁY LETNIE

W trakcie studiów doktoranckich uczestniczyłam w **trzech** szkołach letnich:

- Supramolecular and Colloid Chemistry and Physics for the Life Sciences, On-line Summer School and Workshop, 27-29.07.2020, Rijeka, Chorwacja;
- 23rd International Conference-School Advanced Materials and Technologies. 23-27.08.2021. On-line. Połąga, Litwa;
- Summer School for PhD Students, Międzynarodowa Szkoła Letnia, 18-20.05.2022, Lublin, Polska.

7.4. NAGRODY I WYRÓŻNIENIA

- Stypendium rektora dla doktorantów uzyskane w latach 2020/2021;
- Stypendium doktoranckie z dotacji podmiotowej na dofinansowanie zadań projakościowych w latach 2020/2021 i 2022/2023;
- Pierwsze miejsce za poster naukowy „Adsorption of chosen surfactants at the liquid-gas interface" podczas 9th European Young Engineers Conference. 19-21.04.2021, Warszawa (on-line);
- Nagroda Rektora Uniwersytetu Marii Curie-Skłodowskiej za uznanie dorobku naukowego na rzecz Uniwersytetu Marii Curie-Skłodowskiej w Lublinie za oryginalne i twórcze osiągnięcia naukowe udokumentowane cyklem artykułów opublikowanych w roku akademickim 2021/2022 z zakresu oddziaływań międzycząsteczkowych i termodynamiki procesu adsorpcji, agregacji i zwilżania układów wieloskładnikowych.

7.5. STAŻ NAUKOWY

W trakcie studiów doktoranckich odbyłam **półroczny naukowy staż zagraniczny na Universidad Extremadura** w Hiszpanii w ramach projektu „Międzynarodowe Studia Doktoranckie z Chemii" (nr projektu POWR.03.02.00-00-I005/16).

7.6. AKTYWNOŚĆ ORGANIZACYJNA I CZŁONKOSTWO NAUKOWE

- Członek Wydziałowej Komisji Socjalnej (2022/2023);
- Przedstawiciel doktorantów do Odwoławczej Komisji Dyscyplinarnej dla Doktorantów UMCS (2021/2022);
- Przedstawiciel doktorantów do Rady Wydziału Chemii UMCS (2018/2019);
- Członek Rady Uczelnianej Samorządu Doktorantów UMCS (2018/2019, 2019/2020, 2020/2021, 2021/2022);
- Członek Rady Wydziałowej Samorządu Doktorantów Wydziału Chemii UMCS (2018/2019, 2019/2020, 2020/2021);
- Wiceprzewodnicząca Wydziałowej Rady Samorządu Doktorantów Wydziału Chemii UMCS (2021/2022);
- Członek Polskiego Towarzystwa Chemicznego (2019 – do chwili obecnej);
- Członek Koła Naukowego Alkahest (2018/2019, 2019/2020, 2020/2021).

8. ZAŁĄCZNIKI

Załącznik 1

[D1] E. Rekiel, A. Zdziennicka*, K. Szymczyk, B. Jańczuk, *Thermodynamic Analysis of the Adsorption and Micellization Activity of the Mixtures of Rhamnolipid and Surfactin with Triton X-165*. ***Molecules***, 2022, 27, 3600.

Article

Thermodynamic Analysis of the Adsorption and Micellization Activity of the Mixtures of Rhamnolipid and Surfactin with Triton X-165

Edyta Rekiel, Anna Zdziennicka *, Katarzyna Szymczyk and Bronisław Jańczuk

Department of Interfacial Phenomena, Faculty of Chemistry, Institute of Chemical Sciences,
Maria Curie-Skłodowska University in Lublin, 20-031 Lublin, Poland; edyta.rekiel@poczta.umcs.lublin.pl (E.R.);
katarzyna.szymczyk@mail.umcs.pl (K.S.); bronislaw.janczuk@poczta.umcs.lublin.pl (B.J.)
* Correspondence: anna.zdziennicka@mail.umcs.pl; Tel.: +48-(81)-537-56-70

Abstract: The surface tension of aqueous solutions of Triton X-165 with rhamnolipid or surfactin mixtures was measured. The obtained results were applied for the determination of the concentration and composition of the Triton X-165 and biosurfactants mixture at the water–air interface as well as the contribution of the particular component of the mixtures to water surface tension reduction and the mutual influence of these components on the critical micelle concentration. The determination of these quantities was based on both the commonly used concepts and a new one proposed by us, which assumes that the composition of the mixed monolayer at the water–air interface depends directly on the pressure of the monolayer of the single mixture component and allows us to determine the surface concentration of each mixture component independently of surface tension isotherms shape. Taking into account the composition of the mixed monolayer at the water–air interface, the standard Gibbs adsorption free energy was considered. The obtained results allow us to state that the concentration of both mixture components corresponding to their saturated monolayer and the surface tension of their aqueous solution can be predicted using the surfactants' single monolayer pressure and their mole fraction in the mixed monolayer determined in the proposed way.

Keywords: biosurfactants; rhamnolipid; surfactin; adsorption; micellization; standard Gibbs free energy; standard Gibbs free energy of micellization

1. Introduction

Biosurfactants are characterized by very good interfacial and aggregation properties as well as their biodegradability [1–5]. This promotes their application, among other things, in crude oil recovery [6,7], in the pharmaceutical industry [8], or in natural environment bioremediation [9]. Moreover, they are found in medical [10–12] and household products [10]. In numerous practical applications, the surface tension of the aqueous solution of biosurfactants or their mixtures with classical synthetic surfactants plays a very important role. The proper surface tension value of the aqueous solution required for a given practical application can be obtained at a considerably smaller concentration of biosurfactants than in the case of synthetic surfactants. However, due to the biosurfactants' production costs, their individual practical applications are confined. Therefore, the mixtures of biosurfactants with classical synthetic surfactants are more and more often used in practice [13–16]. From practical and theoretical points of view, it is important to establish the composition and concentration of a biosurfactant and a classical surfactant in the aqueous solution required to achieve the proper surface tension values of this solution on the basis of the surface tension isotherm of the aqueous solution of the mixture components. In practice, it is particularly essential to determine the value of the surface tension of the solution at which the process of the surfactants' aggregation takes place. This problem can be solved to a much greater extent in the case of the mixture of synthetic surfactants than those of

biosurfactants and classical surfactants. To predict the isotherms of the surface tension of the aqueous solution of the biosurfactants and classical surfactant mixture, and thus the required value of the solution surface tension, the relationship between the surface tension isotherm of the aqueous solution of particular components of the mixture and the mixture itself should be known. To study this issue, rhamnolipid (RL), surfactin (SF), and Triton X-165 (TX165) were chosen.

The RL and SF are the most prominent representatives of biosurfactants. Rhamnolipid is produced by *Pseudomonas aeruginosa* [17–19]. In turn, surfactin is produced mainly by *Bacillus subtilis* [8,20,21]. RL reduces the water surface tension due to its adsorption at the water–air interface to a minimal value, even lower than that obtained for the nonionic synthetic surfactants such as Triton [22,23]. The maximal reduction in the water surface tension by SF adsorption at the water–air interface is similar to that of Triton X-100 [22,23]. The critical micelle concentration of RL and SF (CMC) is about two orders of magnitude smaller than that of classical surfactants [22,24]. Biosurfactants can positively affect the adsorption and aggregation properties of classic surfactants. For this reason, the literature reports some studies on the adsorption and aggregation behavior of biosurfactant mixtures with different kinds of synthetic surfactants [16,25,26]. Mostly, they deal with the possible occurrence of synergy in the water surface tension reduction and in the aggregation process. As for the synergistic effects, some surface tension isotherms of the biosurfactant and classic surfactant mixtures, in the concentration range of mixtures of a given composition up to CMC with the linear dependence between the surface tension (γ_{LV}) and the logarithm of the concentration (C), are taken into account [27]. On the other hand, it is difficult to find in the literature isotherms of γ_{LV} of the aqueous solutions of biosurfactant and classic surfactant mixtures in the concentration range at which both the unsaturated and saturated mixed monolayers are formed at the water–air interface. Moreover, the literature lacks a description and/or prediction of the isotherms of the surface tension of the biosurfactants and classical surfactant mixtures as well as the data about the composition of the mixed monolayer at the water–air interface. It should also be mentioned that the analysis of the surface tension of the isotherms of the surfactant mixture based on the isotherm of its particular components only at the constant composition of the mixture, which is mainly investigated, provides a complete explanation of the mixture surface behavior. Therefore, the aim of the study was to measure γ_{LV} of the aqueous solution of the biosurfactant and nonionic classical surfactant mixtures, both at the changing concentration of the mixtures at their constant composition and the constant concentration of one component of the mixture and the variable of the other one. The measurements of γ_{LV} were made in a wide range of composition and concentration. Moreover, the obtained γ_{LV} isotherms were analyzed regarding their possible description and/or prediction to determine the composition of the mixed monolayer at the water–air interface and to find a possible existence of the synergetic effect in the water surface tension and in the CMC reduction. Thus, the mixtures of RL with TX165 and SF with TX165 were applied. The chosen biosurfactants are anionic, including, among others, the –COOH group in their molecules. However, the TX165 molecules contain oxyethylene groups. Under some conditions, the hydrogen ions can be joined with the oxyethylene group and TX165 can behave as the cationic surfactant [27]. Thus, the attractive electrostatic interactions between the RL or SF and TX165 molecules, apart from the formation of hydrogen bonds between them, are possible.

2. Results and Discussion

2.1. Comparison of Some Physicochemical Properties of Solution Components

Surfactants and biosurfactants differ from other substances because of their tendency toward adsorption at different interfaces and their ability to aggregate in a largely polar liquid environment such as water. The adsorption and aggregation properties of surfactants and biosurfactants depend on the type and amount of various chemical groups present in the hydrophobic and hydrophilic parts of their molecules, the size of the molecules, and the presence of an electric charge, as well as the parameters and components of the surface

tension. Similar to RL and SF, chosen by us for studies on the adsorption and aggregation properties of their mixtures with the nonionic TX165 surfactant, the ionic biosurfactants have much better adsorption and aggregation properties than the synthetic surfactants. They reduce the water surface tension to a given value at a concentration considerably smaller than that of TX165 (Figure 1) [22,23]. For example, the reduction in water surface tension to a value equal to 55 mN/m takes place at a TX165 concentration 8.5 times greater than that of RL and 69.8 greater than that of SF (Figure 1). In the case of the critical micelle concentration (CMC) (Table 1) [22,24], the ratio of the TX165 CMC value to RL and SF as well as the CMC of RL to SF is equal to 10.4, 56, and 5.4, respectively.
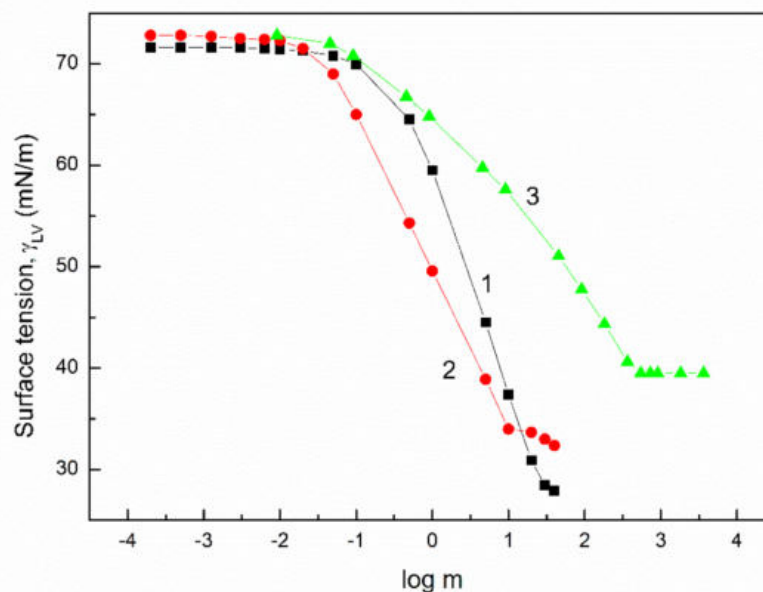
Figure 1. A plot of the surface tension (γ_{LV}) of the aqueous solution of RL (curve 1), SF (curve 2), and TX165 (curve 3) vs. the logarithm from the surfactant weight in mg/dm^3 (m).

What can be the reason for such a large difference between the TX165 and biosurfactants concentration needed to reduce the water surface tension to a given value and between the CMC values? The TX165, RL, and SF tendency to adsorb at the water–air interface is similar because the standard Gibbs free energy of their adsorption calculated from the Langmuir equation modified by de Boer is comparable (Table 1) [22,23]. This indicates that the transition of one TX165, RL, and SF molecule from the bulk phase of the solution to the water–air interface causes similar changes in the Gibbs free energy of the solution. These changes result from the hydration degree of hydrophobic and hydrophilic parts of the biosurfactants and surfactant molecules.

The number of water molecules in direct contact can be approximately established based on the water, biosurfactant, and surfactant contactable area. The minimal contactable area of the water molecule at 293 K is equal to 10 Å^2. The contactable area of the TX165, RL, and SF molecules can be approximately established based on the length of the chemical bonds between the individual atoms in the molecule, the angle between these bonds, as well as the average distance between the biosurfactant, surfactant, and other molecules. It appears that the volume of the surfactant molecule in the aqueous environment can be determined based on the cube in which the surfactant molecule is inscribed, or the sum of the cubes in which the individual parts of the surfactant are inscribed. The volumes of the TX165, RL, and SF moles determined in this way are close to their partial molar volume [24,28] (Table 1). Thus, it was possible to establish the contactable area of TX165, RL, and SF molecules (Table 1). Taking into account the contactable area of the hydrophobic part of these compounds and water, it can be stated that about 36, 30, and 34 water molecules can be contacted directly with the hydrophobic parts of the TX165, RL, and SF

molecules, respectively. As the hydration of the hydrophobic parts of the surfactants exerts the main influence on the standard Gibbs free energy of adsorption, their values for the studied compounds are close. This fact does not account for the difference in the water surface tension reduction by TX165, RL, and SF adsorption at the water–air interface. It is commonly known that the water surface tension results from the Lifshitz–van der Waals and acid–base intermolecular interactions.

Table 1. The different physicochemical properties of water, RL, SF, and TX165.

Properties	Water	TX165	Rhamnolipid	Surfactin
M [g]	18.016	911.000	504.000	1036.340
$V_{molecule}$ [Å^3] *	29.885	1581.170	779.400	1460.440 1739.006 1562.950
V_{mole} [cm^3] *	17.999	952.339	469.433	879.623 1047.403 941.365
$S_{contactable}$ [Å^2] *	58.43	1411.58 363.29	586.59 304.08	1389.02 346.10
γ_{LV}^{min} [mN/m]	–	39.50	27.89	32.37
Γ^{max} [mol/m^2]	–	2.12×10^{-6}	2.01×10^{-6}	1.38×10^{-6}
Γ^{∞} [mol/m^2]	16.600×10^{-6}	4.650×10^{-6}	2.403×10^{-6}	1.782×10^{-6}
$\frac{\Gamma^{max}}{\Gamma^{\infty}}$ *	–	0.4559	0.8365	0.7744
A^{min} [Å^2]	–	78.32	82.60	93.17 120.24
A^0 [Å^2]	10.00	35.70	69.09	93.17
C_{min}^{sat} [M]	–	5.00×10^{-5}	1.98×10^{-6}	9.65×10^{-8}
CMC [M]	–	5.41×10^{-4}	5.21×10^{-5}	9.66×10^{-6}
ΔG_{ads}^0 [kJ/mol] *	–	−44.00	−43.55	−46.22 −51.23
ΔG_{mic}^0 [kJ/mol] *	–	−28.10	−33.80	−37.90
γ_{LV} of tail [mN/m]	72.80	22.00	21.80	24.70
γ_{LV} of head [mN/m]	72.80	35.84	38.39	42.80
γ^{LW} of head [mN/m]	26.85	27.70	35.38	34.25
γ^{AB} of head [mN/m]	45.95	8.14	3.01	8.55
γ^{+} of head [mN/m]	22.975	0.33	0.04	0.37
γ^{-} of head [mN/m]	22.975	50.20	56.74	49.39

* $V_{molecule}$, V_{mole}, $S_{contactable}$, $\frac{\Gamma^{max}}{\Gamma^{\infty}}$, ΔG_{ads}^0, and ΔG_{mic}^0 were calculated. The other parameters were taken from the literature [22–24].

The acid–base intermolecular interactions are associated with hydrogen bonds. According to the van Oss and Constanzo concept [29], the surface tension of biosurfactants and surfactants depends on the orientation of their molecules towards the air phase. This leads to the concept of the head and tail of surfactant surface tension. The surface tension of the tail of TX165, RL, and SF results from the Lifshitz–van der Waals intermolecular interactions and its value is smaller than that of the Lifshitz–van der Waals component of the water surface tension (Table 1) [30–32]. However, the differences between the values of the Lifshitz–van der Waals component for TX165, RL, and SF surface tension are not great for justifying the differences in the water surface tension reduction (Table 1, Figure 1). The difference is found particularly in the concentration range corresponding to that of

the saturated monolayer at the water–air interface (Table 1). It can be assumed that the molecules of surface-active compounds are oriented perpendicular to the water–air interface, and the hydrophobic parts are in the air phase in the saturated monolayer. In such a case, the limiting area occupied by one TX165 molecule is about two times smaller than that of RL and 3.4 times smaller than that of the SF molecule. One TX165 molecule can replace 3.5 molecules of water, seven for RL, and for SF as many as 12 molecules of water at the water–air interface can be replaced. This indicates that at the same concentration of TX165, RL and SF in the monolayer, the ratio of the water–air interface covered by these compounds increases from TX165 to SF. This fact may be one of the reasons for the increase in the degree of surface tension reduction by adsorbing the TX165, RL and SF molecules in the order from TX165 to SF. However, the maximal Gibbs surface excess concentration decreases in the order from TX165 to SF (Table 1) [22,23]. In fact, the maximum fraction of the interface area occupied by the RL molecules is almost twice as large as that of TX165 but the fraction of the area occupied by the SF molecules is slightly smaller than that of RL (Table 1). Taking into account the Lifshitz–van der Waals component (LW) of the water surface tension and the tail of TX165, RL and SF surface tension, it can be stated that the LW component of the water surface tension can change theoretically as a function of TX165, RL, and SF concentration from 26.85 to 22.00 mN/m, from 26.85 to 21.80 mN/m, and from 26.85 to 24.70 mN/m, respectively (Table 1) [24–26]. On the other hand, the acid–base component of the water surface tension can be changed from 45.95 mN/m to zero as a function of their concentrations. It should be mentioned that the LW component of the TX165, RL, and SF head surface tension is greater than for water. The minimal surface tension of the aqueous solution of TX165, RL, and SF is higher than that of their tail (Table 1) [30–32]. This indicates that the hydrogen bonds between the water molecules are not completely reduced by the TX165, RL, and SF adsorption at the water–air interface. It seems also that the ability to reduce the acid–base component of the water surface tension is the main reason for the differences in the surface activity of TX165, RL, and SF. A great difference in the kind and amount of the polar and apolar groups in the hydrophilic parts of the TX165, RL, and SF molecules can be observed.

In the case of the aggregation properties of TX165, RL, and SF, the ability to form aggregates in the aqueous solution increases from TX165 to SF. This is in accordance with the changes in the standard Gibbs free energy of their micellization (Table 1) [16,24–28].

2.2. Surface Tension of TX165 Mixtures with Rhamnolipid and Surfactin

The surface tension of the aqueous solution of the TX165 with RL and TX165 with SF mixtures (γ_{LV}) was considered at both the constant concentration of biosurfactants, the changing TX165 concentration and vice versa (Figures 2–5), and the constant composition of the mixture as a function of its concentration (Figures 6 and 7). However, the concentration of the TX165 + biosurfactant mixtures changed depending on the mixture composition. In other words, the biosurfactant concentration was the same in different compositions of the mixture with TX165. The concentration of TX165 was relative to that of the biosurfactant concentration but different for each mixture composition. The TX165 concentration was selected so as to obtain mixtures with biosurfactant mole fractions equal to 0.2, 0.4, 0.6, and 0.8. Additionally, the surface tension of the TX165 with the biosurfactant mixture, in which the concentration of the particular component was the same as in the solutions of single compounds, was measured [22,24] (Figures 6 and 7).

The shape of the γ_{LV} isotherms of the aqueous solution of the TX165 mixtures with the biosurfactants at their constant concentration in the range from zero to that at which the saturated monolayer of biosurfactants is formed (C_{min}^{sat}) (Table 1) [22] in the absence of TX165 is similar to that of the aqueous solution of single TX165. However, above C_{min}^{sat}, some maxima on the isotherms of surface tension are observed (Figures 2 and 4). These maxima are more and more visible with the increasing values of the constant biosurfactant concentration. In the case of the surface tension isotherms of the aqueous solution of TX165 mixtures with the biosurfactants at a constant TX165 concentration (Figures 3 and 5), the

same relations as at the constant biosurfactant concentration are observed. At a constant TX165 concentration smaller than C_{min}^{sat}, the shape of the γ_{LV} isotherms are similar to that for the single biosurfactants. Above the C_{min}^{sat} of TX165, some maxima on the γ_{LV} isotherms can be seen. They do not indicate a decrease in the TX165 adsorption from its mixture with biosurfactants in the concentration range from zero to that corresponding to the maximal value of γ_{LV}. This may result from the great difference as regards the adsorption activity of TX165 and the biosurfactants.
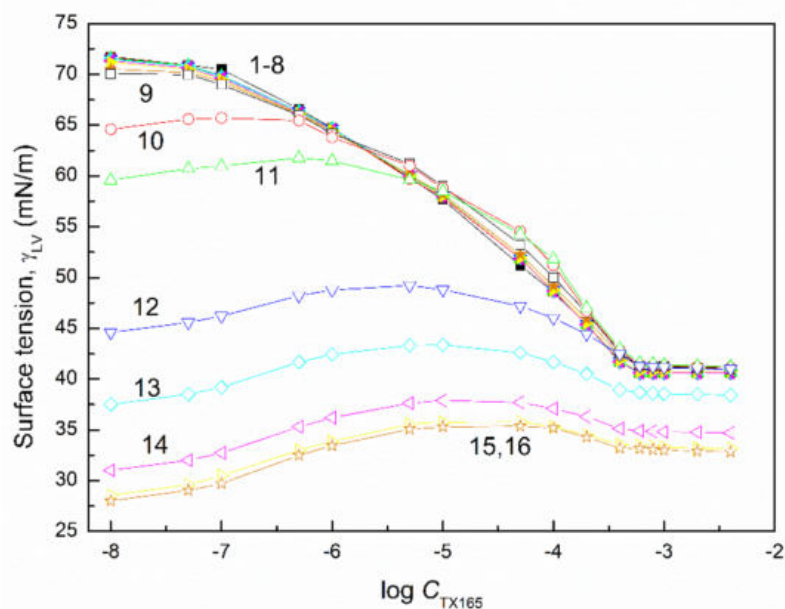
Figure 2. A plot of the surface tension (γ_{LV}) of the aqueous solution of the RL and TX165 mixture vs. the logarithm of the TX165 concentration (C_{TX165}). Curves 1−16 correspond to the constant RL concentration equal to 0.0002, 0.0005, 0.00125, 0.003, 0.00625, 0.01, 0.02, 0.05, 0.1, 0.5, 1, 5, 10, 20, 30, and 40 mg/dm^3, respectively.
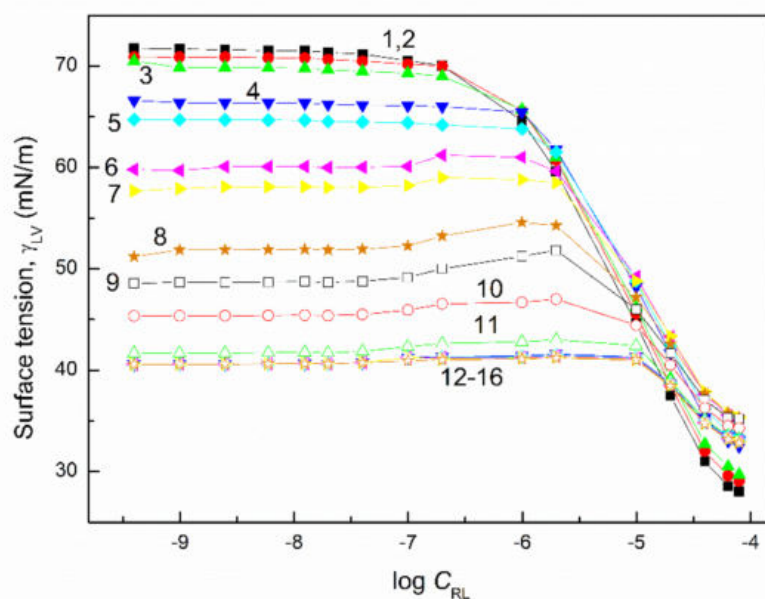
Figure 3. A plot of the surface tension (γ_{LV}) of the aqueous solution of the RL and TX165 mixture vs. the logarithm of the RL concentration (C_{RL}). Curves 1−16 correspond to the constant TX165 concentration equal to 1×10^{-8}, 5×10^{-8}, 1×10^{-7}, 5×10^{-7}, 1×10^{-6}, 5×10^{-6}, 1×10^{-5}, 5×10^{-5}, 1×10^{-4}, 2×10^{-4}, 4×10^{-4}, 6×10^{-4}, 8×10^{-4}, 0.001, 0.002, and 0.004 mole/dm^3, respectively.
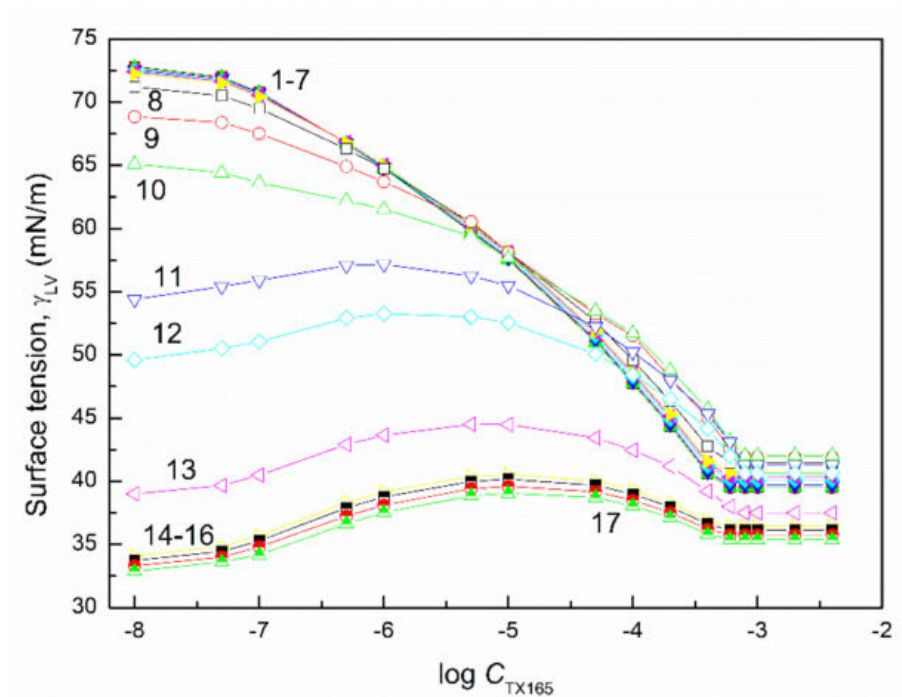
Figure 4. A plot of the surface tension (γ_{LV}) of the aqueous solution of the SF and TX165 mixture vs. the logarithm of the TX165 concentration (C_{TX165}). Curves 1−16 correspond to the constant SF concentration equal to 0.0002, 0.0005, 0.00125, 0.003, 0.00625, 0.01, 0.02, 0.05, 0.1, 0.5, 1, 5, 10, 20, 30, and 40 mg/dm^3, respectively.
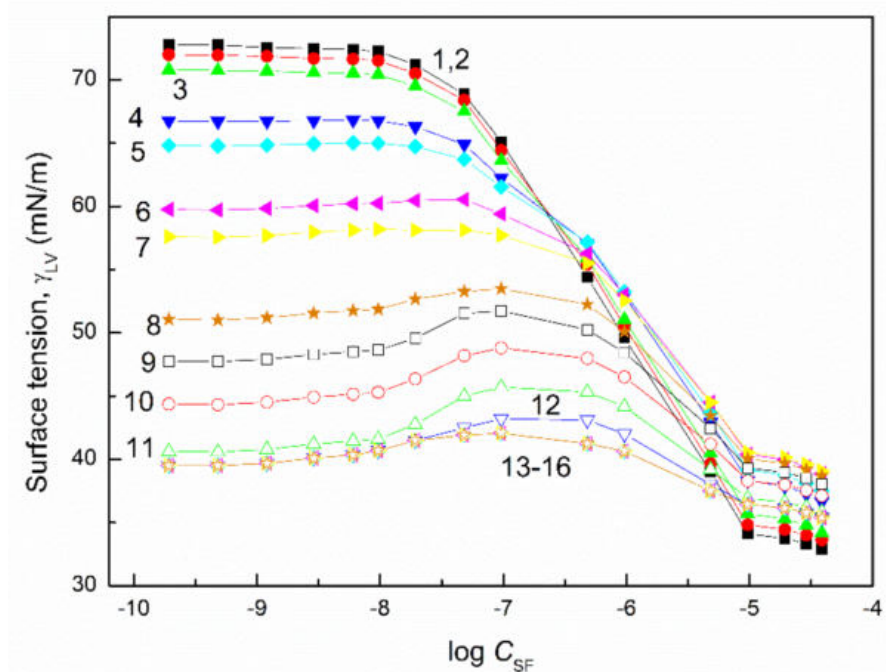
Figure 5. A plot of the surface tension (γ_{LV}) of the aqueous solution of the SF and TX165 mixture vs. the logarithm of the SF concentration (C_{SF}). Curves 1−16 correspond to the constant TX165 concentration equal to 1×10^{-8}, 5×10^{-8}, 1×10^{-7}, 5×10^{-7}, 1×10^{-6}, 5×10^{-6}, 1×10^{-5}, 5×10^{-5}, 1×10^{-4}, 2×10^{-4}, 4×10^{-4}, 6×10^{-4}, 8×10^{-4}, 0.001, 0.002, and 0.004 mole/dm^3, respectively.
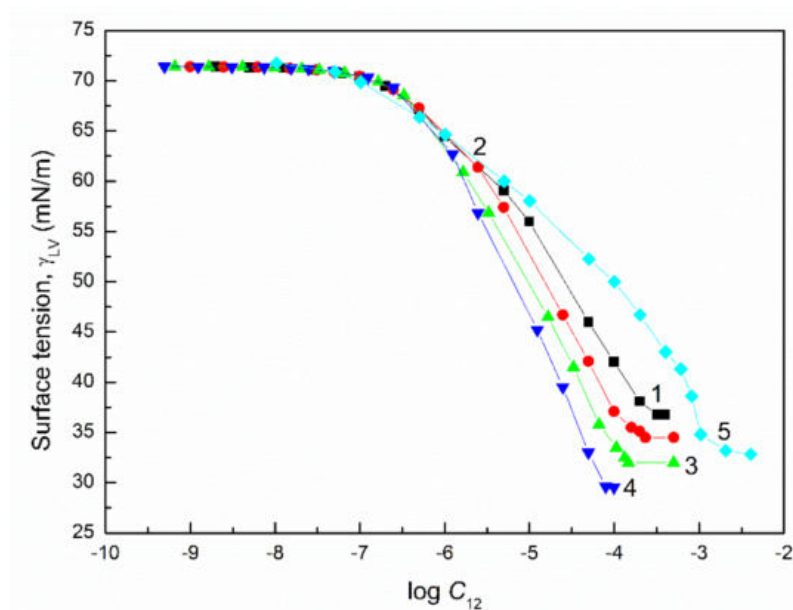
Figure 6. A plot of the surface tension (γ_{LV}) of the aqueous solution of the RL and TX165 mixture vs. the logarithm of its concentration (C_{12}). Curves 1−4 correspond to the RL mole fractions in the mixture equal to 0.2, 0.4, 0.6, and 0.8, respectively. Curve 5 corresponds to the sum of the RL and TX165 concentrations, where the TX165 concentration changed from 0 to 0.004 mole/dm^3 and the RL concentration changed from 3.97×10^{-10} to 7.94×10^{-5} mole/dm^3, as applied in the literature [22,24] for their aqueous solution surface tension measurements.
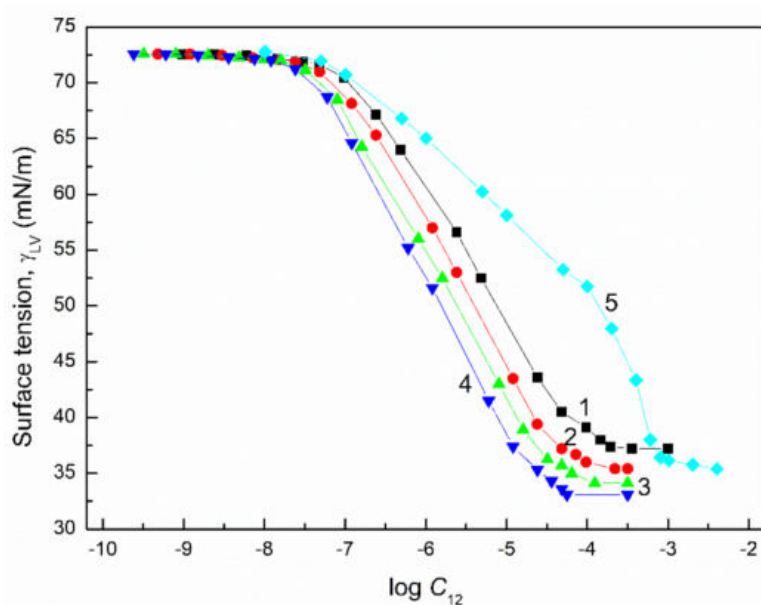
Figure 7. A plot of the surface tension (γ_{LV}) of the aqueous solution of the SF and TX165 mixture vs. the logarithm of its concentrations (C_{12}). Curves 1−4 correspond to the SF mole fractions in the mixture equal to 0.2, 0.4, 0.6, and 0.8, respectively. Curve 5 corresponds to the sum of the SF and TX165 concentrations, where the TX165 concentrations changed from 0 to 0.004 mole/dm^3 and the SF concentration changed from 1.93×10^{-10} to 3.86×10^{-5} mole/dm^3, as applied in the literature [22,24] for their aqueous solution surface tension measurements.

In the case of the aqueous solutions at the constant composition of TX165 mixtures with biosurfactants, the shape of γ_{LV} isotherms are rather similar to those of the aqueous solutions of biosurfactants compared to that of the TX165 solution (Figures 6 and 7). This likely results from the fact that at the comparable concentration of biosurfactants and TX165,

as a result of the higher adsorption activity of biosurfactants than that of TX165, there is a greater effect on the shape of the mixture solution isotherms compared to TX165.

It is very important to describe and/or predict the isotherm of γ_{LV} for a more detailed consideration of the adsorption behavior and properties of the mixed monolayer at the water–air interface. It appears that the isotherms of the surface tension of the aqueous solution of the TX165 mixture with the biosurfactants can be described by the exponential function of the second order. However, in the case of the isotherms on which the maxima of γ_{LV} were observed, it was impossible to describe the isotherms of the surface tension by one exponential function of the second order in the whole mixture concentration range (Figures 2–5). In the case of the aqueous solution of TX165 mixtures with RL and/or SF in which the concentration of one mixture component was constant, the γ_{LV} isotherms were described by the exponential function of the second order obtained, taking into account both the changing concentration of one component of the mixture and the summed concentration of the two components of the mixture (Figures S1–S12). It appears that the values of the surface tension of the aqueous solution of the TX165 with RL or SF mixtures, determined by the exponential function of the second order, in the case in which only the changing concentration of one component of the mixture is taken into account, are closer to those measured than in the case when the total concentration of the mixture is applied. The description of the γ_{LV} isotherms with the maxima by the second-order exponential function is more complicated than in the case of the isotherms without the maxima. These isotherms can be described only by two different second-order exponential functions (Figures S2, S3, S5, S6, S8, S9, S11, S12).

The equation of the exponential function of the second order which includes y_0, A_1, A_2, t_1, and t_2 constants has the form:

$$\gamma_{LV} = y_0 + A_1 \exp\left(\frac{-C}{t_1}\right) + A_2 \exp\left(\frac{-C}{t_2}\right) \tag{1}$$

where C is the concentration of the surfactant or mixture of surfactants.

It was stated that the standard Gibbs free energy of surfactants depends on the surface tension of tails and tail–water interface tension [30–32]. Therefore, it seems that the constants in Equation (1) are associated with the components and parameters of water as well as the tail and head of the surfactants' surface tension. The analysis of the constants in Equation (1) for the aqueous solutions of TX165 and biosurfactant mixture in which the concentration of one component of the mixture is constant and that of the other one is variable is difficult. For these solutions, the concentration and composition of the mixture change. Therefore, the constants in Equation (1) are considered only for the aqueous solution of TX165 with the biosurfactant mixtures at the constant composition and variable concentration (Figures S13–S17). For both the TX165 with RL and TX165 with SF mixtures, the constant y_0 decreases as a function of the mole fraction of biosurfactant in the mixture in the bulk phase. In the case of the TX165 + SF mixture, the relationship between y_0 and the mole fraction of the biosurfactant is almost linear (Figure S13). It seems that this constant is related to the Lifshitz–van der Waals component of the tail of the surfactant's surface tension and water–tail interface tension. The Lifshitz–van der Waals interactions are directly associated with the minimal surface tension value of the surfactants and their mixture's aqueous solution. The y_0 values are close to those of the minimal surface tension of the aqueous solution of the TX165 + RL and TX165 + SF mixtures Figures 6,7 and S13). The other constants in Equation (1) may result from the acid–base components of the surfactants' head surface tension and the electrostatic interactions. The changes of A_1, A_2, t_1, and t_2 as a function of the composition of the TX165 + RL and TX165 + SF mixtures are not linear. Some maxima and minima are observed (Figures S14–S17). However, so far, it has been difficult to express the constants in Equation (1) as a function of some properties of surfactants and biosurfactants.

The isotherms of the γ_{LV} of the aqueous solution of many surfactants are often described by the Szyszkowski equation [27]. However, in the case of the aqueous solu-

tion of surfactant mixtures, fewer attempts to describe the γ_{LV} of these solutions by the Szyszkowski equation are reported in the literature [33]. It is commonly known that γ_{LV} in the Szyszkowski equation depends on the maximal Gibbs surface excess concentration (Γ^{max}), the concentration of surfactants in the bulk phase (C), and the standard Gibbs free energy of adsorption (ΔG^0_{ads}), which is represented by the constant a in this equation. The Szyszkowski equation can be expressed as [27]:

$$\gamma_0 - \gamma_{LV} = RT \ln \Gamma^{max} \ln\left(\frac{C}{a} + 1\right) \tag{2}$$

where γ_0 is the solvent surface tension and n is the parameter used in the Gibbs isotherm equation for the determination of the surface excess concentration of the given surfactants and the mixture of surfactants.

The value of n for the chosen biosurfactants is equal to 2 because they are the 1: 1 type of electrolyte. For TX165 with biosurfactant mixtures, n changes from 1 to 2 as a function of the mixture's composition. The use of the Szyszkowski equation for the calculation of the surface tension of the aqueous solutions of mixtures of non-ionic surfactants with the biosurfactants examined by us is not easy. Firstly, in the case of a series of the aqueous solutions of TX165 mixtures with biosurfactants, in which the concentration of one of the components is constant and the other changes, it is difficult to determine the concentration range of the mixture in which its components are in the monomeric form in the bulk phase. The surface-active substance only in the monomeric form influences the amount of adsorption, which is connected with the water surface tension reduction [27]. This fact is not often taken into account. Thus, it is not possible to describe the surface tension isotherm by the Szyszkowski equation in the whole concentration range of a given surfactant. Secondly, the problem is to establish the γ_0 value for a series of aqueous solutions of TX165 mixtures with RL or SF if the concentration of one component is constant and that of the other one changes. There are two possibilities. One is to take γ_0 as the surface tension of the water and the other is to use γ_0 as the value of the surface tension of the aqueous solution of the single component at its concentration being constant in the aqueous solution of the binary mixture. When solving the Szyszkowski equation in relation to the surface tension of the binary mixture solution at the constant concentration of one of the components, the third problem is what concentration should be used in this equation for calculations—the total or only that of the component with a varying concentration.

It appeared that the best agreement between the values of the surface tension of the TX165 aqueous solutions with the RL and SF mixture calculated from Equation (2) and those measured is obtained if the value of the surface tension of the mixture component at the constant concentration and the values of the variable concentrations of the other mixture component are applied in this equation (Figures S1, S4 and S7). Unfortunately, the γ_{LV} isotherms for the aqueous solution of the TX165 + RL and TX165 + SF mixtures at the constant concentration of one component and variable of the other can be described by Equation (2) if the constant concentration values are smaller than C^{sat}_{min}.

On the other hand, it was possible to describe all γ_{LV} isotherms for the aqueous solutions of the studied binary mixtures of surface-active compounds with the constant composition and the variable concentration (Figures S18–S25). Analyzing the $n\Gamma^{max}$ and a values used for the calculation of the surface tension of the aqueous solution of the binary mixtures of TX165 with the biosurfactants, it can be concluded that the $n\Gamma^{max}$ values change almost linearly with the mixture composition. Moreover, in the case of the a value, a negative deviation from the linear dependence on the mixture composition is observed (Figure S26). It can be stated that using the Szyszkowski equation [27], it is possible not only to describe but also to predict the γ_{LV} isotherms based on the data of the particular component of the surfactant mixtures if the relationship between these data and the mixture composition is known.

From the theoretical and practical points of view, it is more important to predict the surface tension of the aqueous solution of surfactant mixtures than only to describe it.

Among the concepts which can be used for the prediction of γ_{LV} values for the aqueous solutions of surfactant mixtures, the one proposed by Fainerman and Miller seems to be very useful [34,35]. However, while using the Fainerman and Miller concept for the determination of the surface tension of the aqueous solution of surfactant mixtures, the main problem is to establish the values of the area occupied by the mole of each component of the mixture as well as some average values for surfactant mixtures (ω). The ω of the surfactants and their mixtures is equal to $\frac{1}{\Gamma^\infty}$, where Γ^∞ is the limiting concentration of a given component of the surfactant mixtures or mixture in the monolayer at the water–air interface. Γ^∞ is equal to $\frac{1}{NA_0}$, where N is the Avogadro number and A_0 is the limiting area occupied by one surfactant molecule. Assuming that the surfactant molecules at their limiting concentration in the monolayer at the water–air interface are oriented perpendicular to the interface, the A_0 value can be determined based on the bond length between the atoms in the surfactant molecule, the angle between the bonds, and the average allowed distance. The values of A_0 for TX165, RL and SF calculated in this way are close to 35.70, 69.09, and 93.17 Å^2, respectively [22,23]. Knowing the A_0 value of a given surfactant in the mixture, it is easy to calculate its ω value. However, the main problem is calculating the ω values for the surfactant mixtures. If the A_0 values of particular components of the mixture are the same or close, the determination of ω for the surfactant mixtures is easy. However, in our case, there are great differences between the A_0 values of TX165, RL, and SF. It seems reasonable to assume that the Γ^∞_{12} of the TX165 mixtures with RL or SF is equal to $\Gamma^\infty_1 x^S_1 + \Gamma^\infty_2 x^S_2$ where x^S is the mole fraction of the particular surfactants in the mixture and 1, 2, and 12 refer to TX165, the biosurfactant, and the mixture of TX165 with the biosurfactant, respectively. As was stated earlier [33], $x^S_1 = \frac{\pi_1}{\pi_1 + \pi_2}$ and $x^S_2 = \frac{\pi_2}{\pi_1 + \pi_2}$ (π_1 and π_2 are the layers surfactants 1 and 2 pressure, respectively). Taking into account the Γ^∞_{12} values determined in this way, the ω values for the TX165 + RL and TX165 + SF mixtures at a given concentration and composition were deduced. Knowing the ω values for the mixtures and particular components, the surface tension of the aqueous solution of TX165 mixtures with RL and SF was calculated from the Fainerman and Miller equation, which for the binary mixtures has the form [27,28]:

$$\exp\prod = \exp\prod_1 + \exp\prod_2 - 1 \tag{3}$$

where $\prod = \pi\omega/RT$, $\prod_1 = \pi_1\omega_1/RT$ and $\prod_2 = \pi_2\omega_2/RT$ (R is the gas constant and T is the temperature).

It appeared that based on Equation (3) it was possible to predict the surface tension for the aqueous solution of the TX165 mixture with RL or SF if the constant concentration of one component of the mixture was smaller than its C^{sat}_{min} in the whole variable concentration of the other mixture component (Figures S1, S4, S7 and S10). For the aqueous solution of the TX165 and biosurfactant mixture at the concentration of both mixture components higher than their C^{sat}_{min}, the agreement between the measured and calculated (from Equation (3)) values of surface tension is observed only at some mixture concentrations (Figures S3, S6, S9 and S12). In the case of the TX165 mixtures with biosurfactants at a constant composition, the agreement between the values of the measured and calculated (from Equation (3)) surface tension is not observed in the whole range of mixture concentrations. It is possible that due to the stronger interactions between the TX165 molecules and the biosurfactant compared to that between the molecules of the same compound, the surface area occupied by a mole of the mixture is different from that calculated. Such a conclusion is based on the fact that with the hydrophilic part of the TX165, the H$_3$O$^+$ ions can be joined by the hydrogen bonds and the nonionic surfactant can be treated as the cationic one [27]. Therefore the electrostatic interactions can take place between TX165 and the biosurfactants. It seems, however, that despite the strong interactions between the TX165 molecules and those of biosurfactants, the mole fraction of the mixture components in the mixed monolayer at the water–air interface does not differ much from that calculated based on the monolayer pressure of individual compounds. This conclusion confirms the

surface tension isotherms of the aqueous solution of TX165 mixtures with the biosurfactants determined from the following expression [33]:

$$\gamma_{LV} = \gamma_{LV}^1 x_1^S + \gamma_{LV}^2 x_2^S \tag{4}$$

It appeared that for the most studied aqueous solutions of the binary mixtures, the surface tension can be predicted from Equation (4) (Figures S1–S12, S18–S25). The values of γ_{LV} calculated from Equation (4) confirmed that maxima on the γ_{LV} isotherms are possible.

2.3. Concentration and Composition of the Mixed Monolayer

Based on the γ_{LV} isotherms of the aqueous solution of the single surfactants and their mixtures, it is possible to determine the surface concentration of a given surfactant or biosurfactant in both the individual and mixed monolayers at the water–air interface. For this purpose, the Gibbs isotherm equation is most often used for both the aqueous solution of individual surfactants and their mixture, in which the concentration of one component is variable but that of the other is constant, or for the mixtures at a constant composition and variable total concentration.

The Gibbs equation for the aqueous solution of multi-component surfactant mixtures has the form [27]:

$$\Gamma = -\frac{a_i}{nRT}\left(\frac{\partial \gamma_{LV}}{\partial a_i}\right)_{i\neq j,T} = -\frac{C_i}{nRT}\left(\frac{\partial \gamma_{LV}}{\partial C_i}\right)_{i\neq j,T} = -\frac{1}{2.303nRT}\left(\frac{\partial \gamma_{LV}}{\partial \log C_i}\right)_{i\neq j,T} \tag{5}$$

Using Equation (5) for the calculation of the surfactant concentration in the monolayer or the mixed monolayer at the water–air interface, its limitations should be kept in mind. If for the calculation of Γ, the concentration of surfactants in mole/dm^3 is applied, then it is assumed that the coefficient of the surfactant activity is equal to 1 and the mole fraction of the surfactant is equal to $\frac{C_i}{\omega}$, where ω is the number of the water moles in 1 dm^3 at a given temperature. As a matter of fact, the concentration of the surfactants and their mixture is so small that it is not taken into account in the ω calculation. It should also be remembered that Γ is not the total concentration of the surfactants in the monolayer but the so-called Gibbs surface excess concentration. However, the difference between the surfactants' concentration in the surface region and in the bulk phase is so great that Γ can be treated as the total concentration.

For the aqueous solution of TX165 mixtures with RL and SF at the constant concentration of one component and variable of the other one, the isotherms of Γ can be determined in the whole range of variable concentrations of one component of the mixture only when the isotherms of γ_{LV} can be described by one exponential function; in other words, only for the γ_{LV} isotherms on which the maxima are not present. The Γ isotherms of TX165 calculated from Equation (5) at the constant concentration of RL and SF smaller than C_{min}^{sat} have a shape similar to the Γ isotherm of single TX165 (exemplary Figure S27). On the other hand, the shape of the isotherms Γ for RL and SF at a constant concentration of TX165 is similar to that of individual biosurfactants (exemplary Figure S28). Since it is difficult to calculate the Γ isotherms for all tested systems applying Equation (5), conclusions about the interactions between the molecules of the components of the mixed saturated monolayer can hardly be drawn. However, it is possible to calculate the Γ isotherms from those of γ_{LV} with extremes using the Frumkin equation [27,36].

Yet this is the main problem to solve the Frumkin equation against Γ. It has to do with the maximal concentration of each component of the mixture in the surface mixed monolayer at its given composition. It seems reasonable to assume that the maximum concentration in the mixed monolayer of each mixture component at its given concentration in the bulk phase can be approximately equal to the product of the fraction of the surface area occupied by that component and its individual maximum concentration ($x^S \Gamma^{max}$). On the other hand, the water surface tension reduction by the adsorption of a given component of the surfactant mixture at the water–air interface can be expressed by the difference in

the surface tension of water (γ_W) and solution (γ_{LV}) multiplied by the mole fraction of this component in the surface layer ($(\gamma_W - \gamma_{LV})x^S = \pi x^S$). Thus the Frumkin equation can be written in the form:

$$\pi = -RT\Gamma^{max} \ln\left(1 - \frac{\Gamma}{x^S \Gamma^{max}}\right) \tag{6}$$

Taking Equation (6) into account, it was possible to calculate Γ for TX165 and RL as well as for TX165 and SF, even in the case where the maxima are present on the γ_{LV} isotherms (Figures S29–S34). The total Γ for TX165 and RL or SF calculated from Equation (6) for the aqueous solution of TX165 with the biosurfactants mixture at the constant concentration of one component and variable of the other one in the range of the constant concentrations below C_{min}^{sat} is close to the Γ calculated from Equation (5). However, for the aqueous solution of TX165 + RL and TX165 + SF at a constant composition, the differences between the values of Γ determined from Equations (5) and (6) are observed (Figures S35 and S36). There may be two reasons for that. One can refer to the value of n in Equation (5) used for calculations, which is connected to the anionic biosurfactants of the 1:1 type electrolyte, but their molecules in the mixture cannot be completely dissociated and the n value used by us is not proper. The other reason may result from the fact that, as mentioned above, H_3O^+ can be joined with the oxyethylene groups in the hydrophilic part of TX165 molecules [37]. In such a case, RL and SF can be treated as nonionic surfactants. In the calculations of Γ for TX165 and the biosurfactants, there are the x^S values, whose determination is based on the contribution of particular components of the TX165 with RL and SF mixtures to the water surface tension reduction. For the determination of the composition of the mixed monolayer at the water–air interface, the relationship between the x^S values calculated from the contributions of the components to the reduction in the γ_W and their mole fraction in the mixed monolayer is of significant importance. The relative composition of the saturated mixed monolayer is very often calculated from the Hua and Rosen equation of the following form [27,38]:

$$\frac{(x_1^S)^2 \ln\left(x_1^b C_{12}/x_1^S C_1\right)}{\left(1 - x_1^S\right)^2 \ln\left[\left(1 - x_1^b\right)C_{12}/\left(1 - x_1^S\right)C_2\right]} = 1 \tag{7}$$

where indices 1, 2, and 12 refer to TX165, RL, or SF and to the mixtures of TX165 with RL and/or SF, respectively, and b refers to the bulk phase. It proved that the values of x_1^S and x_2^S determined using Equation (7) are similar to those determined in the way mentioned above (Tables S1 and S2 and Figure S37 as an example). As follows from the calculations of x_1^S and x_2^S, the mole fraction of RL and SF in the mixed saturated monolayer is higher than in the bulk phase. This can be more clearly seen in the case of SF than RL. Based on the concept of Hua and Rosen [38], it is possible to determine the parameter of intermolecular interactions in the saturated mixed monolayer (β^σ). The equation resulting from this concept has the form:

$$\beta^\sigma = \frac{\ln\left(x_1^b C_{12}/x_1^S C_1\right)}{\left(1 - x_1^S\right)^2} \tag{8}$$

The calculated values of β^σ indicate that in the case of the TX165 + RL mixture, the synergetic effect in the reduction in water surface tension is more visible than that for the TX165 and SF mixture (Tables S1 and S2). For the TX165 and SF mixture, the β^σ parameter changes from negative to positive values depending on its composition and the surface tension is taken into consideration (Table S2). However, the absolute values of β^σ are close to zero. As mentioned above, the activity of SF adsorption at the water–air interface is much greater than that of TX165. TX165 can not influence the adsorption of SF to such an extent that the synergetic effect in the water surface tension reduction could take place.

2.4. CMC

From the practical point of view, the second important property of surfactants and biosurfactants is their ability to form micelles in the polar environment. The surfactant concentration at which micelles are formed, known as the critical micelle concentration (CMC), can be determined by many methods. Among them, the method based on the γ_{LV} isotherms is often used. Since it was not possible to determine the CMC based on the γ_{LV} isotherms over the whole range of constant concentration values of one component of the mixture of TX165 with RL or TX165 with SF and the variable second component, the CMC was determined only for the mixtures with a constant composition (Figures 6 and 7). The negative deviation of CMC as a function of biosurfactant mole fractions in the mixture with TX165 is observed.

The CMC values obtained from the γ_{LV} isotherms were compared to those calculated for the ideal mixture of surfactants from the following equation [27]:

$$\frac{1}{CMC_{12}} = \frac{x_1^b}{CMC_1} + \frac{1 - x_1^b}{CMC_2} \tag{9}$$

where CMC_1, CMC_2, and CMC_{12} are the critical micelle concentrations of TX165, RL, and SF and their mixtures, respectively.

An insignificant difference between the values of CMC for the mixtures of TX165 with the biosurfactants calculated from Equation (9) and those determined from the γ_{LV} isotherms was found. Based on the comparison of CMC values calculated from Equation (9) and those determined from the γ_{LV} isotherms, it cannot be explicitly stated whether there is a synergistic effect in the aggregation process of the mixed micelles of TX165 with the biosurfactants. Bergström and Eriksson [39] carried out studies on the synergistic effect in the micellization process of the surfactants' binary mixtures. Based on the Poisson–Boltzman theory, they proposed an equation for the calculation of the CMC of the surfactant mixtures. The equation derived by them for the calculation of CMC for the nonionic and ionic surfactant mixtures has the form:

$$CMC_{12}\left(x_2^M\right) = \left(x_2^M\right)^2 \exp\left(1 - x_2^M\right)CMC_2 + \left(1 - x_2^M\right)\exp\left(1 - x_2^M\right)CMC_1 \tag{10}$$

where the x_2^M is the mole fraction of the given component surfactant mixture in the micelles. The mole fraction of the surfactant mixture compounds can be determined from the Hua and Rosen equation [27,38]:

$$\frac{\left(x_1^M\right)^2 \ln(x_1^b CMC_{12}/x_1^M CMC_1)}{\left(1 - x_1^M\right)^2 \ln\left[\left(1 - x_1^b\right)CMC_{12}/\left(1 - x_1^M\right)CMC_2\right]} = 1 \tag{11}$$

Knowing the mole fraction of TX165 and biosurfactant calculated from Equation (11), it is possible to calculate the parameter of intermolecular interactions in the micelle (β^M) [27,38]:

$$\beta^M = \frac{\ln\left(x_1^b CMC_{12}/x_1^M CMC_1\right)}{\left(1 - x_1^M\right)^2} \tag{12}$$

The β^M values calculated from Equation (12) are negative. This indicates synergetic effects in the micelle formation for the TX165 + RL and TX165 + SF mixtures (Table S3). However, the latter condition should confirm this conclusion. As follows, $|\beta^M| > |\ln(CMC_2/CMC_1)|$. This condition is also fulfilled for the TX165 with SF mixtures at mole fractions of SF equal to 0.4, 0.6, and 0.8. In the case of the TX165 + RL mixture, the existence of the synergetic effect in the micelle formation was confirmed by the latter condition only at the mole fractions of RL in the bulk phase, equal to 0.2 and 0.8. Based on the mole fraction of TX165 and biosurfactants, it is possible to calculate the CMC of the studied mixtures. As follows from the calculations, the values of CMC obtained from Equation (10) for the mixtures

of TX165 with RL are close to those determined from the γ_{LV} isotherm (Figure S38). In the case of the TX165 and SF mixture, an insignificant difference between these values is observed (Figure S39).

Taking into account the mole fraction of the TX165 and biosurfactants in the mixture, it is possible to calculate the coefficients of TX165 and biosurfactants activity in the mixed micelles from the following expressions [40]:

$$\ln f_1^M = \beta^M \left(1 - x_1^M\right)^2 \tag{13}$$

$$\ln f_2^M = \beta^M \left(x_1^M\right)^2 \tag{14}$$

Knowing the $\ln f_1$ and $\ln f_2$ values, the CMC of the TX165+RL and TX165+SF mixtures can be calculated from the equation [27]:

$$\frac{1}{\text{CMC}_{12}} = \frac{x_1^b}{f_1 \text{CMC}_1} + \frac{1 - x_1^b}{f_2 \text{CMC}_2} \tag{15}$$

The values of CMC_{12} calculated from Equation (15) for the mixtures of TX165 with RL and SF are close to those determined from the isotherms of the surface tension of their aqueous solutions (Figures S38 and S39).

The compatibility of the CMC values of TX165 mixtures with the biosurfactants determined based on the surface tension of their aqueous solutions with those calculated from Equations (9) and (15) does not indicate the synergistic effect in the micellization process.

On the other hand, the parameter of intermolecular interactions in the micelles determined from the Hua and Rosen theory satisfies, although not in every composition of mixtures, the two conditions for the synergistic effect in the micellization process.

It seems that the lack of reliable evidence of the synergetic effect in the micellization process may result from very great differences in the CMC values of individual components of the mixture, and the theories were proposed for the systems with smaller differences in their surface and volumetric properties.

2.5. Standard Gibbs Free Energy of Adsorption and Micellization

The standard free energy of adsorption (ΔG_{ads}^0) and micellization (ΔG_{amic}^0) is a measure of the surfactants and their mixture tendency to adsorb or aggregate in aqueous media. The literature reports many different methods for ΔG_{ads}^0 determination [27]. Among them, the method based on the constant a is very often applied. The constant a can be determined, among others, by the Szyszkowski and linear Langmuir equations [27]. The dependence between the constant a and ΔG_{ads}^0 has the form:

$$a = \omega \exp \frac{\Delta G_{ads}^0}{RT} \tag{16}$$

Using the Szyszkowski equation, it is possible to describe the γ_{LV} isotherms of the aqueous solutions of TX165 mixtures with biosurfactants, in which the value of the concentration of one component of the mixture was constant but smaller than C_{min}^{sat} and the value of the other was variable, as well as for the mixtures at a constant composition. Thus the constant in this equation was taken into account in the calculation of ΔG_{ads}^0. It appears that ΔG_{ads}^0 for the individual solutions of TX165 and RL calculated based on the constant a from the Szyszkowski equation using Equation (16) are similar to those determined by the other methods [23,30,31]. However, for SF, ΔG_{ads}^0 is smaller than that obtained from the Langmuir equation (Table 1). For the first series of solutions in which the concentration of one component of surfactant was constant and the other was variable, the values of ΔG_{ads}^0 for TX165, RL, and SF in the TX165 + RL and TX165 + SF mixtures were close to those of ΔG_{ads}^0 for these surfactants in their individual solutions. However, in the case of the

aqueous solutions of the TX165 with RL and SF mixture at a constant composition and a variable total concentration, the nonlinear dependence between the ΔG_{ads}^0 and the mole fraction of the biosurfactant in the mixture was obtained. (Figure S40). However, it turned out that the relationship between the ΔG_{ads}^0 and concentration of the biosurfactant in the TX165+RL mixture can be described by the following equation:

$$\Delta G_{ads}^0 = x_1^b \Delta G_{ads,1}^0 + x_2^b \Delta G_{ads,2}^0 + G_{mix}^E \tag{17}$$

where G_{mix}^E is the Gibbs free energy of surfactants mixing.

For the mixed monolayer of the TX165 mixture with RL or SF, the G_{mix}^E can be calculated from the equation:

$$G_{mix}^E = RT \left(x_1^s \ln f_1^S + x_2^s \ln f_2^S \right) \tag{18}$$

The activity coefficients of TX165 (f_1) and RL or SF (f_2) in the mixed monolayer at the water–air interface were determined from the following expressions (Tables S1 and S2) [40]:

$$\ln f_1^S = \beta^\sigma (1 - x_2^s)^2 \tag{19}$$

and

$$\ln f_2^S = \beta^\sigma (x_1^s)^2 \tag{20}$$

In the case of the TX 165+SF mixture, a greater difference between ΔG_{ads}^0 calculated from Equations (16) and (17) is found. This may be a result of great differences in the adsorption activity between TX165 and SF and their molar fractions in the saturated monolayer determined from the Hua and Rosen equation [27,38].

The standard Gibbs free energy of micellization was determined only for the aqueous solution of the TX165 mixture with RL and/or SF in which the composition was constant but the total concentration was variable. For determination of ΔG_{mic}^0, we used the following equation [27]:

$$\Delta G_{mic}^0 = RT \ln \frac{\text{CMC}}{\omega} \tag{21}$$

The values of ΔG_{mic}^0 calculated from Equation (21) do not change linearly as a function of the mole fraction of biosurfactants in the bulk phase. Some binary mixtures of surfactants can be predicted from the ΔG_{mic}^0 components, their mole fraction in the mixture, and the Gibbs free energy of surfactants mixing in the micelle ($G_{mix}^{E,m}$) [40], according to the following equation:

$$\Delta G_{mic}^0 = x_1^b \Delta G_{mic,1}^0 + x_2^b \Delta G_{mic,2}^0 + G_{mix}^{E,m} \tag{22}$$

The $G_{mix}^{E,m}$ fulfils the equation [27,41]:

$$\Delta G_{mix}^{E,m} = RT \left(x_1^M \ln f_1^M + x_2^M \ln f_2^M \right) \tag{23}$$

If the mole fractions of TX165, SF, and RL for the mixtures of TX165+RL and TX165+SF in the bulk phase were used in Equation (22), the calculated values of ΔG_{mic}^0 were higher than those calculated from Equation (21) (Figures S41 and S42). If the values of x_1^M and x_2^M were used in Equation (22) instead of x_1^b and x_2^b, the ΔG_{mic}^0 values calculated from Equation (22) were closer to those calculated from Equation (21) than in the case of x_1^b and x_2^b application. This fact proves the presence of a synergistic effect in the micellization process of tested mixtures.

3. Materials and Methods

Triton X-165 (TX165) ((p- (1,1,3,3-tetramethylbutyl)-phenoxypolyoxyethylene glycol) of a purity over 99% was purchased from FLUKA (Steinheim, Germany). R-95 Rhamnolipid (95%) (RL) and surfactin (≥98%) (SF) were purchased from Sigma-Aldrich (Steinheim, Germany). TX165, RL, and SF were used for the aqueous solution preparation without

further purification. Six series of solutions were prepared for the surface tension measurements. The first series included the aqueous solutions of the RL and TX165 mixture with the constant RL concentration, the values of which ranged from 2×10^{-4} to 40 mg/dm^3, and the variable concentration of TX165 from 1×10^{-8} to 4×10^{-3} mole/dm^3. The second series included the solution in which the concentration of TX165 was constant (in a range from 1×10^{-8} to 4×10^{-3} mole/dm^3) and RL variable, from 2×10^{-4} to 40 mg/dm^3. The third series included the aqueous solutions of the RL mixture with TX165 in which the RL concentration varied from 2×10^{-4} to 40 mg/dm^3. The TX165 mixture was selected so that the molar fractions of TX165 in the mixture were 0.2, 0.4, 0.6, and 0.8. In other words, these were the aqueous solutions of RL and TX165 with a constant composition and variable concentrations. The fourth, fifth, and sixth series were the solutions of the mixture of SF and TX165 of the same concentration as those of the first, second, and third series for the RL and TX 165 mixture. All solutions were prepared using doubly distilled and deionized water (Destamat Bi18E) at an internal specific resistance of 18.2×10^6 Ω·m. The water purity was additionally controlled by the surface tension measurements before the solutions' preparation.

The surface tension (γ_{LV}) of the aqueous solution of rhamnolipid and TX165, as well as the surfactin and TX165 mixtures, was measured by the Krüss K9 tensiometer according to the platinum ring detachment method (du Nouy's method) at 293 K. Before the surface tension measurements, the tensiometer was calibrated using water (γ_{LV} = 72.8 mN/m) and methanol (γ_{LV} = 22.5 mN/m). A more detailed procedure for measuring the surface tension was given earlier [23]. For each concentration of the aqueous solution of RL and TX165, as well as the TX165 and SF mixtures, the surface tension measurements were repeated at least ten times. The standard deviation was ±0.1 mN/m and the uncertainty of the surface tension measurements was in a range from 0.3% to 0.7%.

4. Conclusions

From the measurements of the surface tension of the aqueous solutions of the TX165 + RL and TX165 + SF mixtures at a constant concentration of one mixture component and a variable concentration of the other, it results that maxima are present on the obtained surface tension isotherms, but they are not observed on the surface tension isotherms at the constant mixture composition. The maxima are observed at the constant concentration value of one component mixture close or higher to the CMC. This phenomenon was explained based on the contribution of particular components of the mixture to the reduction in water surface tension. This is important not only from the theoretical but also from the practical point of view.

The isotherms of the surface tension of the aqueous solution of the TX165 with RL or SF mixtures at the constant composition and variable total concentration can be described by the exponential function of the second order and the Szyszkowski equation. The description of the γ_{LV} isotherms of the aqueous solution of the binary mixture of the surfactants by the Szyszkowski equation is a theoretical novelty.

In most cases, the isotherms of the surface tension of the aqueous solution of TX165 + RL and TX165 + SF, on which the maxima are present, can be described by two exponential functions of the second order, one in the range concentration of the mixture component whose concentration is variable from zero to the value corresponding to the maximum of the surface tension, and the other in the concentration range above this, at which the maximum is observed.

The relationship between the constants in the equation of the exponential function of the second order, as well as the components and parameters of the surfactants and biosurfactants tail and head, the surface tension is not excluded.

The isotherms of the surface tension of the aqueous solution of TX165 + RL and TX165 + SF can be predicted by the Fainerman and Miller equation, except for the mixtures in which the concentration of one or two components corresponds to the saturated monolayer at the water–air interface of the aqueous solution of the mixture single components.

The area occupied by one mole of the mixtures at the water–air interface can be deduced based on the contribution of the mixture-given component to the reduction in the water surface tension.

The composition of the mixed monolayer at the water–air interface, as well as the isotherm of the surface tension, can be predicted from the isotherms of the surface tension of the aqueous solution of individual components of the mixture. The prediction of the composition of the mixed monolayer at the water–air interface by means of the simple way proposed by us is comparable to that of the Hua and Rosen equation. Our concept of the composition of the mixed monolayer at the water–air interface determination can be used for the mixture in the concentration range from 0 to CMC in contrast to the Hua and Rosen concept, which is applicable in the concentration range corresponding to the saturated monolayer and in the range of the limited composition of the mixture in the bulk phase.

Using the Hua and Rosen concept, the synergetic effect in the water surface tension reduction was deduced. This effect does not occur in the whole range of the TX165 + RL and TX165 + SF concentrations and is more visible for the TX165 and RL mixture than for the TX165 + SF mixture.

The synergetic effect in the CMC of the studied mixtures was also found using the Hua and Rosen concept.

Taking into account the mole fraction of the given component in the mixed monolayer and its maximal concentration in this monolayer in the Frumkin equation, it is possible to determine isotherms of particular components' adsorption of the studied mixtures as well as the summary concentration.

The changes of the CMC of the TX165 + RL and TX165 + SF mixtures as a function of the biosurfactants mole fraction in the bulk phase can be determined based on the CMC particular components of the mixture and its composition.

The standard Gibbs free energy of the adsorption and micellization of the TX165 + RL does not change linearly as a function of the biosurfactant molar fraction in the mixture in the bulk phase. This energy depends not only on the Gibbs free energy of each component of the studied mixtures but also on their Gibbs free energy of mixing in the mixed monolayer and micelles, respectively.

Supplementary Materials: The following supporting information can be downloaded at: https://www.mdpi.com/article/10.3390/molecules27113600/s1, Table S1: The values of the mole fraction of the surfactants in the mixed monolayer (x_1^S–TX165, x_2^S–RL), parameter of intermolecular interaction (β^σ), activity coefficients (f_1^S and f_2^S), and Gibbs excess free energy of mixing (G_{mix}^E); Table S2: The values of the mole fraction of the surfactants in the mixed monolayer (x_1^S– TX165, x_2^S– SF), parameter of intermolecular interaction (β^σ) activity coefficients (f_1^S and f_2^S), and Gibbs excess free energy of mixing (G_{mix}^E); Table S3: The values of the mole fraction of the surfactants in the mixed micelle (x_1^M- TX165, x_2^M– RL or SF), parameter of intermolecular interaction (β^M), activity coefficients (f_1^M and f_2^M) and Gibbs excess free energy of mixing ($G_{mix}^{E,m}$). Figure S1: A plot of the surface tension (γ_{LV}) of the aqueous solution of RL and TX165 mixture at the constant RL concentration equal to 0.00625 mg/dm^3 vs. the logarithm of the TX165 concentration (C_{TX165}) (a) and the logarithm of the total concentration of the TX16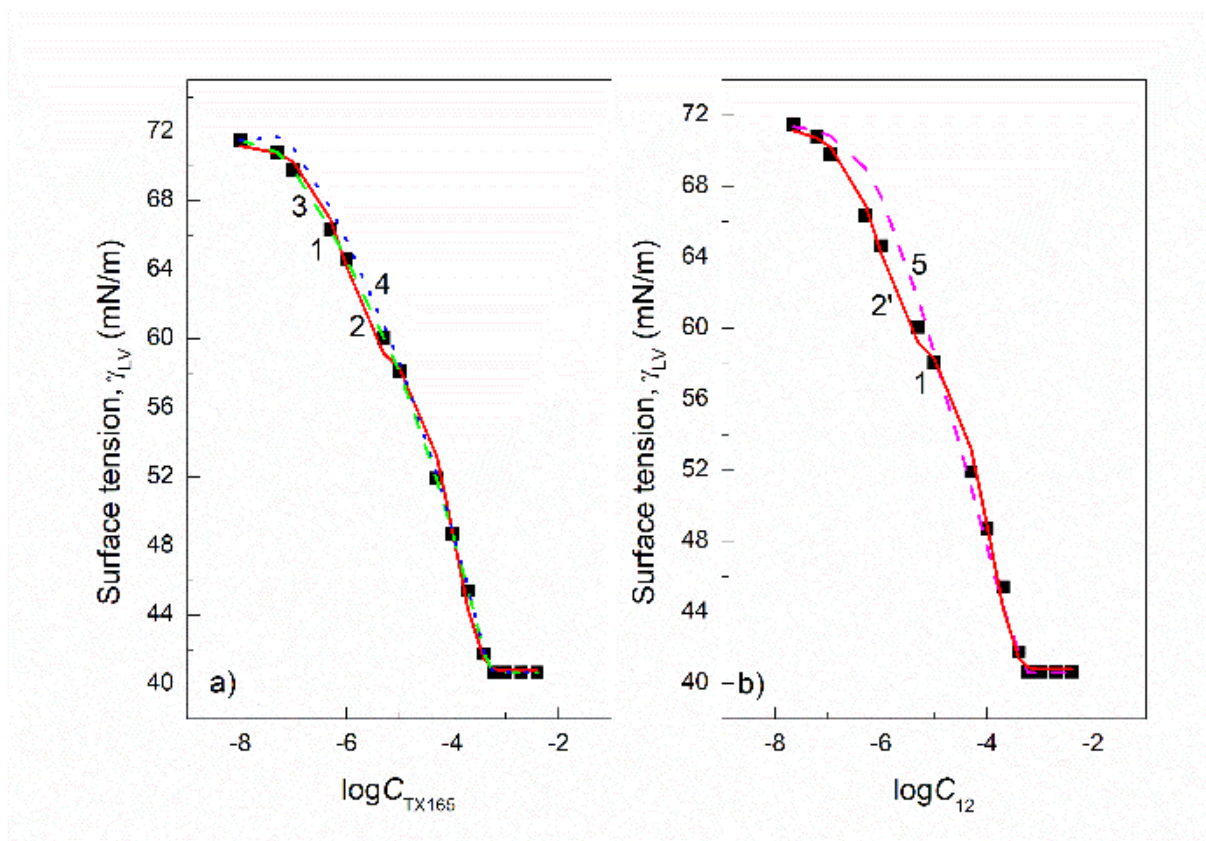5 + RL mixture (C_{12}) (b). Figure S2: A plot of the surface tension (γ_{LV}) of the aqueous solution of RL and TX165 mixture at the constant RL concentration equal to 5 mg/dm^3 vs. the logarithm of the TX165 concentration (C_{TX165}) (a) and the logarithm of the total concentration of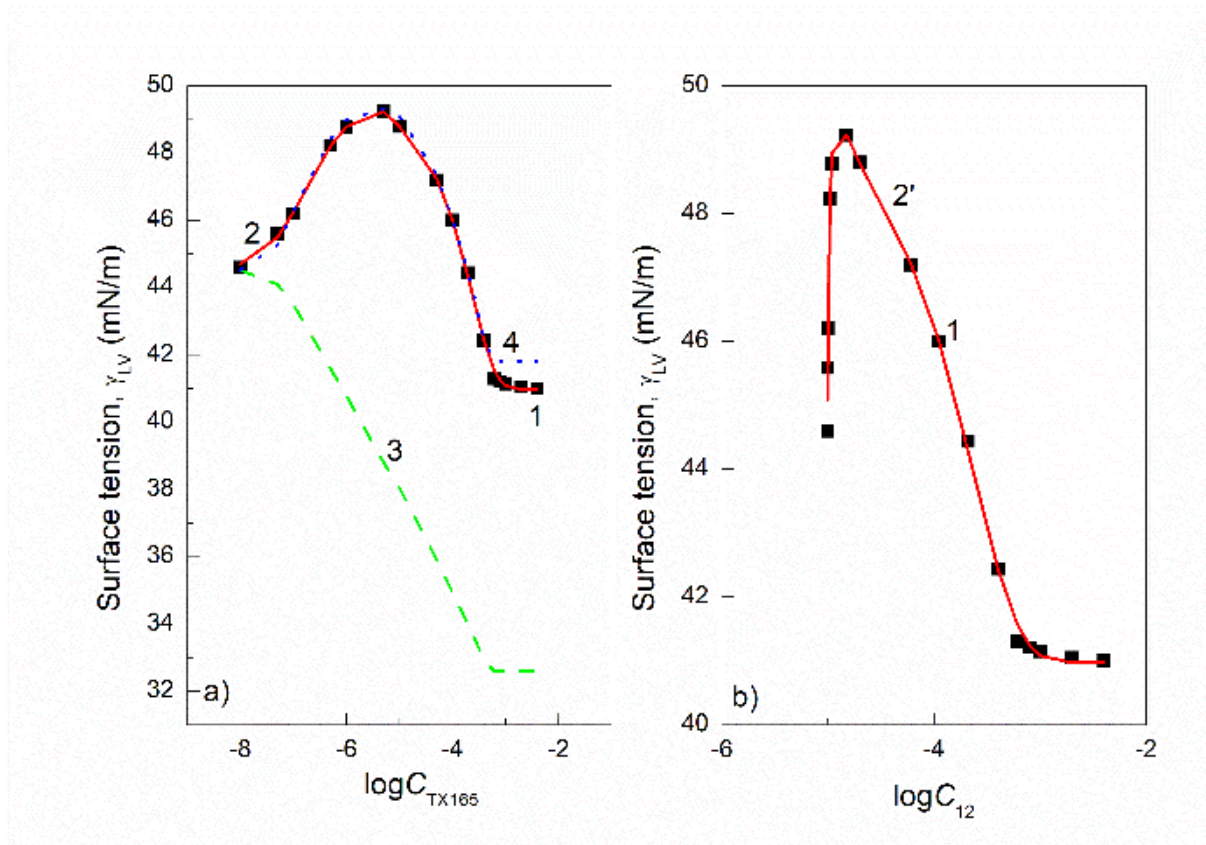 the TX165 +RL mixture (C_{12}) (b); Figure S3: A plot of the surface tension (γ_{LV}) of the aqueous solution of the RL and TX165 mixture at the constant RL concentration equal to 40 mg/dm^3 vs. the logarithm of the TX165 concentration (C_{TX165}) (a) and the logarithm of the total concentration of the TX165 + RL mixture (C_{12}) (b); Figure S4: A plot of the surface tension (γ_{LV}) of the aqueous solution of the SF and TX165 mixture at the constant SF concentration equal to 0.00625 mg/dm^3 vs. the logarithm of the TX165 concentration (C_{TX165}) (a) and the logarithm of the total concentration of the TX165 + SF mixture (C_{12}) (b); Figure S5: A plot of the surface tension (γ_{LV}) of the aqueous solution of the SF and TX165 mixture at the constant SF concentration equal to 5 mg/dm^3 vs. the logarithm of the TX165 concentration (C_{TX165}) (a) and the logarithm of the total concentration of the TX165 + SF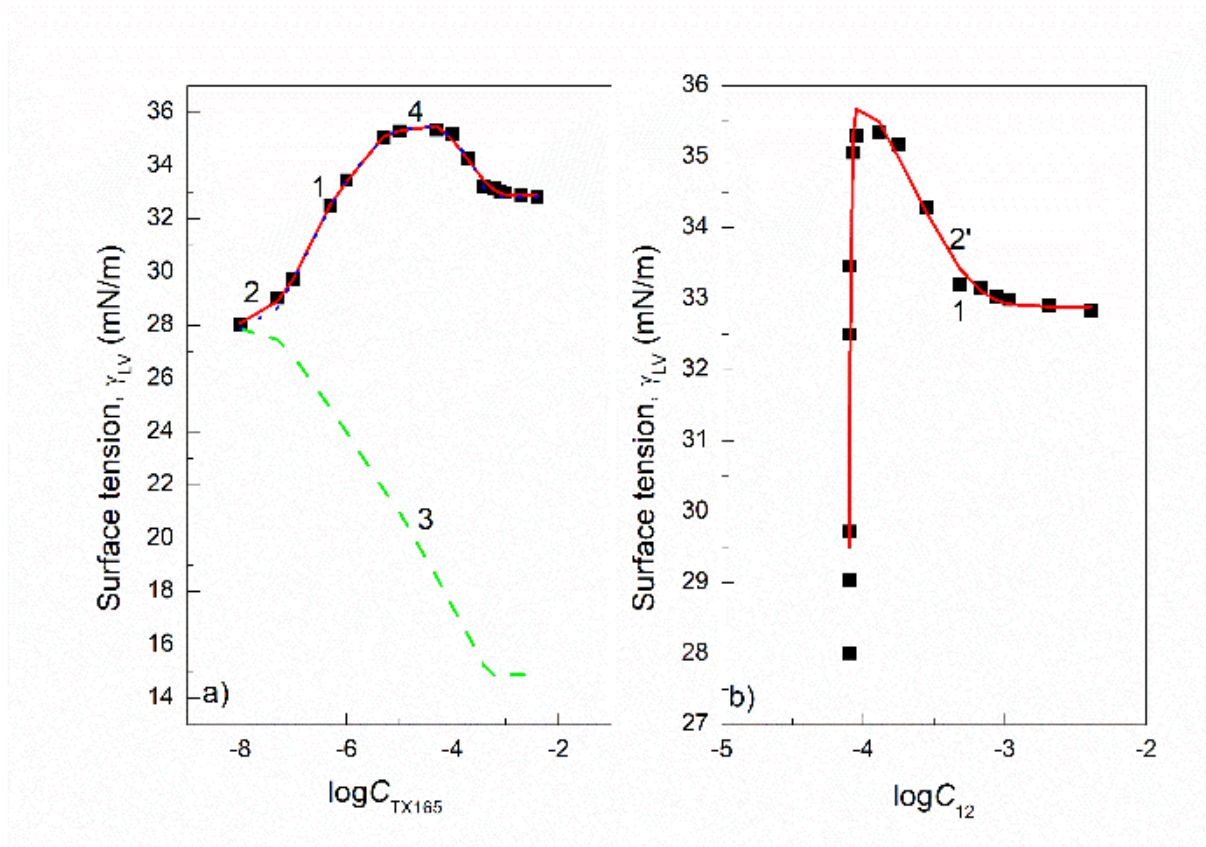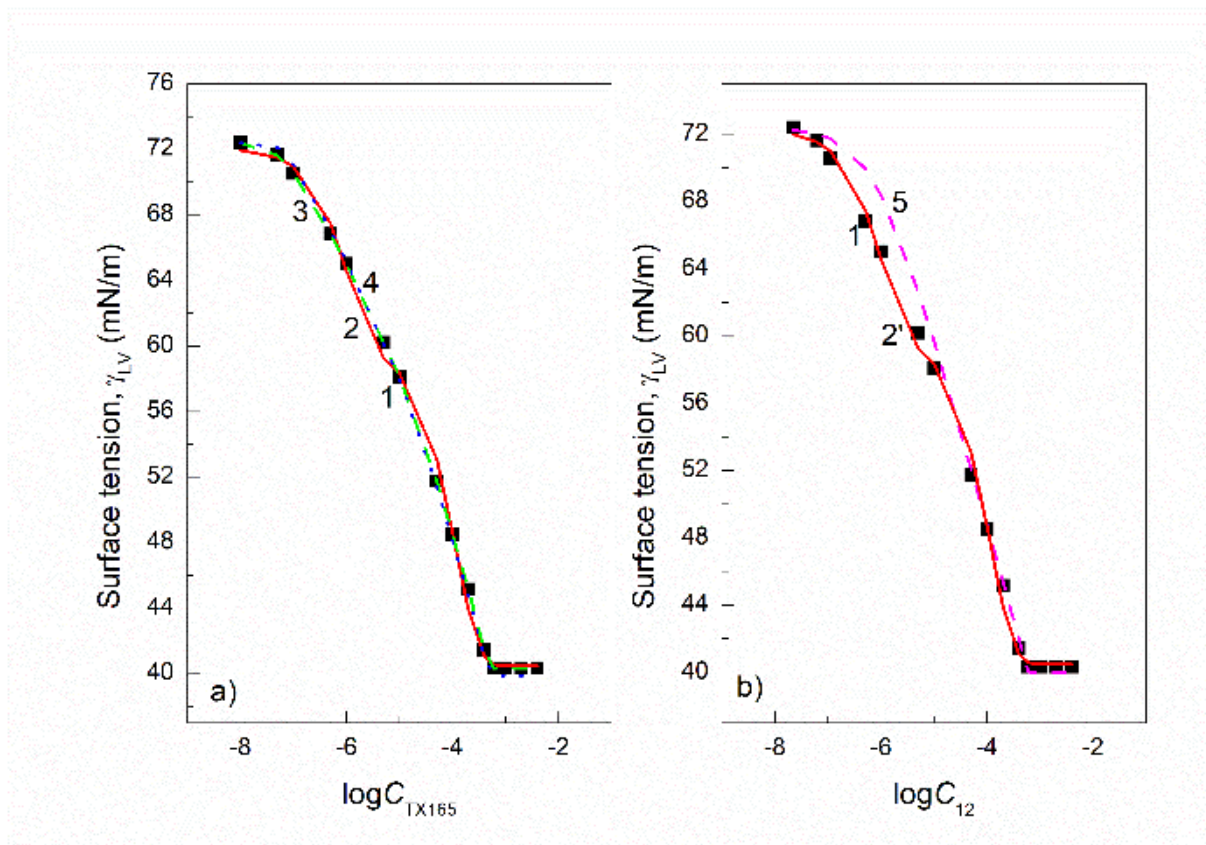 mixture (C_{12}) (b); Figure S6: A plot of the surface tension (γ_{LV}) of the aqueous solution of the SF and TX165 mixture

at the constant SF concentration equal to 40 mg/dm^3 vs. the logarithm of the TX165 concentration (C_{TX165}) (a) and the logarithm of the total concentration of the TX165 + SF mixture (C_{12}) (b); Figure S7: A plot of the surface tension (γ_{LV}) of the aqueous solution of the RL and TX165 mixture at a constant TX165 concentration equal to 5×10^{-7} mole/dm^3 vs. the logarithm of the RL concentrations (C_{RL}) (a) and the logarithm of the total concentration of the TX165 + RL mixture (C_{12}) (b); Figure S8: A plot of the surface tension (γ_{LV}) of the aqueous solution of the RL and TX165 mixture at a constant TX165 concentration equal to 2×10^{-4} mole/dm^3 vs. the logarithm of the RL concentration (C_{RL}) (a) and the logarithm of the total concentration of the TX165 + RL mixture (C_{12}) (b); Figure S9: A plot of the surface tension (γ_{LV}) of the aqueous solution of the RL and TX165 mixture at the constant TX165 concentration equal to 1×10^{-3} mole/dm^3 vs. 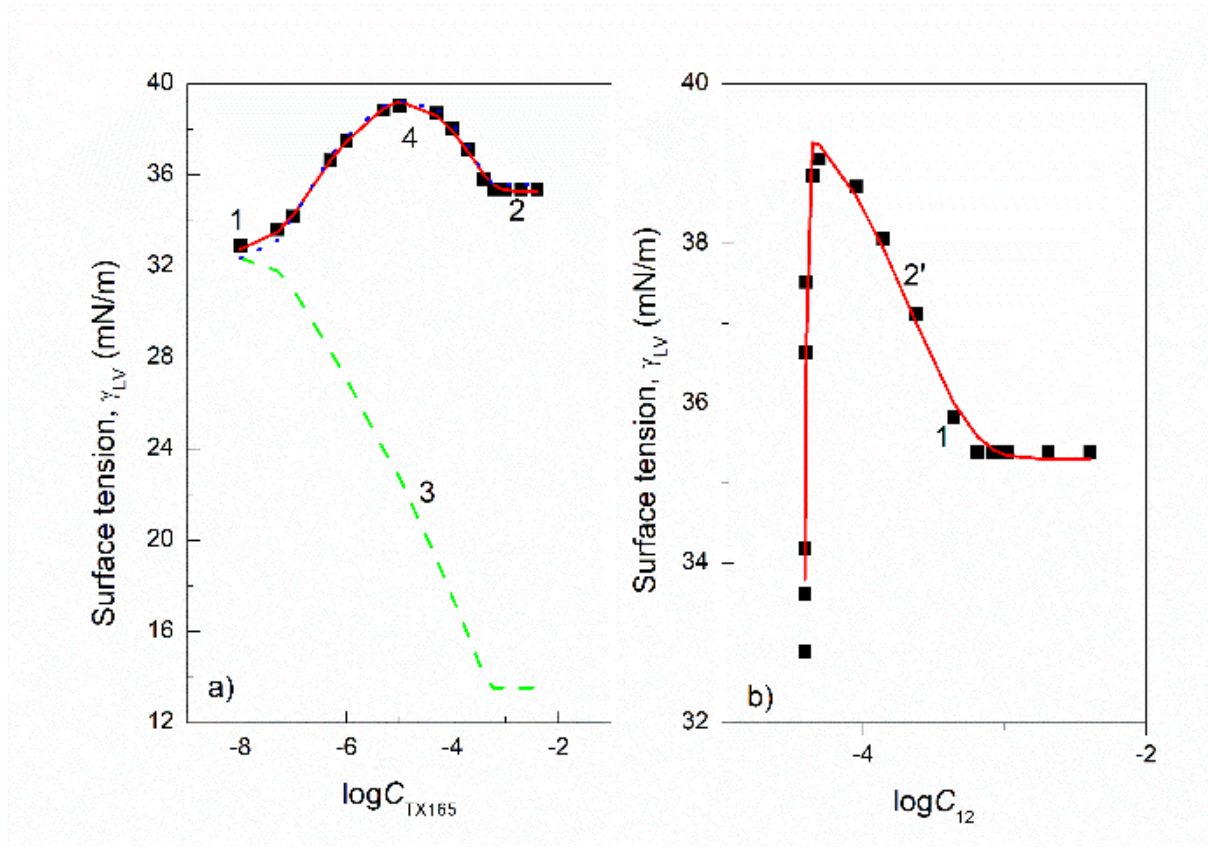the logarithm of the RL concentration (C_{RL}); Figure S10: A plot of the surface tension (γ_{LV}) of the aqueous solution of the SF and TX165 mixture at the constant TX165 concentration equal to 5×10^{-7} mole/dm^3 vs. the logarithm of the SF concentration (C_{SF}) (a) and the logarithm of the total concentration of the TX165 + SF mixture (C_{12}) (b); Figure S11: A plot of the surface tension (γ_{LV}) of the aqueous solution of the SF and TX165 mixture at the constant TX165 concentration equal to 2×10^{-4} mole/dm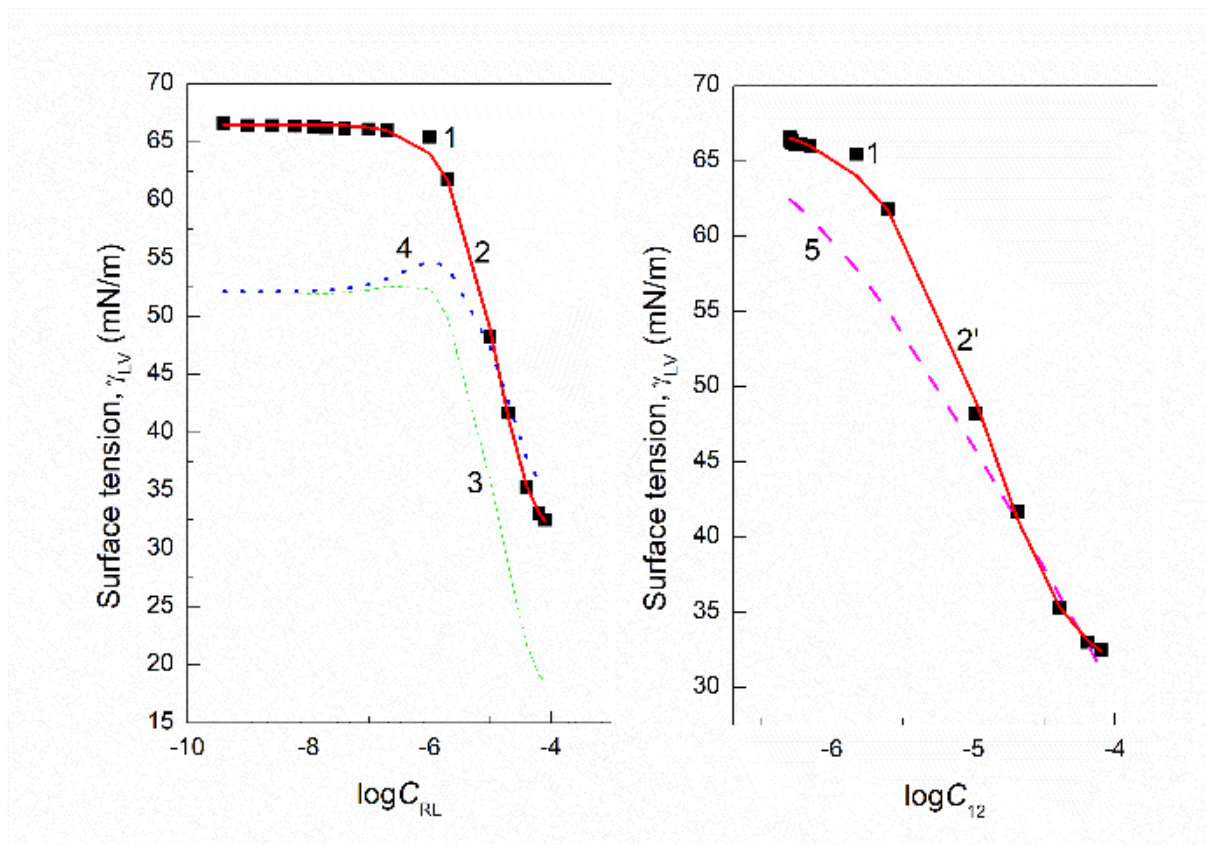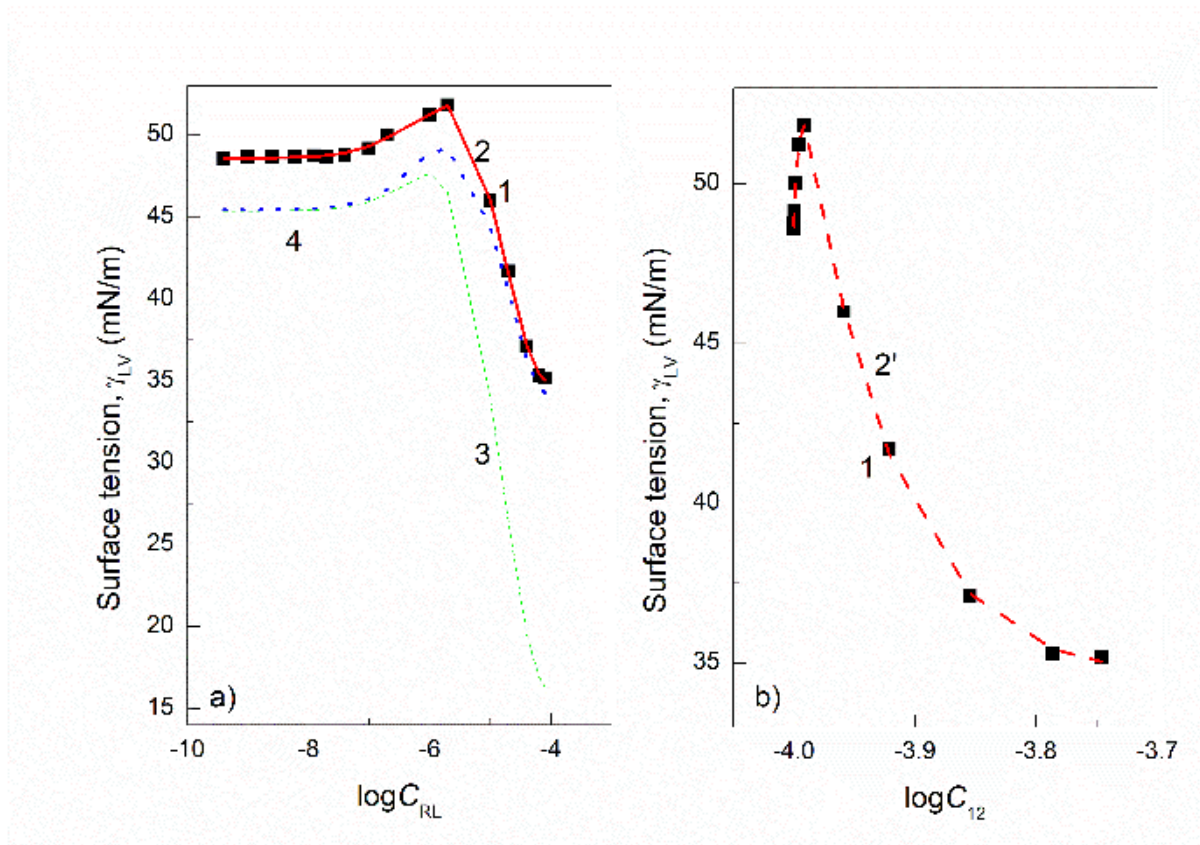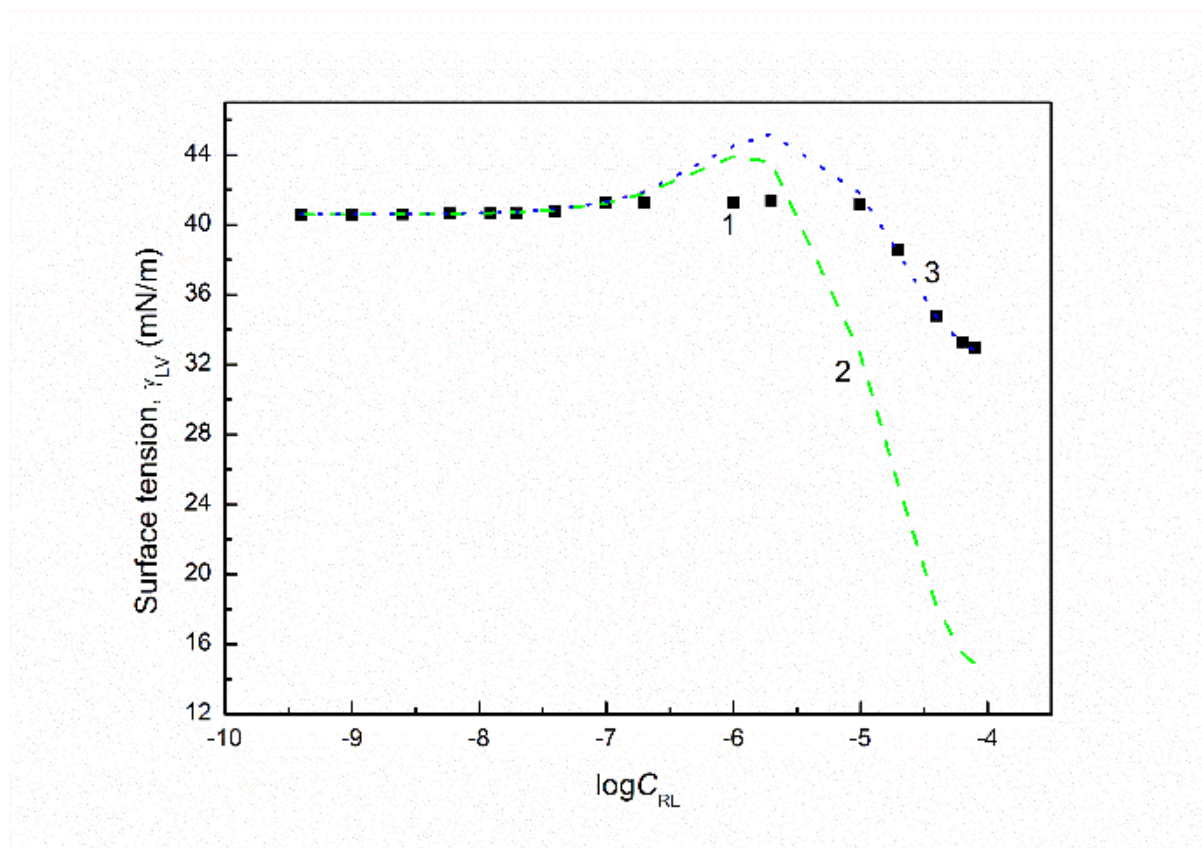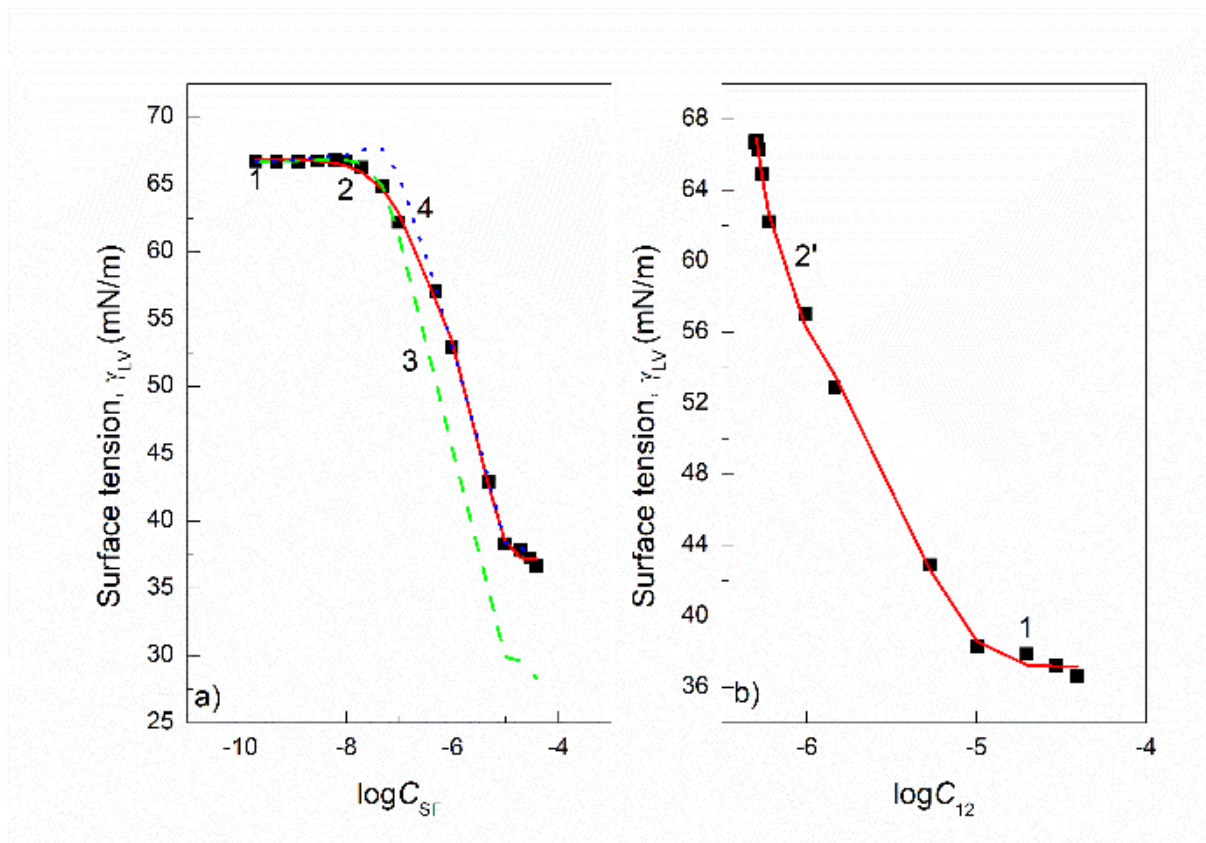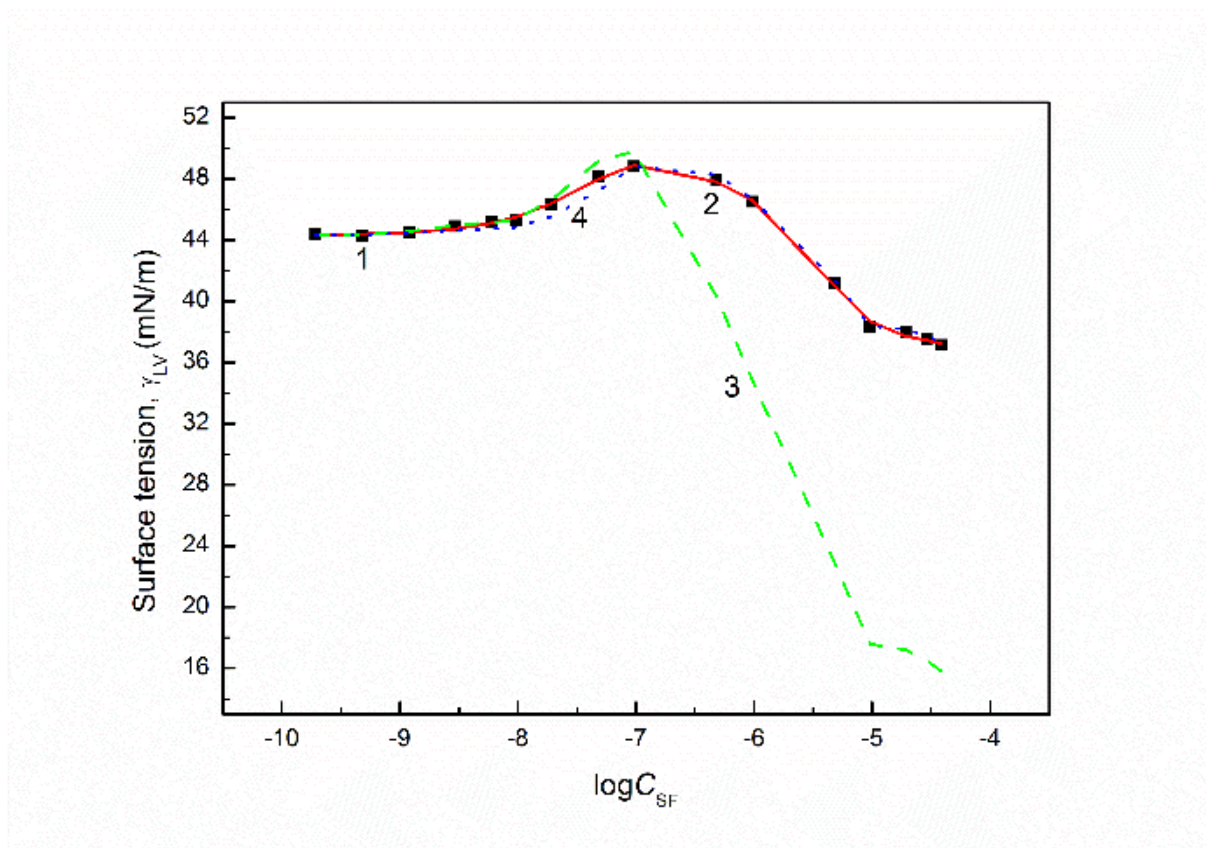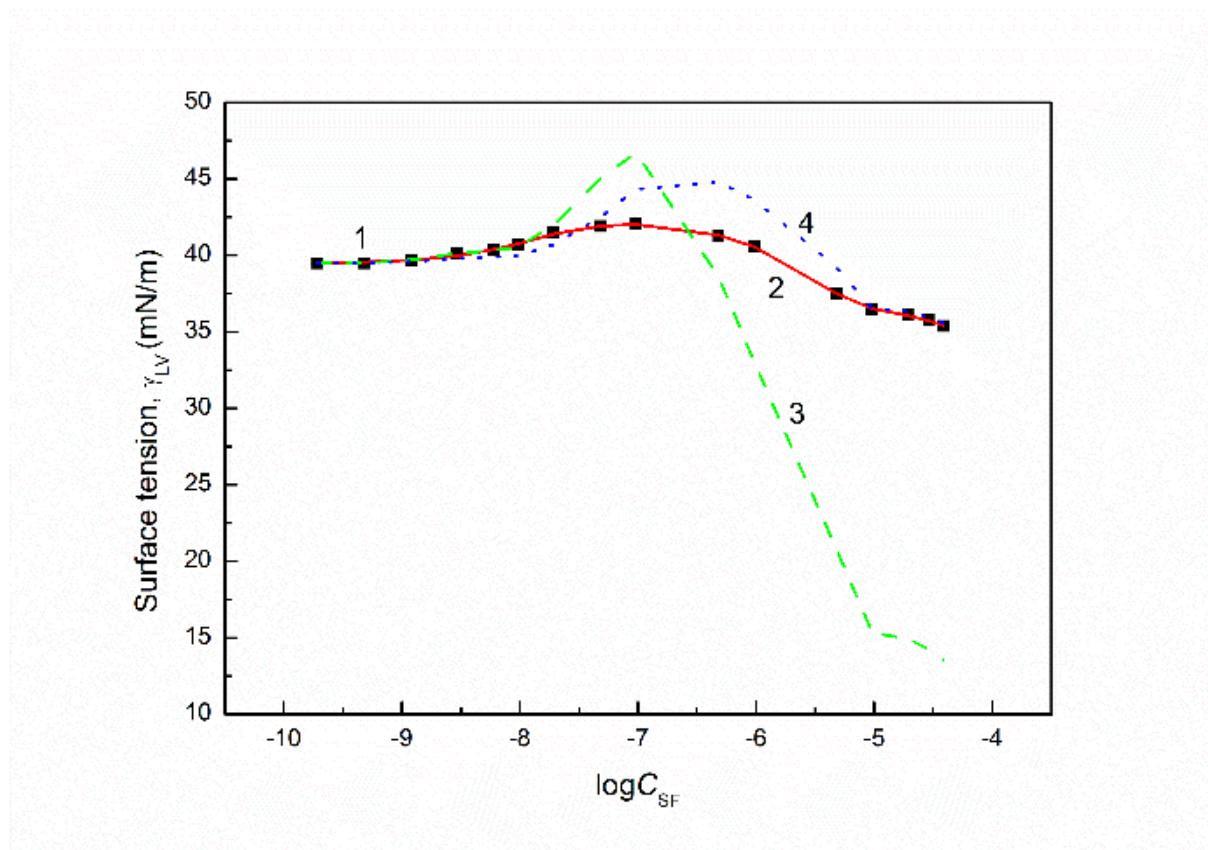^{3} vs. the logarithm of the SF concentration (C_{SF}); Figure S12: A plot of the surface tension (γ_{LV}) of the aqueous solution of the SF and TX165 mixture at the constant TX165 concentration equal to 1×10^{-3} mole/dm^3 vs. the logarithm of the SF concentration (C_{SF}); Figure S13: A plot of the constant y_0 in Equation (1) for the TX165 + RL (curve 1) and TX165 + SF (curve 2) aqueous solutions vs. the biosurfactant mole fraction in the mixture in the bulk phase (x_2^b); Figure S14: A plot of the constant A_1 in Equation (1) for the TX165 + RL (curve 1) and TX165 + SF (curve 2) aqueous solutions vs. the biosurfactant mole fraction in the mixture in the bulk phase (x_2^b); Figure S15: A plot of the constant A_2 in Equation (1) for the TX165 + RL (curve 1) and TX165 + SF (curve 2) aqueous solutions vs. the biosurfactant mole fraction in the mixture in the bulk phase (x_2^b); Figure S16: A plot of the constant t_1 in Equation (1) for the TX165 + RL (curve 1) and TX165 + SF (curve 2) aqueous solutions vs. the biosurfactant mol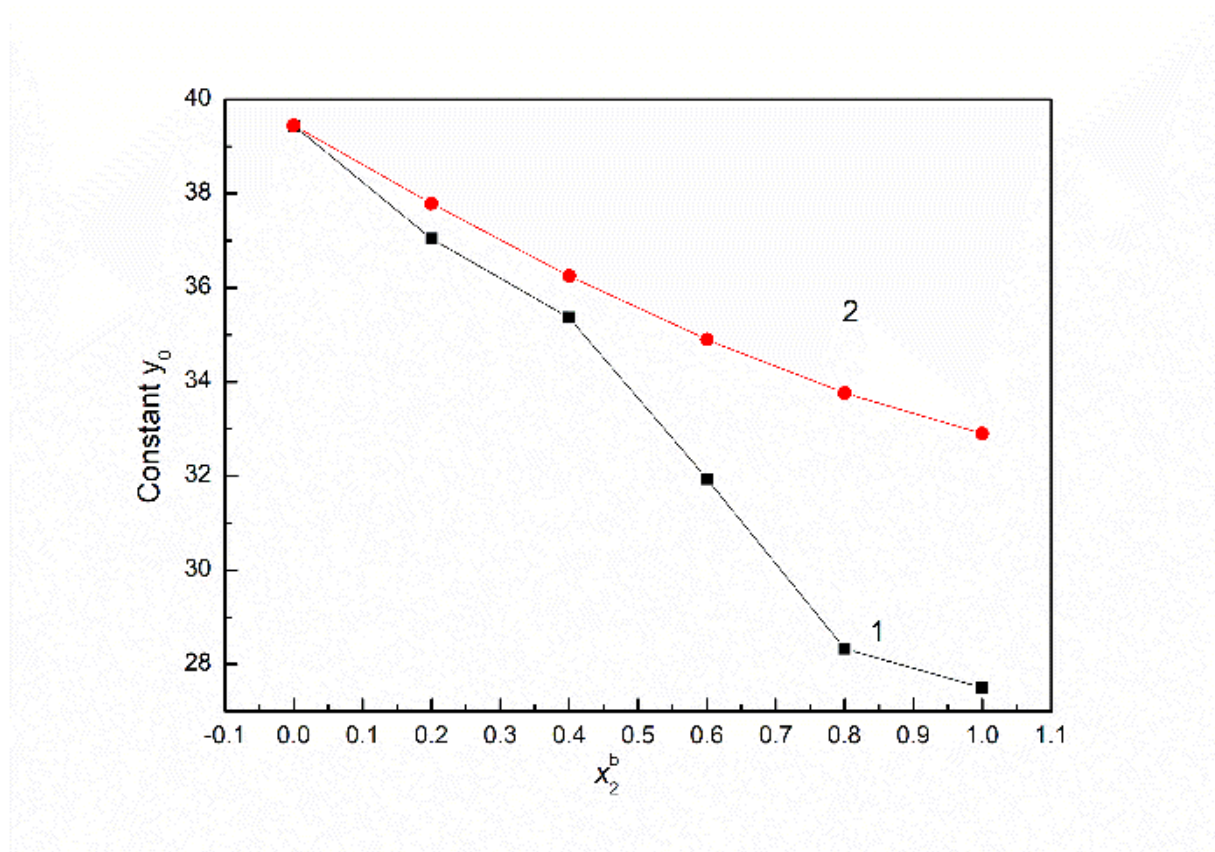e fraction in the mixture in the bulk phase (x_2^b); Figure S17: A plot of the constant t_2 in Equation (1) for the TX165 + RL (curve 1) and TX165 + SF (curve 2) aqueous solutions vs. the biosurfactant mole fraction in the mixture in the bulk phase (x_2^b); Figure S18: A plot of the surface tension (γ_{LV}) of the aqueous solution of the RL and TX165 mixture at the RL mole fraction equal to 0.2 vs. the logarithm of the total concentration of the TX165 + RL mixture (C_{12}); Figure S19: A plot of the surface tension (γ_{LV}) of the aqueous solution of the RL and TX165 mixture at the RL mole fraction equal to 0.4 vs. the logarithm of the total concentration of the TX165 + RL mixture (C_{12}); Figure S20: A plot of the surface tension (γ_{LV}) of the aqueous solution of the RL and TX165 mixture at the RL mole fraction equal to 0.6 vs. the logarithm of the total concentration of the TX165 + RL mixture (C_{12}); Figure S21: A plot of the surface tension (γ_{LV}) of the aqueous solution of the RL and TX165 mixture at the RL mole fraction equal to 0.8 vs. the logarithm of the total concentration of the TX165 + RL mixture (C_{12}); Figure S22: A plot of the surface tension (γ_{LV}) of the aqueous solution of the SF and TX165 mixture at the SF mole fraction equal to 0.2 vs. the logarithm of the total concentration of the TX165 + SF mixture (C_{12}); Figure S23: A plot of the surface tension (γ_{LV}) of the aqueous solution of the SF and TX165 mixture at the SF mole fraction equal to 0.4 vs. the logarithm of the total concentration of the TX165 + SF mixture (C_{12}); Figure S24: A plot of the surface tension (γ_{LV}) of the aqueous solution of the SF and TX165 mixture at the SF mole fraction equal to 0.6 vs. the logarithm of the total concentration of the TX165 + SF mixture (C_{12}); Figure S25: A plot of the surface tension (γ_{LV}) of the aqueous solution of the SF and TX165 mixture at the SF mole fraction equal to 0.8 vs. the logarithm of the total concentration of the TX165 + SF mixture (C_{12}); Figure S26: A plot of the constant a in the Szyszkowski equation (Equation (2)) for the TX165 + RL (curve 1) and TX165 + SF (curve 2) aqueous solutions vs. the biosurfa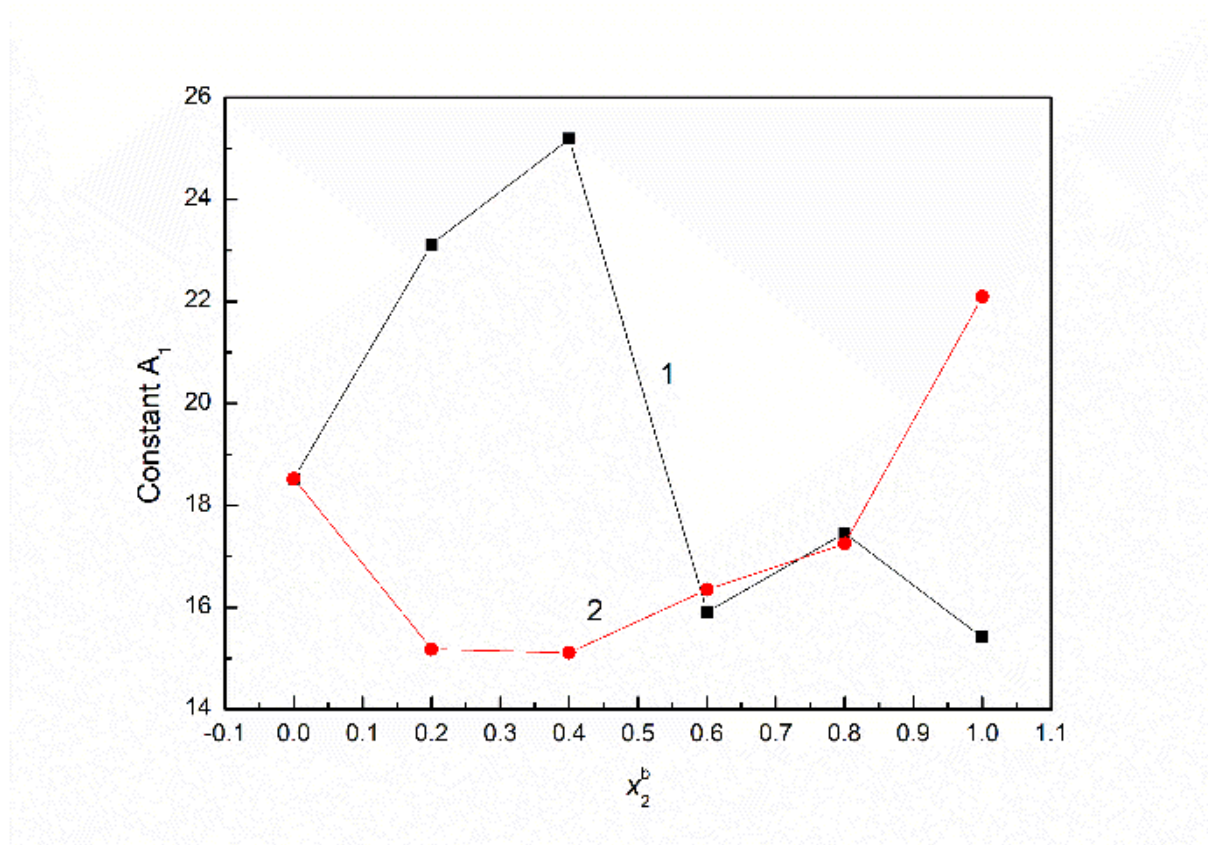ctant mole fraction in the mixture in the bulk phase (x_2^b); Figure S27: A plot of the surface concentration (Γ) of TX165 (curves 1, 1', 2, 2'), RL (curve 3), and SF (curve 5) vs. the logarithm of TX165 concentration (C_{TX165}) at the constant biosurfactant concentration equal to 0.00625 mg/dm^3; Figure S28: A plot of the surface concentration (Γ) of RL (curves 1, 1'), SF (curves 2, 2'), and TX165 (curves 3 and 5) vs. the logarithm of biosurfactant concentration (C) at the constant TX165 concentration equal to 5×10^{-7} mole/dm^3; Figure S29: A plot of the surface concentration (Γ) of TX165 calculated from Equation (6) in the TX165 + RL mixture vs. the logarithm of its concentration (C_{TX165}); Figure S30: A plot of the surface concentration (Γ) of TX165 calculated from Equation (6) in the TX165 + SF mixture vs. the logarithm of its concentration (C_{TX165}); Figure S31: A plot of the surface concentration (Γ) of RL calculated from Equation (6) in the TX165 + RL mixture vs. the logarithm of TX165 concentration (C_{TX165}); Figure S32: A plot of the surface concentration (Γ) of SF calculated from Equation (6) in

the TX165 + SF mixture vs. the logarithm of TX165 concentration (C_{TX165}); Figure S33: A plot of the total surface concentration (Γ) of the TX165 + RL mixture calculated from Equation (6) vs. the logarithm of TX165 concentration (C_{TX165}); Figure S34: A plot of the total surface concentration (Γ) of the TX165 + SF mixture calculated from Equation (6) vs. the logarithm of TX165 concentration (C_{TX165}); Figure S35: A plot of the total surface concentration (Γ) of the TX165 + RL mixture calculated from Equation (6) (curves 1, 2, 3, and 4) and Gibbs surface concentration calculated from Equation (5) vs. the logarithm of the total concentration of TX165 + RL mixture (C_{12}); Figure S36: A plot of the total surface concentration (Γ) of theTX165 + SF mixture calculated from Equation (6) (curves 1, 2, 3, and 4) and Gibbs surface concentration calculated from Equation (5) vs. the logarithm of the total concentration of TX165 + SF mixture (C_{12}); Figure S37: A plot of the TX165 mole fraction in the mixture with RL (curves 1 and 1′) and SF (curves 2 and 2′) (x) at the constant biosurfactant mole fraction in the mixture in the bulk phase equal to 0.2 vs. the total concentration of the TX165 + RL mixture (C_{12}); Figure S38: A plot of the CMC values of TX165 + RL and their mixtures vs. the RL mole fraction in the mixture in the bulk phase (x_2^b); Figure S39: A plot of the CMC values of TX165 + SF and their mixtures vs. the SF mole fraction in the mixture in the bulk phase (x_2^b); Figure S40: A plot of the Gibbs standard free energy of TX165 + RL (curves 1 and 1′) and TX165 + SF (curves 2 and 2′) adsorption at the water–air interface vs. the biosurfactant mole fraction in the mixture in the bulk phase (x_2^b); Figure S41: A plot of the Gibbs standard free energy of TX165 + RL micellization vs. the RL mole fraction in the mixture in the bulk phase (x_2^b) calculated from Equation (21) (curve 1) and form Equation (22) (curves 2 and 3); Figure S42: A plot of the Gibbs standard free energy of TX165 + SF micellization vs. the SF mole fraction in the mixture in the bulk phase (x_2^b) calculated from Equation (21) (curve 1) and form Equation (22) (curves 2 and 3).

References

1. Yuan, L.; Zhang, S.; Wang, Y.; Li, Y.; Wang, X.; Yang, Q. Surfactin inhibits membrane fusion during invasion of epithelial cells by enveloped viruses. *J. Virol.* **2018**, *92*, e0090–e00818. [CrossRef] [PubMed]
2. Ramalingam, V.; Varunkumar, K.; Ravikumar, V.; Rajaram, R. Production and structure elucidation of anticancer potential surfactin from marine actinomycete micromonospora marina. *Process. Biochem.* **2019**, *78*, 169–177. [CrossRef]
3. Khademolhosseini, R.; Jafari, A.; Mousavi, S.M.; Hajfarajollah, H.; Noghabi, K.A.; Manteghian, M. Physicochemical characterization and optimization of glycolipid biosurfactant production by a native strain of Pseudomonas Aeruginosa HAK01 and its performance evaluation for the MEOR process. *RSC Adv.* **2019**, *9*, 7932–7947. [CrossRef] [PubMed]
4. Heerklotz, H.; Seeling, J. Leakage and lysis of lipid membranes induced by the lipopeptide surfactin. *Eur. Biphys. J.* **2007**, *36*, 305–314. [CrossRef] [PubMed]
5. Lang, S. Biological amphiphiles (microbial biosurfactants). *Curr. Opin. Colloid Interface Sci.* **2002**, *7*, 12–20. [CrossRef]
6. Park, T.; Jeon, M.-K.; Lee, K.S.; Kwon, T.-H. Modification of interfacial tension and wettability in oil-brine quartz system by in situ bacterial biosurfactant production at reservoir conditions: Implications for microbial enhanced oil recovery. *Energy Fuels* **2019**, *33*, 4909–4920. [CrossRef]
7. Hadia, N.J.; Ottenheim, C.; Li, S.; Hua, N.Q.; Stubbs, L.P.; Lau, H.C. Experimental investigation of biosurfactant mixtures of surfactin produced by Bacillus Subtilis for EOR Application. *Fuel* **2019**, *251*, 789–799. [CrossRef]
8. Chen, W.-C.; Juang, R.S.; Wei, Y.-H. Applications of a lipopeptide biosurfactant, surfactin, produced by microorganisms. *Biochem. Eng. J.* **2015**, *103*, 158–169. [CrossRef]

9. Cameotra, S.S.; Bollag, J.M. Biosurfactant-enhanced bioremediation of polycyclic aromatic hydrocarbons. *Crit. Rev. Environ. Sci. Technol.* **2003**, *33*, 111–116. [CrossRef]

10. Sarubbo, L.A.; Silva, M.G.C.; Durval, I.J.B.; Bezerra, K.G.O.; Ribeiro, B.G.; Silva, I.A.; Twigg, M.S.; Banat, I.M. Biosurfactants: Production, properties, applications, trends, and general perspectives. *Biochem. Eng. J.* **2022**, *181*, 108377. [CrossRef]

11. Drakontis, C.E.; Amin, S. Biosurfactants: Formulations, properties, and applications. *Curr. Opin. Colloid Interface Sci.* **2020**, *48*, 77–90. [CrossRef]

12. Jemil, N.; Ayed, H.N.; Manresa, A.; Nasri, M.; Hmidet, N. Antioxidant properties, antimicrobial and anti-adhesive activities of DCS1 lipopeptides from Bacillus methylotrophicus DCS1. *BMC Microbiol.* **2017**, *17*, 144. [CrossRef] [PubMed]

13. Shah, M.U.H.; Moniruzzaman, M.; Sivapragasam, M.; Talukder, M.M.R.; Bt Yusup, S.; Goto, M. A binary mixture of a biosurfactant and an ionic liquid surfactant as a green dispersant for oil spill remediation. *J. Mol. Liq.* **2019**, *280*, 111–119. [CrossRef]

14. Chen, M.L.; Penfold, J.; Thomas, R.K.; Smyth, T.J.; Perfumo, A.; Marchant, R.; Banat, I.M.; Stevenson, P.; Parry, A.; Tucker, I.; et al. Mixing Behaviour of the Biosurfactant, Rhamnolipid, with a Conventional Anionic Surfactant, Sodium Dodecyl Benzene Sulfonate. *Langmuir* **2010**, *23*, 17958–17968. [CrossRef] [PubMed]

15. Xu, L.; Amin, S. Microrheological study of ternary surfactant-biosurfactant mixtures. *Int. J. Cosmet. Sci.* **2019**, *41*, 364–370. [CrossRef] [PubMed]

16. Onaizi, S.A.; Nasser, M.S.; Twaiq, F.A. Micellization and interfacial behavior of synthetic surfactant-biosurfactant mixture. *Colloids Surf. A Physicochem. Eng. Asp.* **2012**, *415*, 388–393. [CrossRef]

17. Abalos, A.; Pinazo, A.; Casals, M.R.; Garcia, F.; Maresa, A. Physicochemical and antimicrobial properties of new rhamnolipids produced by Pseudomonas aeruginosa AT10 from soybean oil refinery wastes. *Langmuir* **2001**, *17*, 1367–1371. [CrossRef]

18. Lang, S.; Wullbrandt, D. Rhamnose lipids – biosynthesis, microbial production and application potential. *Appl. Micorbiol. Biotechnol.* **1999**, *51*, 22–32. [CrossRef]

19. Soberón-Chávez, G.; Lépine, F.; Déziel, E. Production of rhamnolipids by Pseudomonas aeruginosa. *Appl. Microbiol. Biotechnol.* **2005**, *68*, 705–717. [CrossRef]

20. Rosenberg, E.; Ron, E.Z. High- and low-molecular-mass microbial surfactants. *Appl. Microbiol. Biotechnol.* **1999**, *52*, 154–162. [CrossRef]

21. Deleu, M.; Razafindralambo, H.; Popineau, Y.; Jocques, P.; Thonart, P.; Paquot, M. Interfacial and emulsifying properties of lipopeptides from Bacillus subtilis. *Coll. Surf. A* **1999**, *152*, 3–10. [CrossRef]

22. Zdziennicka, A.; Jańczuk, B. Thermodynamic parameters of some biosurfactants and surfactants adsorption at water-air interface. *J. Mol. Liq.* **2017**, *243*, 236–244. [CrossRef]

23. Zdziennicka, A.; Szymczyk, K.; Krawczyk, J.; Jańczuk, B. Activity and thermodynamic parameters of some surfactants adsorption at the water–air interface. *Fluid Phase Equilib.* **2012**, *318*, 25–33. [CrossRef]

24. Zdziennicka, A.; Szymczyk, K.; Krawczyk, J.; Jańczuk, B. Critical micelle concentration of some surfactants and thermodynamic parameters of their micellization. *Fluid Phase Equilib.* **2012**, *322-323*, 126–134. [CrossRef]

25. Wang, H.; Gang, H.; Ye, R.; Mu, B. Interaction between biosurfactant surfactin and cationic surfactant cetyl trimethyl ammonium bromide in mixed micelle. *Colloid Polym. Sci.* **2014**, *292*, 3169–3176. [CrossRef]

26. Jian, H.L.; Liao, X.X.; Zhu, L.W.; Zhang, W.M.; Jiang, J.X. Synergism and foaming properties in binary mixtures of a biosurfactant derived from Camellia oleifera Abel and synthetic surfactants. *J. Colloid Interface Sci.* **2011**, *359*, 487–492. [CrossRef]

27. Rosen, M.J. *Surfactants and Interfacial Phenomena*, 3rd ed.; Wiley Intersccience: New York, NY, USA, 2004.

28. Zdziennicka, A.; Krawczyk, J.; Jańczuk, B. Volumetric properties of rhamnolipid and surfactin at different temperatures. *J. Mol. Liq.* **2018**, *255*, 562–571. [CrossRef]

29. Van Oss, C.J.; Constanzo, P.M. Adhesion of anionic surfactants to polymer surfaces and low-energy materials. *J. Adhes. Sci. Technol.* **1992**, *4*, 477–487. [CrossRef]

30. Rekiel, E.; Zdziennicka, A.; Jańczuk, B. Adsorption of surfactin at water with ethanol mixture-air interface. *J. Mol. Liq.* **2020**, *300*, 112240. [CrossRef]

31. Rekiel, E.; Zdziennicka, A.; Jańczuk, B. Adsorption properties of rhamnolipid and ethanol at water/ethanol solution-air interface. *J. Mol. Liq.* **2020**, *308*, 113080. [CrossRef]

32. Szymczyk, K.; Zdziennicka, A.; Jańczuk, B. Properties of some nonionic fluorocarbon surfactants and their mixtures with hydrocarbon ones. *Adv. Coll. Interface Sci.* **2021**, *292*, 102421. [CrossRef] [PubMed]

33. Szaniawska, M.; Szymczyk, K.; Zdziennicka, A.; Jańczuk, B. Adsorption properties and composition of binary Kolliphor mixtures at the water–air interface at different temperatures. *Molecules* **2022**, *27*, 877. [CrossRef] [PubMed]

34. Fainerman, V.B.; Miller, R.; Aksenenko, E.V. Simple model for prediction of surface tension of mixed surfactant solutions. *Adv. Colloid Interface Sci.* **2002**, *96*, 339–359. [CrossRef]

35. Fainerman, V.B.; Miller, R. Simple method to estimate surface tension of mixed surfactant solutions. *J. Phys. Chem. B* **2001**, *105*, 11432–11438. [CrossRef]

36. Adamson, W.; Gast, A.P. *Physical Chemistry of Surfaces*, 6th ed.; Wiley Interscience: New York, NY, USA, 1997.

37. Szymczyk, K.; Zdziennicka, A.; Krawczyk, J.; Jańczuk, B. Behaviour of cetyltrimethyl-ammonium bromide, Triton X-100 and Triton X-114 in mixed monolayer at the (water–air) interface. *J. Chem. Therm.* **2014**, *69*, 85–92. [CrossRef]

38. Rosen, M.J.; Hua, X.Y. Surface concentrations and molecular interactions in binary mixtures of surfactants. *J. Colloid Interface Sci.* **1982**, *86*, 164–172. [CrossRef]

39. Bergström, M.; Eriksson, J.C. Theoretical analysis of synergistic effects in mixed surfactant systems. *Langmuir* **2000**, *16*, 7173–7181. [CrossRef]
40. Szymczyk, K. The properties of binary mixtures of ethoxylated octyl phenols with ethoxylated fluorinated alkanols at the water/air interface. *J. Surf. Deterg.* **2011**, *14*, 415–423. [CrossRef]
41. Atkins, P.; de Paula, J.; Keeler, J. *Physical Chemistry*, 11th ed.; Oxford University Press: Oxford, UK, 2017; pp. 136–147.

Table S1. The values of the the mole fraction of the surfactants in the mixed monolayer (x_1^S − TX165, x_2^S − RL), parameter of intermolecular interaction (β^σ), activity coefficients (f_1^S and f_2^S) and Gibbs excess free energy of mixing (G_{mix}^E).

γ_{LV} [mN/m]	x_1^S	x_2^S	β^σ	f_1^S	f_2^S	G_{mix}^E [kJ/mol]
			$x_2^b = 0.2$			
70	0.6607	0.3393	-2.0802	0.7870	0.4033	-1.1360
65	0.6654	0.3346	-2.3366	0.7698	0.3554	-1.2673
60	0.6539	0.3461	-1.3074	0.8550	0.5718	-0.7208
55	0.4152	0.5848	-2.3955	0.4408	0.6617	-1.4169
			$x_2^b = 0.4$			
70	0.5655	0.4345	-0.6910	0.8777	0.8017	-0.4136
65	0.5406	0.4594	-3.8980	0.4393	0.3201	-2.3582
60	0.5244	0.4756	0.8195	1.2036	1.2528	0.4979
55	0.3418	0.6582	-3.3947	0.2298	0.6726	-1.8604
			$x_2^b = 0.6$			
70	0.4189	0.5811	-0.7973	0.7640	0.8695	-0.4728
65	0.3984	0.6016	0.3979	1.1549	1.0652	0.2323
60	0.3472	0.6528	-0.3991	0.8436	0.9530	-0.2203
55	0.2105	0.7895	-2.1039	0.2694	0.9110	-0.8516
			$x_2^b = 0.8$			
70	0.2840	0.7160	-1.1865	0.5443	0.9088	-0.5877
65	0.2620	0.7380	-0.5808	0.7288	0.9609	-0.2736
60	0.2339	0.7661	-1.0286	0.5468	0.9453	-0.4489
55	0.1736	0.8264	-3.0037	0.1286	0.9135	-1.0497

Table S2. The values of the the mole fraction of the surfactants in the mixed monolayer (x_1^S – TX165, x_2^S – SF), parameter of intermolecular interaction (β^σ) activity coefficients (f_1^S and f_2^S) and Gibbs excess free energy of mixing (G_{mix}^E).

γ_{LV} [mN/m]	x_1^S	x_2^S	β^σ	f_1^S	f_2^S	G_{mix}^E [kJ/mol]
			$x_2^b = 0.2$			
70	0.3518	0.6482	0.3484	1.1576	1.0441	0.1935
65	0.2600	0.7400	0.6884	1.4578	1.0476	0.3226
60	0.1331	0.8669	0.9803	2.0890	1.0175	0.2756
55	0.0585	0.9415	-0.0932	0.9207	0.9997	-0.0125
			$x_2^b = 0.4$			
70	0.1262	0.8738	0.5973	1.5779	1.0096	0.1604
65	0.1139	0.8861	0.4603	1.4353	1.0060	0.1131
60	0.0722	0.9278	0.4892	1.5237	1.0026	0.0798
55	0.0522	0.9478	-1.0516	0.3888	0.9971	-0.1267
			$x_2^b = 0.6$			
70	0.1531	0.8469	-0.8491	0.5439	0.9803	-0.2682
65	0.0947	0.9053	-0.3074	0.7773	0.9972	-0.0642
60	0.0240	0.9760	0.7964	2.1353	1.0005	0.0455
55	0.0203	0.9797	-0.8086	0.4602	0.9997	-0.0391
			$x_2^b = 0.8$			
70	0.0989	0.9011	-1.3348	0.3383	0.9870	-0.2898
65	0.0534	0.9466	-0.6864	0.5406	0.9980	-0.0845
60	0.0114	0.9886	0.5553	1.7207	1.0001	0.0152
55	0.0097	0.9903	-1.0278	0.3650	0.9999	-0.0241

Table S3. The values of the the mole fraction of the surfactants in the mixed micelle (x_1^M- TX165, x_2^M − RL or SF), parameter of intermolecular interaction (β^M), activity coefficients (f_1^M and f_2^M) and Gibbs excess free energy of mixing($G_{mix}^{E,m}$).

			TX165 + SF			
x_2^b	x_1^M	x_2^M	β^M	f_1^M	f_2^M	$G_{mix}^{E,m}$ [kJ/mol]
0.2	0.2597	0.7403	-3.3116	0.1628	0.7998	-1.5509
0.4	0.2463	0.7537	-4.9288	0.0608	0.7416	-2.2286
0.6	0.2192	0.7808	-5.6293	0.0323	0.7629	-2.3474
0.8	0.1371	0.8629	-4.9207	0.0256	0.9117	-1.4177
			TX165 + RL			
x_2^b	x_1^M	x_2^M	β^M	f_1^M	f_2^M	$G_{mix}^{E,m}$ (kJ/mol)
0.2	0.4017	0.5983	-2.8276	0.3634	0.6337	-1.6554
0.4	0.2374	0.7626	-1.4631	0.4270	0.9209	-0.6452
0.6	0.1492	0.8508	-1.4336	0.3543	0.9686	-0.4434
0.8	0.1369	0.8631	-2.5969	0.1445	0.9525	-0.7474

Figure S1. A plot of the surface tension (γ_{LV}) of the aqueous solution of RL and TX165 mixture at the constant RL concentration equal to 0.00625 mg/dm³ vs. the logarithm of the TX165 concentration (C_{TX165}) (a) and the logarithm of the total concentration of the TX165 + RL mixture (C_{12}) (b). Points 1 correspond to the measured values. Curves 2 and 2′ correspond to the value calculated from Eq. (1), curves 3, 4 and 5 correspond to the values calculated from Eqs. (3), (4) and (2), respectively.

Figure S2. A plot of the surface tension (γ_{LV}) of the aqueous solution of RL and TX165 mixture at the constant RL concentration equal to 5 mg/dm³ vs. the logarithm of the TX165 concentration (C_{TX165}) (a) and the logarithm of the total concentration of the TX165 + RL mixture (C_{12}) (b). Points 1 correspond to the measured values. Curves 2 and 2′ correspond to the values calculated from Eq. (1), curves 3 and 4 correspond to the values calculated from Eqs. (3) and (4), respectively.

Figure S3. A plot of the surface tension (γ_{LV}) of the aqueous solution of RL and TX165 mixture at the constant RL concentration equal to 40 mg/dm³ vs. the logarithm of the TX165 concentration (C_{TX165}) (a) and the logarithm of the total concentration of the TX165 + RL mixture (C_{12}) (b). Points 1 correspond to the measured values. Curves 2 and 2′ correspond to the values calculated from Eq. (1), curves 3 and 4 correspond to the values calculated from Eqs. (3) and (4), respectively.

Figure S4. A plot of the surface tension (γ_{LV}) of the aqueous solution of SF and TX165 mixture at the constant SF concentration equal to 0.00625 mg/dm³ vs. the logarithm of the TX165 concentration (C_{TX165}) (a) and the logarithm of the total concentration of the TX165 + SF mixture (C_{12}) (b). Points 1 correspond to the measured values. Curves 2 and 2' correspond to the values calculated from Eq. (1), curves 3, 4 and 5 correspond to the values calculated from Eqs. (3), (4) and (2), respectively.

Figure S5. A plot of the surface tension (γ_{LV}) of aqueous solution of SF and TX165 mixture at the constant SF concentration equal to 5 mg/dm³ vs. the logarithm of the TX165 concentration (C_{TX165}) (a) and the logarithm of the total concentration of the TX165 + SF mixture (C_{12}) (b). Points 1 correspond to the measured values. Curves 2 and 2′ correspond to the values calculated from Eq. (1), curves 3 and 4 correspond to the values calculated from Eqs. (3) and (4), respectively.

Figure S6. A plot of the surface tension (γ_{LV}) of the aqueous solution of SF and TX165 mixture at the constant SF concentration equal to 40 mg/dm³ vs. the logarithm of the TX165 concentration (C_{TX165}) (a) and the logarithm of the total concentration of the TX165 + SF mixture (C_{12}) (b). Points 1 correspond to the measured values. Curves 2 and 2′ correspond to the values calculated from Eq. (1), curves 3 and 4 correspond to the values calculated from Eqs. (3) and (4), respectively.

Figure S7. A plot of the surface tension (γ_{LV}) of the aqueous solution of RL and TX165 mixture at the constant TX165 concentration equal to 5×10^{-7} mole/dm^3 vs. the logarithm of the RL concentrations (C_{RL}) (a) and the logarithm of the total concentration of the TX165 + RL mixture (C_{12}) (b). Points 1 correspond to the measured values. Curves 2 and 2' correspond to the values calculated from Eq. (1), curves 3, 4 and 5 correspond to the values calculated from Eqs. (3), (4) and (2), respectively.

Figure S8. A plot of the surface tension (γ_{LV}) of the aqueous solution of RL and TX165 mixture at the constant TX165 concentration equal to 2×10^{-4} mole/dm³ vs. the logarithm of the RL concentration (C_{RL}) (a) and the logarithm of the total concentration of the TX165 + RL mixture (C_{12}) (b). Points 1 correspond to the measured values. Curves 2 and 2′ correspond to the values calculated from Eq. (1), curves 3 and 4 correspond to the values calculated from Eqs. (3) and (4), respectively.

Figure S9. A plot of the surface tension (γ_{LV}) of the aqueous solution of the RL and TX165 mixture at the constant TX165 concentration equal to 1×10^{-3} mole/dm³ vs. the logarithm of the RL concentration (C_{RL}). Points 1 correspond to the measured values. Curves 2 and 3 correspond to the values calculated from Eqs. (3) and (4), respectively.

Figure S10. A plot of the surface tension (γ_{LV}) of the aqueous solution of the SF and TX165 mixture at the constant TX165 concentration equal to 5×10^{-7} mole/dm³ vs. the logarithm of the SF concentration (C_{SF}) (a) and the logarithm of the total concentration of the TX165 + SF mixture (C_{12}) (b). Points 1 correspond to the measured values. Curves 2 and 2′ correspond to the values calculated from Eq. (1), curves 3 and 4 correspond to the values calculated from Eqs. (3) and (4), respectively.

Figure S11. A plot of the surface tension (γ_{LV}) of the aqueous solution of the SF and TX165 mixture at the constant TX165 concentration equal to 2 × 10^{-4} mole/dm³ vs. the logarithm of the SF concentration (C_{SF}). Points 1 correspond to the measured values. Curves 2, 3 and 4 correspond to the values calculated from Eqs. (1), (3) and (4), respectively.

Figure S12. A plot of the surface tension (γ_{LV}) of the aqueous solution of the SF and TX165 mixture at the constant TX165 concentration equal to 1×10^{-3} mole/dm³ vs. the logarithm of the SF concentration (C_{SF}). Points 1 correspond to the measured values. Curves 2, 3 and 4 correspond to the values calculated from Eqs. (1), (3) and (4), respectively.

Figure S13. A plot of the constant y_0 in Eq. (1) for the TX165 + RL (curve 1) and TX165 + SF (curve 2) aqueous solutions vs. the biosurfactant mole fraction in the mixture in the bulk phase (x_2^b).

Figure S14. A plot of the constant A_1 in Eq. (1) for the TX165 + RL (curve 1) and TX165 + SF (curve 2) aqueous solutions vs. the biosurfactant mole fraction in the mixture in the bulk phase (x_2^b).
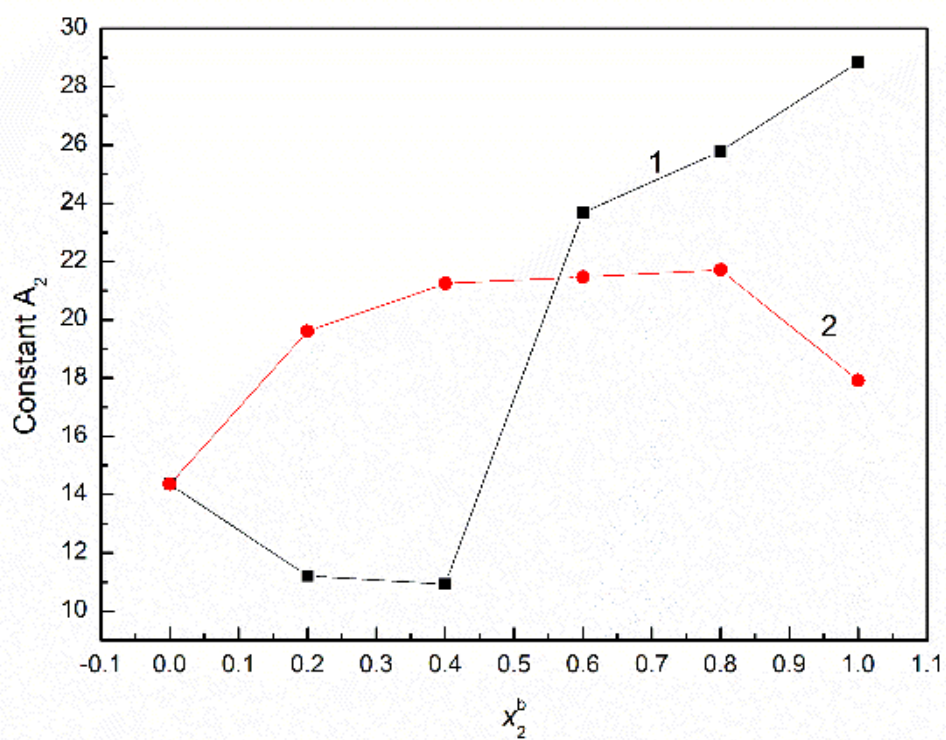
Figure S15. A plot of the constant A_2 in Eq. (1) for the TX165 + RL (curve 1) and TX165 + SF (curve 2) aqueous solutions vs. the biosurfactant mole fraction in the mixture in the bulk phase (x_2^b).
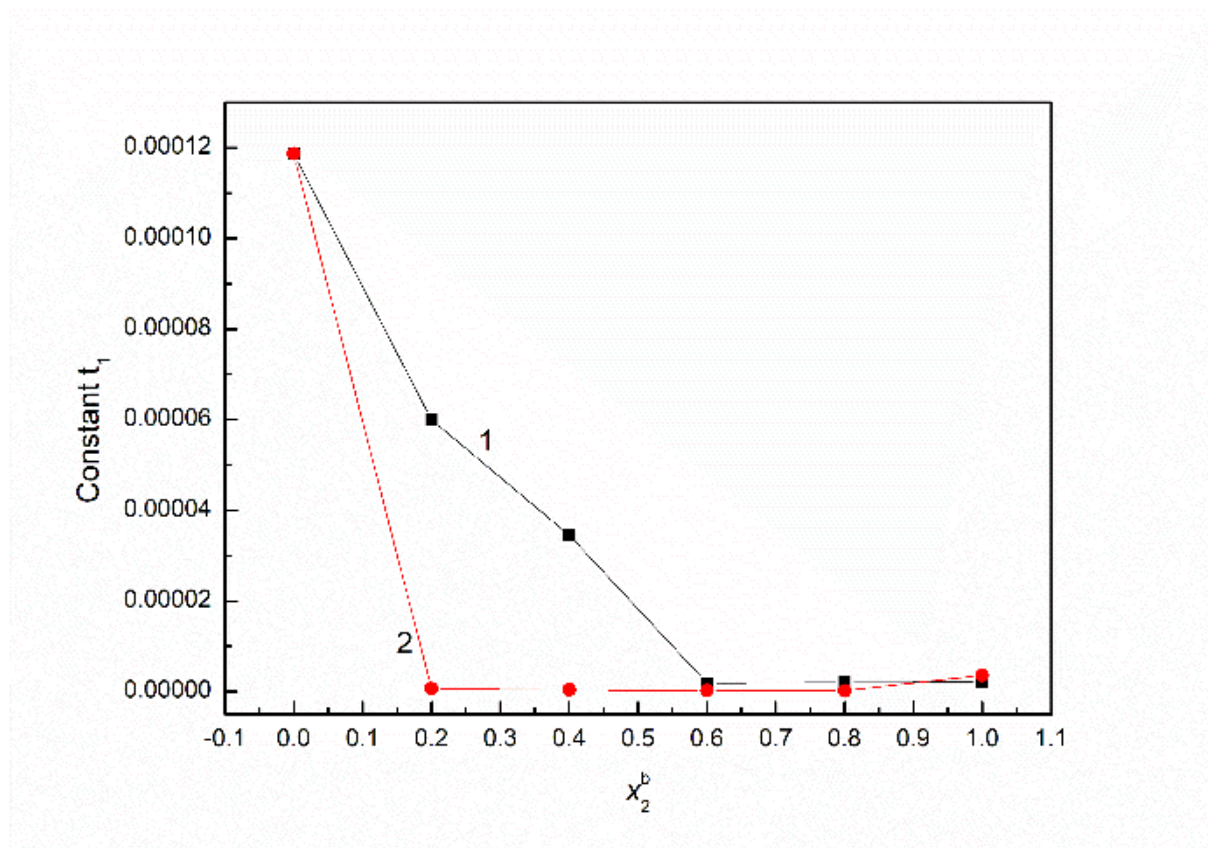
Figure S16. A plot of the constant t_1 in Eq. (1) for the TX165 + RL (curve 1) and TX165 + SF (curve 2) aqueous solutions vs. the biosurfactant mole fraction in the mixture in the bulk phase (x_2^b).
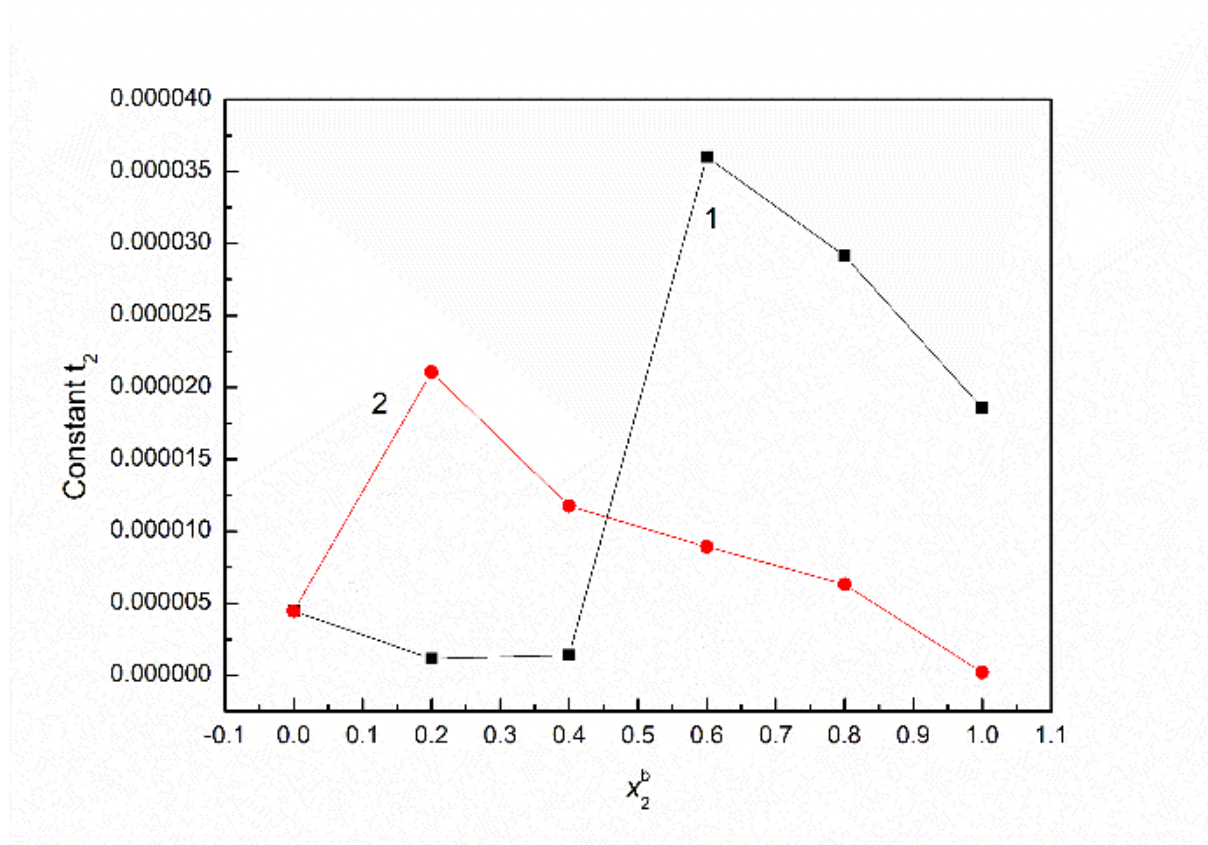
Figure S17. A plot of the constant t_2 in Eq. (1) for the TX165 + RL (curve 1) and TX165 + SF (curve 2) aqueous solutions vs. the biosurfactant mole fraction in the mixture in the bulk phase (x_2^b).

Figure S18. A plot of the surface tension (γ_{LV}) of the aqueous solution of the RL and TX165 mixture at the RL mole fraction equal to 0.2 vs. the logarithm of the total concentration of the TX165 + RL mixture (C_{12}). Points 1 correspond to the measured values. Curves 2, 3, 4 and 5 correspond to the values calculated from Eqs. (2), (1), (3) and (4), respectively.

Figure S19. A plot of the surface tension (γ_{LV}) of the aqueous solution of the RL and TX165 mixture at the RL mole fraction equal to 0.4 vs. the logarithm of the total concentration of the TX165 + RL mixture (C_{12}). Points 1 correspond to the measured values. Curves 2, 3, 4 and 5 correspond to the values calculated from Eqs. (2), (1), (3) and (4), respectively.

Figure S20. A plot of the surface tension (γ_{LV}) of the aqueous solution of the RL and TX165 mixture at the RL mole fraction equal to 0.6 vs. the logarithm of the total concentration of the TX165 + RL mixture (C_{12}). Points 1 correspond to the measured values. Curves 2, 3, 4 and 5 correspond to the values calculated from Eqs. (2), (1), (3) and (4), respectively.
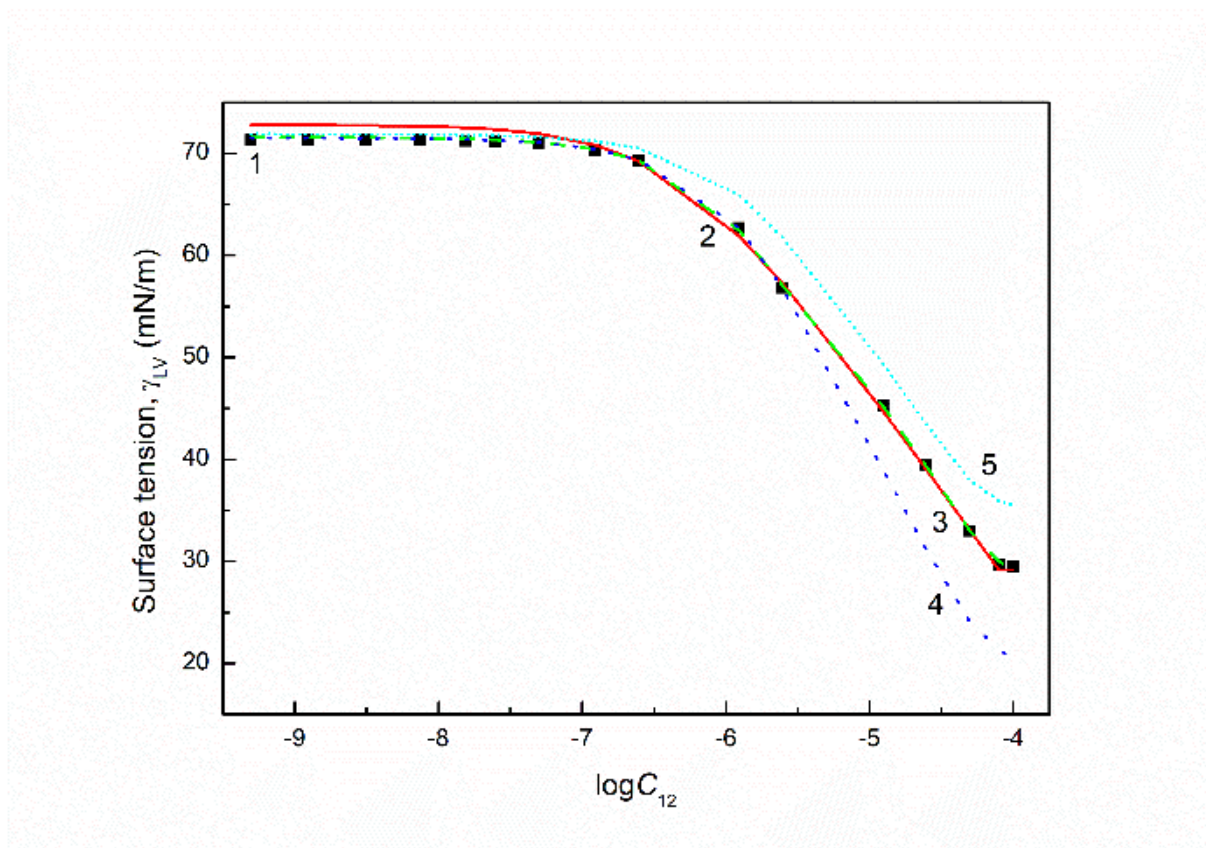
Figure S21. A plot of the surface tension (γ_{LV}) of the aqueous solution of the RL and TX165 mixture at the RL mole fraction equal to 0.8 vs. the logarithm of the total concentration of the TX165 + RL mixture (C_{12}). Points 1 correspond to the measured values. Curves 2, 3, 4 and 5 correspond to the values calculated from Eqs. (2), (1), (3) and (4), respectively.
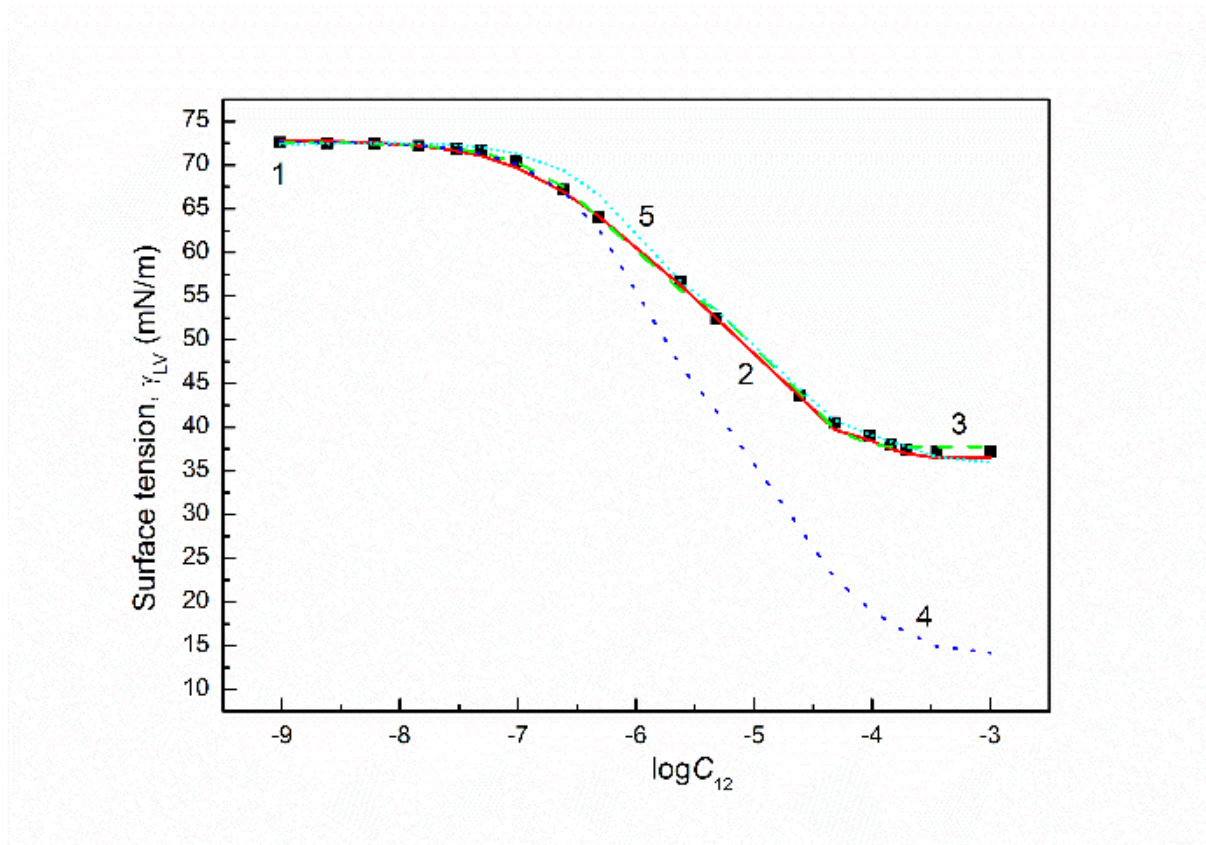
Figure S22. A plot of the surface tension (γ_{LV}) of the aqueous solution of the SF and TX165 mixture at the SF mole fraction equal to 0.2 vs. the logarithm of the total concentration of the TX165 + SF mixture (C_{12}). Points 1 correspond the measured values. Curves 2, 3, 4 and 5 correspond to the values calculated from Eqs. (2), (1), (3) and (4), respectively.

Figure S23. A plot of the surface tension (γ_{LV}) of the aqueous solution of the SF and TX165 mixture at the SF mole fraction equal to 0.4 vs. the logarithm of the total concentration of the TX165 + SF mixture (C_{12}). Points 1 correspond to the measured values. Curves 2, 3, 4 and 5 correspond to the values calculated from Eqs. (2), (1), (3) and (4), respectively.

Figure S24. A plot of the surface tension (γ_{LV}) of the aqueous solution of the SF and TX165 mixture at the SF mole fraction equal to 0.6 vs. the logarithm of the total concentration of the TX165 + SF mixture (C_{12}). Points 1 correspond to the measured values. Curves 2, 3, 4 and 5 correspond to the values calculated from Eqs. (2), (1), (3) and (4), respectively.

Figure S25. A plot of the surface tension (γ_{LV}) of the aqueous solution of the SF and TX165 mixture at the SF mole fraction equal to 0.8 vs. the logarithm of the total concentration of TX165 + SF mixture (C_{12}). Points 1 correspond to the measured values. Curves 2, 3, 4 and 5 correspond to the values calculated from Eqs. (2), (1), (3) and (4), respectively.

Figure S26. A plot of the constant a in the Szyszkowski equation (Eq. (2)) for the TX165 + RL (curve 1) and TX165 + SF (curve 2) aqueous solutions vs. the biosurfactant mole fraction in the mixture in the bulk phase (x_2^b).
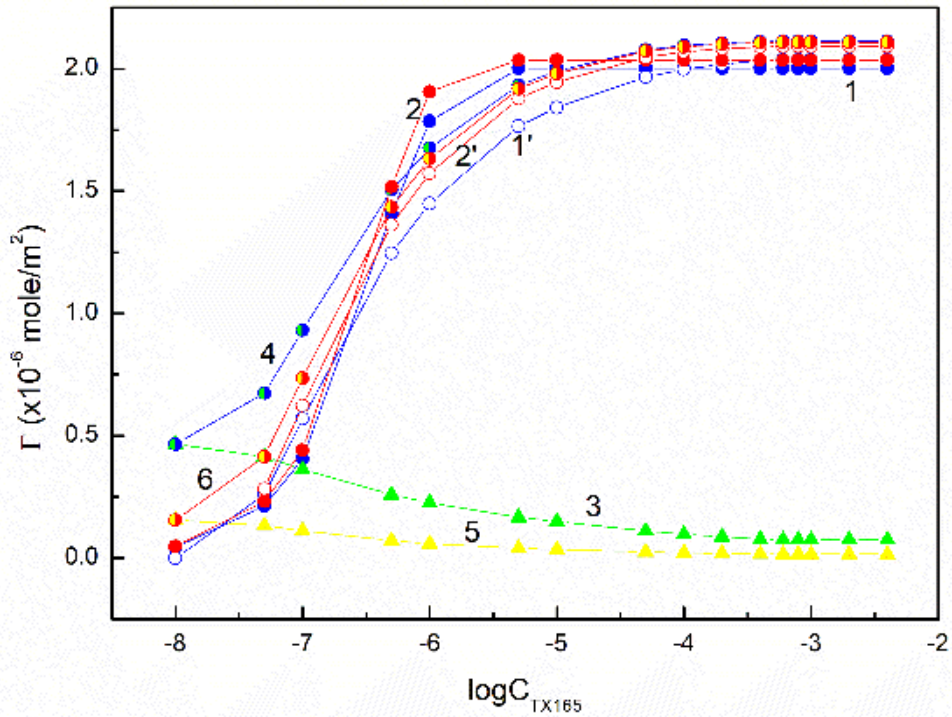
Figure S27. A plot of the surface concentration ($\varGamma$) of TX165 (curves 1, 1', 2, 2'), RL (curve 3) and SF (curve 5) vs. the logarithm of TX165 concentration (C_{TX165}) at the constant biosurfactant concentration equal to 0.00625 mg/dm³. Curves 1 and 2 correspond to the values calculated from Eq. (5), curves 1', 2' 3, 5 to the values calculated from Eq. (6). Curves 4 and 6 correspond to the sum values calculated from Eq. (6) for the TX165 + RL and TX165 + SF mixture, respectively.
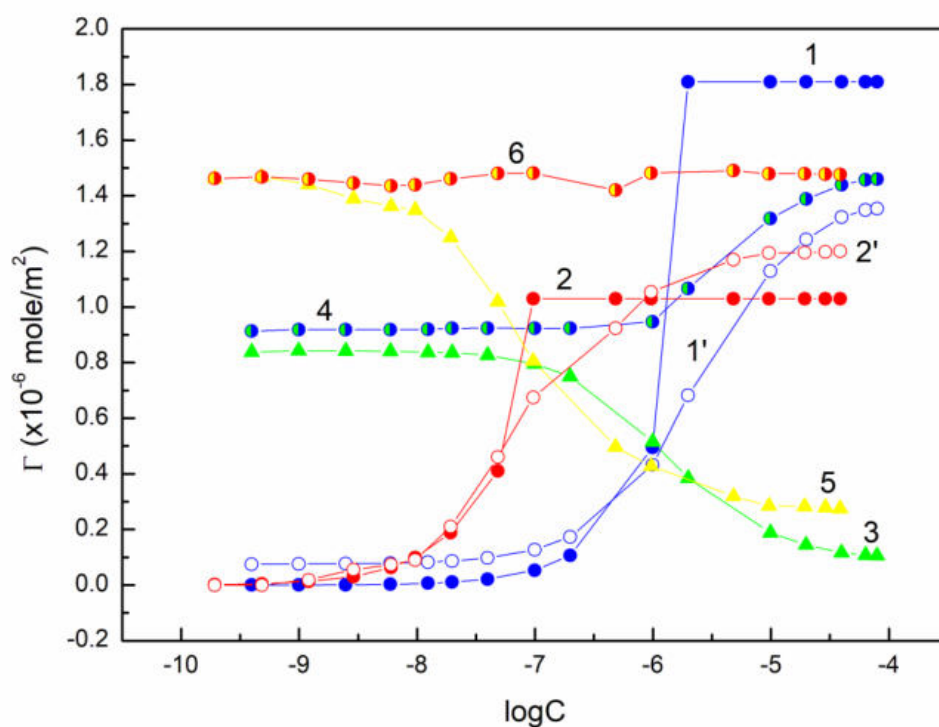
Figure S28. A plot of the surface concentration (Γ) of RL (curves 1, 1'), SF (curves 2, 2') and TX165 (curves 3 and 5) vs. the logarithm of biosurfactant concentration (C) at the constant TX165 concentration equal to 5×10^{-7} mole/dm³. Curves 1 and 2 correspond to the values calculated from Eq. (5), curves 1', 2' 3, 5 to the values calculated from Eq. (6). Curves 4 and 6 correspond to the sum values calculated from Eq. (6) for the TX165 + RL and TX165 + SF mixture, respectively.
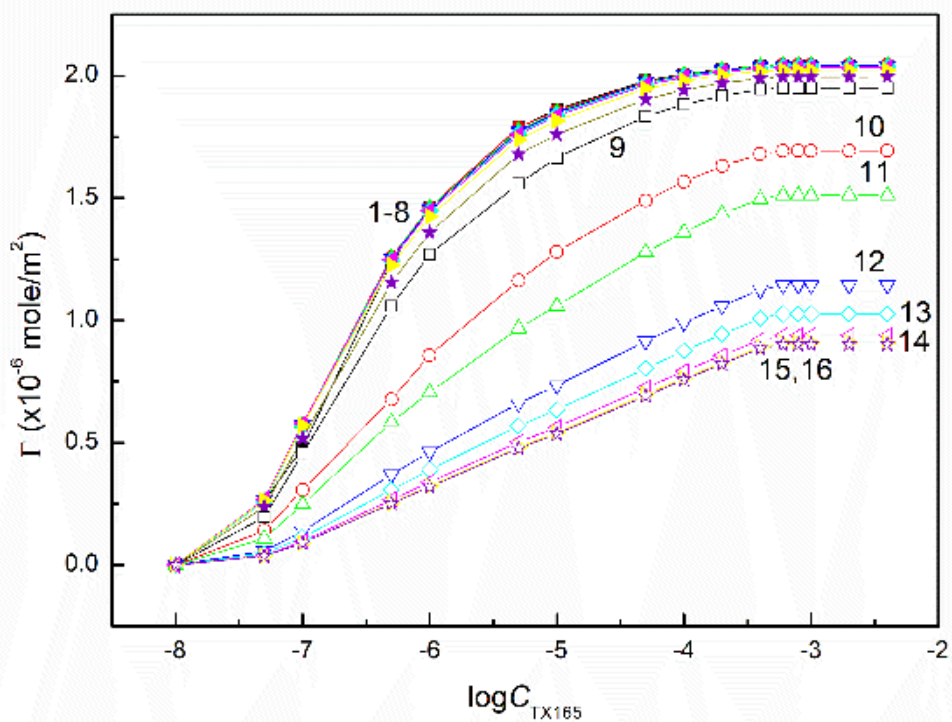
Figure S29. A plot of the surface concentration (Γ) of TX165 calculated from Eq. (6) in the TX165 + RL mixture vs. the logarithm of its concentration (C_{TX165}). Curves $1-16$ correspond to the constant RL concentration equal to 0.0002, 0.0005, 0.00125, 0.003, 0.00625, 0.01, 0.02, 0.05, 0.1, 0.5, 1, 5, 10, 20, 30 and 40 mg/dm³, respectively.
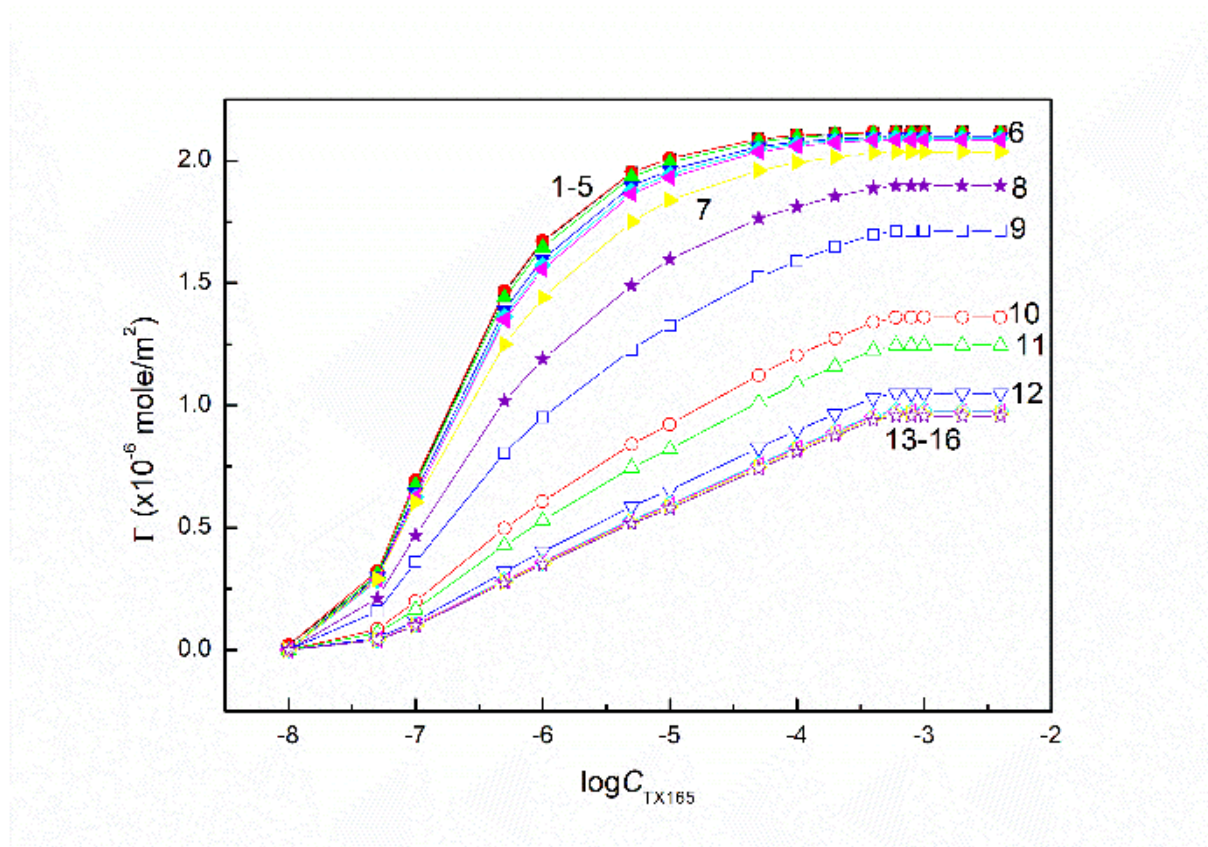
Figure S30. A plot of the surface concentration (Γ) of TX165 calculated from Eq. (6) in the TX165 + SF mixture vs. the logarithm of its concentration (C_{TX165}). Curves $1-16$ correspond to the constant SF concentration equal to 0.0002, 0.0005, 0.00125, 0.003, 0.00625, 0.01, 0.02, 0.05, 0.1, 0.5, 1, 5, 10, 20, 30 and 40 mg/dm³, respectively.
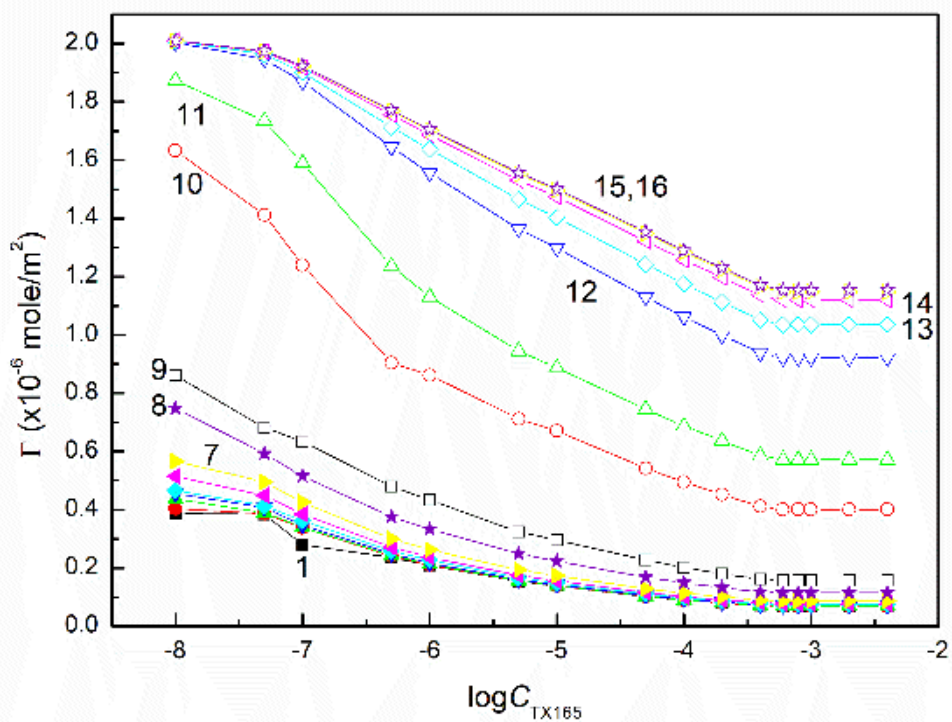
Figure S31. A plot of the surface concentration (Γ) of RL calculated from Eq. (6) in the TX165 + RL mixture vs. the logarithm of TX165 concentration (C_{TX165}). Curves 1 – 16 correspond to the constant RL concentration equal to 0.0002, 0.0005, 0.00125, 0.003, 0.00625, 0.01, 0.02, 0.05, 0.1, 0.5, 1, 5, 10, 20, 30 and 40 mg/dm³, respectively.
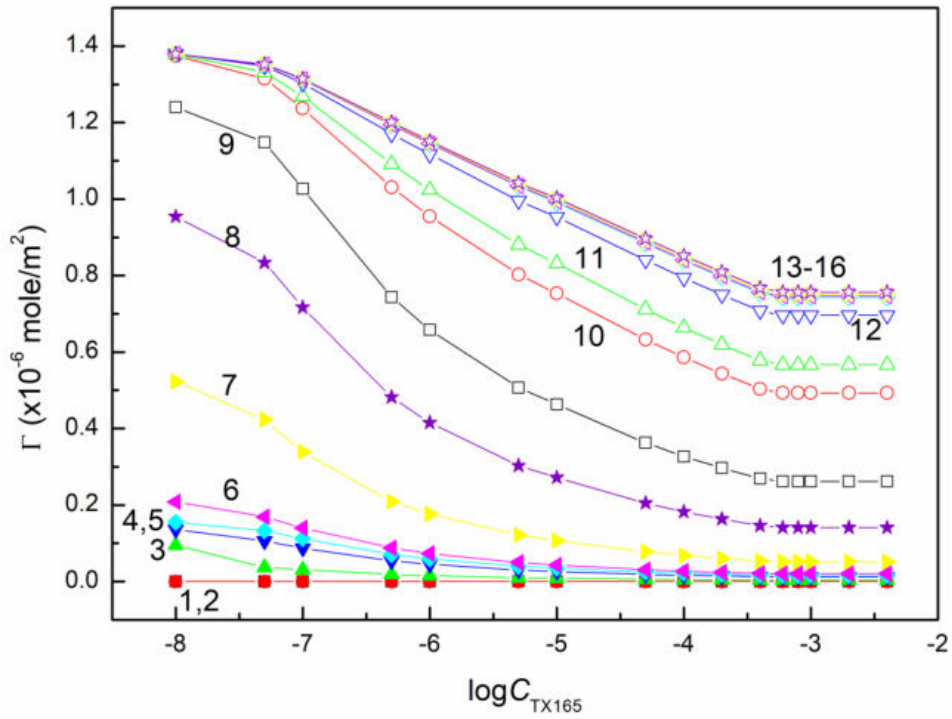
Figure S32. A plot of the surface concentration (Γ) of SF calculated from Eq. (6) in the TX165 + SF mixture vs. the logarithm of TX165 concentration (C_{TX165}). Curves 1 – 16 correspond to the constant SF concentration equal to 0.0002, 0.0005, 0.00125, 0.003, 0.00625, 0.01, 0.02, 0.05, 0.1, 0.5, 1, 5, 10, 20, 30 and 40 mg/dm³, respectively.
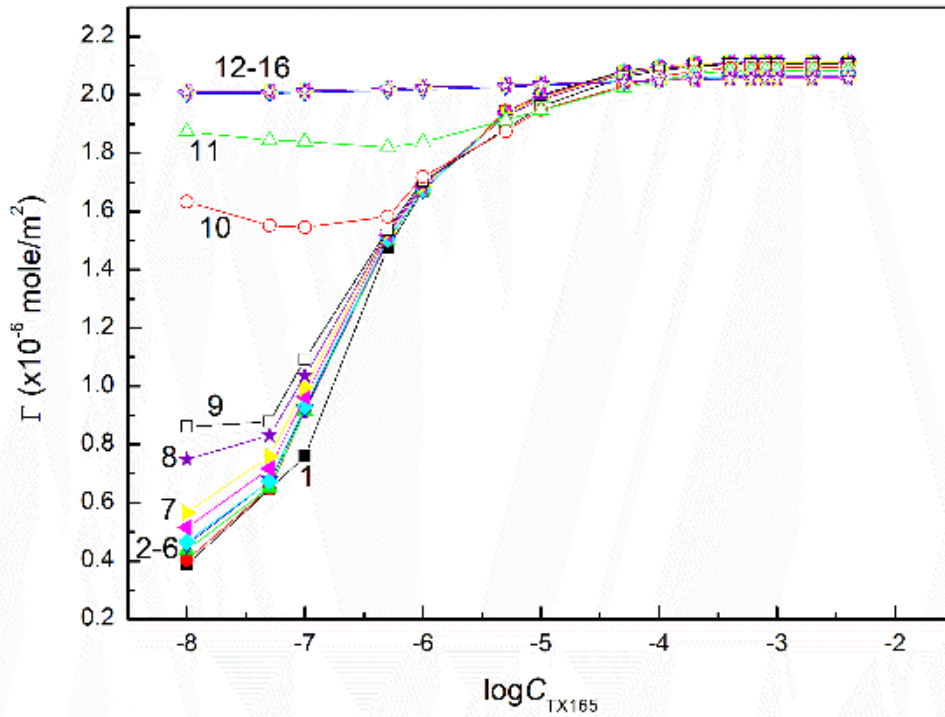
Figure S33. A plot of the total surface concentration (Γ) of the TX165 + RL mixture calculated from Eq. (6) vs. the logarithm of TX165 concentration (C_{TX165}). Curves 1 – 16 correspond to the constant RL concentration equal to 0.0002, 0.0005, 0.00125, 0.003, 0.00625, 0.01, 0.02, 0.05, 0.1, 0.5, 1, 5, 10, 20, 30 and 40 mg/dm³, respectively.
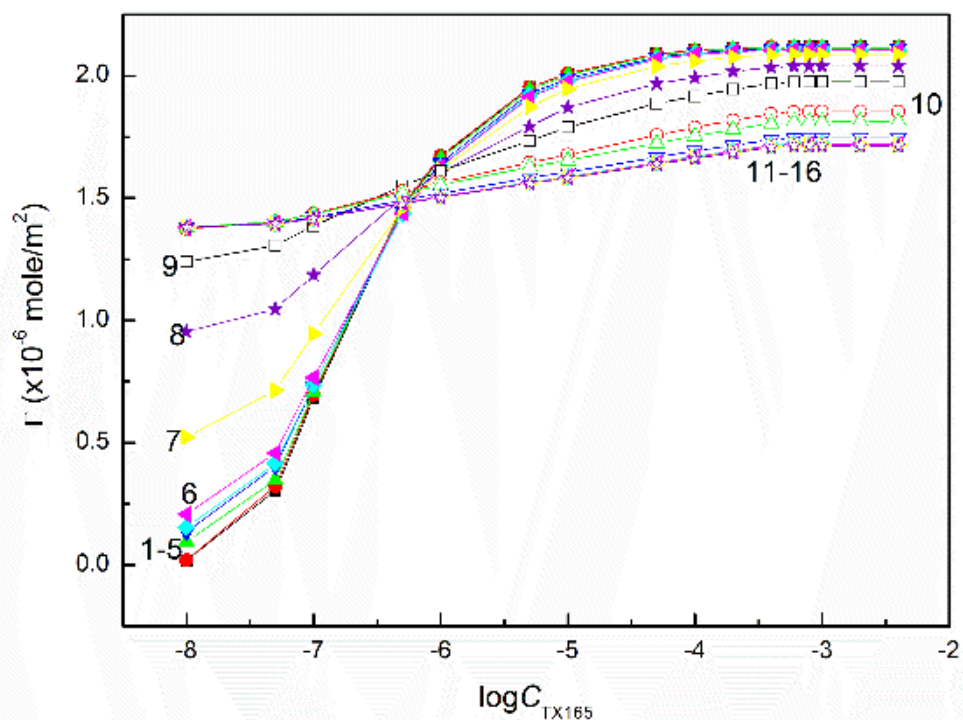
Figure S34. A plot of the total surface concentration (Γ) of the TX165 + SF mixture calculated from Eq. (6) vs. the logarithm of TX165 concentration (C_{TX165}). Curves 1 – 16 correspond to the constant SF concentration equal to 0.0002, 0.0005, 0.00125, 0.003, 0.00625, 0.01, 0.02, 0.05, 0.1, 0.5, 1, 5, 10, 20, 30 and 40 mg/dm³, respectively.
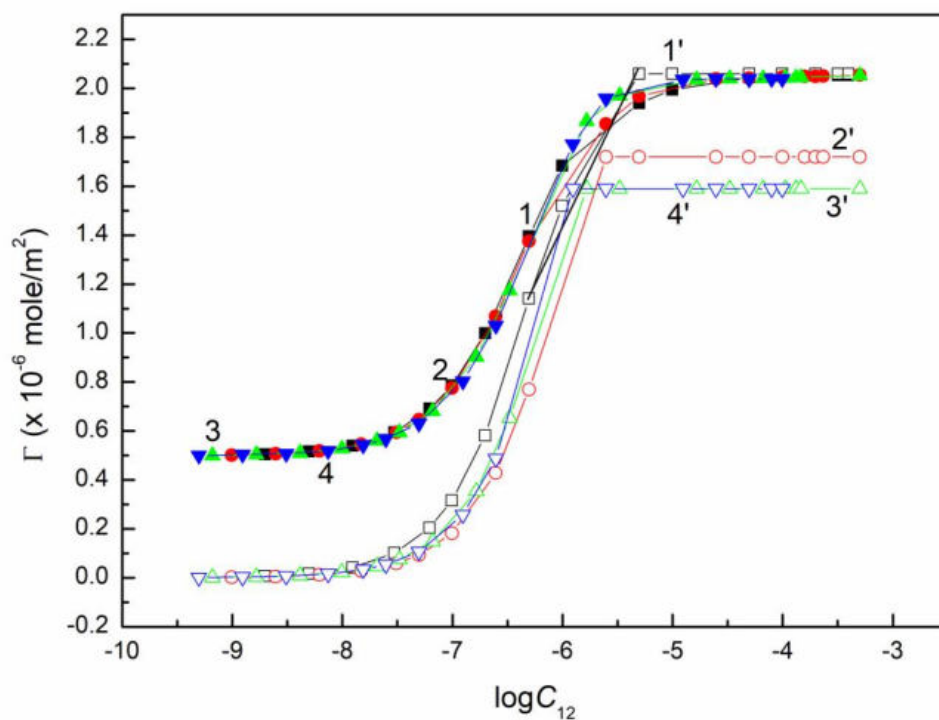
Figure S35. A plot of the total surface concentration (Γ) of the TX165 + RL mixture calculated from Eq. (6) (curves 1, 2, 3 and 4) and Gibbs surface concentration calculated from Eq. (5) vs. the logarithm of the total concentration of RL+TX165 mixture (C_{12}). Curves 1 and 1' correspond to the RL mole fraction in the mixture in the bulk phase equal to 0.2, curves 2 and 2' to 0.4, curves 3 and 3' to 0.6 and curves 4 and 4' correspond to the RL mole fraction in the mixture in the bulk phase equal 0.8, respectively.
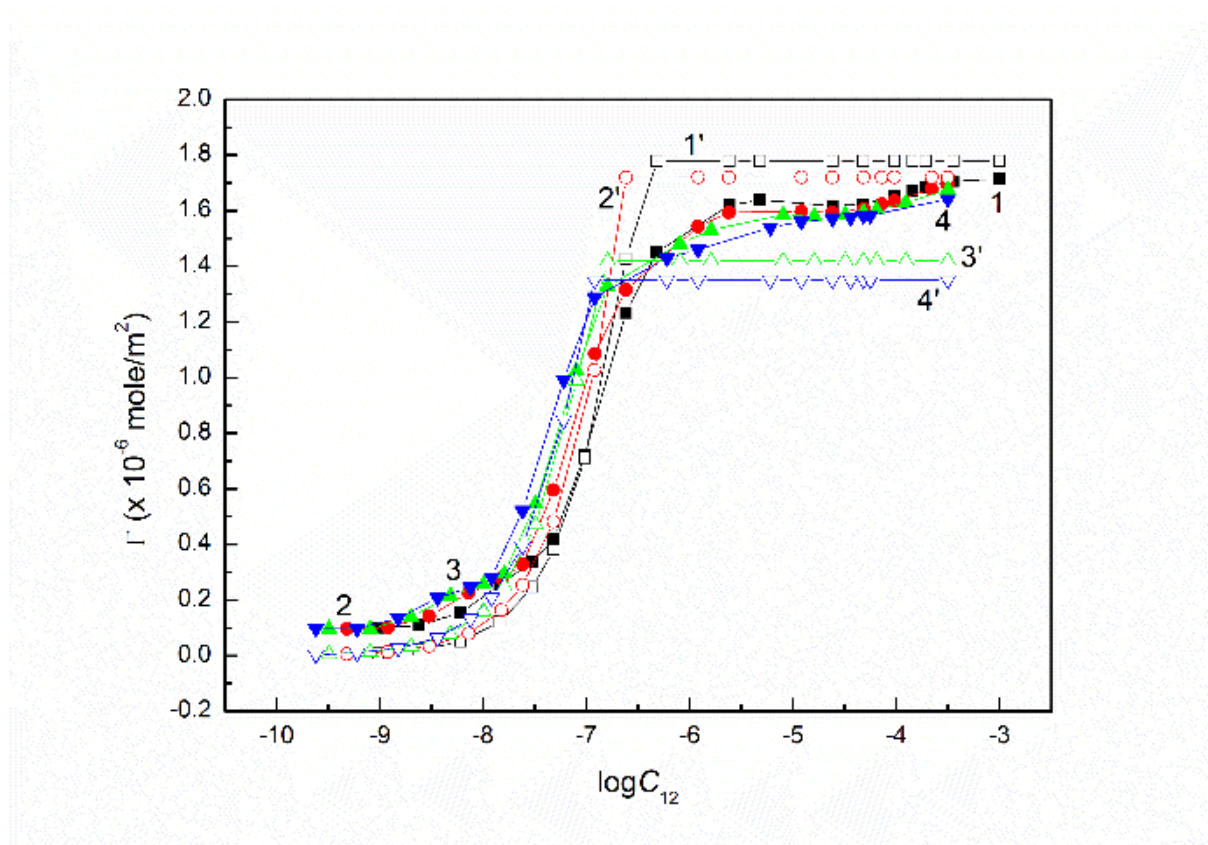
Figure S36. A plot of the total surface concentration (Γ) of the TX165 + SF mixture calculated from Eq. (6) (curves 1, 2, 3 and 4) and Gibbs surface concentration calculated from Eq. (5) vs. the logarithm of the total concentration of TX165 + SF mixture (C_{12}). Curves 1 and 1' correspond to the SF mole fraction in the mixture in the bulk phase equal to 0.2, curves 2 and 2' to 0.4, curves 3 and 3' to 0.6 and curves 4 and 4' correspond to the SF mole fraction in the mixture in the bulk phase equal 0.8, respectively.
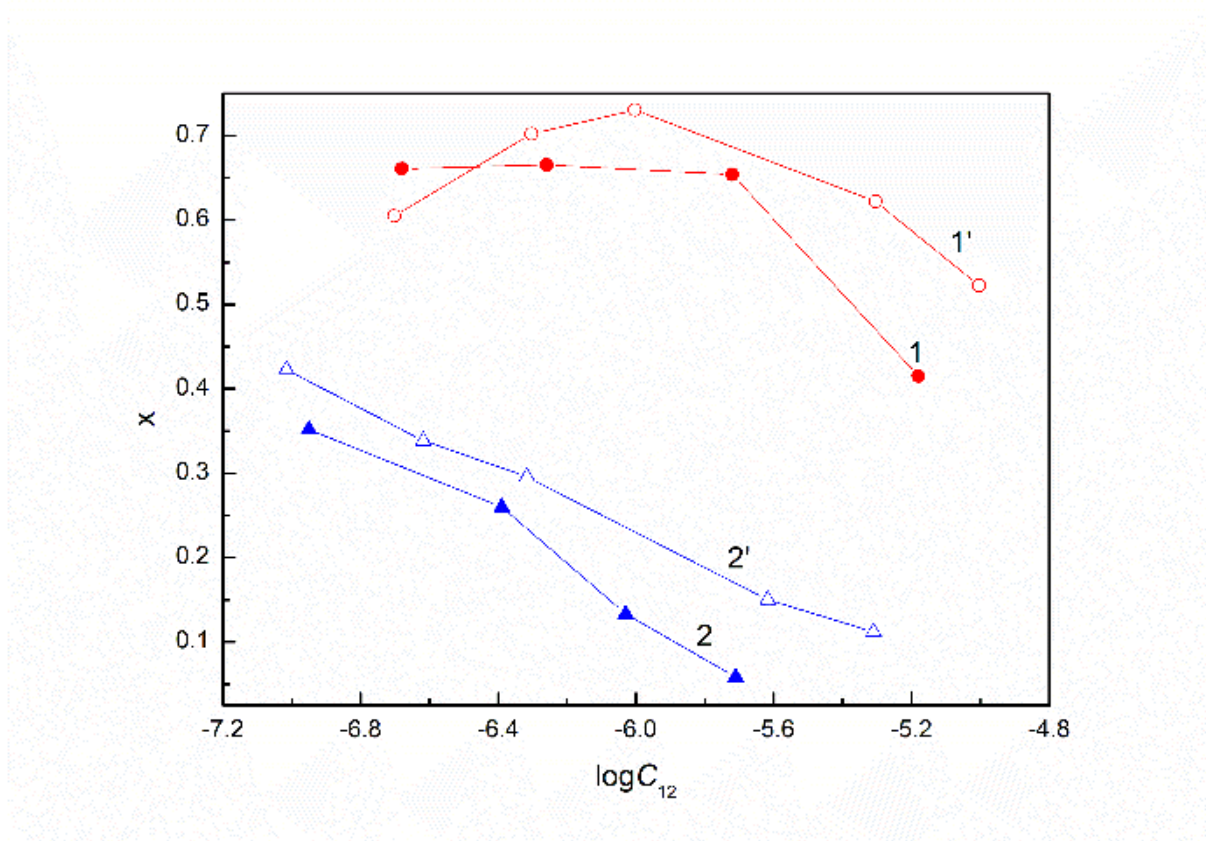
Figure S37. A plot of the TX165 mole fraction in the mixture with RL (curves 1 and 1′) and SF (curves 2 and 2′) (x) at the constant biosurfactant mole fraction in the mixture in the bulk phase equal to 0.2 vs. the total concentration of the TX165 + RL mixture (C_{12}). Curves 1 and 2 correspond to the values obtained from Eq. (7), curves 1′ and 2′ correspond to the values calculated from the expression $x_1^S = \dfrac{\pi_1}{\pi_1 + \pi_2}$
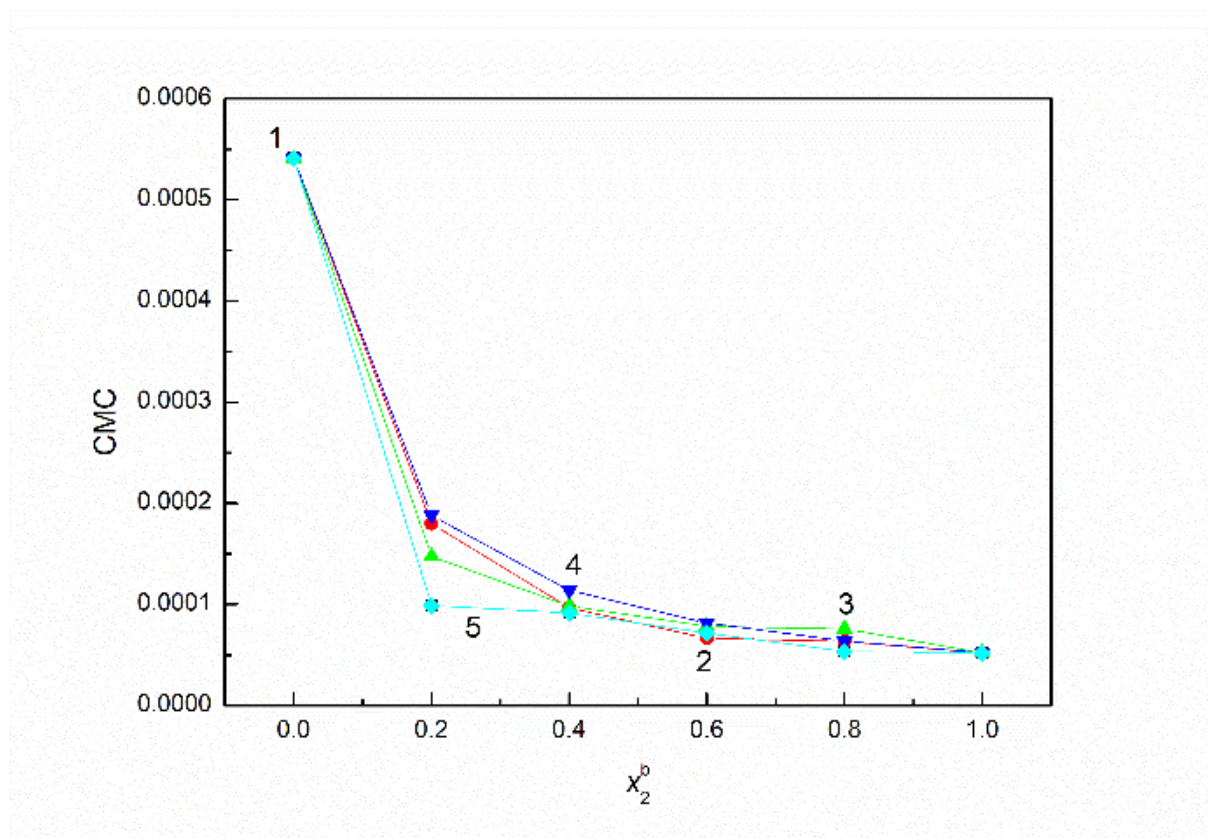
Figure S38. A plot of the CMC values of TX165 + RL and their mixtures vs. the RL mole fraction in the mixture in the bulk phase (x_2^b). Curve 1 corresponds to the CMC values of mixtures determined from surface tension isotherms, curves 2 and 3 correspond to the CMC calculated from Eq. (10), curves 4 and 5 to the values calculated from Eqs. (9) and (15).
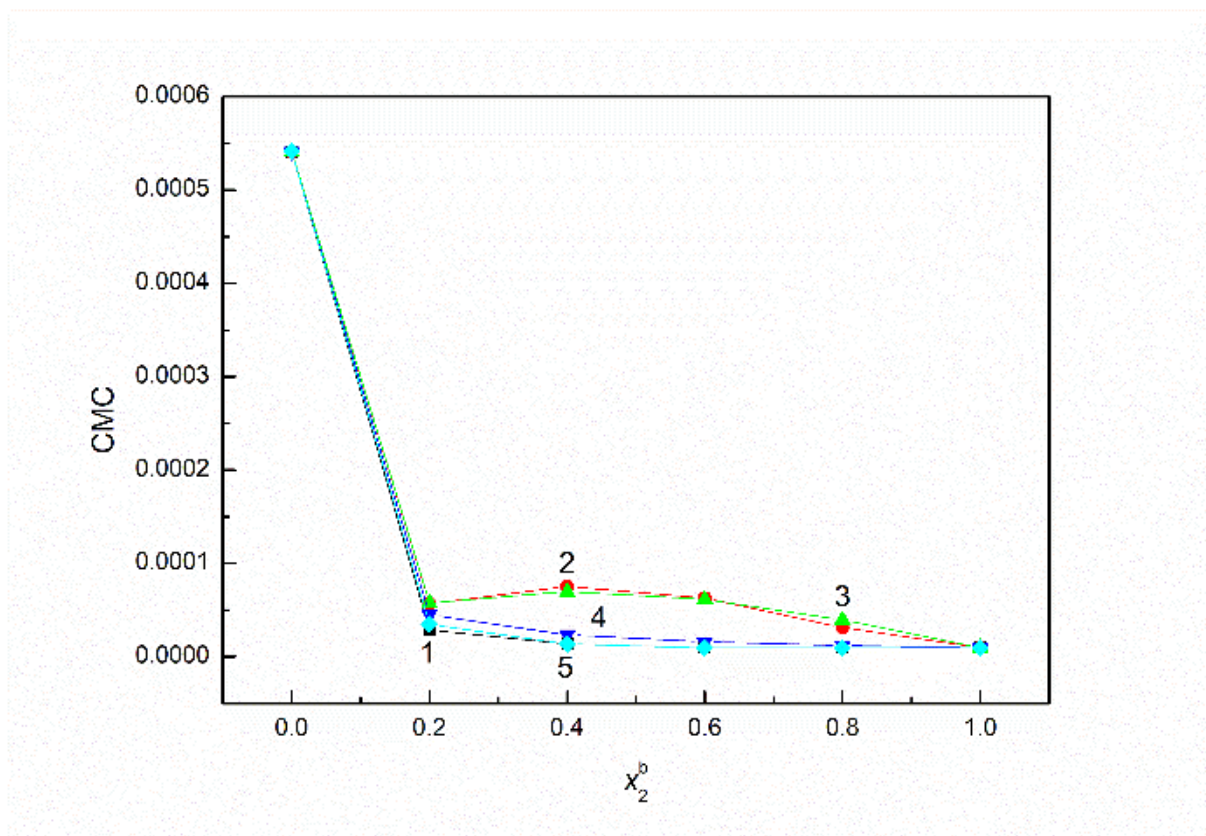
Figure S39. A plot of the CMC values of TX165 + SF and their mixtures vs. the SF mole fraction in the mixture in the bulk phase (x_2^b). Curve 1 corresponds to the CMC values of mixtures determined from surface tension isotherms, curves 2 and 3 correspond to the CMC calculated from Eq. (10), curves 4 and 5 to the values calculated from Eqs. (9) and (15).
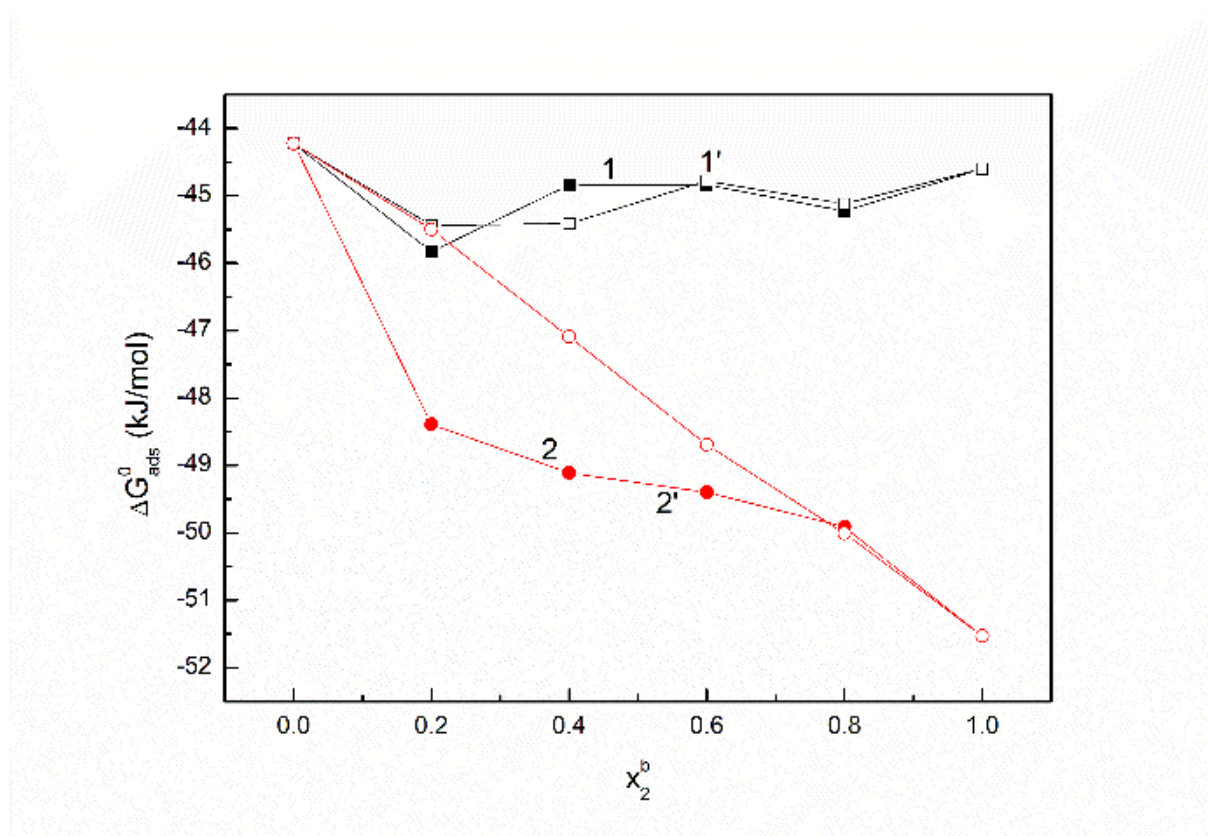
Figure S40. A plot of the Gibbs standard free energy of TX165 + RL (curves 1 and 1′) and TX165 + SF (curves 2 and 2′) adsorption at the water-air interface vs. the biosurfactant mole fraction in the mixture in the bulk phase (x_2^b). Curves 1 and 2 correspond to values calculated from Eq. (16), curves 1′ and 2′ to values calculated from Eq. (17), respectively.
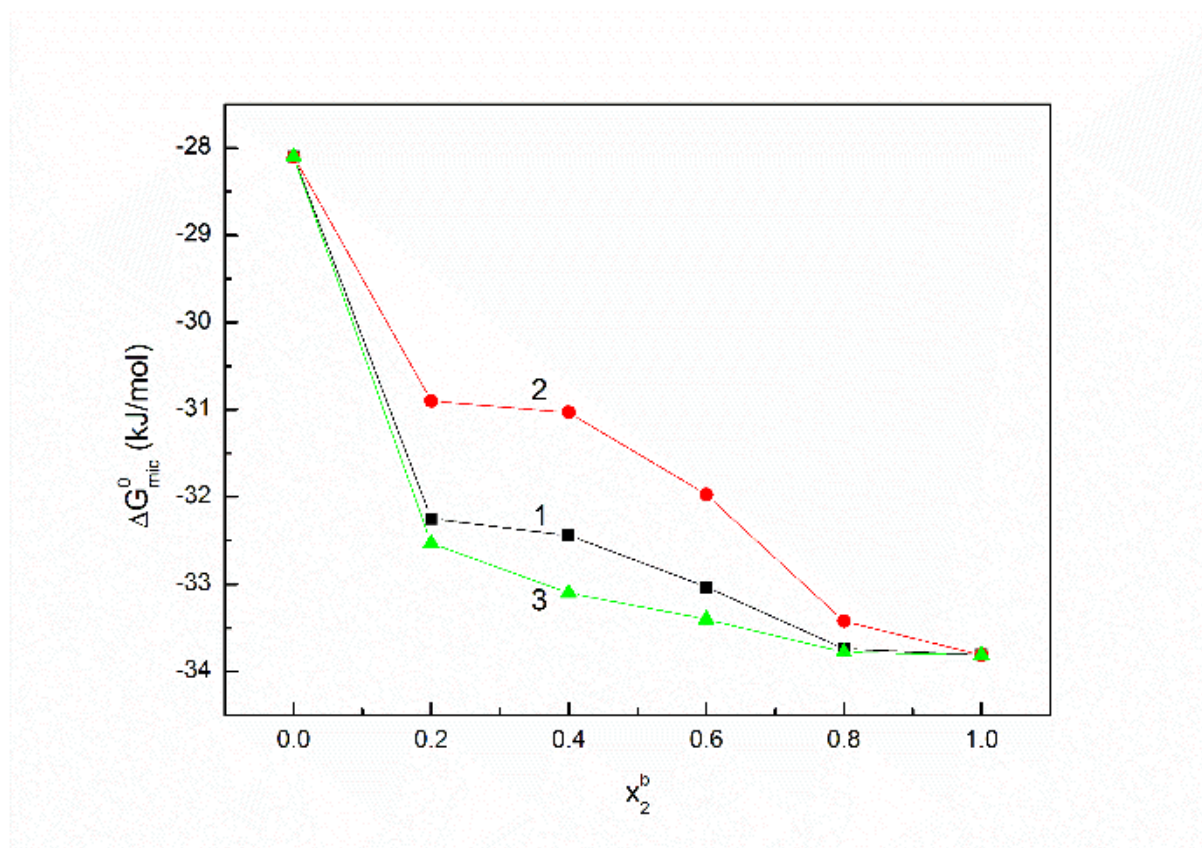
Figure S41. A plot of the Gibbs standard free energy of TX165 + RL micellization vs. the RL mole fraction in the mixture in the bulk phase (x_2^b) calculated from Eq. (21) (curve 1) and form Eq. (22) (curves 2 and 3). Curves 2 and 3 correspond to values calculated taking in the Eq. (22) x_1^b , x_2^b and x_1^M, x_2^M, respectively.
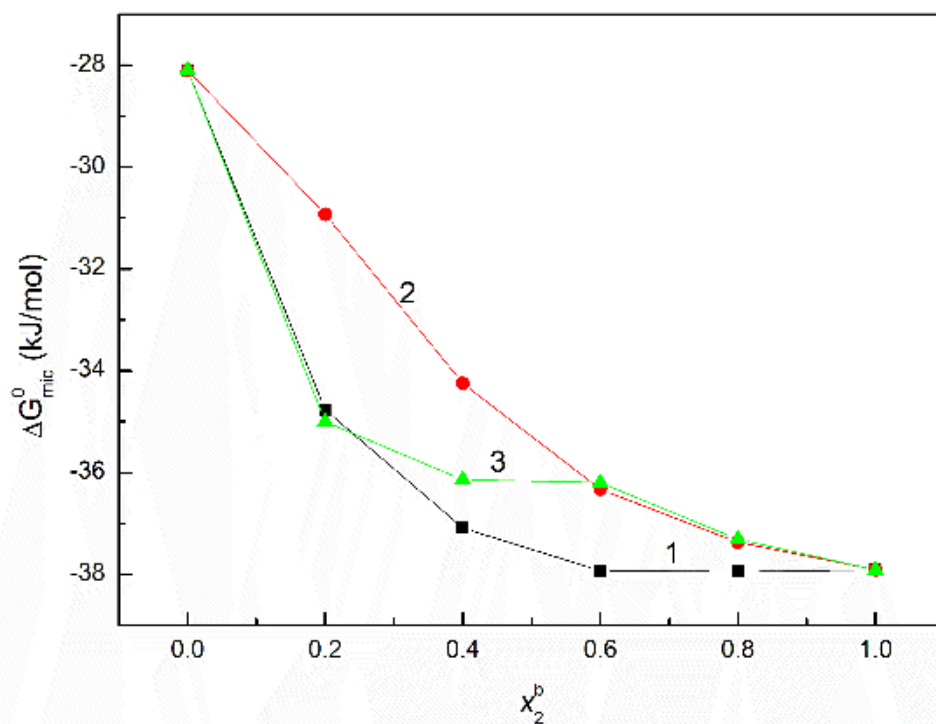
Figure S42. A plot of the Gibbs standard free energy of TX165 + SF micellization vs. the SF mole fraction in the mixture in the bulk phase (x_2^b) calculated from Eq. (21) (curve 1) and form Eq. (22) (curves 2 and 3). Curves 2 and 3 correspond to values calculated taking in the Eq. (22) x_1^b, x_2^b and x_1^M, x_2^M, respectively.

Prof. dr hab. Anna Zdziennicka
Katedra Zjawisk Międzyfazowych
Instytut Nauk Chemicznych
Wydział Chemii UMCS
Pl. M. Curie-Skłodowskiej 3
20-031 Lublin

Lublin, 17.01.2023

OŚWIADCZENIE

Oświadczam, że w pracy

E. Rekiel, **A. Zdziennicka***, K. Szymczyk, B. Jańczuk, *Thermodynamic Analysis of the Adsorption and Micellization Activity of the Mixtures of Rhamnolipid and Surfactin with Triton X-165.* Molecules, 2022, 27, 3600.

mój udział wynosił **30%** i polegał na przygotowaniu koncepcji badań i dobraniu metodologii, interpretacji oraz wizualizacji otrzymanych wyników, weryfikacji procesu pisania pracy oraz przeprowadzonych badań, analizie formalnej, pisaniu oryginalnej wersji manuskryptu, redagowaniu i edycji manuskryptu, współredagowaniu odpowiedzi na recenzje pracy oraz na prowadzeniu korespondencji z czasopismem.

Dr hab. Katarzyna Szymczyk, prof. UMCS
Katedra Zjawisk Międzyfazowych
Instytut Nauk Chemicznych
Wydział Chemii UMCS
Pl. M. Curie-Skłodowskiej 3
20-031 Lublin

Lublin, 17.01.2023

OŚWIADCZENIE

Oświadczam, że w pracy

E. Rekiel, A. Zdziennicka*, **K. Szymczyk**, B. Jańczuk, *Thermodynamic Analysis of the Adsorption and Micellization Activity of the Mixtures of Rhamnolipid and Surfactin with Triton X-165*. Molecules, 2022, 27, 3600.

mój udział wynosił **10%** i polegał na przygotowaniu koncepcji badań i dobraniu metodologii, interpretacji oraz wizualizacji otrzymanych wyników, weryfikacji procesu pisania pracy oraz przeprowadzonych badań, analizie formalnej, pisaniu oryginalnej wersji manuskryptu, redagowaniu i edycji manuskryptu oraz współredagowaniu odpowiedzi na recenzje pracy.

Katarzyna Szymczyk

Prof. dr hab. Bronisław Jańczuk
Katedra Zjawisk Międzyfazowych
Instytut Nauk Chemicznych
Wydział Chemii UMCS
Pl. M. Curie-Skłodowskiej 3
20-031 Lublin

OŚWIADCZENIE

Oświadczam, że w pracy

E. Rekiel, A. Zdziennicka*, K. Szymczyk, **B. Jańczuk**, *Thermodynamic Analysis of the Adsorption and Micellization Activity of the Mixtures of Rhamnolipid and Surfactin with Triton X-165.* Molecules, 2022, 27, 3600;

mój udział wynosił **10%** i polegał na przygotowaniu koncepcji badań i dobraniu metodologii, interpretacji otrzymanych wyników, weryfikacji procesu pisania pracy oraz przeprowadzonych badań, analizie formalnej, pisaniu oryginalnej wersji manuskryptu, redagowaniu i edycji manuskryptu, współredagowaniu odpowiedzi na recenzje pracy.

Załącznik 2

[D2] E. Rekiel, A. Zdziennicka, K. Szymczyk, B. Jańczuk*, *Wetting Properties of Rhamnolipid and Surfactin Mixtures with Triton X-165*. *Molecules*, 2022, 27, 4706.

Article

Wetting Properties of Rhamnolipid and Surfactin Mixtures with Triton X-165

Edyta Rekiel, Anna Zdziennicka, Katarzyna Szymczyk [ID] and Bronisław Jańczuk *[ID]

Department of Interfacial Phenomena, Faculty of Chemistry, Institute of Chemical Sciences,
Maria Curie-Skłodowska University in Lublin, Maria Curie-Skłodowska Sq. 3, 20-031 Lublin, Poland;
edyta.rekiel@poczta.umcs.lublin.pl (E.R.); anna.zdziennicka@mail.umcs.pl (A.Z.);
katarzyna.szymczyk@mail.umcs.pl (K.S.)
* Correspondence: bronislaw.janczuk@poczta.umcs.lublin.pl; Tel.: +48-81-537-5670

Abstract: The wetting properties of the rhamnolipid and surfactin mixtures with Triton X-165 were considered based on the contact angle measurements of their aqueous solution on the polytetrafluoroethylene (PTFE), polymethyl methacrylate (PMMA) and quartz (Q) surfaces. The obtained contact angle isotherms were described by the exponential function of the second order as well as by Szyszkowski equation in some cases. Using the contact angle isotherms of individual biosurfactants and TX165 as well as the earlier obtained isotherms of their surface tension the contact angle isotherms of the biosurfactants mixtures with TX165 were deduced. As follows the presence of the maxima on the contact angle isotherms of the biosurfactants mixtures with TX165 is justified. They do not prove negative adsorption of the biosurfactant and TX165 at the interfaces. However, the mutual exchange of the biosurfactant and TX165 molecules is observed in the layers at the interfaces. The concentration of the studied mixtures at the PTFE-solution interface was established to be close to that at the solution-air one but that at the PTFE-air is equal to zero. However, the concentration of the studied mixtures at the PMMA-solution and quartz-solution is greater than zero. The concentration at the PMMA(quartz)-air and PMMA(quartz)-solution interfaces is smaller than that at the solution-air one.

Keywords: contact angle; biosurfactants; nonionic surfactant; adhesion work; adsorption Gibbs free energy

1. Introduction

The demand for surfactants of useful activity in various fields is constantly growing. Unfortunately, many types of synthetic surfactants, besides their excellent wetting, emulsifying and foaming properties, so useful in their practical application, are dangerous for the natural environment [1]. This is due to the toxic properties of many synthetic surfactants and the difficulty of their degradation. For this reason, biosurfactants, which are mainly produced by bacteria or fungi, are of increasing interest. Biosurfactants are characterized by numerous specific properties, such as great resistance to the temperature, pH and electrolyte concentration changes [2,3]. They exhibit also great adsorption activity at the interfaces and aggregation activity in the water environment [4,5]. Apart from these properties, biosurfactants are characterized by small toxicity and large biodegradability [6]. For this reason, biosurfactants are increasingly used in the petroleum, pharmaceutical, medical and food industries [7–12]. Of the biosurfactants rhamnolipid (RL) and surfactin (SF) are the most widely applied [13–16]. Unfortunately, the relatively high cost of obtaining biosurfactants is an obstacle in their application. In order to reduce the cost of biosurfactants application in practice, their mixtures with non-toxic synthetic surfactants can be used [17–19]. The surfactants mixtures application is correlated, among others to their adsorption, aggregation and wetting properties. However, particularly their wetting properties are least known.

According to the Young's theory [20] the wettability of the solids by different liquids depends on the liquid-air, solid-air and solid-liquid interface tension. In the case of aqueous solution of the surfactants mixture the wettability of solids changes as a function of surfactants mixture concentration due to the adsorption of surfactants at the mentioned interfaces [21,22]. As a result of adsorption, the water-air and solid-water interface tensions change and the solid-air interface tension can also change [23]. These changes depend on the magnitude of the adsorption, the orientation of surfactant molecules in the interface layers, their packing and the composition of the adsorption mixed layers [24].

In the literature it is difficult to find the data about the adsorption properties of the surface layer at the solid-air and solid-water interfaces. In our previous studies [24] it was found out, among others, that in the case of the RL and SF mixtures with Triton X-165 (TX165) the concentration and composition of the mixed monolayer at the water-air interface can be predicted based on the isotherms of the surface tension of the aqueous solution of a particular component of the biosurfactants and TX165 mixtures as well as the tendency of this mixture towards adsorption at the water-air interface.

As mentioned above the wettability of the solids depends not only on the water-air interface tension but also the solid-air and solid-water ones. The contact angle of the liquid on the solids surface is a measure of the wetting process. Thus, the purpose of our studies was to measure the contact angle in the solid-solution drop-air system for the aqueous solution of the biosurfactant with the TX165 mixtures, the possibility to predict the contact angle for the solution mixtures based on the isotherms of the contact angle of individual mixture components as well as the adsorption amount at the solid-air and solid-water interfaces. For these studies polytetrafluoroethylene (PTFE), polymethyl methacrylate (PMMA) and quartz (Q) were chosen. These solids were treated as models for the studies of wetting properties of the biosurfactants mixtures with TX165. Of them PTFE is a low energetic apolar solid, PMMA monopolar and quartz bipolar one. It should be emphasized that PTFE and PMMA are used in medicine as implants [25] and they are also treated as substitutes in human skin wettability [26]. The contact angle isotherms obtained for the studied mixtures were described by the exponential function of the second order and the Szyszkowski equation modified by us. The obtained isotherms were also considered with regard to the contribution of individual mixture components to the water surface tension reduction as well as in the contact angle changes. This contribution was also applied for determination of the adsorption layer composition at the solid-air and solid-water interfaces. The amount of adsorption was calculated using the Gibbs isotherm equation. The isotherms of the Gibbs surface excess concentration were used for the determination of the Gibbs standard free energy of adsorption at the solid-air and solid-water interfaces. This energy was also calculated based on the constant in the Szyszkowski equation.

2. Results and Discussion

2.1. Adsorption and Wetting Properties of TX165, RL and SF

In order to understand the wetting properties of TX165 + RL and TX165 + SF mixtures, it is necessary to determine the influence of individual components of the mixture on the value of the contact angle of their aqueous solutions for different types of solids.

According to van Oss et al. [27,28], solids can be divided into three groups, namely apolar, monopolar and bipolar. This division is related to the surface tension of solids (γ_{SV}). Van Oss et al. proposed that the surface tension of solids and liquids can be treated as the sum of the Lifshitz-van der Waals (γ^{LW}) and acid-base (γ^{AB}) components. The γ^{AB} component was assumed by van Oss et al. [27,28] as equal to the geometric mean of the electron-acceptor (γ^+) and electron-donor (γ^-) parameters. In turn, in the case of the surfactants van Oss and Constanzo [29] assumed that the surfactants surface tension depends on the orientation of their molecules toward the air phase. If the surfactant molecules are oriented toward the air phase by their hydrophobic part, then the surface tension of the surfactant is called the surfactant tail surface tension (γ_T). In the case of the surfactant molecules orientation toward the air phase by the hydrophilic group the

surface tension of surfactants can be expressed as the surfactant head surface tension (γ_H). Taking into account the van Oss et al. approach [27,28] to the surface tension of liquids and solids, particular types of solids can be defined. The surface tension of apolar solids results from only the Lifshitz-van der Waals intermolecular interactions. As the contribution of the dipole and induced dipole interactions to the surface tension is smaller than 2% [27–29], according to Fowkes [30] the surface tension of apolar solids results practically from the London forces. The apolar solids include PTFE. The surface tension of the monopolar solids such as PMMA also results from only the Lifshitz-van der Waals intermolecular interactions but it can interact by the acid-base forces with the adherent medium [27,28]. For the bipolar solids such as quartz, the surface tension results from both the Lifshitz-van der Waals and acid-base intermolecular interactions. The acid-base interactions originate mainly from the hydrogen bond formation called the hydrogen bond interactions.

The knowledge of the surface tension of solids and aqueous solution of the surfactants as well as of the relationship between the solid-solution interface tension (γ_{SL}), the solution and solid surface tension enables the explanation of the wetting properties of surfactants.

In 1805 Young studied the equilibrium state of the liquid drop settled on the solid surface and he stated that this equilibrium depends on the liquid and solid surface tension as well as the solid-liquid interface tension [1,20]. In turn, Dupre described this equilibrium state of the liquid drop settled on the solid surface by the thermodynamic equation, which is commonly called the Young equation [1,20]. From this equation it follows:

$$\cos\theta = \frac{\gamma_{SV} - \gamma_{SL}}{\gamma_{LV}}, \tag{1}$$

where γ_{LV} is the surface tension of pure liquid or solution, γ_{SV} is the solid surface tension and θ the contact angle.

The γ_{SL} in Equation (1) can be replaced with the following relationship [27,28]:

$$\gamma_{SL} = \gamma_{SV} + \gamma_{LV} - W_a = \gamma_{SV} + \gamma_{LV} - 2\left(\sqrt{\gamma_{LV}^{LW}\gamma_{SV}^{LW}} + \sqrt{\gamma_{LV}^{+}\gamma_{SV}^{-}} + \sqrt{\gamma_{LV}^{-}\gamma_{SV}^{+}}\right), \tag{2}$$

where W_a is the adhesion work of the liquid to the solid surface.

Introducing Equation (2) to Equation (1) we obtain:

$$\cos\theta = \frac{-\gamma_{LV} + 2\sqrt{\gamma_{LV}^{LW}\gamma_{SV}^{LW}} + 2\sqrt{\gamma_{LV}^{+}\gamma_{SV}^{-}} + 2\sqrt{\gamma_{LV}^{-}\gamma_{SV}^{+}}}{\gamma_{LV}} \tag{3}$$

In the case of apolar solids Equation (3) assumes the form:

$$\cos\theta = \frac{-\gamma_{LV} + 2\sqrt{\gamma_{LV}^{LW}\gamma_{SV}^{LW}}}{\gamma_{LV}} \tag{4}$$

Equations (3) and (4) are reliable if the layer of the liquid around the liquid drop does not change the solid surface tension [31].

The complete spreading of the liquid over the solid surface takes places if $2\sqrt{\gamma_{LV}^{LW}\gamma_{SV}^{LW}} + 2\sqrt{\gamma_{LV}^{+}\gamma_{SV}^{-}} + 2\sqrt{\gamma_{LV}^{-}\gamma_{SV}^{+}} = 2\gamma_{LV}$ or for apolar solids $2\sqrt{\gamma_{LV}^{LW}\gamma_{SV}^{LW}} = 2\gamma_{LV}$.

In order to prove whether the above mentioned conditions can be fulfilled for the complete spreading of the aqueous solution of biosurfactants and TX165 over the PTFE, PMMA and quartz surfaces, the adhesion work of biosurfactants, TX165 and water to these solid surfaces was calculated based on the components and parameters of the biosurfactants, TX165, water as well as the studied solids surface tension (Tables 1 and 2). The calculations of the adhesion work were made for the surface active agents tail and head orientation toward the solid surface (Table 2). The calculation of W_a of the biosurfactants and TX165 to PTFE indicates that in all cases its values are smaller than that of the cohesion work (W_C) and

the spreading coefficient ($S_{L/S}$) [1] is smaller than zero (Table 2). This points out that it is not possible for the aqueous solutions of the biosurfactants and TX165 to spread over the PTFE surface completely. This conclusion is confirmed by the contact angle values presented in Figures S1–S3 in Supplementary Material. In the case of PMMA at the biosurfactants and TX165 molecules orientation by tail toward the PMMA surface, the $S_{L/S}$ values are positive, however for quartz they are positive at any orientation of the biosurfactants and TX165 molecules to its surface (Table 2). This fact indicates that in the case of the aqueous solutions of TX165, RL and SF at the appropriate concentration, complete spreading of these solutions over the PMMA and quartz surfaces should be observed. Unfortunately, the data presented in Figures S4 and S5 do not confirm this conclusion.

The adhesion work of TX165, RL and SF to the PTFE, PMMA and quartz surface as well as the cohesion work determine the limiting contact angle values of their aqueous solution. In such a case the biosurfactants and TX165 molecules are oriented perpendicularly towards the water-air interface and occupying the limiting area which is related to the geometrical size of the molecule. This limiting area at the water-air interface for TX165 is smaller than that for RL and SF but the SF limiting area is larger than the RL one (Table 3). At such packing of the biosurfactants and TX165 molecules the surface tension of their aqueous solution should be equal to the surfactants tail surface tension (Table 1). Unfortunately, the maximal packing (Γ^{max}) of the TX165, RL and SF molecules corresponds to the minimal area $\left(A^{min} \right)$ occupied by one molecule which is larger than that of the limiting one (A^{∞}). Unexpectedly, the minimal surface area occupied by one molecule of TX165 and SF is larger than the contactable area of the molecule tail $\left(A_T^{cont} \right)$ at its parallel orientation towards the water-air interface. In the case of the RL these areas are comparable (Table 3). This fact suggests that the tail of biosurfactants and TX165 molecules in the saturated monolayer can be oriented parallel towards the water-air interface while the head perpendicularly and/or at an angle to this interface. In the case of TX165 there is the biggest difference between the minimal area occupied by its one molecule in the saturated monolayer at the water-air interface and that of the limiting area considering the used compounds. This can be reflected in the minimal value of the surface tension of the TX165 aqueous solution which is considerably greater than that for the RL and SF solutions (Figures S1–S3). The minimum value of the surface tension of the TX165 aqueous solution is significantly larger than that of the RL and SF solutions (Figures S1–S3) despite slight differences in the values of the surface tension of the TX165, RL and SF tails (Table 1). The differences between the minimal and limiting areas occupied by the biosurfactants and TX165 molecules in the adsorptive monolayer at the water-air interface result from that considering the attractive and repulsive interactions between their molecules. The hydrophilic part of the TX165 molecule is largely hydrated in the aqueous environment, and it can even acquire a positive charge [32,33]. For this reason, repulsive interactions between the TX165 molecules in the adsorptive monolayer at the water-air interface can occur, resulting in an increase in the surface area occupied by one TX165 molecule. In the case of biosurfactants, which can be treated as the 1:1 type electrolyte, due to the specific structure of their molecules head, the electrostatic repulsive interactions between the molecules in the monolayer can be neutralized by the hydrogen bonds formation between these molecules. Therefore, the biosurfactant molecules in the saturated monolayer are more closely packed than the TX165 which affects the surface tension of their solutions.

Table 1. The values of the Lifshitz-van der Waals (γ^{LW}) and acid-base (γ^{AB}) components as well as electron-acceptor (γ^+) and electron-donor (γ^-) parameters of water, TX165, rhamnolipid and surfactin head and tail as well as PTFE, PMMA and quartz surface tension (γ).

Substance	Components and Parameters [mN/m]				γ [mN/m]	Refs.
	γ^{LW}	γ^{AB}	γ^+	γ^-		
SF (head)	34.25	8.55	0.37	49.39	42.80	[24,34]
SF (tail)	24.70	0.00	0.00	0.00	24.70	[24,34]
Water	26.85	45.95	22.975	22.975	72.80	[24,34]
RL (head)	35.38	3.01	0.04	56.74	38.39	[24,34]
RL (tail)	21.80	0.00	0.00	0.00	21.80	[24,34]
TX165 (head)	27.70	8.14	0.33	50.20	35.84	[24,34]
TX165 (tail)	22.00	0.00	0.00	0.00	22.00	[24,34]
PTFE	20.24	0.00	0.00	0.00	20.24	[35]
PMMA	41.28	0.00	0.00	7.28	41.28	[35]
Quartz	38.07	9.63	1.61	14.36	47.70	[35]

The behaviour of the biosurfactant and TX165 molecules at the PTFE-water interface is similar to that at the water-air one. This conclusion is supported by the Gibbs surface excess concentration of biosurfactants and TX165 values at the PTFE-water interface (Γ_{SL}) calculated from the following equation [35]:

$$\Gamma_{SL} = -\frac{C}{nRT}\left[\frac{\partial(-\gamma_{LV}\cos\theta)}{\partial C}\right]_T = -\frac{1}{2.303nRT}\left[\frac{\partial(-\gamma_{LV}\cos\theta)}{\partial \log C}\right]_T, \tag{5}$$

where n is the parameter used in the Gibbs isotherm equation for determination of the surface excess concentration of a given surfactant, C is the surfactant concentration, R is the gas constant and T is the temperature.

The maximal values of Γ_{SL} for TX165 (2×10^{-6} mol/m^2), RL (1.98×10^{-6} mol/m^2) and SF (1.34×10^{-6} mol/m^2) (Table 3) calculated from Equation (5) are similar to those of their Gibbs surface excess concentration at the water-air interface (Γ_{LV}) (TX165 (2.12×10^{-6} mol/m^2), RL (2.01×10^{-6} mol/m^2), and SF (1.382×10^{-6} mol/m^2) [5]) determined from the Gibbs isotherm equation. The similarity of Γ_{SL} to Γ_{LV} was also confirmed on the basis of the Lucassen-Reynders equation, which has the form [36]:

$$\frac{\partial(\gamma_{LV}\cos\theta)}{\partial\gamma_{LV}} = \frac{\Gamma_{SV} - \Gamma_{SL}}{\Gamma_{LV}}, \tag{6}$$

where Γ_{SV} is the Gibbs surface excess concentration at the solid-air interface.

It proved that for PTFE the dependence of adhesion ($\gamma_{LV}\cos\theta$) and surface tension for the biosurfactants and TX165 can be described by the linear equation:

$$\gamma_{LV}\cos\theta = a\gamma_{LV} + b, \tag{7}$$

where a and b are the constants. The constant a was close to -1 (Figure S4). In such case, according to Equation (6) Γ_{SL} is close to Γ_{LV} if the adsorption of the surfactants around the solution drop settled on the PTFE surface does not occur ($\Gamma_{SV} = 0$). For the apolar solids such as PTFE whose surface tension results only from the Lifshitz-van der Waals intermolecular interactions if $a = -1$, the constant b fulfills the equation:

$$b = W_a = \gamma_{LV}(\cos\theta + 1) = 2\sqrt{\gamma_{LV}^{LW}\gamma_{SV}^{LW}}. \tag{8}$$

As follows from Equation (8) if the contact angle is equal to zero, then on one hand, $\gamma_{LV} = \frac{b}{2}$ and on the other hand, $\gamma_{LV} = \sqrt{\gamma_{LV}^{LW}\gamma_{SV}^{LW}}$. From the linear relationship between $\gamma_{LV}\cos\theta$ and γ_{LV} for PTFE, plotted based on the contact angle values for the aqueous solutions of TX165, RL and SF, it results that the constant b value is equal to 47.29 mN/m.

This value is insignificantly higher than W_a of water for PTFE (46.62 mJ/m^2) (Table 2). This indicates that TX165 and biosurfactants reduce only the acid-base component of the water surface tension due to the adsorption of their molecules at the water-air interface. On the other hand, for the contact angle equal to zero, Equation (8) is not suitable since the γ_{LV}^{LW} cannot be higher than γ_{LV}. Hence, it is not possible to determine the critical surface tension of PTFE wetting which corresponds to the contact angle equal to zero from Equation (8). The contact angle equal to zero can occur only if the surface tension of the liquid is equal to that of PTFE and this tension results only from the Lifshitz-van der Waals intermolecular interactions.

Table 2. The values of adhesion work (W_a), solid-liquid interface tension (γ_{SL}) calculated from Equations (1) and (2), respectively and the values of spreading coefficient ($S_{L/S}$).

Substrates	PTFE			PMMA			Quartz		
	W_a	γ_{SL}	$S_{L/S}$	W_a	γ_{SL}	$S_{L/S}$	W_a	γ_{SL}	$S_{L/S}$
SF (head)	52.66	10.38	−32.94	78.48	5.60	−7.12	94.66	−4.16	9.06
SF (tail)	44.72	0.22	−4.68	63.86	2.12	14.46	61.33	11.07	11.93
Water	46.62	46.42	−98.98	92.45	21.63	−53.15	112.43	8.07	−33.17
RL (head)	53.52	5.11	−23.26	77.51	2.16	0.73	94.03	−7.94	17.25
RL (tail)	42.01	0.03	−1.59	60	3.08	16.40	57.62	11.88	14.02
TX165 (head)	47.36	8.72	−24.32	70.73	6.39	−0.95	87.28	−3.74	15.60
TX165 (tail)	42.20	0.04	−1.80	60.27	3.01	16.27	57.88	11.82	13.88

The evidence for the similar behaviour of the biosurfactants and TX165 molecules at the PTFE-water and water-air interface is also the fact that the isotherms of the surface tension of the aqueous solutions and the contact angle of these compounds can be described by the Szyszkowski equation with the similar constants related to the standard Gibbs free energy of adsorption (ΔG_{ads}^0) (Figures S1–S3). The Szyszkowski equation for the isotherm of the solution surface tension can be expressed in the form [1]:

$$\gamma_0 - \gamma_{LV} = RTn\Gamma^{max} \ln\left(\frac{C}{a_1} + 1\right), \tag{9}$$

where γ_0 is the water or the another solvent surface tension, Γ^{max} is the maximal Gibbs surface excess concentration and a_1 is the constant which fulfills the equation [1]:

$$a_1 = \varpi \exp\frac{\Delta G_{ads}^0}{RT}, \tag{10}$$

where ϖ is the number of water moles in 1 dm^3.

If we assume that the thermodynamic equations can be applied for all interfaces, then the surface tension of solids does not depend on the surfactant concentration in the solution and the Szyszkowski equation can be written as:

$$\gamma_{LV}\cos\theta - \gamma_w\cos\theta_W = RTn\Gamma^{max}\ln\left(\frac{C}{a_1} + 1\right), \tag{11}$$

where γ_W is the water surface tension and θ_W is the water contact angle on a given solid.

It appeared that it is possible to obtain almost the same values of Γ^{max} and a_1 for TX165, RL and SF from Equations (10) and (11) (Figures S1–S3 and Table 3). This indicates that the ΔG_{ads}^0 values calculated based on the a_1 constant from Equation (10) are similar (Table 3). Moreover, they are similar to those obtained from the Langmuir equation modified by de Boer, which has the following form (Table 3) [1,37]:

$$\frac{A^0}{A - A^0}\exp\frac{A^0}{A - A^0} = \frac{C}{\varpi}\exp\left(\frac{-\Delta G_{ads}^0}{RT}\right), \tag{12}$$

where A^0 is the limiting area occupied by one molecule of the surfactant and A is the area occupied by one molecule of the surfactant in the monolayer at the interface corresponding to the given C value.

Table 3. The values of the standard Gibbs free energy of the adsorption $\Delta(G_{ads}^0)$, Gibbs excess concentration (maximal—Γ^{max} and limiting—Γ^∞) and the area occupied by TX165, RL and SF at the water-air (W-A), PTFE-water (PTFE-W), PMMA-water (PMMA-W) and quartz-water (Q-W) interfaces (minimal—A^{min} and limiting—A^∞) as well as the contactable area of the tail (A_T^{cont}) and head (A_H^{cont}) of these surfactants molecule.

	ΔG_{ads}^0 [kJ/mol]					
	TX 165		**RL**		**SF**	
Interface	**Equation (12)** [1]	**Equation (10)**	**Equation (12)** [1]	**Equation (10)**	**Equation (12)** [1]	**Equation (10)**
W-A	−44.00	−44.23	−42.57	−44.79	−47.37	−51.53
PTFE-W	−43.89	−42.53	−42.70	−44.59	−51.54	−52.15
PMMA-W	−44.58	−44.11	−43.31	-	−49.52	-
Q-W	−43.58	−42.53	−43.02	-	−50.23	-
	Gibbs surface excess concentration, Γ ($\times 10^{-6}$ mol/m²)					
Interface	Γ^{max}	Γ^∞	Γ^{max}	Γ^∞	Γ^{max}	Γ^∞
W-A	2.12	4.65	2.01	2.403	1.382	1.782
PTFE-W	2.10	4.65	1.98	2.28	1.34	1.75
PMMA-W	1.27	2.80	0.71	0.91	0.55	1.10
PMMA-A	1.00	2.80	0.98	1.20	0.64	1.10
Q-W	0.50	1.03	0.34	0.47	0.51	0.87
Q-A	0.91	1.20	0.69	0.91	0.67	0.87
	Occupied area [Å²]					
	A^{min}	A^∞	A^{min}	A^∞	A^{min}	A^∞
W-A	78.32	35.70	82.60	69.09	120.38	93.14−120.24
PTFE-W	79.06	35.70	82.80	72.82	123.90	93.14−120.24
PMMA-W	130.73	59.30	233.85	182.45	301.87	150.94
PMMA-A	166.03	59.30	169.41	138.36	259.42	150.94
Q-W	332.06	161.19	488.32	353.26	325.55	190.84
Q-A	182.45	138.36	240.62	132.45	247.81	190.84
	Contactable area, A^{cont} [Å²]					
	TX165		**RL**		**SF**	
Surfactant	**Tail**	**Head**	**Tail**	**Head**	**Tail**	**Head**
	61.12	100.61	87.25	72.13	75.95	255.56

[1] The all data concerning the water-air interface (W-A) calculated from Equation (12) were taken from the literature [38].

It should be mentioned that for the calculation of Γ^{max} and a_1 from Equations (10) and (11) the values of C correspond to the monomeric form of the biosurfactants and TX165.

The isotherms of the contact angle of the aqueous solution of biosurfactants and TX165 on the PTFE surface can be described not only by the Szyszkowski equation but also by the exponential function of the second order (Figures 1 and S1–S3). However, it is difficult to find the relationship between the constants in this function presented in figures and some physicochemical properties of solution components. These constants can be related to the components and parameters of the surface active agents and water surface tension similarly to the exponential function of the second order describing the isotherm of the surface tension of the aqueous solution of the surfactants [24].
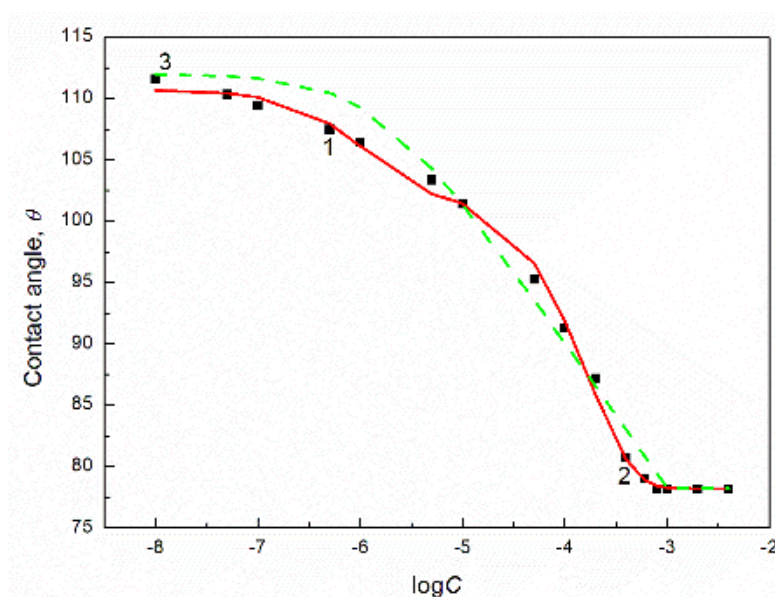
Figure 1. A plot of the TX165 aqueous solution contact angle (*θ*) on PTFE (curves 1–3) vs. the logarithm of TX165 concentration (*C*). Curve 1 corresponds to the measured values, curve 2 to values calculated from the exponential function of the second order:

$$\theta = 24.66595 \exp\left(\frac{-C}{0.000170057}\right) + 7.90722 \exp\left(\frac{-C}{0.0000011843}\right) + 78.1891$$

curve 3 corresponds to the values calculated from Equations (9) and (11), respectively.

The problem of PMMA and quartz wetting by the aqueous solutions of TX165, RL and SF is more complicated than in the case of PTFE. Contrary to PTFE, the surface tension of PMMA is higher than that of both the tail and head of TX165 and RL while in the case of quartz its surface tension is larger than that of the head and tail of all analyzed surface-active substances (Table 1). Moreover, the minimum surface tension of the aqueous solution of the biosurfactants and TX165 is smaller than that of PMMA and quartz (Figures S1–S3). According to van Oss et al. [27–29] it would seem that the aqueous solutions of biosurfactants and TX165 at the appropriate concentration should spread completely over the PMMA and quartz surfaces. Unfortunately, complete spreading over the PMMA and quartz surfaces did not occur for any of the solutions (Figures S5 and S6). It is possible that the reason for this fact is the migration of the biosurfactant and TX165 molecules on the PMMA and quartz surfaces. As the result of this migration, an adsorption layer is formed around the solution drop settled on the PMMA and quartz surfaces which changes their surface tension [38]. This can be confirmed by positive values of the spreading coefficient of the biosurfactants and surfactants on the PMMA and quartz surfaces (Table 2). The possibility of TX165, RL and SF adsorption around the settled solution drop on the PMMA and quartz surfaces is indicated by the curves showing the dependence between the adhesion and the solution surface tension (Figures S7 and S8). The slope of the curves for PMMA and quartz except for that obtained with the TX165 aqueous solution, is positive. In the case of PMMA the slope of the dependence between the adhesion and surface tension is negative for the RL and SF solution at their concentration higher than the critical micelle concentration (CMC) [39]. If the biosurfactants and TX165 are assumed not to adsorb on the PMMA and quartz surfaces around the drop of their solution, their negative adsorption at the solid-water interface takes place according to the Lucassen-Reynders equation [36]. This is impossible in practice. Probably due to the presence of the adsorption layer at the PMMA-air and quartz-air interfaces, the contact angle isotherm of the aqueous TX165, RL and SF solutions can not be described by Equation (11). It is interesting that using the difference between the contact angle for water and solution in the Szyszkowski equation

instead of the layer pressure at the PMMA-water interface (PMMA(quartz)-water minus PMMA(solution)-solution interface tension), it was possible to describe the isotherm of the contact angle of the aqueous solution of TX165 for PMMA and quartz (Figures S7 and S8). Moreover, the values of the standard Gibbs free energy of adsorption calculated from Equation (10) based on the constant a_1 obtained in this way are close to the standard Gibbs free energy of adsorption values for TX165 at the PMMA-water and quartz-water interfaces calculated from the Langmuir equation modified by de Boer [1,37]. It should be mentioned that for the aqueous solution of RL it was impossible to describe the contact angle isotherm of its solution for PMMA and quartz as well as for the aqueous solution of SF for PMMA.

According to the Lucassen-Reynders equation, the positive slope of the curves obtained from the relationship between the adhesion and surface tension indicates that the adsorption of the surfactant at the solid-water interface is smaller than at the solid-air one [36]. This may be due to the very strong interactions of water molecules with the solid surface which is reflected in the W_a values (Table 2), hindering the adsorption of surfactants. Due to these interactions of water molecules with the PMMA and quartz surfaces, there is smaller adsorption of TX165, RL and SF at the PMMA-water and quartz-water interfaces than at the water-air one (Table 3) [34]. The comparison of the minimal (A^{min}) and limiting areas (A^{∞}) of TX165, RL and SF molecules occupied at these interfaces with the contactable area (A^{cont}) of their molecules shows that they are oriented parallel to the PMMA and quartz surfaces (Table 3).

2.2. Contact Angle of Biosurfactants Mixtures with TX165

According to Equation (4) [27,28] in the case of apolar solids such as PTFE whose surface tension results only from the Lifshitz-van der Waals intermolecular interactions, the contact angle of surfactants aqueous solutions depends on the surface tension of the solution, the Lifshitz-van der Waals component of this tension and the PTFE surface tension. In turn, the surface tension of the aqueous solution depends on the components and parameters of the surface tension of all its constituents. Indeed, Equation (4) is applied for the calculation of the contact angle of liquids and solutions if the surface tension of apolar solids is not changed by the liquid vapour layer formed around the liquid drop settled on the solid surface. This proved that the liquid vapour having the surface tension larger than that of the solid does not change it. To explain the wetting properties of the TX165 + RL and TX165 + SF mixtures in the PTFE-aqueous solution of these mixtures-air system, the contact angle of hypothetical liquids on the PTFE surface, whose surface tension results only from the Lifshitz-van der Waals interactions, was calculated from Equation (4). Then it was assumed that the surface tension of hypothetical liquids results also from the Lifshitz-van der Waals intermolecular interactions and is equal to the Lifshitz-van der Waals components of water and tail of the biosurfactants and TX165. Taking into account the Lifshitz-van der Waals component for the water surface tension and that of RL, SF and TX165 head, the contact angle was calculated from Equation (4). As follows the contact angle for water, RL, SF and TX165 is equal to 42.57, 22.01, 35.86 and 23.32 degrees, respectively. These contact angle values indicate that it is impossible to achieve the complete spreading of the aqueous solution of the biosurfactants with the TX165 mixtures over the PTFE surface. This suggestion is confirmed by the contact angle values larger than zero (Figures 2 and 3) as well as data presented in Figures S9 and S10. The minimal values of the surface tension of the aqueous solution of RL, SF and TX165 are higher than the Lifshitz-van der Waals component of water surface tension (Figures S1–S3) [40]. On the other hand, the Lifshitz-van der Waals component of the surface of the aqueous solution of the biosurfactants and TX165 does not depend on the solution concentration and is close to the Lifshitz-van der Waals component of water surface tension. This indicates that at the water-air interface the biosurfactants and TX165 do not reduce the LW component of water surface tension by their adsorption. However, they reduce its AB component but not to zero. On the other hand, the minimal surface tension of the aqueous solution of biosurfactants and TX165 mixtures is not smaller than the surface tension of the aqueous

solution of individual mixture component. This may be the reason that the contact angle values of the studied mixtures aqueous solution are not smaller than those for the single biosurfactants and TX165 solutions (Figures 2, 3 and S1–S3).

Figure 2. A plot of the contact angle (θ) of aqueous solution of TX165 + RL mixtures on the PTFE surface vs. the logarithm of the TX165 concentration (*C*). Curves 1–16 correspond to the constant RL concentration equal to 0.0002, 0.0005, 0.00125, 0.003, 0.00625, 0.01, 0.02, 0.05, 0.1, 0.5, 1, 5, 10, 20, 30 and 40 mg/dm^3, respectively.
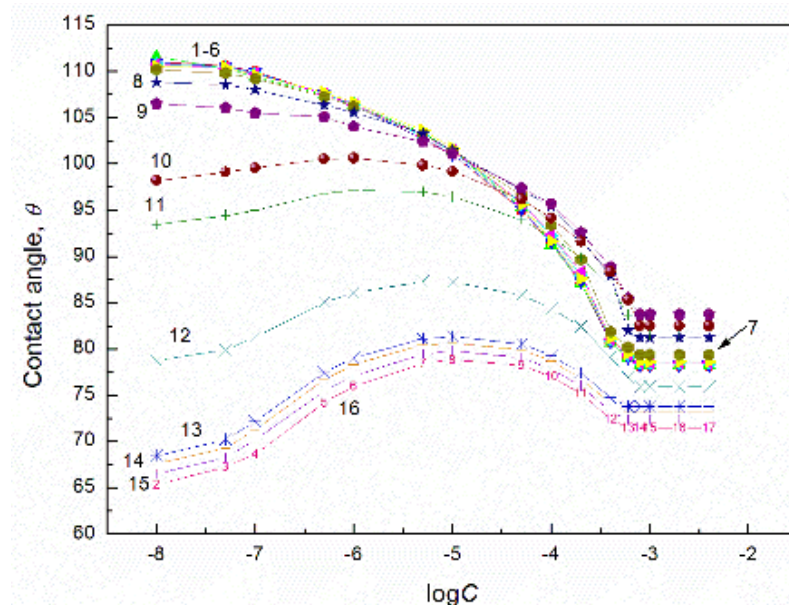
Figure 3. A plot of the contact angle (θ) of aqueous solution of TX165 + SF mixtures on the PTFE surface vs. the logarithm of the TX165 concentration (*C*). Curves 1–16 correspond to the constant SF concentration equal to 0.0002, 0.0005, 0.00125, 0.003, 0.00625, 0.01, 0.02, 0.05, 0.1, 0.5, 1, 5, 10, 20, 30 and 40 mg/dm^3, respectively.

It was found earlier that the surface tension of the biosurfactants with the TX165 mixtures depends on the contribution of particular components of the mixture to the reduction of water surface tension which is proportional to that of water surface tension by its single components [24]. As the contact angle isotherms of the aqueous solution of biosurfactants mixture for PTFE are similar to the surface tension isotherm, it can be possible

to predict the contact angle of the mixture based on that of its particular components. In the other words, the contact angle of the aqueous solution of the surfactants mixture on the PTFE surface should depend on the sum of the products of the contact angle of the mixture components at the appropriate concentration and the fraction of the mixed layer at the PTFE-water interface (X). Thus, it can be written:

$$\theta = \theta_1 X_1 + \theta_2 X_2, \tag{13}$$

where indices 1 and 2 refer to components 1 and 2 of the mixture.

This proved that the relationship between the adhesion and surface tension for all tested aqueous solutions of the biosurfactants with the TX165 mixture for PTFE is linear, and the line slope is close to -1. In that case, according to the Lucassen-Reynders equation (Equation (6)) [36], the concentration of the TX165 + biosurfactant mixture at the PTFE-water interface is similar to that at the water-air one. Assuming that the composition of the mixed layers at the PTFE-water and water-air interfaces is nearly the same, it is possible to calculate X_1 and X_2 from the following expression:

$$X_1 = \frac{\pi_1}{\pi_1 + \pi_2} \text{ and } X_2 = \frac{\pi_2}{\pi_1 + \pi_2} \tag{14}$$

where π_1 and π_2 are the pressures of the monolayer at the water-air interface of the single components of the surfactant mixtures.

Thus for the PTFE-solution drop-air systems in which the concentration of the biosurfactant and/or TX165 in the bulk phase of the solution corresponds to the unsaturated single monolayer at the water-air interface (C_{unsat}), the θ values calculated from Equation (13) based on Equation (14) are close to those measured (Figures 4 and S11–S13). Unfortunately, at the concentration of one or two components of the TX165 + biosurfactant mixture higher than C_{unsat} there is smaller agreement between the measured and calculated contact angle values than in the case mentioned above. Then the composition of the mixed layer at the PTFE-water interface can be slightly different from that at the water-air one, despite the equal total concentration of the surfactant mixture at these interfaces.
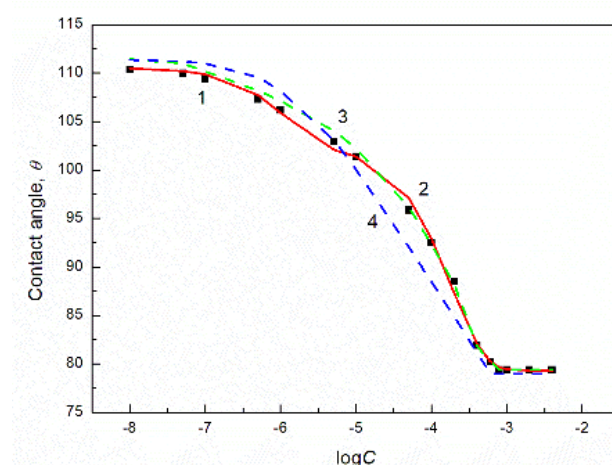
Figure 4. A plot of the contact angle (θ) of aqueous solution of TX165 + RL on PTFE at the constant RL concentration equal to 0.00625 vs. the logarithm of TX165 concentration (C). Points 1 correspond to the measured values, curves 2 correspond the values calculated form the exponential function of the second order:

$$\theta = 23.28064 \exp\left(\frac{-C}{0.00018624}\right) + 7.93008 \exp\left(\frac{-C}{0.00000117916}\right) + 79.31736$$

and curves 3 and 4 correspond to values calculated from Equations (13) and (9), respectively.

It should be emphasized that the contact angle isotherms for all studied solutions on the PTFE surface can be described by the exponential function of the second order (Figures 4 and S11–S13 as an example). At the concentration of one or two components in the solution bulk phase higher than C_{unsat} the isotherms of θ, on which the maxima are observed, can be described by the two exponential functions—one from the initial contact angle value to the maximal one and the other from the maximal value to the final one (Figures S11–S13). Similarly to the aqueous solution of RL, SF and TX165 the contact angle isotherm of the aqueous solution of the TX165 + biosurfactant mixtures on the PTFE surface can be described by the modified Szyszkowski equation (Equation (11)) (Figures S11–S13). Unfortunately, Equation (11) is fulfilled only for the solution in which the constant concentration of one component of the mixture is equal to C_{unsat}. It is worth noting that the calculated values of the standard Gibbs free energy of adsorption of individual components of the TX165 + biosurfactant mixture from equation (10) based on the obtained constant values from the Szyszkowski equation (Equation (11)) are similar to those calculated from the modified Langmuir equation for the water-air interface [1].

This suggests that the adsorption of the biosurfactants and TX165 mixtures at the PTFE-water interface affects only on the contribution of the acid-base interaction to the PTFE-water interface tension. This suggestion is confirmed by the relationship between the adhesion and the surface tension (Figure S14). The dependence shows that not only the adsorption of the TX165 + biosurfactant mixture at the PTFE-water and water-air interfaces is similar but also that the adhesion work of the solution to the PTFE surface does not depend on the mixture composition and concentration. The values of the adhesion work of solution mixtures are close to that of water to the PTFE surface.

Some authors [41,42] suggest that in the case of the linear relationship between the adhesion and surface tension with the slope equal to −1, the value equal to half of the work adhesion obtained from this relationship is equal to the critical surface tension of solid wetting. In the case of the aqueous solution of the biosurfactant and TX165 mixtures the value of the half of the adhesion work of the solution to the PTFE surface is equal to 23.75 mJ/m^2. According to the above considerations it is impossible to acquire the complete spreading of the studied mixture over the PTFE surface which is further confirmed by the isotherms of the solution contact angle.

The wetting process of PMMA and quartz by the aqueous solution of TX165 + RL and TX165 + SF is more complicated than that of PTFE. As mentioned above the surface tension of the surfactants tail is smaller than that of PMMA and quartz. In the case of the surfactant head surface tension, its value is insignificantly higher than the surface tension of PMMA only for SF. Thus, theoretically it is possible to obtain the complete spreading of the aqueous solution of the TX165 + RL and TX165 + SF mixtures over the PMMA and quartz surface. However, no complete spreading over the surface for the mentioned solids was obtained (Figures 5–8 and S15–S18).

As mentioned above the values of the spreading coefficient of the biosurfactants and TX165 over the PMMA and quartz surface are positive independent of the way of molecules orientation towards their surface (except for the TX165 head-PMMA system) (Table 2). Thus, it is possible that the biosurfactants and TX165 can penetrate from the solution drop settled on the quartz or PMMA surface, changing the surface tension of PMMA and quartz around the drop. In that case the surface tension of the PMMA and quartz is variable as a function of the aqueous solution of the biosurfactants and TX165 mixtures concentration and composition. This suggestion is confirmed by the relationships between the adhesion and surface tension for both PMMA and quartz (Figures S19–S22). The slope of the curves of these relationships changes as a function of the composition and concentration of the solution of the studied mixtures. It depends also on the type of the solids and for PMMA it changes even from negative to positive values. This indicates that the slope of the curve representing the dependence between the adhesion and surface tension for the solution of TX165 + biosurfactant mixture at the same composition and concentration is different for PMMA and quartz (Figures S19–S22). According to the

Lucassen-Reynders equation (Equation (6)) the changes of the slope of this dependence as a function of the composition and the concentration of the solution of the biosurfactant and TX165 mixture are due to those in the correlation between the adsorption of this mixture at the solid-air and solid-liquid interfaces. This relation influences on the isotherm of the contact angle. Similarly to PTFE, the maxima on the isotherms of the contact angle of the aqueous solution of the TX165 + RL and TX165 + SF mixtures on the PMMA and quartz surfaces are present for the solutions whose concentration of one and/or two mixture components is higher than C_{unsat} (Figures S15–S18). These maxima can be explained based on the contact angle isotherms calculated from Equation (13) (Figures 9 and S23–S26).

Figure 5. A plot of the contact angle (θ) of aqueous solution of TX165 + RL mixtures on the PMMA surface vs. the logarithm of the TX165 concentration (C). Curves 1–16 correspond to the constant RL concentration equal to 0.0002, 0.0005, 0.00125, 0.003, 0.00625, 0.01, 0.02, 0.05, 0.1, 0.5, 1, 5, 10, 20, 30 and 40 mg/dm^3, respectively.
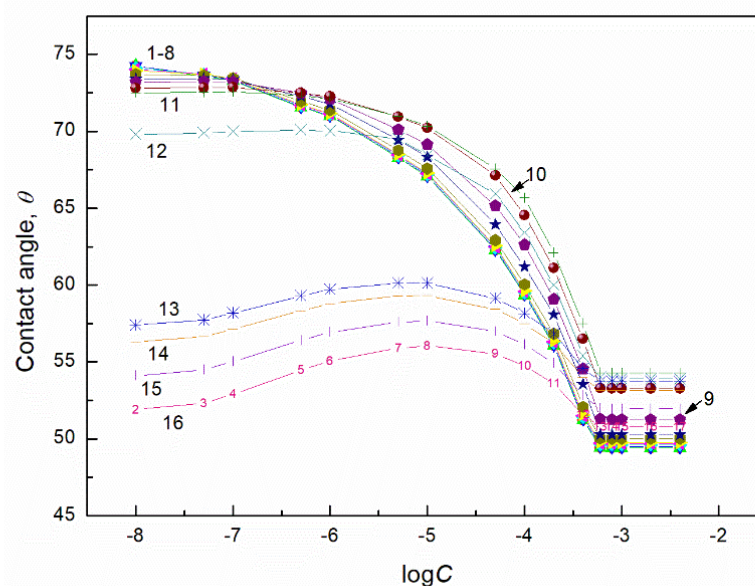
Figure 6. A plot of the contact angle (θ) of aqueous solution of TX165 + SF mixtures on the PMMA surface vs. the logarithm of the TX165 concentration (C). Curves 1–16 correspond to the constant SF concentration equal to 0.0002, 0.0005, 0.00125, 0.003, 0.00625, 0.01, 0.02, 0.05, 0.1, 0.5, 1, 5, 10, 20, 30 and 40 mg/dm^3, respectively.

Figure 7. A plot of the contact angle (θ) of aqueous solution of TX165 + RL mixtures on the quartz surface vs. the logarithm of the TX165 concentration (*C*). Curves 1–16 correspond to the constant RL concentration equal to 0.0002, 0.0005, 0.00125, 0.003, 0.00625, 0.01, 0.02, 0.05, 0.1, 0.5, 1, 5, 10, 20, 30 and 40 mg/dm^3, respectively.
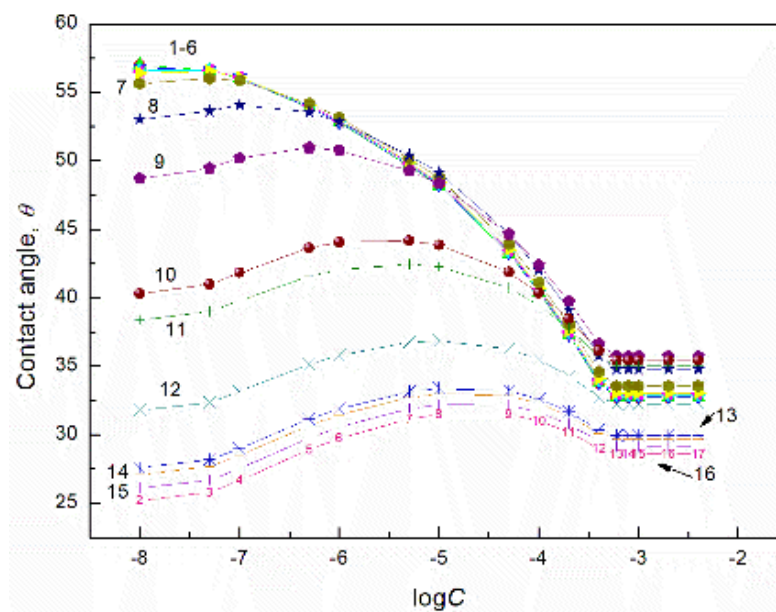
Figure 8. A plot of the contact angle (θ) of aqueous solution of TX165 + SF mixtures on the quartz surface vs. the logarithm of the TX165 concentration (*C*). Curves 1–16 correspond to the constant SF concentration equal to 0.0002, 0.0005, 0.00125, 0.003, 0.00625, 0.01, 0.02, 0.05, 0.1, 0.5, 1, 5, 10, 20, 30 and 40 mg/dm^3, respectively.
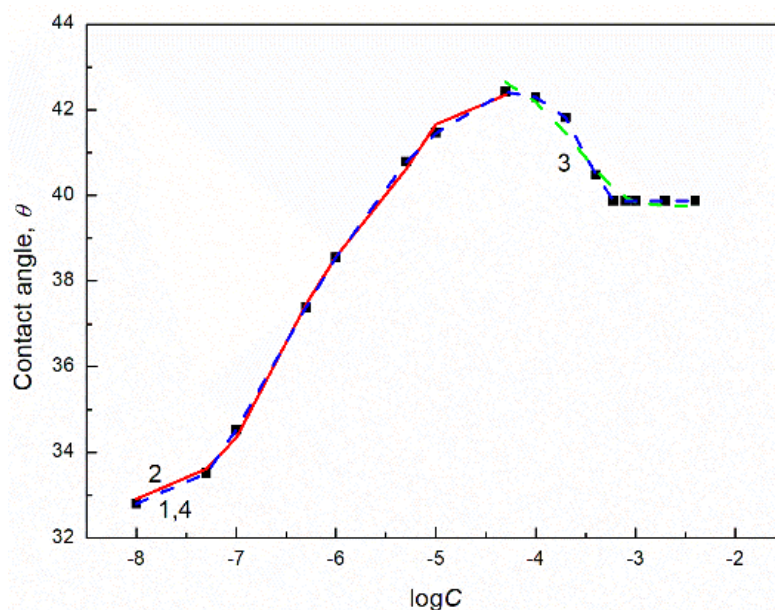
Figure 9. A plot of the contact angle (θ) for TX165 + RL for PMMA at the constant RL concentration equal to 40 mg/dm³ vs. the logarithm of TX165 concentration (C). Points 1 correspond to the measured values, curve 2 corresponds the values calculated from two exponential functions of the second order: $\left(\theta = -5.28316\exp\left(\frac{-C}{0.0000028661}\right) - 4.34766\exp\left(\frac{-C}{0.0000054396}\right) + 42.35076\right)$, $\left(\theta = 1.73099\exp\left(\frac{-C}{0.00028}\right) + 1.73099\exp\left(\frac{-C}{0.00028}\right) + 39.75775\right)$, and curves 3 and 4 correspond to values calculated from Equations (13) and (9), respectively.

In most cases the theoretical isotherms of the contact angle are similar to those obtained from the measured contact angle even at the solution concentration of particular components of the mixture higher than C_{unsat} (Figures 9 and S23–S26). The agreement between the isotherm obtained from the calculations and measurements of the contact angle suggests that the particular components contribution to the contact angle is proportional to the reduction of water surface tension. Moreover the composition of the surface mixed monolayer at the solid-air and the solid-water interfaces is similar despite different concentrations. If there is no such agreement, there can be differences in the composition of the interface layers at the solid-air and solid-water interfaces. It should be mentioned that all isotherms of the contact angle of the aqueous solution of TX165 + RL and TX165 + SF on the PMMA and quartz surface can be described by the exponential function of the second order (Figures 9 and S23–S26). In the case of the solution at the concentration of one or two components of a given mixture higher than C_{unsat}, the isotherms of the contact angle were described by the two exponential functions: one in the concentration range of the component at the variable concentration with its value from zero to that corresponding to the maximal value and the other one from the maximum to the limited concentration value. In the case of the solutions at the constant concentration smaller than C_{unsat}, the contact angle isotherm can be also described by the modified Szyszkowski equation (Figures 9 and S23–S26). The values of the standard Gibbs free energy of adsorption obtained from this equation are higher than those obtained for the individual components of the mixture.

2.3. Composition and Concentration of the Mixed Layer at the Solid-Air and Solid-Water Interfaces

The dependence between the adhesion and surface tension of the aqueous solutions of TX165 + RL and TX165 + SF both at the constant biosurfactants concentration and variable TX165 and vice versa for PTFE can be expressed by one linear dependence (Figure S14). Its slope is close to −1. Thus according to the Lucassen-Renders equation [35] (Equation (6)) the Gibbs surface excess concentration of the biosurfactants and TX165 mixture at the PTFE-water interface is close to that at the water-air one. As a matter of fact, there should be

satisfied the condition that the surface tension of PTFE does not depend on the concentration and composition of the biosurfactants and TX165 mixtures. The constant b in the linear equation describing the dependence between the adhesion and surface tension is close to the adhesion work of water to the PTFE surface (Table 2). This means that $2\sqrt{\gamma_W^{LW}\gamma_W^{LSV}}$ is close to $\gamma_{LV}(\cos\theta + 1)$. Thus it follows that the mixtures of the biosurfactants with TX165 do not reduce the Lifshitz-van der Waals component of the water surface tension (Table 1) and that the surface tension of PTFE does not depend on the concentration and composition of the TX165 + RL and TX165 + SF mixtures. The linear dependence between the adhesion and surface tension at the slope equal to -1 does not prove that despite the same concentration of the biosurfactants mixture with TX165 at the water-air and the PTFFE-water interfaces, the composition of the mixed monolayer is the same. For this reason the Gibbs surface excess concentration of the biosurfactants and TX165 mixtures at the PTFE-water interface was calculated from Equation (5). However, it was possible to calculate the Gibbs surface excess concentration at the PTFE-water interface only in the range of the constant concentration value of one component of the mixture smaller than C_{unsat}. For such a case the dependence between the adhesion tension and the variable concentration of the other component of the mixture can be expressed by the exponential function of the second order. The maximal excess concentration of the biosurfactant or TX165 was determined from the linear dependence between the concentration logarithm and the adhesion tension. In the case of the constant concentration of one component of the mixture and variable of the other one at which the maxima on the contact angle isotherm are present, the Gibbs surface excess concentration of the biosurfactants and TX165 was calculated from the following expression:

$$\Gamma_1^{max} X_1 + \Gamma_2^{max} X_2 = \Gamma_{12}. \tag{15}$$

It seems reasonable to assume that the contribution of the particular component mixture to its total concentration at the PTFE-water interface similarly to the contact angle should be proportional to that of this component in the water surface tension reduction. Thus for the calculation of Γ_{12} the values of X_1 and X_2 determined in the above mentioned way were used in Equation (15) (Figure S27).

As follows from the comparison of the Gibbs surface excess concentration of the biosurfactants and TX165 at the PTFE-water and the water-air interfaces the composition of its mixed monolayer at the PTFE-water interface is somehow different from that at the water-air one [24] (Figures S28–S31). It should be remembered that the adsorption mechanism for the same surfactant at the PTFE-water and water-air interfaces is different. In the adsorption at the PTFE-water interface the hydrophobic interactions between PTFE and the surfactant tail play a very important role. They depend on the PTFE-water and the tail-water interface tension and the contactable area of the surfactant tail. Hence, these differences in the composition of the mixed monolayer at the PTFE-water and water-air interfaces are likely to take place. Nevertheless, as indicated by the values of the Gibbs standard free energy of adsorption of the biosurfactants and TX165, calculated from both the Langmuir equation modified by de Boer and based on the modified Szyszkowski equation, the tendency for the biosurfactant and TX165 to adsorb at the PTFE-water interface is similar to that at the water-air one (Table 4) [24].

In the case of the monopolar PMMA and bipolar quartz the determination of the biosurfactants and TX165 adsorption is more complicated than at the PTFE-water interface.

Table 4. The values of standard Gibbs free energy of adsorption of TX165, RL and SF (ΔG_{ads}^0) at the PTFE-water, PMMA-water, quartz-water, PMMA-air and quartz-air interfaces calculated from Equations (10) and (12) respectively.

	ΔG_{ads}^0 [kJ/mol]									
	PTFE-W		PMMA-A		PMMA-W		Q-A		Q-W	
Mixture	Equation (12)	Equation (10)	Equation (12)	Equation (10)	Equation (12)	Equation (10)	Equation (12)	Equation (10)	Equation (12)	Equation (10)
TX165 + RL (const RL)	−43.63	−42.91	−42.89	−42.11	−42.90	−41.91	−35.79	-	−44.16	−43.44
TX165 + SF (const SF)	−44.17	−43.84	−43.47	−42.74	−44.05	−43.25	−46.35	−45.15	−46.18	−46.00
TX165 + RL (const TX165)	−42.13	−41.51	−42.66	−42.15	−45.36	−45.14	−46.07	−45.81	−48.51	−48.01
TX165 + SF (const TX165)	−49.42	−48.15	−48.71	−49.05	−49.33	−49.11	−51.16	−50.25	−52.64	−51.13

Based on the relationship between the adhesion and surface tension of the aqueous solution of the biosurfactants and TX165 mixture for PMMA and quartz, the amount of the adsorbed mixture at the solid-water interface cannot be deduced contrary to PTFE. There is no linear dependence between the adhesion and surface tension for PMMA and quartz. Moreover, the curves representing this dependence can assume the positive slope which would suggest the negative adsorption (Figures S19–S22). The values of adhesion work obtained from the van Oss at al. [27–29] and Young-Dupre equations [1,20] for all studied solutions to the PMMA and quartz surface indicate that $2\sqrt{\gamma_{LV}^{LW}\gamma_{SV}^{LW}} + 2\sqrt{\gamma_{LV}^{+}\gamma_{SV}^{-}} + 2\sqrt{\gamma_{LV}^{-}\gamma_{SV}^{+}} > \gamma_{LV}(\cos\theta + 1)$. This means that the surface tension of PMMA and quartz changes as a function of composition and concentration of the biosurfactants and TX165 mixture. This satisfies the equation:

$$2\sqrt{\gamma_{LV}^{LW}\gamma_{SV}^{LW}} + 2\sqrt{\gamma_{LV}^{+}\gamma_{SV}^{-}} + 2\sqrt{\gamma_{LV}^{-}\gamma_{SV}^{+}} - \gamma_{LV}(\cos\theta + 1) = \pi. \tag{16}$$

As follows at the first approximation $\pi \approx \frac{\gamma_W - \gamma_{LV}}{2}$. Taking into account Equation (16) and the Young equation it was possible to determine the PMMA-solution and quartz-solution interface tension as well as the PMMA-surface layer and quartz-surface layer interface tensions. Then the Gibbs surface excess concentrations of SF, RL and TX165 at these interfaces could be determined using the following equations:

$$\Gamma_{SV} = -\frac{C}{nRT}\left[\frac{\partial\gamma_{SV}}{\partial C}\right]_T = -\frac{1}{2.303nRT}\left[\frac{\partial\gamma_{SV}}{\partial\log C}\right]_T, \tag{17}$$

$$\Gamma_{SL} = -\frac{C}{nRT}\left[\frac{\partial\gamma_{SL}}{\partial C}\right]_T = -\frac{1}{2.303nRT}\left[\frac{\partial\gamma_{SL}}{\partial\log C}\right]_T. \tag{18}$$

Based on Equations (17) and (18) it was possible to calculate the Γ_{SV} and Γ_{SL} values at the constant concentration of one mixture component smaller than its C_{unsat}. In the other case the Γ_{SV} and Γ_{SL} values were determined from expression (15) (Figures S32–S35).

It appeared that the values of Γ_{SV} and Γ_{SL} are significantly smaller than that of Γ_{LV} [24] (Figures S32–S35). As follows from the single surfactants layer at the PMMA-air, PMMA-water, quartz-air and quartz-water interfaces the molecules of biosurfactants and TX165 in the mixed layer are oriented parallel towards the interface. However, the Gibbs surface excess concentration of TX165 in the saturated mixed monolayer at the PMMA-air, quartz-air as well as the PMMA-water and quartz-water interfaces is higher than that for the biosurfactants. This may result from three cases: (1) the oxyethylene groups in

the TX165 molecule can be connected with hydrogen ions, (2) active electric interactions occur between the oxyethylene group and hydrogen ions, (3) interactions of particularly negatively charged quartz surface and/or –CO groups on the PMMA surface take place. On the other hand, one molecule of biosurfactants can remove more water molecules from the interface than one molecule of TX165 (Table 3). The relationship between the values of Γ_{SV} and Γ_{SL} explains the slope of the curves representing the dependence between the adhesion and surface tension (Figures S19–S22, S36 and S37). In the case of quartz this slope is positive for all studied solutions because Γ_{SV} is higher than Γ_{SL}. This may result from the fact that the heads of the biosurfactants and TX165 molecules interact strongly with the water ones (Table 2). The interactions of the biosurfactants and TX165 molecules with the PMMA and quartz surface through the water phase depend on the solid-tail, solid-head as well as the water-tail and water-head interactions and the contactable area of tail and head [43]. These interactions are associated with the interface tension. As the water-head of the biosurfactant and/or the water-head of TX165 interface tension is negative, it reduces the possibility of surfactants to adsorb at the PMMA-water and quartz-water interfaces compared to the PMMA-air and quartz-air interfaces. This is more evident in the case of the systems including quartz instead of PMMA. Despite smaller adsorption of the biosurfactants and TX165 mixture at the PMMA-air, quartz-air, PMMA-water and quartz-water interfaces than at the water-air one, the values of standard Gibbs free energy of adsorption calculated from the Langmuir equation modified by de Boer Equation (12) are similar to those of the standard Gibbs free energy of adsorption at the water-air interface. It is worth mentioning that the values of the standard Gibbs free energy of adsorption determined based on the Szyszkowski equation are close to those calculated from the Langmuir equation (Table 4). It should be pointed out that the values of Γ_{SV} and Γ_{SL} calculated from the modified Szyszkowski equation in which instead of the difference between the interface tension of water and solution that between the contact angle for water and solution were applied on the PMMA and quartz surface. The difference between the contact angle of water on the surfaces of PMMA and quartz and the solution is close to that between the PMMA (quartz)-water and PMMA (quartz)-solution and/or between the surface tension of PMMA (quartz)-air in the presence of the water drop and the solution (Figure S38).

3. Materials and Methods

Triton X-165 (p-(1,1,3,3-tetramethylbutyl)-phenoxypolyoxyethylene glycol) of purity over 99% was purchased from FLUKA. R-95 Rhamnolipid (95%) (RL) and surfactin ($\geq$98%) (SF) were purchased from Sigma-Aldrich. Nonionic TX165 and biosurfactants were used without further purification. Four series of the aqueous solutions of TX165 with the biosurfactant mixture were prepared for the contact angle measurements on the PTFE, PMMA and Q surface. The first and second series included the aqueous solutions of the mixture of TX165 with RL and SF, in which the biosurfactant concentration was constant and that of TX165 was variable. The third and fourth series included the solutions of the mixture of TX165 with RL and SF in which the concentration of TX165 was constant and concentration of the biosurfactant changed. The range of biosurfactants concentration in all series of solutions was from 0 to 40 mg/dm^3, and that of TX165 from 0 to 4×10^{-3} mole/dm^3. The range of the biosurfactants and TX165 concentration in the aqueous solution included the value of CMC of the given surface active agent. The water used for preparation of all solutions was doubly distilled and deionized (Destamat Bi18E). The internal specific resistance of water was 18.2×10^6 $\Omega \cdot$m. Before the solution preparation the water purity was additionally controlled by the surface tension measurements.

The polymers used for the contact angle measurements were obtained from Mega-Tech, Poland and the quartz solids from Conductance, Poland. Before the contact angle measurements the surfaces of the polymers and quartz plates were prepared according to the procedure described earlier [34], which was used twice for each plate. Then the plates were dried and placed in a desiccator with the molecular sieve.

The advancing contact angle (θ) for the aqueous solutions of TX165 + biosurfactant mixture on the PTFE, PMMA and quartz surfaces was measured by the sessile drop method at 293 $\pm$ 0.1 K using the DSA30 measuring system (Krüss, Hamburg, Germany) with a thermostated chamber. For determination of the contact angle values both tangential and circle fittings were used. The procedure for measuring the contact angle was described in detail previously [35]. The drop volume of 7 μL was used for all contact angles measurements. The contact angle measurements for each solution on the PTFE, PMMA and quartz surfaces were repeated 10 times. The standard deviation of the contact angle values was related to the concentration of the biosurfactants and TX165 in the solution. At the concentration corresponding to the unsaturated mixed monolayers at the water-air interface the standard deviation was smaller than 1.5° but at that corresponding to the saturated mixed monolayer was larger, being close to 2°.

4. Conclusions

Based on of the measurements of the contact angle and the thermodynamic analysis of the obtained results, a number of conclusions can be drawn.

In no case the aqueous solutions of the TX165 and biosurfactants mixtures spread completely over the PTFE, PMMA and quartz surface. In the case of PMMA and quartz this results from the fact that around the solution drop settled on the PMMA and quartz surface the mixed biosurfactant and TX165 layer is formed, changing their.

The contact angle isotherms of the aqueous solution of TX165 with RL and SF can be described by the exponential function of the second order even when the maxima are present on them. In that case there can be used two exponential functions: one for the solution concentration from zero to that corresponding the maximum and the other one from the concentration corresponding to the maximum and the final concentration.

In most cases the contact angle isotherms can be predicted from those of the surface tension of the aqueous solution of individual TX165, RL and SF.

In the PTFE-aqueous solution of the biosurfactant mixture with the TX165 drop-air system, the contact angle changes as a result of the acid-base component of water surface tension reduction due to its adsorption at the water-air interface.

In some cases it is possible to describe the isotherms of the contact angle by the Szyszkowski equation using: (1) the difference between the adhesion tension of water and solution for the PTFE-solution system, (2) the difference between the contact angle for water and solution in the PMMA-air, PMMA-solution, quartz-air and quartz-solution systems.

The adsorption of the biosurfactant + TX165 mixture at the PTFE-water interface is comparable with that at the water-air one, but there are some differences in the surface layers composition.

The adsorption of the biosurfactant mixtures with TX165 at the PMMA-air, PMMA-water, quartz-air and quartz-water interfaces is smaller than at the water-air one. In the case of the systems including quartz, the adsorption of the biosurfactant + TX165 mixture at the quartz-air interface is larger than that at the quartz-water interface.

The standard Gibbs free energy of adsorption of biosurfactant + TX165 mixture at the PTFE-water, PMMA-air, PMMA-water, quartz-air and quartz-water interfaces is comparable to that at the water-air interface.

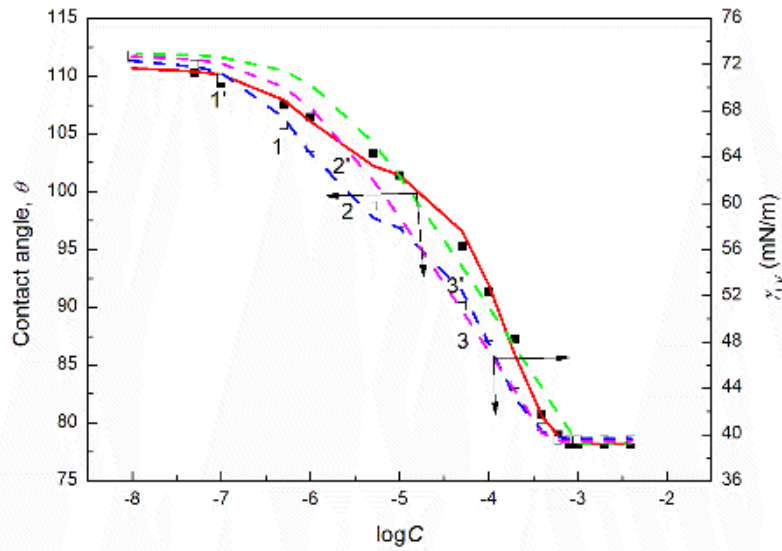**Supplementary Materials:** The following supporting information can be downloaded at: https://www.mdpi.com/article/10.3390/molecules27154706/s1, Figure S1: A plot of the TX165 aqueous solution contact angle (θ) surface tension (γ_{LV}) (curves 1–3) and contact angle (θ) on PTFE (curves 1′–3′) vs. the logarithm of TX165 concentration (*C*). Curves 1 and 1′ correspond to the measured values, curves 2 and 2′ to values calculated from the exponential function of the second order, curves 3 and 3′ correspond to the values calculate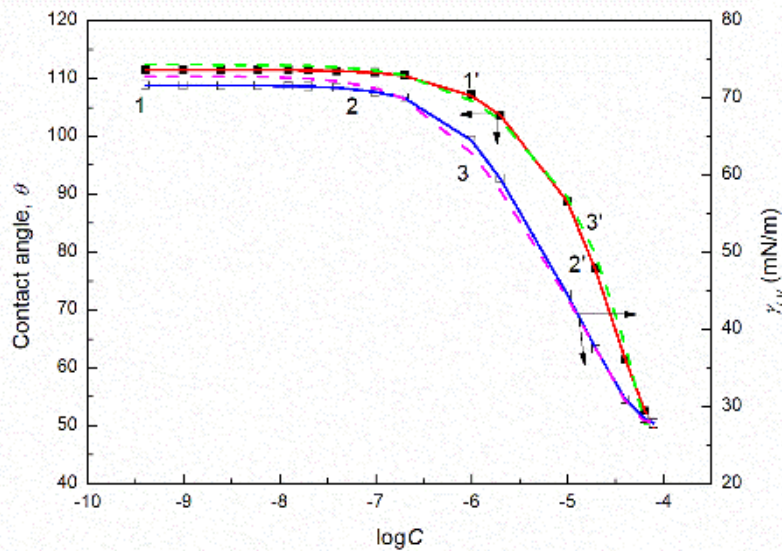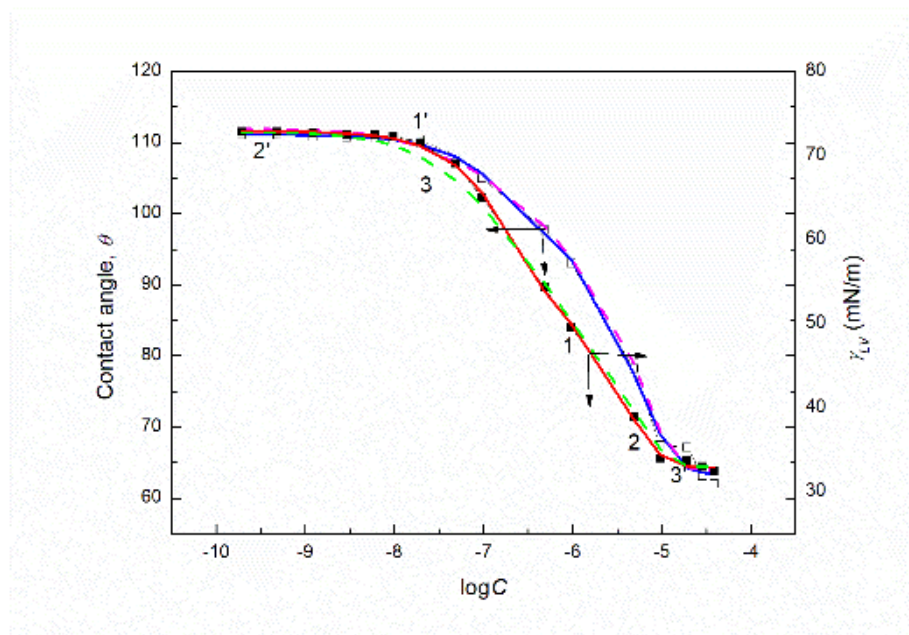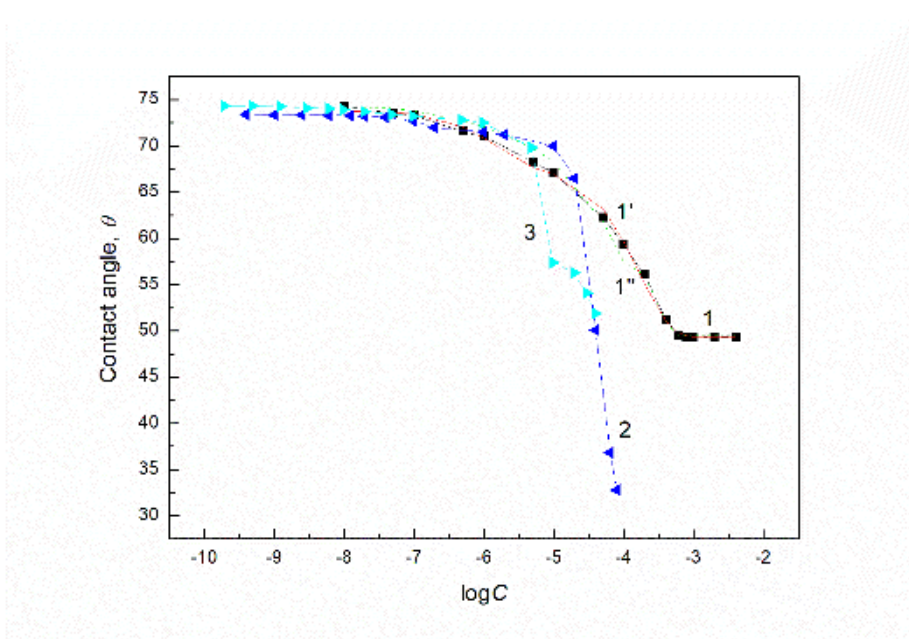d from Equations (9) and (11), respectively; Figure S2: A plot of the RL aqueous solution surface tension (γ_{LV}) (curves 1–3) and contact angle (θ) on PTFE (curves 1′–3′) vs. the logarithm of RL concentration (*C*). Curves 1 and 1′ correspond to the measured values, curves 2 and 2′ to values calculated from the exponential function of the second order, curves 3 and 3′ correspond to the values calculated from Equations (9) and (11), respectively; Figure S3:
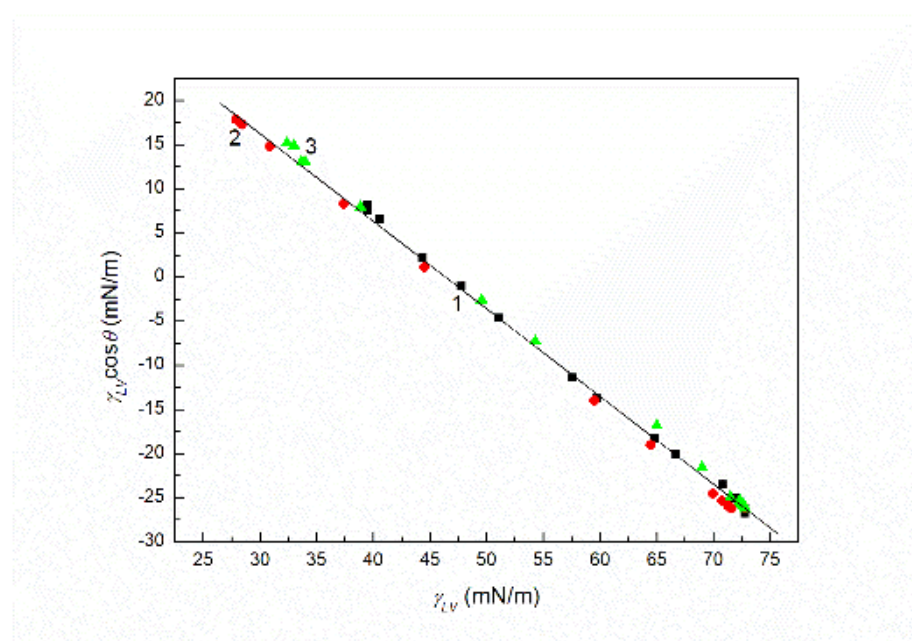
A plot of the SF aqueous solution surface tension (γ_{LV}) (curves 1–3) and contact angle (θ) on PTFE (curves 1′–3′) vs. the logarithm of SF concentration (*C*). Curves 1 and 1′ correspond the measured values, curves 2 and 2′ to values calculated from the exponential function of the second order, curves 3 and 3′ correspond to the values calculated from Equations (9) and (11), respectively; Figure S4: A plot of the contact angle (θ) of aqueous solution of TX165 (curves 1, 1′ and 1″), RL (curve 2) and SF (curve 3) on PMMA vs. the logarithm of surfactant concentration (*C*). Curves 1, 2 and 3 correspond to the measured values, curves 1′ and 1″ correspond to the values calculated from the exponential function of the second order and Equation (9), respectively; Figure S5: A plot of the contact angle (θ) of aqueous solution of TX165 (curves 1, 1′ and 1″), RL (curve 2) and SF (curve 3 and 3′) on quartz vs. the logarithm of surfactant concentration (*C*). Curves 1, 2 and 3 correspond to the measured values, curves 1′, and 3′ correspond to the values calculated from the exponential function of the second order and curve 1″ corresponds to the values calculated from Equation (9); Figure S6: A plot of the adhesion tension ($\gamma_{LV}\cos\theta$) vs. the surface tension (γ_{LV}) of aqueous solut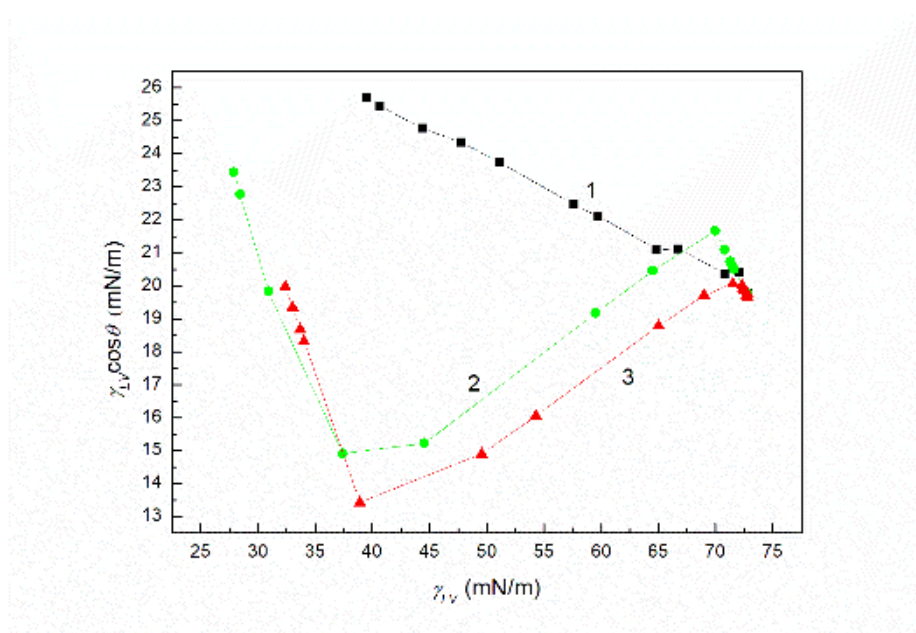ions of TX165, RL and SF for PTFE; Figure S7: A plot of the adhesion tension ($\gamma_{LV}\cos\theta$) vs. the surface tension (γ_{LV}) of aqueous solutions of TX165 (curve 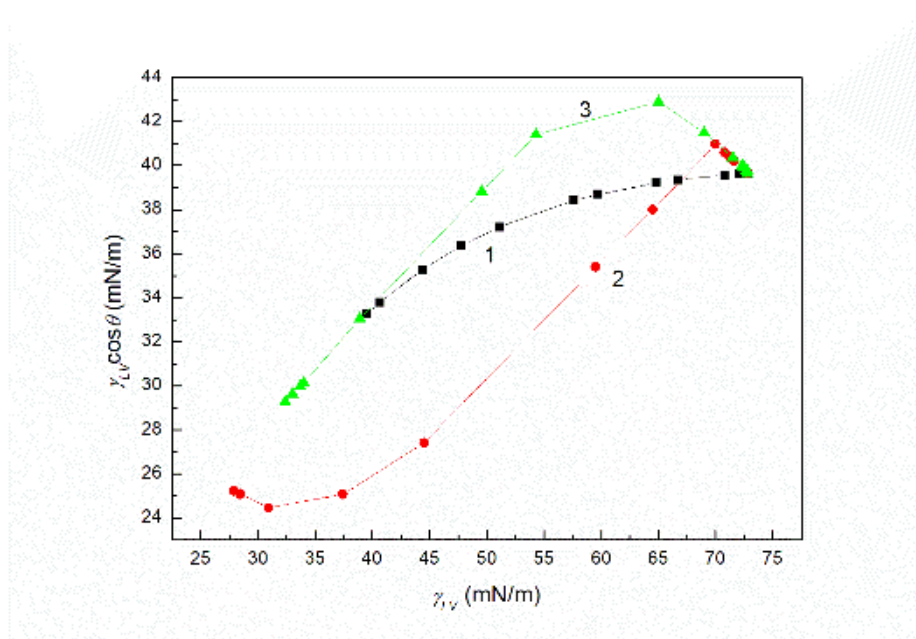1), RL (curve 2) and SF (curve 3) for PMMA; Figure S8: A plot of the adhesion tension ($\gamma_{LV}\cos\theta$) vs. the surface tension (γ_{LV}) of aqueous solutions of TX16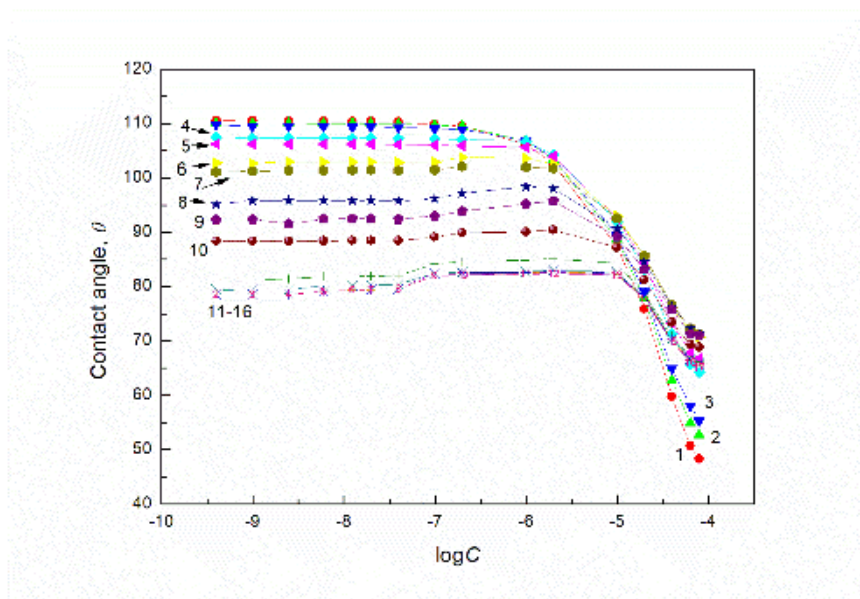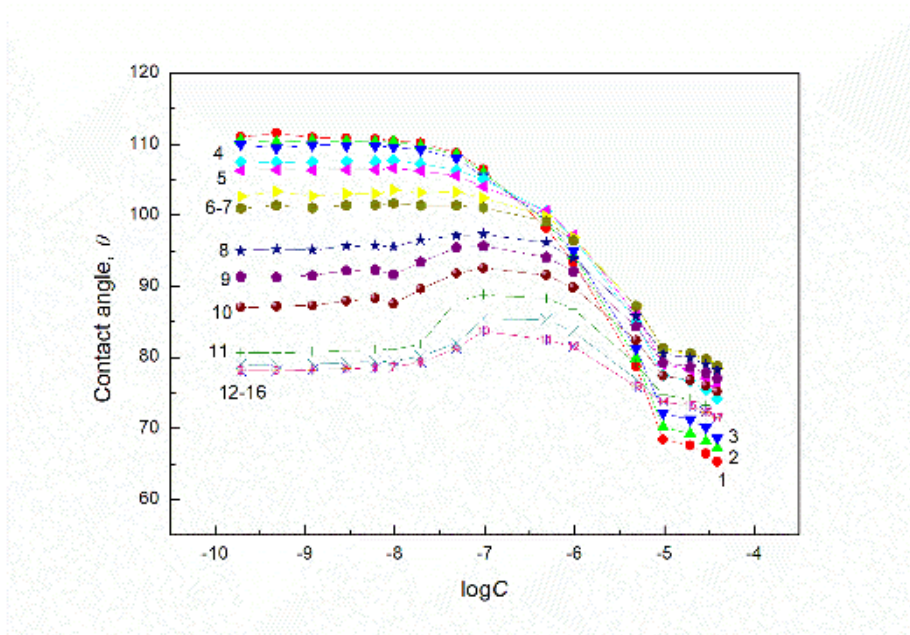5 (curve 1), RL (curve 2) and SF (curve 3) for quartz; Figure S9: A plot of the contact angle (θ) of aqueous solution of TX165 + RL mixtures on the PTFE surface vs. the logarithm of the RL concentration (*C*). Curves 1–16 correspond to the constant TX165 concentration equal to $1 \times 10^{-8}, 5 \times 10^{-8}, 1 \times 10^{-7}$, $5 \times 10^{-7}, 1 \times 10^{-6}, 5 \times 10^{-6}, 1 \times 10^{-5}, 5 \times 10^{-5}, 1 \times 10^{-4}, 2 \times 10^{-4}, 4 \times 10^{-4}, 6 \times 10^{-4}, 8 \times 10^{-4}$, 0.001, 0.002 and 0.004 mole/dm^3, respectively; Figure S10: A plot of the contact angle (θ) of aqueous solution of TX165 + SF mixtures on the PTFE surface vs. the logarithm of the SF concentration (*C*). Curves 1–16 correspond to the constant TX165 concentration equal to $1 \times 10^{-8}, 5 \times 10^{-8}, 1 \times 10^{-7}$, $5 \times 10^{-7}, 1 \times 10^{-6}, 5 \times 10^{-6}, 1 \times 10^{-5}, 5 \times 10^{-5}, 1 \times 10^{-4}, 2 \times 10^{-4}, 4 \times 10^{-4}, 6 \times 10^{-4}, 8 \times 10^{-4}$, 0.001, 0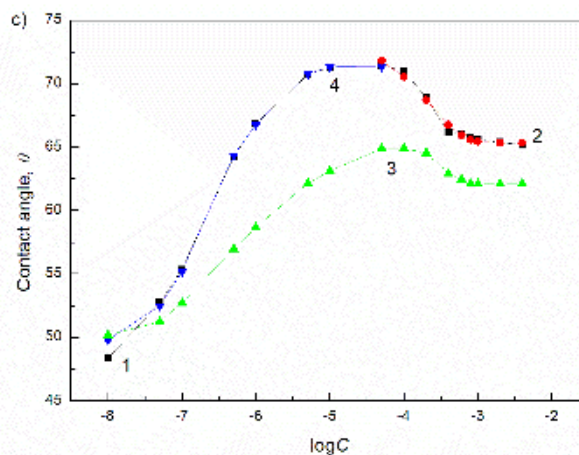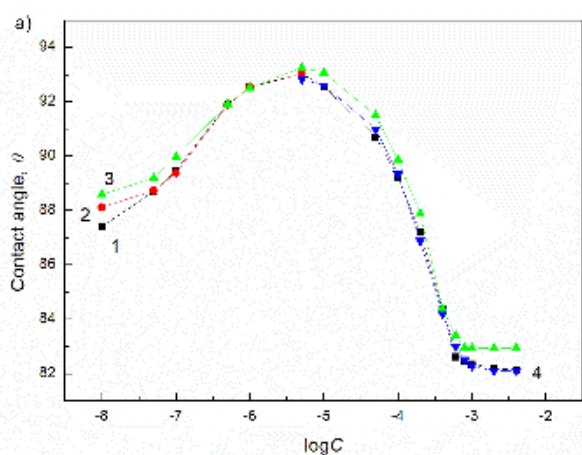.002 and 0.004 mole/dm^3, respectively; Figure S11: A plot of the contact angle (θ) of aqueous solution of TX165 + RL on PTFE at the constant RL concentration equal to 5 (a) and 40 mg/dm^3 (b) vs. the logarithm of TX165 concentration (*C*). Points 1 correspond to the measured values, curves 2–4 correspond the values calculated form the exponential function of the second order,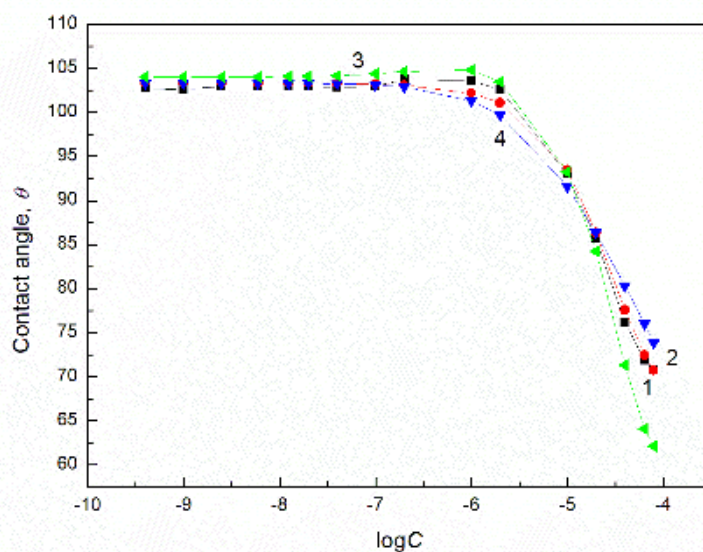 Equations (13) and (9), respectively; Figure S12: A plot of the contact angle (θ) of aqueous solution of TX165 + RL on PTFE at the constant TX165 concentration equal to 5×10^{-6} mole/dm^3 vs. the logarithm of RL concentration (*C*). Points 1 correspond to the measured values, curves 2–4 correspond the values calculated form the exponential function of the second order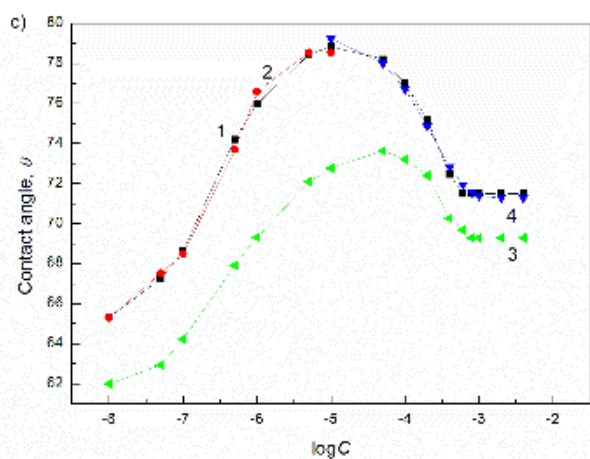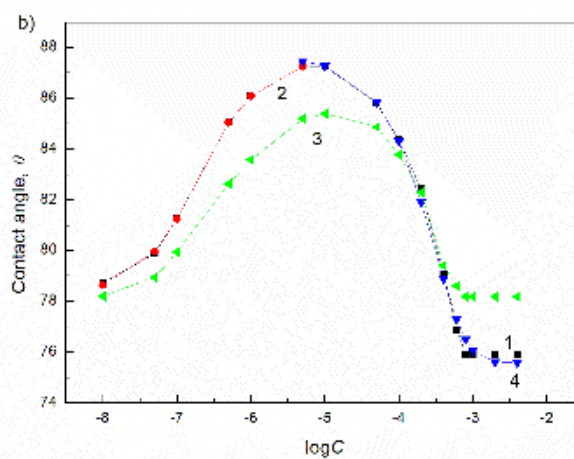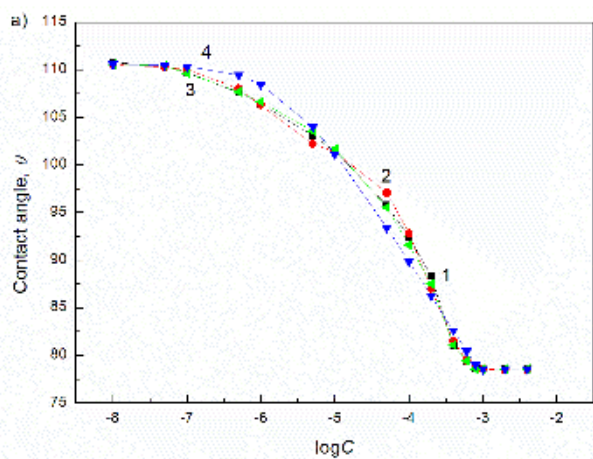, Equations (13) and (9), respectively; Figure S13: A plot of the contact angle (θ) of aqueous solution of TX165 + SF on PTFE at the constant SF concentration equal to 0.00625 (a), 5 (b) and 40 mg/dm^3 (c) vs. the logarithm of TX165 concentration (*C*). Points 1 correspond to the measured values, curves 2–4 correspond the values calculated form the exponential function of the se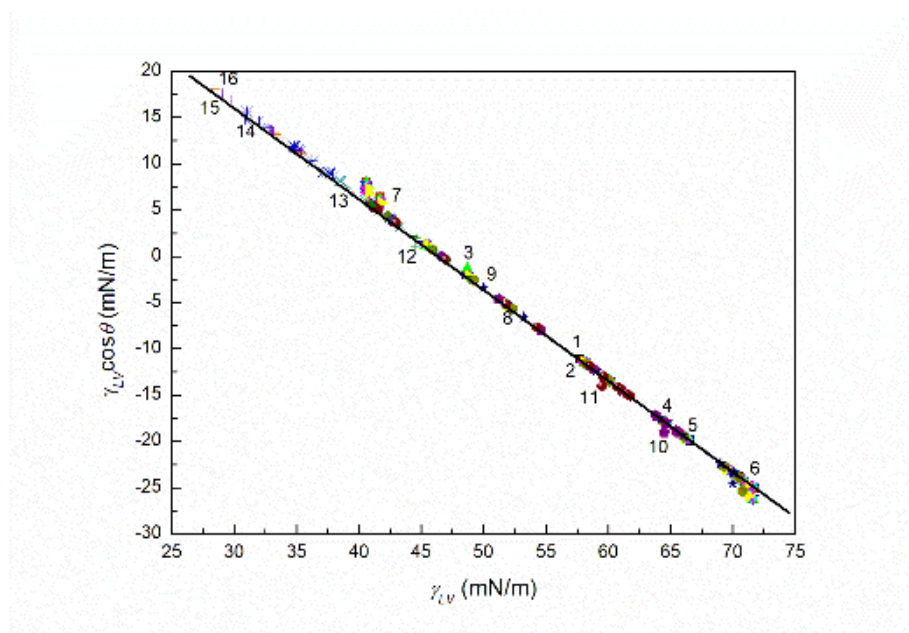cond order, Equations (13) and (9), respectively; Figure S14: A plot of the adhesion tension ($\gamma_{LV}\cos\theta$) vs. the surface tension (γ_{LV}) of aqueous solutions of TX165 + RL and TX165 + SF mixtures both at the constant b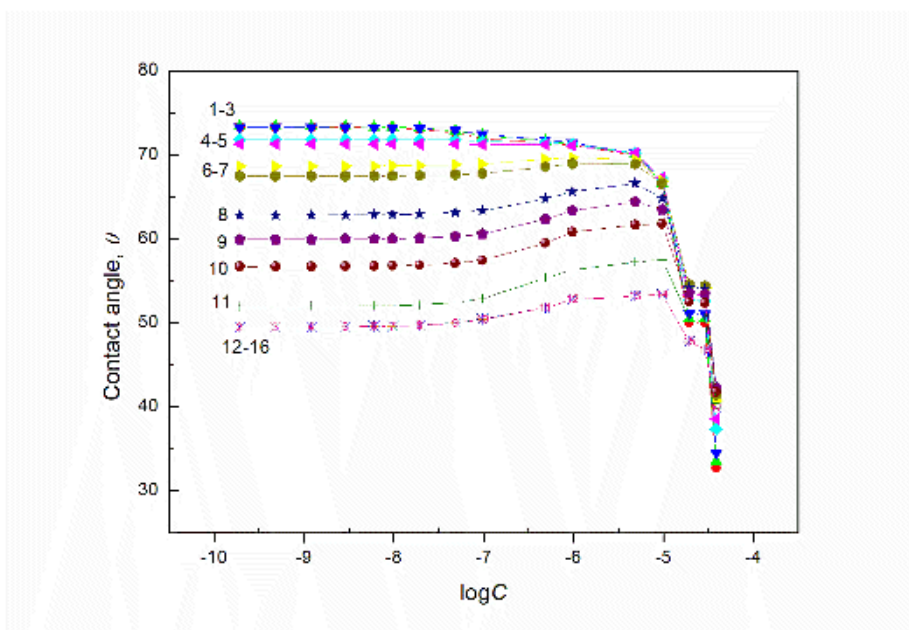iosurfactant and TX165 concentration for PTFE; Figure S15: A plot of the contact angle (θ) of aqueous solution of TX165 + RL mixtures on the PMMA surface vs. the logarithm of RL concentration (*C*). Curves 1–16 correspond to the constant TX165 concentration equal to $1 \times 10^{-8}, 5 \times 10^{-8}, 1 \times 10^{-7}, 5 \times 10^{-7}, 1 \times 10^{-6}, 5 \times 10^{-6}, 1 \times 10^{-5}, 5 \times 10^{-5}, 1 \times 10^{-4}$, $2 \times 10^{-4}, 4 \times 10^{-4}, 6 \times 10^{-4}, 8 \times 10^{-4}$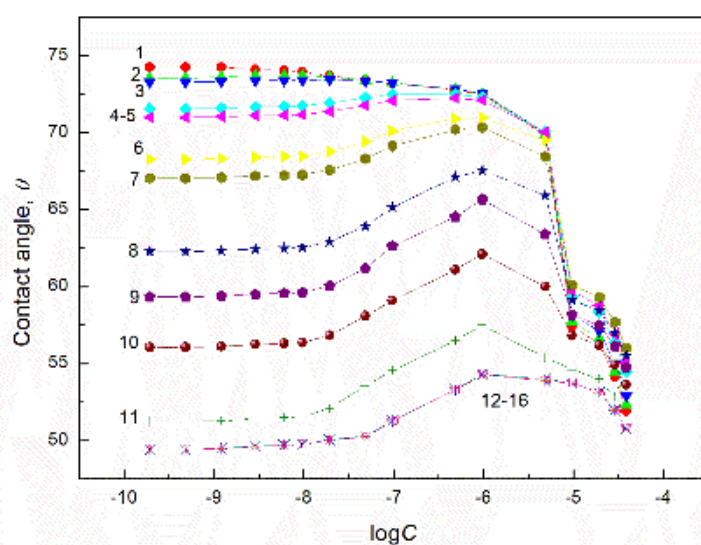, 0.001, 0.002 and 0.004 mole/dm^3, respectively; Figure S16: A plot of the contact angle (θ) of aqueous solution of TX165 + SF mixtures on the PMMA surface vs. the logarithm of the SF concentration (*C*). Curves 1–16 correspond to the constant TX165 concentration equal to $1 \times 10^{-8}, 5 \times 10^{-8}, 1 \times 10^{-7}, 5 \times 10^{-7}, 1 \times 10^{-6}, 5 \times 10^{-6}, 1 \times 10^{-5}, 5 \times 10^{-5}, 1 \times 10^{-4}$, $2 \times 10^{-4}, 4 \times 10^{-4}, 6 \times 10^{-4}, 8 \times 10^{-4}$, 0.001, 0.002 and 0.004 mole/dm^3, respectively; Figure S17: A plot of the contact angle (θ) of aqueous solution of TX165 + RL mixtures on the quartz surface vs. the logarithm of the RL concentration (*C*). Curves 1–16 correspond to the constant TX165 concentration equal to $1 \times 10^{-8}, 5 \times 10^{-8}, 1 \times 10^{-7}, 5 \times 10^{-7}, 1 \times 10^{-6}, 5 \times 10^{-6}, 1 \times 10^{-5}, 5 \times 10^{-5}, 1 \times 10^{-4}$, $2 \times 10^{-4}, 4 \times 10^{-4}, 6 \times 10^{-4}, 8 \times 10^{-4}$, 0.001, 0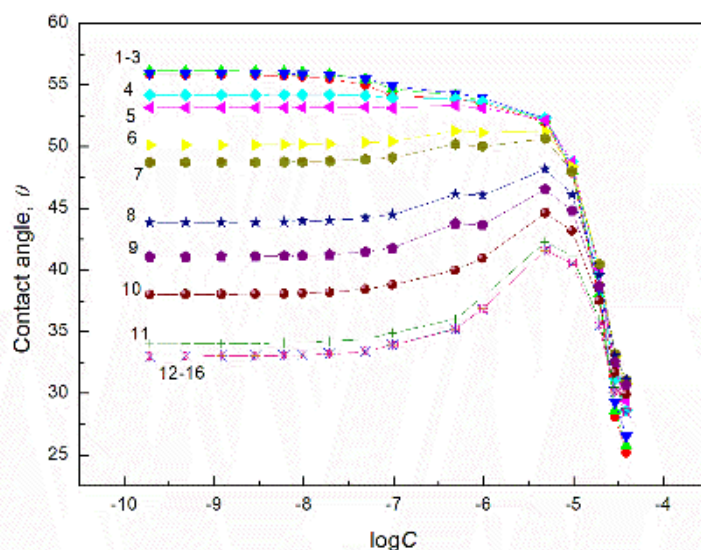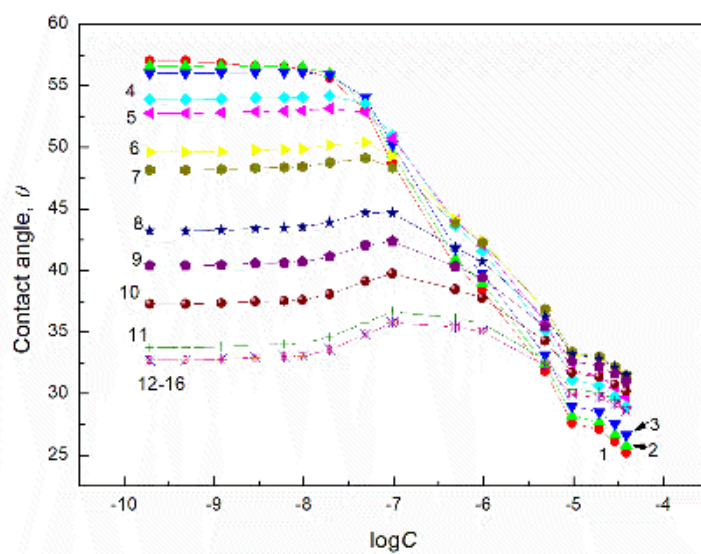.002 and 0.004 mole/dm^3, respectively; Figure S18: A plot of the contact angle (θ) of aqueous solution of TX165 + SF mixtures on the quartz surface vs. the logarithm of the SF concentration (*C*). Curves 1–16 correspond to the constant TX165 concentration equal to $1 \times 10^{-8}, 5 \times 10^{-8}, 1 \times 10^{-7}, 5 \times 10^{-7}, 1 \times 10^{-6}, 5 \times 10^{-6}, 1 \times 10^{-5}, 5 \times 10^{-5}, 1 \times 10^{-4}$, $2 \times 10^{-4}, 4 \times 10^{-4}, 6 \times 10^{-4}, 8 \times 10^{-4}$, 0.001, 0.002 and 0.004 mole/dm^3, respectively; Figure S19: A plot of the adhesion tension ($\gamma_{LV}\cos\theta$) vs. the surface tension (γ_{LV}) of aqueous solutions of TX165 + RL at the constant concentration of RL (a) and TX165 (b) at all studied concentration for PMMA; Figure S20: A plot of the adhesion tension ($\gamma_{LV}\cos\theta$) vs. the surface tension (γ_{LV}) of

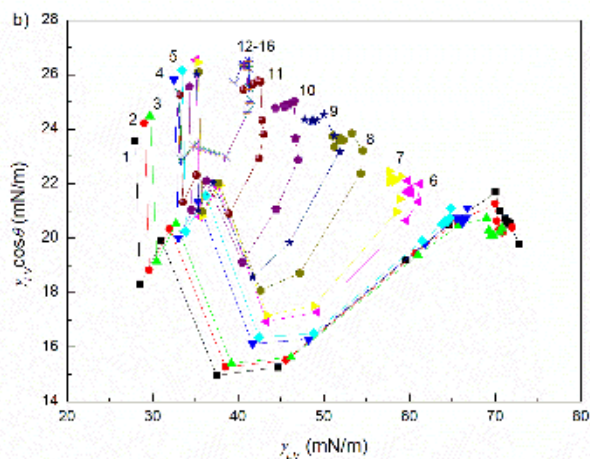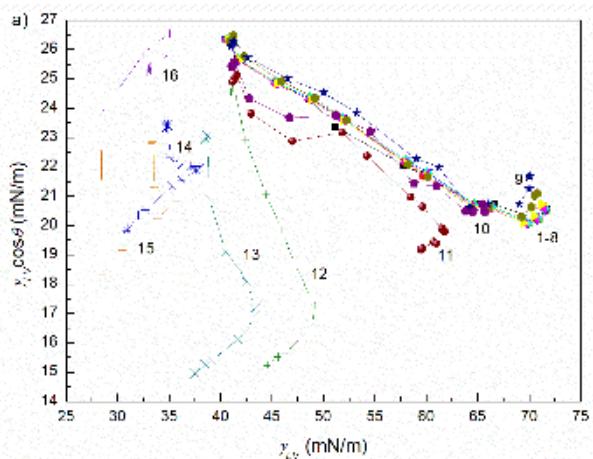aqueous solutions of TX165 + SF at the constant concentration of SF (a) and TX165 (b) at all studied concentration for PMMA; Figure S21: A plot of the adhesion tension ($\gamma_{LV} \cos \theta$) vs. the surface tension (γ_{LV}) of aqueous solutions of TX165 + RL at the constant concentration of RL (a) and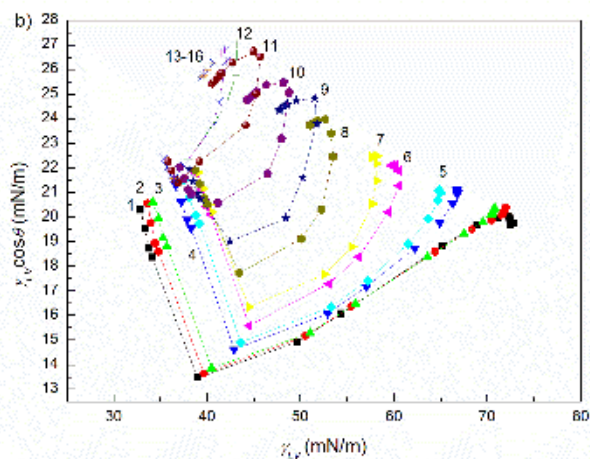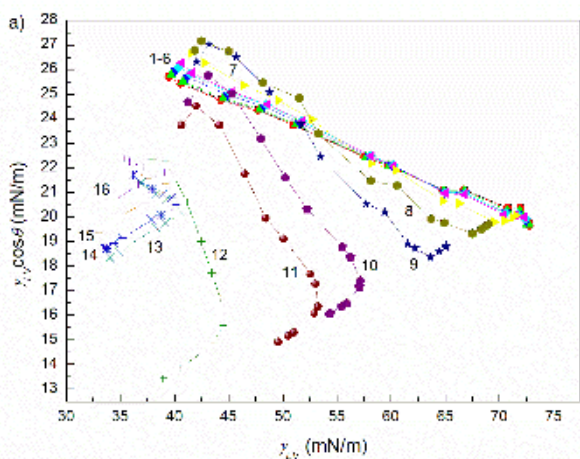 TX165 (b) at all studied concentration for quartz; Figure S22: A plot of the adhesion tension ($\gamma_{LV} \cos \theta$) vs. the surface tension (γ_{LV}) of aqueous solutions of TX165 + SF at the constant concentration of SF (a) and TX16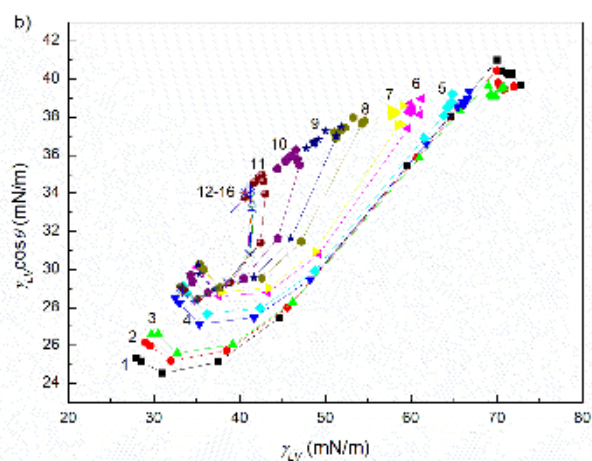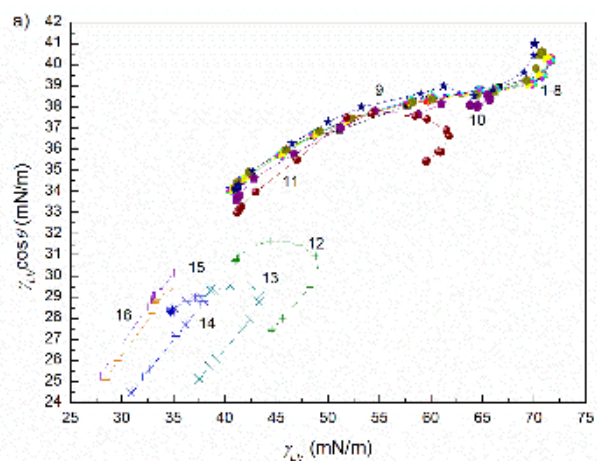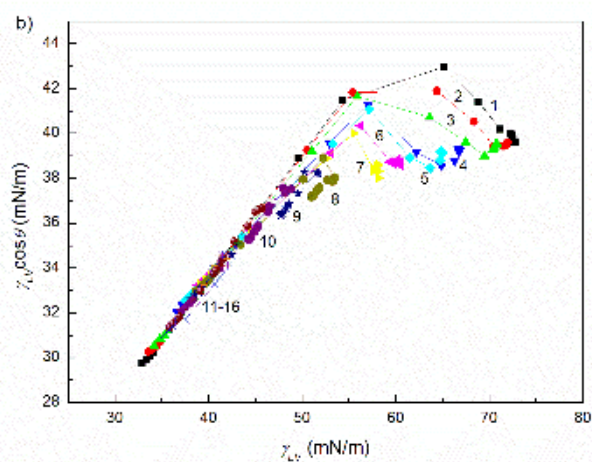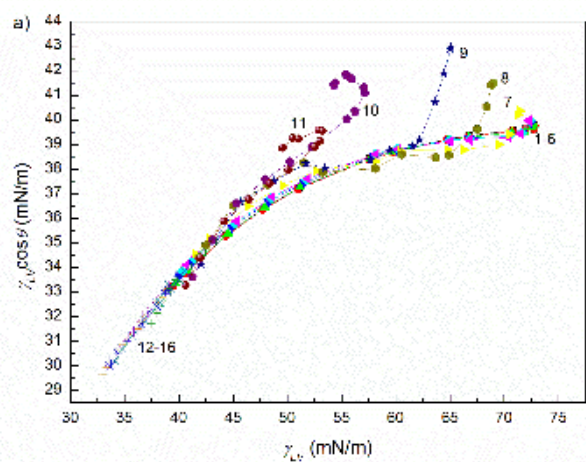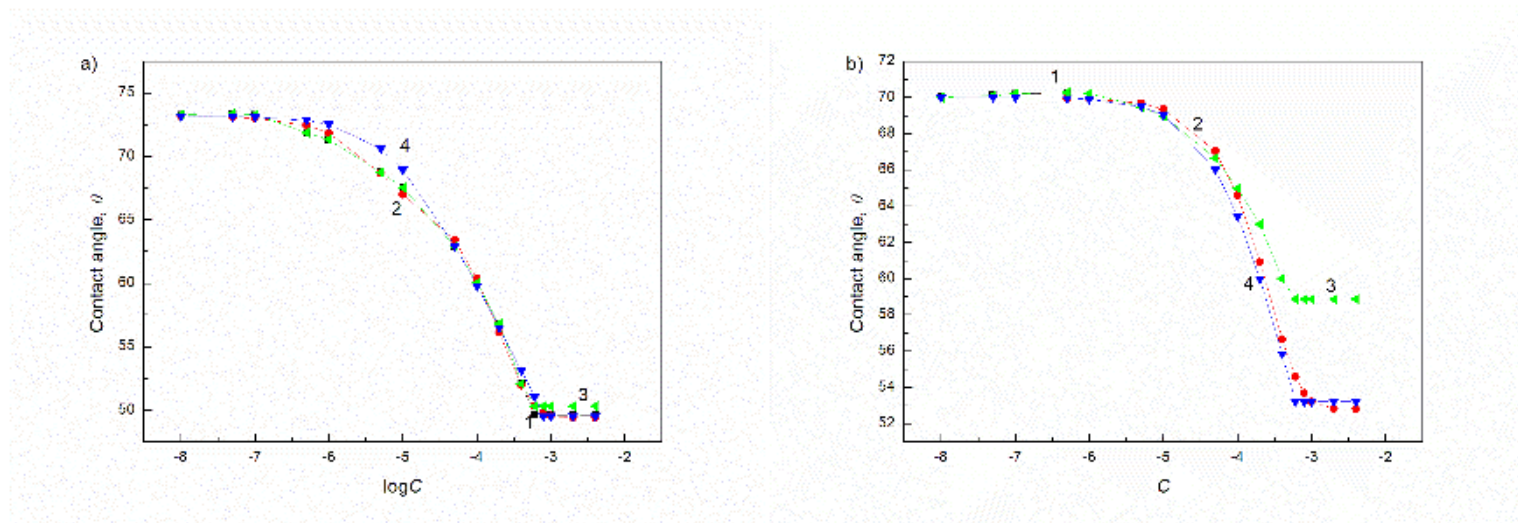5 (b) at all studied concentration for quartz; Figure S23: A plot of the contact angle (θ) for TX165 + RL for PMMA at the constant RL concentration equal to 0.00625 (a), 5 (b) mg/dm^3 vs. the logarithm of TX165 concentration (*C*). Points 1 correspond to the measured values, curves 2–4 correspond the values calculated form the exponential function of the second order, Equations (13) and (9), respectively; Figure S24: A plot of the contact angle (θ) for TX165 + SF for PMMA at the constant SF concentration equal to 0.00625 (a), 5 (b) and 40 mg/dm^3 (c) vs. the logarithm of TX165 concentration (*C*). Points 1 correspond to the measured values, curves 2–4 correspond the values calculated form the exponential function of the second order, Equations (13) and (9), respectively; Figure S25: A plot of the contact angle (θ) for TX165 + RL for quartz at the constant RL concentration equal to 0.00625 (a), 5 (b) and 40 mg/dm^3 (c) vs. the logarithm of TX165 concentration (*C*). Points 1 correspond to the measured values, curves 2–4 correspond the values calculated form the exponential function of the second order, Equations (13) and (9), respectively; Figure S26: A plot of the contact angle (θ) for TX165 + SF for quartz at the constant SF concentration equal to 0.00625 (a), 5 (b) and 40 mg/dm^3 (c) vs. the logarithm of TX165 concentration (*C*). Points 1 correspond to the measured values, curves 2–4 correspond the values calculated form the exponential function of the second order, 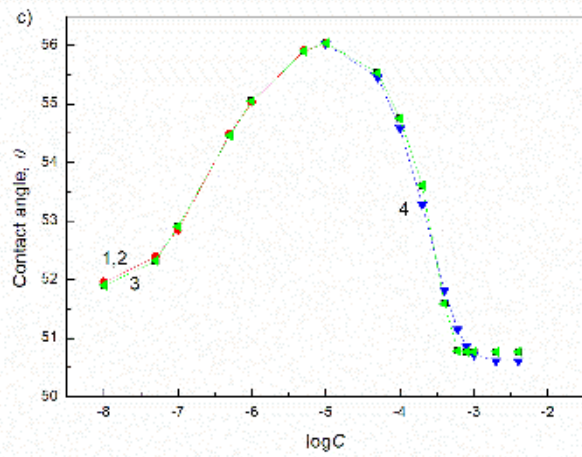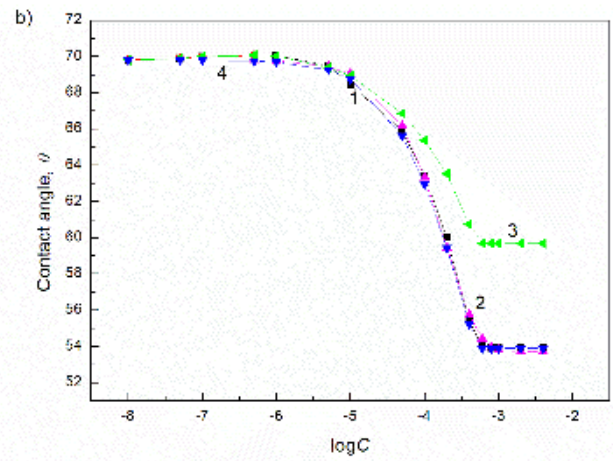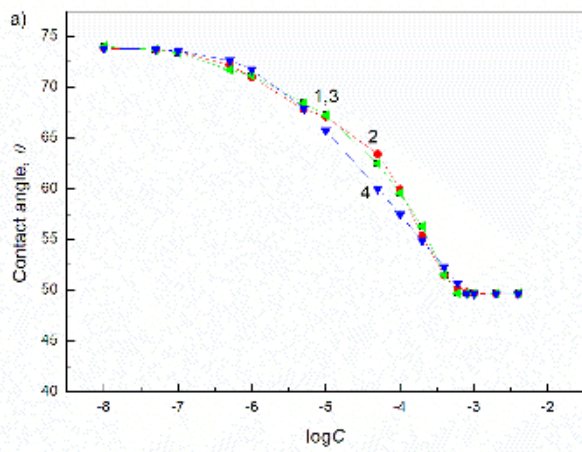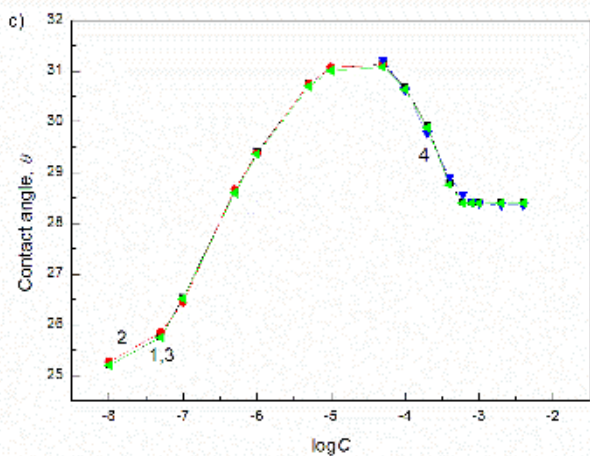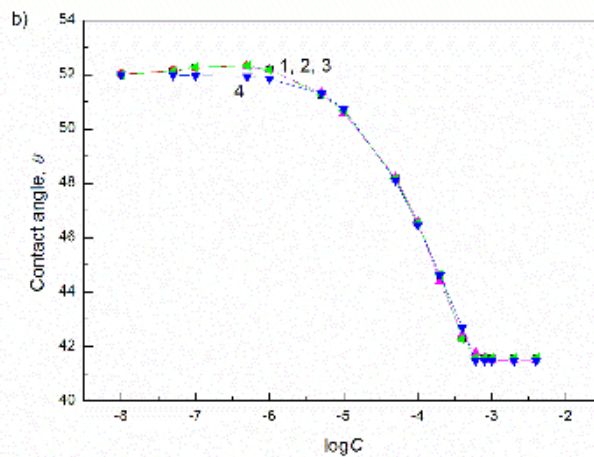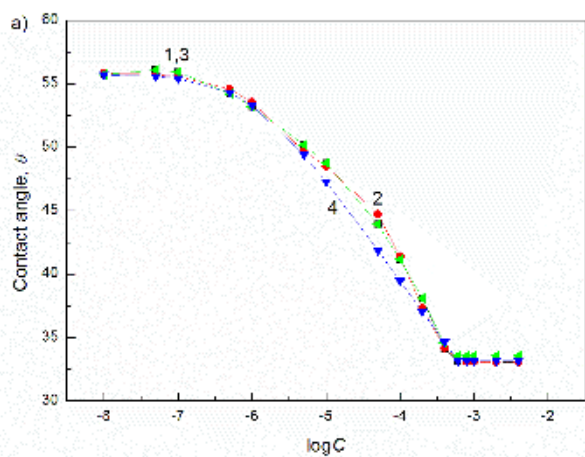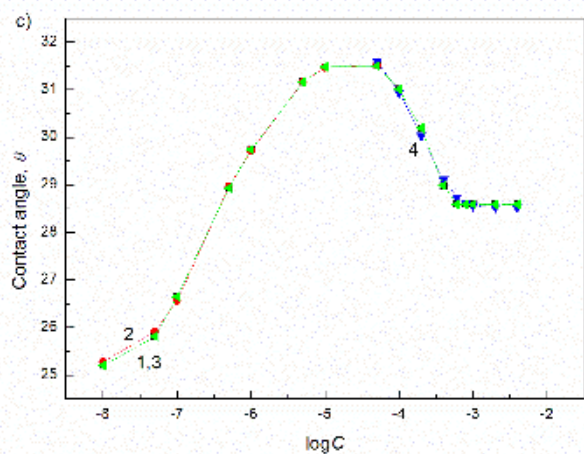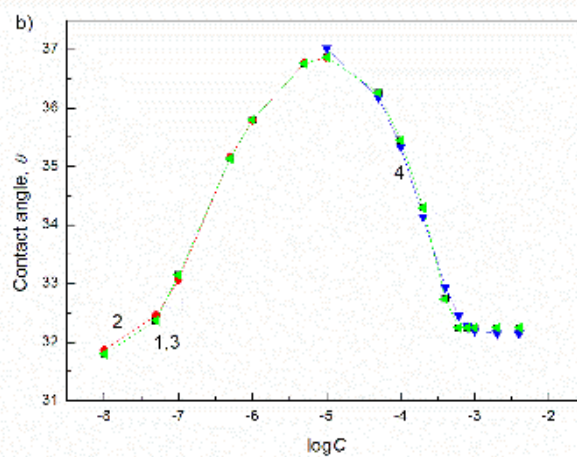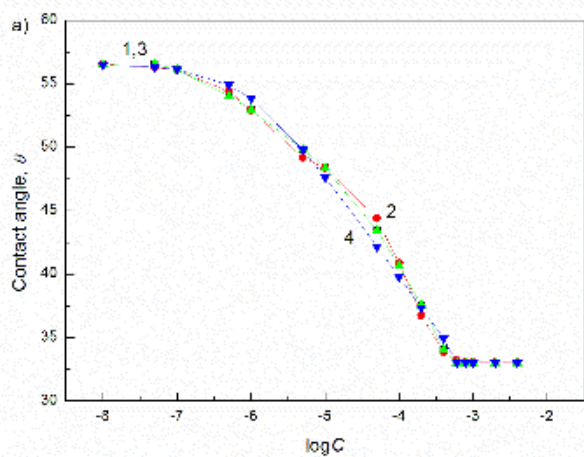Equations (13) and (9), respectively; Figure S27: A plot of the Gibbs surface excess concentration at the PTFE-water interface (Γ_{SL}) for TX165 (a, c), RL (b) and SF (d) vs. the logarithm of surfactant concentration (*C*) calculated from Equations (5) and (15); Figure S28: A plot of the Gibbs surface excess concentration at the PTFE-water interface (Γ_{SL}) for TX165 (curve 1), RL (2) and their sum (curve 3) vs. the logarithm of surfactant concentration (*C*) at the constant RL equal to 0.0002 (a), 0.00625 (b), 5 (c) and 40 mg/dm^3 (d); Figure S29: A plot of the Gibbs surface excess concentration at the PTFE-water interface (Γ_{SL}) for TX165 (curve 1), RL (2) and their sum (curve 3) vs. the logarithm of surfactant concentration (*C*) at the constant TX165 concentration equal to 5×10^{-7} (a), 1×10^{-6} (b), 2×10^{-4} (c) and 1×10^{-3} mole/dm^3 (d); Figure S30: A plot of the Gibbs surface excess concentration at the PTFE-water interface (Γ_{SL}) for TX165 (curve 1), SF (2) and their sum (curve 3) vs. the logarithm of surfactant concentration (*C*) at the constant SF concentration eq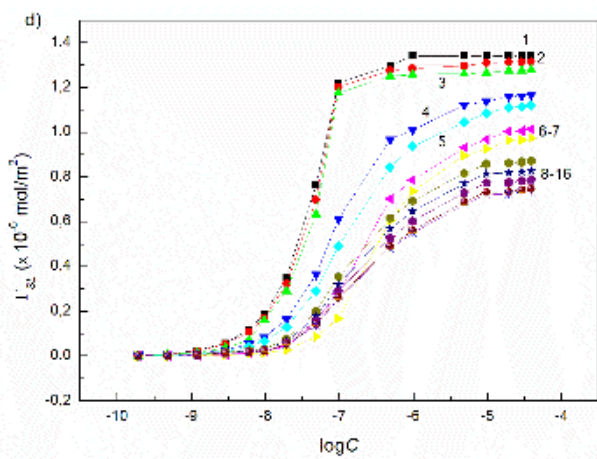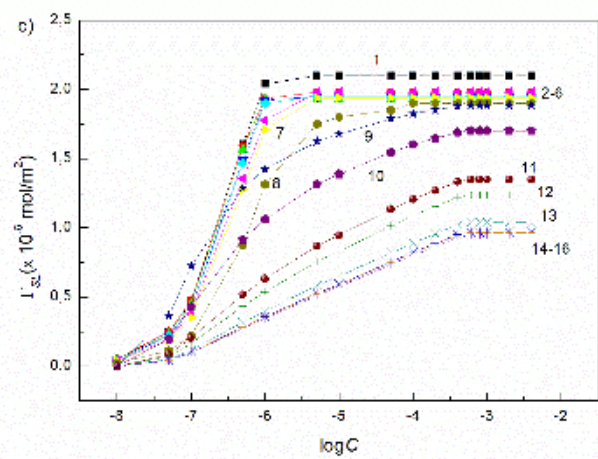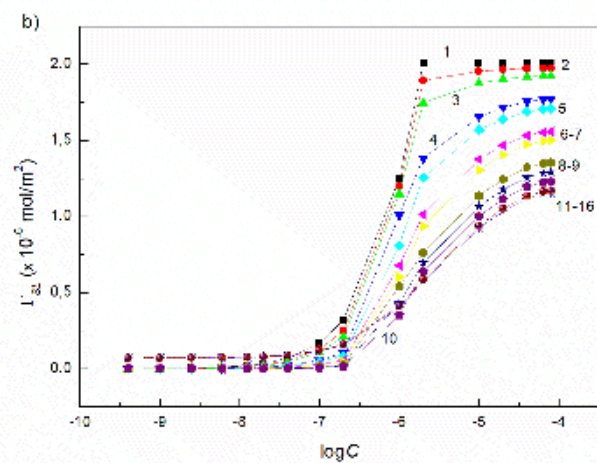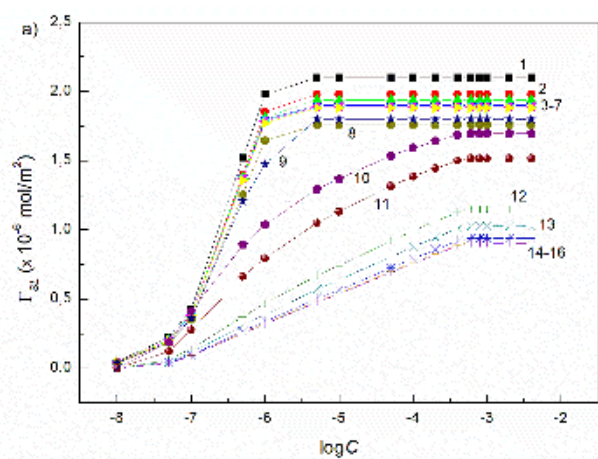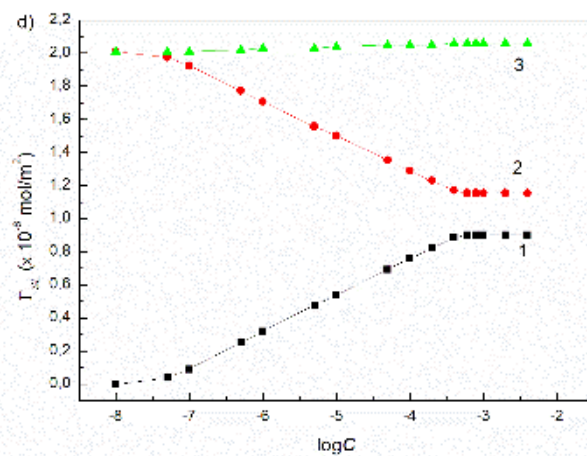ual to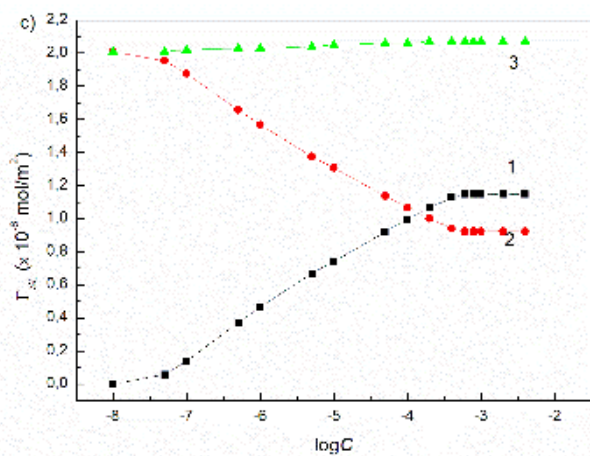 0.0002 (a), 0.00625 (b), 5 (c) and 40 mg/dm^3 (d); Figure S31: A plot of the Gibbs surface excess concentration at the PTFE-water interface (Γ_{SL}) for TX165 (curve 1), SF (2) and their sum (curve 3) vs. the logarithm of surfactant concentration (*C*) at the constant TX165 concentration equal to 5×10^{-7} (a), 1×10^{-6} (b), 2×10^{-4} (c) and 1×10^{-3} mole/dm^3 (d); Figure S32: A plot of the Gibbs surface excess concentration at the PMMA-water interface (Γ_{SL}) vs. the logarithm of surfactant concentration (*C*) for TX165 + RL (a,b) and TX165 +SF (c,d) at the constant TX165 concentration (b, d) and RL (a) as well as SF (c); Figure S33: A plot of the Gibbs surface excess concentration at the PMMA-air interface (Γ_{SV}) vs. the logarithm of surfactant concentration (*C*) for TX165 + RL (a, b) and TX165 +SF (c, d) at the constant TX165 concentration (b, d) and RL (a) as well as SF (c); Figure S34: A plot of the Gibbs surface excess concentration at the quartz-water interface (Γ_{SL}) vs. the logarithm of surfactant concentration (*C*) for TX165 + RL (a,b) and TX165 +SF (c,d) at the constant TX165 concentration (b,d) and RL (a) as well as SF (c); Figure S35: A plot of the Gibbs surface excess concentration at the quartz-air interface (Γ_{SV}) vs. the logarithm of surfactant concentration (*C*) for TX165 + RL (a, b) and TX165 +SF (c, d) at the constant TX165 concentration (b,d) and RL (a) as well as SF (c); Figure S36: The difference between the Gibbs surface excess concentration at the PMMA-water and PMMA-air interface vs. the logarithm of surfactant concentration (*C*) for TX165 + RL (a) and TX165 +SF (b). Curves 1–4 correspond to the constant biosurfactant concentration equal to 0.0002, 0.00625, 5 and 40 mg/dm^3; Figure S37: A plot of the difference between the Gibbs surface excess concentration at the quartz-water and quartz-air interface vs. the logarithm of surfactant concentration (*C*) for TX165 + RL (a) and TX165 +SF (b). Curves 1–4 correspond to the constant biosurfactant concentration equal to 0.0002, 0.00625, 5 and 40 mg/dm^3; Figure S38: A plot of the difference between the values of the PMMA(quartz)-air interface tension ($\Delta\gamma_{SV}$) at the TX165 + biosurfactant mixture concentration equal to zero and equal to a given value (curve 1) and between the PMMA(quartz)-water (curve 2) and PMMA(quartz)-solution (curve 2) ($\Delta\gamma_{SL}$) as well as the difference between the values of contact angle of the water and solution on the PMMA (a,b) and quartz (c,d) ($\Delta\gamma_{\theta}$) (curve 3) at the constant RL and SF concentration equal to 0.00625 mg/dm^3 vs. the logarithm of surfactant concentration (*C*).

References

1. Rosen, M.J. *Surfactants and Interfacial Phenomena*, 3rd ed.; Wiley Intersccience: New York, NY, USA, 2004.
2. Marchant, R.; Banat, I.M. Biosurfactants: A sustainable replacement for chemical surfactants. *Biotechnol. Lett.* **2012**, *34*, 1597–1605. [CrossRef] [PubMed]
3. Banat, I.M.; Makkar, R.S.; Cameotra, S.S. Potential commercial applications of microbial surfactants. *Appl. Microbiol. Biotechnol.* **2000**, *53*, 495–508. [CrossRef] [PubMed]
4. Ishigami, Y.; Osman, M.; Nakahara, H.; Sano, Y.; Ishiguro, R.; Matsumoto, M. Significance of β-sheet formation for micellization and surface adsorption of surfactin. *Colloids Surf. B* **1995**, *4*, 341–348. [CrossRef]
5. Zdziennicka, A.; Jańczuk, B. Thermodynamic parameters of some biosurfactants and surfactants adsorption at water-air interface. *J. Mol. Liq.* **2017**, *243*, 236–244. [CrossRef]
6. Tânia, M.S.; Lima, T.M.S.; Procópio, L.C.; Brandão, F.D.; Carvalho, A.M.X.; Tótola, M.R.; Borges, A.C. Biodegradability of bacterial surfactants. *Biodegradation* **2011**, *3*, 585–592. [CrossRef]
7. Sarubbo, L.A.; Maria da Gloria, C.S.; Durval, I.J.B.; Bezerra, K.G.O.; Ribeiro, B.G.; Silva, I.A.; Twigg, M.S.; Banat, I.M. Biosurfac-tants: Production, properties, applications, trends, and general perspectives. *Biochem. Eng. J.* **2022**, *181*, 108377. [CrossRef]
8. Drakontis, C.E.; Amin, S. Biosurfactants: Formulations, properties, and applications. *Curr. Opin. Colloid Interface Sci.* **2020**, *48*, 77–90. [CrossRef]
9. Mulligan, C.N. Environmental applications for biosurfactants. *Environ. Pollut.* **2005**, *133*, 183–198. [CrossRef]
10. Seydlová, G.; Svobodová, J. Review of surfactin chemical properties and the potential biomedical applications. *Cent. Eur. J. Med.* **2008**, *3*, 123–133. [CrossRef]
11. Rodrigues, L.; Banat, I.M.; Teixeira, J.; Oliveira, R. Biosurfactants: Potential applications in medicine. *J. Antimicrob. Chemother.* **2006**, *57*, 609–618. [CrossRef]
12. Nitschke, M.; Costa, S.G.V.A.O. Biosurfactants in food industry. *Trends Food Sci. Technol.* **2007**, *18*, 252–259. [CrossRef]
13. Sekhon Randhawa, K.K.; Rahman, P.K.S.M. Rhamnolipid biosurfactants—Past, present, and future scenario of global market. *Front. Microbiol.* **2014**, *5*, 454. [CrossRef] [PubMed]
14. Bafghi, M.K.; Fazaelipoor, M.H. Application of rhamnolipid in the formulation of a detergent. *J. Surfactant Deterg.* **2012**, *15*, 679–684. [CrossRef]
15. Chen, W.C.; Juang, R.-S.; Wei, Y.-H. Applications of a lipopeptide biosurfactant, surfactin, produced by microorganisms. *Biochem. Eng. J.* **2015**, *103*, 158–169. [CrossRef]
16. Shaligram, N.S.; Singhal, R.S. Surfactin—A review on biosynthesis, fermentation, purification and applications. *Food Technol. Biotechnol.* **2010**, *48*, 119–134.
17. Shah, M.U.H.; Moniruzzaman, M.; Sivapragasam, M.; Talukder, M.M.; Bt Yusup, S.; Goto, M. A binary mixture of a biosurfactant and an ionic liquid surfactant as a green dispersant for oil spill remediation. *J. Mol. Liq.* **2019**, *280*, 111–119. [CrossRef]
18. Chen, M.L.; Penfold, J.; Thomas, R.K.; Smyth, T.J.; Perfumo, A.; Marchant, R.; Banat, I.M.; Stevenson, P.; Parry, A.; Tucker, I.; et al. Mixing Behaviour of the Biosurfactant, Rhamnolipid, with a Conventional Anionic Surfactant, Sodium Dodecyl Benzene Sulfonate. *Langmuir* **2010**, *23*, 17958–17968. [CrossRef]
19. Xu, L.; Amin, S. Microrheological study of ternary surfactant-biosurfactant mixtures. *Int J. Cosmet Sci* **2019**, *41*, 364–370. [CrossRef]
20. Adamson, W.; Gast, A.P. *Physical Chemistry of Surfaces*, 6th ed.; Wiley Interscience: New York, NY, USA, 1997.
21. Mańko, D.; Zdziennicka, A.; Jańczuk, B. Surface tension of polytetrafluoroethylene and its wetting by aqueous solution of some surfactants and their mixtures. *Appl. Surf. Sci.* **2017**, *392*, 117–125. [CrossRef]
22. Szymczyk, K.; Zdziennicka, A.; Krawczyk, J.; Jańczuk, B. Correlation between wetting, adhesion and adsorption in the polymer–aqueous solutions of ternary surfactant mixtures–air systems. *Appl. Surf. Sci.* **2014**, *288*, 488–496. [CrossRef]
23. Szymczyk, K.; González-Martín, M.L.; Morales Bruque, J.; Jańczuk, B. Effect of two hydrocarbon and one fluorocarbon surfactant mixtures on the surface tension and wettability of polymers. *J. Colloid Interface Sci.* **2014**, *47*, 180–187. [CrossRef] [PubMed]

24. Rekiel, E.; Zdziennicka, A.; Szymczyk, K.; Jańczuk, B. Thermodynamic Analysis of the Adsorption and Micellization Activity of the Mixtures of Rhamnolipid and Surfactin with Triton X-165. *Molecules* **2022**, *27*, 3600. [CrossRef]

25. Godin, M.S.; Della Torre, T. The use of expanded polytetrafluoroethylene (e-PTFE) implants in rhinoplasty. *Oper. Tech. Otolayngol. Head Neck. Surg.* **2008**, *19*, 285–289. [CrossRef]

26. Krawczyk, J. Surface free energy of the human skin and its critical surface tension of wetting in the skin/surfactant aqueous solution/air system. *Skin Res. Technol.* **2015**, *21*, 214–223. [CrossRef]

27. van Oss, C.J.; Chaudhury, M.K.; Good, R.J. Monopolar surfaces. *Adv. Colloid Interface Sci.* **1987**, *28*, 35–64. [CrossRef]

28. van Oss, C.J. *Interfacial Forces in Aqueous Media*, 1st ed.; Marcel Dekker: New York, NY, USA, 1994.

29. van Oss, C.J.; Constanzo, P.M. Adhesion of anionic surfactants to polymer surfaces and low-energy materials. *J. Adhes. Sci. Technol.* **1992**, *4*, 477–487. [CrossRef]

30. Fowkes, F.M. Attractive forces at interfaces. *Ind. Eng. Chem.* **1964**, *56*, 40–52. [CrossRef]

31. Szymczyk, K.; Zdziennicka, A.; Krawczyk, J.; Jańczuk, B. Wettability, adhesion, adsorption and interface tension in the polymer/surfactant aqueous solution system: II. Work of adhesion and adsorption of surfactant at polymer–solution and solution–air interfaces. *Colloids Surf. A Physicochem. Eng. Asp.* **2012**, *402*, 139–145. [CrossRef]

32. Beyer, K. Phase structures, water binding, and molecular dynamics in liquid crystalline and frozen states of the system Triton X-100-D2O: A deuteron and carbon NMR study. *J. Colloid Interface Sci.* **1982**, *86*, 73–89. [CrossRef]

33. Desai, T.R.; Dixit, S.G. Interaction and Viscous Properties of Aqueous Solutions of Mixed Cationic and Nonionic Surfactants. *J. Colloid Interface Sci.* **1996**, *177*, 471–477. [CrossRef]

34. Zdziennicka, A.; Krawczyk, J.; Szymczyk, K.; Jańczuk, B. Macroscopic and microscopic properties of some surfactants and biosurfactants. *Int. J. Mol. Sci.* **2018**, *19*, 1934. [CrossRef] [PubMed]

35. Rekiel, E.; Zdziennicka, A.; Jańczuk, B. Mutual influence of ethanol and surfactin on their wetting and adhesion properties. *Colloids Surf. A Physicochem. Eng. Asp.* **2021**, *627*, 127161. [CrossRef]

36. Lucassen-Reynders, E.H. Contact angles and adsorption on solids. *J. Phys. Chem.* **1963**, *67*, 969–972. [CrossRef]

37. Boer, J.H. *The Dynamical Character of Adsorption*, 1st ed.; Oxford University Press: London, UK, 1953.

38. Zdziennicka, A.; Szymczyk, K.; Krawczyk, J.; Jańczuk, B. Activity and thermodynamic parameters of some surfactants adsorption at the water–air interface. *Fluid. Phase Equilib.* **2012**, *318*, 25–33. [CrossRef]

39. Zdziennicka, A.; Krawczyk, J.; Jańczuk, B. Volumetric properties of rhamnolipid and surfactin at different temperatures. *J. Mol. Liq.* **2018**, *255*, 562–571. [CrossRef]

40. Rekiel, E.; Zdziennicka, A.; Jańczuk, B. Adsorption of surfactin at water with ethanol mixture-air interface. *J. Mol. Liq.* **2020**, *300*, 112240. [CrossRef]

41. Zisman, W.A. Contact angle wettability and adhesion. In *Advances in Chemistry Series*; Fowkes, F.M., Ed.; American Chemical Society: Washington, DC, USA, 1964; Volume 43, pp. 1–51.

42. Bernett, M.K.; Zisman, W.A. Relation of wettability by aqueous solutions to the surface constitution of low-energy solids. *J. Phys. Chem.* **1959**, *63*, 1241–1246. [CrossRef]

43. Szymczyk, K.; Zdziennicka, A.; Jańczuk, B. Properties of some nonionic fluorocarbon surfactants and their mixtures with hydrocarbon ones. *Adv. Colloid Interface Sci.* **2021**, *292*, 102421. [CrossRef]

Wetting properties of rhamnolipid and surfactin mixtures with Triton X-165

Edyta Rekiel [1], Anna Zdziennicka [1], Katarzyna Szymczyk [1] and Bronisław Jańczuk [1,*]

Department of Interfacial Phenomena, Institute of Chemical Sciences, Faculty of Chemistry, Maria Curie-Skłodowska University in Lublin. Maria Curie-Skłodowska Sq.3, 20-031 Lublin, Poland

*Correspondence: bronislaw.janczuk@poczta.umcs.lublin.pl ; Tel.: (48-81) 537-56-70

Figure S1. A plot of the TX165 aqueous solution contact angle (θ) surface tension (γ_{LV}) (curves 1 - 3) and contact angle (θ) on PTFE (curves 1' - 3') vs. the logarithm of TX165 concentration (C). Curves 1 and 1' correspond to the measured values, curves 2 and 2' to values calculated from the exponential function of the second order, curves 3 and 3' correspond to the values calculated from Eqs. (9) and (11), respectively.

Figure S2. A plot of the RL aqueous solution surface tension (γ_{LV}) (curves 1 - 3) and contact angle (θ) on PTFE (curves 1' - 3') vs. the logarithm of RL concentration (C). Curves 1 and 1' correspond to the measured values, curves 2 and 2' to values calculated from the exponential function of the second order, curves 3 and 3' correspond to the values calculated from Eqs. (9) and (11), respectively.

Figure S3. A plot of the SF aqueous solution surface tension (γ_{LV}) (curves 1 - 3) and contact angle (θ) on PTFE (curves 1' - 3') vs. the logarithm of SF concentration (C). Curves 1 and 1' correspond the measured values, curves 2 and 2' to values calculated from the exponential function of the second order, curves 3 and 3' correspond to the values calculated from Eqs. (9) and (11), respectively.

Figure S4. A plot of the contact angle (θ) of aqueous solution of TX165 (curves 1, 1' and 1"), RL (curve 2) and SF (curve 3) on PMMA vs. the logarithm of surfactant concentration (C). Curves 1, 2 and 3 correspond to the measured values, curves 1' and 1" correspond to the values calculated from the exponential function of the second order and Eq. (9), respectively.
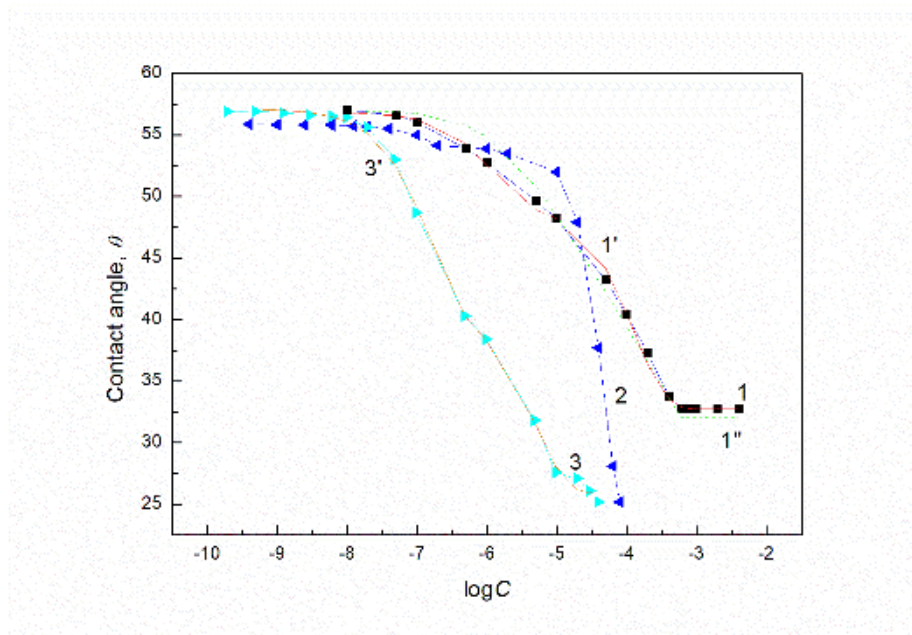
Figure S5. A plot of the contact angle (θ) of aqueous solution of TX165 (curves 1, 1' and 1"), RL (curve 2) and SF (curve 3 and 3') on quartz vs. the logarithm of surfactant concentration (C). Curves 1, 2 and 3 correspond to the measured values, curves 1', and 3' correspond to the values calculated from the exponential function of the second order and curve 1" corresponds to the values calculated from Eq. (9).

Figure S6. A plot of the adhesion tension ($\gamma_{LV}\cos\theta$) vs. the surface tension (γ_{LV}) of aqueous solutions of TX165 (points 1), RL (points 2) and SF (points 3) for PTFE.

Figure S7. A plot of the adhesion tension ($\gamma_{LV}\cos\theta$) vs. the surface tension (γ_{LV}) of aqueous solutions of TX165 (curve 1), RL (curve 2) and SF (curve 3) for PMMA.

Figure S8. A plot of the adhesion tension ($\gamma_{LV}\cos\theta$) vs. the surface tension (γ_{LV}) of aqueous solutions of TX165 (curve 1), RL (curve 2) and SF (curve 3) for quartz.

Figure S9. A plot of the contact angle (θ) of aqueous solution of TX165 + RL mixtures on the PTFE surface vs. the logarithm of the RL concentration (C). Curves 1 – 16 correspond to the constant TX165 concentration equal to 1×10^{-8}, 5×10^{-8}, 1×10^{-7}, 5×10^{-7}, 1×10^{-6}, 5×10^{-6}, 1×10^{-5}, 5×10^{-5}, 1×10^{-4}, 2×10^{-4}, 4×10^{-4}, 6×10^{-4}, 8×10^{-4}, 0.001, 0.002 and 0.004 mole/dm^3, respectively.

Figure S10. A plot of the contact angle (θ) of aqueous solution of TX165 + SF mixtures on the PTFE surface vs. the logarithm of the SF concentration (C). Curves 1 – 16 correspond to the constant TX165 concentration equal to 1×10^{-8}, 5×10^{-8}, 1×10^{-7}, 5×10^{-7}, 1×10^{-6}, 5×10^{-6}, 1×10^{-5}, 5×10^{-5}, 1×10^{-4}, 2×10^{-4}, 4×10^{-4}, 6×10^{-4}, 8×10^{-4}, 0.001, 0.002 and 0.004 mole/dm^3, respectively.

Figure S11. A plot of the contact angle (θ) of aqueous solution of TX165 + RL on PTFE at the constant RL concentration equal to 5 (a) and 40 mg/dm³ (c) vs. the logarithm of TX165 concentration (C). Points 1 correspond to the measured values, curves 2 – 4 correspond the values calculated form the exponential function of the second order, Eqs. (13) and (9), respectively.

Figure S12. A plot of the contact angle (θ) of aqueous solution of TX165 + RL on PTFE at the constant TX165 concentration equal to 5 x 10⁻⁶ mole/dm³ vs. the logarithm of RL concentration (C). Points 1 correspond to the measured values, curves 2 – 4 correspond the values calculated form the exponential function of the second order, Eqs. (13) and (9), respectively.

Figure S13. A plot of the contact angle (θ) of aqueous solution of TX165 + SF on PTFE at the constant SF concentration equal to 0.00625 (a), 5 (b) and 40 mg/dm³ (c) vs. the logarithm of TX165 concentration (C). Points 1 correspond to the measured values, curves 2 – 4 correspond the values calculated form the exponential function of the second order, Eqs. (13) and (9), respectively.

Figure S14. A plot of the adhesion tension ($\gamma_{LV}\cos\theta$) vs. the surface tension (γ_{LV}) of aqueous solutions of TX165 + RL and TX165 + SF mixtures both at the constant biosurfactant and TX165 concentration for PTFE.

Figure S15. A plot of the contact angle (θ) of aqueous solution of TX165 + RL mixtures on the PMMA surface vs. the logarithm of RL concentration (C). Curves 1 – 16 correspond to the constant TX165 concentration equal to 1×10^{-8}, 5×10^{-8}, 1×10^{-7}, 5×10^{-7}, 1×10^{-6}, 5×10^{-6}, 1×10^{-5}, 5×10^{-5}, 1×10^{-4}, 2×10^{-4}, 4×10^{-4}, 6×10^{-4}, 8×10^{-4}, 0.001, 0.002 and 0.004 mole/dm³, respectively.

Figure S16. A plot of the contact angle (θ) of aqueous solution of TX165 + SF mixtures on the PMMA surface vs. the logarithm of the SF concentration (C). Curves 1 – 16 correspond to the constant TX165 concentration equal to 1×10^{-8}, 5×10^{-8}, 1×10^{-7}, 5×10^{-7}, 1×10^{-6}, 5×10^{-6}, 1×10^{-5}, 5×10^{-5}, 1×10^{-4}, 2×10^{-4}, 4×10^{-4}, 6×10^{-4}, 8×10^{-4}, 0.001, 0.002 and 0.004 mole/dm^3, respectively.

Figure S17. A plot of the contact angle (θ) of aqueous solution of TX165 + RL mixtures on the quartz surface vs. the logarithm of the RL concentration (C). Curves 1 – 16 correspond to the constant TX165 concentration equal to 1×10^{-8}, 5×10^{-8}, 1×10^{-7}, 5×10^{-7}, 1×10^{-6}, 5×10^{-6}, 1×10^{-5}, 5×10^{-5}, 1×10^{-4}, 2×10^{-4}, 4×10^{-4}, 6×10^{-4}, 8×10^{-4}, 0.001, 0.002 and 0.004 mole/dm^3, respectively.

Figure S18. A plot of the contact angle (θ) of aqueous solution of TX165 + SF mixtures on the quartz surface vs. the logarithm of the SF concentration (C). Curves 1 – 16 correspond to the constant TX165 concentration equal to 1 × 10^{-8}, 5 × 10^{-8}, 1 × 10^{-7}, 5 × 10^{-7}, 1 × 10^{-6}, 5 × 10^{-6}, 1 × 10^{-5}, 5 × 10^{-5}, 1 × 10^{-4}, 2 × 10^{-4}, 4 × 10^{-4}, 6 × 10^{-4}, 8 × 10^{-4}, 0.001, 0.002 and 0.004 mole/dm^3, respectively.

Figure S19. A plot of the adhesion tension ($\gamma_{LV}\cos\theta$) vs. the surface tension (γ_{LV}) of aqueous solutions of TX165 + RL at the constant concentration of RL (a) and TX165 (b) at all studied concentration for PMMA.

Figure S20. A plot of the adhesion tension ($\gamma_{LV}\cos\theta$) vs. the surface tension (γ_{LV}) of aqueous solutions of TX165 + SF at the constant concentration of SF (a) and TX165 (b) at all studied concentration for PMMA.

Figure S21. A plot of the adhesion tension ($\gamma_{LV}\cos\theta$) vs. the surface tension (γ_{LV}) of aqueous solutions of TX165 + RL at the constant concentration of RL (a) and TX165 (b) at all studied concentration for quartz.

Figure S22. A plot of the adhesion tension ($\gamma_{LV}\cos\theta$) vs. the surface tension (γ_{LV}) of aqueous solutions of TX165 + SF at the constant concentration of SF (a) and TX165 (b) at all studied concentration for quartz.

Figure S23. A plot of the contact angle (θ) for TX165 + RL for PMMA at the constant RL concentration equal to 0.00625 (a) and 5 (b) vs. the logarithm of TX165 concentration (C). Points 1 correspond to the measured values, curves 2 – 4 correspond the values calculated from the exponential function of the second order, Eqs. (13) and (9), respectively.

Figure S24. A plot of the contact angle (θ) for TX165 + SF for PMMA at the constant SF concentration equal to 0.00625 (a), 5 (b) and 40 mg/dm³ (c) vs. the logarithm of TX165 concentration (C). Points 1 correspond to the measured values, curves 2 – 4 correspond the values calculated form the exponential function of the second order, Eqs. (13) and (9), respectively.

Figure S25. A plot of the contact angle (θ) for TX165 + RL for quartz at the constant RL concentration equal to 0.00625 (a), 5 (b) and 40 mg/dm³ (c) vs. the logarithm of TX165 concentration (C). Points 1 correspond to the measured values, curves 2 – 4 correspond the values calculated form the exponential function of the second order, Eqs. (13) and (9), respectively.

Figure S26. A plot of the contact angle (*θ*) for TX165 + SF for quartz at the constant SF concentration equal to 0.00625 (a), 5 (b) and 40 mg/dm³ (c) vs. the logarithm of TX165 concentration (*C*). Points 1 correspond to the measured values, curves 2 – 4 correspond the values calculated form the exponential function of the second order, Eqs. (13) and (9), respectively.

Figure S27. A plot of the Gibbs surface excess concentration at the PTFE-water interface (Γ_{SL}) for TX165 (a, c), RL (b) and SF (d) vs. the logarithm of surfactant concentration (C) calculated from Eqs. (5) and (15).

Figure S28. A plot of the Gibbs surface excess concentration at the PTFE-water interface (Γ_{SL}) for TX165 (curve 1), RL (2) and their sum (curve 3) vs. the logarithm of surfactant concentration (C) at the constant RL concentration equal to 0.0002 (a), 0.00625 (b), 5 (c) and 40 mg/dm^3 (d).

Figure S29. A plot of the Gibbs surface excess concentration at the PTFE-water interface (Γ_{SL}) for TX165 (curve 1), RL (2) and their sum (curve 3) vs. the logarithm of surfactant concentration (C) at the constant TX165 concentration equal to 5×10^{-7} (a), 1×10^{-6} (b), 2×10^{-4} (c) and 1×10^{-3} mole/dm^3 (d).

Figure S30. A plot of the Gibbs surface excess concentration at the PTFE-water interface (Γ_{SL}) for TX165 (curve 1), SF (2) and their sum (curve 3) vs. the logarithm of surfactant concentration (C) at the constant SF concentration equal to 0.0002 (a), 0.00625 (b), 5 (c) and 40 mg/dm³ (d).

Figure S31. A plot of the Gibbs surface excess concentration at the PTFE-water interface (Γ_{SL}) for TX165 (curve 1), SF (2) and their sum (curve 3) vs. the logarithm of surfactant concentration (C) at the constant TX165 concentration equal to 5×10^{-7} (a), 1×10^{-6} (b), 2×10^{-4} (c) and 1×10^{-3} mole/dm³ (d).

Figure S32. A plot of the Gibbs surface excess concentration at the PMMA-water interface (Γ_{SL}) vs. the logarithm of surfactant concentration (C) for TX165 + RL (a, b) and TX165 +SF (c, d) at the constant TX165 concentration (b, d) and RL (a) as well as SF (c).

Figure S33. A plot of the Gibbs surface excess concentration at the PMMA-air interface (Γ_{SV}) vs. the logarithm of surfactant concentration (C) for TX165 + RL (a, b) and TX165 +SF (c, d) at the constant TX165 concentration (b, d) and RL (a) as well as SF (c).

Figure S34. A plot of the Gibbs surface excess concentration at the quartz-water interface (Γ_{SL}) vs. the logarithm of surfactant concentration (C) for TX165 + RL (a, b) and TX165 +SF (c, d) at the constant TX165 concentration (b, d) and RL (a) as well as SF (c).

Figure S35. A plot of the Gibbs surface excess concentration at the quartz-air interface (Γ_{SV}) vs. the logarithm of surfactant concentration (C) for TX165 + RL (a, b) and TX165 +SF (c, d) at the constant TX165 concentration (b, d) and RL (a) as well as SF (c).

Figure S36. The difference between the Gibbs surface excess concentration at the PMMA-water and PMMA-air interface vs. the logarithm of surfactant concentration (C) for TX165 + RL (a) and TX165 +SF (b). Curves 1 – 4 correspond to the constant biosurfactant concentration equal to 0.0002, 0.00625, 5 and 40 mg/dm³.

Figure S37. A plot of the difference between the Gibbs surface excess concentration at the quartz-water and quartz-air interface vs. the logarithm of surfactant concentration (C) for TX165 + RL (a) and TX165 +SF (b). Curves 1 – 4 correspond to the constant biosurfactant concentration equal to 0.0002, 0.00625, 5 and 40 mg/dm³.

Figure S38. A plot of the difference between the values of the PMMA(quartz)-air interface tension ($\Delta\gamma_{SV}$) at the TX165 + biosurfactant mixture concentration equal to zero and equal to a given value (curve 1) and between the PMMA(quartz)-water (curve 2) and PMMA(quartz)-solution (curve 2) ($\Delta\gamma_{SL}$) as well as the difference between the values of contact angle of the water and solution on the PMMA (a, b) and quartz (c, d) ($\Delta\gamma_\theta$) (curve 3) at the constant RL and SF concentration equal to 0.00625 mg/dm3 vs. the logarithm of surfactant concentration (C).

Prof. dr hab. Anna Zdziennicka
Katedra Zjawisk Międzyfazowych
Instytut Nauk Chemicznych
Wydział Chemii UMCS
Pl. M. Curie-Skłodowskiej 3
20-031 Lublin

Lublin, 17.01.2023

OŚWIADCZENIE

Oświadczam, że w pracy

E. Rekiel, **A. Zdziennicka**, K. Szymczyk, B. Jańczuk*, *Wetting Properties of Rhamnolipid and Surfactin Mixtures with Triton X-165*. Molecules, 2022, 27, 4706;

mój udział wynosił **25%** i polegał na przygotowaniu koncepcji badań i dobraniu metodologii, przeprowadzeniu badań, interpretacji oraz wizualizacji otrzymanych wyników, weryfikacji procesu pisania pracy oraz przeprowadzonych badań, analizie formalnej, pisaniu oryginalnej wersji manuskryptu, redagowaniu i edycji manuskryptu, współredagowaniu odpowiedzi na recenzje pracy.

Anna Zdziennicka

Dr hab. Katarzyna Szymczyk, prof. UMCS
Katedra Zjawisk Międzyfazowych
Instytut Nauk Chemicznych
Wydział Chemii UMCS
Pl. M. Curie-Skłodowskiej 3
20-031 Lublin

Lublin, 17.01.2023

OŚWIADCZENIE

Oświadczam, że w pracy

E. Rekiel, A. Zdziennicka, **K. Szymczyk**, B. Jańczuk*, *Wetting Properties of Rhamnolipid and Surfactin Mixtures with Triton X-165*. Molecules, 2022, 27, 4706;

mój udział wynosił **10%** i polegał na przygotowaniu koncepcji badań i dobraniu metodologii, interpretacji oraz wizualizacji otrzymanych wyników, analizie formalnej, pisaniu oryginalnej wersji manuskryptu oraz redagowaniu i edycji manuskryptu.

Katarzyna Szymczyk

Prof. dr hab. Bronisław Jańczuk
Katedra Zjawisk Międzyfazowych
Instytut Nauk Chemicznych
Wydział Chemii UMCS
Pl. M. Curie-Skłodowskiej 3
20-031 Lublin

Lublin, 17.01.2023

OŚWIADCZENIE

Oświadczam, że w pracy

E. Rekiel, A. Zdziennicka, K. Szymczyk, **B. Jańczuk***, *Wetting Properties of Rhamnolipid and Surfactin Mixtures with Triton X-165*. Molecules, 2022, 27, 4706;

mój udział wynosił **10%** i polegał na przygotowaniu koncepcji badań i dobraniu metodologii, interpretacji otrzymanych wyników, weryfikacji procesu pisania pracy oraz przeprowadzonych badań, analizie formalnej, pisaniu oryginalnej wersji manuskryptu, redagowaniu i edycji manuskryptu, współredagowaniu odpowiedzi na recenzje pracy oraz prowadzeniu korespondencji z czasopismem.

Załącznik 3

[D3] E. Rekiel, A. Zdziennicka*, B. Jańczuk, *Adsorption properties of rhamnolipid and ethanol at water/ethanol solution-air interface.* ***Journal of Molecular Liquids***, 2020, 308, 113080.

Adsorption properties of rhamnolipid and ethanol at water/ethanol solution-air interface

Edyta Rekiel, Anna Zdziennicka *, Bronisław Jańczuk

Department of Interfacial Phenomena, Institute of Chemical Sciences, Faculty of Chemistry, Maria Curie-Skłodowska University in Lublin, Maria Curie-Skłodowska Sq. 3, 20-031 Lublin, Poland

A B S T R A C T

The water/ethanol solutions of surfactants and/or their mixtures are very often used in practice. Alcohol changes largely, among others adsorption, aggregation and wetting properties of the surfactants. Therefore, measurements of the surface tension of the water/ethanol solution of rhamnolipid were made. For this purpose the du Noüy ring method was applied. The measured values of the surface tension of rhamnolipid water/ethanol solution were compared to those calculated using the Miller et al., Connors equations as well as independent adsorption method. These results were also analyzed taken into account the contributions of the adsorbed rhamnolipid and ethanol in the mixed film pressure at the water/ethanol solution-air interface. This analysis allowed us to determine the mutual effect of rhamnolipid and ethanol on their adsorption at the solution-air interface. The adsorption of the rhamnolipid and ethanol was discussed on the basis of the Gibbs, Langmuir and Frumkin equations of the adsorption isotherm. The tendency of rhamnolipid and ethanol to adsorb at the solution-air interface was discussed based on the Gibbs free energy of adsorption which was determined using different methods. The obtained results and their analysis show that there is not a synergetic effect in the water surface tension reduction by the ethanol and rhamnolipid mixture adsorption.

© 2020 Elsevier B.V. All rights reserved.

1. Introduction

The short chain alcohols are often applied as additives and/or co-surfactants in the systems including surfactant or surfactants mixtures [1]. In their molecules there is present the –OH group whose properties are similar to this group in the water. Apart from this group a short hydrocarbon tail is found in the alcohol molecules. Thus, it can be stated that the alcohol molecules contain both hydrophobic and hydrophilic parts. For this reason the short chain alcohols are capable of adsorbing at the water-air interface [2–5]. They can also aggregate at a proper concentration in the aqueous solution [2–15]. The molecules of short chain alcohols present in the aqueous solutions of surfactants and their mixtures can change hydration of the head and tail of the surfactant molecules and thus the conditions for adsorption as well as the aggregation of surfactants [1,2]. The molecules of alcohol influence also on the structure of water by changing its dielectric constant [2,6]. These changes of the hydration of surfactants molecules and water structure induced by short chain alcohols influence, among others, on the surfactant adsorption at the water-air interface [16–18]. However, there is no consensus on the trend of changes in the amount of even classical surfactant

adsorption at the water-air interface in literature [1,16–18]. In the case of biosurfactants it is very difficult to find the studies dealing with the effect of short chain alcohols on their adsorption at the water-air interface. Biosurfactants are increasingly used in various fields [19–27]. In many cases, they are applied in different solutions, for example in ethanol. Among biosurfactants, rhamnolipid is of significant importance. Rhamnolipid, which is produced mainly by *Pseudomonas aeruginosa* during cultivation on glucose, glycerol or triglycerides (representing glycolipids) [28–33], is characterized by very interesting properties [19,20,26,27]. It should be noted that there are many types of rhamnolipid but all of them have the same functional groups in their molecules (-COOH, –CO, –OH, –CH$_2$– and –CH$_3$) [34]. The number of these groups depends on the type of rhamnolipid. The adsorption, aggregation and wetting properties of mono–rhamnolipid are the most often studied [34,35]. However, the literature presents different opinions about these properties. As a matter of fact, they depend on the presence of other substances in the rhamnolipid aqueous solution. From the practical point of view it is important to be familiar with the influence of ethanol on the adsorption properties of rhamnolipid. Therefore, the aim of our studies was to determine the mutual influence of mono-rhamnolipid and ethanol on their adsorption at the water/ethanol solution-air interface, the composition of the mixed monolayer and thermodynamics of the adsorption. For this purpose the measurements of the surface tension of water/ethanol solution of rhamnolipid were conducted. These measurements were made in the range of complete

mixing of ethanol with water and mono-rhamnolipid in the range from 0 to 40 mg/dm³. On the basis of the obtained results the mutual influence of ethanol and rhamnolipid on their adsorption at the solution-air interface was discussed.

2. Experimental

2.1. Materials

Ethanol (ET) (96% pure) was purchased from POCH and purified by the method described earlier [5]. R-95 Rhamnolipid (RL) purchased from SIGMA-ALDRICH was used without further purification. For preparation of water/ethanol solutions of rhamnolipid, deionized water of the internal specific resistance of 18.2 x 10⁶Ω m (doubly distilled, Destemat Bi18E) was applied. A mixture of water and ethanol at ethanol concentration from 0 to 17.13 mol/dm³ was used as the solvent for rhamnolipid. The concentration of rhamnolipid in this solvent was in the range from 0 to 40 mg/dm³. Two series of rhamnolipid solutions in the water/ethanol solution were prepared for the surface tension measurements. One series included the solutions with a constant concentration of rhamnolipid and different ethanol concentration whereas the other one included solutions with a varying concentration of rhamnolipid and the constant concentration of ethanol.

2.2. Measurements

For the measurements of the equilibrium surface tension (γ_{LV}) of the water/ethanol solution of RL, the Krüss K9 tensiometer was used. The tensiometer was calibrated on the basis of water and methanol before the measurements. It was assumed that the water surface tension at 293 K was equal to 72.8 and methanol to 22.5 mN/m. The surface tension measurements were described in detail earlier [5]. For each water/ethanol solution of rhamnolipid, at least 10 measurements were made. The standard deviation depending on the ethanol and rhamnolipid concentration was in the range from ±0.1 to ±0.25 mN/m and the uncertainty of the surface tension measurements was equal from 0.3 to 0.7%.

3. Results and discussion

The surface tension of the solutions depends on the number of the components and their concentration as well as solution components surface tension and the kind of intermolecular interactions
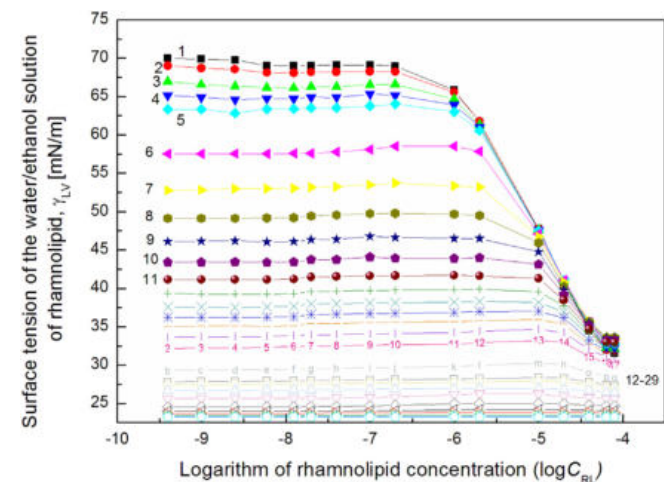
Fig. 1. A plot of surface tension (γ_{LV}) of the water/ethanol solution of RL vs. the logarithm of RL concentration ($\log C_{RL}$). Curves 1–29 correspond to the constant ET concentration equal to 0.06692; 0.1338; 0.2677; 0.4015; 0.535; 1.0706; 1.6062; 2.1416; 2.677; 3.2124; 3.7478; 4.2832; 4.8185; 5.3538; 5.8893; 6.6925; 7.7245; 8.5664; 10.2797; 11.968; 12.145; 13.3794; 14.5696; 15.4064; 16.084; 16.3777; 16.648; 16.8988 and 17.13 M.
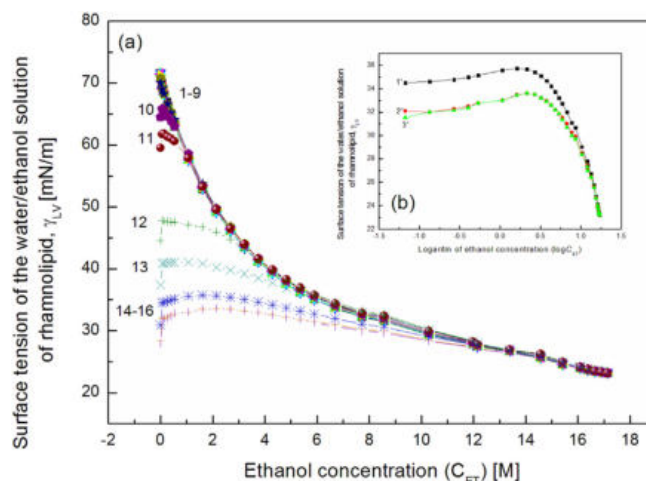
Fig. 2. A plot of surface tension (γ_{LV}) of the water/ethanol solution of RL vs. the ET concentration (C_{ET}) (a) and vs. the logarithm of ethanol concentration (b). Curves 1–16 correspond to the constant RL concentration equal to 0.0002; 0.0005; 0.00125; 0003; 0.00625; 0.01; 0.02; 0.05; 0.1; 0.5; 1; 5; 10; 20; 30 and 40 mg/dm³, curves 1′ – 3′ correspond to the constant RL concentration equal to 20, 30 and 40 mg/dm³.

contributing to this tension. Thus, the surface tension of the water-ethanol solution of rhamnolipid depends on the components and parameters of the water, ethanol and rhamnolipid surface tension and their concentration in the solution (Figs. 1 and 2). The surface tension of water at 293 K is equal to 72.8 mN/m [36] (Table 1) and according to the van Oss et al. [37–39] it results from the Lifshitz-van der Waals (LW) and hydrogen bond intermolecular interactions [38]. The hydrogen bonds interactions is treated as a Lewis acid-base one (AB). Thus, the surface tension of water consists of two components – the Lifshitz-van der Waals (γ_W^{LW}) and Lewis acid-base (γ_W^{AB}). In turn, the AB components are a function of two parameters: electron-acceptor (γ_W^+) and electron-donor (γ_W^-) ($\gamma_W^{AB} = 2\sqrt{\gamma_W^+\gamma_W^-}$). Van Oss et al. [37–39] treated water as a model liquid and assumed that the values of electron-acceptor and electron-donor parameters of the acid-base components of its surface tension are the same. The ethanol surface tension also results from the Lifshitz-van der Waals and hydrogen bond intermolecular interactions, however the electron-acceptor parameter of its acid-base component is considerably lower than the electron-donor one [40,41]. In the case of mono-rhamnolipid, according to the van Oss and Constanzo [42] the surface tension depends on the orientation of its molecules towards the air phase. In the hydrophobic part of mono-rhamnolipid two octyl groups are present. Therefore, if the mono-rhamnolipid molecules are oriented by the hydrophobic part towards the air phase, at the first approximation, its surface tension should be equal to the octane surface tension. Thus the surface tension of mono-rhamnolipid is close to 21.8 mN/m [36,43]. In turn, the surface tension of RL at the molecules orientation by head

Table. 1
The Lifshitz-van der Waals (γ^{LW}) and acid-base (γ^{AB}) components as well as the electron-acceptor (γ^+) and the electron-donor (γ^-) parameters of water, ethanol and rhamnolipid head and tail surface tension (γ).

Substance	Components and parameters [mN/m]				γ [mN/m]	Ref.
	γ^{LW}	γ^{AB}	γ^+	γ^-		
RL (head)	35.38	3.01	0.04	46.74	38.39	[44]
RL (tail)	21.80	0.00	0.00	0.00	21.80	[43]
Water	26.85	45.95	22.975	22.975	72.80	[44]
Ethanol	21.40	1.80	0.09	9.00	23.20	[40,41]

towards the air phase includes the Lifshitz-van der Waals and acid-base components. Similar to ethanol, the electron-acceptor parameter of the RL acid-base component is considerably lower than that of the electron-donor (Table 1) [44]. However, it should be remembered that mono-rhamnolipid can include other rhamnolipids [26,45,46]. The Lifshitz-van der Waals component of RL head is the largest of the substances being in the solution (Table 1). It is known that the adsorption of amphiphilic substances at the polar liquid–air interface depends largely on the interactions of the surfactant tail with the polar solvent molecules [1]. Due to the adsorption, the monolayer of surface active agent is formed. In this layer the amphiphilic molecules are oriented by the hydrophobic part towards the air phase. Thus, the surface tension of the water should change theoretically from 72.8 to 21.8 mN/m if the water surface is completely covered by the RL molecules. However, in practice, at 293 K the maximal coverage of water surface by the RL molecules is lower than the limiting one [34] and the water surface tension affected by RL is changed only from 72.8 to 27.89 mN/m [34]. Indeed, the surface tension of the water-ethanol mixture changes from the surface tension of water to that of ethanol (Table 1). In the case of the water/ethanol solution of RL the changes of the water surface tension depend on the mutual influence of ethanol and RL on their adsorption at the solution-air interface.

ET and RL independent adsorption at the water-air interface was assumed. In such case the surface tension of the solution can be calculated from the following expression:

$$\gamma_{LV} = \gamma_{LV}^{RL} + \gamma_{LV}^{ET} - \gamma_W \qquad (1)$$

where
γ_{LV} is the surface tension of water/ethanol solution of RL, γ_{LV}^{RL} is the surface tension of aqueous solution of RL, γ_{LV}^{ET} is the surface tension of water/ethanol mixture and γ_W is the water surface tension.

From the comparison of the measured water/ethanol solution of RL surface tension and those calculated from Eq. (1) (Figs. S1 and S2, and as an example Figs. S3–S8) it results that in any case the calculated values are the same as those measured. For better understanding the relationship between the calculated and measured surface tension values, four cases of the ET and RL concentration range will be considered. The first case refers to the concentration range of ethanol (C_{ET}^{unsat}) [5] and RL (C_{RL}^{unsat}) [34] in which the unsaturated monolayer at the water-air interface is formed by ET without RL and RL without ET. The second one includes the solutions at the concentration of RL equal to C_{RL}^{unsat} and ET at the concentration at which its saturated monolayer at the water-air interface in the absence of RL is formed (C_{ET}^{sat}). The third case regards the solutions at the concentration of ET equal to C_{ET}^{unsat} and RL to the concentration at which its saturated monolayer at the water-air interface in the absence of ET is formed (C_{RL}^{sat}). The fourth case occurs when the concentration of ET is equal to C_{ET}^{sat} and RL to C_{RL}^{sat} [5,34]. The differences between the values of the surface tension calculated from Eq. (1) and those measured are the lowest for the first case (Figs. S3 and S6) and the highest for the fourth one (Figs. S5 and S8). The calculated values are always lower than the measured ones. The γ_{LV} values calculated from Eq. (1) do not explain the increase of γ_{LV} as a function of ET concentration in the range of C_{ET}^{unsat} at the constant RL concentration equal to C_{RL}^{sat}.

To explain this fact the γ_{LV} values were calculated from the expression:

$$\gamma_{LV} = \gamma_W - x_{ET} - x_{RL}\pi_{RL} \qquad (2)$$

where π_{ET} [5] is equal to $\gamma_W - \gamma_{LV}^{ET}$, π_{RL} [34] is equal to $\gamma_W - \gamma_{LV}^{RL}$, x_{ET} is the fraction of ethanol pressure in the mixed ET/RL monolayer at the solution-air interface and x_{RL} is the fraction of the RL pressure in the

RL/ET mixed monolayer. π_{ET} and π_{RL} were calculated on the basis of the ET and RL pressure in their single solution at the water-air interface.

It was assumed that $x_{ET} = \dfrac{\pi_{ET}}{\pi_{ET} + \pi_{RL}}$ and $x_{RL} = \dfrac{\pi_{RL}}{\pi_{ET} + \pi_{RL}}$. The values of x_{ET} and x_{RL} can be also determined from Eq. (2) on the basis of the measured values of solution surface tension called as real ones by us.

The γ_{LV} values calculated from Eq. (2) (Figs. S3–S10) are close to those measured if the concentration of ET is equal to C_{ET}^{unsat} and RL to C_{RL}^{unsat}. In the cases when the concentration of ET is equal to C_{ET}^{unsat} and RL to C_{RL}^{sat} or ET to C_{ET}^{sat} and RL to C_{RL}^{unsat} as well as ET concentration is equal to C_{ET}^{sat} and RL to C_{RL}^{sat}, there are some differences between the values of γ_{LV} calculated from Eq. (2) and those measured. However, the maxima are present on the calculated isotherms of surface tension. They are more evident on the curves showing the changes of solution surface tension as a function of ET concentration at the constant RL concentration equal to C_{RL}^{sat} (Figs. S8 and S9). These maxima result from the ET and RL mutual influence on their adsorption at the solution-air interface. To explain this influence the real fractions of ET an RL pressure in the mixed monolayer were calculated from Eq. (2) (Figs. S11 and S12, exemplary Figs. S13–S18). For the calculations, it was assumed that the contribution of ET and RL to the pressure of the ET/RL mixed monolayer is proportional to their pressure in the individual solutions. The values of x_{ET} and x_{RL} determined in such a way were compared to those obtained from the expressions: $x_{ET} = \dfrac{\pi_{ET}}{\pi_{ET} + \pi_{RL}}$ and $x_{RL} = \dfrac{\pi_{RL}}{\pi_{ET} + \pi_{RL}}$ (Figs. S13–S20). As follows, independent adsorption does not take place even at the concentration of ET equal to C_{ET}^{unsat} and RL to C_{RL}^{unsat}. On the other hand, in this case RL reduces adsorption of ET. However, this decrease is not remarkable. The decrease of ET adsorption by RL causes a slight increase of solution surface tension (Figs. 1 and 2) in comparison to the individual ET solution at the same concentration [5]. In the range of ET concentration equal to C_{ET}^{sat}, independently of RL concentration, its adsorption at the solution-air interface is reduced. However, the presence of RL molecules in the monolayer causes an increase of solution surface tension compared to the solution of single ET. To understand the mechanism of ET and RL adsorption at the water/ethanol solution of RL-air interface, the changes of the hydration of ET and RL molecules as well as the dielectric constant as a function of solution composition were analyzed. The hydration of the hydrocarbon tail of ET and RL increases the tendency of their molecules to adsorption at the solution-air-interface. However, the hydration of the polar part of ET and RL molecules decreases their tendency to adsorption. The exchanges of water molecules joined with the hydrophilic part of RL molecules into the ethanol ones result in greater possibility of RL adsorption at the solution-air interface. Thus at the RL and ET concentration equal to C_{ET}^{unsat} and C_{RL}^{unsat} the increase of RL adsorption may take place. The increase of ET concentration can cause dehydration of not only the head but also the tail of RL molecules which, in result, decreases RL adsorption properties. It should be mentioned that the dielectric constant of the solution decreases with increasing ET concentration which affects the RL adsorption properties.

It is commonly known that the ET molecules aggregate in water at the proper concentration [2,5,6]. Thus ET and RL can form mixed aggregates. The aggregates formation can be associated with greater changes of solution Gibbs free energy than the adsorption of RL at the solution-air interface. The exchange of the water molecules hydrating the RL tail on the ET ones which are oriented by the –OH group towards the water molecules, formation of mixed aggregates and decrease of dielectric constant increases the hydrophilic properties of RL tail. This causes a decrease of RL adsorption properties. Probably for this reason the surface tension of the studied solutions at the ET concentration equal to its critical aggregation concentration (CAC) [5] (Table 2) differs only slightly from that of ET solution without RL. As a matter of fact, the contribution of RL to the pressure of the mixed monolayer at the solution-

Table 2

The values of the RL CMC, ethanol CAC, maximal surface excess concentration (Γ^{max}), limiting surface concentration (Γ^{∞}), concentration at Γ^{max}, surface tension at CMC (γ^{CMC}) and at CAC (γ^{CAC}), minimal surface tension (γ^{min}) and minimal area occupied by one molecule of ethanol and rhamnolipid (A^0).

Substance	CMC or CAC	Γ^{max} $\times 10^{-6}$ mol/m^2	Γ^{∞}	γ^{CMC} or γ^{CAC} [mN/m]	C at Γ^{max}	γ^{min} [mN/m]	A^0 [Å^2]	Ref.
RL	26.24 mg/dm^3	2.01	2.401	29.08	5 mg/dm^3	27.89	69.08	[34,43]
Ethanol	7.04 M or 0.167	7.91	7.91	31.72	3.7478 M	23.20	21.00	[5]

air interface decreases practically to zero when the concentration fraction of ET grows to 1.

To prove in which range of ET and RL concentration, the contribution of ET and RL to the mixed monolayer pressure is or is not proportional to that of the monolayer of single ET and RL, the calculations of the solution surface tension were done using the Fainerman and Miller method [47,48]. For the calculation of γ_{LV} of the studied solution, surface tension of aqueous solution of individual ethanol [5] and rhamnolipid [35] as well as the number of their moles per unit area were used (Table 1). This number was determined based on the limiting area of ET and RL molecules at their perpendicular orientation at the solution-air interface. It should be emphasized that the Fainerman and Miller method [47,48] was firstly proposed for prediction of the surface tension of solution of the surfactant mixtures from the same homologous series. It appeared that this method is useful for other systems.

The values of γ_{LV} calculated from the Fainerman and Miller equation [47,48] (Figs. S21 and S22, S3–S8) are only slightly different from the measured ones in three other cases. The first one includes the ET and RL concentration equal to C_{ET}^{unsat} and C_{RL}^{unsat}. The second one includes the whole range of the ET concentration and RL concentration equal to C_{RL}^{unsat}. In turn, the third case includes the whole range of RL concentration and ET concentration equal to C_{ET}^{unsat}. Otherwise, there are great differences between the measured and calculated values of γ_{LV}. These facts confirm the above mentioned statements dealing with the contribution of ET and RL to the pressure of the mixed monolayer at the solution-air interface.

For the surface tension calculation of mixture liquids in the whole range of their concentration, the Connors method can be also used [49]. In our case there is a mixture of water, ethanol and rhamnolipid. To show the extent to which RL affects the applicability of this method, the surface tension of the studied solutions was calculated (Figs. S3–S8, S23). In the whole range of ET concentration and RL concentration equal to C_{RL}^{unsat}, the values of surface tension of water/ethanol solution of RL calculated from the Connors equation and those measured are compatible. Thus, using the Connors equation it is impossible to predict the increase of solution surface tension as a function of RL concentration at its constant concentration equal to C_{RL}^{sat}.

3.1. Concentration of ethanol and rhamnolipid in the mixed monolayer

The literature presents numerous equations applied for determination of the isotherm of surface active agents concentration in the surface region at the solution-air interface. The Gibbs isotherm equation [1,50], applied the most frequently, allows to establish the Gibbs surface excess concentration (Γ). It should be noted that for the surfactants in the range of their low concentration, Γ is practically equal to the total surface concentration of a given surfactant. Thus, the Gibbs surface excess concentration of RL can be treated as a total one. In the case of water/ethanol mixture, the Gibbs surface excess concentration only in the range of C_{ET}^{unsat} is, in the first approximation, close to that of the total one. The Gibbs isotherm of ET excess concentration shows a maximum. However, this isotherm does not approach zero if the ET mole fraction approaches 1. To solve the Gibbs isotherm equation the changes of $\frac{d\gamma_{LV}}{da}$ or $\frac{d\gamma_{LV}}{dC}$ or $\frac{d\gamma_{LV}}{dx}$ or $\frac{d\gamma_{LV}}{d\log a}$ or $\frac{d\gamma_{LV}}{d\log C}$ or $\frac{d\gamma_{LV}}{d\log x}$ must be known. In the case when the maxima or plateau are present on the surface tension

isotherms, it is difficult to find the function describing these isotherms. For ET at the constant RL concentration equal to C_{RL}^{unsat} and for RL at the constant concentration of ET equal to C_{ET}^{unsat} the changes of solution surface tension as a function of ET and/or RL concentration can be described by the second order exponential function. Therefore, it was possible to calculate the Gibbs surface excess concentration for ET (Γ_{ET}) and RL (Γ_{RL}) using $\frac{d\gamma_{LV}}{da}$ and $\frac{d\gamma_{LV}}{dC}$, respectively. The maximal value of RL Gibbs excess concentration (Γ_{RL}^{max}) was determined using $\frac{d\gamma_{LV}}{d\log C}$ in the Gibbs isotherm equation. In the case of the constant RL concentration equal to C_{RL}^{sat} and ET to C_{ET}^{sat}, it was difficult to obtain the correct values of Γ_{RL} and Γ_{ET}. It should be mentioned that the presence of plateau and/or the increase of the surface tension of solution as the function of ET concentration at the constant RL concentration and/or as a function of RL concentration at the constant ET one does not prove that it is caused by the decrease of ET and RL concentration in the surface region at the solution-air interface. To solve this problem, the isotherms of the surface tension of aqueous solution of ET and RL were calculated individually based on the ET and RL contribution in the pressure of the ET/RL mixed monolayer determined from Eq. (2) (Figs. S24 and S25). It appeared that there are insignificant differences between the values of Γ_{ET} or Γ_{RL} determined in a such way and those obtained from the isotherms of measured surface tension of the solution (Figs. S26 and S27). Unfortunately, in this case it was impossible to determine the Γ_{ET} and Γ_{RL} values for the all studied systems. As the pressure of the surface monolayer is directly connected with the surface concentration of surface active agents, it seems that Γ_{ET} and Γ_{RL} in the mixed monolayer, at the first approximation, can be determined on the basis of the Γ_{ET} and Γ_{RL} for their single solution using x_{ET} and x_{RL} [5,34] calculated from Eq. (2). In fact, the total concentration of ET (Γ_{ET}^{Tot}) was used in the calculations [5]. The ET total concentration in the surface layer calculated in this way was compared to the values obtained on the basis of the measured surface tension as well as determined from ET contribution to the pressure of the mixed monolayer at the solution-air interface. To determine the total concentration of ET in the surface layer, firstly the isotherm of Guggenheim-Adam was established (Fig. S28). Next, Γ_{ET}^{Tot} was obtained from the following expression [51]:

$$\Gamma_{ET}^{Tot} = \Gamma_{ET}^{GA} + C \cdot h \qquad (3)$$

where Γ_{ET}^{GA} is the surface excess concentration of Guggenheim-Adam, C is the ET concentration and h is the length of the ET molecule.

It appeared that in many cases the theoretical isotherms of the ethanol total concentration determined in two different ways were similar (Fig. S29). There is also a compatibility between the isotherms of the RL surface excess concentration determined by the above mentioned methods (Fig. S30).

Knowing the Γ_{ET}^{max} and Γ_{RL}^{max} values, it is possible to determine the isotherm of ET and RL concentration in the surface region at the solution-air interface from the Frumkin equation [1,50]. For the calculation of Γ_{ET}, $\Gamma_{ET}^{max} = 7.91 \times 10^{-6}$ mol/m^2 was applied for all systems. For Γ_{RL} calculations, the values of Γ_{RL}^{max} obtained from the Gibbs isotherm equation were applied. If the measured values of the surface tension were taken into account, real values of Γ_{ET} and Γ_{RL} were obtained in many cases (Figs. S31 and S32). If the values of γ_{LV} determined from

the ET and RL contribution to the surface pressure of the ET/RL mixed monolayer were used for the calculation of Γ_{ET} and Γ_{RL}, they were similar to the theoretical ones, at the first approximation, and for some systems to those obtained based on the measured surface tension and Gibbs isotherm equation [1,50] (Figs. S33–S38).

The calculations of ET and RL concentration in the surface region indicated that in the case of ET or RL concentration in the bulk phase equal to C_{ET}^{sat} or C_{RL}^{sat}, it is impossible to obtain real values of the concentration using the measured values in the Gibbs and/or Frumkin equations. The knowledge of ET and RL contribution to the pressure of their mixed monolayer is useful to determine the surface concentration of ET and RL. As follows from the calculations, at the concentration equal to C_{ET}^{unsat} and C_{RL}^{unsat}, the decrease of ET and increase of RL adsorption at the solution-air interface takes place in comparison to those resulting from the ET and RL contribution to the pressure of their mixed monolayer proportional to that of individual layers. At the concentration of ET equal to C_{ET}^{sat}, the decrease of RL adsorption by ethanol is observed. If the ET concentration is higher than CAC [5] the small adsorption of RL takes place even if the surface tension of water/ethanol solution of RL is only slightly larger than that for individual ET. If the mole fraction of ET approaches the unity there is practically no RL adsorption. The determined values of Γ_{ET} and Γ_{RL} confirm the above mentioned statement that the changes of the head and tail hydration of RL molecules and changes of the solution dielectric constant as a function of its composition play a main role in the adsorption of ET and RL at the solution-air interface. No synergetic effect was found in the ET and RL adsorption. The coverage of the water surface by the ET and RL mixtures does not exceed that by single ET and RL [5,34]. At the concentration of ET equal to C_{ET}^{sat}, even if the summary concentration of ET and RL is changed, the coverage of the water surface by the mixed monolayer is practically

constant. It should be remembered that the cross section of the RL head is more than three times higher than that of the ET one.

3.2. Standard Gibbs free energy of adsorption

The literature presents numerous different methods for determination of Gibbs free energy of adsorption (ΔG_{ads}^0) [1,50]. As it is known, this energy depends on the standard enthalpy and entropy of adsorption. Enthalpy is connected to creation and disruption of chemical bonds. In the solution, the changes of enthalpy during the adsorption of ET and RL result mainly from formation and disruption of hydrogen bonds. The changes of adsorption enthalpy in such systems are generally small and they can assume both negative and positive values [1]. Therefore, the changes of ΔG_{ads}^0 during the surface active substances adsorption result from the changes of solution entropy. The entropy changes of the water/ethanol solution of RL can result from dehydration of ET and RL molecules, creation of hydrogen bonds between the ET molecules and the head of RL ones, orientation of ET and RL molecules in the surface region, changes of the water structure by the ET and RL molecules as well as changes of the intermolecular distance.

Among the methods used for ΔG_{ads}^0 determination, the de Boer-Langmuir equation and linear form of the Langmuir equation are applied [1,50,52]. These equations were used for determination of ET and RL ΔG_{ads}^0 values on the basis of all surface excess concentration isotherms (Tables 3 and 4). In the case of ET for determination of ΔG_{ads}^0 the equation proposed by us was also used. This equation has the form [53]:

$$\Delta G_{ads}^0 = RT \ \ln a_{CAC} - \frac{\gamma_0 - \gamma_{LV}^{CAC}}{\Gamma_{ET}^{max}} \tag{4}$$

Table 3
The Gibbs free energy of ethanol adsorption (ΔG_{ads}^0) calculated from the de Boer-Langmuir, linear Langmuir equations and Eqs. (4) and (5) on the basis of the different surface concentration isotherms.

C_{RL} [mg/dm³]	ΔG_{ads}^0 [mJ/mol]							
	A	B	C	D	Eqs. (4) and (5)			
					E	F	G	H
0.0002	−10.16	−10.91	−10.17	−10.51	−7.34[a]	−11.60[a]	−7.79[a]	−7.87[a]
					−9.55[b]	−13.80[b]	−9.99[b]	−10.07[b]
0.0005	−9.56	−10.35	−10.23	−10.57	−7.38[a]	−11.68[a]	−7.80[a]	−7.91[a]
					−9.58[b]	−13.88[b]	−10.00[b]	−10.11[b]
0.00125	−9.53	−11.27	−10.29	−10.63	−7.35[a]	−11.73[a]	−7.77[a]	−7.89[a]
					−9.55[b]	−13.93[b]	−9.97[b]	−10.09[b]
0.003	−9.51	−9.49	−10.18	−10.68	−7.32[a]	−11.59[a]	−7.74[a]	−7.89[a]
					−9.52[b]	−13.79[b]	−9.94[b]	−10.09[b]
0.00625	−9.46	−9.47	−10.15	−10.67	−7.32[a]	−11.54[a]	−7.75[a]	−7.87[a]
					−9.52[b]	−13.74[b]	−9.96[b]	−10.07[b]
0.01	−9.46	−10.34	−10.14	−10.61	−7.28[a]	−11.54[a]	−7.75[a]	−7.88[a]
					−9.48[b]	−13.74[b]	−9.95[b]	−10.08[b]
0.02	−9.46	−9.52	−10.01	−10.61	−7.22[a]	−11.48[a]	−7.72[a]	−7.88[a]
					−9.42[b]	−13.68[b]	−9.92[b]	−10.08[b]
0.05	−9.43	−9.51	−9.78	−10.46	−7.14[a]	−11.39[a]	−7.69[a]	−7.86[a]
					−9.34[b]	−13.59[b]	−9.89[b]	−10.06[b]
0.1	−9.40	−9.54	−9.40	−10.35	−7.03[a]	−11.24[a]	−7.59[a]	−7.86[a]
					−9.23[b]	−13.44[b]	−9.79[b]	−10.06[b]
0.5	−9.04	−9.6		−9.76	−6.27[a]	−10.93[a]	−7.02[a]	−7.81[a]
					−8.47[b]	−13.14[b]	−9.22[b]	−10.01[b]
1	−8.54	−9.56		−10.02	−5.64[a]	−10.42[a]	−6.55[a]	−7.70[a]
					−7.84[b]	−12.62[b]	−8.75[b]	−9.91[b]

A - ΔG_{ads}^0 calculated from the de Boer-Langmuir equation on the basis of ethanol total surface concentration at the solution-air interface determined from the measured values of the studied solution surface tension (for $A^0 = 21.00$ Å² – Table 2). B - ΔG_{ads}^0 calculated from the de Boer-Langmuir equation on the basis of ethanol total surface concentration at the solution-air interface determined form the isotherm of the solution surface tension resulting only from contribution of ethanol in the reduction of water surface tension ($\gamma_{LV} = \gamma_W - x_{ET}\pi_{ET}$; see Eq. (2)) (for $A^0 = 21.00$ Å² – Table 2). C - ΔG_{ads}^0 calculated from the de Boer-Langmuir equation on the basis of ethanol total surface concentration at the solution-air interface determined from the Frumkin equation on the measured values of studied solution surface tension (for $A^0 = 21.00$ Å² – Table 2). D - ΔG_{ads}^0 calculated from the de Boer-Langmuir equation on the basis of ethanol total surface concentration at the solution-air interface determined from the Frumkin equation based on the solution surface tension calculated from Eq. (2) (for $A^0 = 21.00$ Å² – Table 2). E - ΔG_{ads}^0 calculated from Eq. (4) ([a]) and Eq. (5) ([b]), respectively, based on ethanol CAC (Table 2), surface tension of solution and ethanol Γ at CAC (Γ- see A). F - ΔG_{ads}^0 calculated from Eq. (4) ([a]) and Eq. (5) ([b]), respectively, based on ethanol CAC (Table 2), surface tension of solution and ethanol Γ at CAC (Γ- see B). G - ΔG_{ads}^0 calculated from Eq. (4) ([a]) and Eq. (5) ([b]), respectively, based on ethanol CAC (Table 2), surface tension of solution and ethanol Γ at CAC (Γ- see C). H - ΔG_{ads}^0 calculated from Eq. (4) ([a]) and Eq. (5) ([b]), respectively, based on ethanol CAC (Table 2), surface tension of solution and ethanol Γ at CAC (Γ- see D).

Table 4
The Gibbs free energy of rhamnolipid adsorption (ΔG_{ads}^0) calculated from the de Boer-Langmuir and linear Langmuir equations on the basis of different surface concentration isotherms.

C_{ET} [M]	ΔG_{ads}^0 [mJ/mol]					
	A	B	C	D	E	F
0.06692	−42.69	−41.86	−43.90	−42.89	−57.28	−46.64
0.1338	−40.70	−41.66	−41.70	−42.64	−56.70	−46.39
0.2677	−40.08	−41.44	−41.08	−42.40	−55.93	−46.15
0.4015	−39.65	−41.19	−40.69	−42.09	−54.98	−45.76
0.535	−39.30	−40.96	−40.37	−41.82	−54.15	−45.39
1.0706	−38.18	−40.56	−39.14	−41.27	−52.14	−43.62
1.6062	−37.17	−39.87	−38.10	−40.46	−50.34	−42.02
2.1416	−36.22	−39.64	−37.15	−40.31	−50.34	−41.55
2.677	−35.27	−39.25	−36.22	−40.02	−50.89	−41.44
3.2124	−34.32	−38.75	−35.41	−39.65	−50.34	−41.46
3.7478	−33.44	−38.39	−34.78	−39.42	−50.34	−41.20
4.2832	−32.61	−38.12	−34.25	−39.27	−50.89	−41.30

A - ΔG_{ads}^0 calculated from the de Boer-Langmuir equation on the basis of the rhamnolipid surface concentration at the solution-air interface determined from the measured values of the studied solution surface tension (for $A^0 = 69.08$ Å^2 – Table 2). B - ΔG_{ads}^0 calculated from the de Boer-Langmuir equation on the basis of the rhamnolipid surface concentration at the solution-air interface determined from the isotherm of the solution surface tension resulting from the contribution of rhamnolipid in the reduction of water surface tension ($\gamma_{LV} = \gamma_W - x_{RL}\pi_{RL}$; see Eq. (2)) (for $A^0 = 69.08$ Å^2 – Table 2). C - ΔG_{ads}^0 calculated from the linear Langmuir equation on the basis of the rhamnolipid surface concentration at the solution-air interface determined from the measured values of studied solution surface tension (for $A^0 = 69.08$ Å^2 – Table 2). D - ΔG_{ads}^0 calculated from the linear Langmuir equation on the basis of the rhamnolipid surface concentration at the solution-air interface determined from the solution surface tension calculated from Eq. (2) (for $A^0 = 69.08$ Å^2 – Table 2). E - ΔG_{ads}^0 calculated from the linear Langmuir equation on the basis of the rhamnolipid surface concentration at the solution-air interface determined from Frumkin equation and the measured values of the studied solution surface tension (for $A^0 = 69.08$ Å^2 – Table 2). F - ΔG_{ads}^0 calculated from the linear Langmuir equation on the basis of the rhamnolipid surface concentration at the solution-air interface determined form the Frumkin equation based on the solution surface tension calculated from Eq. (2) (for $A^0 = 69.08$ Å^2 – Table 2).

or

$$\Delta G_{ads}^0 = RT \ \ln x_{CAC} - \frac{\gamma_0 - \gamma_{LV}^{CAC}}{\Gamma_{ET}^{max}} \tag{5}$$

Unfortunately, it was impossible to obtain real ΔG_{ads}^0 values for ethanol at the RL concentration equal to C_{RL}^{sat} and for RL at the ethanol concentration equal to C_{ET}^{sat}.

It appeared that there are some differences in the ΔG_{ads}^0 values for a given system depending on the calculation methods and kind of isotherm of surface excess concentration taken for this calculation. Moreover, the values of ΔG_{ads}^0 for ET calculated from Eq. (5), in the first approximation, are similar to those determined from de Boer-Langmuir and linear Langmuir equations. Unfortunately, the values of ET and RL ΔG_{ads}^0 obtained from the Frumkin surface excess concentration isotherms [1] are less probable than those calculated from the Langmuir equations [1,50,52]. As a matter of fact, there were obtained two series of ΔG_{ads}^0 values for ET depending whether their activity (a) or mole fraction (x) was applied in the calculations. If the activity was used (Eq. (4)) then the absolute value of ΔG_{ads}^0 was lower than that obtained from Eq. (5) (Fig. S39). Comparing the ΔG_{ads}^0 values for ET to those obtained in a single solution [5] it can be stated that the values calculated from Eq. (5) are similar to those calculated based on the de Boer-Langmuir equation [52]. This is reasonable because in the de Boer-Langmuir equation [52] the activity coefficient for the adsorbing substance at the water-air interface is assumed to be equal to 1. It is interesting to point that in the range of constant RL concentration equal to C_{RL}^{unsat}, the values of ET ΔG_{ads}^0 are practically constant. In the case of RL the absolute values of its ΔG_{ads}^0 at the water/ethanol solution-air interface contrary to ET ΔG_{ads}^0 decrease with the increasing ET concentration in the bulk phase from the value corresponding to ΔG_{ads}^0 of single RL [34] to the value lower by about 10 kJ/mol (Fig. S40). As the absolute value

of ΔG_{ads}^0 for single RL at the water-air interface is about four time larger than that of ΔG_{ads}^0 for single ET, it is probable that at the constant low ethanol concentration the RL affects the ET adsorption to a larger extent than vice versa. This confirms the statement presented above. In turn, the increase of ET concentration affects the RL adsorption to a larger extent than RL the ET adsorption at the solution-air interface.

4. Conclusions

From the measurements of the surface tension of the water/ethanol solution of rhamnolipid and consideration of the ethanol and rhamnolipid contribution to the pressure of the mixed monolayer at the solution-air interface, it results that this contribution is not equal to pressure part of ethanol and rhamnolipid in the mixed monolayer resulting from their independent adsorption at the solution air interface. In the range of ethanol and rhamnolipid concentration corresponding to the unsaturated single monolayer, the rhamnolipid adsorption is more favorable than that of ethanol. At the ethanol concentration corresponding to its saturated monolayer a reverse dependence takes place. On the basis of the ethanol and rhamnolipid contribution to the pressure of mixed monolayer at the solution-air interface resulting from their independent adsorption it is impossible to predict the surface tension of the water/ethanol solution of rhamnolipid, but this tension can be predicted by the Fainerman and Miller equation in the whole range of ethanol concentration if the constant concentration of rhamnolipid corresponds to its unsaturated monolayer and vice versa. Otherwise there are differences between the calculated and measured values of surface tension of the studied solutions. Similarly to the values of surface tension calculated from the Fainerman and Miller equation those determined from the Connors equation are in good agreement with the measured ones in the same range of ethanol and rhamnolipid concentration as that mentioned above. The tendency towards ethanol adsorption at the solution-air interface decreases as a function of rhamnolipid concentration and vice versa. The standard Gibbs free energy of ethanol adsorption at the solution-air interface can be determined not only using the de Boer-Langmuir and linear Langmuir equations but also on the basis of the ethanol critical aggregation concentration and the surface tension at this concentration.

CRediT authorship contribution statement

Edyta Rekiel: Formal analysis, Writing - original draft. **Anna Zdziennicka:** Formal analysis, Writing - original draft, Writing - review & editing. **Bronisław Jańczuk:** Formal analysis, Writing - original draft.

Declaration of competing interest

The authors have no financial or personal relationships with other people or organizations that could inappropriately influence their work or state.

Appendix A. Supplementary data

Supplementary data to this article can be found online at https://doi.org/10.1016/j.molliq.2020.113080.

References

[1] J.M. Rosen, Surfactants and Interfacial Phenomena, 3rd ed. Wiley Interscience, New York, 2004.
[2] R. Zana, Aqueous surfactant-alcohol systems: a review, Adv. Colloid Interf. Sci. 57 (1995) 1–64.
[3] Y.F. Yano, Correlation between surface and bulk structures of alcohol-water mixtures, J. Colloid Interface Sci. 284 (2005) 255–259.
[4] P. Lavi, A. Marmur, Adsorption isotherms for concentrated aqueous-organic solutions (CAOS), J. Colloid Interface Sci. 230 (2000) 107–113.

[5] A. Chodzińska, A. Zdziennicka, B. Jańczuk, Volumetric and surface properties of short chain alcohols in aqueous solution-air systems at 293K, J. Solut. Chem. 41 (12) (2012) 2226–2245.

[6] A.B. Roney, B. Space, E.W. Castner, R.L. Napoleon, R.B. Moore, A molecular dynamics study of aggregation phenomena in aqueous n-propanol, J. Phys. Chem. B 108 (2004) 7389–7401.

[7] R. Zana, M.J. Eljebari, Fluorescence probing of self-association of alcohols in aqueous solution, J. Phys. Chem. 97 (1993) 11134–11136.

[8] H. Hayashi, Y. Udagawa, Mixing state of 1-propanol aqueous solutions studied by small-angle X-ray scattering: a new parameter reflecting the shape of SAXS curve, Bull. Chem. Soc. Jpn. 65 (1992) 155–159.

[9] K. Yoshida, T. Yamaguchi, Low-frequency Raman spectroscopy of aqueous solutions of aliphatic alcohols, Z. Naturforsch. 56a (2001) 529–536.

[10] G. Raina, G.U. Kulkarni, C.N.R. Rao, Surface enrichment in alcohol−water mixtures, J. Phys. Chem. A 105 (2001) 10204–10207.

[11] C.M. Romero, M.S. Paéz, Surface tension of aqueous solutions of alcohol and polyols at 298.15 K, Phys. Chem. Liq. 44 (2006) 61–65.

[12] M. Araton, T. Toyomasu, M. Villeneuve, Y. Uchizono, T. Takiue, K. Motomura, N. Ikeda, Thermodynamic study on the surface formation of the mixture of water and ethanol, J. Colloid Interface Sci. 191 (1997) 146–153.

[13] G. Vázquez, E. Alvarez, J.M. Navaza, Surface tension of alcohol+water from 20 to 50 °C, J. Chem. Eng. Data 40 (1995) 611–614.

[14] J. Fidler, P.M. Rodger, Solvation structure around aqueous alcohols, J. Phys. Chem. B 103 (1999) 7695–7703.

[15] H. Tamaka, K. Gubbins, Structure and thermodynamic properties of water-methanol mixtures: role of the water-water interaction, J. Chem. Phys. 97 (1992) 2626–2632.

[16] J.-B. Huang, M. Mao, B.-Y. Zhu, The surface physico-chemical properties of surfactants in ethanol–water mixtures, Colloids Surf. A Physicochem. Eng. Asp. 155 (1999) 339–348.

[17] A. Pan, B. Naskar, G.K.S. Prameela, B.V.N. Phani Kumar, A.B. Mandal, S.C. Bhattacharya, S.P. Moulik, Amphiphile behavior in mixed solvent media I: self-aggregation and ion association of sodium dodecylsulfate in 1,4-dioxane–water and methanol–water media, Langmuir 28 (2012) 13830–13843.

[18] A.I. Kovtun, S.L. Khil'ko, S.A. Zholob, V.I. Rybachenko, Effect of lower alcohols on adsorption characteristics of sodium dodecyl sulfate solutions at liquid as interfaces, Colloid J 72 (2010) 389–395.

[19] A. Abalos, A. Pinazo, M.R. Casals, F. Garcia, A. Manresa, Physicochemical and antimicrobial properties of new rhamnolipids produced by Pseudomonas aeruginosa AT10 from soybean oil refinery wastes, Langmuir 17 (2001) 1367–1371.

[20] O. Pornsunthorntwee, S. Chavadej, R. Rujiravanit, Solution properties and vesicle formation of rhamnolipid biosurfactants produced by Pseudomonas aeruginosa SP4, Colloids Surf B Biointerfaces 72 (2009) 6–15.

[21] T. Stipcevic, A. Piljac, G. Piljac, Enhanced healing of full-thickness burn wounds using di-rhamnolipid, Burns 32 (2006) 24–34.

[22] T. Stipcevic, T. Piljac, R.R. Isseroff, Di-rhamnolipid from Pseudomonas aeruginosa displays differential effects on human keratinocyte and fibroblast cultures, J. Dertmatol. Sci. 40 (2005) 141–143.

[23] R. Makkar, S. Cameotra, An update on the use of unconventional substrates for biosurfactant production and their new applications, Appl. Microbiol. Biotechnol. 58 (2002) 428–434.

[24] C.C. Lai, Y.C. Huang, Y.H. Wei, J.S. Chang, Biosurfactant-enhanced removal of total petroleum hydrocarbons from contaminated soil, J. Hazardous Mater 167 (2009) 609–614.

[25] C.N. Mulligan, Environmental applications for biosurfactants, Environ. Pollut. 133 (2005) 183–198.

[26] B. Thanomsub, W. Pumeechockchai, A. Limtrakul, P. Arunrattiyakorn, W. Petchleelaha, T. Nitoda, Chemical structures and biological activities of rhamnolipids produced by Pseudomonas aeruginosa B189 isolated from milk factory waste, Bioresour. Technol. 97 (2006) 2457–2461.

[27] M. Benincasa, A. Abalos, I. Oliveira, A. Manresa, Chemical structure, surface properties and biological activities of the biosurfactant chemical structures and biological activities of rhamnolipids produced by Pseudomonas aeruginosa LBI from soapstock, Antonie van Leeuwenhoec 85 (2004) 1–8.

[28] Y.H. Wei, Ch.L. Cheng, Ch.Ch. Chien, H.M. Wan, Enhanced di-rhamnolipid production with an indigenous isolate Pseudomonas aeruginosa J16, Process Biochem. 43 (2008) 769–774.

[29] H. Chong, Q. Li, Microbial production of rhamnolipids:opportunities, challenges and strategies, Microb. Cell Factories 16 (137) (2017) 1–12.

[30] T.B. Lotfabad, H. Abassi, R. Ahmadkhaniha, R. Roostaazad, R. Masooma, H.S. Zahiri, G. Ahamdian, H. Vali, K.A. Noghabi, Structural characterization of a rhamnolipid-type biosurfactant produced by Pseudomonas aeruginosa MR01: enhancement of di-rhamnolipid proportion using gamma irradiation, Colloids Surf B Biointerfaces 81 (2010) 397–405.

[31] G.S. Shreve, R. Makula, Characterization of a new rhamnolipid biosurfactant complex from Pseudomonas isolate DYNA270, Biomolecules 9 (885) (2019) 1–11.

[32] A.M. Abbdel-Mawgoud, F. Lépine, E. Déziel, Rhamnolipids: diversity of structures, microbial origins and roles, Appl. Microbiol. Biotechnol. 86 (2010) 1323–1336.

[33] C. Chayabutra, J. Wu, L.K. Ju, Rhamnolipid production by Pseudomonas aeruginosa under denitrification: effects of limiting nutrients and carbon substrates, Biotechnol. Bioeng. 72 (2001) 25–33.

[34] D. Mańko, A. Zdziennicka, B. Jańczuk, Thermodynamic properties of rhamnolipid micellization and adsorption, Colloids and Sur. B 119 (2014) 22–29.

[35] S.S. Helvaci, S. Peker, G. Özdemir, Effect of electrolytes on the surface behaviour of rhamnoipids R1 and R2, Colloids Surf. B 35 (2004) 225–233.

[36] F.M. Fowkes, Attractive forces at interfaces, Ind. Eng. Chem. 56 (1964) 40–52.

[37] C.J. Van Oss, Interfacial Forces in Aqueous Media, Marcel Dekker, New York, NY, USA, 1994.

[38] C.J. Van Oss, R.J. Good, Surface tension and the solubility of polymers and biopolymers: the role of polar and apolar interfacial free energies, J. Macromol. Sci. 26 (1989) 1183–1203.

[39] C.J. Van Oss, M.K. Chaudhury, R.J. Good, Monopolar surfaces, Adv. Colloid Interf. Sci. 28 (1987) 35–64.

[40] A. Zdziennicka, The wettability of polytetrafluoroethylene and polymethylmethacrylate by aqueous solutions of Triton X-100 and short chain alcohol mixtures, Appl. Surface Sci. 255 (2009) 7369–7379.

[41] A. Zdziennicka, B. Jańczuk, Behaviour of cationic surfactants and short chain alcohols in mixed surface layers at water-air and polymer-water interfaces with regard to polymer wettability. II wettability of polymers, J. Colloid Interface Sci. 350 (2010) 568–576.

[42] C.J. van Oss, P.M. Constanzo, Adhesion of anionic surfactants to polymer surfaces and low-energy materials, J. Adhes. Sci. Technol. (4) (1992) 477–487.

[43] A. Zdziennicka, B. Jańczuk, Thermodynamic parameters of some biosurfactants and surfactants adsorption at water-air interface, J. Mol. Liquids 243 (2017) 236–244.

[44] A. Zdziennicka, B. Jańczuk, Wetting and adhesion properties of rhamnolipid and surfactin, Int. J. Adhes. Adhes. 84 (2018) 275–282.

[45] G. Soberón-Chávez, F. Lépine, E. Déziel, Production of rhamnolipids by Pseudomonas aeruginosa, Appl. Microbiol. Biotechnol. 68 (2005) 705–717.

[46] E. Dézíel, F. Lépine, S. Milot, R. Villemur, Mass spectrometry monitoring of rhamnolipids from a growing culture of Pseudomonas aeruginosa strain 57RP, Biochim. Biophys. Acta 1485 (2000) 143–152.

[47] V.B. Fainerman, R. Miller, E.V. Aksenenko, Simple model for prediction of surface tension of mixed surfactant solutions, Adv. Colloid Interf. Sci. 96 (2002) 339–359.

[48] V.B. Fainerman, R. Miller, Simple method to estimate surface tension of mixed surfactant solutions, J. Phys. Chem. B 105 (2001) 11432–11438.

[49] K.A. Connors, K.A. Wright, Dependence of surface tension on composition of binary aqueous-organic solutions, Anal. Chem. 61 (1989) 194–198.

[50] A.W. Adamson, A.P. Gast, Physical Chemistry of Surfaces, 6th ed Wiley-Interscience, New York, 1997.

[51] A. Zdziennicka, Surface behavior of Triton X-165 and short chain alcohol mixtures, Langmuir 26 (3) (2010) 1860–1869.

[52] J.H. de Boer, The Dynamic Character of Adsorption, Oxford University, Oxford, 1953.

[53] E. Rekiel, A. Zdziennicka, B. Jańczuk, Adsorption of surfactin at water with ethanol mixture-air interface, J. Mol. Liq. 300 (2020) 112240.

ADSORPTION PROPERTIES OF RHAMNOLIPID AND ETHANOL AT WATER/ETHANOL SOLUTION-AIR INTERFACE

EDYTA REKIEL, ANNA ZDZIENNICKA* AND BRONISŁAW JAŃCZUK

Department of Interfacial Phenomena, Institute of Chemical Sciences, Faculty of Chemistry, Maria Curie-Skłodowska University in Lublin, Maria Curie-Skłodowska Sq. 3, 20-031 Lublin, Poland

Running title: Adsorption

*To whom correspondence should be addressed

phone   (48-81) 537-56-70   fax   (48-81) 533-3348

e-mail   aniaz@hektor.umcs.lublin.pl
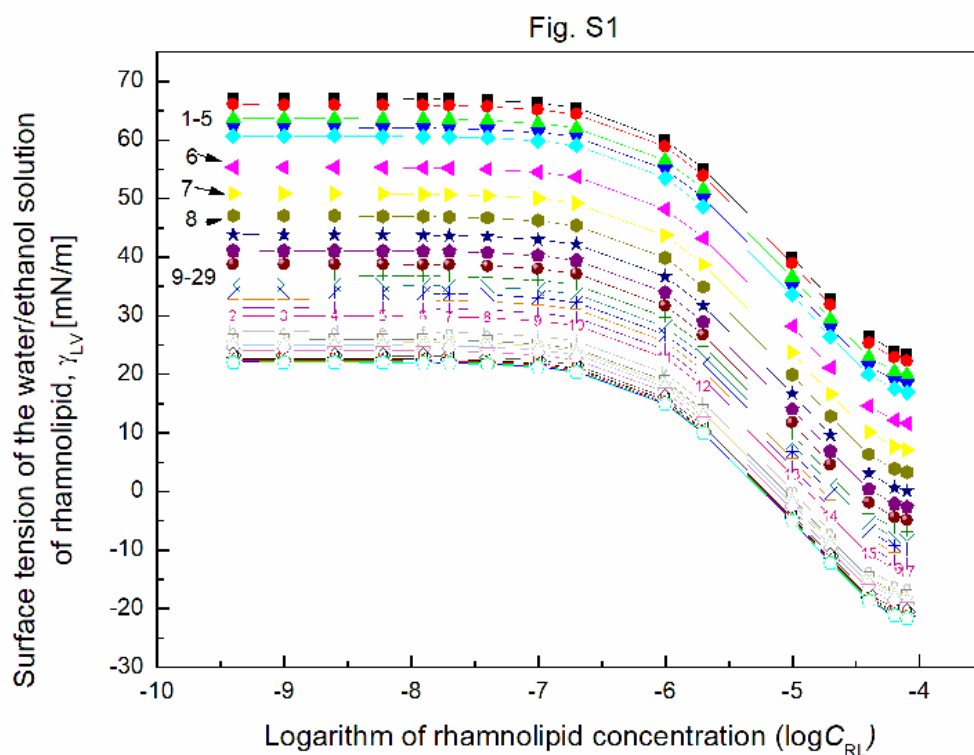
Fig. S1. A plot of surface tension (γ_{LV}) of the water/ethanol solution of RL vs. the logarithm of RL concentration ($\log C_{RL}$) calculated from Eq. (1). Curves 1 – 29 correspond to the constant ET concentration equal to 0.06692; 0.1338; 0.2677; 0.4015; 0.535; 1.0706; 1.6062; 2.1416; 2.677; 3.2124; 3.7478; 4.2832; 4.8185; 5.3538; 5.8893; 6.6925; 7.7245; 8.5664; 10.2797; 11.968; 12.145; 13.3794; 14.5696; 15.4064; 16.084; 16.3777; 16.648; 16.8988 and 17.13 M.
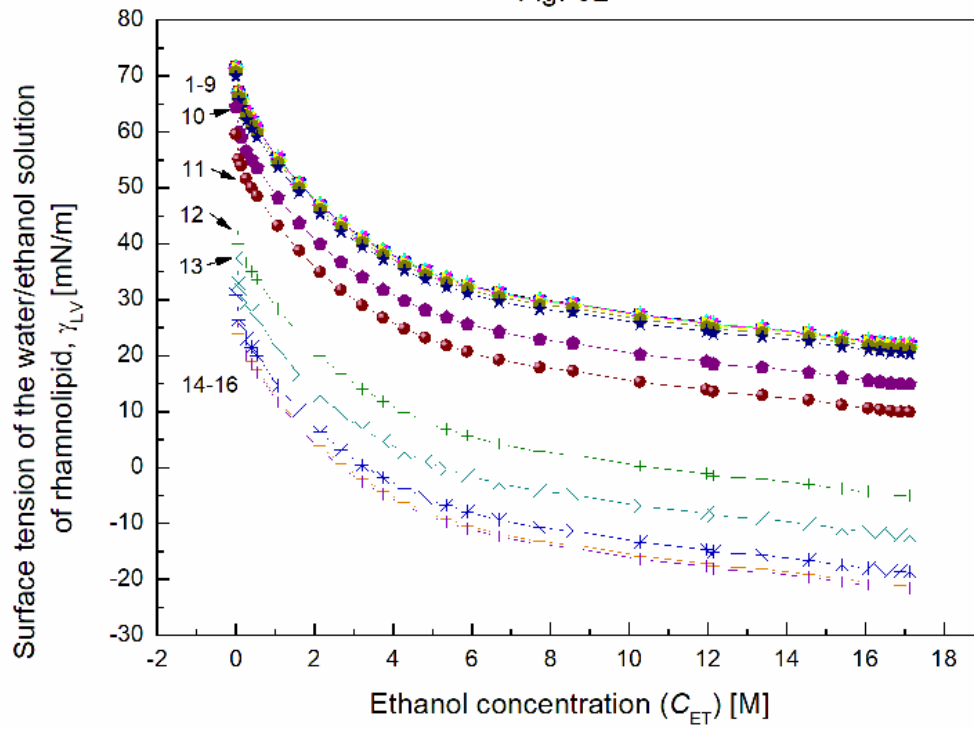
Fig. S2. A plot of surface tension (γ_{LV}) of the water/ethanol solution of RL vs. the ET concentration (C_{ET}) calculated from Eq. (1). Curves 1 – 16 correspond to the constant RL concentration equal to 0.0002; 0.0005; 0.00125; 0003; 0.00625; 0.01; 0.02; 0.05; 0.1; 0.5; 1; 5; 10; 20; 30 and 40 mg/dm³.
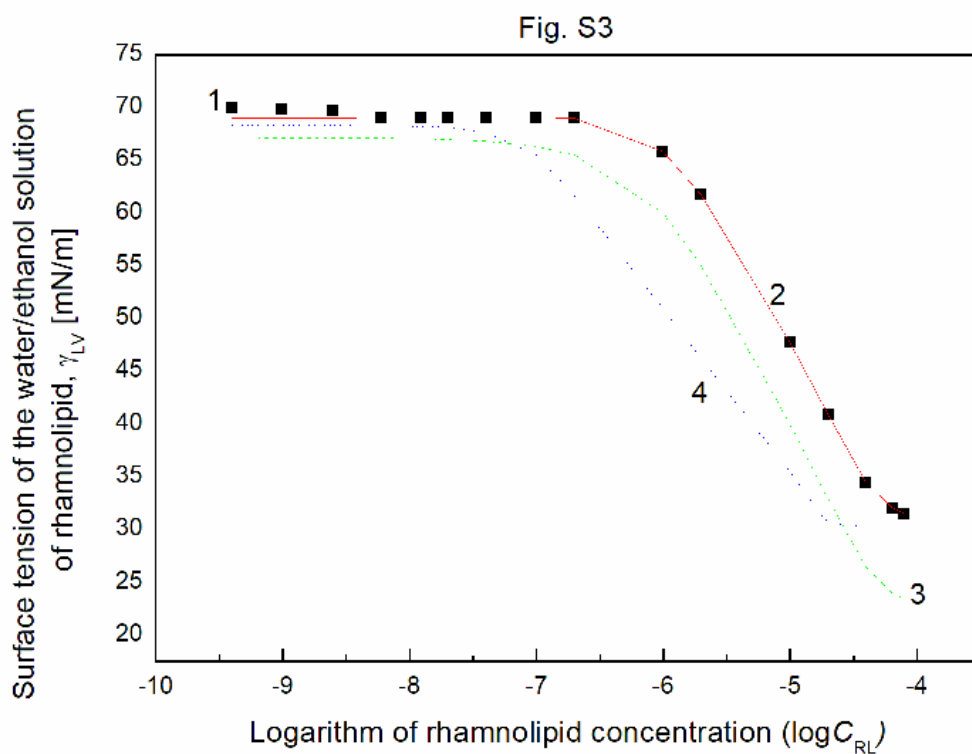
Fig. S3. A plot of surface tension (γ_{LV}) of the water/ethanol solution of RL vs. the logarithm of RL concentration (logC_{RL}) at the constant ET concentration equal to 0.06692 M. Points 1 correspond to the measured values, line 2 corresponds to the values calculated from Eq. (2), line 3 corresponds to the values calculated from Eq. (1) and line 4 to those calculated from the Fainerman and Miller equation.
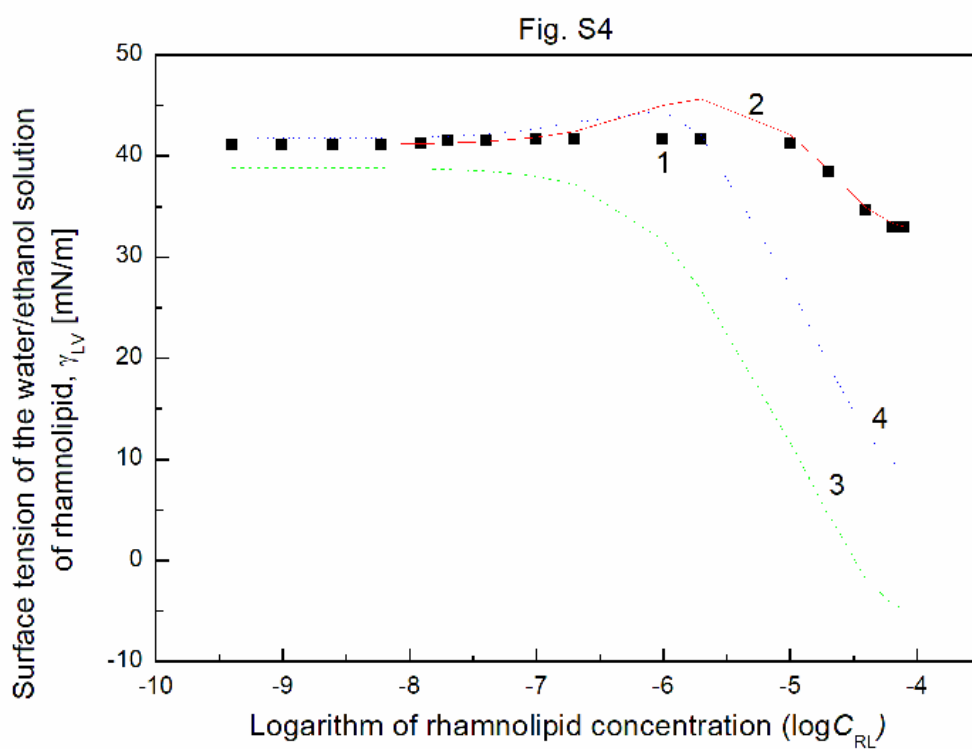
Fig. S4. A plot of surface tension (γ_{LV}) of the water/ethanol solution of RL vs. the logarithm of RL concentration ($\log C_{RL}$) at the constant ET concentration equal to 3.7478 M. Points 1 correspond to the measured values, lines 2 corresponds to the values calculated from Eq. (2), line 3 corresponds to the values calculated from Eq. (1) and line 4 to those calculated from the Fainerman and Miller equation.
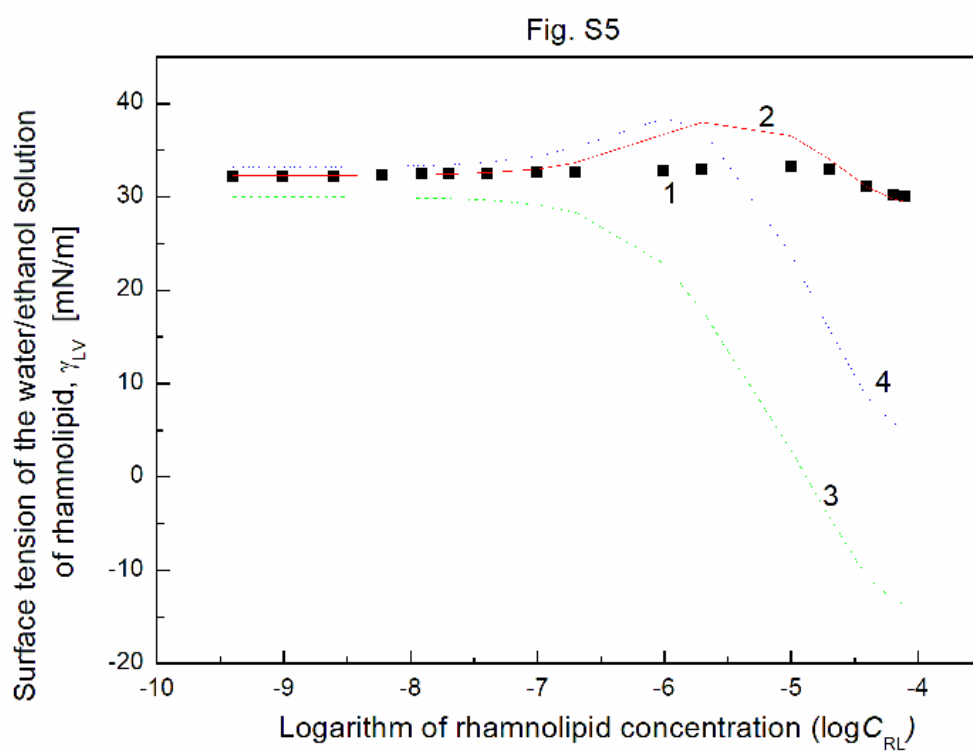
Fig. S5. A plot of surface tension (γ_{LV}) of the water/ethanol solution of RL vs. the logarithm of RL concentration ($\log C_{RL}$) at the constant ET concentration equal to 7.7245 M. Points 1 correspond to the measured values, lines 2 corresponds to the values calculated from Eq. (2), line 3 corresponds to the values calculated from Eq. (1) and line 4 to calculated from the Fainerman and Miller equation.
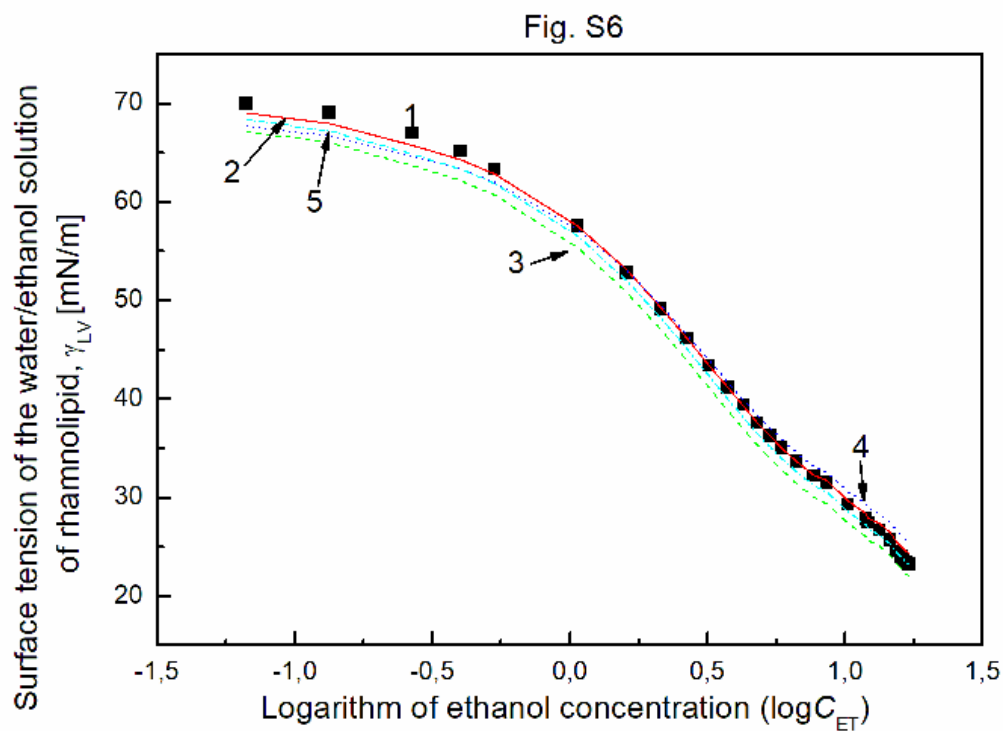
Fig. S6. A plot of surface tension (γ_{LV}) of the water/ethanol solution of RL vs. the ET concentration ($\log C_{ET}$) at the constant RL concentration equal to 0.0002 mg/dm^3. Points 1 correspond to the measured values, line 2 corresponds to the values calculated from Eq. (2), line 3 corresponds to the values calculated from Eq. (1), line 4 to those calculated from the Fainerman and Miller equation and line 5 to the values calculated from the Connors equation.
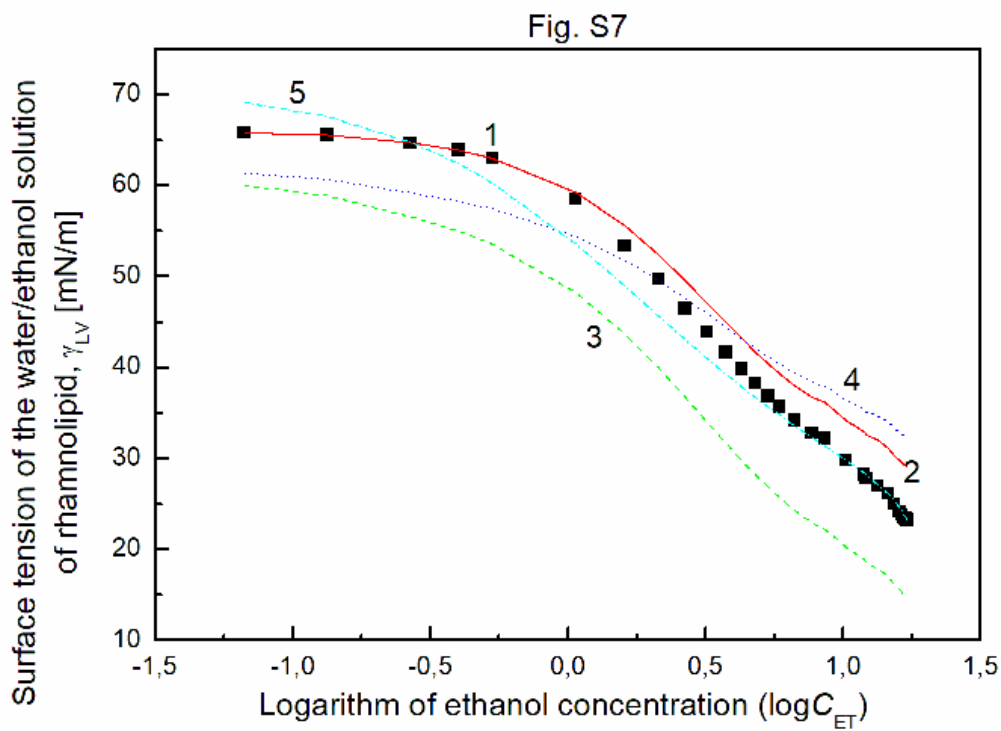
Fig. S7. A plot of surface tension (γ_{LV}) of the water/ethanol solution of RL vs. the ET concentration ($\log C_{ET}$) at the constant RL concentration equal to 0.5 mg/dm³. Points 1 correspond to the measured values, line 2 corresponds to the values calculated from Eq. (2), line 3 corresponds to the values calculated from Eq. (1), line 4 to those calculated from the Fainerman and Miller equation and line 5 to the values calculated from the Connors equation.
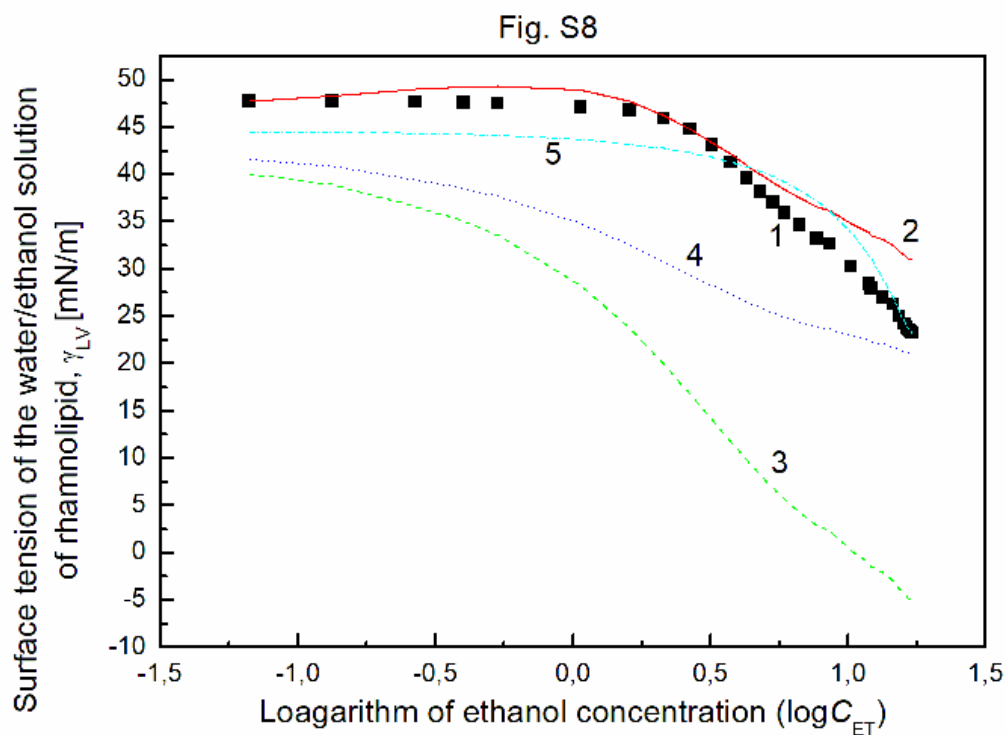
Fig. S8. A plot of surface tension (γ_{LV}) of the water/ethanol solution of RL vs. the ET concentration ($\log C_{ET}$) at the constant RL concentration equal to 5 mg/dm^3. Points 1 correspond to the measured values, line 2 corresponds to the values calculated from Eq. (2), line 3 corresponds to the values calculated from Eq. (1), line 4 to those calculated from the Fainerman and Miller equation and line 5 to the values calculated from the Connors equation.
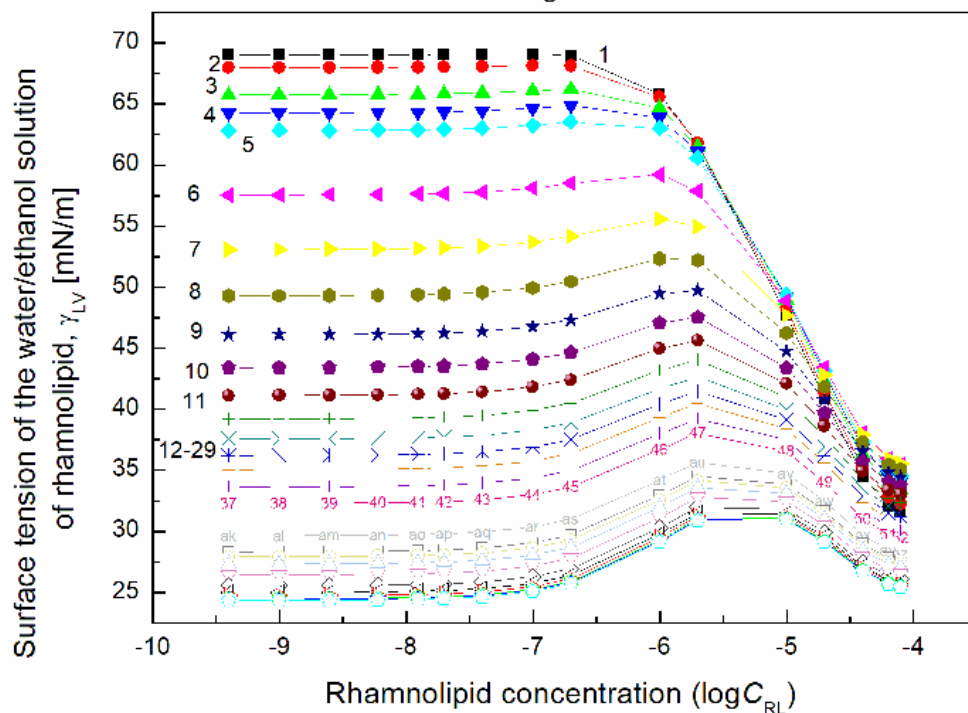
Fig. S9. A plot of surface tension (γ_{LV}) of the water/ethanol solution of RL vs. the logarithm of RL concentration (logC_{RL}) calculated from Eq. (2). Curves 1 – 29 correspond to the constant ET concentration equal to 0.06692; 0.1338; 0.2677; 0.4015; 0.535; 1.0706; 1.6062; 2.1416; 2.677; 3.2124; 3.7478; 4.2832; 4.8185; 5.3538; 5.8893; 6.6925; 7.7245; 8.5664; 10.2797; 11.968; 12.145; 13.3794; 14.5696; 15.4064; 16.084; 16.3777; 16.648; 16.8988 and 17.13 M.
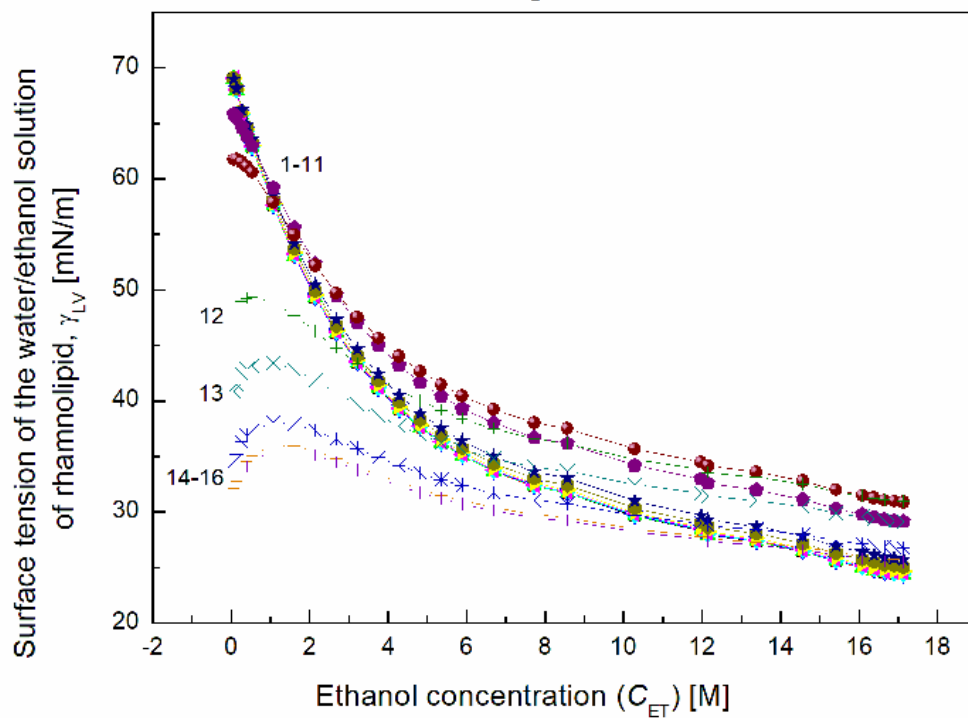
Fig. S10. A plot of surface tension (γ_{LV}) of the water/ethanol solution of RL vs. the ET concentration (C_{ET}) (a) calculated from Eq. (2). Curves 1 – 16 correspond to the constant RL concentration equal to 0.0002; 0.0005; 0.00125; 0003; 0.00625; 0.01; 0.02; 0.05; 0.1; 0.5; 1; 5; 10; 20; 30 and 40 mg/dm^3.
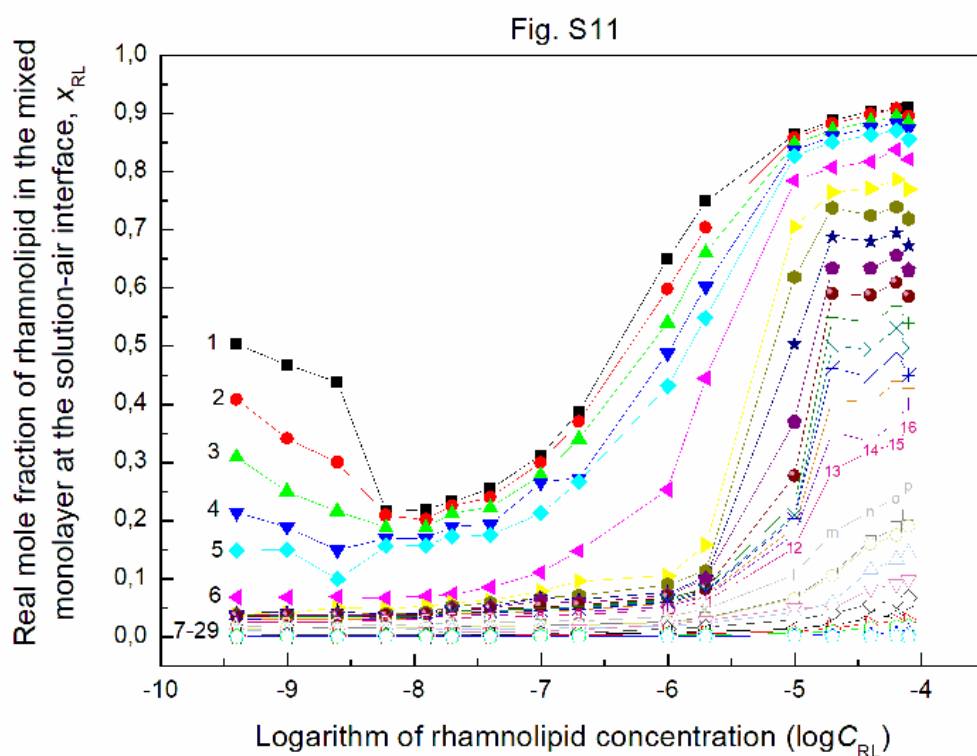
Fig. S11. A plot of real mole fraction of RL in the mixed monolayer at the solution-air interface calculated from Eq. (2) vs. the logarithm of RL concentration ($\log C_{RL}$). Curves 1 – 29 correspond to the constant ET concentration equal to 0.06692; 0.1338; 0.2677; 0.4015; 0.535; 1.0706; 1.6062; 2.1416; 2.677; 3.2124; 3.7478; 4.2832; 4.8185; 5.3538; 5.8893; 6.6925; 7.7245; 8.5664; 10.2797; 11.968; 12.145; 13.3794; 14.5696; 15.4064; 16.084; 16.3777; 16.648; 16.8988 and 17.13 M.
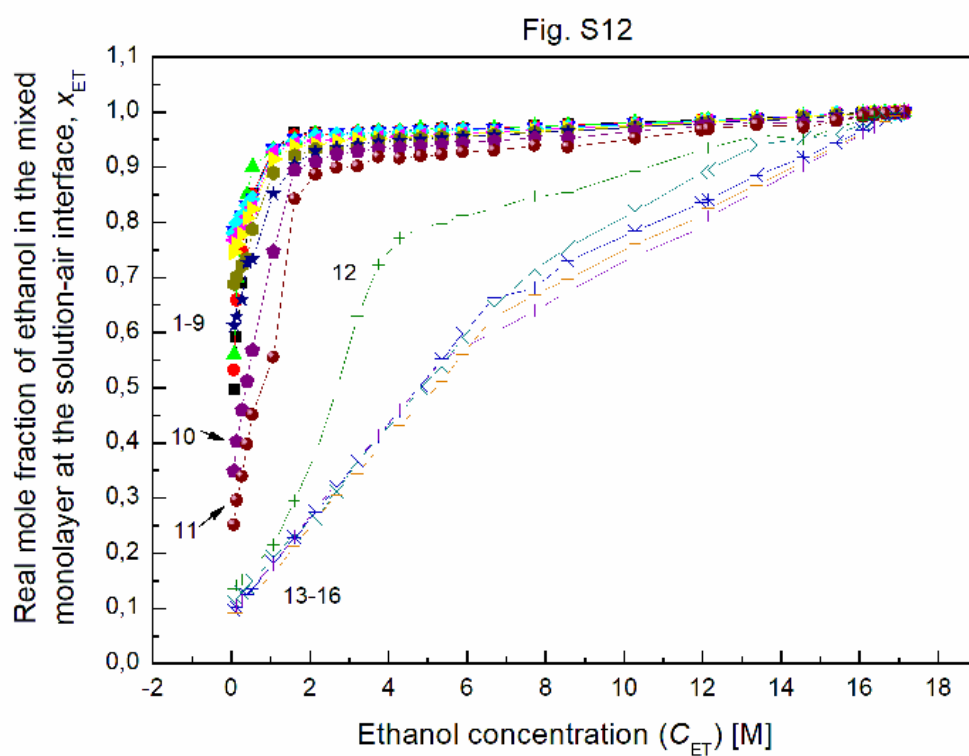
Fig. S12. A plot of real mole fraction of ethanol in the mixed monolayer at the solution-air interface calculated from Eq. (2) vs. the ET concentration (C_{ET}). Curves 1 – 16 correspond to the constant RL concentration equal to 0.0002; 0.0005; 0.00125; 0003; 0.00625; 0.01; 0.02; 0.05; 0.1; 0.5; 1; 5; 10; 20; 30 and 40 mg/dm^3.
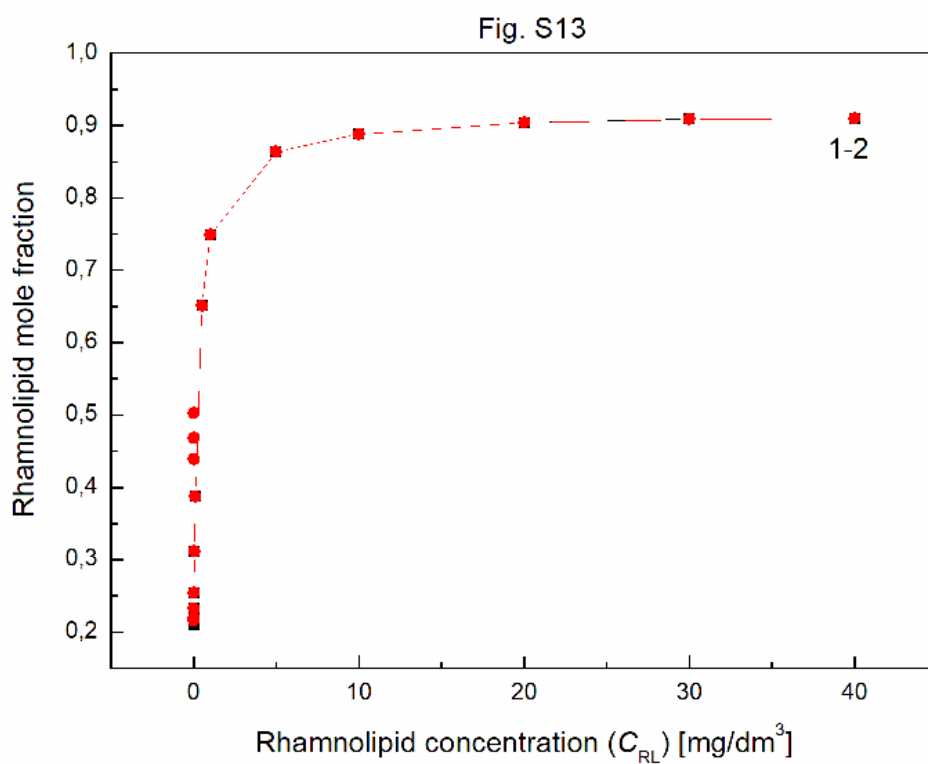
Fig. S13. A comparison of RL mole fraction determined on the basis of the monolayer pressure of the individual RL and ET at the water-air interface (curve 1) and those calculated from Eq. (2) (curve 2) at the constant ET concentration equal to 0.06692 M.
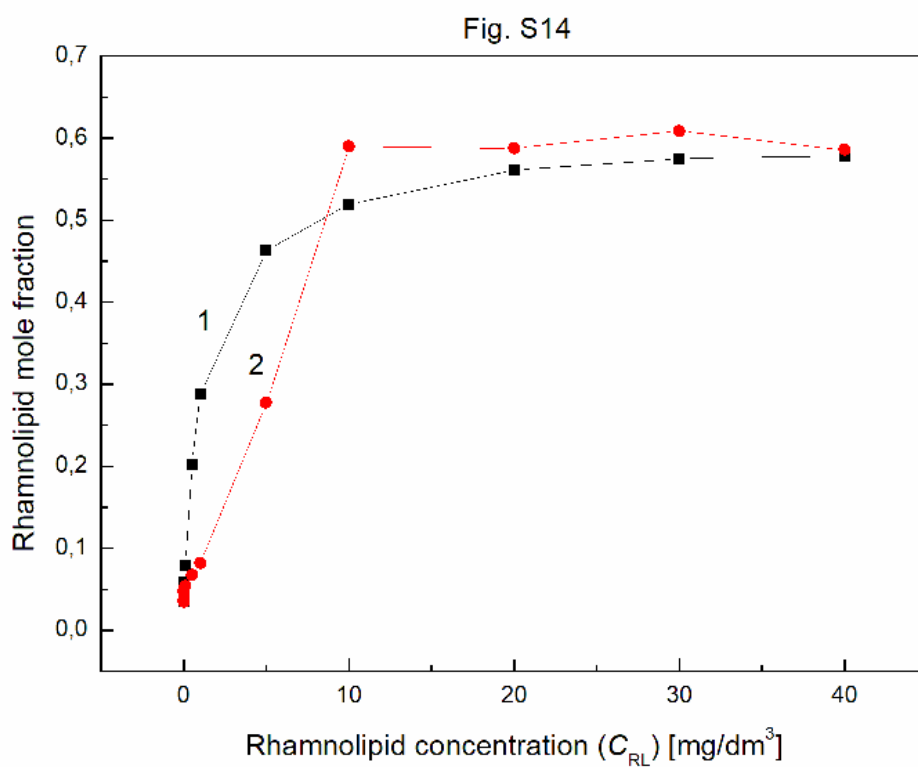
Fig. S14. A comparison of RL mole fraction determined on the basis of the monolayer pressure of the individual RL and ET at the water-air interface (curve 1) and those calculated from Eq. (2) (curve 2) at the constant ET concentration equal to 3.7478 M.
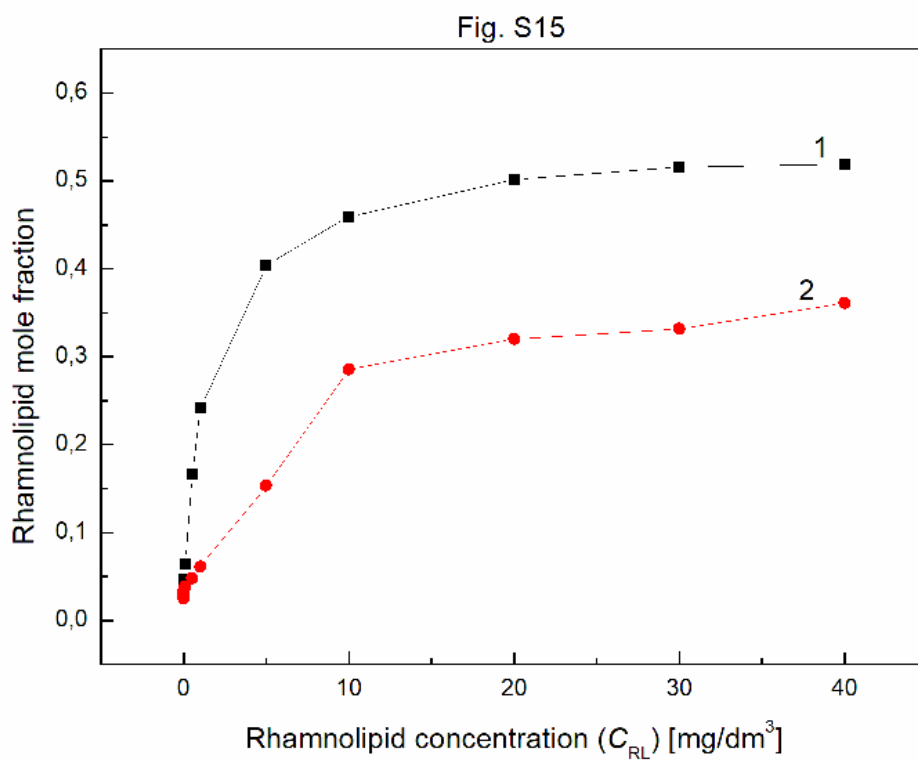
Fig. S15. A comparison of RL mole fraction determined on the basis of the monolayer pressure of the individual RL and ET at the water-air interface (curve 1) and those calculated from Eq. (2) (curve 2) at the constant ET concentration equal to 7.7245 M.
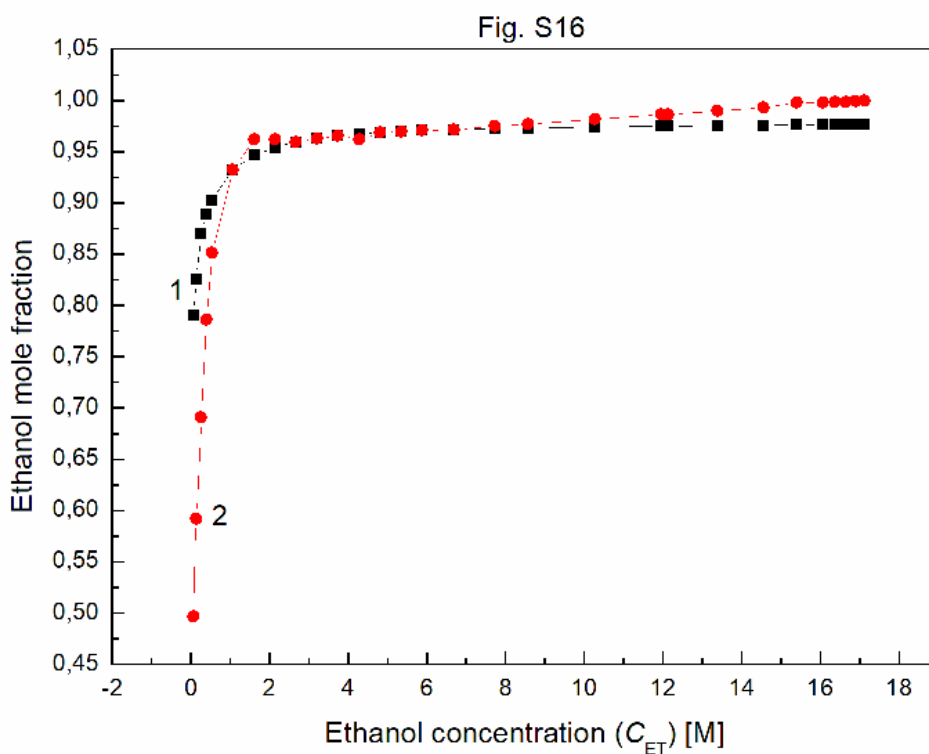
Fig. S16. A comparison of ET mole fraction determined on the basis of the monolayer pressure of the individual RL and ET at the water-air interface (curve 1) and those calculated from Eq. (2) (curve 2) at the constant RL concentration equal to 0.0002 mg/dm^3.
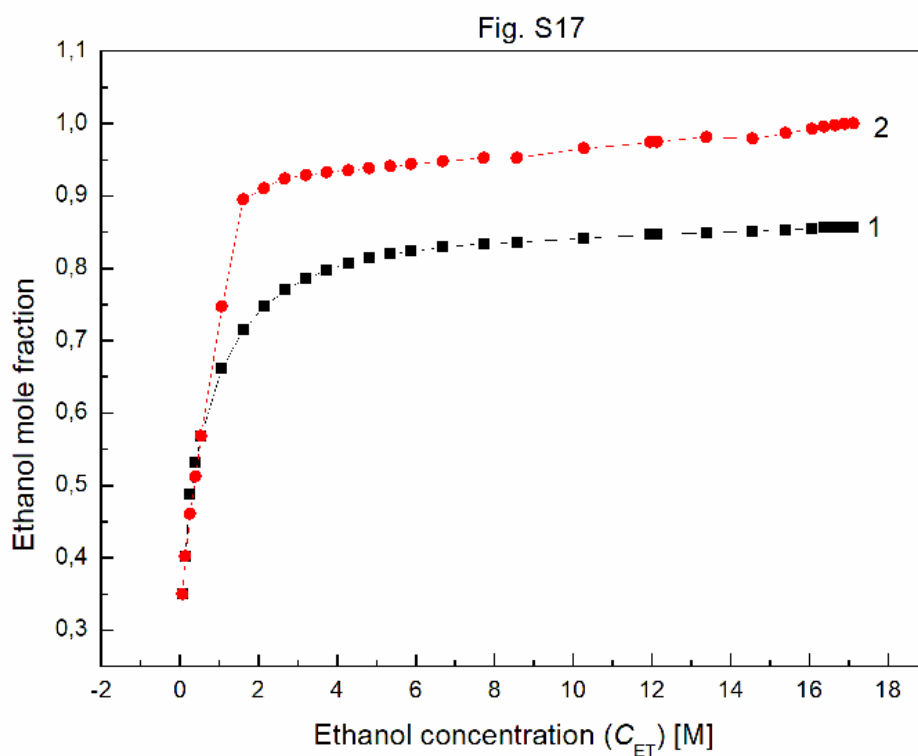
Fig. S17. A comparison of ET mole fraction determined on the basis of the monolayer pressure of the individual RL and ET at the water-air interface (curve 1) and those calculated from Eq. (2) (curve 2) at the constant RL concentration equal to 0.5 mg/dm^3.
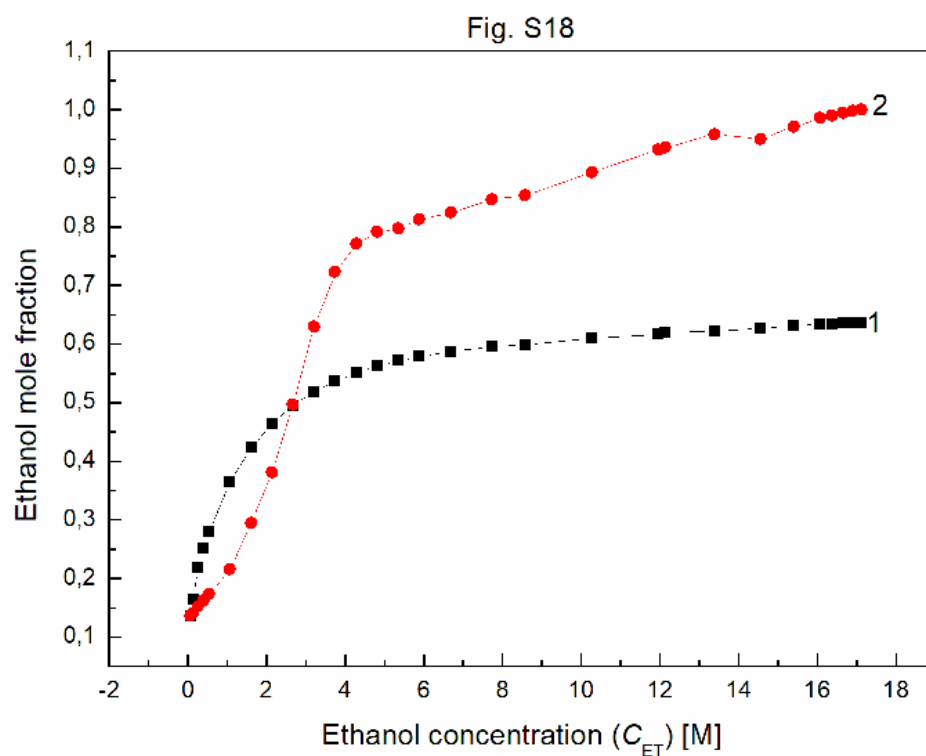
Fig. S18. A comparison of ET mole fraction determined on the basis of the monolayer pressure of the individual RL and ET at the water-air interface (curve 1) and those calculated from Eq. (2) (curve 2) at the constant RL concentration equal to 5 mg/dm^3.
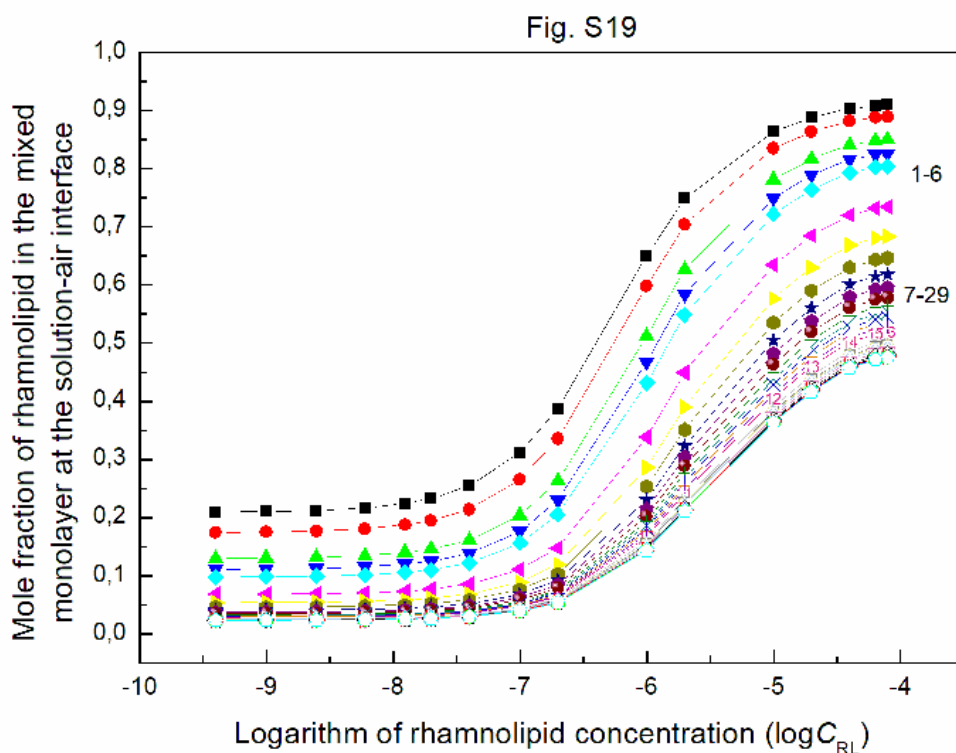
Fig. S19. A plot of mole fraction of RL in the mixed monolayer at the solution-air interface determined on the basis of the monolayer pressure of the individual RL and ET at the water-air interface vs. the logarithm of RL concentration ($\log C_{RL}$). Curves 1 – 29 correspond to the constant ET concentration equal to 0.06692; 0.1338; 0.2677; 0.4015; 0.535; 1.0706; 1.6062; 2.1416; 2.677; 3.2124; 3.7478; 4.2832; 4.8185; 5.3538; 5.8893; 6.6925; 7.7245; 8.5664; 10.2797; 11.968; 12.145; 13.3794; 14.5696; 15.4064; 16.084; 16.3777; 16.648; 16.8988 and 17.13 M.
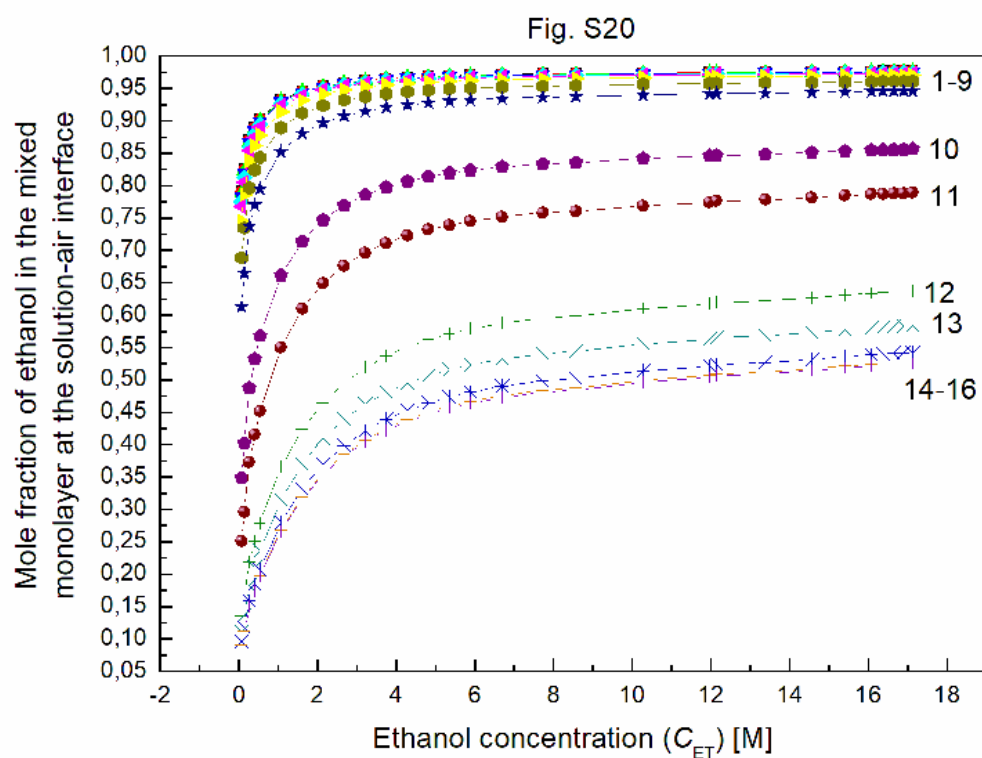
Fig. S20. A plot of mole fraction of ethanol in the mixed monolayer at the solution-air interface determined on the basis of the monolayer pressure of the individual RL and ET at the water-air interface vs. the ET concentration (C_{ET}). Curves 1 – 16 correspond to the constant RL concentration equal to 0.0002; 0.0005; 0.00125; 0003; 0.00625; 0.01; 0.02; 0.05; 0.1; 0.5; 1; 5; 10; 20; 30 and 40 mg/dm^3.
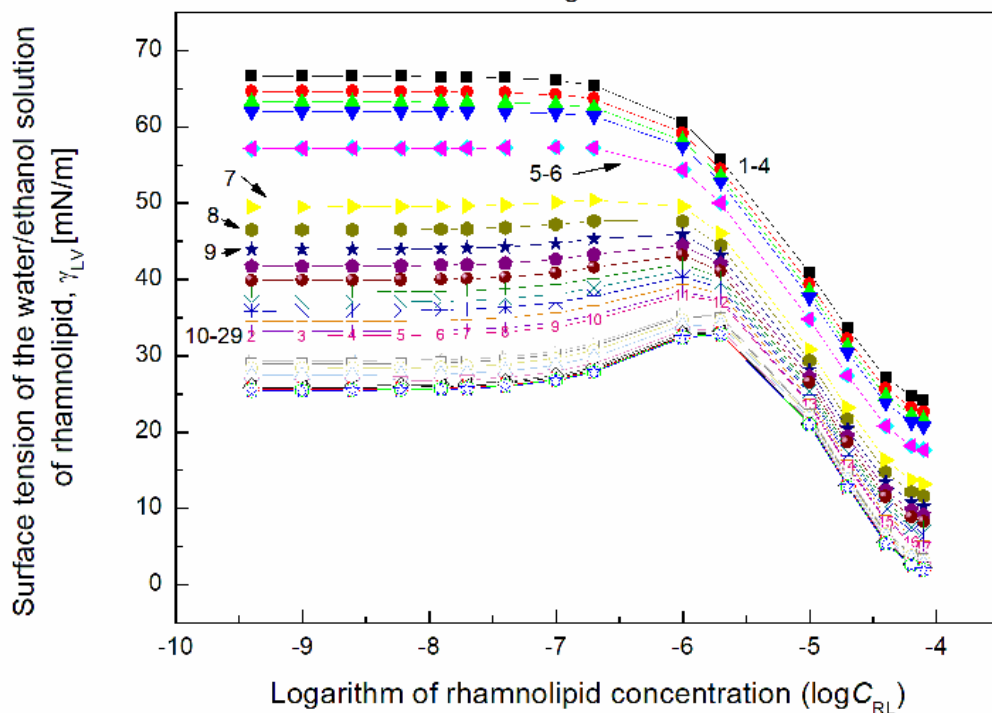
Fig. S21. A plot of surface tension (γ_{LV}) of the water/ethanol solution of RL calculated from the Fainerman and Miller equation vs. the logarithm of RL concentration ($\log C_{RL}$). Curves 1 – 29 correspond to the constant ET concentration equal to 0.06692; 0.1338; 0.2677; 0.4015; 0.535; 1.0706; 1.6062; 2.1416; 2.677; 3.2124; 3.7478; 4.2832; 4.8185; 5.3538; 5.8893; 6.6925; 7.7245; 8.5664; 10.2797; 11.968; 12.145; 13.3794; 14.5696; 15.4064; 16.084; 16.3777; 16.648; 16.8988 and 17.13 M.
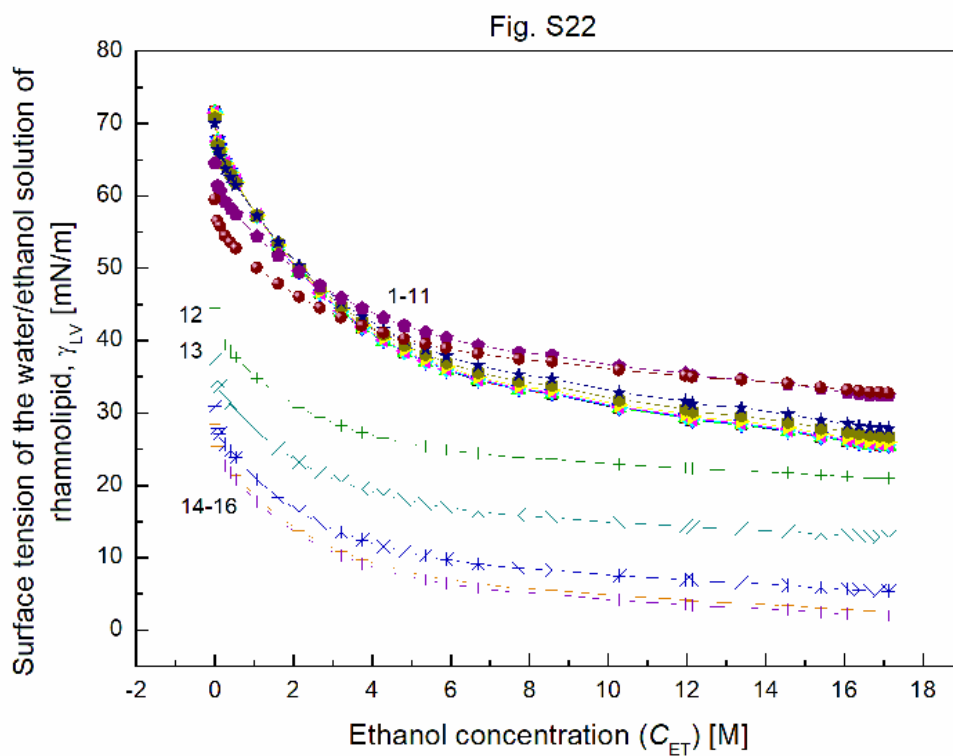
Fig. S22. A plot of surface tension (γ_{LV}) of the water/ethanol solution of RL calculated from the Fainerman and Miller equation vs. the ET concentration (C_{ET}). Curves 1 – 16 correspond to the constant RL concentration equal to 0.0002; 0.0005; 0.00125; 0003; 0.00625; 0.01; 0.02; 0.05; 0.1; 0.5; 1; 5; 10; 20; 30 and 40 mg/dm³.
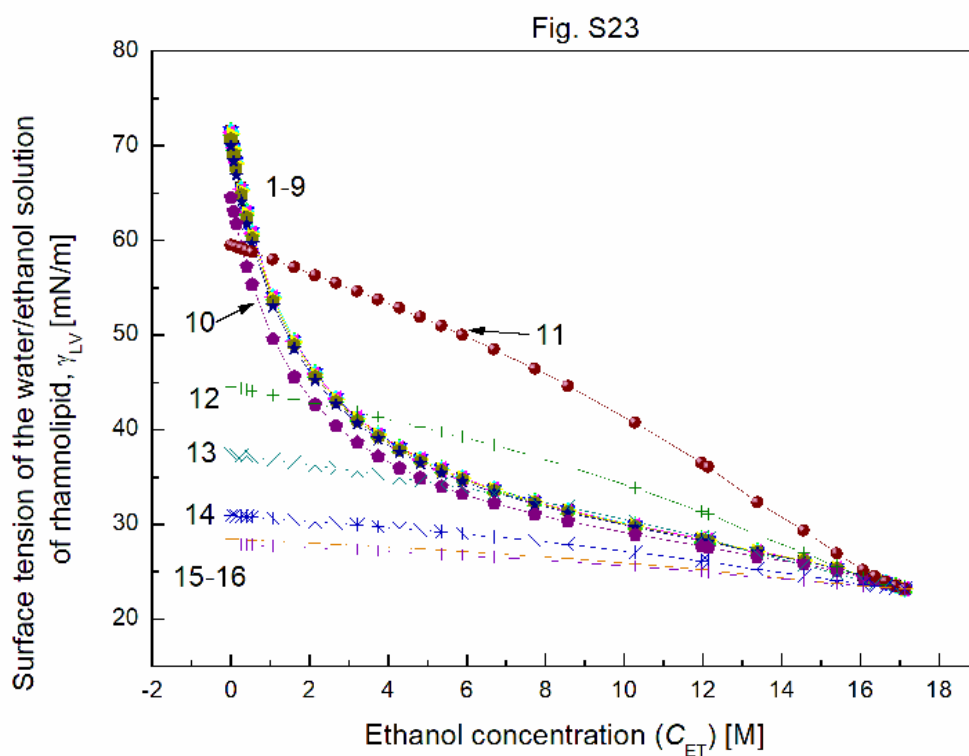
Fig. S23. A plot of surface tension (γ_{LV}) of the water/ethanol solution of RL calculated from the Connors equation vs. the ET concentration (C_{ET}). Curves 1 – 16 correspond to the constant RL concentration equal to 0.0002; 0.0005; 0.00125; 0003; 0.00625; 0.01; 0.02; 0.05; 0.1; 0.5; 1; 5; 10; 20; 30 and 40 mg/dm^3.
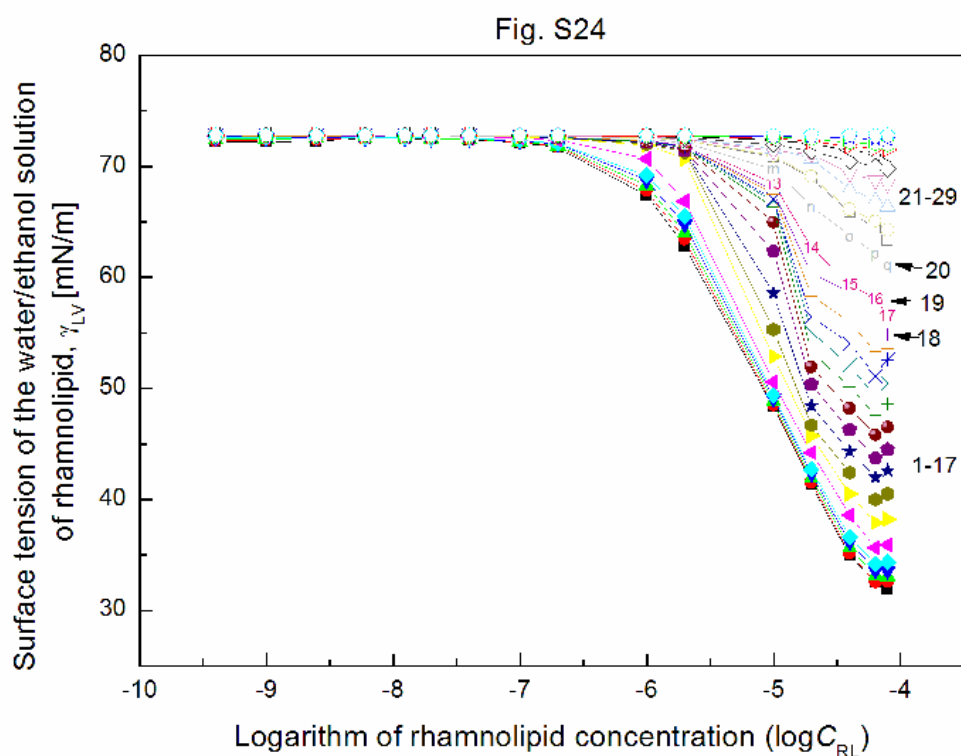
Fig. S24. A plot of surface tension (γ_{LV}) of the water/ethanol solution of RL calculated on the basis of RL and ET contribution to the mixed monolayer pressure at the solution-air interface vs. the logarithm of RL concentration (logC_{RL}). Curves 1 – 29 correspond to the constant ET concentration equal to 0.06692; 0.1338; 0.2677; 0.4015; 0.535; 1.0706; 1.6062; 2.1416; 2.677; 3.2124; 3.7478; 4.2832; 4.8185; 5.3538; 5.8893; 6.6925; 7.7245; 8.5664; 10.2797; 11.968; 12.145; 13.3794; 14.5696; 15.4064; 16.084; 16.3777; 16.648; 16.8988 and 17.13 M.
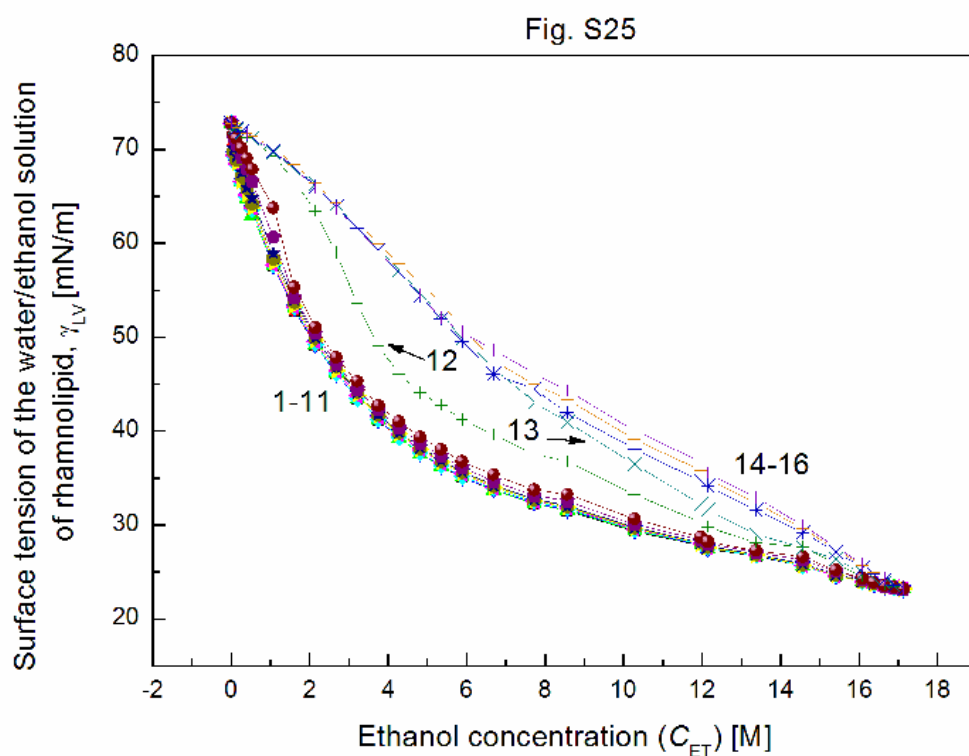
Fig. S25. A plot of surface tension (γ_{LV}) of the water/ethanol solution of RL calculated on the basis of RL and ET contribution to the mixed monolayer pressure at the solution-air interface vs. the ET concentration (C_{ET}). Curves 1 – 16 correspond to the constant RL concentration equal to 0.0002; 0.0005; 0.00125; 0003; 0.00625; 0.01; 0.02; 0.05; 0.1; 0.5; 1; 5; 10; 20; 30 and 40 mg/dm^3.
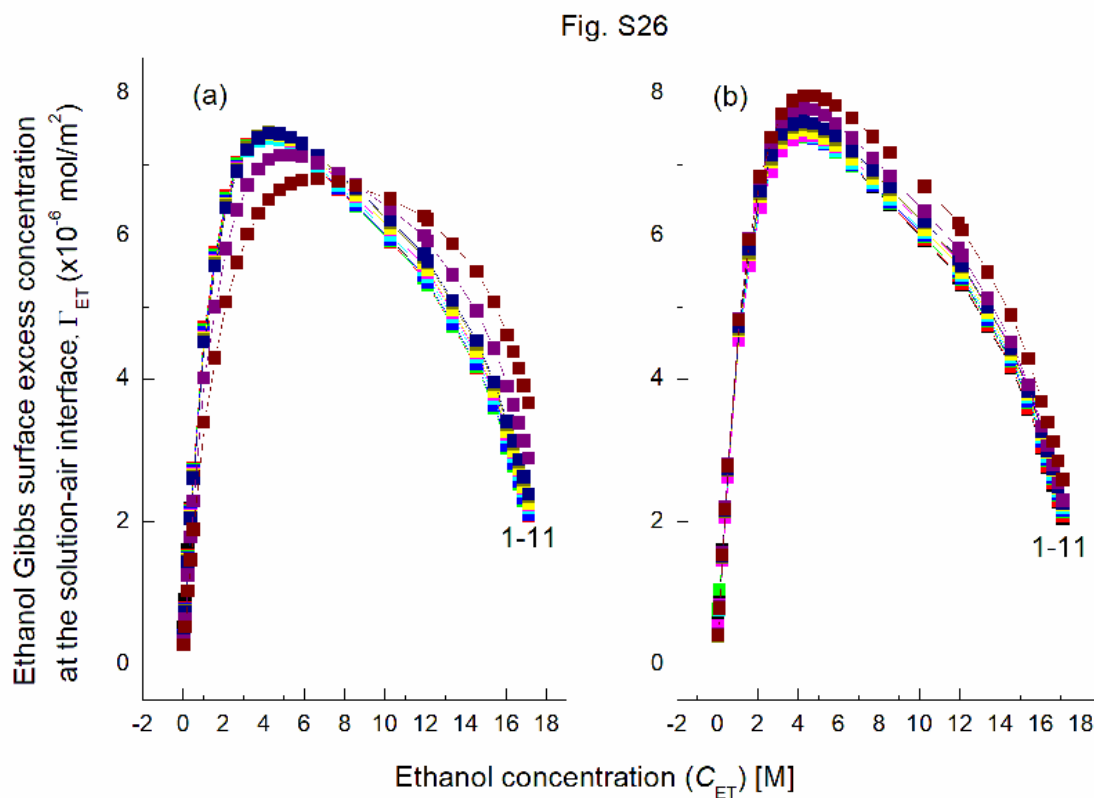
Fig. S26. A plot of ethanol Gibbs surface excess concentration at the solution-air interface calculated on the basis of the measured surface tension of the studied solution (a) and calculated on the basis of the ET contribution to the mixed monolayer pressure at the solution-air interface (b) vs. the ET concentration (C_{ET}). Curves 1 – 11 correspond to the constant RL concentration equal to 0.0002; 0.0005; 0.00125; 0003; 0.00625; 0.01; 0.02; 0.05; 0.1; 0.5 and mg/dm^3.
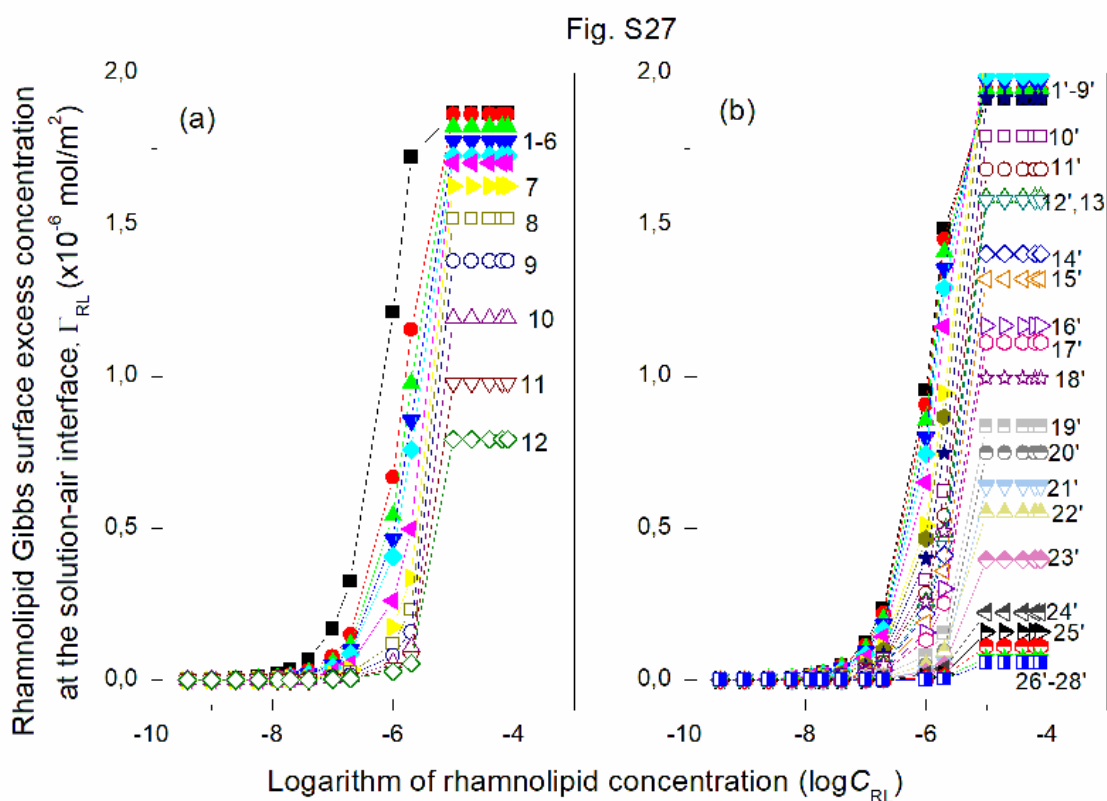
Fig. S27. A plot of RL Gibbs surface concentration at the solution-air interface calculated on the basis of the measured surface tension of the studied solution (a) and calculated from the RL contribution to the mixed monolayer pressure at the solution-air interface (b) vs. the logarithm of RL concentration ($\log C_{RL}$). Curves 1 – 12 correspond to the constant ET concentration equal to 0.06692; 0.1338; 0.2677; 0.4015; 0.535; 1.0706; 1.6062; 2.1416; 2.677; 3.2124; 3.7478 and 4.2832 M. Curves 1' – 28' correspond to the constant ET concentration equal to 0.06692; 0.1338; 0.2677; 0.4015; 0.535; 1.0706; 1.6062; 2.1416; 2.677; 3.2124; 3.7478, 4.2832; 4.8185; 5.3538; 5.8893; 6.6925; 7.7245; 8.5664; 10.2797; 11.968; 12.145; 13.3794; 14.5696; 15.4064; 16.084; 16.3777; 16.648 and 16.8988 M.
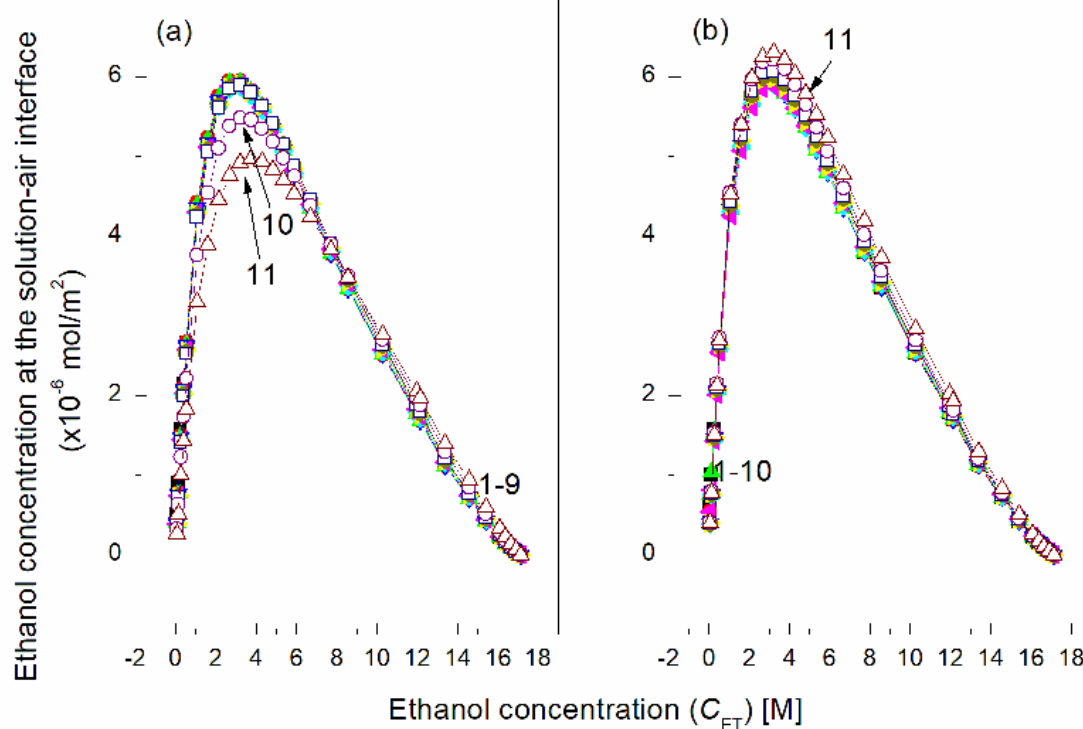
Fig. S28. A plot of ethanol concentration at the solution-air interface calculated from the Gugenheim-Adam equation on the basis of the ethanol Gibbs surface excess concentration determined from the measured surface tension of the studied solution (a) and calculated based on the ET contribution to the mixed monolayer pressure at the solution-air interface (b) vs. the ET concentration (C_{ET}). Curves 1 – 11 correspond to the constant RL concentration equal to 0.0002; 0.0005; 0.00125; 0003; 0.00625; 0.01; 0.02; 0.05; 0.1; 0.5 and 1 mg/dm^3.
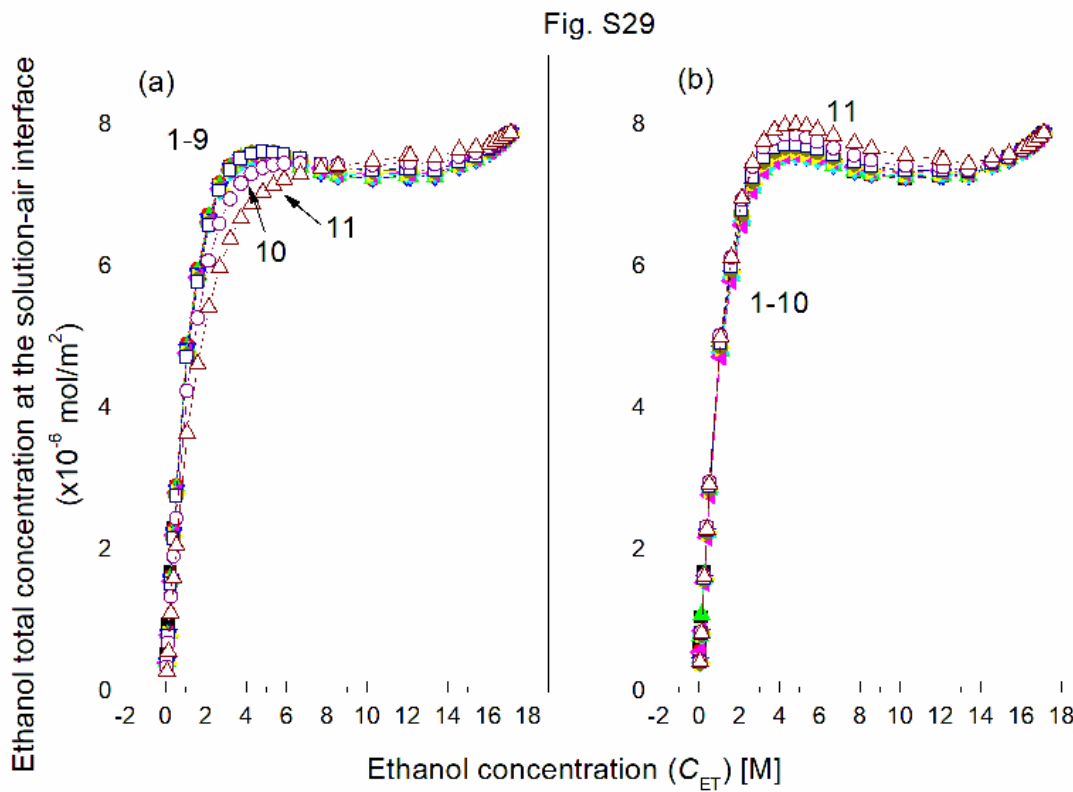
Fig. S29. A plot of total ethanol concentration at the solution-air interface calculated from Eq. (3) based on the data presented in Fig. S28a (a) and Fig. S28b (b) vs. the ET concentration (C_{ET}). Curves 1 – 11 correspond to the constant RL concentration equal to 0.0002; 0.0005; 0.00125; 0003; 0.00625; 0.01; 0.02; 0.05; 0.1; 0.5 and 1 mg/dm^3.
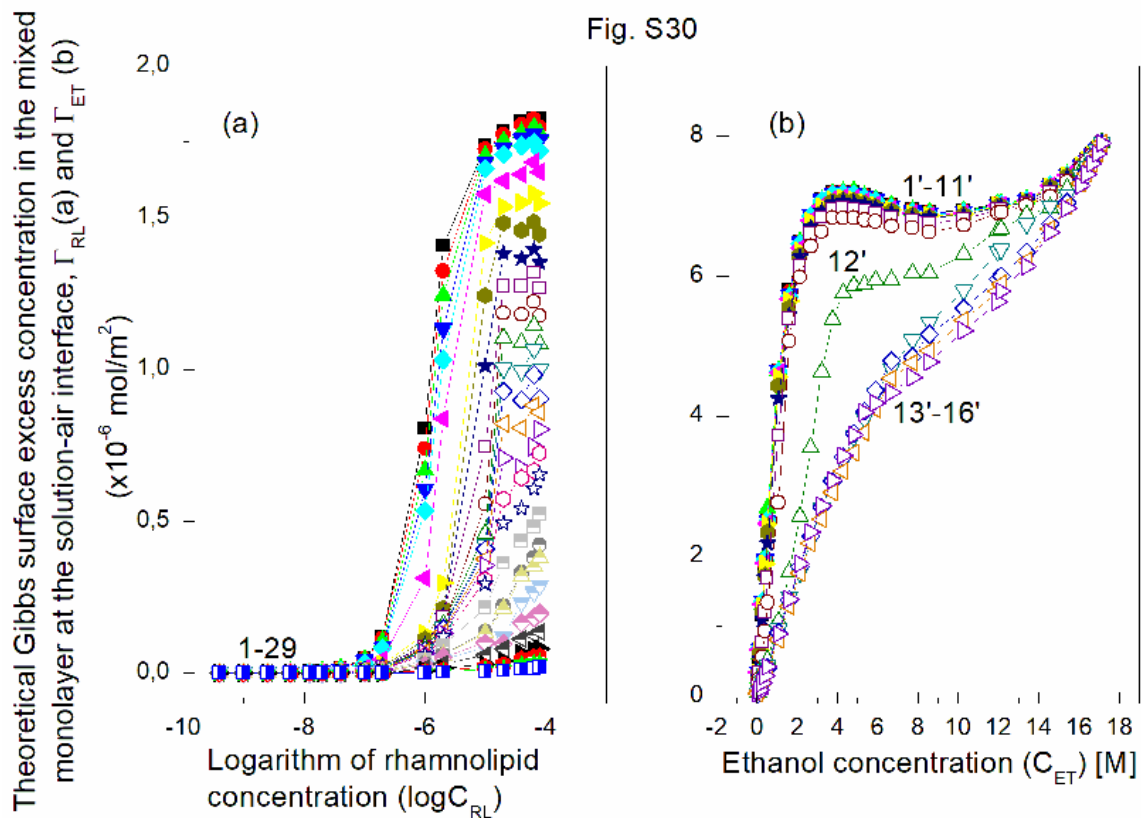
Fig. S30. A plot of theoretical RL (a) and ET (b) Gibbs surface excess concentration in the mixed monolayer at the solution-air interface calculated on the basis of the Gibbs surface excess concentration of individual RL and ET vs. the logarithm of RL ($\log C_{RL}$) and ET ($\log C_{ET}$) concentration. Curves 1 – 29 correspond to the constant ET concentration equal to 0.06692; 0.1338; 0.2677; 0.4015; 0.535; 1.0706; 1.6062; 2.1416; 2.677; 3.2124; 3.7478; 4.2832; 4.8185; 5.3538; 5.8893; 6.6925; 7.7245; 8.5664; 10.2797; 11.968; 12.145; 13.3794; 14.5696; 15.4064; 16.084; 16.3777; 16.648; 16.8988 and 17.13 M. Curves 1' – 16' correspond to the constant RL concentration equal to 0.0002; 0.0005; 0.00125; 0003; 0.00625; 0.01; 0.02; 0.05; 0.1; 0.5; 1; 5; 10; 20; 30 and 40 mg/dm^3.
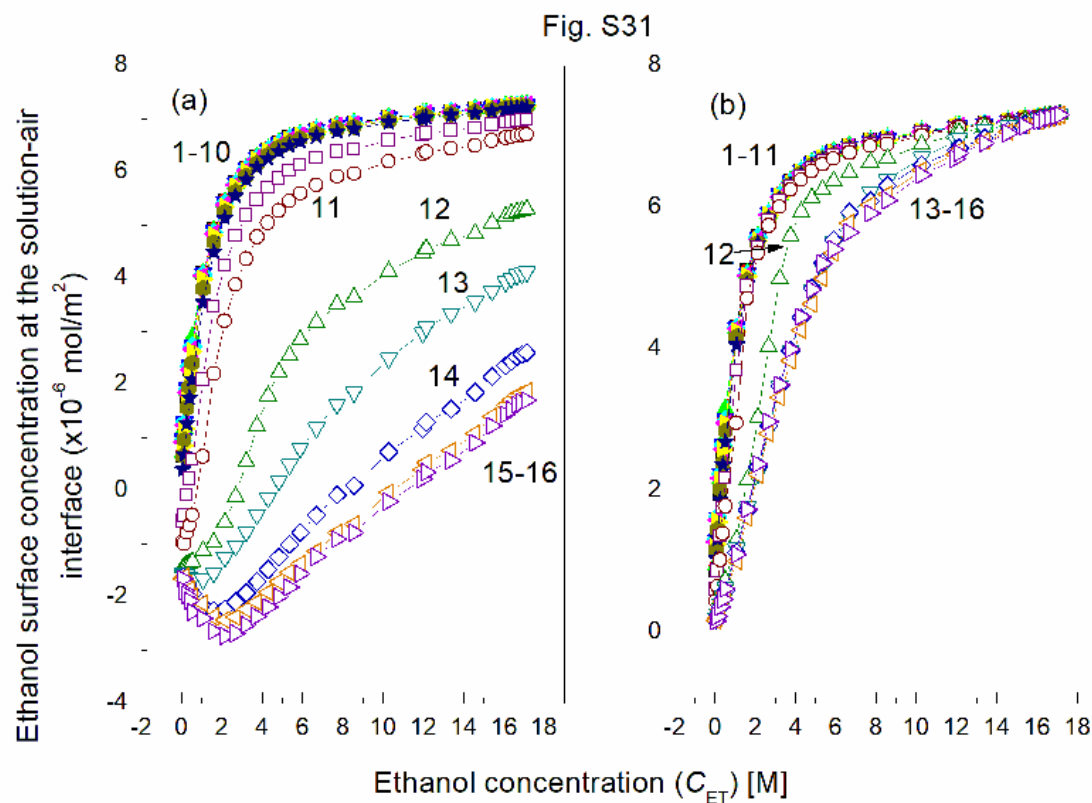
Fig. S31. A plot of ET surface concentration at the solution-air interface calculated from the Frumkin equation on the basis of the measured surface tension of the studied solution (a) and calculated from ethanol contribution to the mixed monolayer pressure (b) vs. the ET concentration (C_{ET}). Curves 1 – 16 correspond to the constant RL concentration equal to 0.0002; 0.0005; 0.00125; 0003; 0.00625; 0.01; 0.02; 0.05; 0.1; 0.5; 1; 5; 10; 20; 30 and 40 mg/dm³.
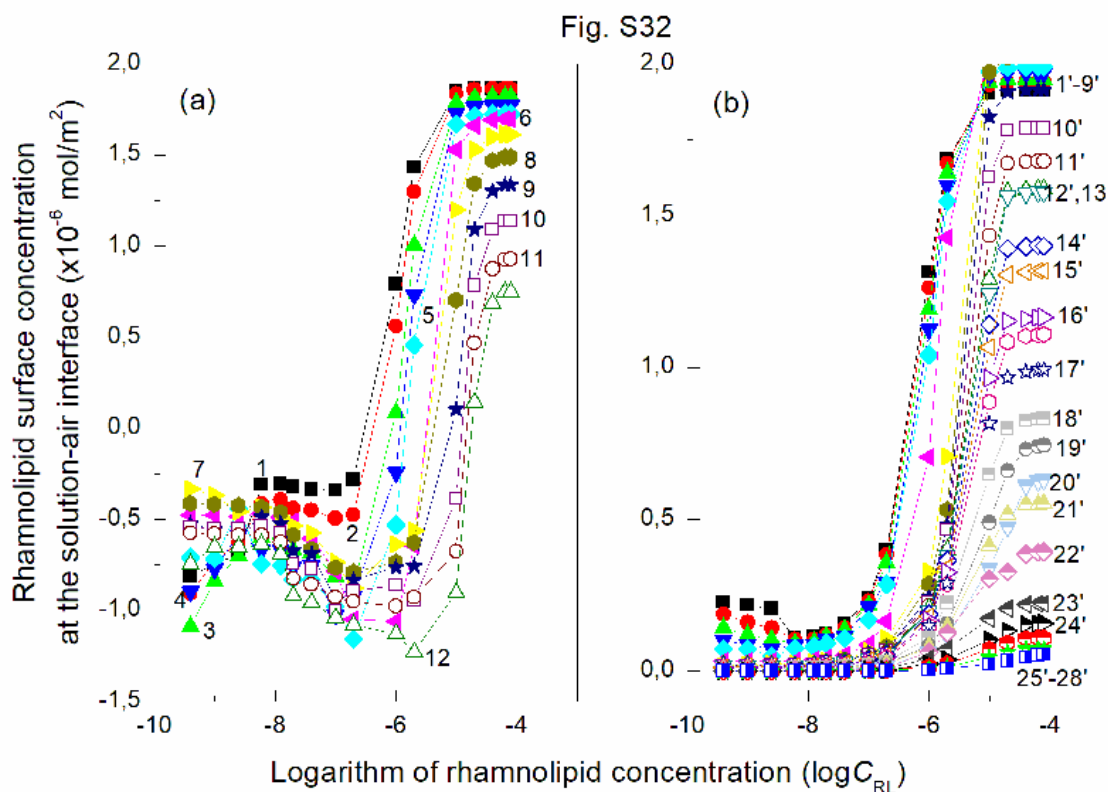
Fig. S32. A plot of RL surface concentration at the solution-air interface calculated from the Frumkin equation on the basis of the measured surface tension of the studied solution (a) and calculated from the RL contribution to the mixed monolayer pressure (b) vs. the logarithm of RL concentration ($\log C_{RL}$). Curves 1 – 12 correspond to the constant ET concentration equal to 0.06692; 0.1338; 0.2677; 0.4015; 0.535; 1.0706; 1.6062; 2.1416; 2.677; 3.2124; 3.7478 and 4.2832 M. Curves 1' – 28' correspond to the constant ET concentration equal to 0.06692; 0.1338; 0.2677; 0.4015; 0.535; 1.0706; 1.6062; 2.1416; 2.677; 3.2124; 3.7478, 4.2832; 4.8185; 5.3538; 5.8893; 6.6925; 7.7245; 8.5664; 10.2797; 11.968; 12.145; 13.3794; 14.5696; 15.4064; 16.084; 16.3777; 16.648 and 16.8988 M.
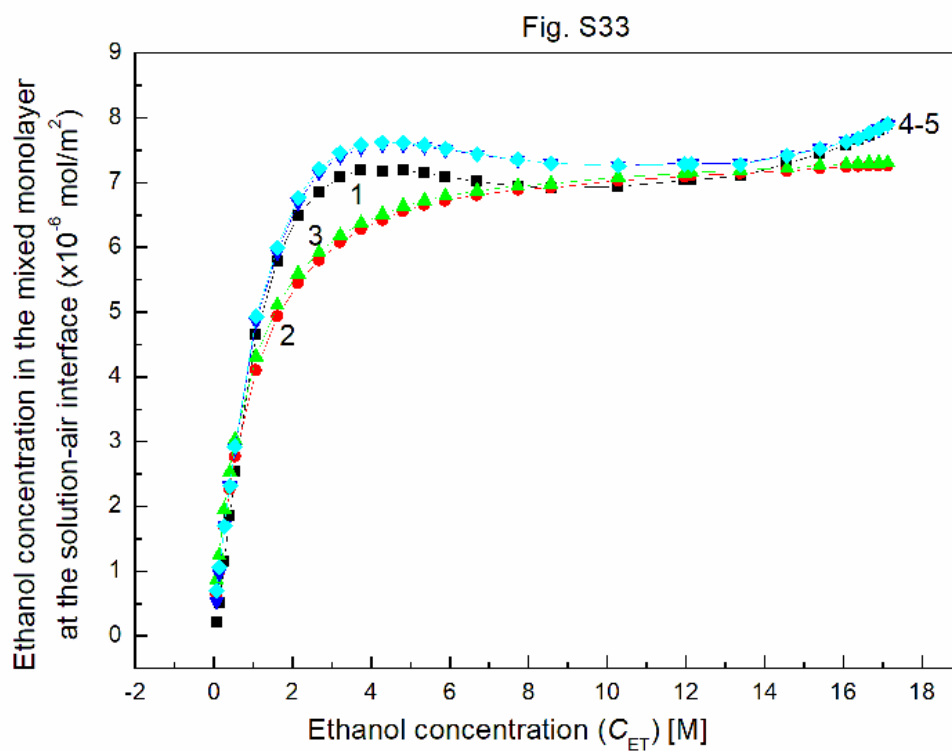
Fig. S33. A plot of ET concentration in the mixed monolayer at the solution-air interface vs. the ET concentration (C_{ET}) at the constant RL concentration equal to 0.0002 mg/dm³. Curves 1 -5 correspond to the values from Figs. S30b, S31, S29, respectively.
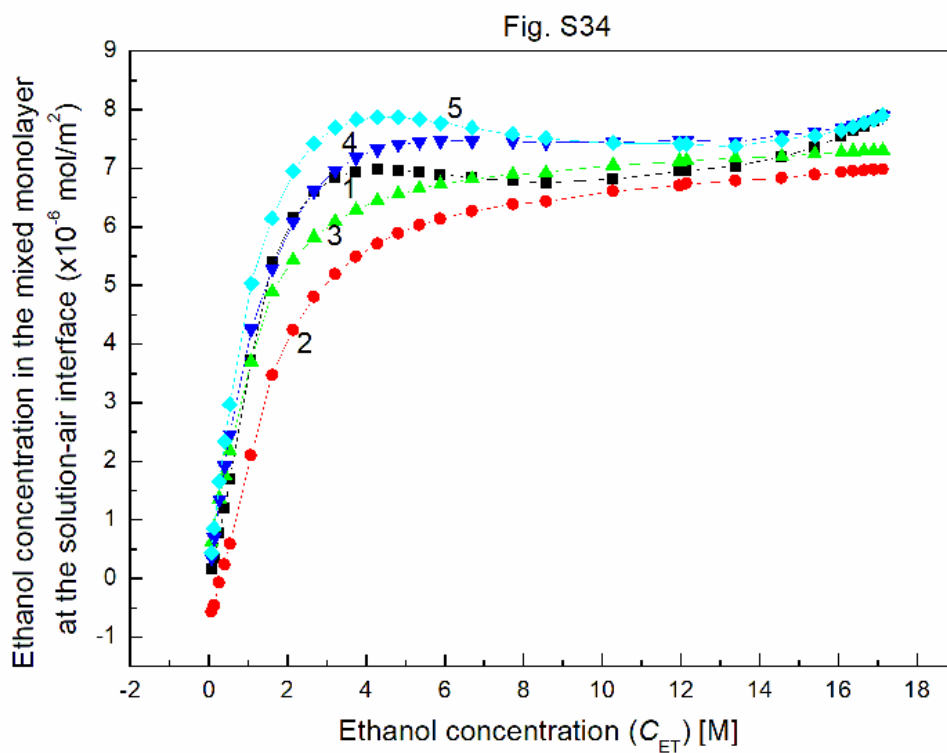
Fig. S34. A plot of ET concentration in the mixed monolayer at the solution-air interface vs. the ET concentration (C_{ET}) at the constant RL concentration equal to 0.5 mg/dm³. Curves 1 -5 correspond to the values from Figs. S30b, S31, S29, respectively.
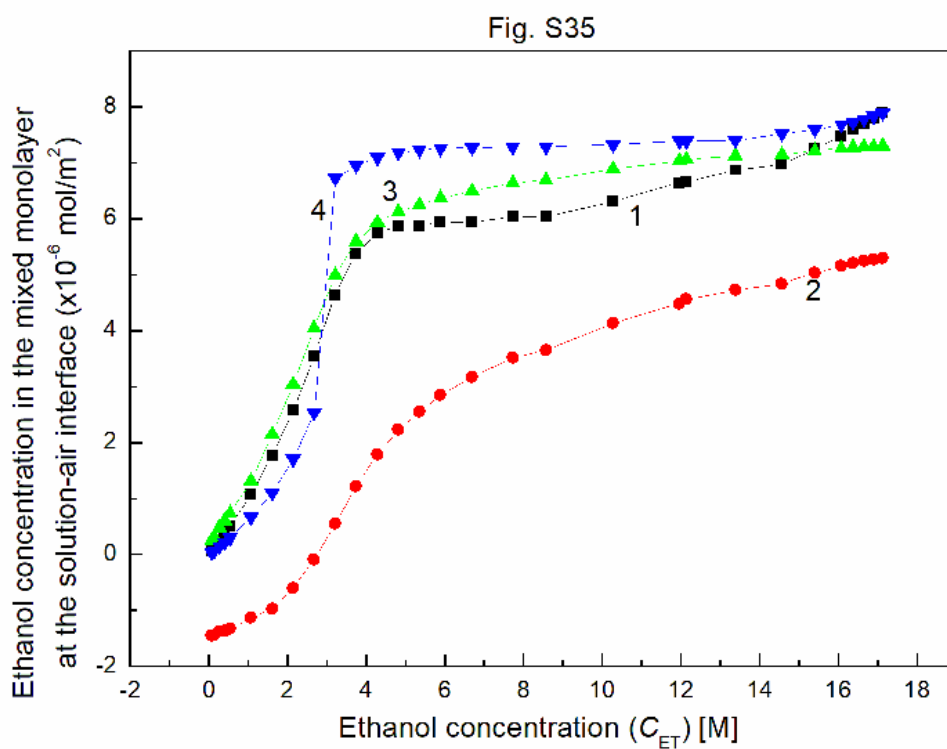
Fig. S35. A plot of ET concentration in the mixed monolayer at the solution-air interface vs. the ET concentration (C_{ET}) at the constant RL concentration equal to 5 mg/dm^3. Curves 1 -5 correspond to the values from Figs. S30b, S31, S29, respectively.
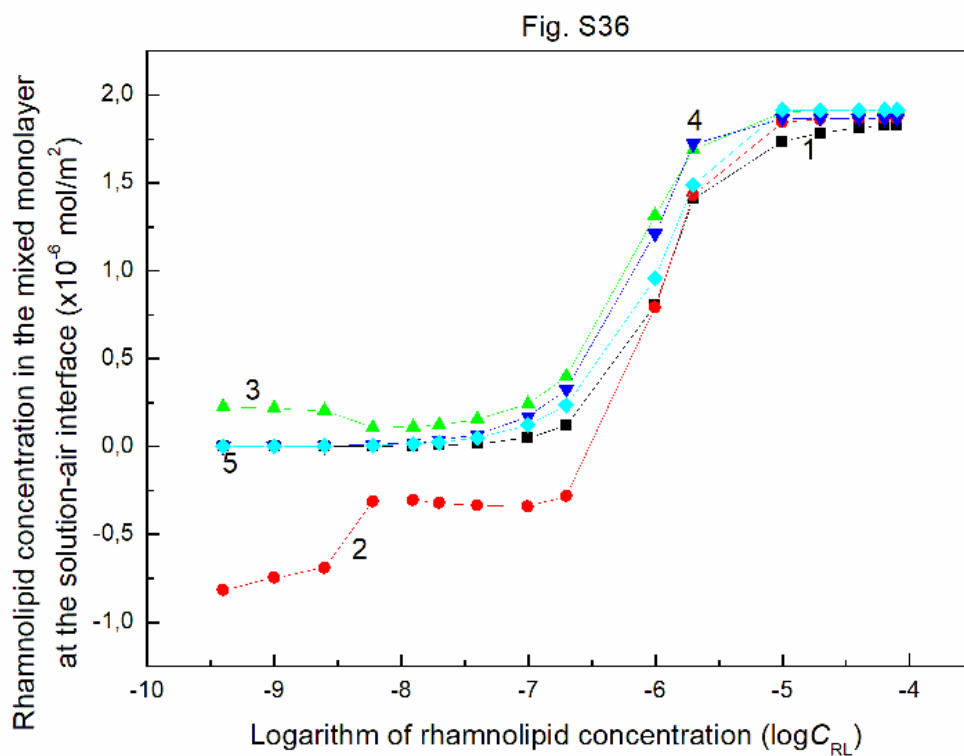
Fig. S36. A plot of RL concentration in the mixed monolayer at the solution-air interface vs. the logarithm of RL concentration ($\log C_{RL}$) at the constant ET concentration equal to 0,06692 M. Curves 1 -5 correspond to the values from Figs. S30a, S32, S27, respectively.
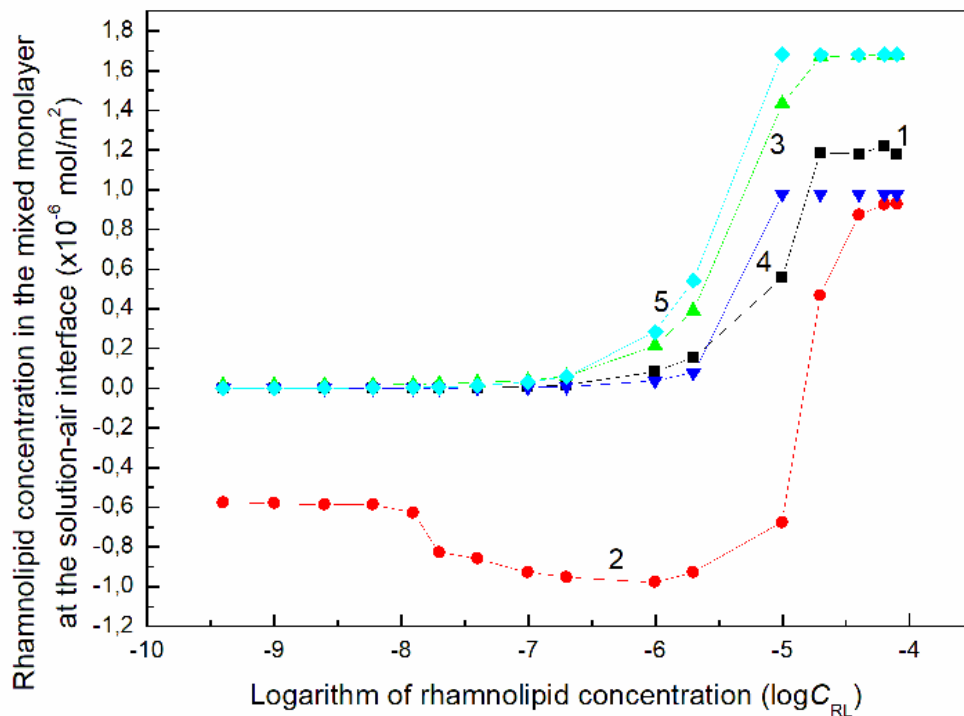
Fig. S37. A plot of RL concentration in the mixed monolayer at the solution-air interface vs. the logarithm of RL concentration ($\log C_{RL}$) at the constant ET concentration equal to 3.7478 M. Curves 1 -5 correspond to the values from Figs. S30a, S32, S27, respectively.
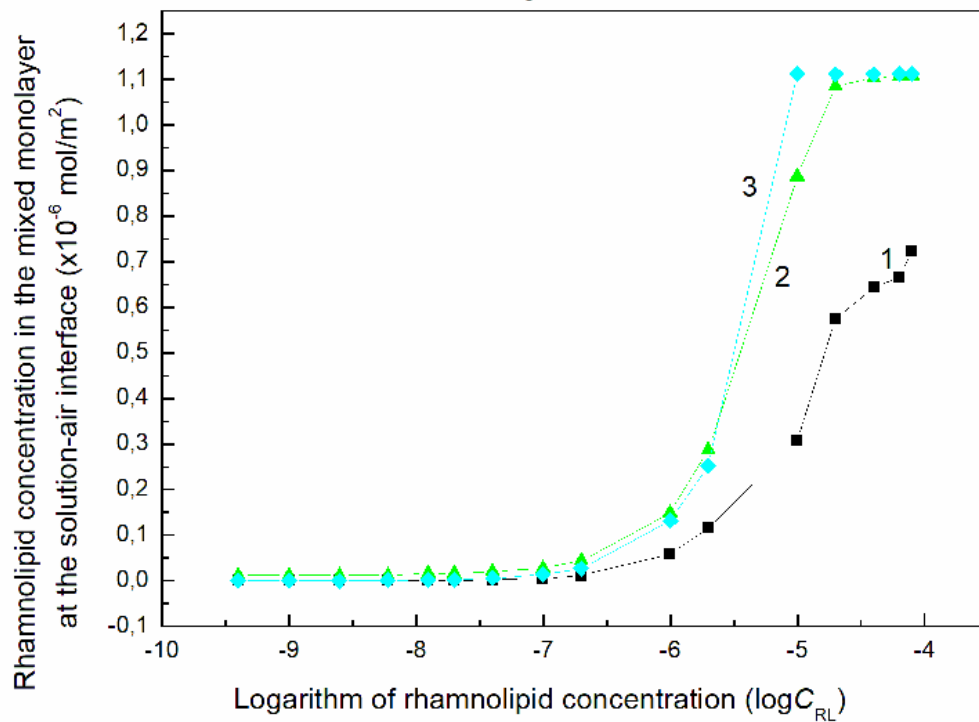
Fig. S38. A plot of RL concentration in the mixed monolayer at the solution-air interface vs. the logarithm of RL concentration ($\log C_{RL}$) at the constant ET concentration equal to 7.7245 M. Curves 1 -5 correspond to the values from Figs. S30a, S32, S27, respectively.
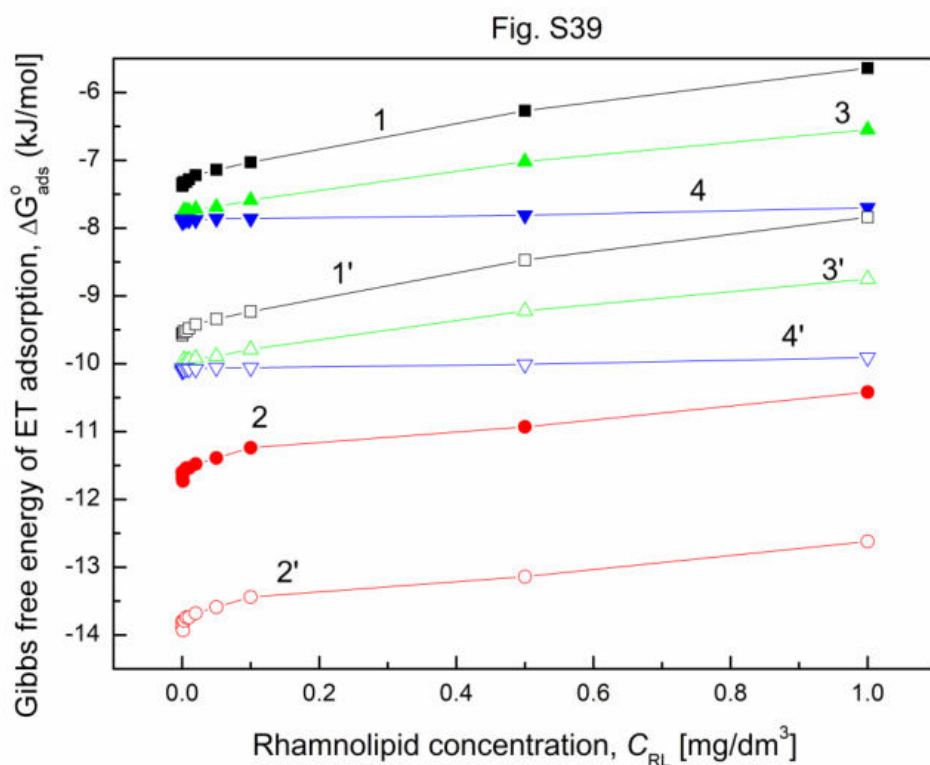
Fig. S39. A plot of ET Gibbs free energy of adsorption (ΔG_{ads}^{0}) at the solution-air interface vs. the RL concentration (C_{RL}) calculated from Eq. (4) (curves 1 – 4) and from Eq. (5) (curves 1' – 5'). Curves 1 and 1'; curves 2 and 2', curves 3 and 3', curves 4 and 4' correspond to the ΔG_{ads}^{0} values calculated based on ethanol CAC (Table 2), surface tension of solution and ethanol Γ at CAC according to point A, B, C and D in Table 3, respectively.
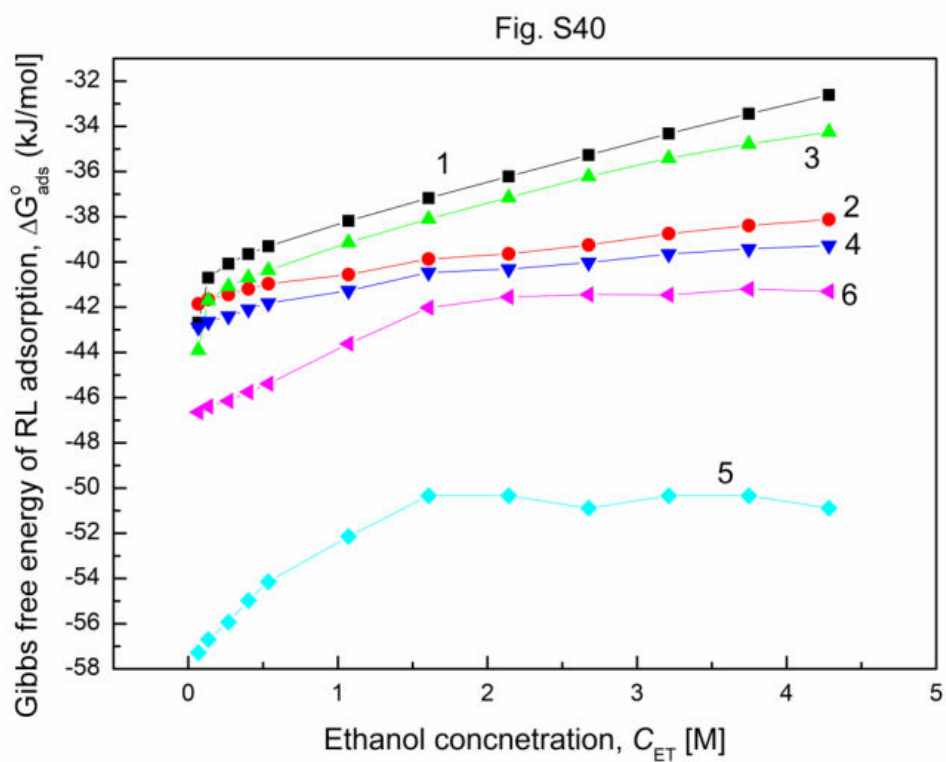
Fig. S40. A plot of RL Gibbs free energy of adsorption (ΔG_{ads}^{0}) at the solution-air interface vs. the ET concentration (C_{ET}) calculated from the de Boer-Langmuir and linear Langmuir equations on the basis of different surface concentration isotherms. Description of the curves 1 – 6 correspond to points 1, B, C, D, E and F in Table 4.

Prof. dr hab. Anna Zdziennicka
Katedra Zjawisk Międzyfazowych
Instytut Nauk Chemicznych
Wydział Chemii UMCS
Pl. M. Curie-Skłodowskiej 3
20-031 Lublin

Lublin, 17.01.2023

OŚWIADCZENIE

Oświadczam, że w pracy

E. Rekiel, **A. Zdziennicka***, B. Jańczuk, *Adsorption properties of rhamnolipid and ethanol at water/ethanol solution-air interface.* Journal of Molecular Liquids, 2020, 308, 113080;

mój udział wynosił **30%** i polegał na analizie formalnej otrzymanych wyników, pisaniu oryginalnej wersji manuskryptu, redagowaniu i edytowaniu manuskryptu, współredagowaniu odpowiedzi na recenzje pracy oraz na prowadzeniu korespondencji z czasopismem.

Prof. dr hab. Bronisław Jańczuk
Katedra Zjawisk Międzyfazowych
Instytut Nauk Chemicznych
Wydział Chemii UMCS
Pl. M. Curie-Skłodowskiej 3
20-031 Lublin

Lublin, 17.01.2023

OŚWIADCZENIE

Oświadczam, że w pracy

E. Rekiel, A. Zdziennicka*, **B. Jańczuk**, *Adsorption properties of rhamnolipid and ethanol at water/ethanol solution-air interface*. Journal of Molecular Liquids, 2020, 308, 113080;

mój udział wynosił **15%** i polegał na analizie formalnej otrzymanych wyników, pisaniu oryginalnej wersji manuskryptu oraz współredagowaniu odpowiedzi na recenzje pracy.

Załącznik 4

[D4] E. Rekiel, A. Zdziennicka*, B. Jańczuk, *Adsorption of surfactin at water with ethanol mixture-air interface*. ***Journal of Molecular Liquids***, 2020, 300, 112240.

Adsorption of surfactin at water with ethanol mixture-air interface

Edyta Rekiel, Anna Zdziennicka *, Bronisław Jańczuk

Department of Interfacial Phenomena, Institute of Chemical Sciences, Faculty of Chemistry, Maria Curie-Skłodowska University in Lublin, Maria Curie-Skłodowska Sq. 3, 20-031 Lublin, Poland

ABSTRACT

The addition of alcohol to surfactant changes, among others, its adsorption properties, therefore the surface tension of water/ethanol solution of surfactin was measured at 293 K using the ring detachment method. The measurements were made in the range of surfactin concentration from 0 to 40 mg/dm^3 and in the whole range of ethanol concentration so their molecules were present in solution in the monomeric and aggregated forms. The values of solution surface tension were also predicted using the Miller et al., Connors and independent adsorption methods. Based on these measurement results, the surfactin Gibbs surface excess concentration at the solution-air interface was determined. The ethanol Gibbs surface excess concentration was established using the Gibbs and Guggenheim-Adam concepts as well as that of the total concentration one. Taking into account the Gibbs surface excess concentration of surfactin and total ethanol concentration, the fraction of the area occupied by surfactin and ethanol at the solution-air interface was deduced. Additionally, composition of mixed monolayer at the solution-air interface was calculated and compared to the theoretical composition resulting from the independent adsorption of surfactin and ethanol. Based on the Gibbs surface excess concentration of ethanol and surfactin, the Gibbs standard free energy of adsorption was calculated using different methods. The obtained results and their consideration indicate that there is a mutual influence of surfactin and ethanol on their adsorption at the solution-air interface which depends on the concentration of both surfactin and alcohol.

© 2019 Elsevier B.V. All rights reserved.

1. Introduction

Biosurfactants are produced by microorganisms mainly on their cell surfaces or they are excreted extracellularly [1,2]. Their molecules consist of two parts having different affinity for the solvents. One part has affinity for water and other polar liquids and the other for apolar ones. Owing to this structure of their molecules biosurfactants form micelles at the concentration called the critical micelle concentration and adsorb at different interfaces [3,4]. Except for these two characteristics they have other unusual properties, for example high biodegradability, effectiveness at extreme temperature, bactericidal and virucidal [5–7]. Such useful biosurfactants properties make them facilitate solubilisation, emulsification, detergency and dispersion therefore they are used in cosmetics, pharmaceuticals, detergents, foods, plant protection products as well as are used in solid bioremediation [8–14]. Of the biosurfactants, the surfactin plays a very important role. Surfactin produced by *Bacillus subtilis* and belonging to the cyclic lipopeptides was discovered by Arima et al. [15]. In its molecules there is present heptapeptide with the chiral sequence LLDLLDL that is combined with β-hydroxyfatty acid having a chain length of 12 to 16 carbon atoms [11,16]. It is interesting that in the aqueous solution and at the

solution-air interface surfactin has a β-sheet structure with characteristic horse-saddle conformation [17]. Probably because of this conformation surfactin exhibits biological activity [18]. Despite biological activity surfactin is also surface active. It reduces the water surface tension to about 30 mN/m [17,19], similarly to synthetic non-ionic Tritons [20]. However it has very low CMC [17,19,21]. This causes that surfactin can have wide application in industry, environmental protection and everyday life [22–25]. In many processes and products surfactin can be used in various solvents. Unfortunately, it is difficult to find in the literature its aggregation and adsorption properties in solvents different from water. Ethanol is an exceptionally often used solvent. Depending on the concentration this alcohol can act as a co-solvent or a co-surfactant [26,27]. It is known that ethanol influences on the behaviour of classical surfactants in the aqueous solution and in the surface layer at the water-air interface but this influence is not fully explained [27–37]. At the concentration called the critical aggregation concentration short chain alcohols form aggregates [26,27]. Thus modification of surfactants behaviour in the bulk phase and their adsorption at the water-air interface by alcohols depends on the form in which alcohols are present in solution.

As it is difficult to find in the literature investigations on biosurfactants properties in the alcohol presence, it seems interesting to determine changes of adsorption properties of surfactin in the mixed water-ethanol solvent in the whole range of ethanol

---

concentration. For this purpose the measurements of surface tension of water/ethanol solution of surfactin were made at 293 K at the constant surfactin or ethanol concentration. On the basis of the obtained results, the Gibbs surface excess concentration, the fraction of the area occupied by surfactin and ethanol molecules at the solution-air interface, composition of the mixed monolayer as well as the standard Gibbs free energy of surfactin and ethanol adsorption were taken into account. Additionally, the measured values of solution surface tension were compared to those predicted theoretically based on the independent adsorption as well as Miller et al. [38,39] and Connors equations [40,41].

2. Experimental

2.1. Materials

Ethanol (96% purity) was bought from POCH and it was purified by the method described earlier [27]. Surfactin (≥98.0%) was bought from Sigma-Aldrich and used without further purification. The solutions were prepared with the addition of deionized water of internal specific resistance of 18.2 x $10^6 \Omega$ m (doubly distilled, Destemat Bi18E). Surface tension measurements were used to control water purity. The series of aqueous solutions of surfactin and ethanol with the addition of water were prepared in the concentration range of ethanol from 0 to 17.13 M and that of surfactin from 2×10^{-4} to 40 mg/dm^3.

2.2. Methods

The surface tension of the mixture of biosurfactant with water and ethyl alcohol was measured with the Krüss K9 tensiometer using the du Nouy's method (platinum ring detachment method). Before the measurements of solution surface tension the tensiometer was tested using water and methanol whose surface tension at 293 K was equal to 72.8 and 22.5 mN/m, respectively. For each measurement the ring was cleaned in distilled water and heated in the Bunsen burner flame to red colour. More than 10 successive measurements were performed. The jacketed vessel with thermostatic water bath was used to control the temperature with ±0.01 K. Depending on the range of surfactin and ethanol concentration, the uncertainty of measurements was equal from 0.3 to 0.7%.

3. Results and discussion

3.1. Solution surface tension

Surface tension of water/ethanol solution of surfactin (SF) depends on both surfactin and ethanol (ET) concentration (Figs. 1 and 2). The isotherms of the surface tension obtained at the constant SF concentration can be divided into two parts (Fig. 1). The first part corresponds to the ethanol concentration from 0 to its critical aggregation concentration (CAC) which is equal to 7.04 M [27] and the other from CAC to "pure" ethanol. It is unexpected that the surface tension values of studied solution at each constant surfactin concentration in the range of alcohol concentration from CAC to 17.13 M are close to those for the individual aqueous ethanol solution [27]. This fact suggests that surfactin does not adsorb at the solution-air interface in this range of alcohol concentration. On the other hand, it should be stressed that the value of surface tension of surfactin tail is only 1.5 mN/m higher than that of the surface tension of ethanol (23.2 mN/m) at 293 K (Table 1).

The changes of the surface tension of water/ethanol solution of surfactin as a function of biosurfactant or ethanol concentration can be explained based on the components and parameters of the surface tension of water and ethanol as well as that of surfactin head and tail (Table 1). According to van Oss et al. [46] the surface tension of the liquid or solid results from the Lifshitz-van der Waals and hydrogen bond intermolecular interactions. Indeed this approach does not include the electrostatic interaction which can also influence the surface tension

of liquid. However, in the case of our systems these interactions can be neglected.

Van Oss and Constanzo [47] stated that in the case of the surfactants the surface tension depends on the orientation of their molecules toward the gas phase. Thus the surface tension of tail and head can be used. The values of the Lifshitz-van der Waals component of the water and ethanol surface tension are close to each other and insignificantly lower than that of surfactin tail while the Lifshitz-van der Waals component of surfactin head is considerably higher than that of water and ethanol. The molecules of the ET and SF should be oriented by the hydrophobic tail toward the air in the adsorption monolayer at the solution-air interface. As the Lifshitz-van der Waals components of water, ethanol and surfactin tail are at the first approximation similar, the increase of ET and SF concentration in the solution causes the decrease of acid-base component of the water surface tension resulting from the intermolecular interactions of hydrogen bond. For this reason,

Fig. 1. A plot of the surface tension of water/ethanol solution of surfactin (γ_{LV}) vs. the logarithm of ethanol concentration (C_A). Curves 1–16 correspond to the constant surfactin concentrations equal to 0.0002; 0.0005; 0.00125; 0003; 0.00625; 0.01; 0.02; 0.05; 0.1; 0.5; 1; 5; 10; 20; 30 and 40 mg/dm^3.
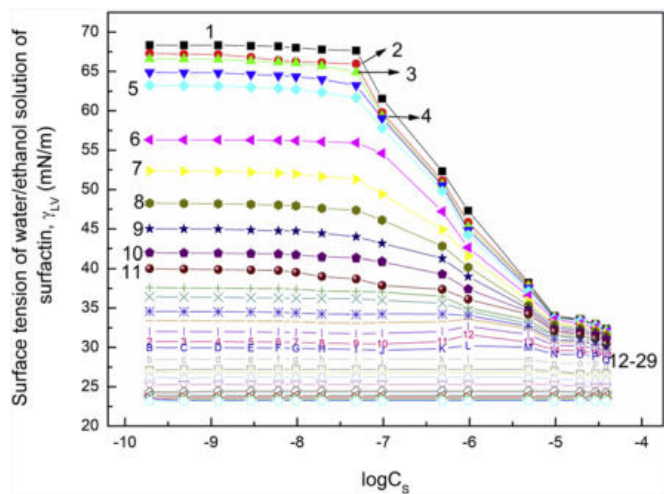
Fig. 2. A plot of the surface tension of water/ethanol solution of surfactin (γ_{LV}) vs. the logarithm of surfactin concentration (C_S). Curves 1–29 correspond to the constant ethanol concentrations equal to 0.06692; 0.1338; 0.2677; 0.4015; 0.535; 1.0706; 1.6062; 2.1416; 2.677; 3.2124; 3.7478; 4.2832; 4.8185; 5.3538; 5.8893; 6.6925; 7.7245; 8.5664; 10.2797; 11.968; 12.145; 13.3794; 14.5696; 15.4064; 16.084; 16.3777; 16.648; 16.8988 and 17.13 M.

Table 1
The Lifshitz-van der Waals (γ^{LW}) and acid-base (γ^{AB}) components as well as the electron-acceptor (γ^+) and the electron-donor (γ^-) parameters of water, ethanol and surfactin head and tail surface tension (γ).

Substance	Components and parameters [mN/m]				γ [mN/m]	Ref.
	γ^{LW}	γ^{AB}	γ^+	γ^-		
SF (head)	34.25	8.55	0.37	49.39	42.80	[42]
SF (tail)	24.70	0.00	0.00	0.00	24.70	[19]
Water	26.85	45.95	22.975	22.975	72.80	[43]
Ethanol	21.40	1.80	0.09	9.00	23.20	[44,45]

the solution surface tension decreases at both the constant surfactin and ethanol concentration. Indeed at the constant SF concentration, the surface tension decreases from the surface tension of aqueous solution of surfactin at each constant concentration to the ethanol surface tension. In the case of the solution at the constant ET concentration (Fig. 2) the surface tension changes from the surface tension of aqueous solution of alcohol at the given concentration [27] to the value which is in the range of surface tension of aqueous solution of surfactin at the concentration equal to 40 mg/dm³ [19] to the surface tension of ethanol depending on the ethanol concentration. As a matter of fact the changes of surface tension of water/ethanol solution of surfactin at the constant ET and SF concentrations depend on surfactin and ethanol adsorption at the solution-air interface. The mutual influence of alcohol and surfactin on their adsorption at the solution-air interface can be shown by the determination of the surface tension based on independent adsorption and Miller et al. [38,39] as well as Connors [40,41] equations (Eqs. (S1)–(S3)).

As follows from these calculations independent adsorption (Eq. (S3)) takes place if the ET and SF concentrations are in the range in which their unsaturated monolayer at the water-air interface is formed (Figs. S1–S45). On the other hand, the results obtained from the calculations of surface tension using the Miller et al. approach [38,39] (Eq. (S1)) indicate whether solution behaves as ideal or not ideal. In this case calculations of the surface tension of the solution were made for two different values of the area occupied by the surfactin molecules at the solution-air interface. The value of the area occupied by surfactin equal to 7.24×10^5 m²/mol corresponds to its maximal Gibbs surface concentration equal to 1.38×10^{-6} mol/m² while that equal to 5.61×10^5 m²/mol corresponds to 1.782×10^{-6} mol/m² [19].

To show the applicability of the Miller et al. [38,39] (Eq. (S1)) and Connors [40,41] (Eq. (S2)) equations as well as independent adsorption (Eq. (S3)) for prediction of the solution surface tension in the whole range of ET and SF concentrations the absolute values of deviation from the measured ones were calculated (Tables S1a and S1b). In fact, the absolute deviation values measured and calculated from the Connors equation [40,41] (Eq. (S2)) values of the solution surface tension practically do not depend on the constant SF concentration contrary to the case of the constant ET concentration. In the case of solution at the constant SF concentration the consistence between the calculated and measured values of surface tension increases with the increasing constant ET concentration. This confirms the above mentioned conclusion that the surface tension of water/ethanol solution of surfactin above the ethanol CAC [27] depends only on the ethanol adsorption at the solution-air interface individually or together with the SF head. This conclusion is also confirmed by the deviation of absolute values of measured ones and those obtained from the independent adsorption (Eq. (S3)) as well as the Miller et al. equation [38,39] (Eq. (S1)). In this case the absolute deviation increases with the increase of both ET and SF concentrations. It should be also mentioned that the better prediction is obtained from the Miller et al. equation [38,39] (Eq. (S1)) if the value of surface occupied by SF molecule equal to 5.61×10^5 m²/mol [19] was used in it.

3.2. Adsorption of ethanol and surfactin at the solution-air interface

Adsorption of SF and ET at the solution-air interface causes the changes of solution surface tension. Adsorption at the solution-air interface is usually determined from the Gibbs adsorption isotherm which can be used in a different mathematical form [48]. Therefore the ethanol Gibbs surface excess concentration was calculated from the Gibbs equation [3] applying mole concentration, mole fraction and ethanol activity assuming that it does not depend on the SF concentration (Figs. S46–S59). Indeed using different alcohol concentration units in the Gibbs isotherm equation, different values of maximal ethanol Gibbs surface excess concentration at the solution-air interface were obtained. They decrease in the function of SF concentration in the solution (Fig. S60). However, the isotherms of maximal ethanol Gibbs surface excess concentration are different depending on the concentration units applied for their determination. As it was stated earlier, the most probable values of ethanol Gibbs surface excess concentration were obtained if in the Gibbs isotherm equation ethanol activity was used [27]. Therefore only these values were taken into account in the case of alcohol adsorption (Figs. S46–S59). Since the SF concentration is considerably lower than that of ET, only the mole concentration of surfactin was used for its Gibbs surface excess concentration determination assuming that the SF activity coefficient is close to 1 according to the asymmetrical definition of its chemical potential. In the case of surfactin the Gibbs surface excess concentration is practically equal to its total concentration in the surface layer at the solution-air interface (Fig. S61). However, in the case of ethanol its Gibbs surface excess concentration is not equal to the ethanol total concentration and the values of Gibbs surface excess concentration at high alcohol concentration are not real. In the case of ethanol to obtain the real surface excess concentration the Guggenheim-Adam equation should be applied [27,48]. However, to take into account the changes of solution surface tension under the influence of the SF and ET adsorption, the total concentration of SF and ET should be known. Thus the total concentration of ethanol at the surface monolayer at the solution-air interface (Γ_γ) was calculated from the following equation [35]:

$$\Gamma_\gamma = \Gamma^V + C_2 h \tag{1}$$

where Γ^V is the surface excess concentration of Guggenheim-Adam calculated from the Gibbs surface excess concentration of ethanol assuming that the Gibbs surface was chosen in such a way that the number of alcohol mole in the real system was comparable to that in the reference system having the same volume, C_2 is the ethanol concentration and h is the thickness of adsorption layer and is equal to 4.61 Å.

Knowing the total concentration of ET and SF in the monolayer at the solution-air interface (Figs. S46–S59 and S61) it was possible to determine the area fraction occupied by SF and ET molecules as well as the composition of this monolayer [49] (Figs. S62–S64). The fraction of the area occupied by ethanol and surfactin molecules as well as the composition of the formed monolayer depend on the mutual interaction between the ethanol and surfactin molecules. To show the mutual influence of the SF and ET on their adsorption at the solution-air interface, the specific concentration of ethanol and surfactin should be taken into account. In the case of alcohol its concentration corresponding to the maximal Gibbs surface excess concentration at the solution-air interface ($C_{A-0} = 3.74$ M) and the concentration equal to its CAC for the aqueous solution of single ethanol ($C_{CAC} = 7.04$ M) [27] should be considered. However, for surfactin the first concentration in its individual aqueous solution corresponding to its saturated monolayer at the solution-air interface ($C_{SF-0} = 0.1$ M) and surfactin CMC = 9.66×10^{-6} M should be useful for the consideration of the surfactin adsorption at the solution-air interface [19].

The tendency to adsorb SF and ET at the solution-air interface depends on the mutual interactions of the water, SF and ET molecules in the bulk phase which influences on Gibbs free energy of the solution.

It is known that the ET and SF molecules in water are hydrated. The hydration process of SF tail and head is different. The water molecules around tail are in a different way oriented than around the head. In the case of the SF head the water molecules are attached by hydrogen bonds. It is possible that even 9 water molecules can be directly joined with the SF head. This suggestion is based on the fact that the limiting area occupied by the SF molecule oriented perpendicular to the interface is equal to 93.17 Å^2 [19] and to water 10 Å^2 [50]. The SF tail is surrounded by water molecules due to the Lifshitz-van der Waals intermolecular interactions between the water molecules and tail. The presence of the ethanol molecules can change hydration of both SF tail and head. The replacement of the water molecules joined with the SF head by the ET molecules causes the increase of head hydrophobic properties. However, the replacement of the water molecules hydrating the SF tail by ethanol ones causes the increase of its hydrophilic properties. In the range of ET concentrations from 0 to C_{A-0} and SF from 0 to C_{S-0} the sum of total ethanol concentration and SF in the monolayer is higher than that resulting from the independent adsorption of ET and SF at the solution-air interface (Figs. S65). It is possible that at low concentrations of ET and SF the replacement of the water molecules joined with the SF head by ethanol ones is more favorable than those surrounding the SF tail. This causes that the hydrophobicity of SF molecules may increase. For this reason the adsorption of SF increases insignificantly at the solution-air interface what is confirmed by the ratio of surfactin Gibbs surface excess concentration at the solution-air interface to its concentration in the absence of ethanol (Fig. S66). As the ethanol molecules can adsorb independently and together with the SF ones, the total adsorption of ethanol at the solution-air interface is somewhat higher than the independent one (Figs. S67).

The increase of the ethanol concentration in the solution can cause the total replacement of the water molecules hydrating the surfactin tail and head. As results from this dehydration, the tail becomes hydrophilic but the head hydrophobic. In such case the adsorption of SF is inhibited and/or its small adsorption takes place but the SF molecules in the monolayer at the solution-air interface are oriented by head toward the air phase and therefore the solution surface tension at the alcohol concentration higher than its CAC is close to that of the aqueous solution of individual alcohol. To confirm the above conclusion the surface layer composition was determined and compared to that of the theoretical one resulting from independent adsorption of SF and ET at the solution-air interface (Figs. S68–S81). It appears that at each concentration of SF and low ET concentration in the solution, the mole fraction of SF in the real adsorbed monolayer at the solution-air interface is higher than in the theoretical one resulting from the independent adsorption of SF and ET. With increasing of SF concentration an increase of the range of ET concentrations in which the mole fraction of SF in the real monolayer is higher than that in the theoretical one is observed. As mentioned above, at the SF concentration corresponding to its unsaturated monolayer in the absence of the alcohol, the increase of SF mole fraction in the monolayer is associated with the increase of its adsorption at the solution-air interface compared to SF adsorption from its aqueous solution (Fig. S66). At the SF concentration corresponding to its saturated monolayer at the solution-air interface in the absence of ET [19], the mole fraction of SF is associated with a decrease of SF adsorption. However, this decrease is smaller than it results from the independent adsorption of SF and ET. In the case of ethanol adsorption a reversed conclusion can be drawn (Figs. S68–S81). It means that the range of low SF and ET concentrations in the solution the adsorption of ethanol increases but to a smaller extent than surfactin. At the ethanol concentration higher than that corresponding to the Gibbs maximal surface excess concentration but lower than its CAC [27] the greater decrease of ethanol adsorption than that of SF takes place. As a matter of fact at the concentration of alcohol higher than CAC the adsorption of SF at the solution-air interface was not observed. To sum up it can be stated that there is mutual influence of ethanol and SF on their adsorption at the solution-air interface, but the influence of ethanol is greater than that of SF. At low alcohol and SF concentrations the increase of adsorption of both components takes place.

3.3. Standard Gibbs free energy of surfactin and ethanol adsorption at the solution-air interface

The tendency to adsorb particular components of solution at the solution-air interface can be expressed by the standard Gibbs free energy of adsorption (ΔG_{ads}^0). This energy depends on the changes of the orientation and configuration of the molecules in solution and in the surface region as well as on the formation and breaking chemical bonds during the adsorption process. There are many different methods for determination of the standard Gibbs free energy of adsorption. Among them, the Langmuir equation modified by de Boer is very often used [3,51,52]. It is also possible to determine ΔG_{ads}^0 from the linear form of Langmuir isotherm adsorption equation [3,52]. Both equations were applied for determination of SF ΔG_{ads}^0 (Fig. S82, Table 2).

The values of SF ΔG_{ads}^0 obtained at different constant ethanol concentrations increase as a function of ET concentration. At a low ET concentration, these values are comparable to that obtained for SF in its individual aqueous solution. It is interesting that the values of ΔG_{ads}^0 for SF at the concentration of alcohol higher than its CAC [27] are not positive. This can indicate that SF adsorption at the ET concentration higher than CAC takes place but as mentioned above the orientation of the SF molecules in the surface monolayer is by the head directed toward the air phase. Indeed there are differences between the SF ΔG_{ads}^0 values at the same concentration of alcohol calculated from the linear and modified by de Boer Langmuir equation [3,51,52]. These differences increase with increasing ethanol concentration.

Of course, it results from the fact that at the higher ethanol concentration no independent adsorption of ET and SF occurs. The ΔG_{ads}^0 of ethanol was also determined from the Langmuir equation modified by de Boer (Fig. S83, Table 2). The ΔG_{ads}^0 values of alcohol increase with increasing SF concentration in the solution (Table 2). However, it was possible only in the range of SF concentration from 0.0002 to 20 mg/dm^3. At the SF concentration corresponding to its unsaturated monolayer at the solution-air interface in the absence of alcohol [19], the ΔG_{ads}^0 values of ethanol are close to that of ethanol ΔG_{ads}^0 in the absence of SF [27].

Taking into account the Gibbs-Duhem equation for the surface region as well as the symmetrical and asymmetrical definitions of the chemical potential it is possible to make the following equation [19]:

$$\Delta G_{ads}^0 = RT ln X_{CMC} - \frac{\gamma_0 - \gamma_{LV}^{CMC}}{\Gamma_{max}} \tag{2}$$

where
R is the gas constant, T is the absolute temperature, X_{CMC} is the molar fraction of the surfactant at CMC, γ_0 is the surface tension of the solvent, γ_{LV}^{CMC} is the surface tension of solution at CMC and Γ_{max} is the maximal Gibbs surface excess concentration of surfactant at the solution-air interface.

It is interesting whether this equation can be applied for determination of ethanol Gibbs free energy of adsorption based on its CAC. In such a case, Eq. (2) can be written in two forms:

$$\Delta G_{ads}^0 = RT ln a_{CAC} - \frac{\gamma_0 - \gamma_{LV}^{CAC}}{\Gamma_{max}} \tag{3}$$

where in this case γ_0 is the surface tension of the aqueous solution of surfactin at the given concentration and a_{CAC} is the ethanol activity at which its aggregation process takes place. If it is assumed that in the aggregated ethanol pseudophase, its activity coefficient is close to unity,

Table 2

The values of the Gibbs standard free energy of adsorption (ΔG^0_{ads}) for surfactin calculated from the Langmuir equation modified by de Boer and its linear form as well as for ethanol calculated from the Langmuir equation modified by de Boer and based on Eqs. (3) and (4).

Ethanol concentration [M]	ΔG^0_{ads} for surfactin [kJ/mol]		Surfactin concentration [mg/dm³]	ΔG^0_{ads} for ethanol [kJ/mol]		
	Modified Langmuir equation	Linear Langmuir equation		Modified Langmuir equation	Eq. (4)	Eq. (3)
0	−47.37	−48.60	0	−9.28	−9.97	−7.77
0.06692	−48.47	−50.31	0.0002	−9.58	−10.04	−7.84
0.1338	−48.36	−50.22	0.0005	−9.59	−10.13	−7.93
0.2677	−48.13	−50.10	0.00125	−9.59	−10.11	−7.91
0.4015	−47.90	−49.95	0.003	−9.57	−10.13	−7.93
0.5350	−47.67	−49.82	0.00625	−9.56	−10.08	−7.88
1.0706	−46.75	−49.31	0.01	−9.56	−10.10	−7.90
1.6062	−45.83	−48.63	0.02	−9.55	−9.99	−7.79
2.1416	−44.91	−48.16	0.05	−9.46	−9.75	−7.55
2.6770	−43.99	−47.64	0.1	−8.83	−9.28	−7.08
3.2124	−43.07	−47.13	0.5	−7.42	−7.96	−5.76
3.7478	−42.15	−46.63	1	−6.39	−7.31	−5.11
4.2832	−41.23	−46.10	5	−4.04	−5.90	−3.70
4.8185	−40.31	−45.49	10	−4.60	−5.23	−3.03
5.3538	−39.39	−45.07	20		−5.17	−2.97
5.8893	−38.47	−44.58	30			
6.6925	−37.09	−43.83	40			
7.7245	−35.34	−42.82				
8.5664	−33.93	−41.88				
10.2797	−31.22	−40.42				
11.9680	−28.97	−39.29				

from Eq. (3) there is obtained:

$$\Delta G^0_{ads} = RT\ln X_{CAC} - \frac{\gamma_0 - \gamma^{CAC}_{LV}}{\Gamma_{max}} \tag{4}$$

Taking into account Eqs. (3) and (4) the ΔG^0_{ads} values of ethanol were calculated and are presented in Table 2. As follows from this table it results that the values of ethanol ΔG^0_{ads} calculated from Eq. (4) are at the first approximation close to those calculated from the Langmuir equation modified by de Boer. However, the values calculated from Eq. (3) are higher than those calculated from the modified Langmuir equation at the given constant SF concentration.

4. Conclusions

From the measured values of surface tension of the water/ethanol solution of SF and their consideration it results that there is mutual influence of the ET and SF on the surface tension. The surface tension of solution at the SF concentration corresponding to its unsaturated monolayer in the absence of ethanol and concentration of alcohol from 0 to that corresponding to the maximal Gibbs excess surface concentration can be predicted from the independent adsorption of SF and ET at the solution-air interface. The surface tension can be also predicted using the Miller et al. equation in the same range of ET and SF concentrations.

On the other hand, the surface tension of aqueous solution can be described by the Connors equation choosing the proper values of constants in this equation.

There is mutual influence of SF and ET on their adsorption at the solution-air interface. However, ethanol influences on the SF adsorption to a greater extent that in the reverse way. The adsorption of both SF and ET at their low concentrations is higher than their independent adsorption. Probably it results from the proper dehydration of the head and tail of SF by the alcohol molecules. The adsorption of SF at the solution-air interface was detected only at the ethanol concentration from 0 to its critical aggregation concentration because the solution surface tension at the ethanol concentration higher than CAC is close to its surface tension in the absence of SF. However, it does not exclude the SF adsorption which was confirmed by the values ΔG^0_{ads} of SF. The ΔG^0_{ads} of ethanol can be determined not only by the modified Langmuir equation but also based on its CAC values.

CRediT authorship contribution statement

Edyta Rekiel: Investigation, Resources, Writing - original draft. **Anna Zdziennicka:** Validation, Writing - review & editing. **Bronisław Jańczuk:** Validation, Writing - review & editing.

Declaration of competing interest

The authors have no financial or personal relationships with other people or organizations that could inappropriately influence their work or state.

Appendix A. Supplementary data

Supplementary data to this article can be found online at https://doi.org/10.1016/j.molliq.2019.112240.

References

[1] J.D. Desai, I.M. Banat, Microbial production of surfactants and their commercial potential, Microbiol. Mol. Biol. Rev. 61 (1997) 47–64.

[2] R. Marchant, I.M. Banat, Biosurfactants: a sustainable replacement for chemical surfactants? Biotechnol. Lett. 34 (2012) 1597–1605.

[3] J.M. Rosen, Surfactants and Interfacial Phenomena, 3rd ed. Wiley Interscience, New York, 2004.

[4] R. Marchant, I.M. Banat, Microbial biosurfactants: challenges and opportunities for future exploitation, Trends Biotechnol. 30 (2012) 558–565.

[5] D. Vollenbroich, M. Ozel, J. Vater, R.M. Kamp, G. Pauli, Mechanism of inactivation of enveloped viruses by the biosurfactant surfactin from Bacillus subtilis, Biologicals 25 (1997) 289–297.

[6] A. Abalos, A. Pinazo, M.R. Casals, F. Garcia, A. Manresa, Physicochemical and antimicrobial properties of new rhamnolipids produced by *Pseudomonas aeruginosa* AT10 from soybean oil refinery wastes, Langmuir 17 (2001) 1367–1371.

[7] M. Benincasa, A. Abalos, I. Oliveira, A. Manresa, Chemical structure, surface properties and biological activities of the biosurfactant chemical structures and biological activities of rhamnolipids produced *by Pseudomonas aeruginosa* LBI from soap stock, Antonie van Leeuwenhoek 85 (2004) 1–8.

[8] R. Makkar, S. Cameotra, An update on the use of unconventional substrates for biosurfactant production and their new applications, Appl. Microbiol. Biotechnol. 58 (2002) 428–434.

[9] C.C. Lai, Y.C. Huang, Y.H. Wei, J.S. Chang, Biosurfactant-enhanced removal of total petroleum hydrocarbons from contaminated soil, J. Hazard. Mater. 167 (2009) 609–614.

[10] C.N. Mulligan, Environmental applications for biosurfactants, Environ. Pollut. 133 (2005) 183–198.

[11] G. Seydlová, J. Svobodová, Review of surfactin chemical properties and the potential biomedical applications, Central European Journal of Medicine 3 (2) (2008) 123–133.

[12] L. Rodrigues, I.M. Banat, J. Teixeira, R. Oliveira, Biosurfactants: potential applications in medicine, J. Antimicrob. Chemother. 57 (2006) 609–618.

[13] M. Nitschke, S.G.V.A.O. Costa, Biosurfactants in food industry, Trends Food Sci. Technol. 18 (2007) 252–259.

[14] M. Pacwa-Płociniczak, G.A. Płaza, Z. Piotrowska-Seget, S.S. Cameotra, Environmental applications of biosurfactants: recent advances, Int. J. Mol. Sci. 12 (2011) 633–654.

[15] K. Arima, A. Kakinuma, G. Tamura, Surfactin, a crystalline peptide lipid surfactant produced by *Bacillus subtilis*: isolation, characterization and its inhibition of fibrin clot formation, Biochem. Biophys. Res. Commun. 31 (1968) 488–494.

[16] N.S. Shaligram, R.S. Singhal, Surfactin – a review on biosynthesis, fermentation, purification and applications, Food Technol. Biotechnol. 48 (2) (2010) 119–134.

[17] Y. Ishigami, M. Osman, H. Nakahara, Y. Sano, R. Ishiguro, M. Matsumoto, Significance of β-sheet formation for micellization and surface adsorption of surfactin, Colloids Surf. B: Biointerfaces 4 (1995) 341–348.

[18] J.M. Bonmatin, M. Genest, H. Labbé, M. Ptak, Solution three-dimensional structure of surfactin: a cyclic lipopeptide studied by 1H-NMR, distance geometry, and molecular dynamics, Biopolymers 34 (1994) 975–986.

[19] A. Zdziennicka, B. Jańczuk, Thermodynamic parameters of some biosurfactants and surfactants adsorption at water-air interface, J. Mol. Liq. 243 (2017) 236–244.

[20] A. Zdziennicka, K. Szymczyk, J. Krawczyk, B. Jańczuk, Critical micelle concentration of some surfactants and thermodynamic parameters of their micellization, Fluid Phase Equilib. 322–323 (2012) 126–134.

[21] A. Zdziennicka, J. Krawczyk, B. Jańczuk, Volumetric properties of rhamnolipid and surfactin at different temperatures, J. Mol. Liq. 255 (2018) 562–571.

[22] P. Singh, S.S. Cameotra, Potential applications of microbial surfactants in biomedical sciences, Trends Biotechnol. 22 (2004) 142–146.

[23] G. Seydlova, R. Čabala, J. Svobodová, Sufactin – novel solutions for global issues, in: S. Olsztyńska-Janos (Ed.), Biomedical Engineering, Trends, Research and Technologies, INTECH 2011, pp. 305–330 , chapter 13.

[24] J.-F. Liu, S.M. Mbadinga, S.-Z. Yang, J.-D. Gu, B.-Z. Mu, Chemical structure, property and potential applications of biosurfactants produced by *Bacillus subtilis* in petroleum recovery and spill mitigation, Int. J. Mol. Sci. 16 (2015) 4814–4837.

[25] W.C. Chen, R.-S. Juang, Y.-H. Wei, Applications of a lipopeptide biosurfactant, surfactin, produced by microorganisms, Biochem. Eng. J. 103 (2015) 158–169.

[26] R. Zana, M.J. Eljebari, Fluorescence probing of self-association of alcohols in aqueous solution, J. Phys. Chem. 97 (1993) 11134–11136.

[27] A. Chodzińska, A. Zdzienicka, B. Jańczuk, Volumetric and surface properties of short chain alcohols in aqueous solution-air systems at 293 K, J. Solut. Chem. 41 (12) (2012) 2226–2245.

[28] R. Zana, Aqueous surfactant-alcohol systems: a review, Adv. Colloid Interf. Sci. 57 (1995) 1–64.

[29] R. Zana, S. Yiv, C. Strazielle, P. Lianos, Effect of alcohol on the properties of micellar systems: I. Critical micellization concentration, micelle molecular weight and ionization degree, and solubility of alcohols in micellar solutions, J. Colloid Interface Sci. 80 (1981) 208–222.

[30] D.E. Guveli, J.B. Kayes, S.S. Davis, Hydrodynamic studies of micellar systems of alkyltrimethyl-ammonium bromides and the effect of added 1-alkanols, J. Colloid Interface Sci. 72 (1979) 130–138.

[31] D. Attwood, V. Mosquera, J. Rodriguez, M. Garcia, M.J. Suarez, Effect of alcohols on the micellar properties in aqueous solution of alkyltrimethylammonium bromides, Colloid Polym. Sci. 272 (1994) 584–591.

[32] G.M. Førland, J. Samseth, H. Høiland, K. Mortensen, The effect of medium chain length alcohols on the micellar properties of sodium dodecyl sulfate in sodium chloride solutions, J. Colloid Interface Sci. 164 (1994) 163–167.

[33] M. Tomšič, M. Bešter-Rogač, A. Jamnik, W. Kunz, D. Touraud, Trenary systems of nonionic surfactant Brij 35, water and various simple alcohols: structural investigations by small-angle X-ray scattering and dynamic light scattering, J. Colloid Interface Sci. 294 (2006) 194–211.

[34] A. Zdziennicka, B. Jańczuk, Behaviour of anionic surfactants and short chain alcohols mixtures in monolayer at water-air interface, J. Surfactant Deterg. 14 (2011) 257–267.

[35] A. Zdziennicka, Surface behavior of Triton X-165 and short chain alcohol mixtures, Langmuir 26 (3) (2010) 1860–1869.

[36] M. Bielawska, A. Chodzińska, B. Janczuk, A. Zdziennicka, Determination of CTAB CMC in mixed water + short-chain alcohol solvent by surface tension, conductivity, density and viscosity measurements, Colloids Surf. A Physicochem. Eng. Asp. 424 (2013) 81–88.

[37] A. Zdziennicka, The adsorption tendency of cetylpyridinium bromide at water-air interface and micelles formation in the presence of propanol, Colloids Surf. A Physicochem. Eng. Asp. 325 (2008) 93–100.

[38] V.B. Fainerman, R. Miller, E.V. Aksenenko, Simple model for prediction of surface tension of mixed surfactant solutions, Adv. Colloid Interf. Sci. 96 (2002) 339–359.

[39] V.B. Fainerman, R. Miller, Simple method to estimate surface tension of mixed surfactant solutions, J. Phys. Chem. B 105 (2001) 11432–11438.

[40] K.A. Connors, K.A. Wright, Dependence of surface tension on composition of binary aqueous-organic solutions, Anal. Chem. 61 (1989) 194–198.

[41] D. Khossravi, K.A. Connors, Solvent effects on chemical processes. 3. Surface tension of binary aqueous organic solvent, J. Solut. Chem. 22 (1993) 321–330.

[42] A. Zdziennicka, B. Jańczuk, Wetting and adhesion properties of rhamnolipid and surfactin, Int. J. Adhes. Adhes. 84 (2018) 275–282.

[43] A. Zdziennicka, K. Szymczyk, J. Krawczyk, B. Jańczuk, Some remarks on the solid surface tension determination from contact angle measurements, Appl. Surf. Sci. 405 (2017) 88–101.

[44] A. Zdziennicka, The wettability of polytetrafluoroethylene and polymethylmethacrylate by aqueous solutions of Triton X-100 and short chain alcohol mixtures, Appl. Surf. Sci. 255 (2009) 7369–7379.

[45] A. Zdziennicka, B. Jańczuk, Behaviour of cationic surfactants and short chain alcohols in mixed surface layers at water-air and polymer-water interfaces with regard to polymer wettability. II Wettability of polymers, J. Colloid Interface Sci. 350 (2010) 568–576.

[46] C.J. van Oss, Interfacial Forces in Aqueous Media, Marcel Dekker, New York, 1994.

[47] C.J. van Oss, P.M. Constanzo, Adhesion of anionic surfactants to polymer surfaces and low-energy materials, J. Adhes. Sci. Technol. 6 (1992) 477–487.

[48] J. Ościk, Adsorption, PWN, Warsaw, 1982.

[49] A. Zdziennicka, B. Jańczuk, Properties of n-octyl-β-D-glucopyranoside and sodium dodecylsulfate mixed monolayer at the water-air interface, J. Mol. Liq. 280 (2019) 259–267.

[50] A.J. Groszek, Selective adsorption at graphite/hydrocarbon interfaces, Proc. R. Soc. Lond. A Math. Phys. Sci. 314 (1970) 473–478.

[51] J.H. de Boer, The Dynamic Character of Adsorption, Oxford University, Oxford, 1953.

[52] A.W. Adamson, A.P. Gast, Physical Chemistry of Surfaces, 6th ed. Wiley-Interscience, New York, 1997.

ADSORPTION OF SURFACTIN AT WATER WITH ETHANOL MIXTURE-AIR INTERFACE

EDYTA REKIEL, ANNA ZDZIENNICKA* AND BRONISŁAW JAŃCZUK

Department of Interfacial Phenomena, Institute of Chemical Sciences, Faculty of Chemistry, Maria Curie-Skłodowska University in Lublin, Maria Curie-Skłodowska Sq. 3, 20-031 Lublin, Poland

Running title: Adsorption

*To whom correspondence should be addressed

phone   (48-81) 537-56-70   fax   (48-81) 533-3348

e-mail   aniaz@hektor.umcs.lublin.pl

Equations used for the solution surface tension calculations:

1. Miller et al. equation:
   For calculation of the studied solution surface tension there was applied the equation proposed by Miller et al. [1,2] based on the surface tension of individual surfactants. This equation has the following form:

   $$\exp \overline{\overline{\Pi}} = \exp \overline{\Pi}_1 + \exp \overline{\Pi}_2 - 1 \tag{S1}$$

   where $\overline{\overline{\Pi}} = \Pi\omega/RT$, $\overline{\Pi}_1 = \Pi_1\omega_1/RT$, $\overline{\Pi}_2 = \Pi_2\omega_2/RT$ are the dimensionless surface pressures of the mixture and individual solutions of surfactin and ethanol, respectively, ω_1, ω_2 and ω is the molar surface area of the surfactin and ethanol and their mixture, respectively. In the case of ethanol ω_2 was assumed to be equal to 1.26 x 10^5 m^2/mol. Depending on the surfactin orientation, there were applied the values of ω_1 equal to 5.61 x 10^5 m^2/mol and 7.24 x 10^5 m^2/mol.

2. Calculations of the solution surface tension from the Connors equation [3,4]:

   $$\gamma = \gamma_0 - (\gamma_0 - \gamma_s)\left[1 + \frac{\beta(1-X)}{1-\alpha(1-X)}\right]X \tag{S2}$$

   were made at the given constat surfactin concentration.
   γ_0 is the surface tension of aqueous solution of pure surfactin at the given concentration, γ_s is the surface tension of "pure" ethanol, X is the ethanol mole fraction and α and β are the empirical constants.

3. In the case of independent adsorption there was applied the following equation:

   $$\gamma_{LV} = \gamma_W - \pi_1 - \pi_2 \tag{S3}$$

   where γ_{LV} is the surface tension of aqueous solution of surfactin and ethanol, γ_W is the water surface tension, π_1 is the difference between the water and aqueous solution of surfactin surface tension and π_2 is the difference between the water and aqueous solution of ethanol surface tension.

References

[1] V.B. Fainerman, R. Miller, E.V. Aksenenko, Simple model for prediction of surface tension of mixed surfactant solutions, Advances in Colloid and Interface Science, 96 (2002) 339–359.

[2] V.B. Fainerman, R. Miller, Simple method to estimate surface tension of mixed surfactant solutions, Journal of Physical Chemistry B, 105 (2001) 11432–11438.

[3] K.A. Connors, K.A. Wright, Dependence of surface tension on composition of binary aqueous-organic solutions, Analytical Chemistry, 61 (1989) 194–198.

[4] D. Khossravi, K.A. Connors, Solvent effects on chemical processes. 3. Surface tension of binary aqueous organic solvent, Journal of Solution Chemistry, 22 (1993) 321–330.

Table S1a. The absolute deviation between the calculated from the Miller et al., Connors equations as well as from the independent adsorption and the measured values of water/ethanol aqueous solutions of surfactin surface tension at the constant surfactin concentration.

SF concentration [mg/dm^3]	Miller et al. equation for SF ω = 5.61 x 10^5 m^2/mol	Miller et al. equation for SF ω = 7.24 x 10^5 m^2/mol	Independent adsorption	Connors equation
0.0002	0.32	0.32	0.32	1.76
0.0005	0.31	0.31	0.31	1.76
0.00125	0.52	0.60	0.33	1.28
0.003	0.95	1.20	0.39	1.20
0.00625	1.18	1.50	0.42	1.27
0.01	1.41	1.80	0.45	1.27
0.02	2.89	3.73	1.00	1.19
0.05	5.95	7.28	3.35	1.15
0.1	7.20	7.93	6.22	1.18
0.5	2.92	2.67	14.77	1.89
1	3.28	5.65	18.01	2.06
5	13.02	15.46	26.18	1.61
10	16.89	19.29	29.51	1.92
20	17.03	19.42	29.61	0.30
30	17.49	19.87	30.00	2.55
40	17.90	20.28	30.34	2.40

Table S1b. The absolute deviation between the calculated from the Miller et al., Connors equations as well as from the independent adsorption and the measured values of water/ethanol aqueous solutions of surfactin surface tension at the constant ethanol concentration.

| Ethanol concentration [M]	Miller et al. equations for SF ω= 5.61 x 10^5 m^2/mol	Miller et al. equations for SF ω = 7.24 x 10^5 m^2/mol	Independent adsorption	Connors equation
0.06692	1.32	1.43	1.99	1.28
0.1338	1.63	1.77	2.19	1.82
0.2677	2.66	2.83	4.01	2.76
0.4015	0.30	1.68	4.87	4.55
0.5350	3.07	3.34	5.06	4.35
1.0706	4.19	4.74	6.64	5.13
1.6062	6.28	6.79	8.33	5.28
2.1416	6.21	7.05	9.57	4.74
2.6770	6.89	7.87	10.72	4.16
3.2124	7.47	8.56	11.65	3.38
3.7478	7.77	8.96	12.20	2.81
4.2832	8.11	9.39	13.02	2.49
4.8185	8.09	9.44	13.60	2.31
5.3538	8.50	9.91	13.98	1.98
5.8893	8.63	10.09	14.34	1.88
6.6925	8.71	10.18	14.66	1.74
7.7245	8.76	10.20	14.90	1.57
8.5664	8.78	10.17	14.89	1.35
10.2797	8.42	9.83	15.35	1.05
11.9680	8.29	9.71	15.39	0.97
12.1450	8.28	9.72	15.43	1.04
13.3794	8.19	9.65	15.42	0.78
14.5696	8.10	9.60	15.45	0.68
15.4064	8.02	9.55	15.48	0.62
16.0840	7.96	9.51	15.50	0.47
16.3777	7.93	9.50	15.51	0.41
16.6480	7.90	9.47	15.50	0.33
16.8988	7.91	9.48	15.51	0.15
17.1300	7.87	9.45	15.50	0.00
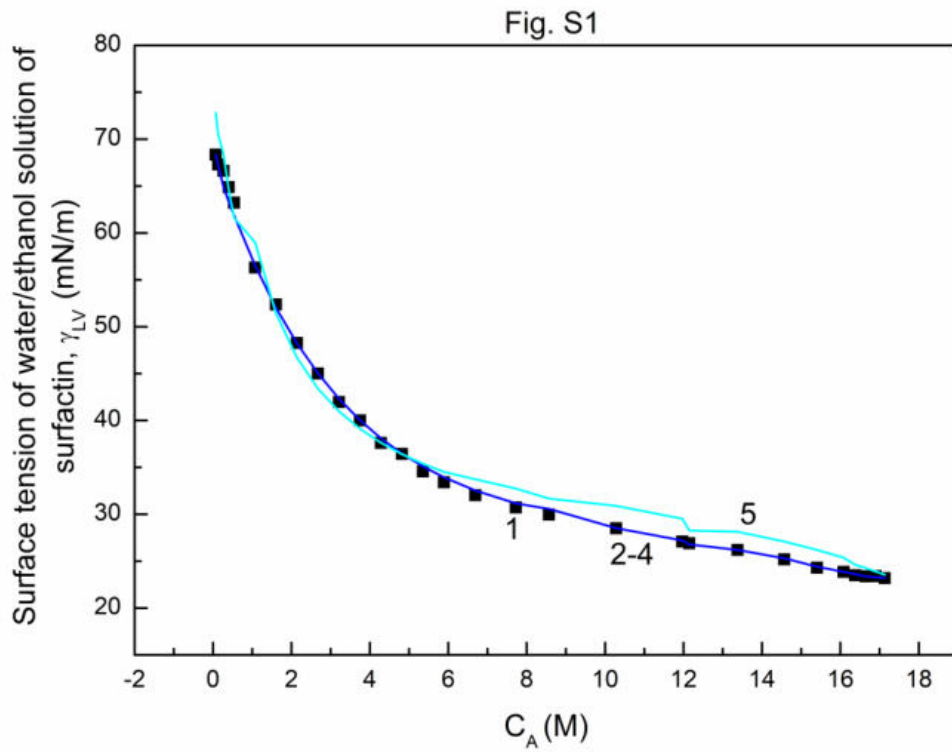
Fig. S1. A plot of the surface tension of water/ethanol solution of surfactin (γ_{LV}) at the constant surfactin concentration equal to 0.0002 mg/dm^3 vs. the logarithm of ethanol concentration (C_A). Points 1 correspond to the measured values, lines 2 and 3 correspond to the values calculated from the Miller et al. equation for ω equal to 5.61 x 10^5 m^2/mol and 7.24 x m^2/mol, line 4 corresponds to the value resulting from independent adsorption and line 5 corresponds to the value calculated from the Connors equation.
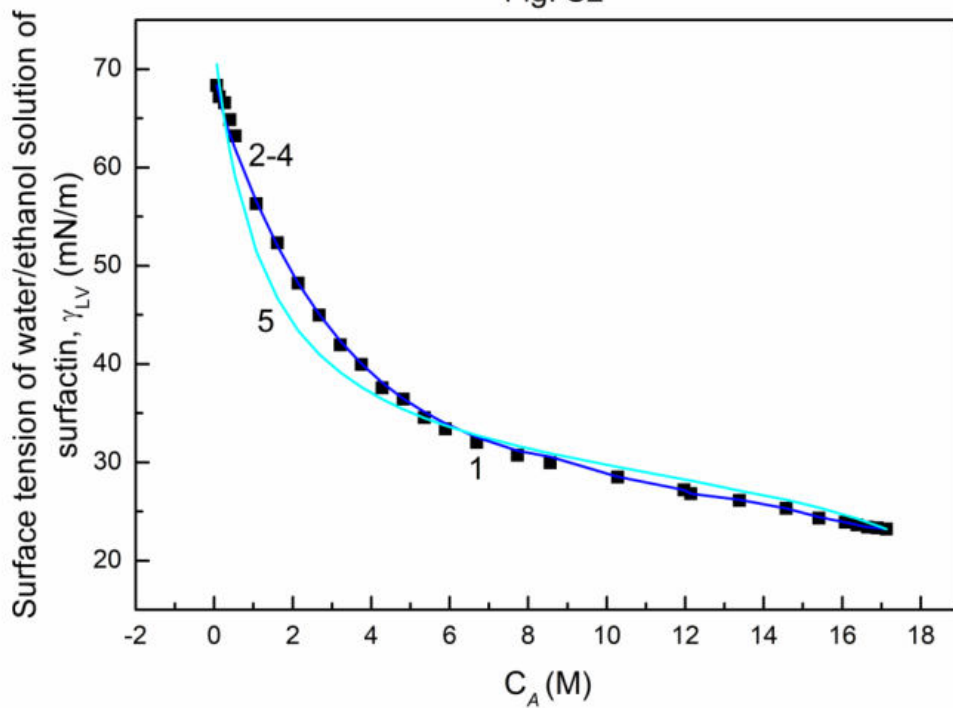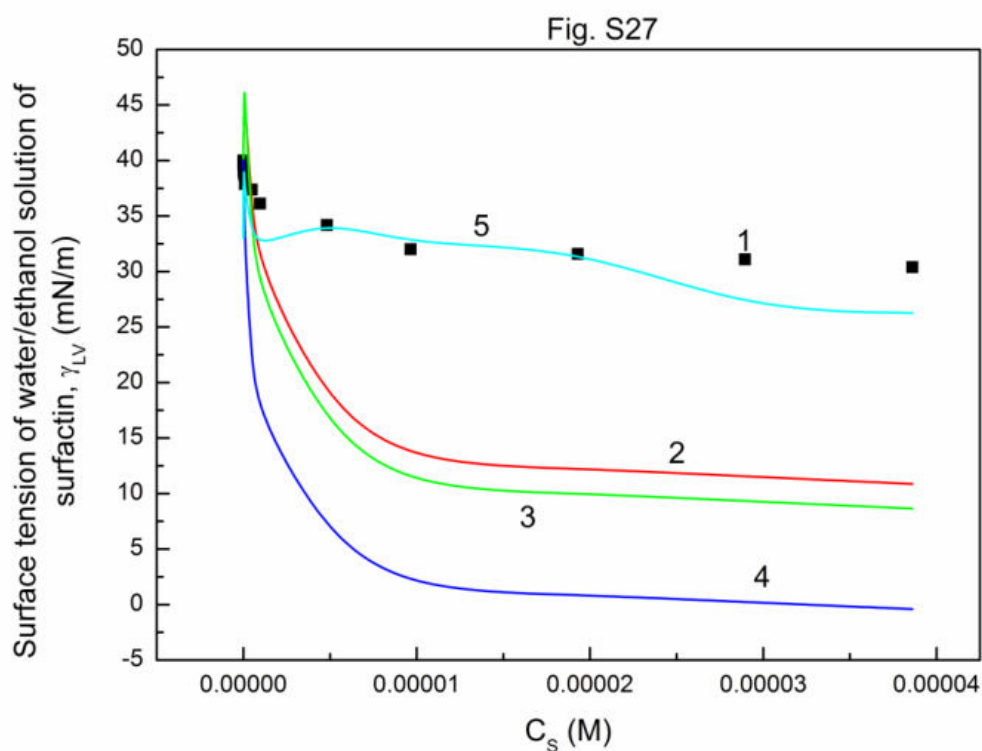
Fig. S2. A plot of the surface tension of water/ethanol solution of surfactin (γ_{LV}) at the constant surfactin concentration equal to 0.0005 mg/dm^3 vs. the logarithm of ethanol concentration (C_A). Points 1 correspond to the measured values, lines 2 and 3 correspond to the values calculated from the Miller et al. equation for ω equal to 5.61 x 10^5 m^2/mol and 7.24 x m^2/mol, line 4 corresponds to the value resulting from independent adsorption and line 5 corresponds to the value calculated from the Connors equation.
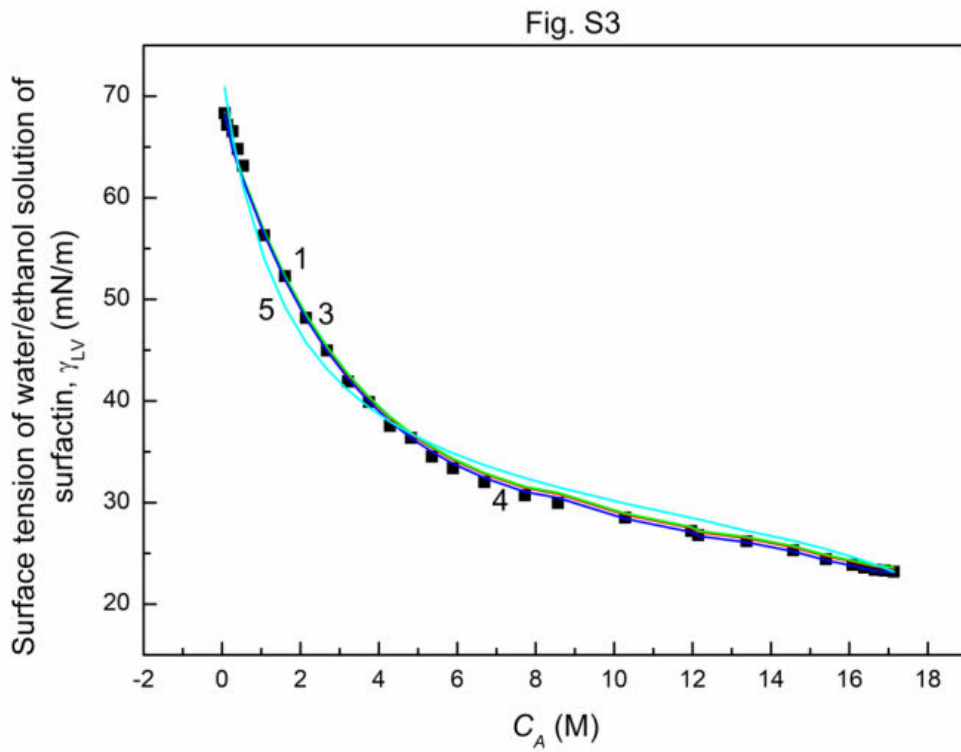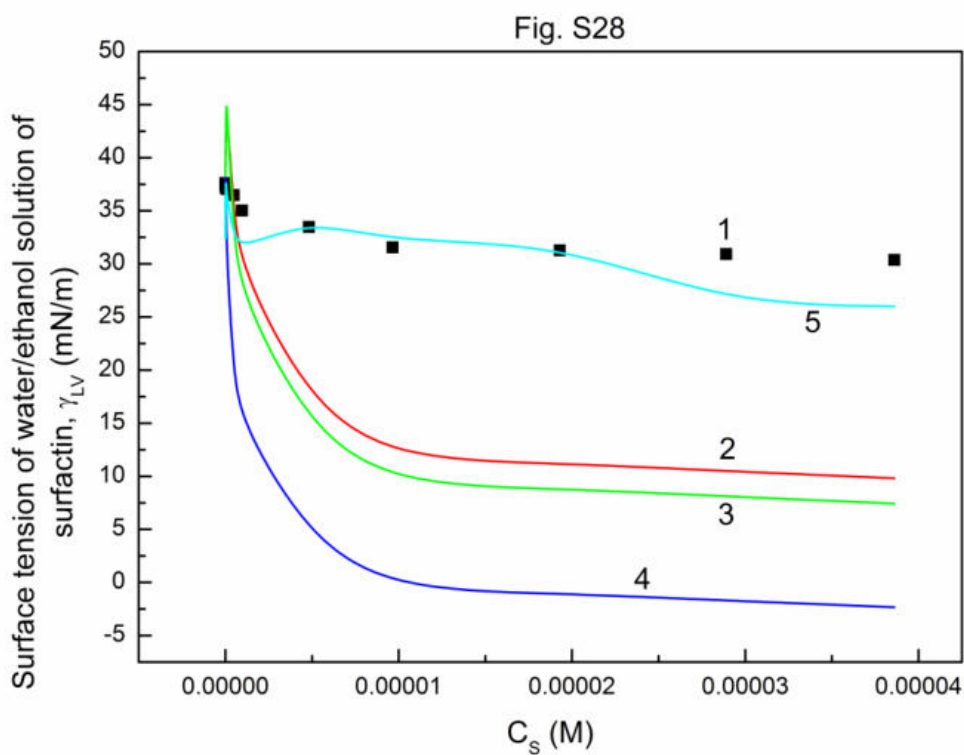
Fig. S3. A plot of the surface tension of water/ethanol solution of surfactin (γ_{LV}) at the constant surfactin concentration equal to 0.00125 mg/dm^3 vs. the logarithm of ethanol concentration (C_A). Points 1 correspond to the measured values, lines 2 and 3 correspond to the values calculated from the Miller et al. equation for ω equal to 5.61 x 10^5 m^2/mol and 7.24 x m^2/mol, line 4 corresponds to the value resulting from independent adsorption and line 5 corresponds to the value calculated from the Connors equation.
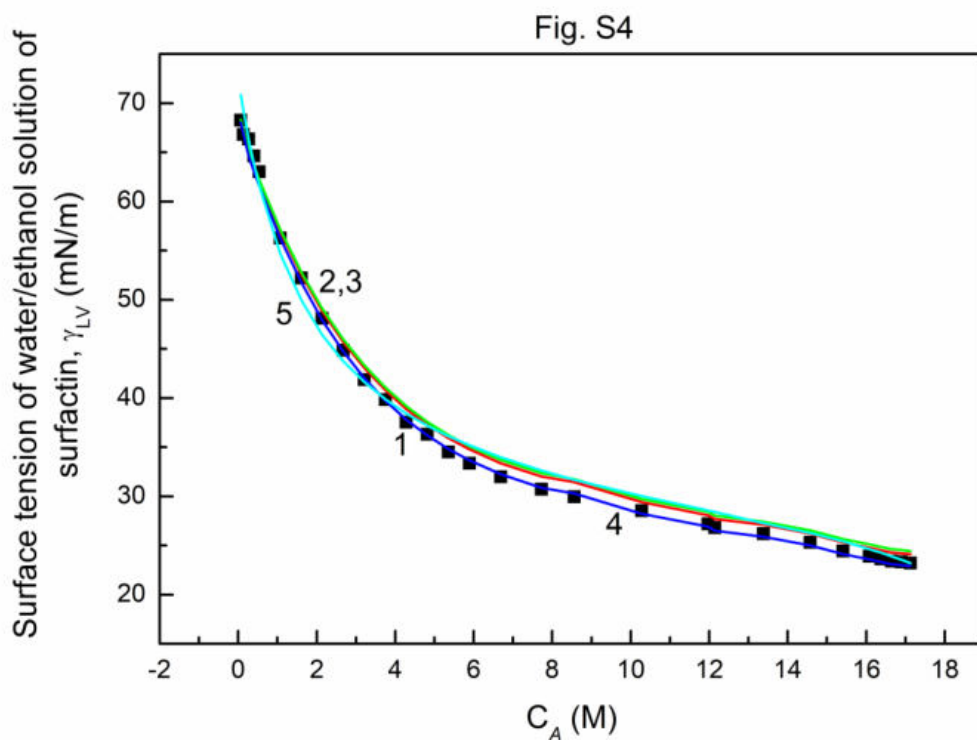
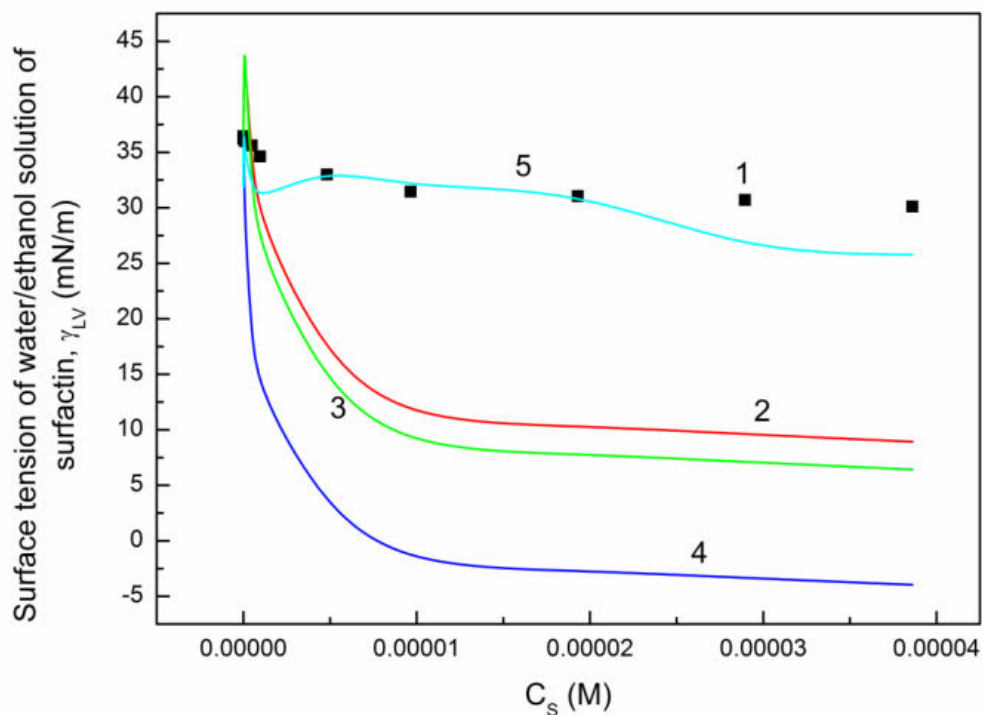Fig. S4. A plot of the surface tension of water/ethanol solution of surfactin (γ_{LV}) at the constant surfactin concentration equal to 0.003 mg/dm^3 vs. the logarithm of ethanol concentration (C_A). Points 1 correspond to the measured values, lines 2 and 3 correspond to the values calculated from the Miller et al. equation for ω equal to 5.61 x 10^5 m^2/mol and 7.24 x m^2/mol, line 4 corresponds to the value resulting from independent adsorption and line 5 corresponds to the value calculated from the Connors equation.
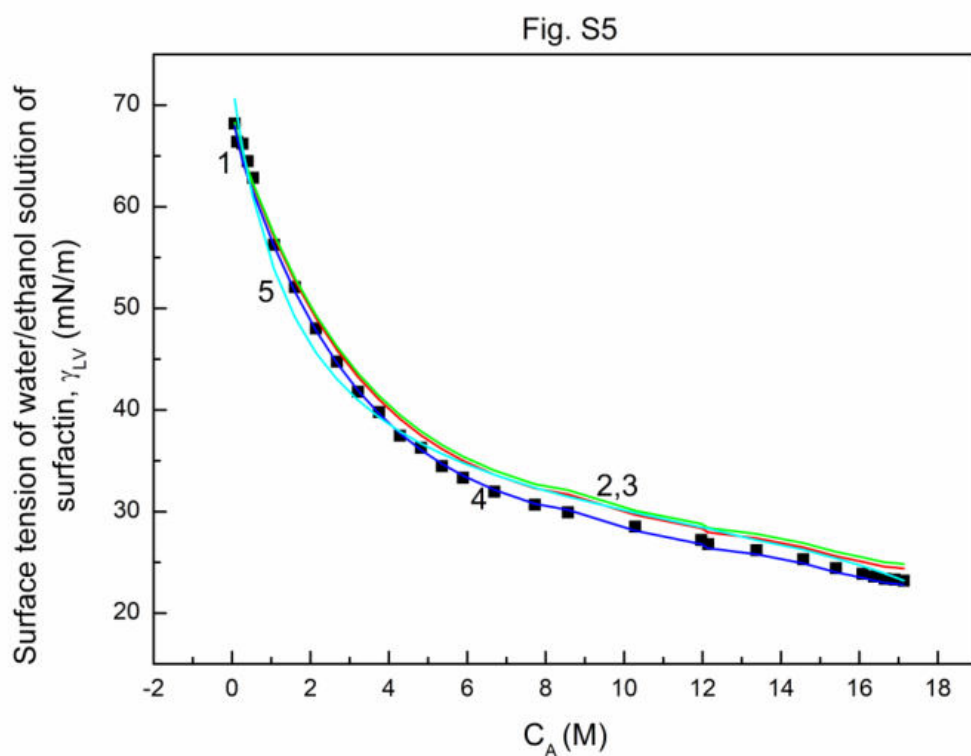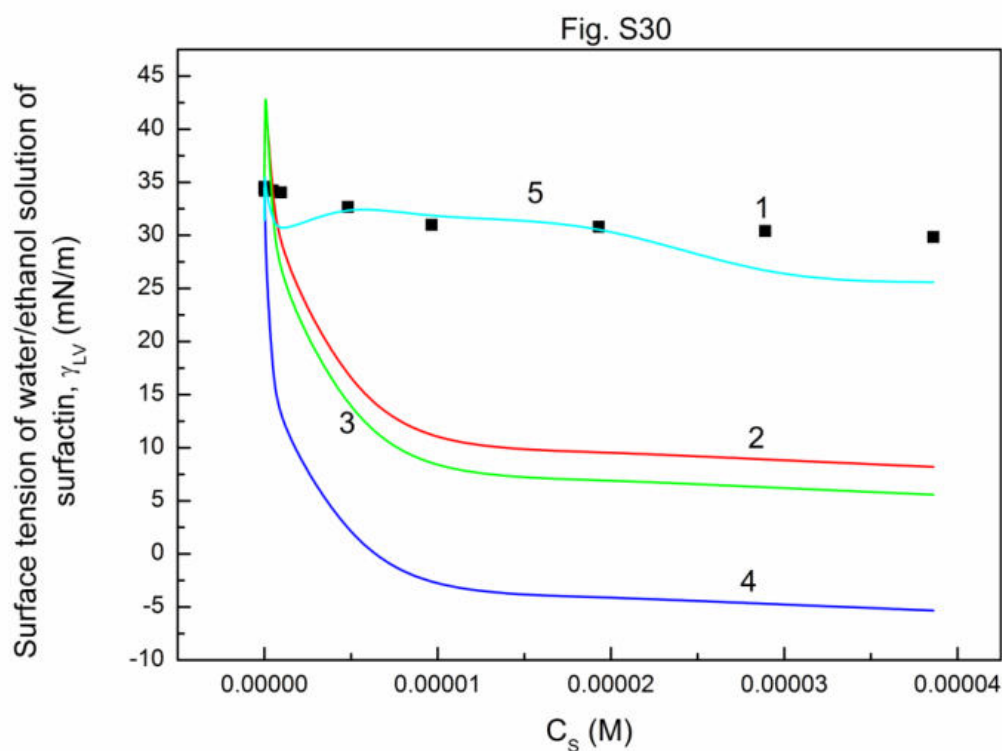
Fig. S5. A plot of the surface tension of water/ethanol solution of surfactin (γ_{LV}) at the constant surfactin concentration equal to 0.00625 mg/dm^3 vs. the logarithm of ethanol concentration (C_A). Points 1 correspond to the measured values, lines 2 and 3 correspond to the values calculated from the Miller et al. equation for ω equal to 5.61 x 10^5 m^2/mol and 7.24 x m^2/mol, line 4 corresponds to the value resulting from independent adsorption and line 5 corresponds to the value calculated from the Connors equation.
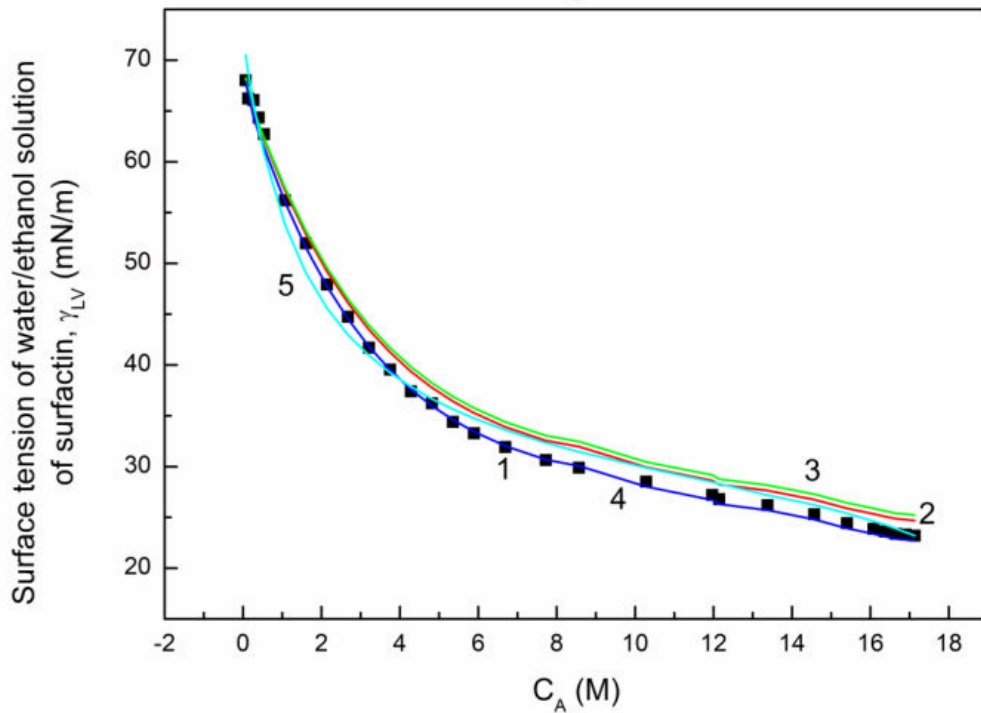
Fig. S6. A plot of the surface tension of water/ethanol solution of surfactin (γ_{LV}) at the constant surfactin concentration equal to 0.01 mg/dm^3 vs. the logarithm of ethanol concentration (C_A). Points 1 correspond to the measured values, lines 2 and 3 correspond to the values calculated from the Miller et al. equation for ω equal to 5.61 x 10^5 m^2/mol and 7.24 x m^2/mol, line 4 corresponds to the value resulting from independent adsorption and line 5 corresponds to the value calculated from the Connors equation.
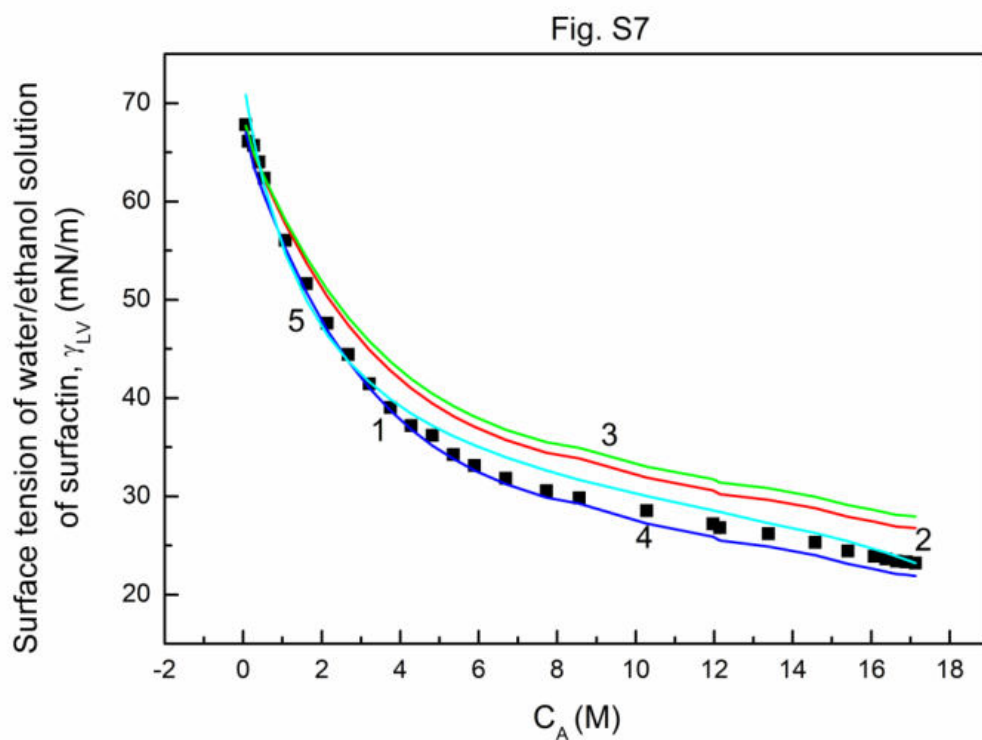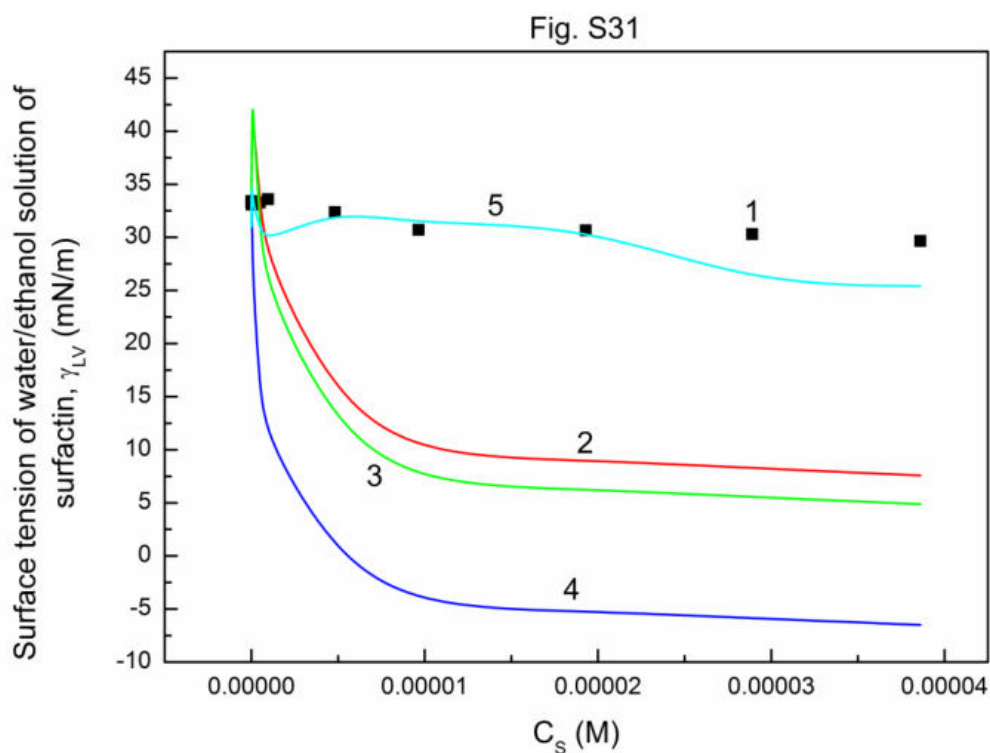
Fig. S7. A plot of the surface tension of water/ethanol solution of surfactin (γ_{LV}) at the constant surfactin concentration equal to 0.02 mg/dm^3 vs. the logarithm of ethanol concentration (C_A). Points 1 correspond to the measured values, lines 2 and 3 correspond to the values calculated from the Miller et al. equation for ω equal to 5.61 x 10^5 m^2/mol and 7.24 x m^2/mol, line 4 corresponds to the value resulting from independent adsorption and line 5 corresponds to the value calculated from the Connors equation.
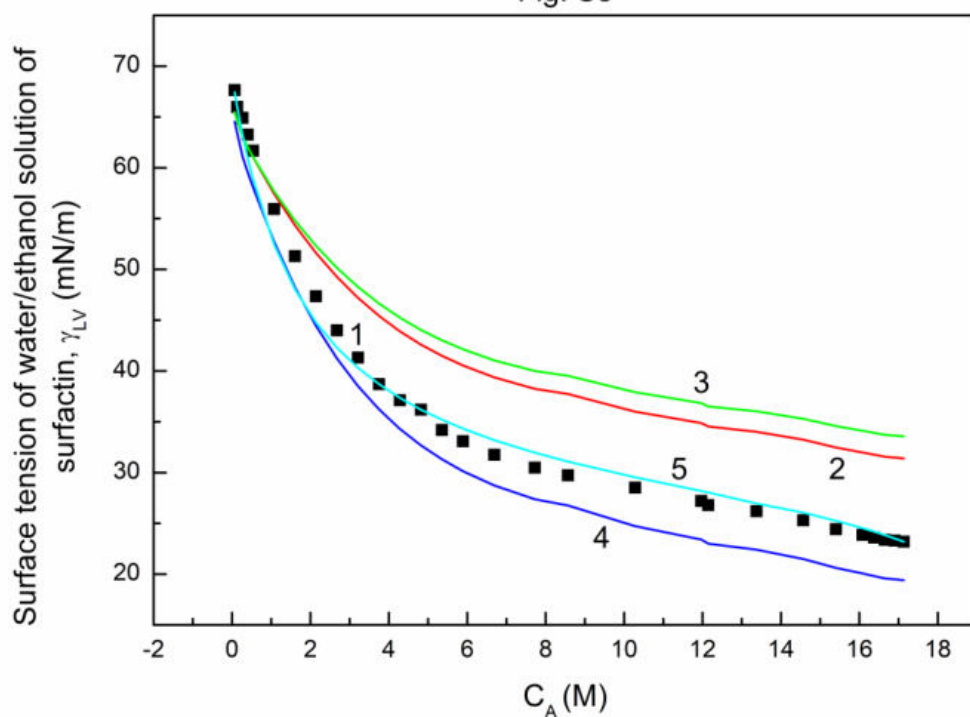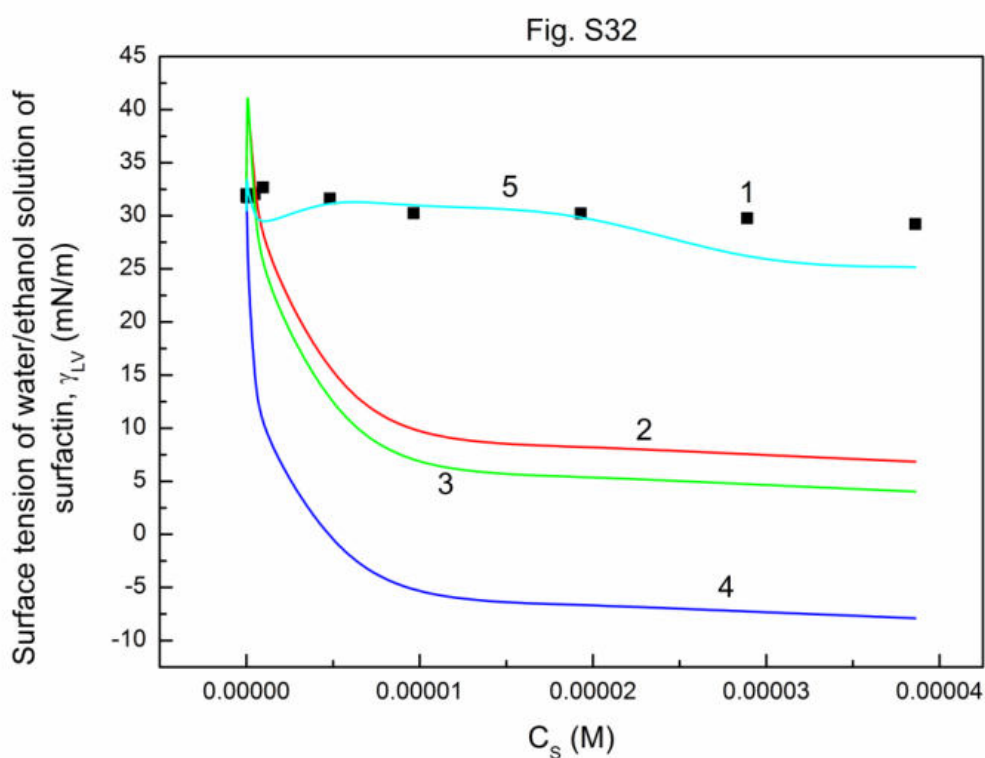
Fig. S8. A plot of the surface tension of water/ethanol solution of surfactin (γ_{LV}) at the constant surfactin concentration equal to 0.05 mg/dm^3 vs. the logarithm of ethanol concentration (C_A). Points 1 correspond to the measured values, lines 2 and 3 correspond to the values calculated from the Miller et al. equation for ω equal to 5.61 x 10^5 m^2/mol and 7.24 x m^2/mol, line 4 corresponds to the value resulting from independent adsorption and line 5 corresponds to the value calculated from the Connors equation.
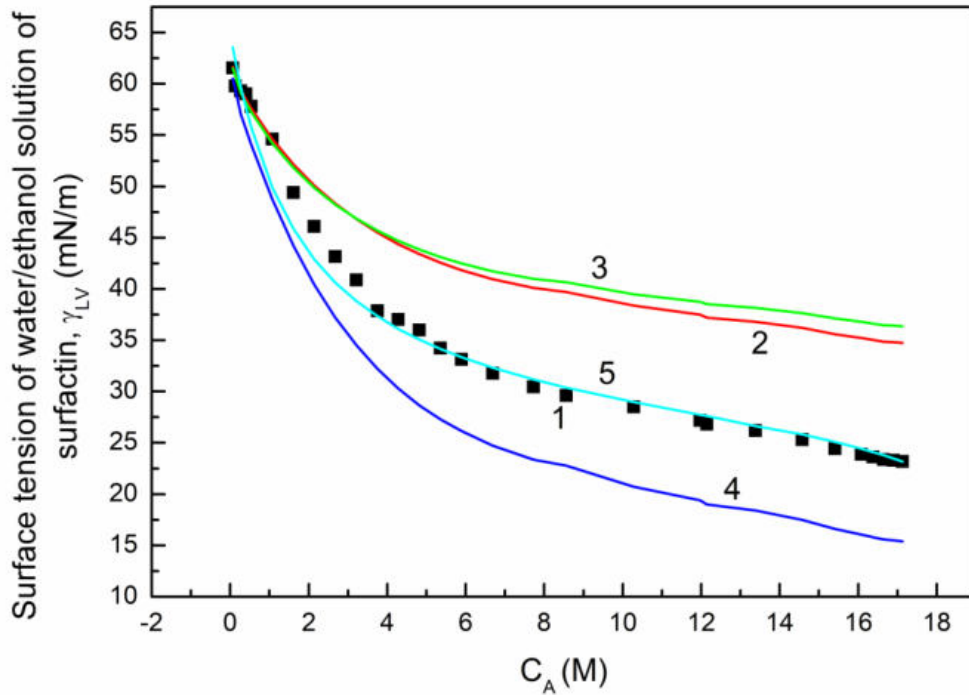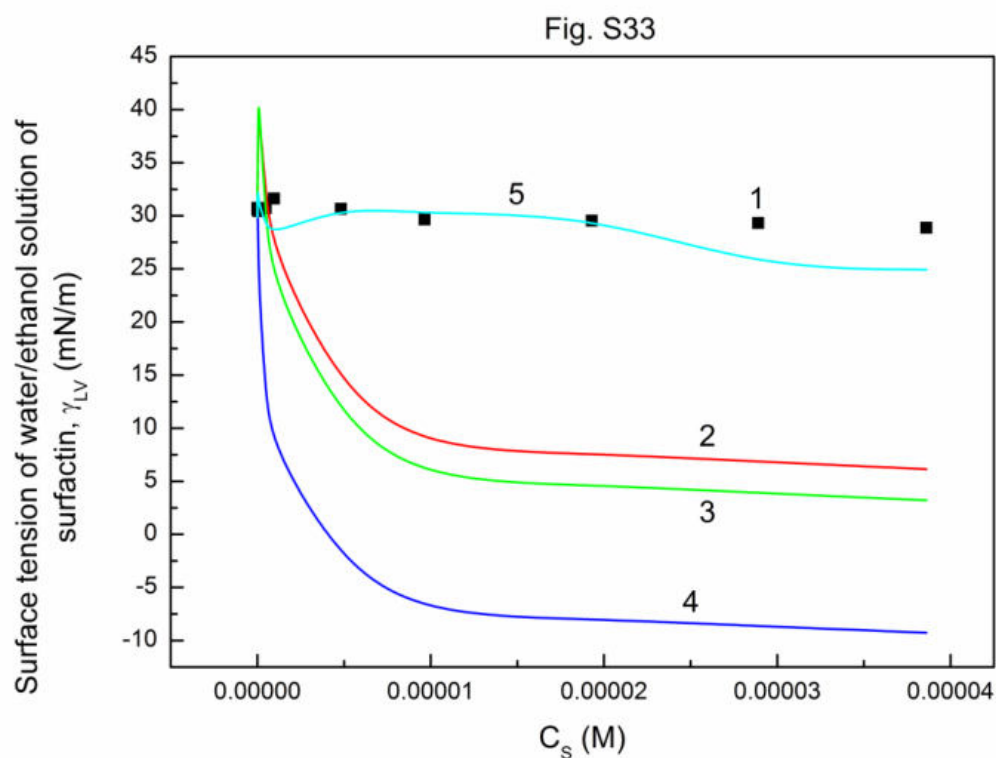
Fig. S9. A plot of the surface tension of water/ethanol solution of surfactin (γ_{LV}) at the constant surfactin concentration equal to 0.1 mg/dm^3 vs. the logarithm of ethanol concentration (C_A). Points 1 correspond to the measured values, lines 2 and 3 correspond to the values calculated from the Miller et al. equation for ω equal to 5.61 x 10^5 m^2/mol and 7.24 x m^2/mol, line 4 corresponds to the value resulting from independent adsorption and line 5 corresponds to the value calculated from the Connors equation.
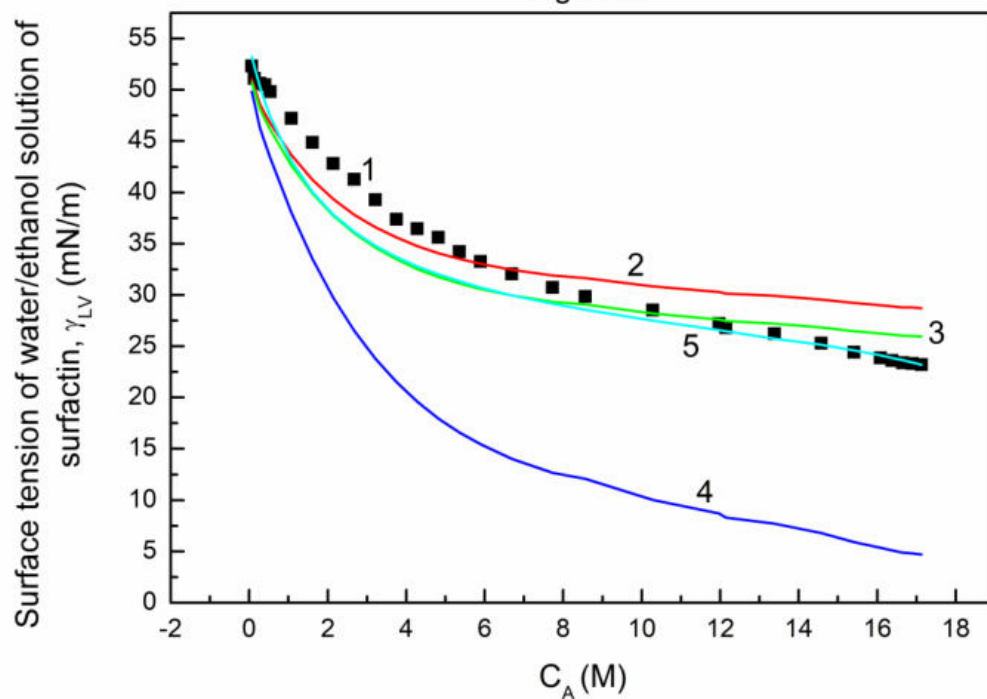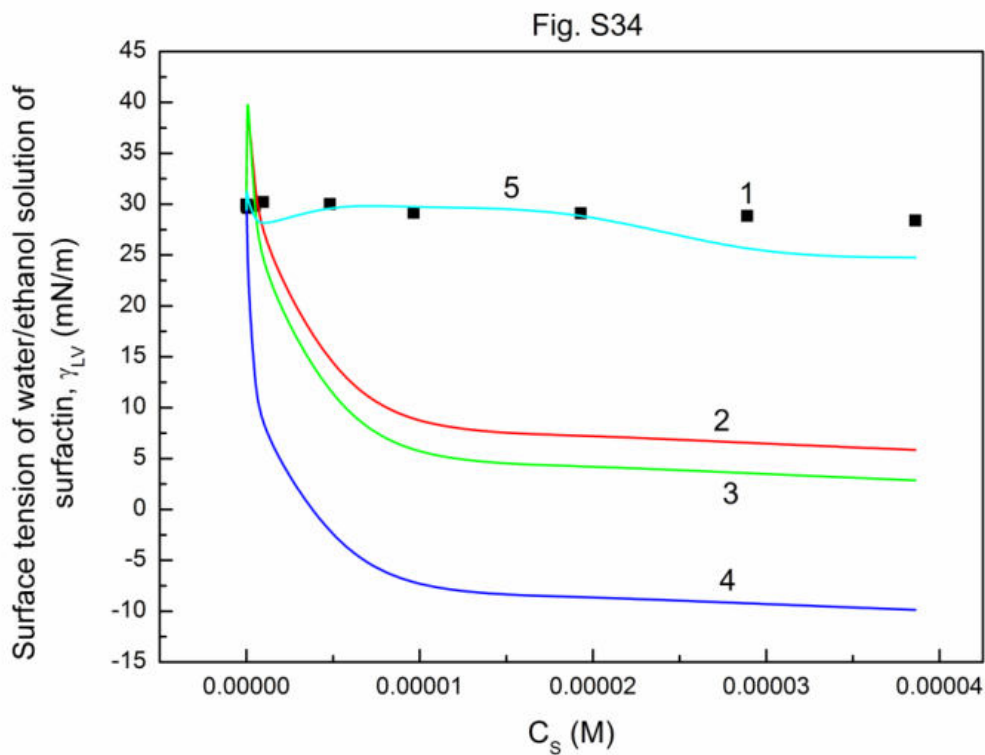
Fig. S10. A plot of the surface tension of water/ethanol solution of surfactin (γ_{LV}) at the constant surfactin concentration equal to 0.5 mg/dm^3 vs. the logarithm of ethanol concentration (C_A). Points 1 correspond to the measured values, lines 2 and 3 correspond to the values calculated from the Miller et al. equation for ω equal to 5.61 x 10^5 m^2/mol and 7.24 x m^2/mol, line 4 corresponds to the value resulting from independent adsorption and line 5 corresponds to the value calculated from the Connors equation.
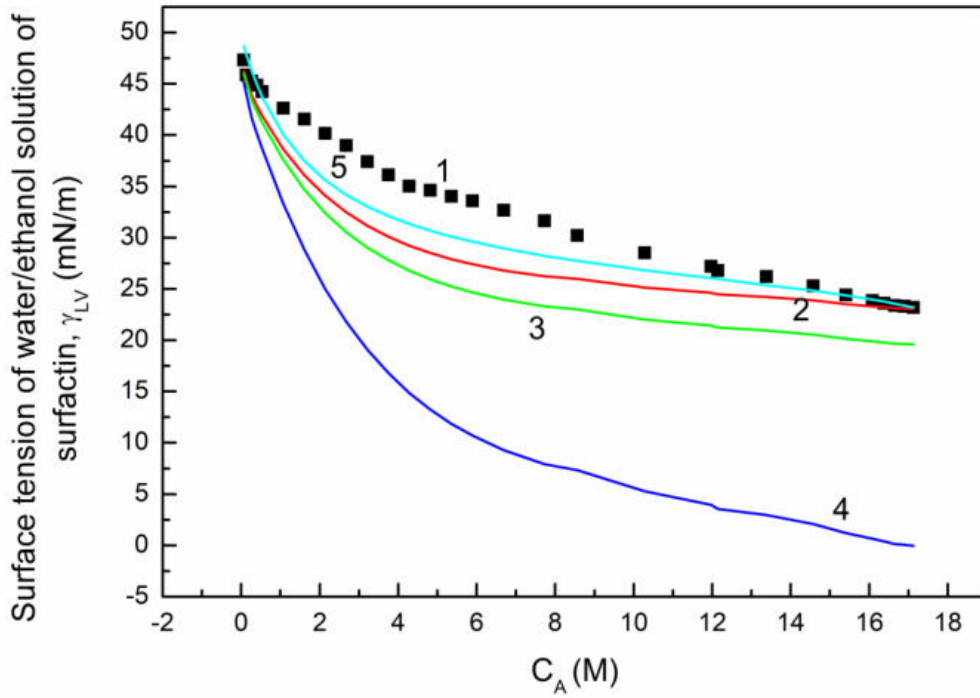
Fig. S11. A plot of the surface tension of water/ethanol solution of surfactin (γ_{LV}) at the constant surfactin concentration equal to 1 mg/dm^3 vs. the logarithm of ethanol concentration (C_A). Points 1 correspond to the measured values, lines 2 and 3 correspond to the values calculated from the Miller et al. equation for ω equal to 5.61 x 10^5 m^2/mol and 7.24 x m^2/mol, line 4 corresponds to the value resulting from independent adsorption and line 5 corresponds to the value calculated from the Connors equation.
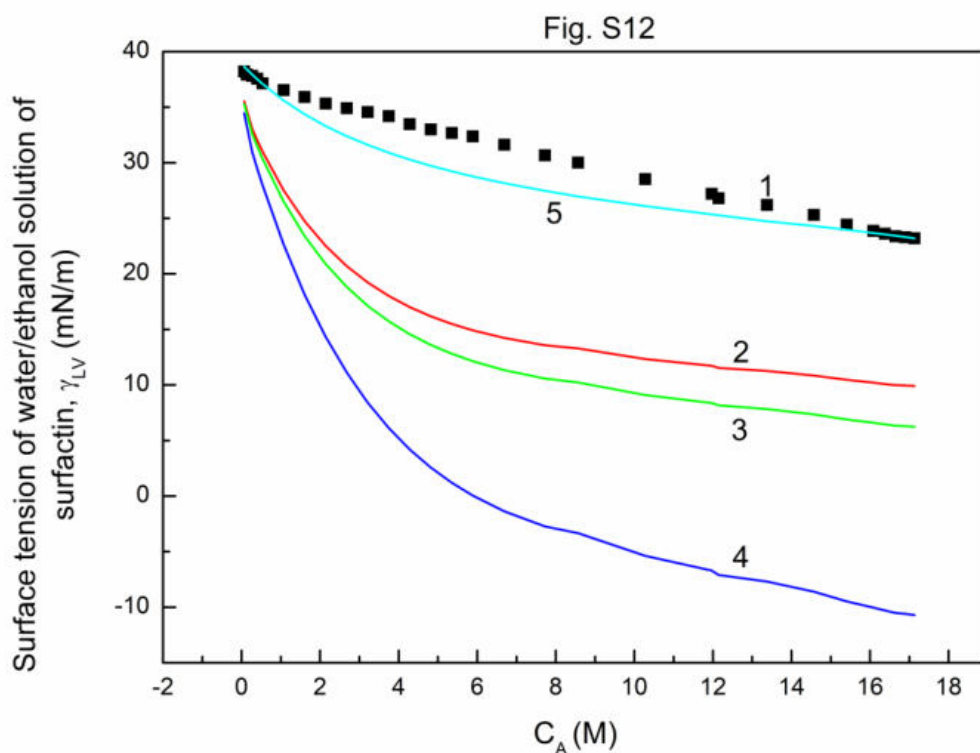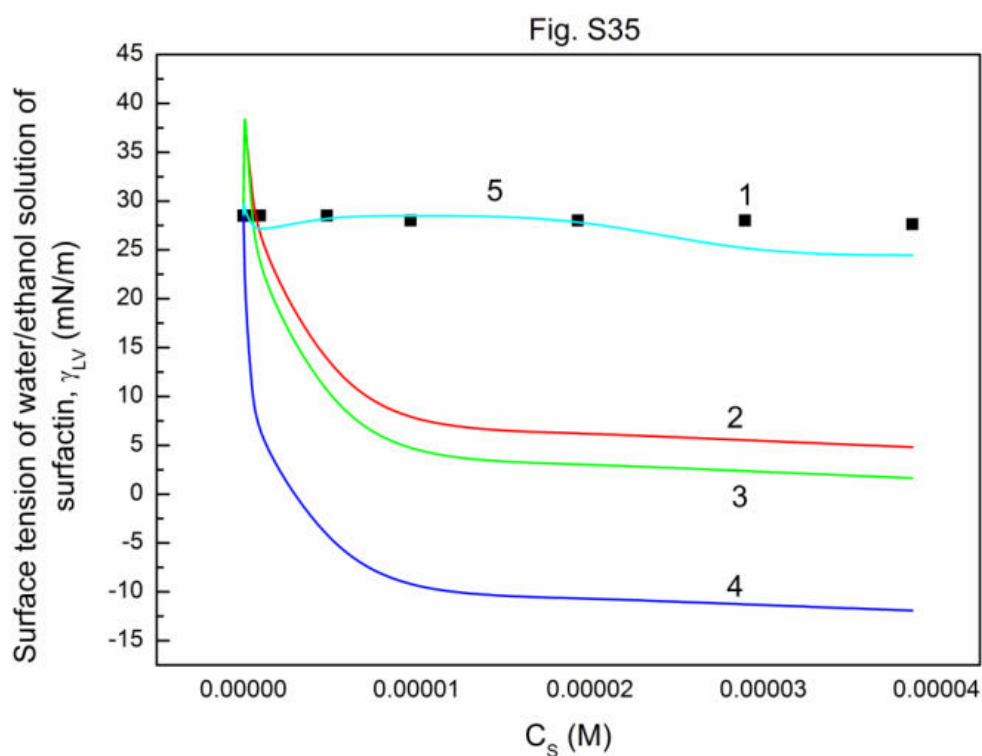
Fig. S12. A plot of the surface tension of water/ethanol solution of surfactin (γ_{LV}) at the constant surfactin concentration equal to 5 mg/dm^3 vs. the logarithm of ethanol concentration (C_A). Points 1 correspond to the measured values, lines 2 and 3 correspond to the values calculated from the Miller et al. equation for ω equal to 5.61 x 10^5 m^2/mol and 7.24 x m^2/mol, line 4 corresponds to the value resulting from independent adsorption and line 5 corresponds to the value calculated from the Connors equation.
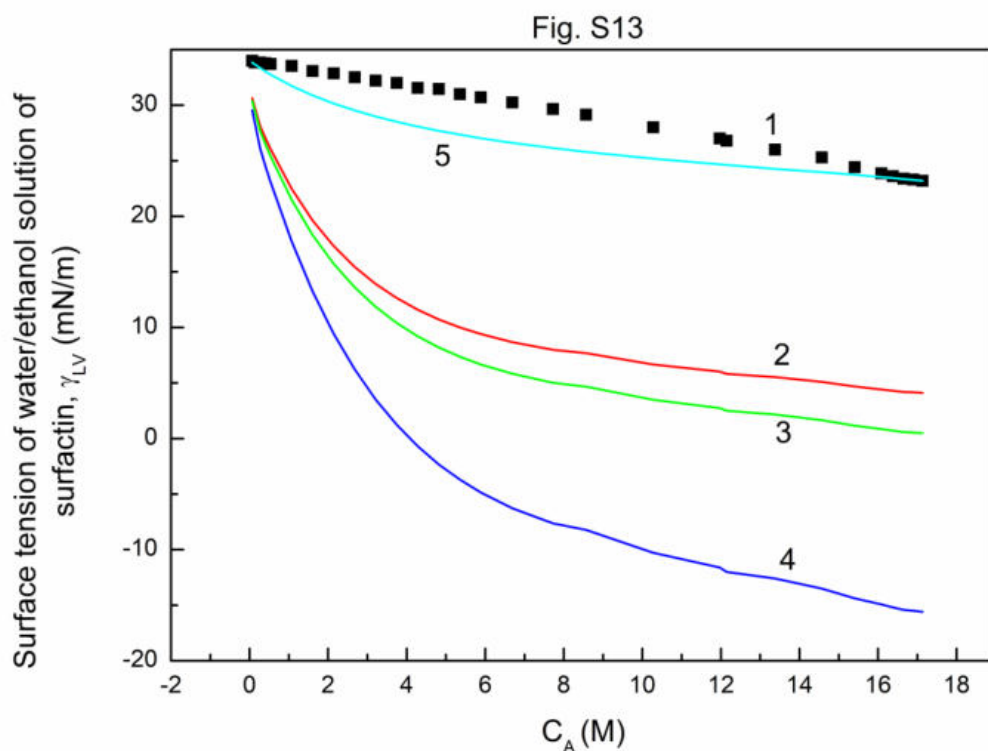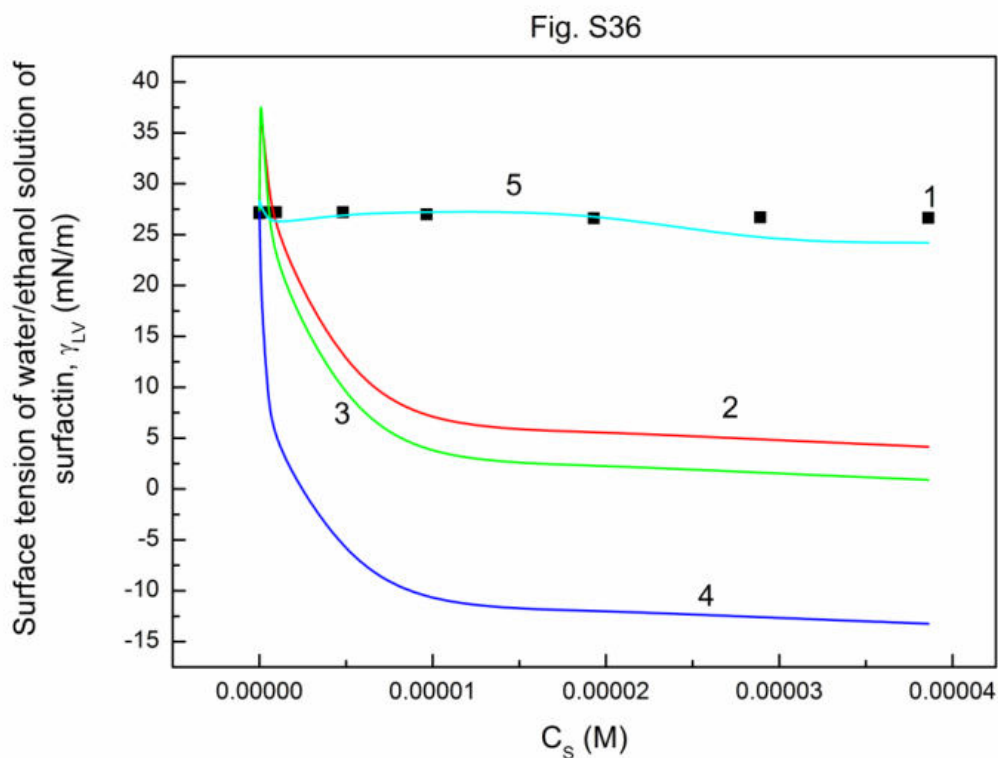
Fig. S13. A plot of the surface tension of water/ethanol solution of surfactin (γ_{LV}) at the constant surfactin concentration equal to 10 mg/dm^3 vs. the logarithm of ethanol concentration (C_A). Points 1 correspond to the measured values, lines 2 and 3 correspond to the values calculated from the Miller et al. equation for ω equal to 5.61 x 10^5 m^2/mol and 7.24 x m^2/mol, line 4 corresponds to the value resulting from independent adsorption and line 5 corresponds to the value calculated from the Connors equation.
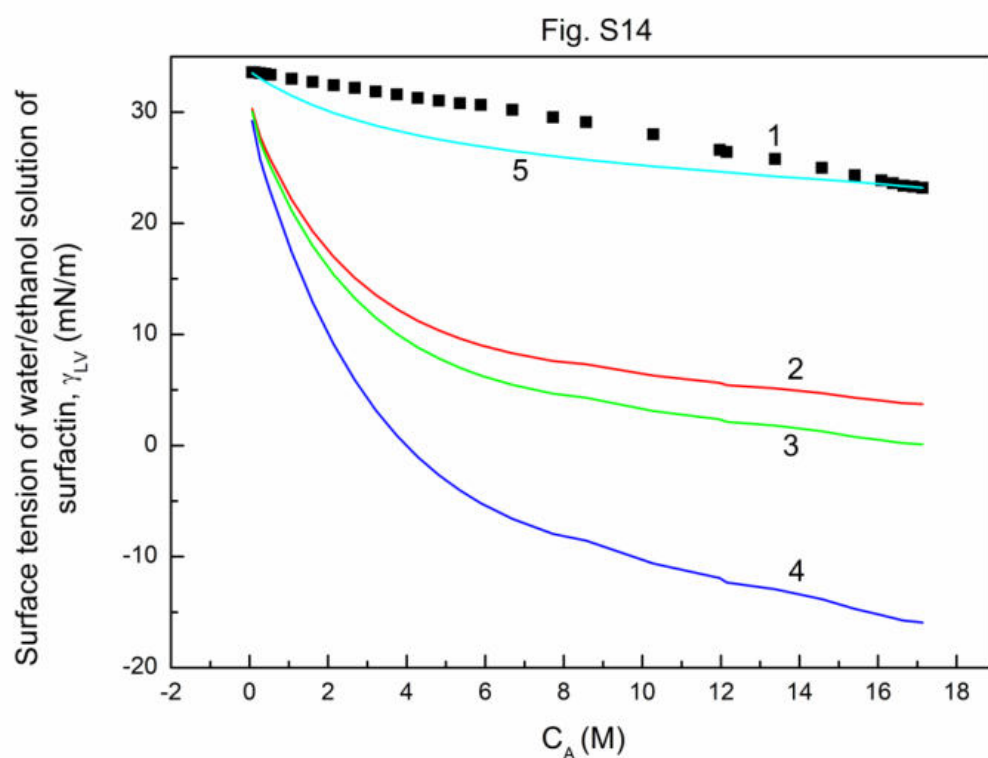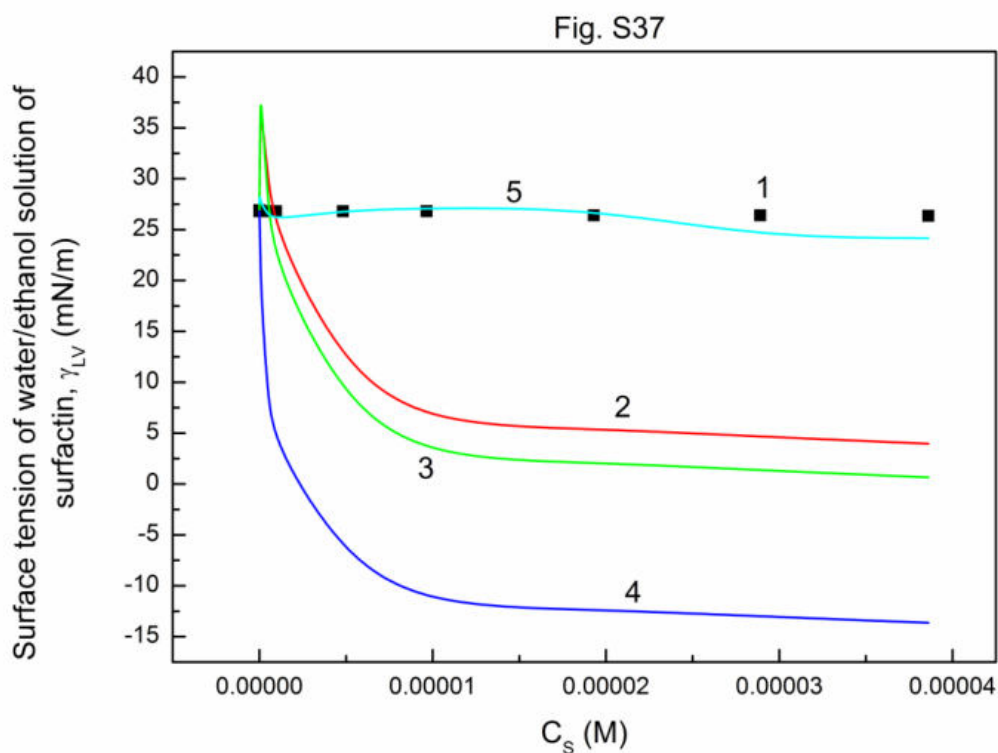
Fig. S14. A plot of the surface tension of water/ethanol solution of surfactin (γ_{LV}) at the constant surfactin concentration equal to 20 mg/dm^3 vs. the logarithm of ethanol concentration (C_A). Points 1 correspond to the measured values, lines 2 and 3 correspond to the values calculated from the Miller et al. equation for ω equal to 5.61 x 10^5 m^2/mol and 7.24 x m^2/mol, line 4 corresponds to the value resulting from independent adsorption and line 5 corresponds to the value calculated from the Connors equation.
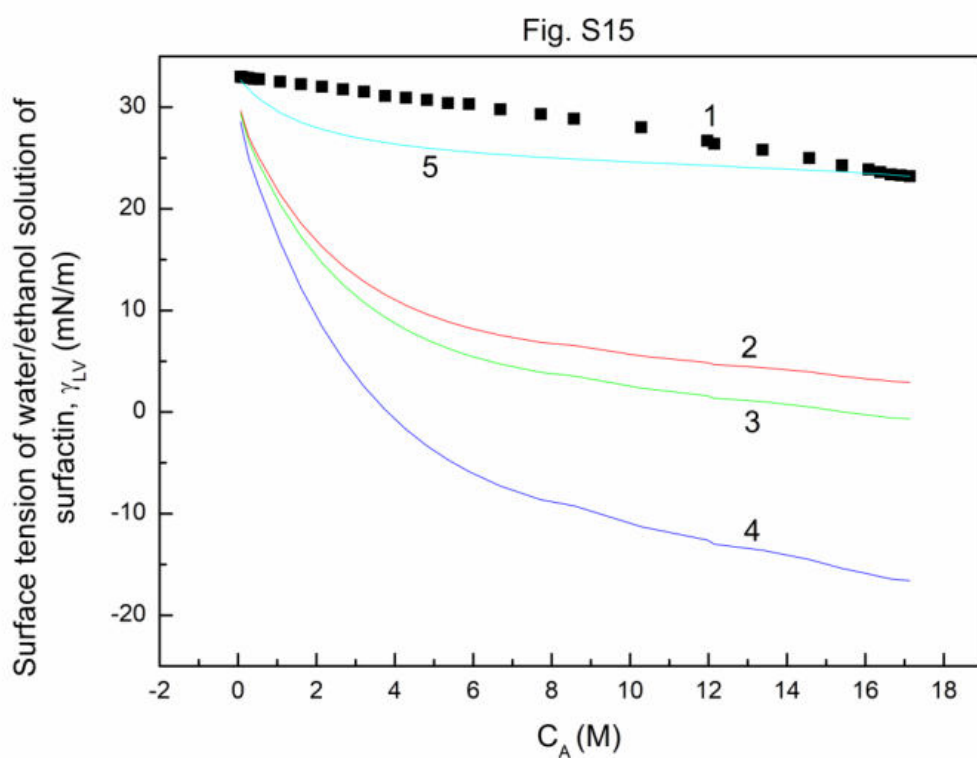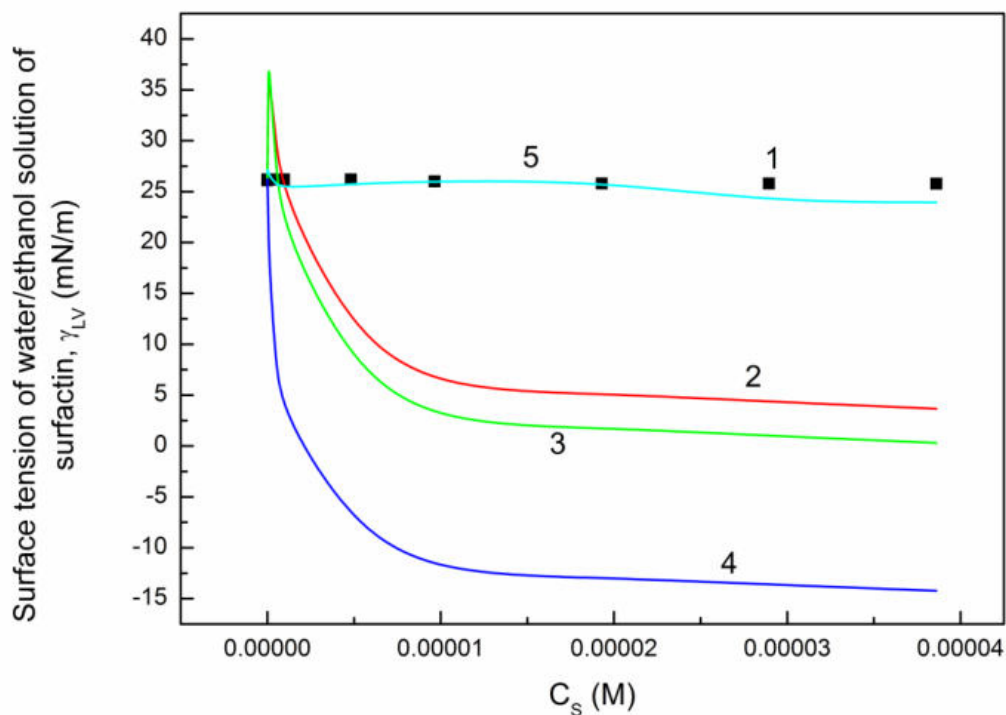
Fig. S15. A plot of the surface tension of water/ethanol solution of surfactin (γ_{LV}) at the constant surfactin concentration equal to 30 mg/dm^3 vs. the logarithm of ethanol concentration (C_A). Points 1 correspond to the measured values, lines 2 and 3 correspond to the values calculated from the Miller et al. equation for ω equal to 5.61 x 10^5 m^2/mol and 7.24 x m^2/mol, line 4 corresponds to the value resulting from independent adsorption and line 5 corresponds to the value calculated from the Connors equation.
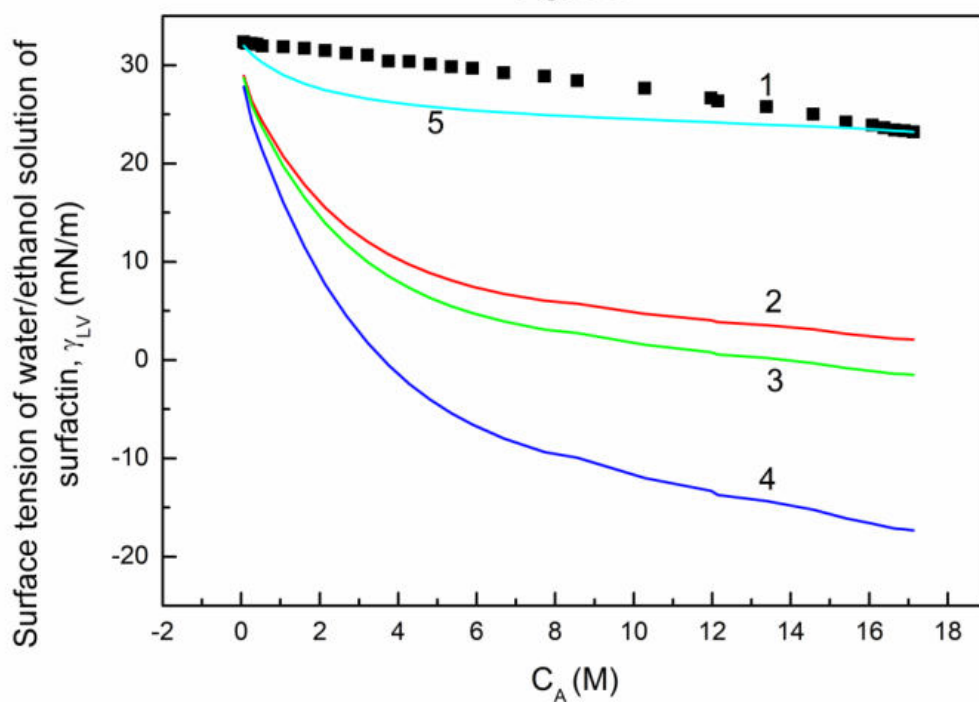
Fig. S16. A plot of the surface tension of water/ethanol solution of surfactin (γ_{LV}) at the constant surfactin concentration equal to 40 mg/dm^3 vs. the logarithm of ethanol concentration (C_A). Points 1 correspond to the measured values, lines 2 and 3 correspond to the values calculated from the Miller et al. equation for ω equal to 5.61 x 10^5 m^2/mol and 7.24 x m^2/mol, line 4 corresponds to the value resulting from independent adsorption and line 5 corresponds to the value calculated from the Connors equation.
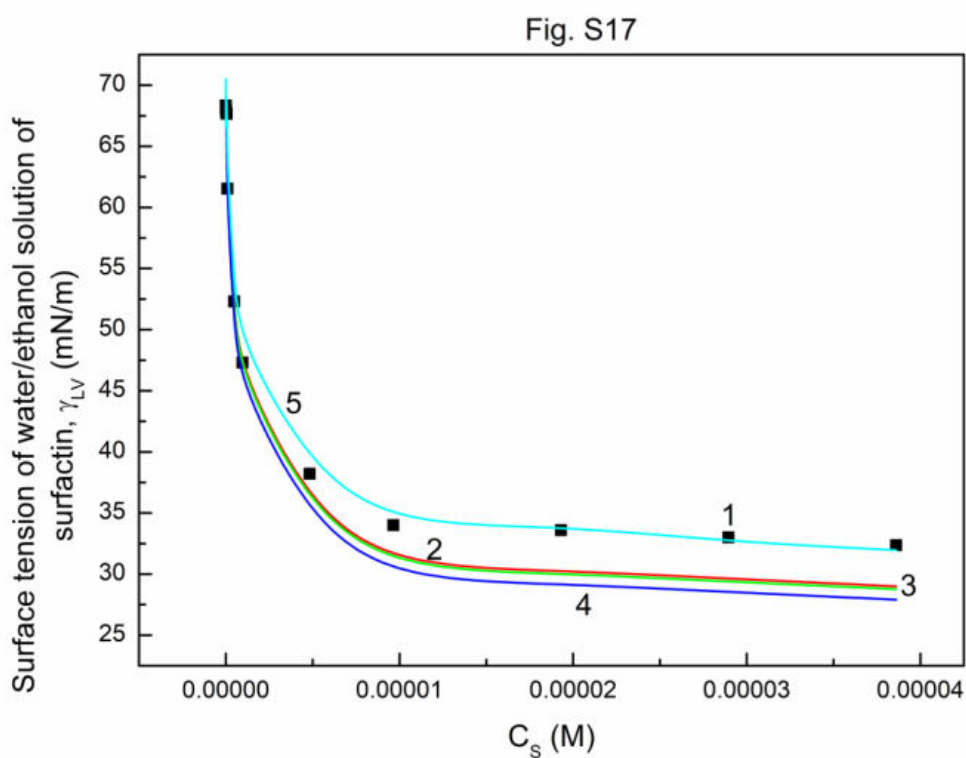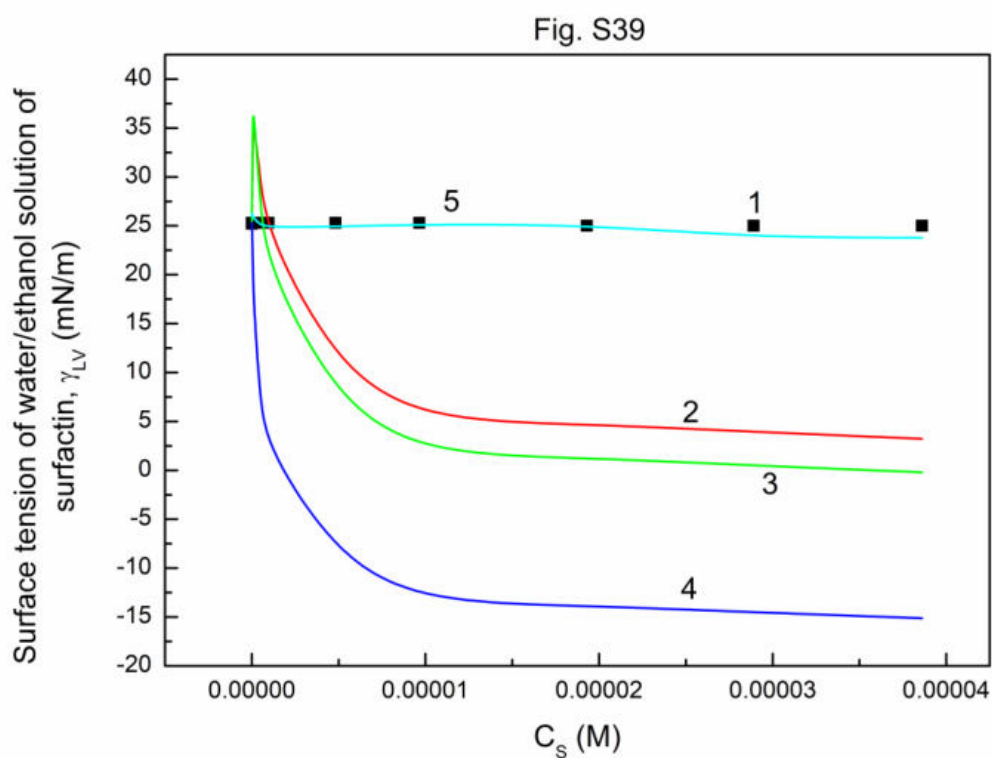
Fig. S17. A plot of the surface tension of water/ethanol solution of surfactin (γ_{LV}) at the constant ethanol concentration equal to 0.06692 M vs. the logarithm of surfactin concentration (C_S). Points 1 correspond to the measured values, lines 2 and 3 correspond to the values calculated from the Miller et al. equation for ω equal to 5.61 x 10^5 m^2/mol and 7.24 x m^2/mol, line 4 corresponds to the value resulting from independent adsorption and line 5 corresponds to the value calculated from the Connors equation.
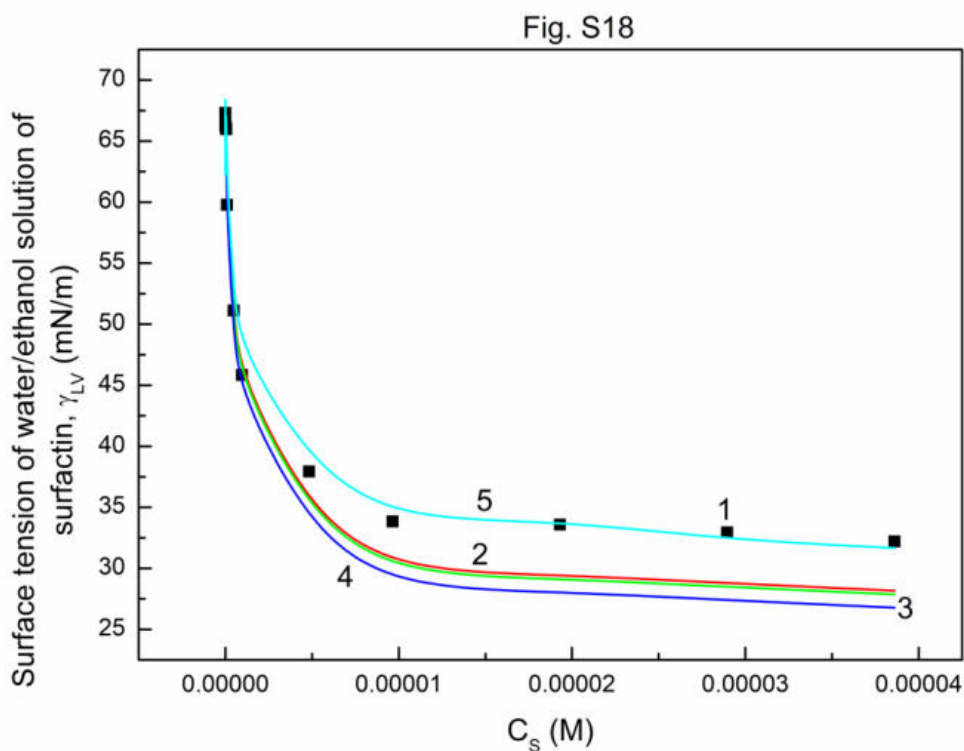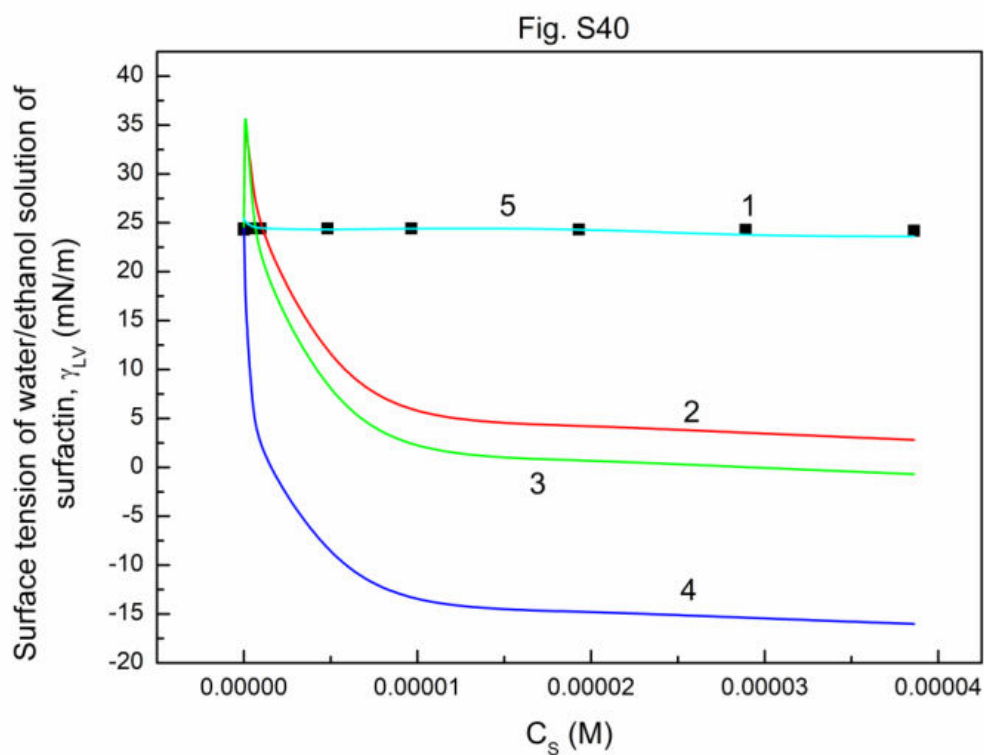
Fig. S18. A plot of the surface tension of water/ethanol solution of surfactin (γ_{LV}) at the constant ethanol concentration equal to 0.1338 M vs. the logarithm of surfactin concentration (C_S). Points 1 correspond to the measured values, lines 2 and 3 correspond to the values calculated from the Miller et al. equation for ω equal to 5.61 x 10^5 m^2/mol and 7.24 x m^2/mol, line 4 corresponds to the value resulting from independent adsorption and line 5 corresponds to the value calculated from the Connors equation.
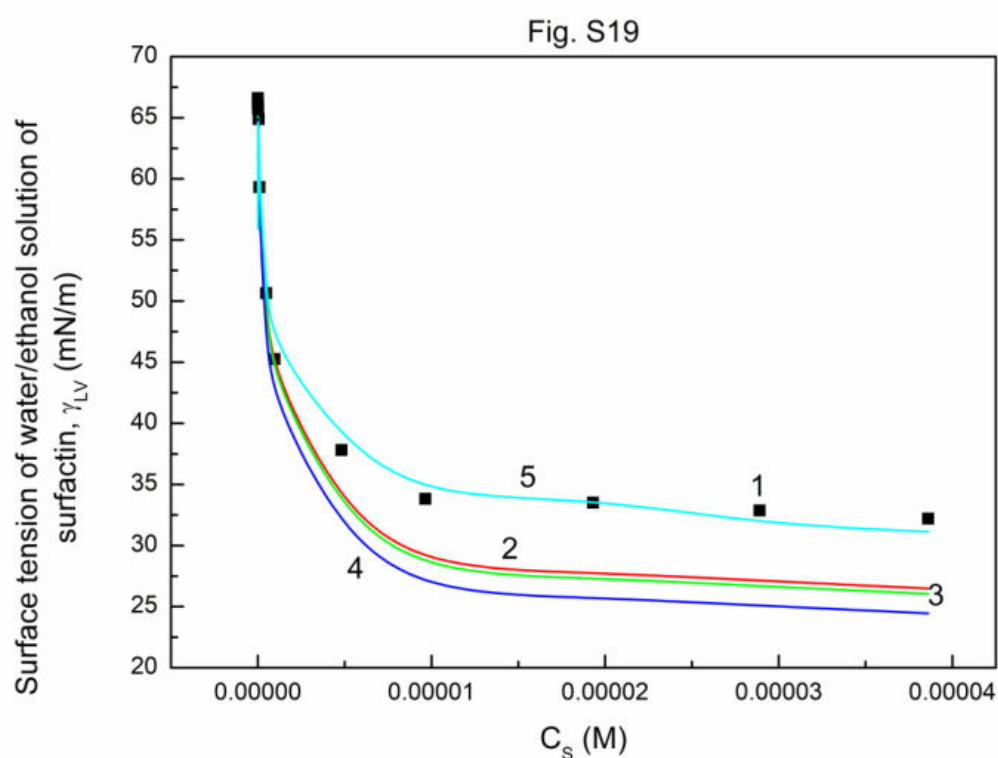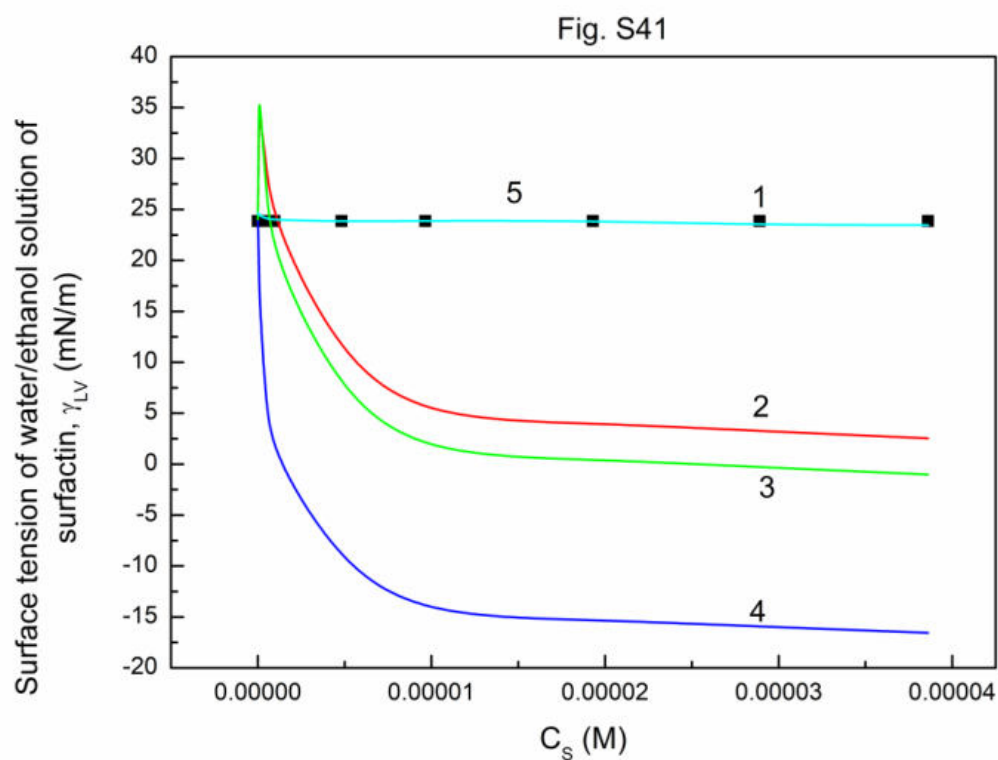
Fig. S19. A plot of the surface tension of water/ethanol solution of surfactin (γ_{LV}) at the constant ethanol concentration equal to 0.2677 M vs. the logarithm of surfactin concentration (C_S). Points 1 correspond to the measured values, lines 2 and 3 correspond to the values calculated from the Miller et al. equation for ω equal to 5.61 x 10^5 m^2/mol and 7.24 x m^2/mol, line 4 corresponds to the value resulting from independent adsorption and line 5 corresponds to the value calculated from the Connors equation.
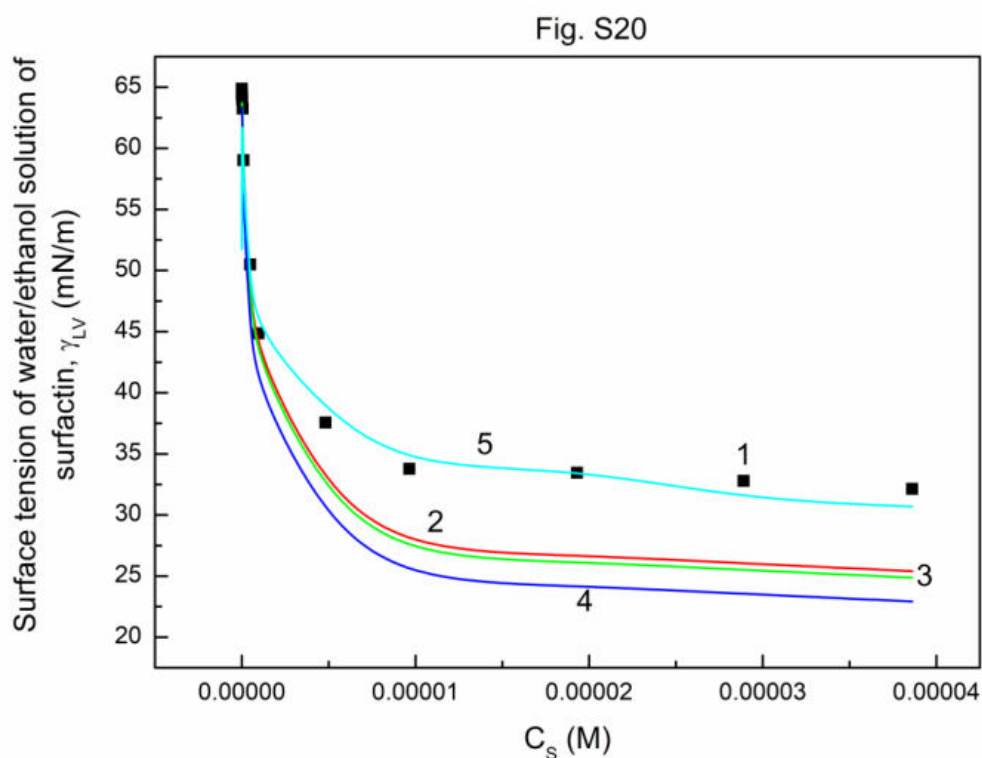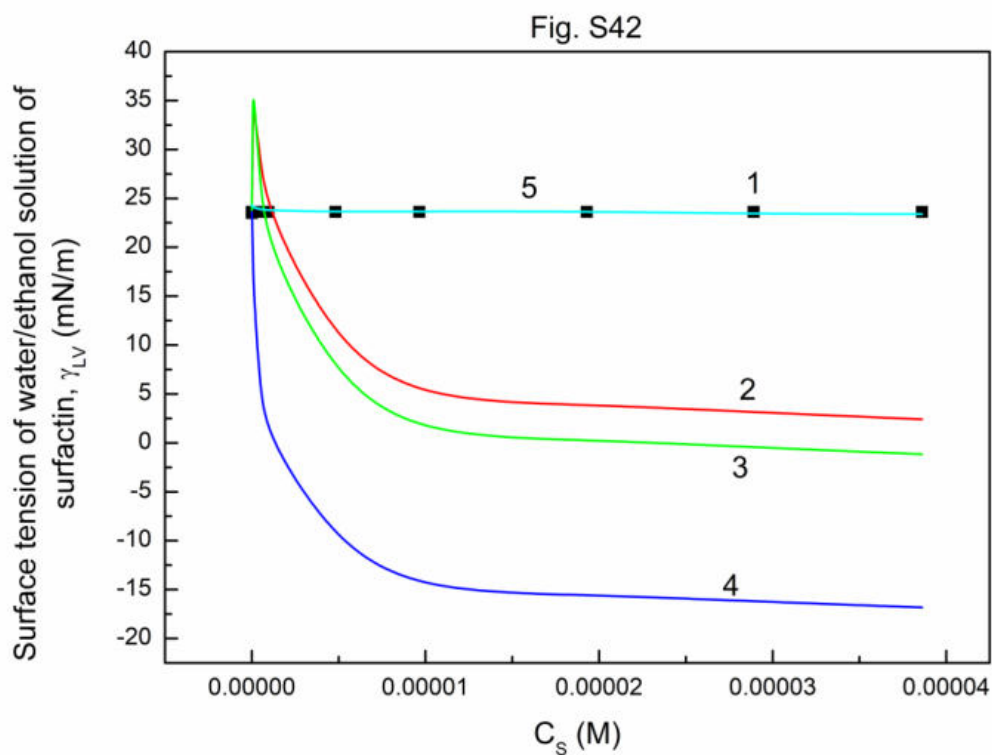
Fig. S20. A plot of the surface tension of water/ethanol solution of surfactin (γ_{LV}) at the constant ethanol concentration equal to 0.4015 M vs. the logarithm of surfactin concentration (C_S). Points 1 correspond to the measured values, lines 2 and 3 correspond to the values calculated from the Miller et al. equation for ω equal to 5.61 x 10^5 m^2/mol and 7.24 x m^2/mol, line 4 corresponds to the value resulting from independent adsorption and line 5 corresponds to the value calculated from the Connors equation.
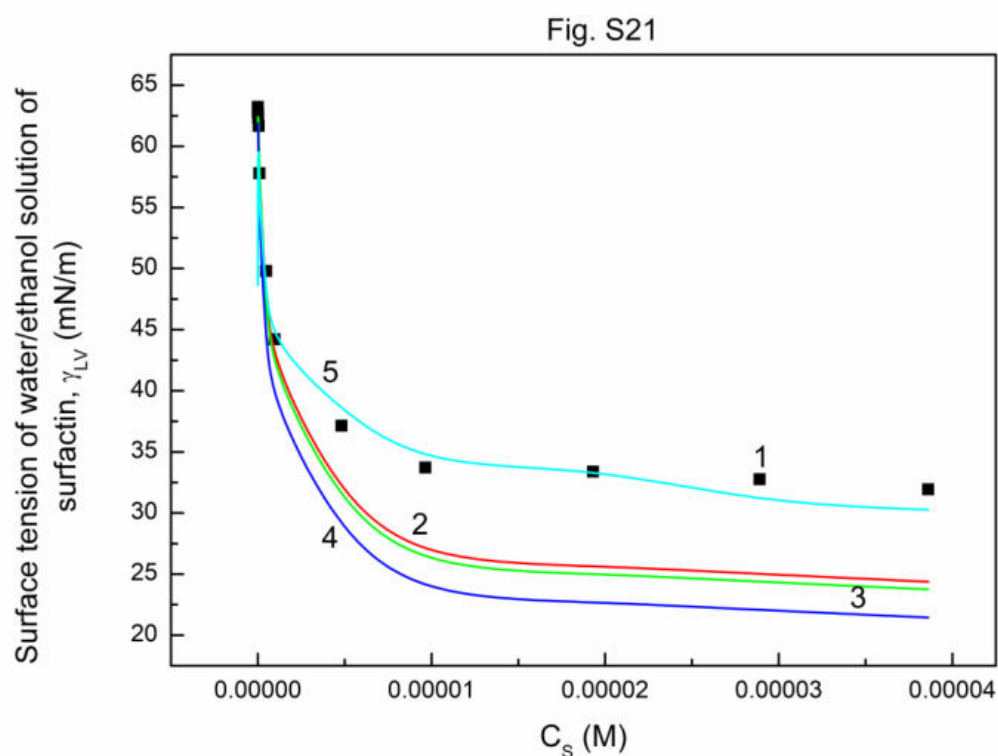
Fig. S21. A plot of the surface tension of water/ethanol solution of surfactin (γ_{LV}) at the constant ethanol concentration equal to 0.535 M vs. the logarithm of surfactin concentration (C_S). Points 1 correspond to the measured values, lines 2 and 3 correspond to the values calculated from the Miller et al. equation for ω equal to 5.61 x 10^5 m^2/mol and 7.24 x m^2/mol, line 4 corresponds to the value resulting from independent adsorption and line 5 corresponds to the value calculated from the Connors equation.
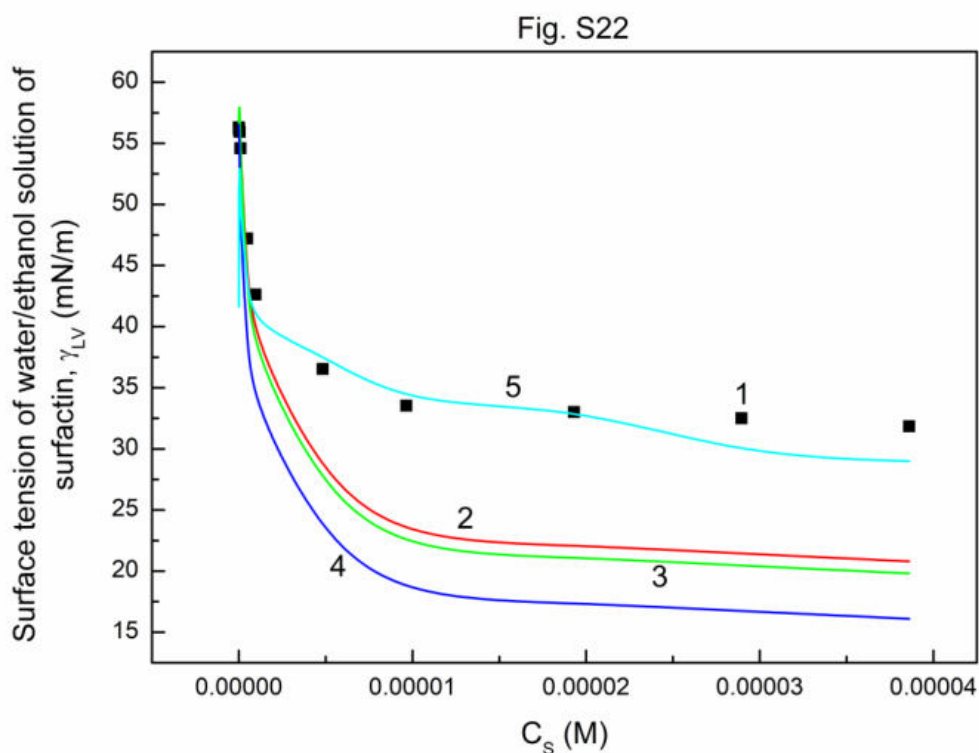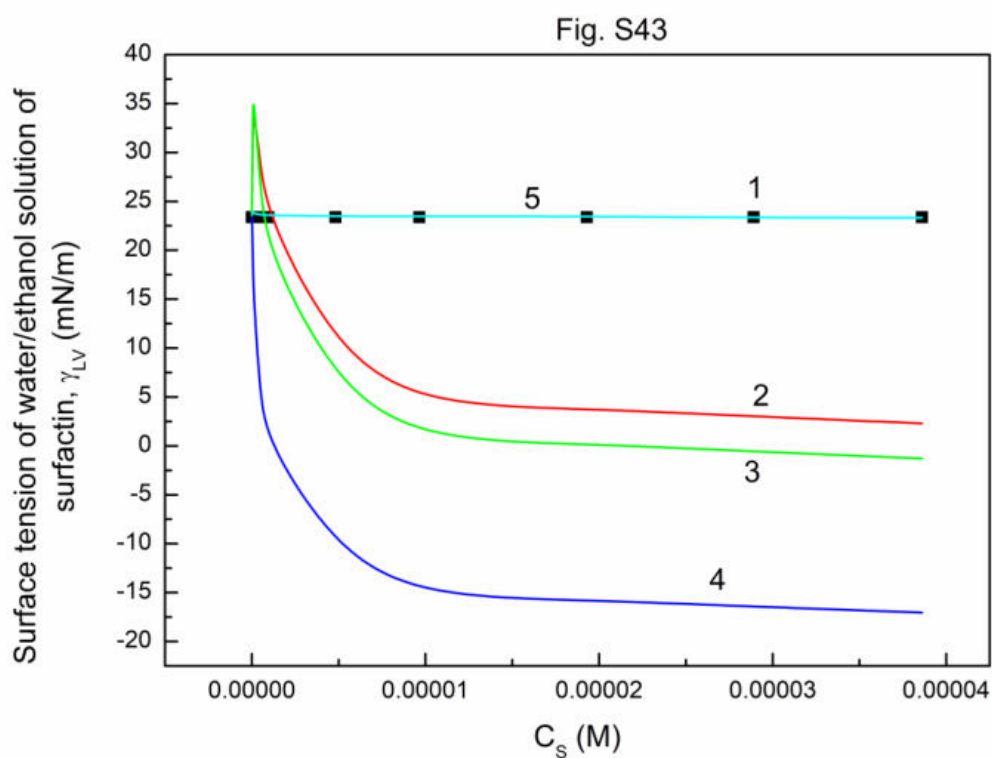
Fig. S22. A plot of the surface tension of water/ethanol solution of surfactin (γ_{LV}) at the constant ethanol concentration equal to 1.0706 M vs. the logarithm of surfactin concentration (C_S). Points 1 correspond to the measured values, lines 2 and 3 correspond to the values calculated from the Miller et al. equation for ω equal to 5.61 x 10^5 m^2/mol and 7.24 x m^2/mol, line 4 corresponds to the value resulting from independent adsorption and line 5 corresponds to the value calculated from the Connors equation.
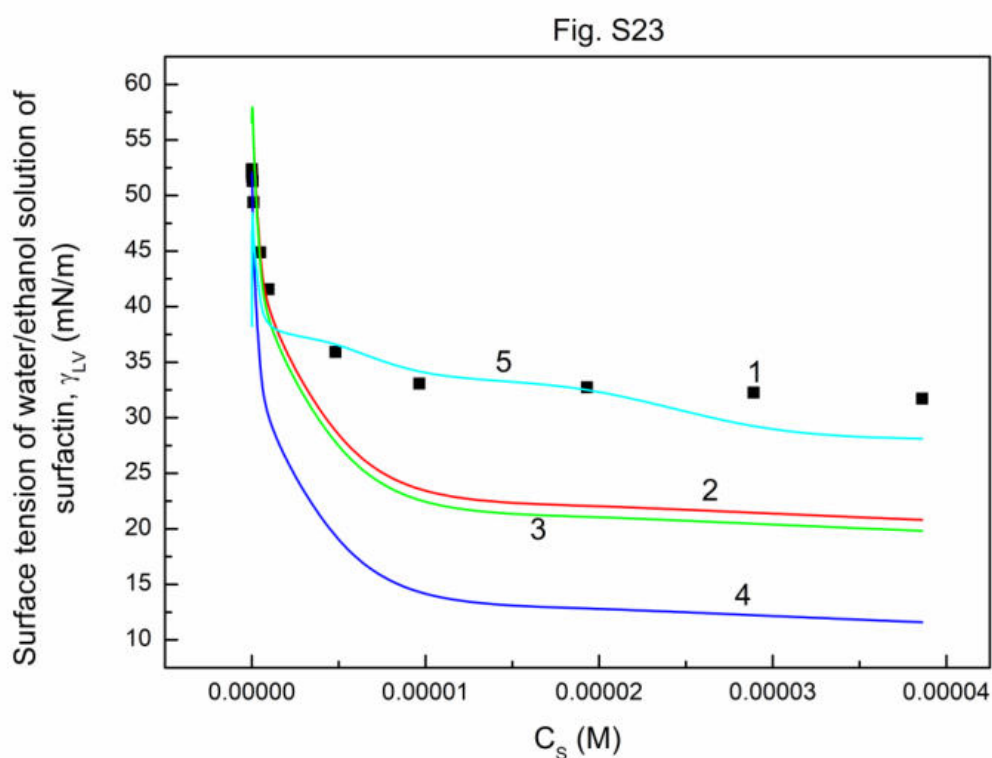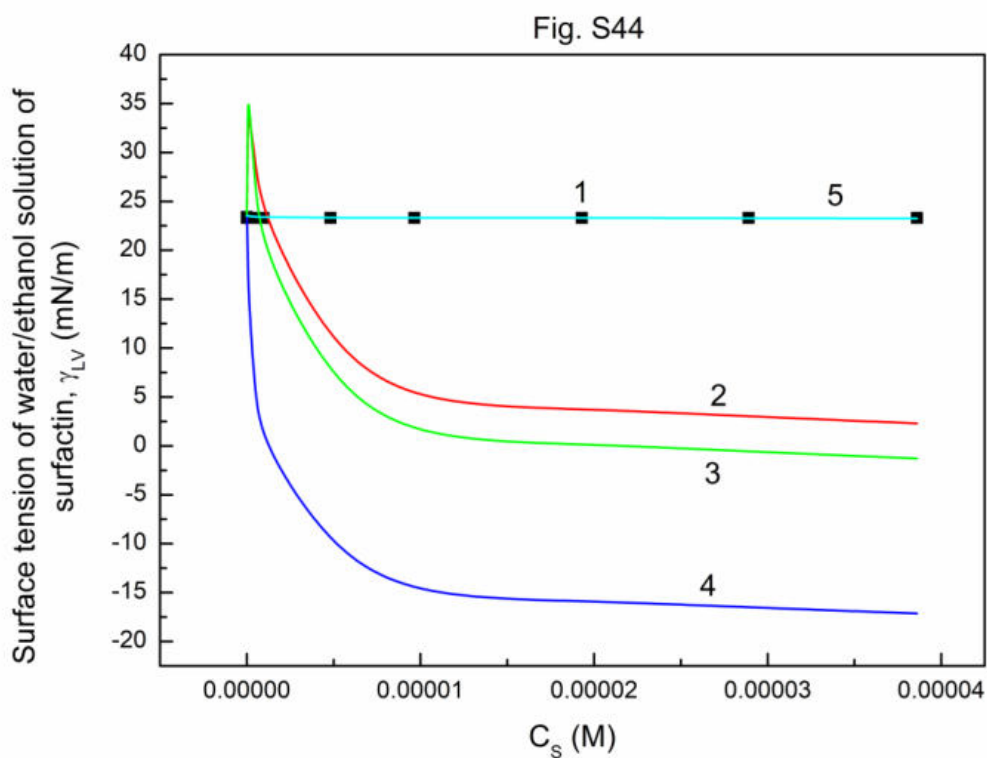
Fig. S23. A plot of the surface tension of water/ethanol solution of surfactin (γ_{LV}) at the constant ethanol concentration equal to 1.6062 M vs. the logarithm of surfactin concentration (C_S). Points 1 correspond to the measured values, lines 2 and 3 correspond to the values calculated from the Miller et al. equation for ω equal to 5.61 x 10^5 m^2/mol and 7.24 x m^2/mol, line 4 corresponds to the value resulting from independent adsorption and line 5 corresponds to the value calculated from the Connors equation.
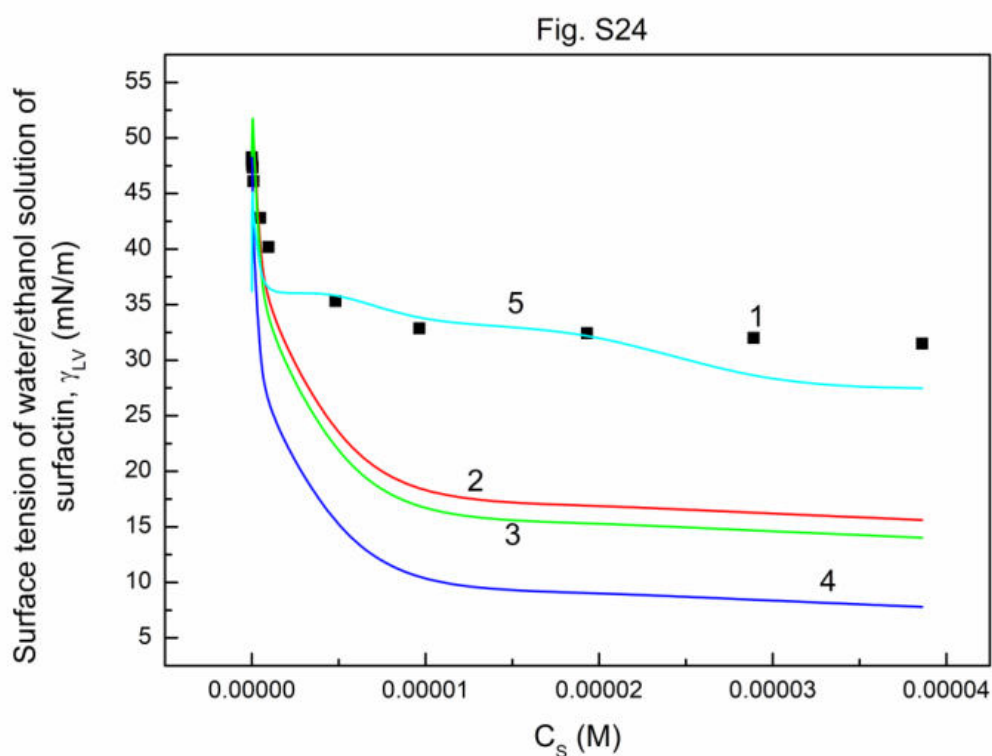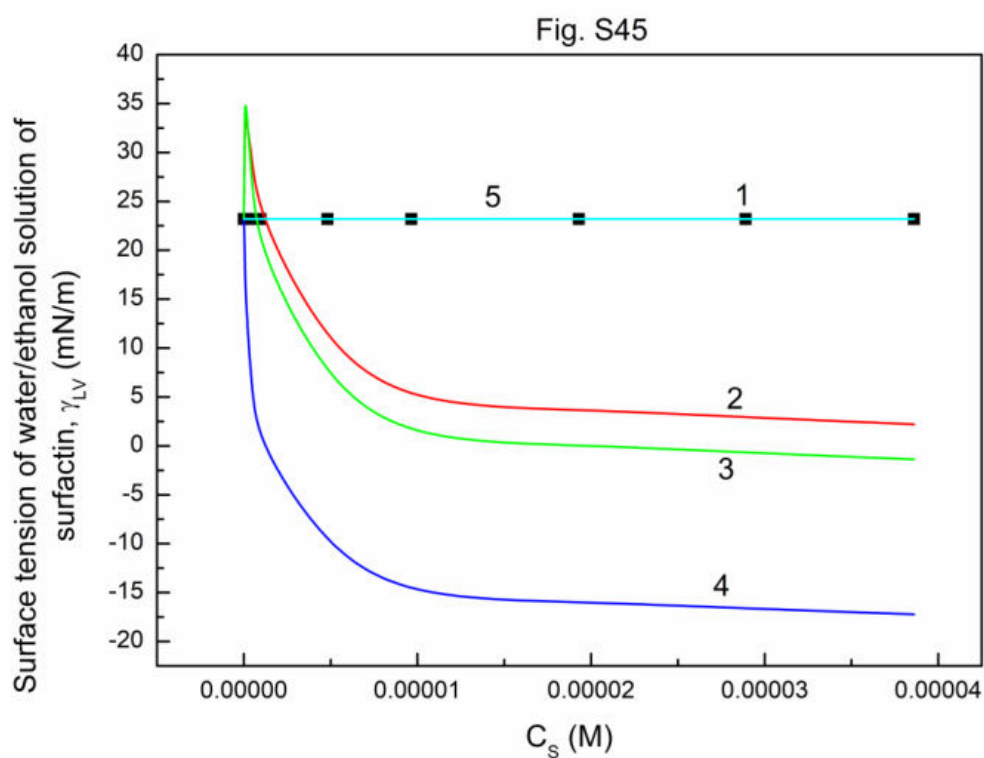
Fig. S24. A plot of the surface tension of water/ethanol solution of surfactin (γ_{LV}) at the constant ethanol concentration equal to 2.1416 M vs. the logarithm of surfactin concentration (C_S). Points 1 correspond to the measured values, lines 2 and 3 correspond to the values calculated from the Miller et al. equation for ω equal to 5.61 x 10^5 m^2/mol and 7.24 x m^2/mol, line 4 corresponds to the value resulting from independent adsorption and line 5 corresponds to the value calculated from the Connors equation.
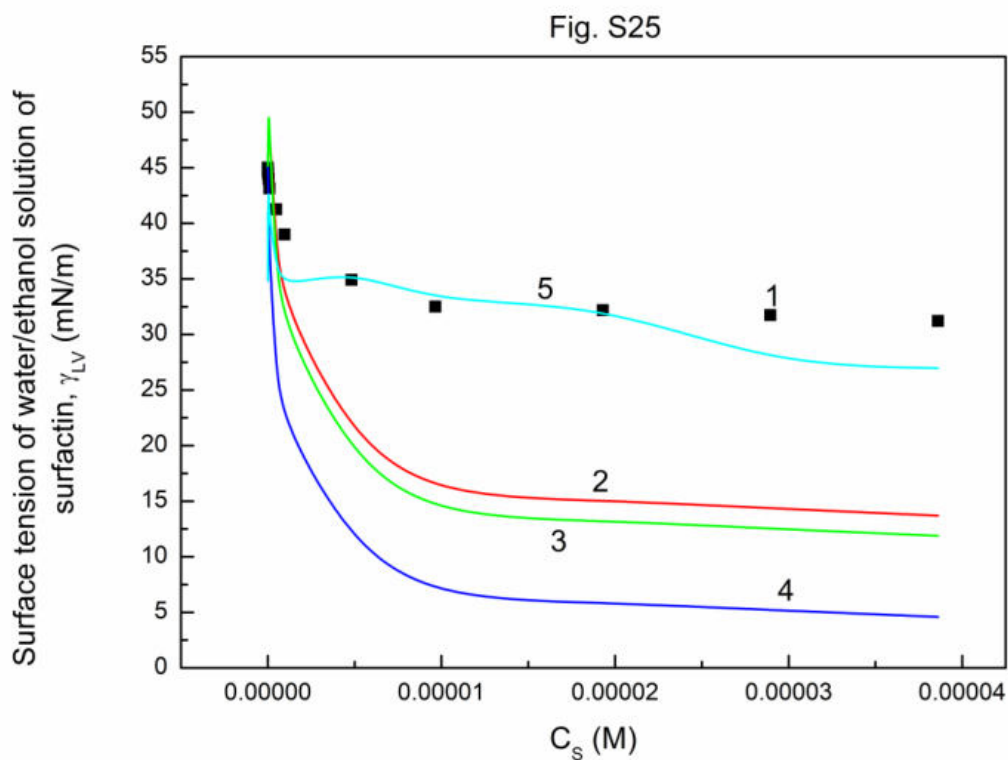
Fig. S25. A plot of the surface tension of water/ethanol solution of surfactin (γ_{LV}) at the constant ethanol concentration equal to 2.677 M vs. the logarithm of surfactin concentration (C_S). Points 1 correspond to the measured values, lines 2 and 3 correspond to the values calculated from the Miller et al. equation for ω equal to 5.61 x 10^5 m^2/mol and 7.24 x m^2/mol, line 4 corresponds to the value resulting from independent adsorption and line 5 corresponds to the value calculated from the Connors equation.
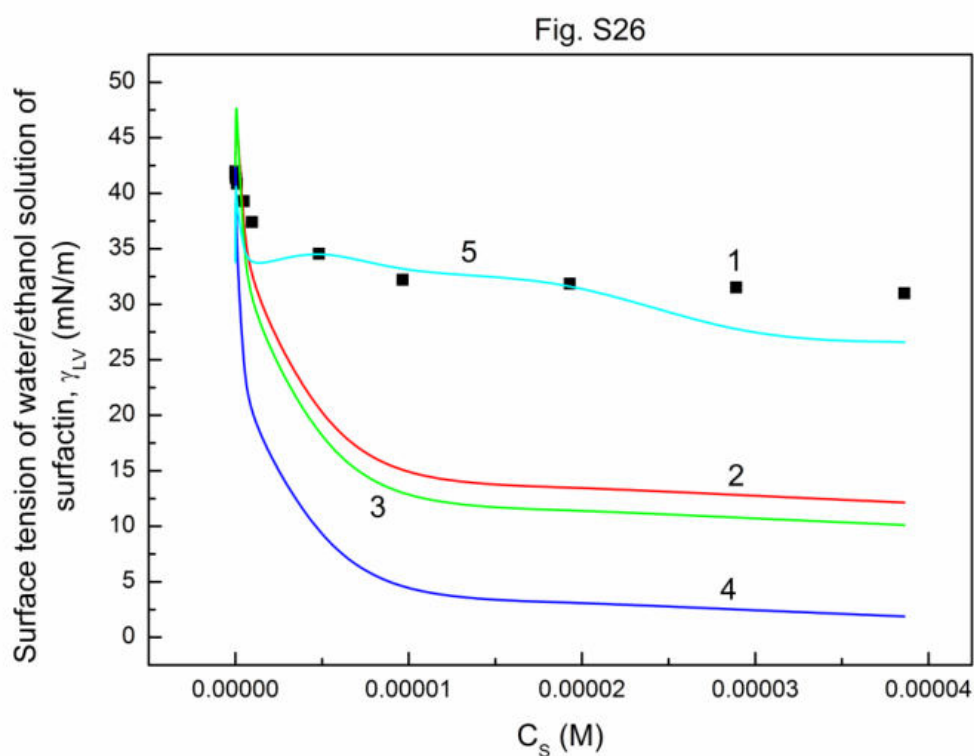
Fig. S26. A plot of the surface tension of water/ethanol solution of surfactin (γ_{LV}) at the constant ethanol concentration equal to 3.2124 M vs. the logarithm of surfactin concentration (C_S). Points 1 correspond to the measured values, lines 2 and 3 correspond to the values calculated from the Miller et al. equation for ω equal to 5.61 x 10^5 m^2/mol and 7.24 x m^2/mol, line 4 corresponds to the value resulting from independent adsorption and line 5 corresponds to the value calculated from the Connors equation.

Fig. S27. A plot of the surface tension of water/ethanol solution of surfactin (γ_{LV}) at the constant ethanol concentration equal to 3.7478 M vs. the logarithm of surfactin concentration (C_S). Points 1 correspond to the measured values, lines 2 and 3 correspond to the values calculated from the Miller et al. equation for ω equal to 5.61 x 10^5 m^2/mol and 7.24 x m^2/mol, line 4 corresponds to the value resulting from independent adsorption and line 5 corresponds to the value calculated from the Connors equation.

Fig. S28. A plot of the surface tension of water/ethanol solution of surfactin (γ_{LV}) at the constant ethanol concentration equal to 4.2832 M vs. the logarithm of surfactin concentration (C_S). Points 1 correspond to the measured values, lines 2 and 3 correspond to the values calculated from the Miller et al. equation for ω equal to 5.61 x 10^5 m^2/mol and 7.24 x m^2/mol, line 4 corresponds to the value resulting from independent adsorption and line 5 corresponds to the value calculated from the Connors equation.

Fig. S29. A plot of the surface tension of water/ethanol solution of surfactin (γ_{LV}) at the constant ethanol concentration equal to 4.8185 M vs. the logarithm of surfactin concentration (C_S). Points 1 correspond to the measured values, lines 2 and 3 correspond to the values calculated from the Miller et al. equation for ω equal to 5.61 x 10^5 m^2/mol and 7.24 x m^2/mol, line 4 corresponds to the value resulting from independent adsorption and line 5 corresponds to the value calculated from the Connors equation.

Fig. S30. A plot of the surface tension of water/ethanol solution of surfactin (γ_{LV}) at the constant ethanol concentration equal to 5.3538 M vs. the logarithm of surfactin concentration (C_S). Points 1 correspond to the measured values, lines 2 and 3 correspond to the values calculated from the Miller et al. equation for ω equal to 5.61 x 10^5 m^2/mol and 7.24 x m^2/mol, line 4 corresponds to the value resulting from independent adsorption and line 5 corresponds to the value calculated from the Connors equation.

Fig. S31. A plot of the surface tension of water/ethanol solution of surfactin (γ_{LV}) at the constant ethanol concentration equal to 5.8893 M vs. the logarithm of surfactin concentration (C_S). Points 1 correspond to the measured values, lines 2 and 3 correspond to the values calculated from the Miller et al. equation for ω equal to 5.61 x 10^5 m^2/mol and 7.24 x m^2/mol, line 4 corresponds to the value resulting from independent adsorption and line 5 corresponds to the value calculated from the Connors equation.

Fig. S32. A plot of the surface tension of water/ethanol solution of surfactin (γ_{LV}) at the constant ethanol concentration equal to 6.6925 M vs. the logarithm of surfactin concentration (C_S). Points 1 correspond to the measured values, lines 2 and 3 correspond to the values calculated from the Miller et al. equation for ω equal to 5.61 x 10^5 m^2/mol and 7.24 x m^2/mol, line 4 corresponds to the value resulting from independent adsorption and line 5 corresponds to the value calculated from the Connors equation.

Fig. S33. A plot of the surface tension of water/ethanol solution of surfactin (γ_{LV}) at the constant ethanol concentration equal to 7.7245 M vs. the logarithm of surfactin concentration (C_S). Points 1 correspond to the measured values, lines 2 and 3 correspond to the values calculated from the Miller et al. equation for ω equal to 5.61 x 10^5 m^2/mol and 7.24 x m^2/mol, line 4 corresponds to the value resulting from independent adsorption and line 5 corresponds to the value calculated from the Connors equation.

Fig. S34. A plot of the surface tension of water/ethanol solution of surfactin (γ_{LV}) at the constant ethanol concentration equal to 8.5664 M vs. the logarithm of surfactin concentration (C_S). Points 1 correspond to the measured values, lines 2 and 3 correspond to the values calculated from the Miller et al. equation for ω equal to 5.61 x 10^5 m^2/mol and 7.24 x m^2/mol, line 4 corresponds to the value resulting from independent adsorption and line 5 corresponds to the value calculated from the Connors equation.

Fig. S35. A plot of the surface tension of water/ethanol solution of surfactin (γ_{LV}) at the
constant ethanol concentration equal to 10.2797 M vs. the logarithm of surfactin
concentration (C_S). Points 1 correspond to the measured values, lines 2 and 3
correspond to the values calculated from the Miller et al. equation for ω equal to 5.61
x 10^5 m^2/mol and 7.24 x m^2/mol, line 4 corresponds to the value resulting from
independent adsorption and line 5 corresponds to the value calculated from the
Connors equation.

Fig. S36. A plot of the surface tension of water/ethanol solution of surfactin (γ_{LV}) at the constant ethanol concentration equal to 11.968 M vs. the logarithm of surfactin concentration (C_S). Points 1 correspond to the measured values, lines 2 and 3 correspond to the values calculated from the Miller et al. equation for ω equal to 5.61 x 10^5 m^2/mol and 7.24 x m^2/mol, line 4 corresponds to the value resulting from independent adsorption and line 5 corresponds to the value calculated from the Connors equation.

Fig. S37. A plot of the surface tension of water/ethanol solution of surfactin (γ_{LV}) at the constant ethanol concentration equal to 12.145 M vs. the logarithm of surfactin concentration (C_S). Points 1 correspond to the measured values, lines 2 and 3 correspond to the values calculated from the Miller et al. equation for ω equal to 5.61 x 10^5 m^2/mol and 7.24 x m^2/mol, line 4 corresponds to the value resulting from independent adsorption and line 5 corresponds to the value calculated from the Connors equation.

Fig. S38. A plot of the surface tension of water/ethanol solution of surfactin (γ_{LV}) at the constant ethanol concentration equal to 13.3794 M vs. the logarithm of surfactin concentration (C_S). Points 1 correspond to the measured values, lines 2 and 3 correspond to the values calculated from the Miller et al. equation for ω equal to 5.61 x 10^5 m^2/mol and 7.24 x m^2/mol, line 4 corresponds to the value resulting from independent adsorption and line 5 corresponds to the value calculated from the Connors equation.

Fig. S39. A plot of the surface tension of water/ethanol solution of surfactin (γ_{LV}) at the constant ethanol concentration equal to 14.5696 M vs. the logarithm of surfactin concentration (C_S). Points 1 correspond to the measured values, lines 2 and 3 correspond to the values calculated from the Miller et al. equation for ω equal to 5.61 x 10^5 m^2/mol and 7.24 x m^2/mol, line 4 corresponds to the value resulting from independent adsorption and line 5 corresponds to the value calculated from the Connors equation.

Fig. S40. A plot of the surface tension of water/ethanol solution of surfactin (γ_{LV}) at the constant ethanol concentration equal to 15.4064 M vs. the logarithm of surfactin concentration (C_S). Points 1 correspond to the measured values, lines 2 and 3 correspond to the values calculated from the Miller et al. equation for ω equal to 5.61 x 10^5 m^2/mol and 7.24 x m^2/mol, line 4 corresponds to the value resulting from independent adsorption and line 5 corresponds to the value calculated from the Connors equation.

Fig. S41. A plot of the surface tension of water/ethanol solution of surfactin (γ_{LV}) at the constant ethanol concentration equal to 16.084 M vs. the logarithm of surfactin concentration (C_S). Points 1 correspond to the measured values, lines 2 and 3 correspond to the values calculated from the Miller et al. equation for ω equal to 5.61 x 10^5 m^2/mol and 7.24 x m^2/mol, line 4 corresponds to the value resulting from independent adsorption and line 5 corresponds to the value calculated from the Connors equation.

Fig. S42. A plot of the surface tension of water/ethanol solution of surfactin (γ_{LV}) at the constant ethanol concentration equal to 16.3777 M vs. the logarithm of surfactin concentration (C_S). Points 1 correspond to the measured values, lines 2 and 3 correspond to the values calculated from the Miller et al. equation for ω equal to 5.61 x 10^5 m^2/mol and 7.24 x m^2/mol, line 4 corresponds to the value resulting from independent adsorption and line 5 corresponds to the value calculated from the Connors equation.

Fig. S43. A plot of the surface tension of water/ethanol solution of surfactin (γ_{LV}) at the constant ethanol concentration equal to 16.648 M vs. the logarithm of surfactin concentration (C_S). Points 1 correspond to the measured values, lines 2 and 3 correspond to the values calculated from the Miller et al. equation for ω equal to 5.61 x 10^5 m^2/mol and 7.24 x m^2/mol, line 4 corresponds to the value resulting from independent adsorption and line 5 corresponds to the value calculated from the Connors equation.

Fig. S44. A plot of the surface tension of water/ethanol solution of surfactin (γ_{LV}) at the constant ethanol concentration equal to 16.8988 M vs. the logarithm of surfactin concentration (C_S). Points 1 correspond to the measured values, lines 2 and 3 correspond to the values calculated from the Miller et al. equation for ω equal to 5.61 x 10^5 m^2/mol and 7.24 x m^2/mol, line 4 corresponds to the value resulting from independent adsorption and line 5 corresponds to the value calculated from the Connors equation.

Fig. S45. A plot of the surface tension of water/ethanol solution of surfactin (γ_{LV}) at the constant ethanol concentration equal to 17.13 M vs. the logarithm of surfactin concentration (C_S). Points 1 correspond to the measured values, lines 2 and 3 correspond to the values calculated from the Miller et al. equation for ω equal to 5.61 x 10^5 m²/mol and 7.24 x m²/mol, line 4 corresponds to the value resulting from independent adsorption and line 5 corresponds to the value calculated from the Connors equation.
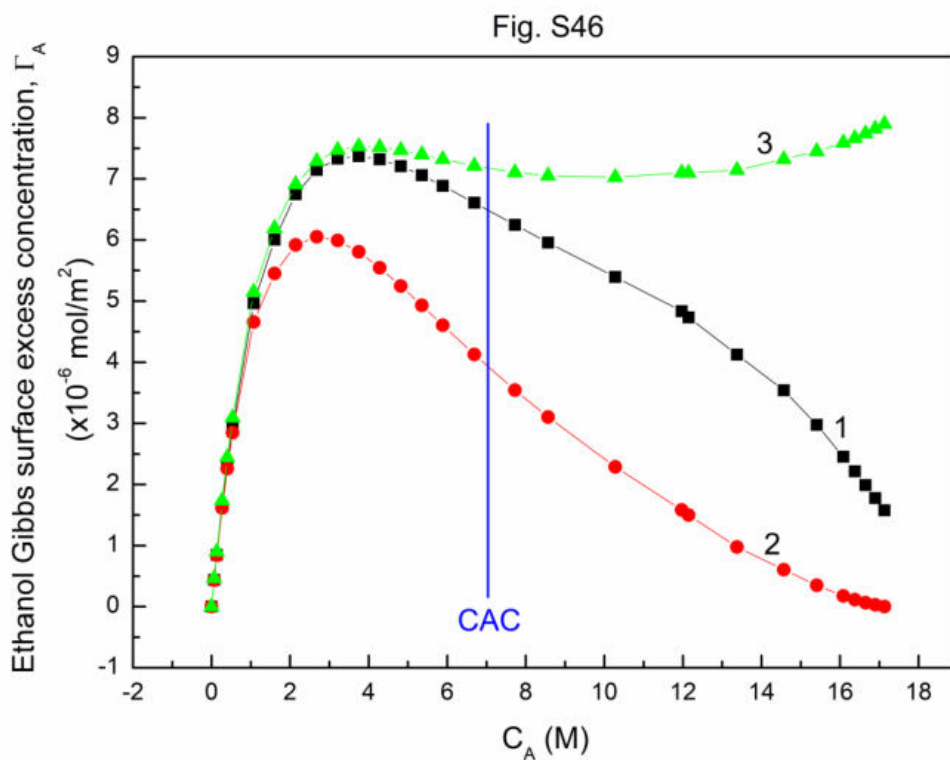
Fig. S46. A plot of the ethanol surface excess concentration calculated from the Gibbs equation based on its activity (curve 1), the Guggenheim-Adam equation (curve 2) and the total ethanol concentration calculated from Eq. (1) (curve 3) vs. the logarithm of ethanol concentration (C_A) at the constant surfactin concentration equal to 0.0002 mg/dm^3.
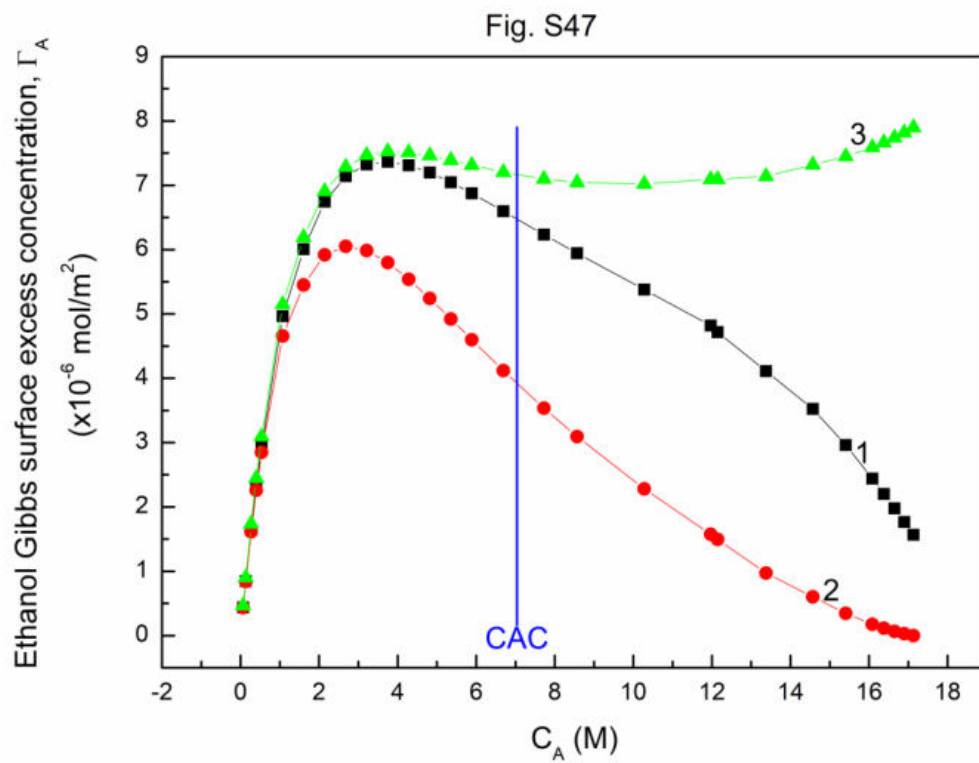
Fig. S47. A plot of the ethanol surface excess concentration calculated from the Gibbs equation based on its activity (curve 1), the Guggenheim-Adam equation (curve 2) and the total ethanol concentration calculated from Eq. (1) (curve 3) vs. the logarithm of ethanol concentration (C_A) at the constant surfactin concentration equal to 0.0005 mg/dm^3.
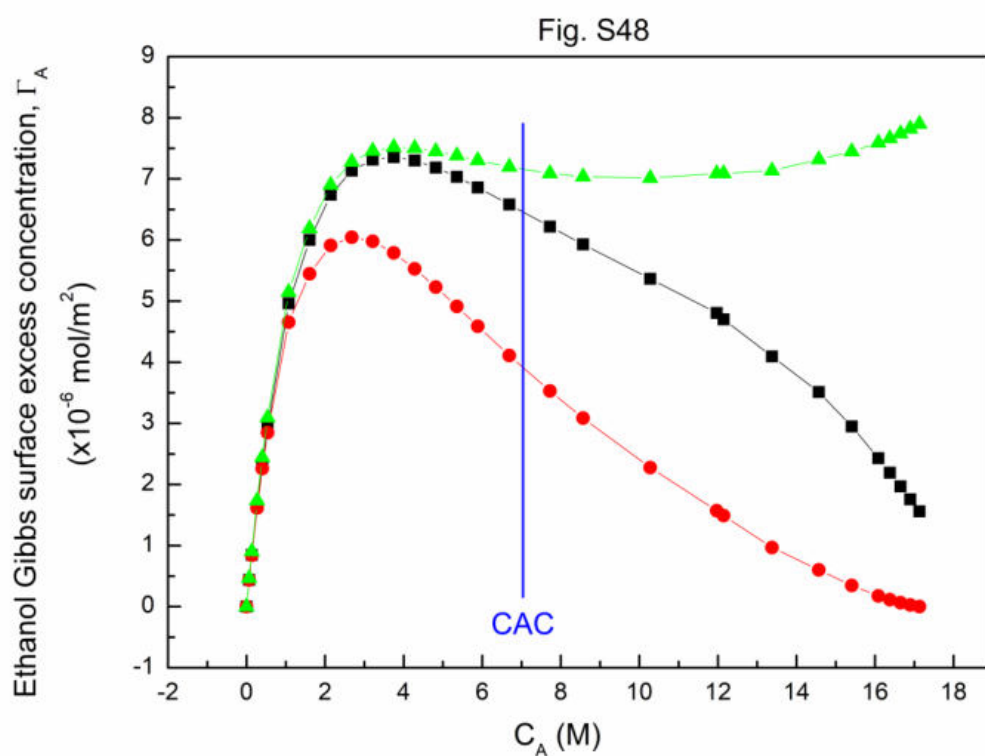
Fig. S48. A plot of the ethanol surface excess concentration calculated from the Gibbs
equation based on its activity (curve 1), the Guggenheim-Adam equation (curve 2) and
the total ethanol concentration calculated from Eq. (1) (curve 3) vs. the logarithm of
ethanol concentration (C_A) at the constant surfactin concentration equal to 0.00125
mg/dm^3.
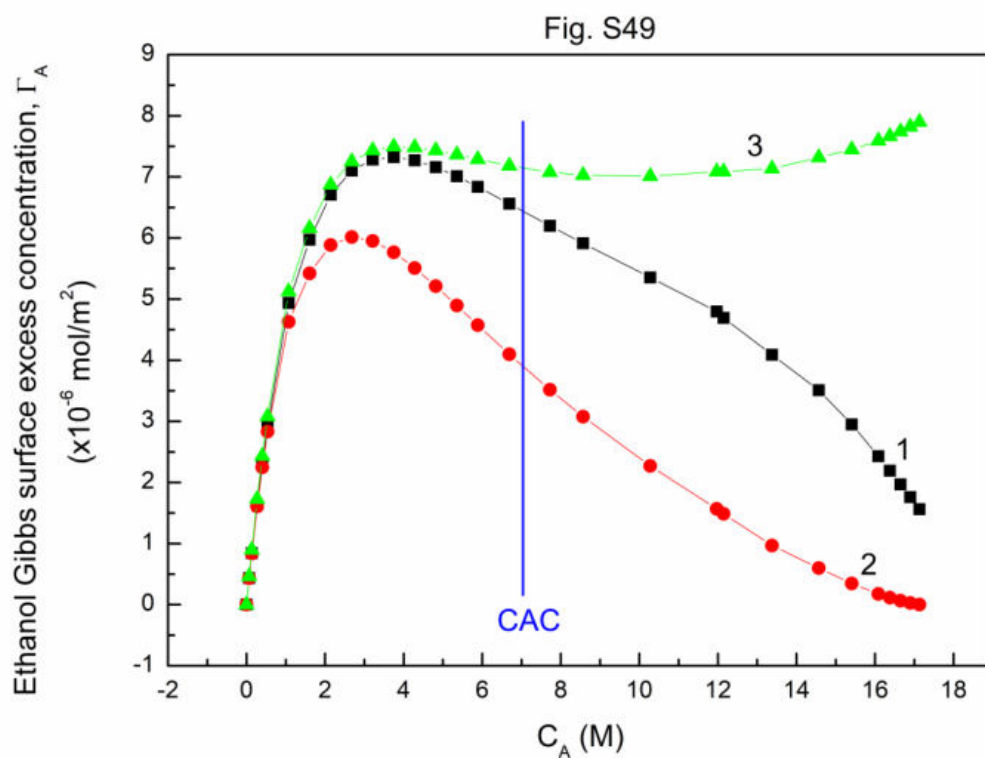
Fig. S49. A plot of the ethanol surface excess concentration calculated from the Gibbs equation based on its activity (curve 1), the Guggenheim-Adam equation (curve 2) and the total ethanol concentration calculated from Eq. (1) (curve 3) vs. the logarithm of ethanol concentration (C_A) at the constant surfactin concentration equal to 0.003 mg/dm^3.
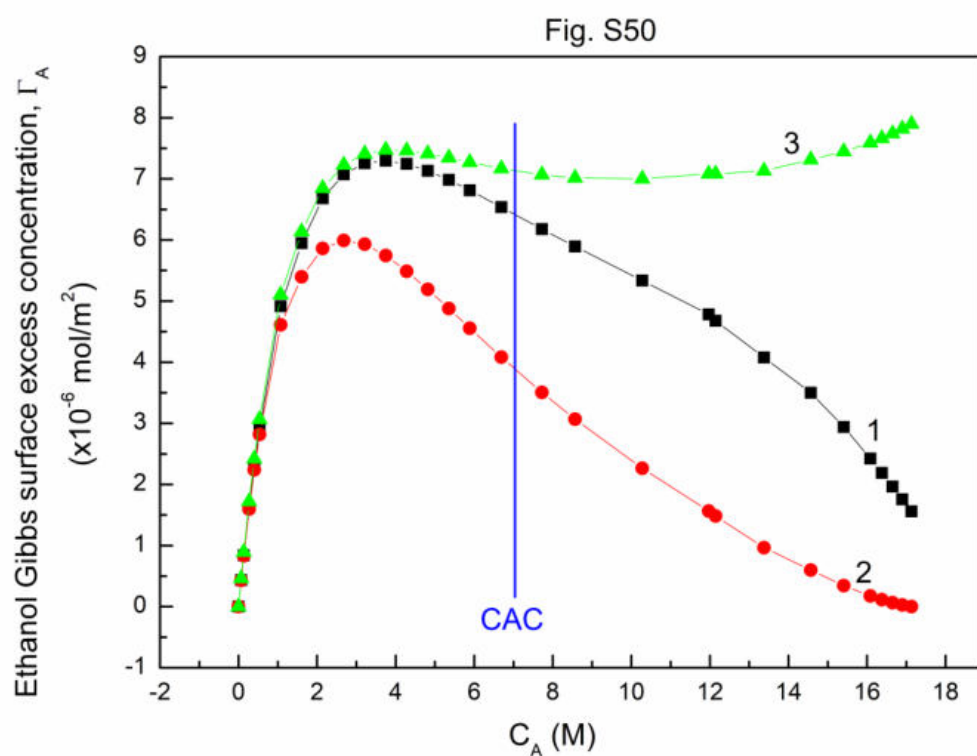
Fig. S50. A plot of the ethanol surface excess concentration calculated from the Gibbs equation based on its activity (curve 1), the Guggenheim-Adam equation (curve 2) and the total ethanol concentration calculated from Eq. (1) (curve 3) vs. the logarithm of ethanol concentration (C_A) at the constant surfactin concentration equal to 0.00625 mg/dm^3.
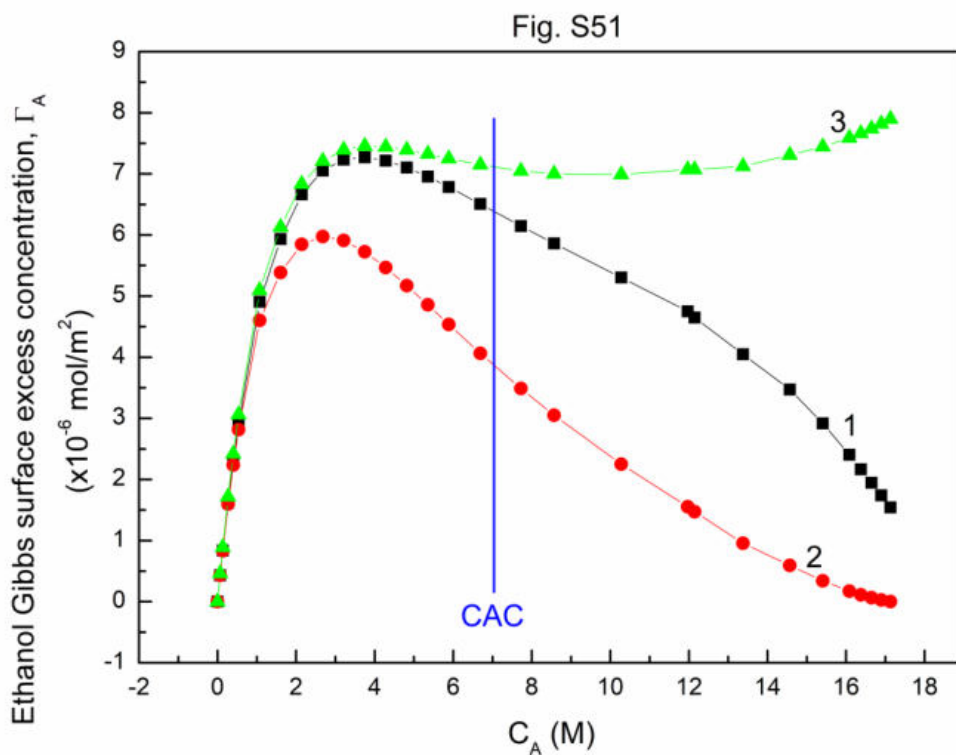
Fig. S51. A plot of the ethanol surface excess concentration calculated from the Gibbs equation based on its activity (curve 1), the Guggenheim-Adam equation (curve 2) and the total ethanol concentration calculated from Eq. (1) (curve 3) vs. the logarithm of ethanol concentration (C_A) at the constant surfactin concentration equal to 0.01 mg/dm^3.
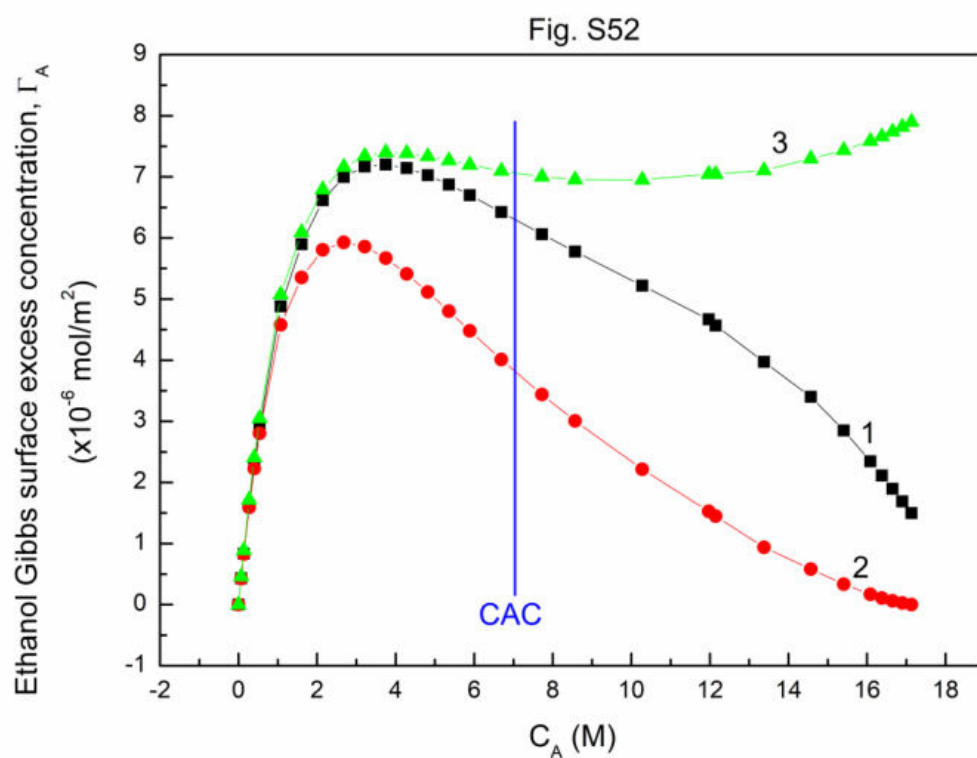
Fig. S52. A plot of the ethanol surface excess concentration calculated from the Gibbs equation based on its activity (curve 1), the Guggenheim-Adam equation (curve 2) and the total ethanol concentration calculated from Eq. (1) (curve 3) vs. the logarithm of ethanol concentration (C_A) at the constant surfactin concentration equal to 0.02 mg/dm^3.
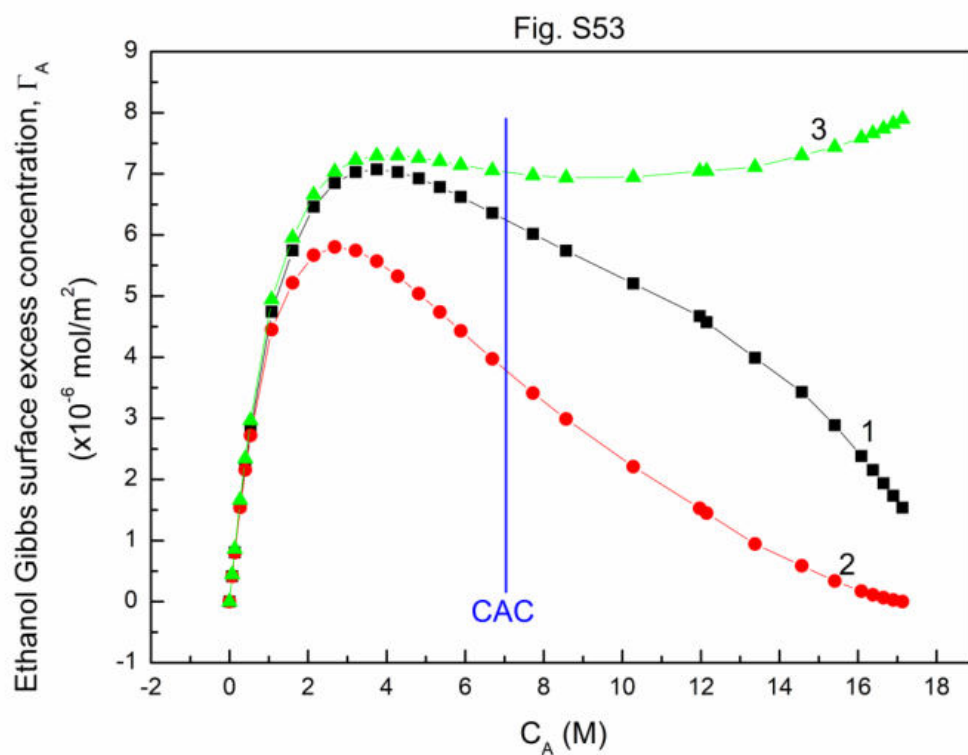
Fig. S53. A plot of the ethanol surface excess concentration calculated from the Gibbs equation based on its activity (curve 1), the Guggenheim-Adam equation (curve 2) and the total ethanol concentration calculated from Eq. (1) (curve 3) vs. the logarithm of ethanol concentration (C_A) at the constant surfactin concentration equal to 0.05 mg/dm^3.
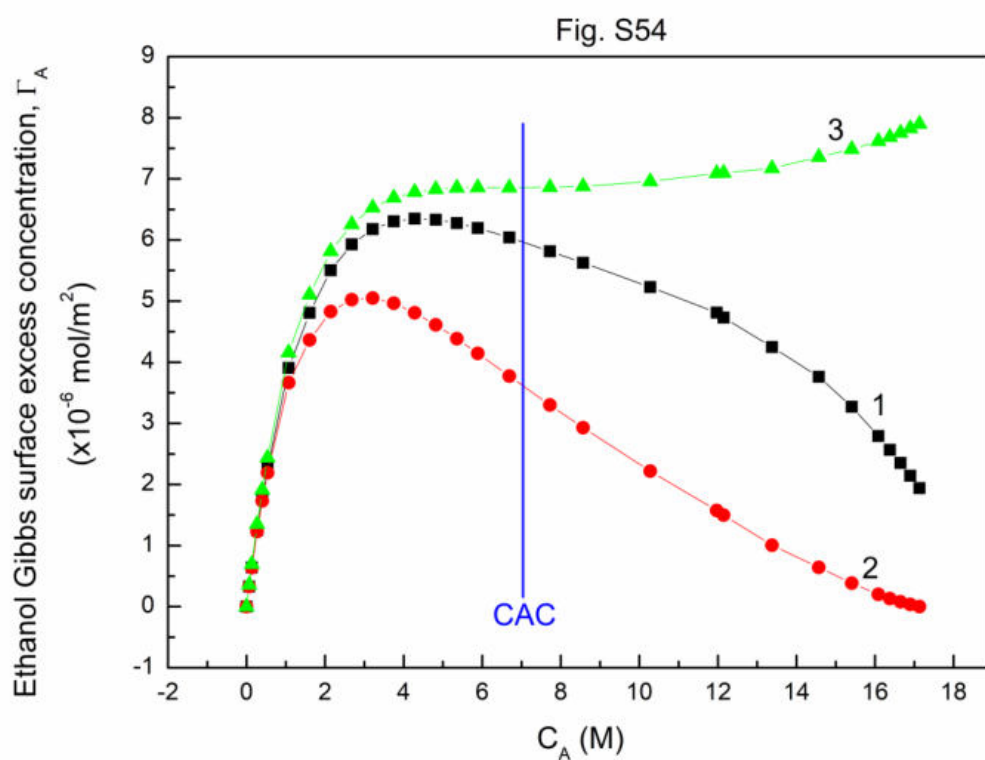
Fig. S54. A plot of the ethanol surface excess concentration calculated from the Gibbs equation based on its activity (curve 1), the Guggenheim-Adam equation (curve 2) and the total ethanol concentration calculated from Eq. (1) (curve 3) vs. the logarithm of ethanol concentration (C_A) at the constant surfactin concentration equal to 0.1 mg/dm^3.
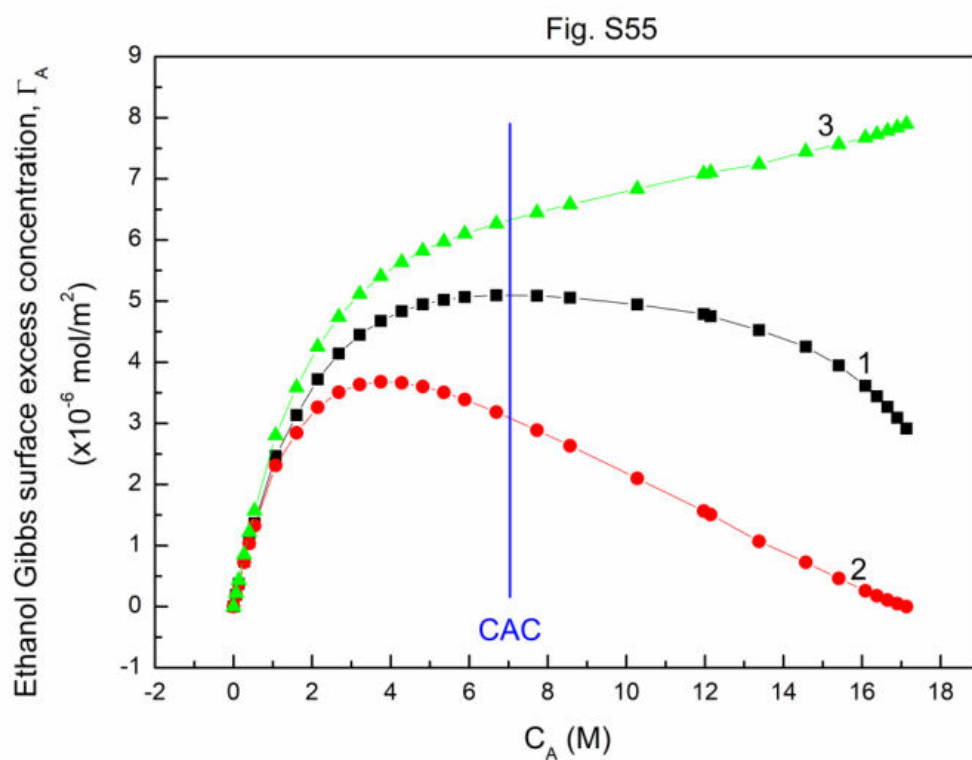
Fig. S55. A plot of the ethanol surface excess concentration calculated from the Gibbs equation based on its activity (curve 1), the Guggenheim-Adam equation (curve 2) and the total ethanol concentration calculated from Eq. (1) (curve 3) vs. the logarithm of ethanol concentration (C_A) at the constant surfactin concentration equal to 0.2 mg/dm^3.
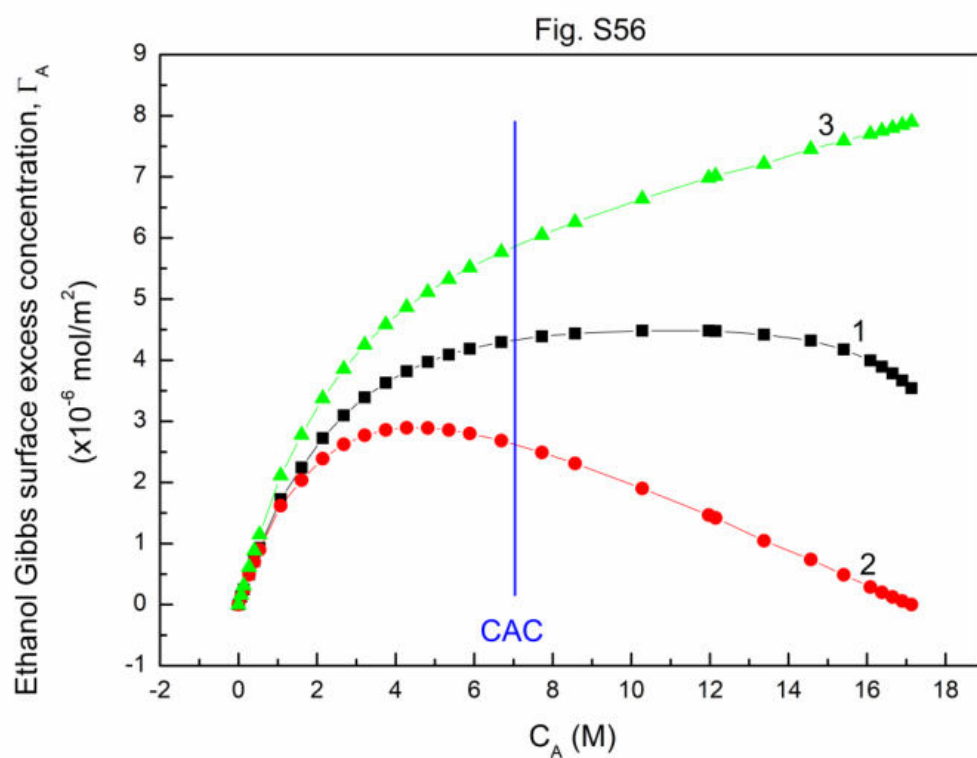
Fig. S56. A plot of the ethanol surface excess concentration calculated from the Gibbs
equation based on its activity (curve 1), the Guggenheim-Adam equation (curve 2) and
the total ethanol concentration calculated from Eq. (1) (curve 3) vs. the logarithm of
ethanol concentration (C_A) at the constant surfactin concentration equal to 1 mg/dm^3.
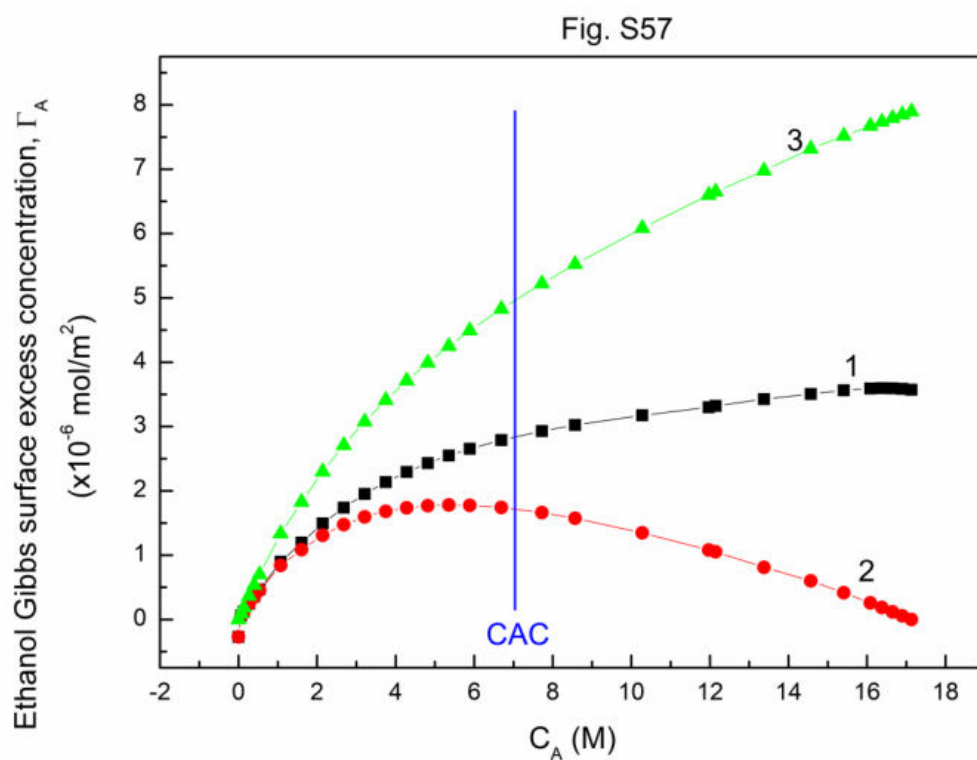
Fig. S57. A plot of the ethanol surface excess concentration calculated from the Gibbs equation based on its activity (curve 1), the Guggenheim-Adam equation (curve 2) and the total ethanol concentration calculated from Eq. (1) (curve 3) vs. the logarithm of ethanol concentration (C_A) at the constant surfactin concentration equal to 5 mg/dm^3.
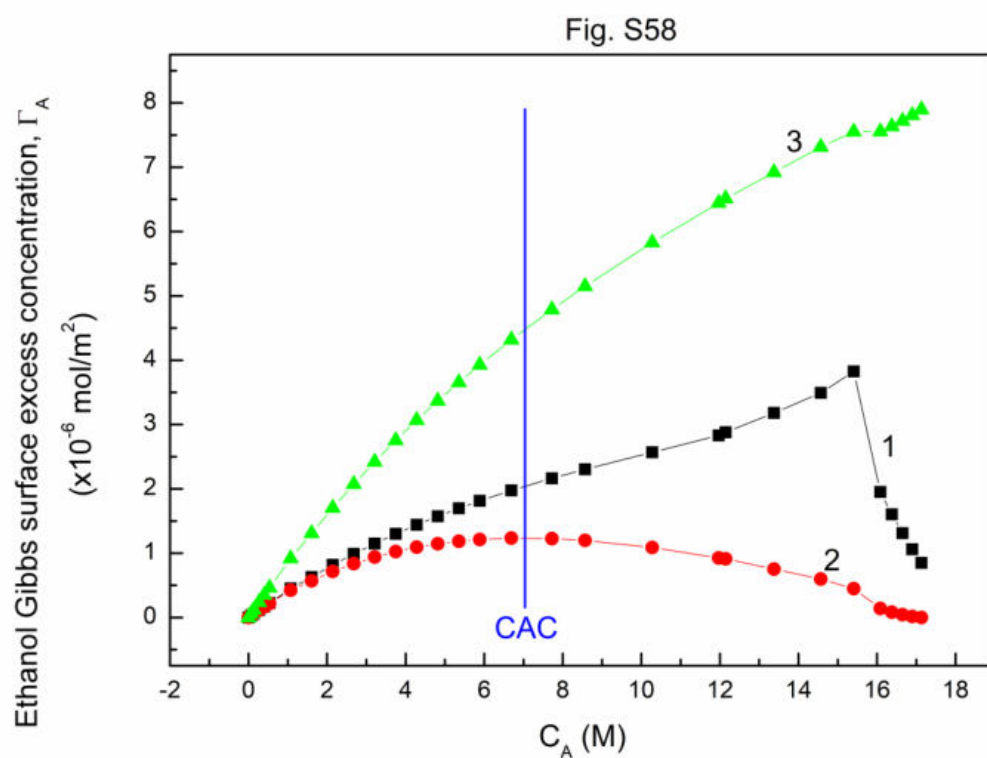
Fig. S58. A plot of the ethanol surface excess concentration calculated from the Gibbs equation based on its activity (curve 1), the Guggenheim-Adam equation (curve 2) and the total ethanol concentration calculated from Eq. (1) (curve 3) vs. the logarithm of ethanol concentration (C_A) at the constant surfactin concentration equal to 10 mg/dm^3.
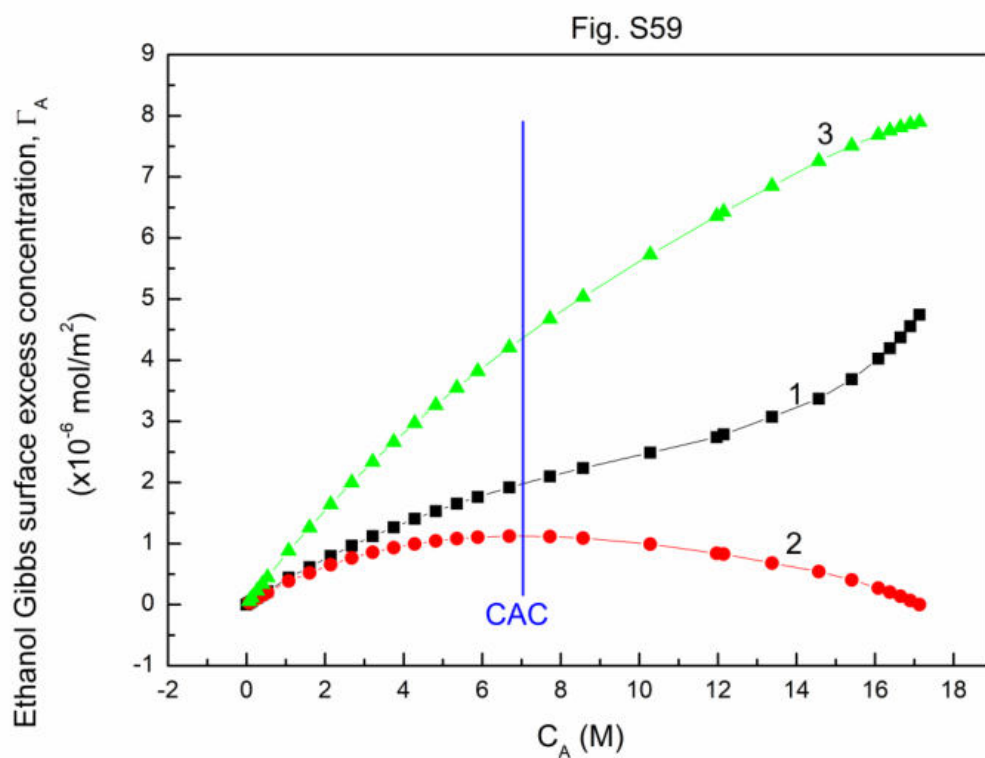
Fig. S59. A plot of the ethanol surface excess concentration calculated from the Gibbs equation based on its activity (curve 1), the Guggenheim-Adam equation (curve 2) and the total ethanol concentration calculated from Eq. (1) (curve 3) vs. the logarithm of ethanol concentration (C_A) at the constant surfactin concentration equal to 20 mg/dm^3.
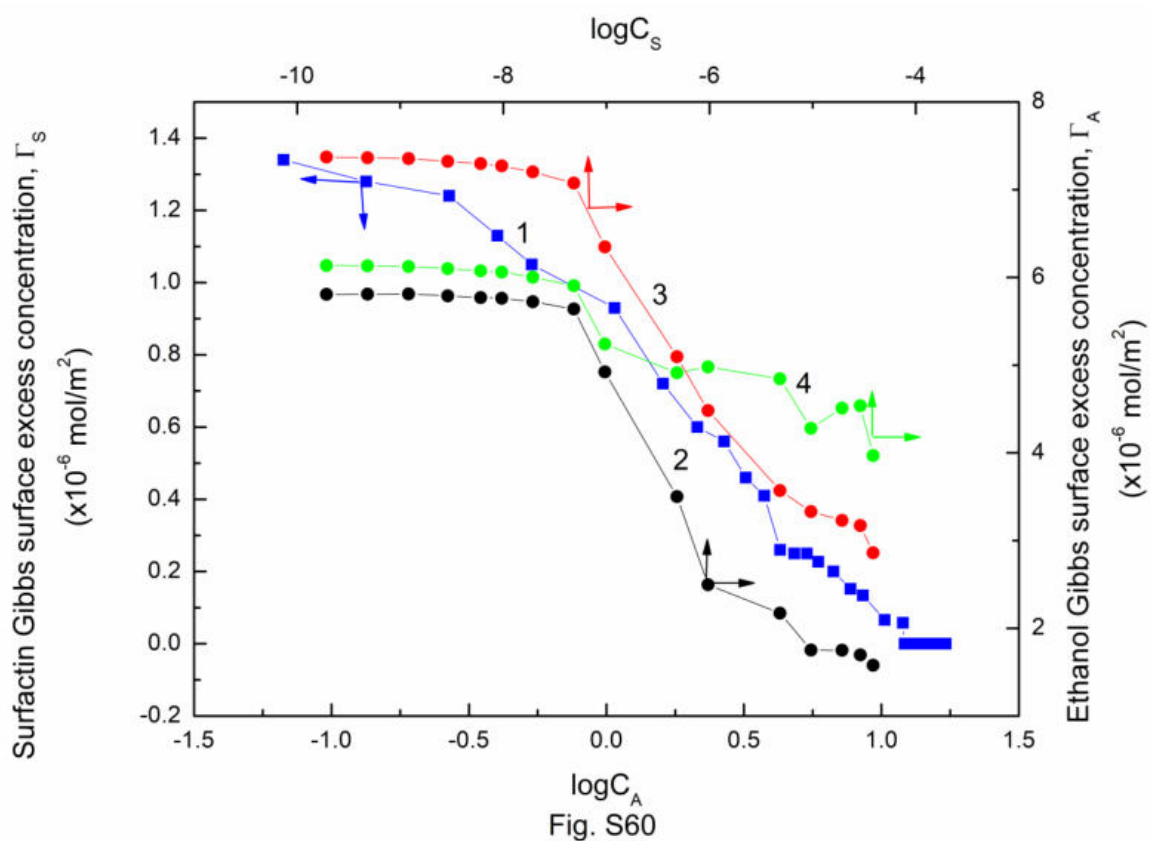
Fig. S60. A plot of the maximal Gibbs surface excess concentration of surfactin (curve 1) vs. the logarithm of ethanol concentration (C_A) and ethanol (curves 2 – 4) vs. the logarithm of surfactin concentration (C_S). Curves 2 – 4 correspond to the values of ethanol maximal Gibbs surface excess concentration calculated from the Gibbs equation based on the ethanol mole fraction, activity and mole concentration.
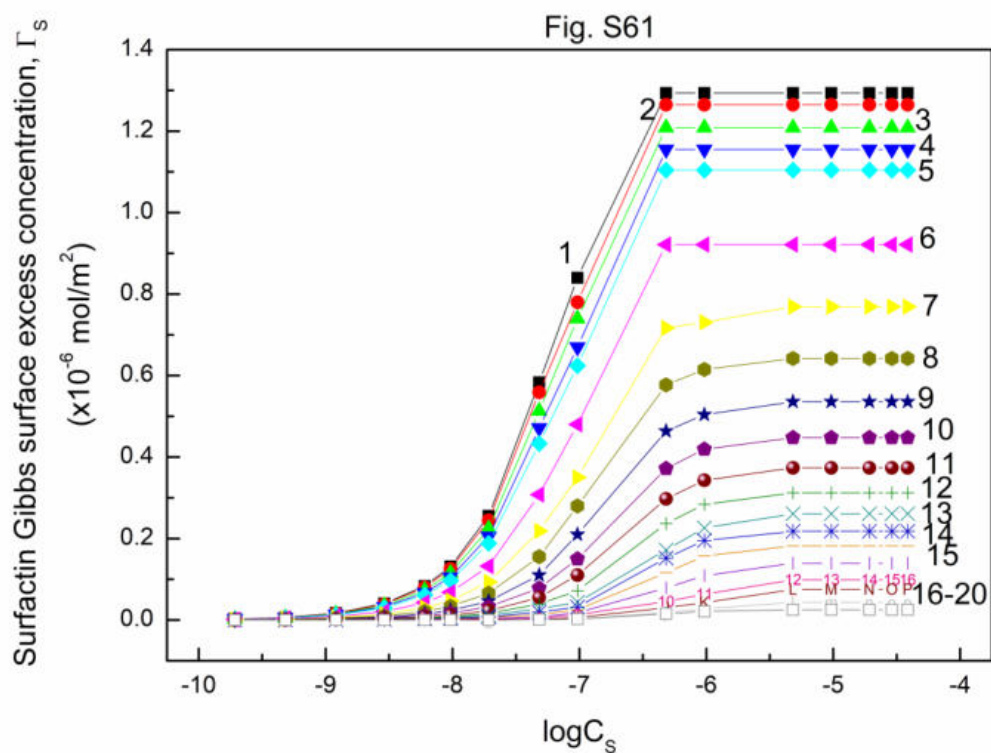
Fig. S61. A plot of the surfactin Gibbs surface excess concentration calculated from the Gibbs equation vs. the logarithm of surfactin concentration (C_S). Curves $1 - 20$ correspond to the constant ethanol concentrations equal to 0.06692; 0.1338; 0.2677; 0.4015; 0.535; 1.0706; 1.6062; 2.1416; 2.677; 3.2124; 3.7478; 4.2832; 4.8185; 5.3538; 5.8893; 6.6925; 7.7245; 8.5664; 10.2797 and 11.968 M.
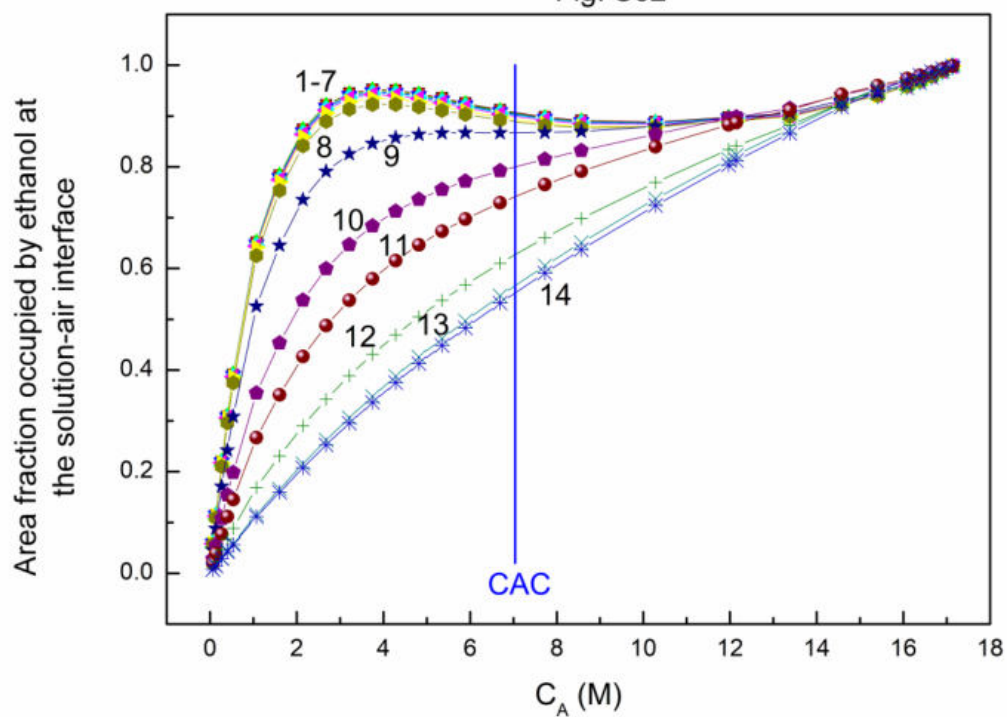
Fig. 62. A plot of the area fraction occupied by ethanol at the solution-air interface vs. the ethanol concentration (C_A). Curves 1 – 14 correspond to the constant surfactin concentrations equal to 0.0002; 0.0005; 0.00125; 0003; 0.00625; 0.01; 0.02; 0.05; 0.1; 0.5; 1; 5; 10 and 20 mg/dm^3.
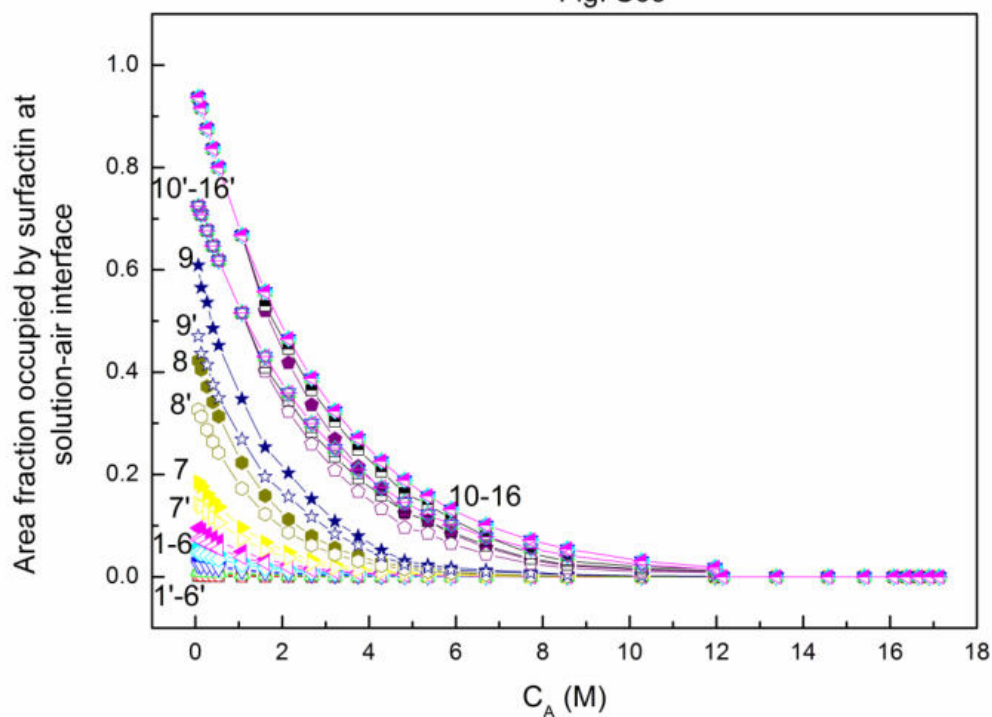
Fig. S63. A plot of the area fraction occupied by surfactin at the solution-air interface vs. the ethanol concentration (C_A). Curves 1 – 14 and 1' – 14' were obtained for surfactin limiting Gibbs surface excess concentration equal to 1.38 and 1.79 x 10^{-6} mol/m^2 depending on the hydrophilic part of surfactin molecule configuration. Curves 1 – 14 and 1' - 14' correspond to the constant surfactin concentrations equal to 0.0002; 0.0005; 0.00125; 0003; 0.00625; 0.01; 0.02; 0.05; 0.1; 0.5; 1; 5; 10 and 20 mg/dm^3.
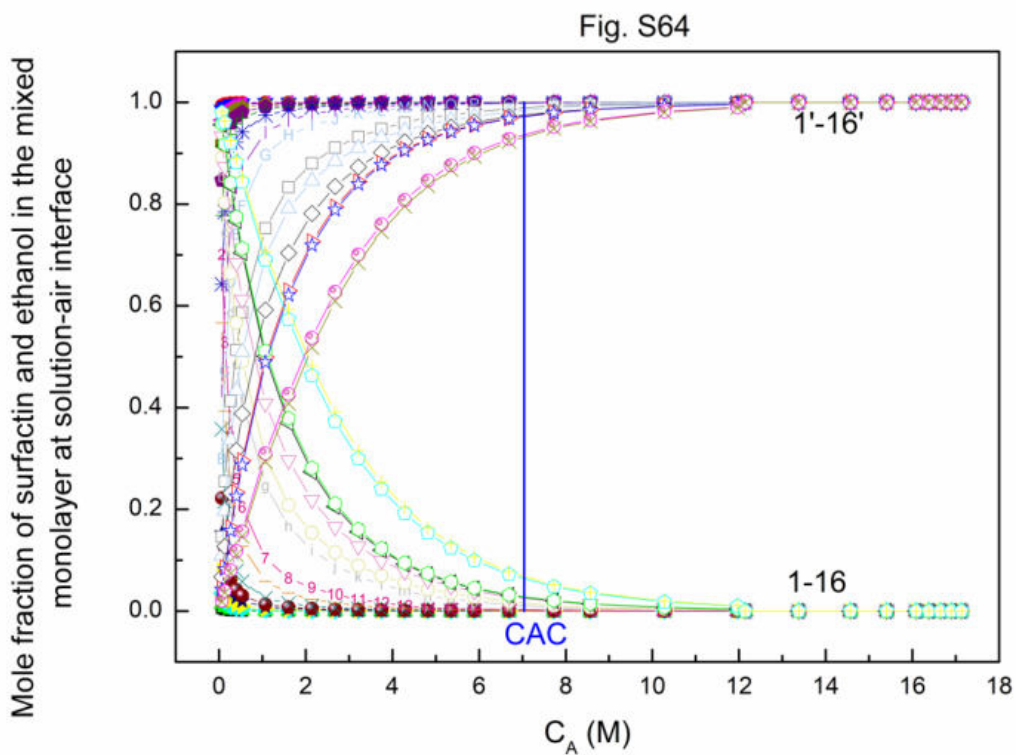
Fig. 64. The mole fraction of surfactin (curves 1- 16) and ethanol (curves 1'-16') in the mixed monolayer at the solution-air interface vs. the ethanol concentration. Curves 1 – 16 and 1' – 16' correspond to the constant surfactin concentration equal to 0.0002; 0.0005; 0.00125; 0003; 0.00625; 0.01; 0.02; 0.05; 0.1; 0.5; 1; 5; 10; 20; 30 and 40 mg/dm^3.
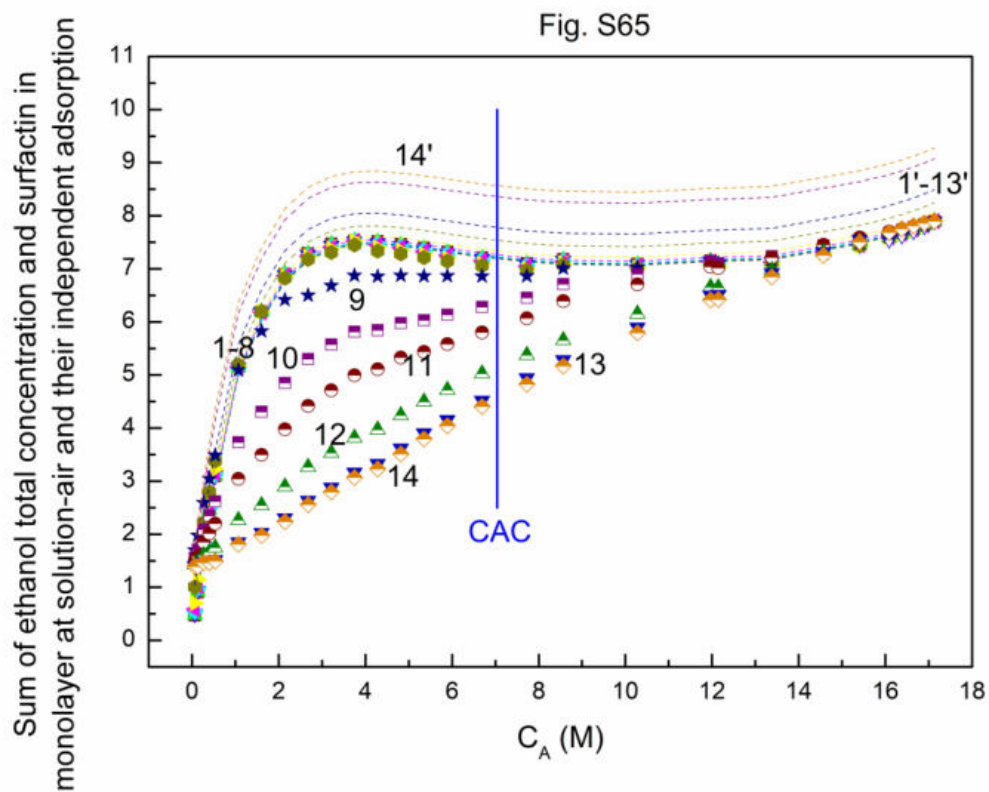
Fig. S65. Comparison of the sum of ethanol total concentration and surfactin in the monolayer at the solution-air interface (points 1 – 14) to that resulting from their independent adsorption (lines 1' – 14'). Points 1 – 14 and lines 1' – 14' correspond to the constant surfactin concentration equal to 0.0002; 0.0005; 0.00125; 0003; 0.00625; 0.01; 0.02; 0.05; 0.1; 0.5; 1; 5; 10 and 20 mg/dm^3.
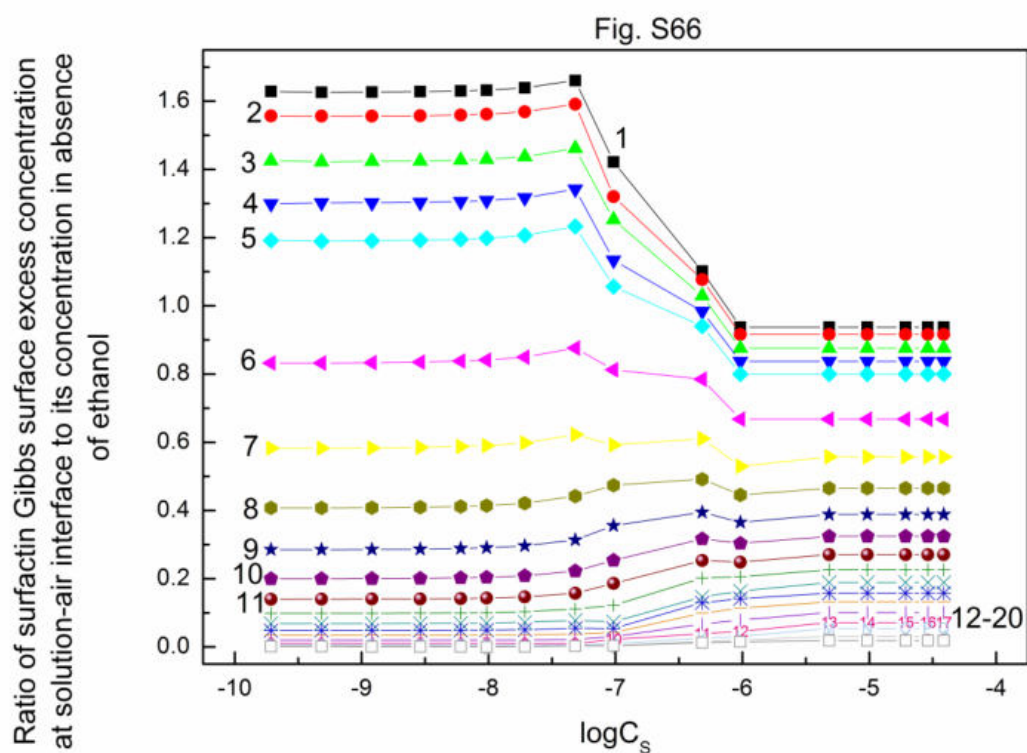
Fig. S66. A plot of the ratio of surfactin Gibbs surface excess concentration at the solution-air interface to its concentration in the absence of ethanol vs. the logarithm of surfactin concentration (C_S). Curves 1 – 20 correspond to the constant ethanol concentrations equal to 0.06692; 0.1338; 0.2677; 0.4015; 0.535; 1.0706; 1.6062; 2.1416; 2.677; 3.2124; 3.7478; 4.2832; 4.8185; 5.3538; 5.8893; 6.6925; 7.7245; 8.5664; 10.2797 and 11.968 M.
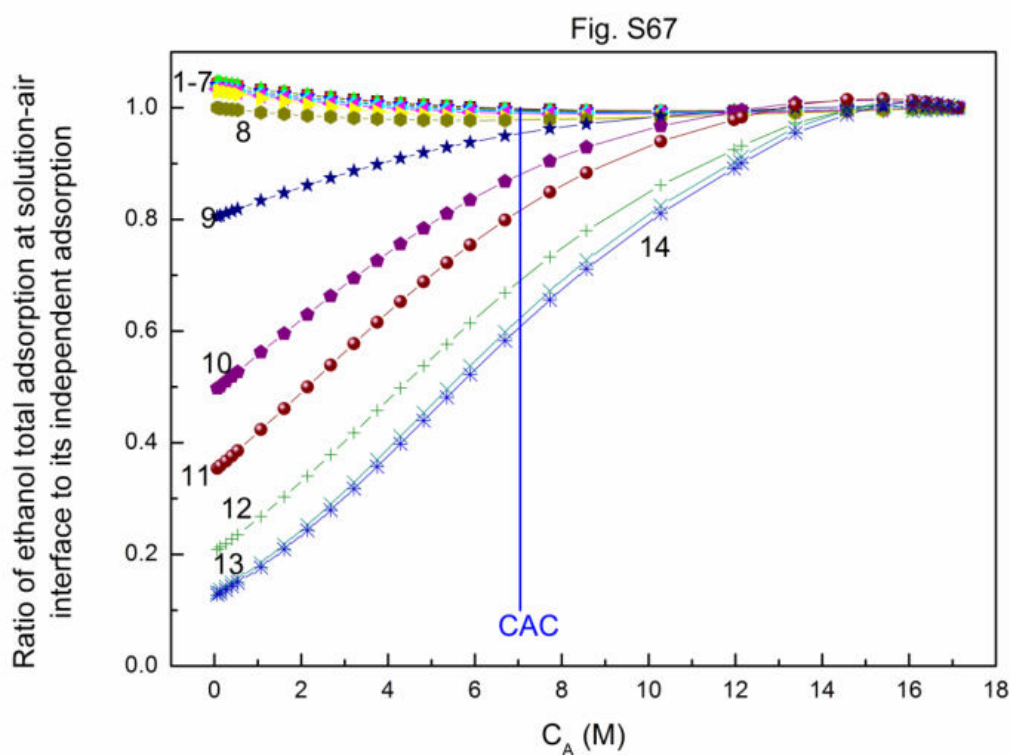
Fig. S67. A plot of the ratio of ethanol total adsorption at the solution-air interface to its independent adsorption in the absence of surfactin vs. the ethanol concentration (C_A). Curves 1 - 14 correspond to the constant surfactin concentration equal to 0.0002; 0.0005; 0.00125; 0003; 0.00625; 0.01; 0.02; 0.05; 0.1; 0.5; 1; 5; 10 and 20 mg/dm^3.
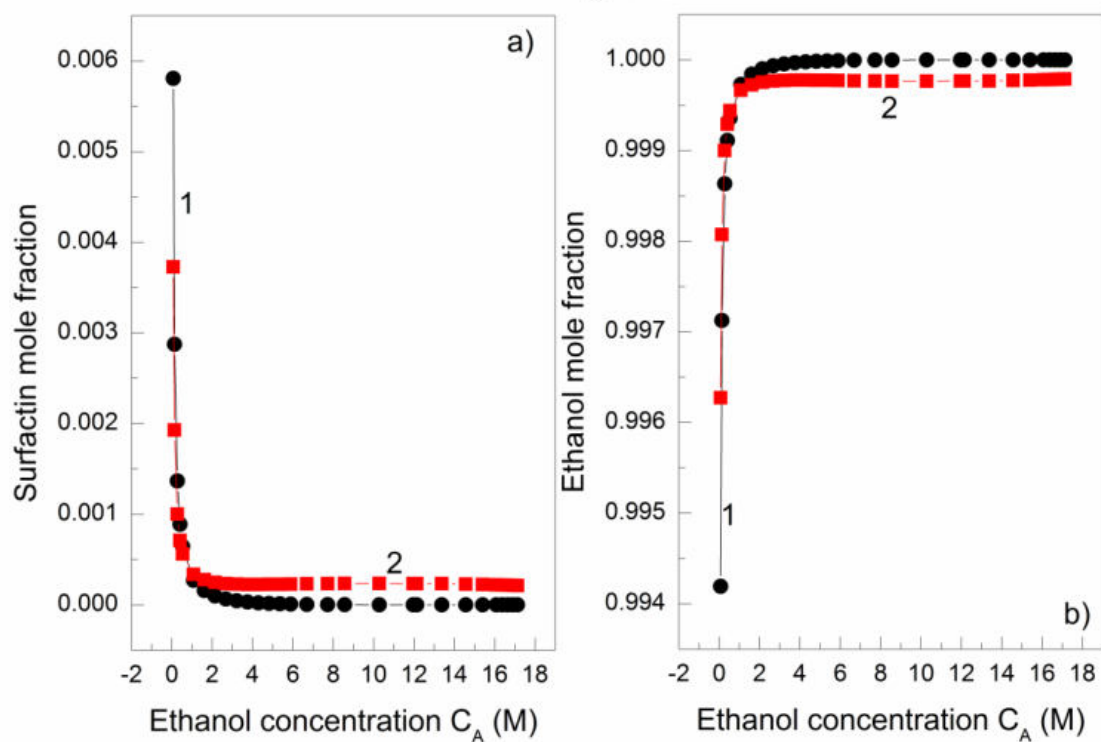
Fig. S68. Comparison of the surfactin (a) and ethanol (b) mole fraction in the real adsorbed monolayer at the solution-air interface (curve 1) and theoretical resulting from independent surfactin and ethanol adsorption (curve 2) vs. the ethanol concentration (C_A) at the constant surfactin concentration equal to 0.0002 mg/dm^3.
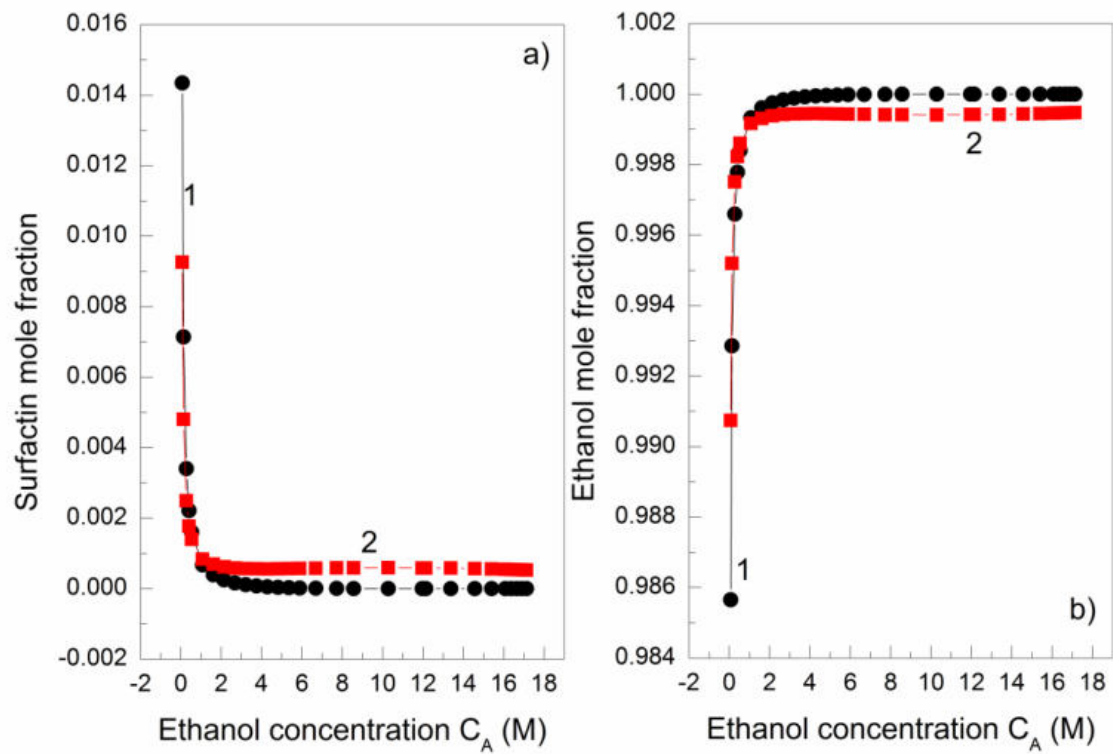
Fig. S69. Comparison of the surfactin (a) and ethanol (b) mole fraction in the real adsorbed
monolayer at the solution-air interface (curve 1) and theoretical resulting from
independent surfactin and ethanol adsorption (curve 2) vs. the ethanol concentration
(C_A) at the constant surfactin concentration equal to 0.0005 mg/dm^3.
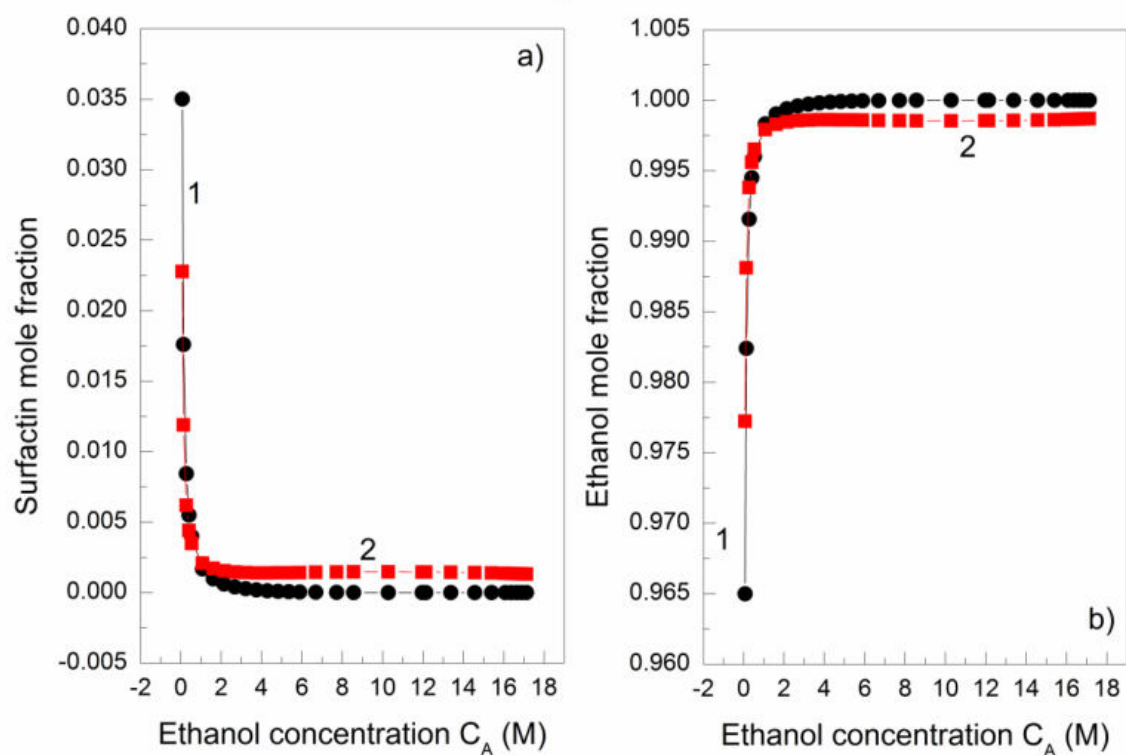
Fig. S70. Comparison of the surfactin (a) and ethanol (b) mole fraction in the real adsorbed monolayer at the solution-air interface (curve 1) and theoretical resulting from independent surfactin and ethanol adsorption (curve 2) vs. the ethanol concentration (C_A) at the constant surfactin concentration equal to 0.00125 mg/dm^3.
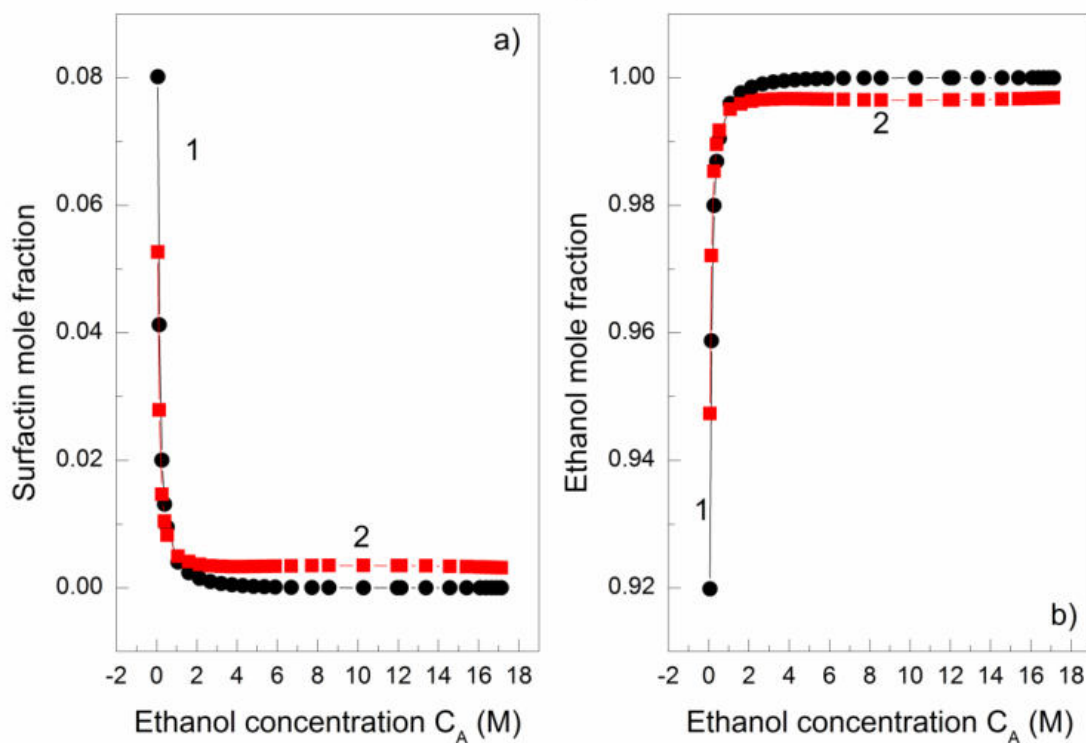
Fig. S71. Comparison of the surfactin (a) and ethanol (b) mole fraction in the real adsorbed monolayer at the solution-air interface (curve 1) and theoretical resulting from independent surfactin and ethanol adsorption (curve 2) vs. the ethanol concentration (C_A) at the constant surfactin concentration equal to 0.003 mg/dm^3.
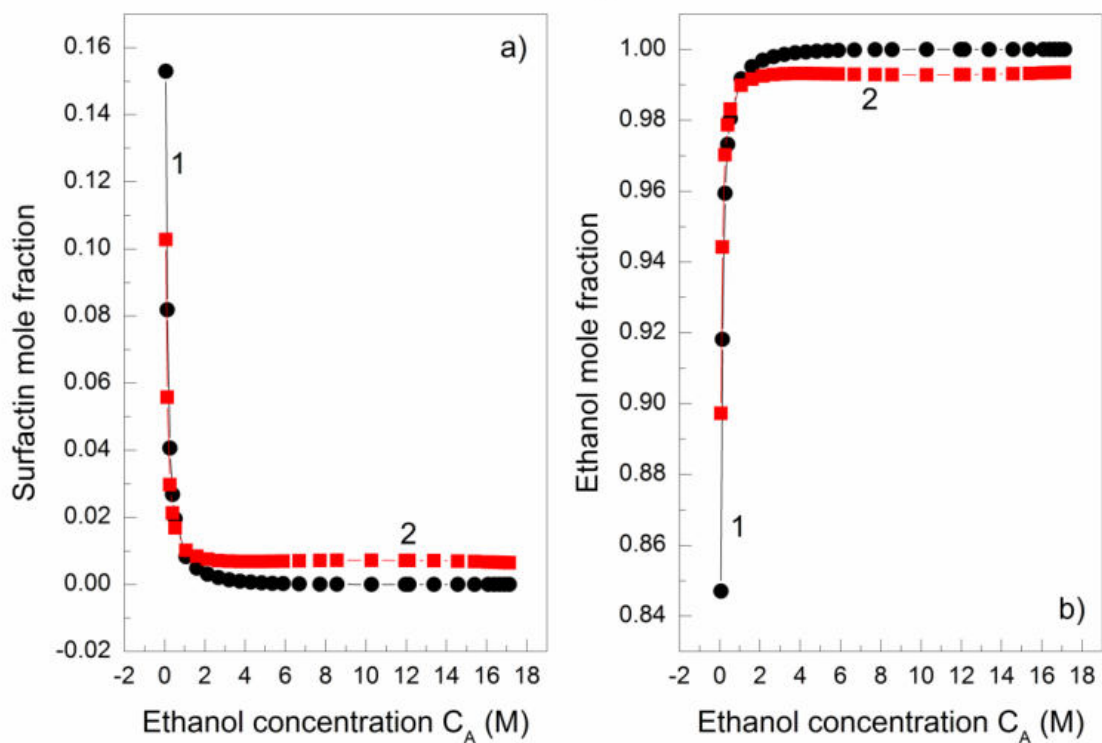
Fig. S72. Comparison of the surfactin (a) and ethanol (b) mole fraction in the real adsorbed monolayer at the solution-air interface (curve 1) and theoretical resulting from independent surfactin and ethanol adsorption (curve 2) vs. the ethanol concentration (C_A) at the constant surfactin concentration equal to 0.00625 mg/dm^3.
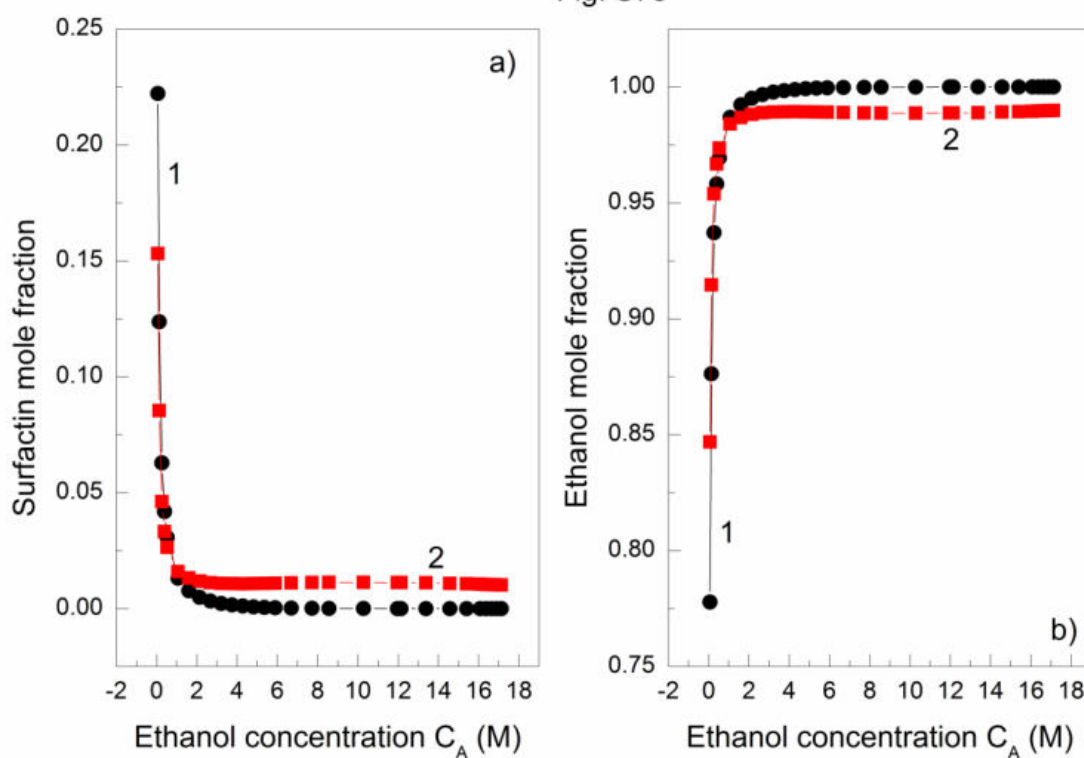
Fig. S73. Comparison of the surfactin (a) and ethanol (b) mole fraction in the real adsorbed monolayer at the solution-air interface (curve 1) and theoretical resulting from independent surfactin and ethanol adsorption (curve 2) vs. the ethanol concentration (C_A) at the constant surfactin concentration equal to 0.01 mg/dm^3.
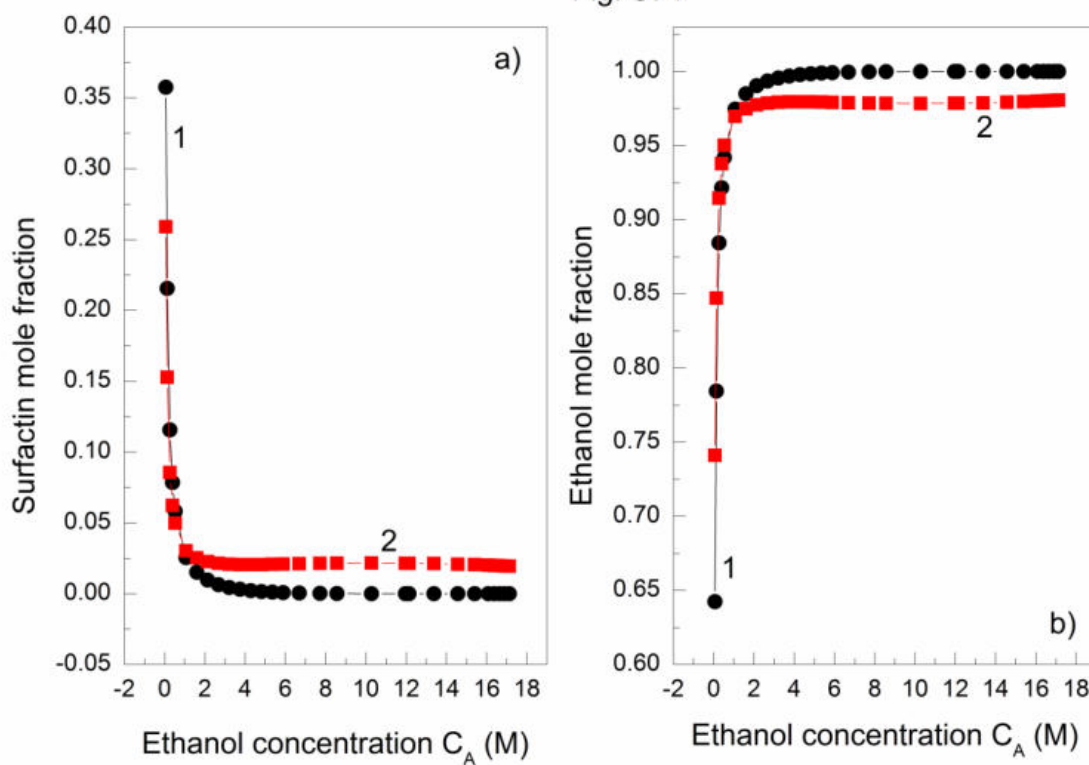
Fig. S74. Comparison of the surfactin (a) and ethanol (b) mole fraction in the real adsorbed monolayer at the solution-air interface (curve 1) and theoretical resulting from independent surfactin and ethanol adsorption (curve 2) vs. the ethanol concentration (C_A) at the constant surfactin concentration equal to 0.02 mg/dm^3.
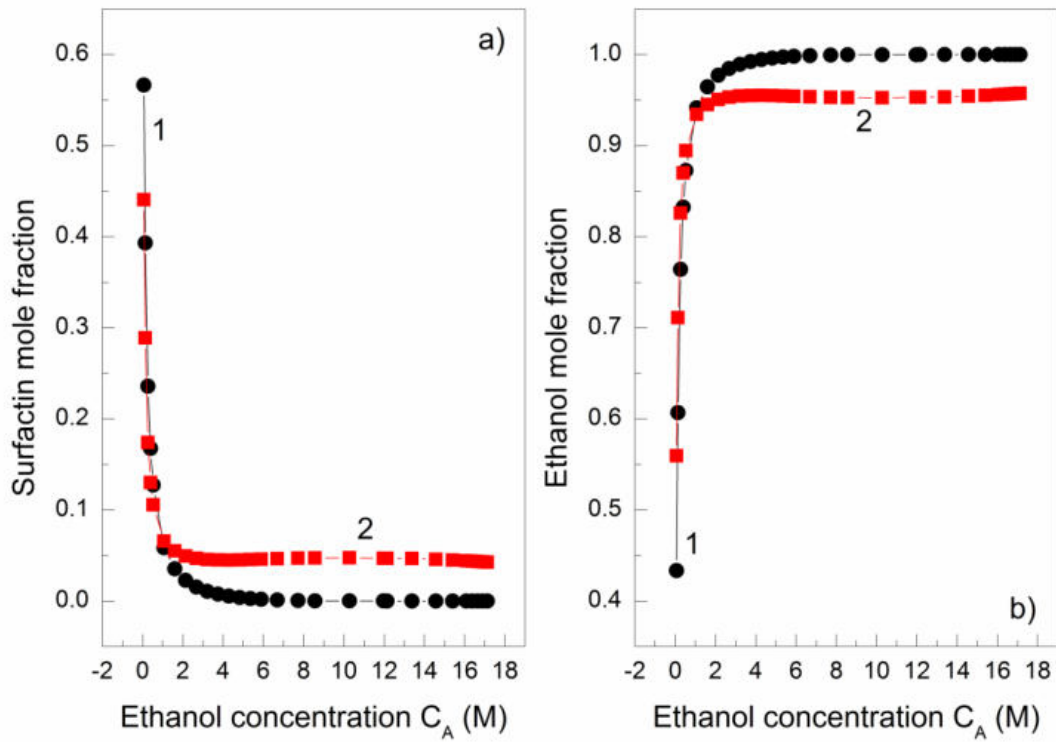
Fig. S75. Comparison of the surfactin (a) and ethanol (b) mole fraction in the real adsorbed monolayer at the solution-air interface (curve 1) and theoretical resulting from independent surfactin and ethanol adsorption (curve 2) vs. the ethanol concentration (C_A) at the constant surfactin concentration equal to 0.05 mg/dm^3.
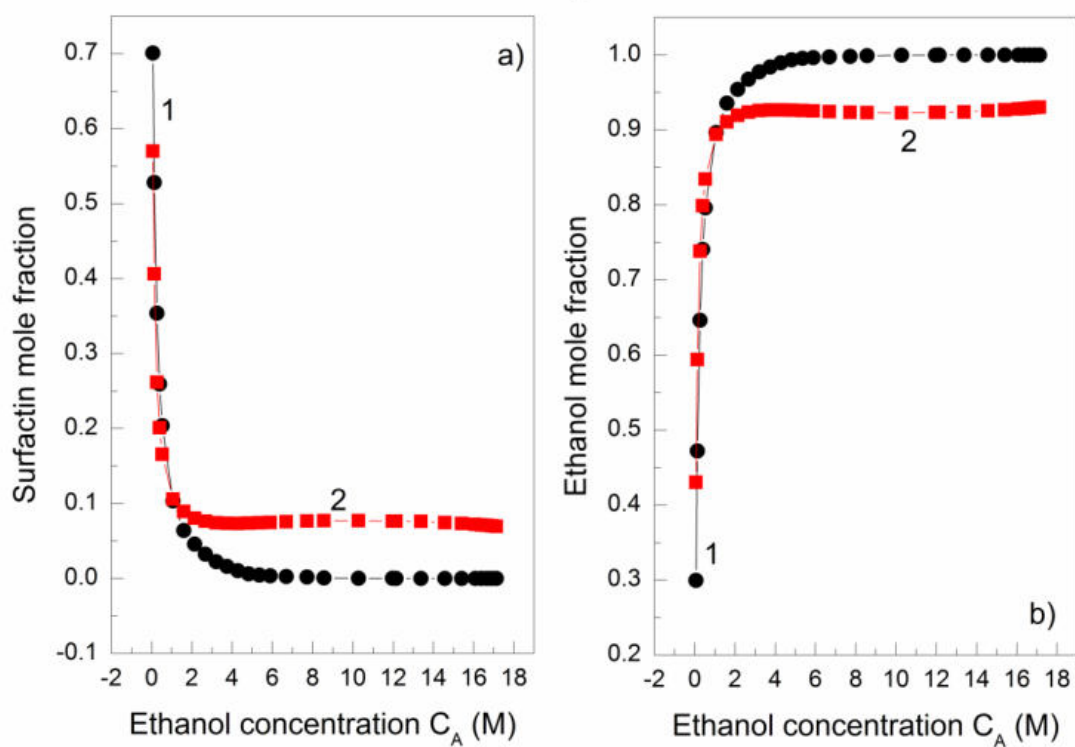
Fig. S76. Comparison of the surfactin (a) and ethanol (b) mole fraction in the real adsorbed monolayer at the solution-air interface (curve 1) and theoretical resulting from independent surfactin and ethanol adsorption (curve 2) vs. the ethanol concentration (C_A) at the constant surfactin concentration equal to 0.1 mg/dm^3.
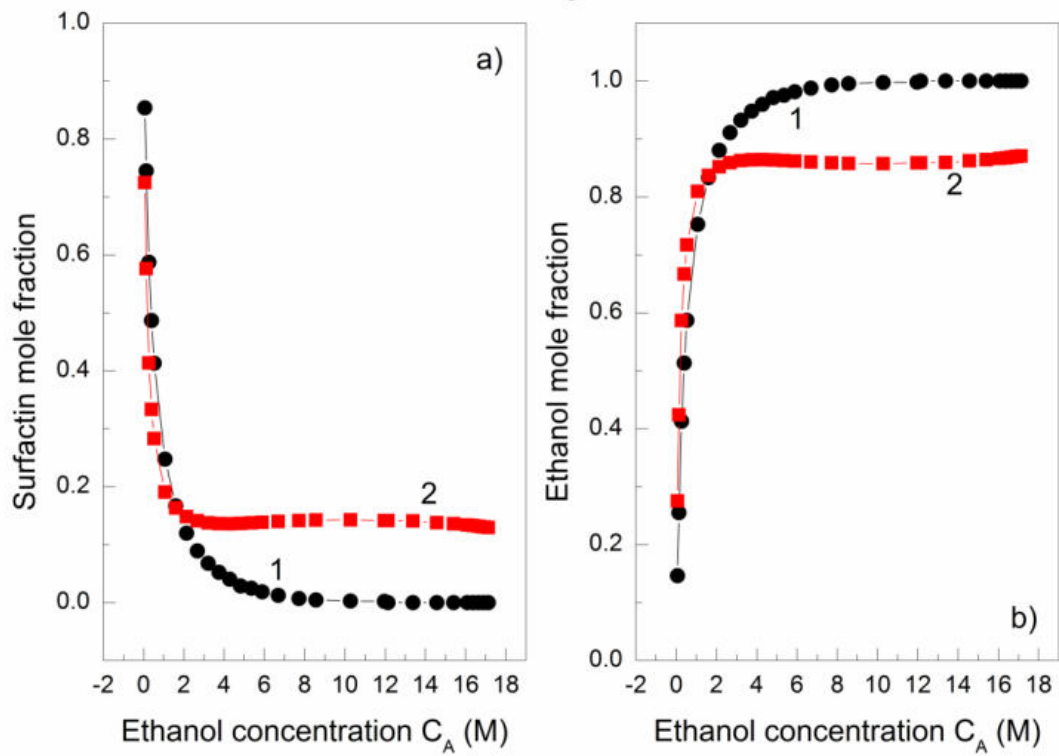
Fig. S77. Comparison of the surfactin (a) and ethanol (b) mole fraction in the real adsorbed monolayer at the solution-air interface (curve 1) and theoretical resulting from independent surfactin and ethanol adsorption (curve 2) vs. the ethanol concentration (C_A) at the constant surfactin concentration equal to 0.5 mg/dm^3.
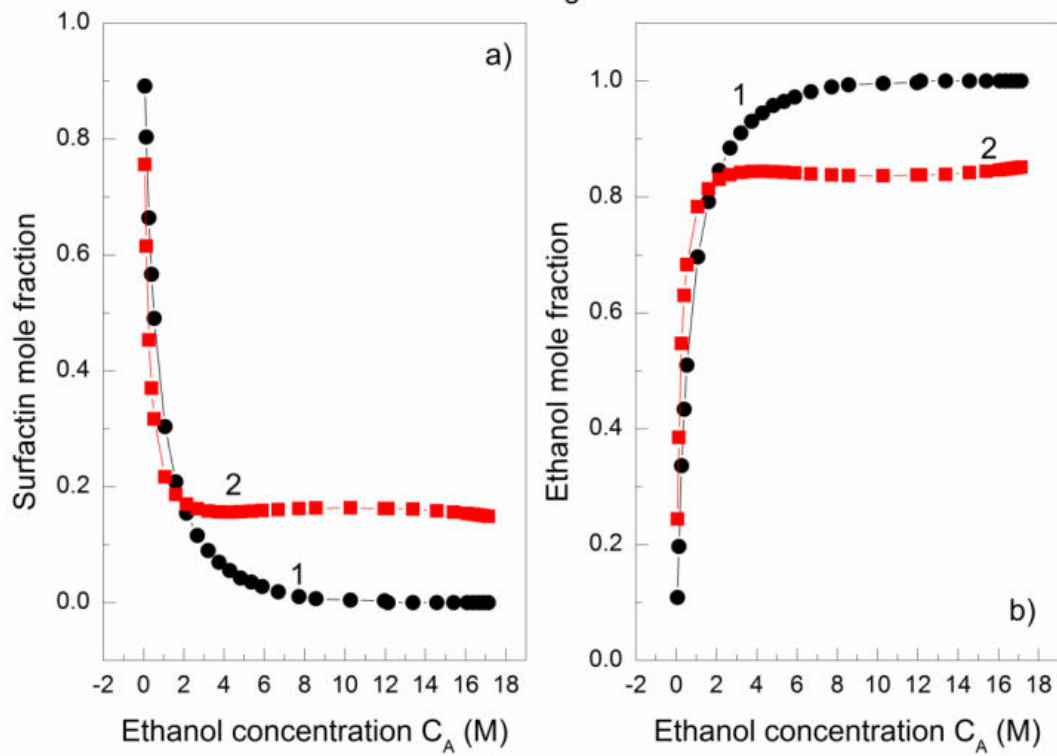
Fig. S78. Comparison of the surfactin (a) and ethanol (b) mole fraction in the real adsorbed monolayer at the solution-air interface (curve 1) and theoretical resulting from independent surfactin and ethanol adsorption (curve 2) vs. the ethanol concentration (C_A) at the constant surfactin concentration equal to 1 mg/dm^3.
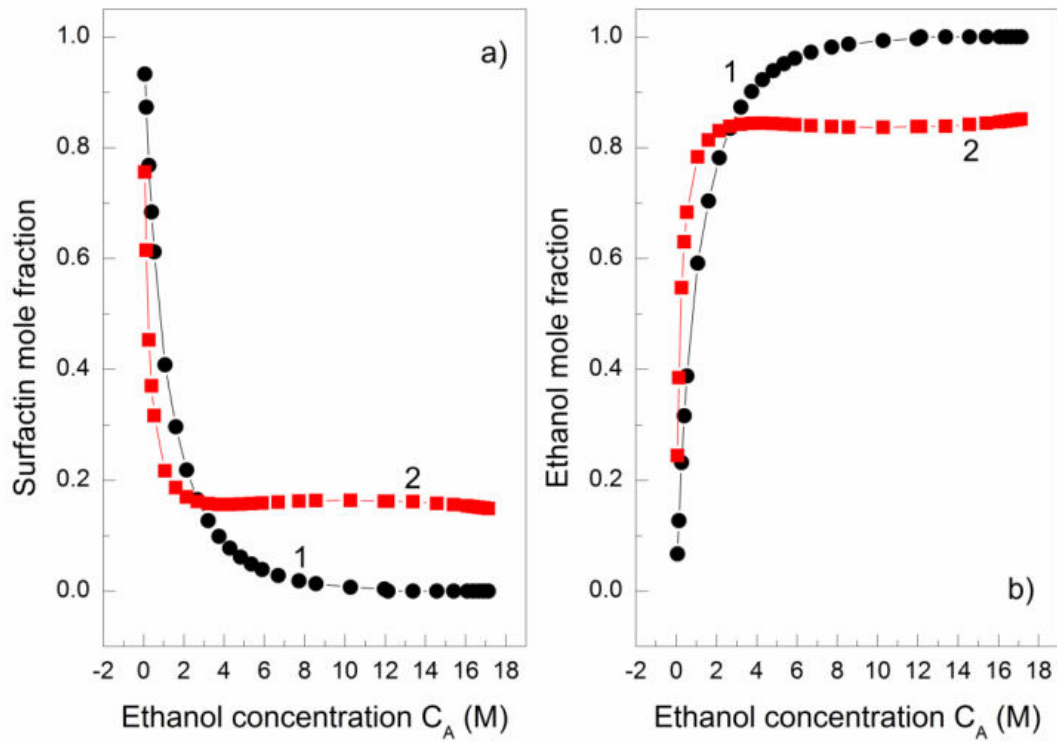
Fig. S79. Comparison of the surfactin (a) and ethanol (b) mole fraction in the real adsorbed monolayer at the solution-air interface (curve 1) and theoretical resulting from independent surfactin and ethanol adsorption (curve 2) vs. the ethanol concentration (C_A) at the constant surfactin concentration equal to 5 mg/dm^3.
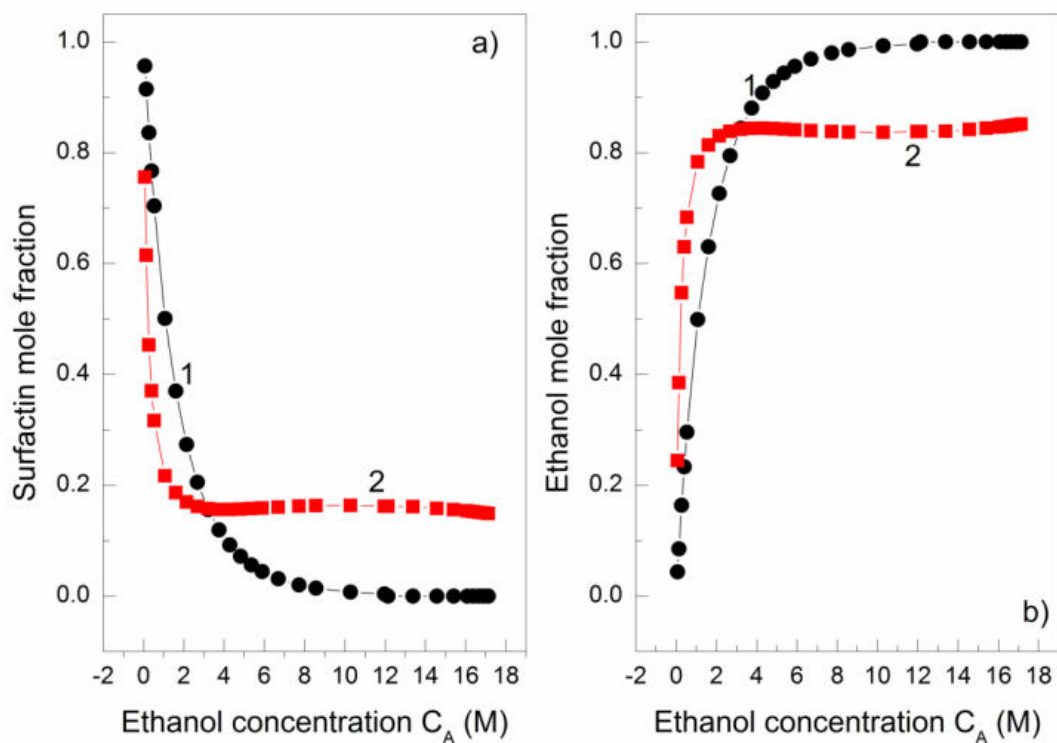
Fig. S80. Comparison of the surfactin (a) and ethanol (b) mole fraction in the real adsorbed monolayer at the solution-air interface (curve 1) and theoretical resulting from independent surfactin and ethanol adsorption (curve 2) vs. the ethanol concentration (C_A) at the constant surfactin concentration equal to 10 mg/dm^3.
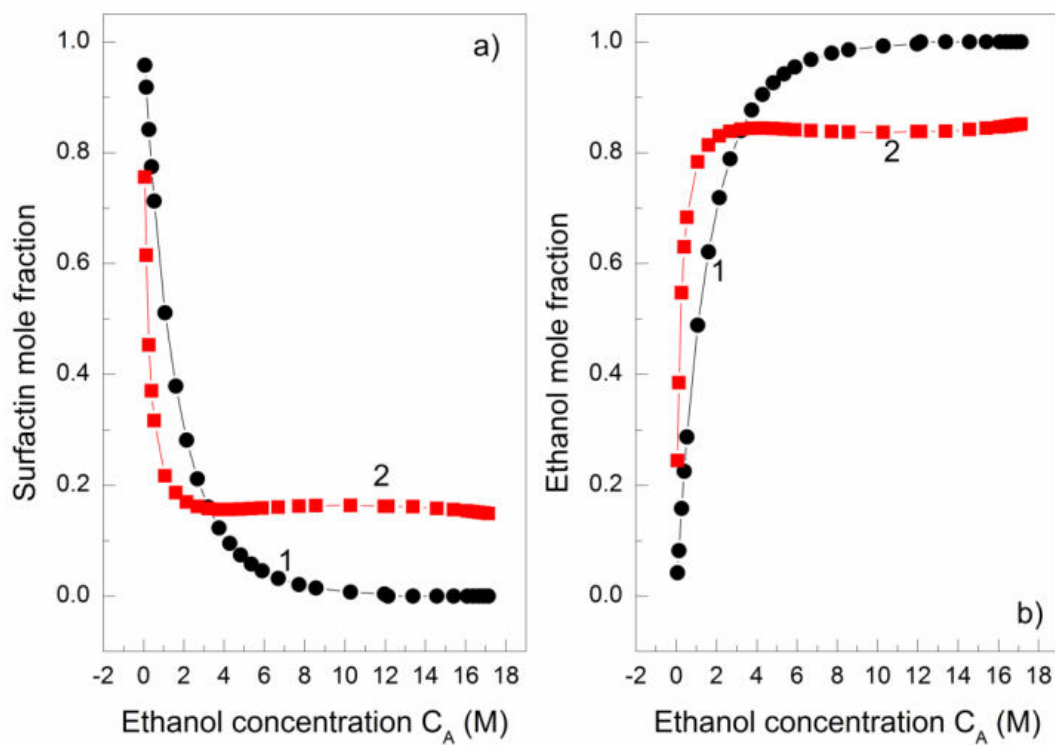
Fig. S81. Comparison of the surfactin (a) and ethanol (b) mole fraction in the real adsorbed monolayer at the solution-air interface (curve 1) and theoretical resulting from independent surfactin and ethanol adsorption (curve 2) vs. the ethanol concentration (C_A) at the constant surfactin concentration equal to 20 mg/dm^3.
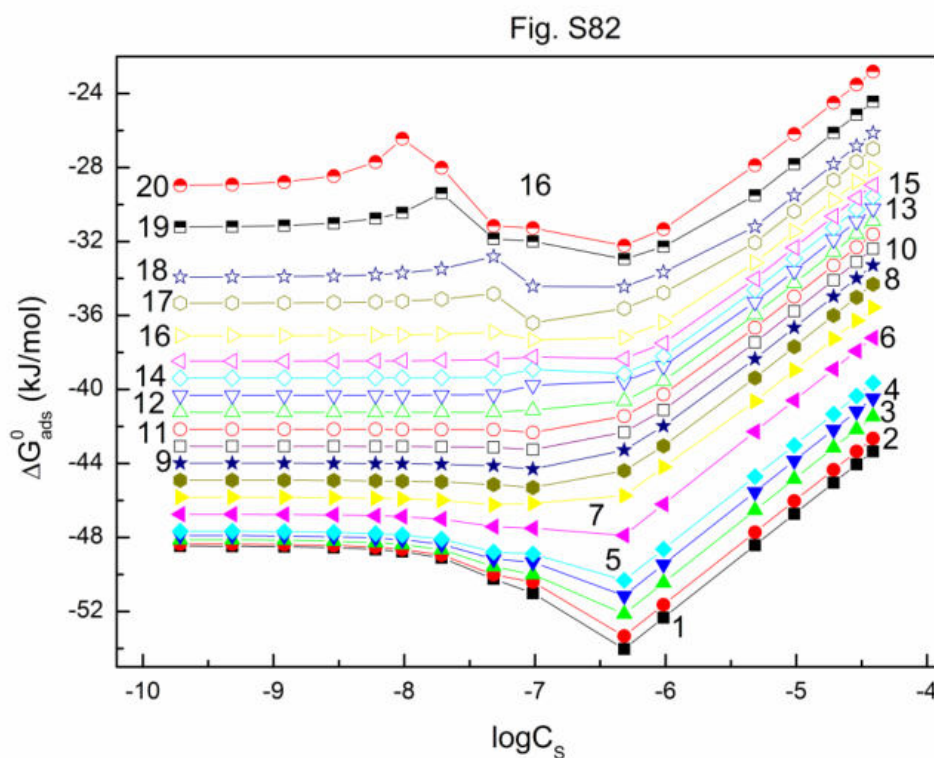
Fig. S82. A plot of the surfactin Gibbs standard free energy of adsorption (ΔG_{ads}^0) calculated from the Langmuir equation modified by de Boer vs. the logarithm of surfactin concentration (C_S). Curves 1 – 20 correspond to the constant ethanol concentrations equal to 0.06692; 0.1338; 0.2677; 0.4015; 0.535; 1.0706; 1.6062; 2.1416; 2.677; 3.2124; 3.7478; 4.2832; 4.8185; 5.3538; 5.8893; 6.6925; 7.7245; 8.5664; 10.2797 and 11.968 M.
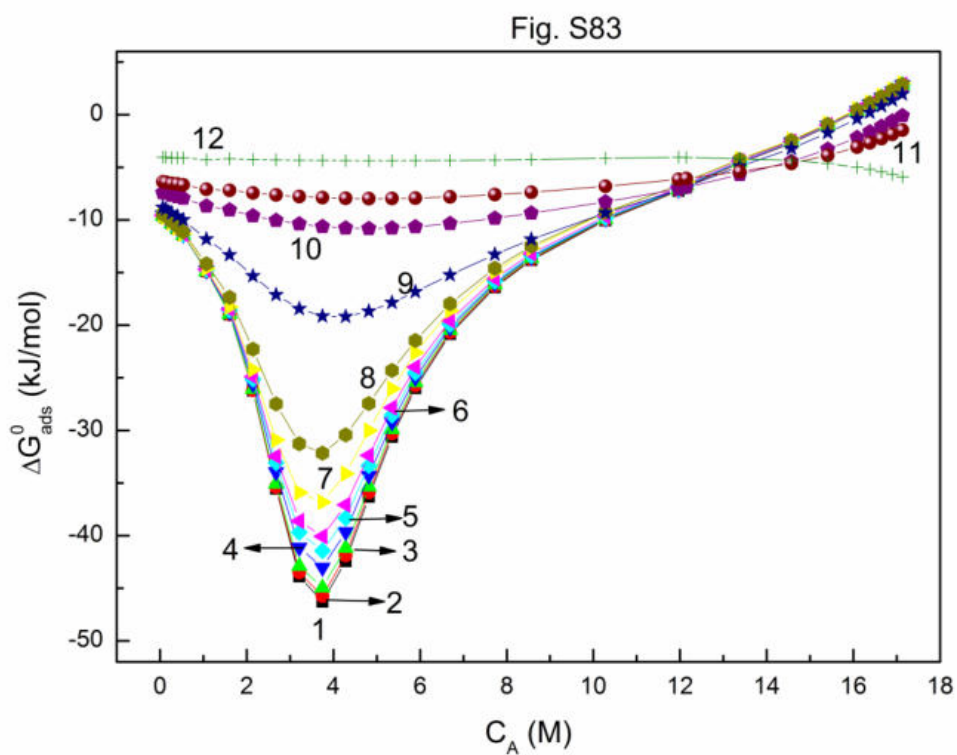
Fig. S83. A plot of the ethanol Gibbs standard free energy of adsorption (ΔG^0_{ads}) calculated from the Langmuir equation modified by de Boer vs. the logarithm of ethanol concentration (C_A). Curves 1 – 12 correspond to the constant surfactin concentrations equal to 0.0002; 0.0005; 0.00125; 0003; 0.00625; 0.01; 0.02; 0.05; 0.1; 0.5; 1 and 5 mg/dm^3.

Prof. dr hab. Anna Zdziennicka
Katedra Zjawisk Międzyfazowych
Instytut Nauk Chemicznych
Wydział Chemii UMCS
Pl. M. Curie-Skłodowskiej 3
20-031 Lublin

Lublin, 17.01.2023

OŚWIADCZENIE

Oświadczam, że w pracy

E. Rekiel, **A. Zdziennicka***, B. Jańczuk, *Adsorption of surfactin at water with ethanol mixture-air interface*. Journal of Molecular Liquids, 2020, 300, 112240;

mój udział wynosił **35%** i polegał na weryfikacji procesu pisania pracy oraz przeprowadzonych badań, redagowaniu i edycji manuskryptu, współredagowaniu odpowiedzi na recenzje pracy oraz prowadzeniu korespondencji z czasopismem.

Prof. dr hab. Bronisław Jańczuk
Katedra Zjawisk Międzyfazowych
Instytut Nauk Chemicznych
Wydział Chemii UMCS
Pl. M. Curie-Skłodowskiej 3
20-031 Lublin

Lublin, 17.01.2023

OŚWIADCZENIE

Oświadczam, że w pracy

E. Rekiel, A. Zdziennicka*, **B. Jańczuk**, *Adsorption of surfactin at water with ethanol mixture-air interface*. Journal of Molecular Liquids, 2020, 300, 112240;

mój udział wynosił **10%** i polegał na weryfikacji procesu pisania pracy oraz przeprowadzonych badań, redagowaniu i edycji manuskryptu oraz współredagowaniu odpowiedzi na recenzje pracy.

Bronisław Jańczuk

Załącznik 5

[D5] E. Rekiel, A. Zdziennicka*, B. Jańczuk, *Mutual influence of ethanol and surfactin on their wetting and adhesion properties*, ***Colloids and Surfaces A: Physicochemical and Engineering Aspects***, 2021, 627, 127161.

Mutual influence of ethanol and surfactin on their wetting and adhesion properties

Edyta Rekiel, Anna Zdziennicka [*], Bronisław Jańczuk

Department of Interfacial Phenomena, Institute of Chemical Sciences, Faculty of Chemistry, Maria Curie-Skłodowska University in Lublin, Maria Curie-Skłodowska Sq. 3, 20-031 Lublin, Poland

HIGHLIGHTS

- Ethanol (ET) improves wetting properties of surfactin (SF).
- Wetting properties of SF and ET mixture depend on components and parameters of γ_{LV} and γ_{SV}.
- Complete wetting of PMMA and quartz by SF and ET mixture solution occurs at $\gamma_{LV} \neq \gamma_{SV}$.
- Adsorption of ET and SF at PMMA-W and quartz-W interfaces is lower than at W-A one.
- Tendency of SF to adsorb at interfaces is low at ET concentration higher than its CAC.

GRAPHICAL ABSTRACT
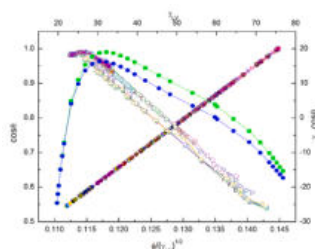
ARTICLE INFO

ABSTRACT

The measurements of the contact angle of aqueous solution of ethanol and surfactin mixture in the whole range of ethanol concentration on PTFE, PMMA and quartz were made at changing ethanol concentration and constant of surfactin and vice versa. Based on the obtained results, the Young-Dupre and van Oss et al. equations, the intermolecular interactions parameter between the solution and solid phases was determined and used to explain the possibility to form the ethanol and surfactin mixed layer beyond the solution drop settled on the PMMA and/ or quartz surface. This layer pressure and that at the PMMA-solution, the quartz-solution interface was determined using the Young-Dupre and van Oss et al. equations and applied for the ethanol and surfactin Frumkin isotherm adsorption determination. The Gibbs adsorption isotherm was also determined. The ethanol and surfactin Gibbs and Frumkin isotherms at the solid-solution, solid-air interfaces were compared to those at the solution-air one. From these isotherms of surfactin and ethanol adsorption at three interfaces, the slope of the linear dependence between the adhesion and surface tension was explained. The Gibbs isotherm was applied for determination of the Gibbs standard free energy of ethanol and surfactin adsorption at the solid-air and solid-water interfaces.

1. Introduction

Ethanol (ET) is very often added to the aqueous solution of different

kinds of surfactants to change their adsorption, aggregation, and wetting properties depending on the surfactants practical use [1–5]. ET is miscible with water over the whole concentration range. This is due to

---

the fact that the dipole moment of the –OH group in the ET and water molecule is almost the same and the alkyl group in ET is too short to limit its solubility in water [2,6]. Moreover, the angle between the alkyl and –OH groups in the ET molecule is similar to the angle between the –OH groups in the water molecule [2]. ET added to water changes its density, viscosity and dielectric constant [6]. The changes of these water properties affected by ET are not linear [2,3,6]. For example, the isotherm of the viscosity of the water-ET mixture has the maximum [6]. When water and ET are mixed, there takes place volume contraction, which is the smallest when the ratio of moles of water to ET is one to one. [3,6]. ET shows the activity of adsorption at different interfaces [3]. It is interesting that the standard Gibbs free energy of ET adsorption at the water-air interface is similar to those of classical surfactants having alkyl group in the tail [1,7]. This indicates that contribution of –CH$_3$ and –CH$_2$– groups to the standard Gibbs free energy of adsorption is the same as in the case of classical surfactants [1,6]. In the water environment ET forms small aggregates at its concentration called as the critical aggregation concentration (CAC) [2,3,6–15].

These specific properties of ET have promoted research on its effects on various surfactant properties [1–3,16–30]. The current studies do not always provide the same conclusions about the role of ET in the behaviour of surfactants at various interfaces and in the bulk phase. Compared to surfactants, ET can be treated as an additive, co-surfactant and co-solvent depending on its concentration in the aqueous solution of surfactants [1,3].

The previous studies suggest that ET can increase or decrease the adsorption of surfactants at various interfaces, decrease or increase the CMC of surfactants depending on its concentration, and thus affect the wetting properties of aqueous surfactant solutions [1–3,23,25,28]. Unfortunately, these studies concern mostly to the classic surfactants, which have a negative impact on the environment [1–3,16–30]. For this reason, biosurfactants are becoming more and more popular [31–33] not only from the theoretical point of view. As biosurfactants are non-toxic, have antibacterial properties and are easily degradable [34,35], they are increasingly used in various fields [36–42]. They are very often used in practice in an alcoholic solution. Among the biosurfactants surfactin plays a very important role [39–41]. The specific properties of the surfactin can result in the increase of its practical applications [39–41].

Surfactin is a very active surface agent and forms micelles at its low concentration in the aqueous solution [42]. The CMC of surfactin is much lower = than even nonionic classical surfactants such as Tritons [42,43]. However, the wetting properties of surfactin are worse than those of these surfactants. As the ET influences on the adsorption properties of surfactin and these properties decide about wetting surfactants properties, the studies of the ET influence on wetting behaviour can be developed from the theoretical and practical points of view. For this reason, the purpose of our studies was to establish the wetting properties of the aqueous solution of ethanol and surfactin mixture on apolar, monopolar, and bipolar solids in the whole range of ET concentration in the solution. As an apolar solid polytetrafluoroethylene (PTFE), monopolar poly(methyl methacrylate) (PMMA) and bipolar quartz were used. The wetting properties were established based on the advancing contact angle measurements of the aqueous solution of ET and SF mixture. The contact angles were measured as a function of ET concentration at the constant SF one and vice versa. The obtained results were discussed based on the mutual adsorption of ET and SF at the interfaces.

2. Experimental

2.1. Materials

96% pure ethanol was purchased from POCH (Poland). Before being used for the research, it was purified by the previously described method [44]. 98% (HPLC) pure surfactin (C$_{53}$H$_{93}$N$_7$O$_{13}$, molecular weight

1036.34 g) (Fig. S1) purchased from Sigma-Aldrich was used in the study without further purification. Deionized water of internal specific resistance of 18.2×10^6 Ω m (doubly distilled, Destemat Bi18E) was used to prepare aqueous solutions of a mixture of ethanol and surfactin. The method of these solutions preparation was described earlier [44].

PTFE and PMMA were purchased from Mega-Tech, Poland and the quartz solids from Conductance, Poland. The method of the PMMA, PTFE and quartz plates preparation and cleaning them or advancing contact angle measurements on their surfaces is presented in the literature [45].

2.2. Methods

The advancing contact angle of the aqueous solution of ET and SF mixture on the PTFE, PMMA and quartz surfaces (θ) was measured by the sessile drop method using the DSA30 measuring system (Krüss) in a thermostated chamber at 293 ± 0.1 K. The contact angle measurements were made for the aqueous solution of ET and SF mixture as a function of ET concentration at the constant SF one and vice versa. The conditions and procedure of the contact angle measurements of the aqueous solution of different mixtures of surface active agents on the PTFE, PMMA and quartz surface are discussed in the literature. [45]. For each concentration of the solution, the contact angle on the given solid was measured for 30 drops. Depending on the concentration of solution the standard deviation was in the range from 1 to 2°.

3. Calculations

On the basis of the contact angle values (θ) it is possible to calculate the intermolecular interactions parameter across the solid-liquid interface (ϕ), the Gibbs surface excess concentration of surface active agents at the solid-air (Γ_{SV}) and solid-solution interface (Γ_{SL}), the total surface concentration of surfactants as well as adhesion work of the aqueous solution of surface active agents to the solid surface (W_a) and the standard Gibbs free energy of adsorption of surface active agents at the solid-air and solid-solution interfaces (ΔG^0_{ads}).

For the calculations of ϕ parameter, the Young equation [1,46] as well as the Girifalco and Good [47] and van Oss et al. approaches were used [48,49]. The Young equation has the form [1,46]:

$$\gamma_{SV} - \gamma_{SL} = \gamma_{LV} cos\theta \tag{1}$$

The form of the Girifalco and Good equation is as follows [47]:

$$\gamma_{SL} = \gamma_{SV} + \gamma_{LV} - 2\phi\sqrt{\gamma_{SV}\gamma_{LV}} \tag{2}$$

where: γ_{SV}, γ_{LV} and γ_{SL} are the solid-air, liquid-air and solid-air interface tensions, respectively.

Recently, the consideration of Girifalco and Good [47] dealing with the interface tension has been criticized by Bormashenko [50]. However, based on these equations many approaches to the wetting process were found. Among them, these proposed by Fowkes [51], Kaelble [52], Owens and Wendt [53], Wu [54,55], van Oss et al. [48,49], Neumann et al. [56,57] and Chibowski [58] are commonly successfully used for the solid surface tension determination from the contact angle measurements as well as for explanation of the wetting properties of the surface active agents. From this reason, we used this equation for consideration of the intermolecular interactions across the solid-liquid interface.

Based on Eq. (2) and the assumption that ϕ can be expressed as a sum of two components resulting from the Lifshitz-van der Waals intermolecular interactions and hydrogen bonds, van Oss et al. [48,49] proposed the following equation:

$$\gamma_{SL} = \gamma_{SV} + \gamma_{LV} - 2\sqrt{\gamma^{LW}_{SV}\gamma^{LW}_{LV}} - 2\sqrt{\gamma^+_{SV}\gamma^-_{LV}} - 2\sqrt{\gamma^-_{SV}\gamma^+_{LV}} \tag{3}$$

where LW, "+ " and "-" refer to the Lifshitz-van der Waals component of

the solid or liquid surface tension and to the electron-acceptor and electron-donor parameters of the acid-base component of the surface tension, respectively.

From Eqs. (1) and (2) it results that:

$$\phi = \frac{\gamma_{LV}(cos\theta + 1)}{2\sqrt{\gamma_{SV}\gamma_{LV}}} \tag{4}$$

or

$$cos\theta = 2\frac{\phi}{\sqrt{\gamma_{LV}}}\sqrt{\gamma_{SV}} - 1 \tag{5}$$

Comparing Eqs. (2) and (3) we obtain:

$$\phi = \frac{\sqrt{\gamma_{SV}^{LW}\gamma_{LV}^{LW}} + \sqrt{\gamma_{SV}^{+}\gamma_{LV}^{-}} + \sqrt{\gamma_{SV}^{-}\gamma_{LV}^{+}}}{\sqrt{\gamma_{SV}\gamma_{LV}}} \tag{6}$$

In the case of apolar solids Eq. (6) assumes the form:

$$\phi = \frac{\sqrt{\gamma_{SV}^{LW}\gamma_{LV}^{LW}}}{\sqrt{\gamma_{SV}\gamma_{LV}}} \tag{7}$$

Taking into account the measured values of the contact angle of the aqueous solution of surfactin and ethanol mixture on the PTFE, PMMA and quartz surface, the surface tension of the studied solutions as well as components and parameters of solids surface tension from literature [44, 45] the values of the parameter of the intermolecular interactions across the solid-solution interface were calculated from the above presented equations.

The adsorption of surfactin and ethanol at the PTFE-solution, PMMA-air, PMMA-solution, quartz-air and quartz-solution interfaces was considered on the basis of the Lucassen-Reynders [59] as well as the Gibbs and Frumkin equations [1,46].

The Lucassen-Reynders equation can be expressed as [59]:

$$\frac{\partial(\gamma_{LV}cos\theta)}{\partial\gamma_{LV}} = \frac{\Gamma_{SV} - \Gamma_{SL}}{\Gamma_{LV}} \tag{8}$$

Eq. (8) can be solved if the relation between the adhesion ($\gamma_{LV}cos\theta$) and the surface tension (γ_{LV}) can be described by a proper function. It appeared that in many cases this dependence was linear:

$$\gamma_{LV}cos\theta = a\gamma_{LV} + b \tag{9}$$

On the basis of Eqs. (8) and (9), the Γ_{SL} values for the PTFE-solution interface were calculated using the measured values of the contact angle and the surface tension of the aqueous solution of surfactin and ethanol mixture taken from literature [44]. In the case of PMMA and quartz only the differences between the Gibbs surface excess concentration of surfactin or ethanol at the solid-air and solid-solution interfaces were determined from Eqs. (8) and (9).

The Gibbs surface excess concentration of surfactin and ethanol was also calculated from the Gibbs isotherm equation which for the PTFE-solution interface has the following form:

$$\Gamma_{SL} = -\frac{a}{nRT}\frac{\partial(-\gamma_{LV}cos\theta)}{\partial a} = -\frac{C}{nRT}\frac{\partial(-\gamma_{LV}cos\theta)}{\partial C}$$
$$= -\frac{1}{2.303nRT}\frac{\partial(-\gamma_{LV}cos\theta)}{\partial logC} \tag{10}$$

For calculation of Γ_{SL} for ethanol, the dependence between the adhesion surface tension and the activity (a) was used. The γ_{SL} value at the PMMA-solution and the quartz-solution interfaces was used in the Gibbs isotherm equation for the calculation of Γ_{SL} for surfactin and ethanol and it has the form:

$$\Gamma_{SL} = -\frac{a}{nRT}\frac{\partial\gamma_{SL}}{\partial a} = -\frac{C}{nRT}\frac{\partial\gamma_{SL}}{\partial C} = -\frac{1}{2.303nRT}\frac{\partial\gamma_{SL}}{\partial logC} \tag{11}$$

where: R is the gas constant, T is the temperature and n is the number depending on the type of surfactants (for the nonionic surfactant it is

equal to 1 and for the ionic surfactant of the type 1:1 electrolyte it is equal to 2).

The values of γ_{SL} used in this equation were obtained from Eq. (3) based on the components and parameters of the PMMA and quartz surface tension taken from the literature [45].

The Gibbs surface excess concentration of ethanol and surfactin at the PMMA-air and quartz-air interfaces was calculated from the Gibbs isotherm equation which has the form:

$$\Gamma_{SV} = -\frac{C}{nRT}\frac{\partial\gamma_{SV}}{\partial a} = -\frac{C}{nRT}\frac{\partial\gamma_{SV}}{\partial C} = -\frac{1}{2.303nRT}\frac{\partial\gamma_{SV}}{\partial logC} \tag{12}$$

Indeed, the Gibbs surface excess concentration at the above mentioned interfaces was calculated using the ethanol activity and the mole concentration for surfactin.

The total concentration of ethanol and surfactin was calculated from the Frumkin equation [1,46] which for the solid-air and solid-liquid interface can be expressed in the forms:

$$\gamma_{SW} - \gamma_{SV,f} = \pi = RT\Gamma_{SV,f}^{max}\ln f_0 (1 - \frac{\Gamma_{SV,f}}{\Gamma_{SV,f}^{max}}) \tag{13}$$

$$\gamma_{SW} - \gamma_{SL} = \pi = RT\Gamma_{SL}^{max}\ln f_0 (1 - \frac{\Gamma_{SL}}{\Gamma_{SL}^{max}}) \tag{14}$$

where: π is the pressure of the adsorbed layer, $\gamma_{SV,f}$ is the solid/adsorbed layer surface tension, $\Gamma_{SV,f}$ and $\Gamma_{SV,f}^{max}$ are the surface concentration of surface active agent at the solid-air interface, and the maximal concentration of this agent and Γ_{SL} and Γ_{SL}^{max} are the concentration of surface active agent at the solid-solution interface and the maximal concentration of this agent.

The γ_{SW} and γ_{SL} values used for calculation of surface concentration of ethanol and surfactin were determined from Eq. (3) based on the literature values of components and parameters of the solids surface tension. However, the $\gamma_{SV,f}$ values were determined on the basis of the Young-Dupre [46] and van Oss et al. [48,49] equations. The Young-Dupre equation can be written in the form [46]:

$$W_a = \gamma_{LV}(cos\theta + 1) \tag{15}$$

The van Oss et al. equation has the form [48,49]:

$$W_a = 2\sqrt{\gamma_{SV}^{LW}\gamma_{LV}^{LW}} + 2\sqrt{\gamma_{SV}^{+}\gamma_{LV}^{-}} + 2\sqrt{\gamma_{SV}^{-}\gamma_{LV}^{+}} \tag{16a}$$

For PTFE which is the apolar solid, Eq. (16a) can be expressed as [48, 49]:

$$W_a = 2\sqrt{\gamma_{SV}^{LW}\gamma_{LV}^{LW}} \tag{16b}$$

The differences between the adhesion work of the aqueous solution of surfactin and ethanol mixture calculated from Eqs. (15) and (16a) were treated as the adsorbed layer pressure at the PMMA-air and quartz-air interfaces.

The standard Gibbs free energy of ethanol and surfactin adsorption (ΔG_{ads}^{0}) at the solid-air and solid-solution interfaces was calculated from the Langmuir equation modified by de Boer [60] which can be written as:

$$\frac{A_0}{A - A_0}exp\frac{A_0}{A - A_0} = \frac{C}{\omega}\exp f_0 (\frac{-\Delta G_{ads}^{0}}{RT}) \tag{17}$$

where: ω is the number of water moles in 1 dm^3.

The values of the area occupied by a molecule of ethanol or surfactin (A) used in Eq. (17) were calculated based on the Gibbs surface excess concentration and the limiting area of these substrates (A_0) taken from the literature [44].

4. Results and discussion

The wettability of the solid by liquids and/or different kinds of the solutions depends on the difference between the adhesion work of liquid or solution to solid surface (W_a) and the cohesion work of liquid or solution (W_c) [46]. In the wetting process, the important role is played by the surface layer formation at the solid-liquid, solid-air, and liquid-air interfaces. The properties of even a single liquid in the interface region are different from those in the bulk phase [46]. In the case of the aqueous solution of the surface active agents and their mixture, the properties of the surface region depend on the surfactants adsorption at the interfaces as well as density and orientation of their molecules in the surface layers [1]. The formation of the surface layer at the solution-air interface causes a decrease of the interface tension [1,46]. This decrease influences on the wettability of the solid by the solution. However, a large decrease of the solution-air interface tension due to the adsorption of the surfactant at this interface does not prove that the surfactant is characterized by good wetting properties with regards to a given type of the solid [1,46]. The way of the surfactants molecule orientation at the solid-air and solid-solution interfaces and the surface tension of the surfactants tail and head decide about their wetting properties to a great extent. Short chain alcohols are very often added to the solution to improve the wetting properties of a given surfactant.

4.1. Contact angle

Surfactin (SF) adsorbing at the water-air interface reduces the water surface tension to minimal value comparable to that obtained by the aqueous solution of Tritons (Table S1) [61]. However, this value is achieved at the SF concentration many times lower than that of Tritons [42,61]. On the other hand, at the SF concentration in water at which the minimal value of solution surface tension was achieved, complete spreading of this solution drop over the apolar PTFE, monopolar PMMA and bipolar quartz is not observed [45]. Moreover, the minimal value of contact angle of SF solution on these solids is higher than that of Tritons solution and similar to the contact angle values of some ionic surfactants [62]. The surface tension value of the SF tail does not differ significantly from the one obtained for Tritons tail and some ionic classical surfactants [43,45]. Greater differences are between the components and parameters of the head surface tension of SF and Tritons and other surfactants (Table 1).

The addition of ethanol (ET) to surfactin (SF) solution changes the wetting properties of the solution considerably (Figs. 1–6). The aqueous solution of SF and ET mixture spreads over PMMA (Figs. 3 and 4) and quartz (Figs. 5 and 6) surface completely at the ET concentration at which it is present in the solution in the aggregated form independently of SF concentration [6]. In the case of PTFE, a significant decrease of the contact angle (θ) as a function of ET concentration is observed (Figs. 1 and 2). However, complete spreading does not take place. The surface tension of PTFE [3] is smaller than that of ET [3] (Table 1), water as well

Fig. 1. A plot of the contact angle (θ) of the water/ethanol solution of SF vs. the ethanol concentration (C_{ET}) for PTFE. Curves 1 – 17 correspond to the constant SF concentration equal to 0; 0.0002; 0.0005; 0.00125; 0003; 0.00625; 0.01; 0.02; 0.05; 0.1; 0.5; 1; 5; 10; 20; 30 and 40 mg/dm^3.
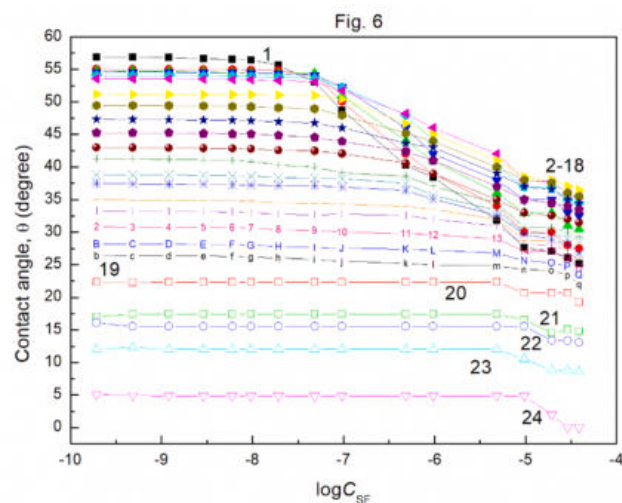

Fig. 2. A plot of the contact angle (θ) of the water/ethanol solution of SF vs. the logarithm of surfactin concentration (C_{SF}) for PTFE. Curves 1 – 30 correspond to the constant ET concentration equal to 0; 0.06692; 0.1338; 0.2677; 0.4015; 0.535; 1.0706; 1.6062; 2.1416; 2.677; 3.2124; 3.7478; 4.2832; 4.8185; 5.3538; 5.8893; 6.6925; 7.7245; 8.5664; 10.2797; 11.968; 12.145; 13.3794; 14.5696; 15.4064; 16.084; 16.3777; 16.648; 16.8988 and 17.13 M.

as the SF tail and head [45]. Thus, it is impossible to achieve complete spreading of PTFE by the aqueous solution of SF and ET mixture.

In the case of PMMA and quartz, their surface tension (γ_{SV}) is lower than that of water but larger than that of ET and SF tail and insignificantly different from that of SF head [3] (Table 1). For this reason complete spreading of PMMA and quartz surface can occur by the solution of SF and ET mixture at the proper ET concentration (Figs. 4–6).

The relationship between the contact angle and the solution-air (γ_{LV}), solid-air (γ_{SV}) and solid-solution (γ_{SL}) interface tensions can be explained on the basis of the Young consideration dealing with the equilibrium state of the liquid drop settled on the solid surface (Eq. (1)) as well as the Girifalco and Good consideration dealing with the interface tension (Eq. (2)) [47].

The values of the solid-solution interface tension which influence on the contact angle greatly depend, among others, on the parameter of intermolecular interactions across the solid-solution interface (ϕ). This

Table 1
The values of the Lifshitz-van der Waals (γ^{LW}) and acid-base (γ^{AB}) components as well as the electron-acceptor (γ^+) and the electron-donor (γ^-) parameters of the water, ethanol, PTFE, PMMA and quartz surface tension (γ) as well the SF head and tail surface tension taken from literature [44,45].

Substrate	Components and parameters				γ [mN/m]
	γ^{LW} [mN/m]	γ^{AB} [mN/m]	γ^+ [mN/m]	γ^- [mN/m]	
PTFE	20.24	0.00	0.00	0.00	20.24
PMMA	41.28	0.00	0.00	7.28	41.28
Quartz	38.07	9,63	1.61	14.36	47.70
Water	26.85	45.95	22.975	22.975	72.80
Ethanol	21.40	1.80	0.09	9.00	23.20
SF head	34.25	8.55	0.37	49.39	42.80
tail	24.70	0.00	0.00	0.00	24.70

Fig. 3. A plot of the contact angle (θ) of the water/ethanol solution of SF vs. the ethanol concentration (C_{ET}) for PMMA. Curves 1 – 17 correspond to the constant SF concentration equal to 0; 0.0002; 0.0005; 0.00125; 0003; 0.00625; 0.01; 0.02; 0.05; 0.1; 0.5; 1; 5; 10; 20; 30 and 40 mg/dm^3.
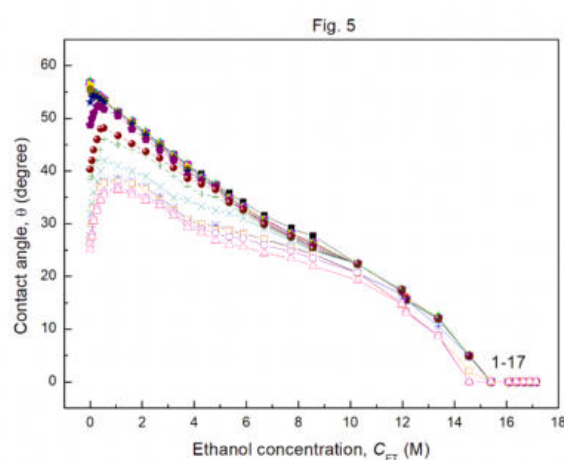
Fig. 5. A plot of the contact angle (θ) of the water/ethanol solution of SF vs. the ethanol concentration (C_{ET}) for quartz. Curves 1 – 17 correspond to the constant SF concentration equal to 0; 0.0002; 0.0005; 0.00125; 0003; 0.00625; 0.01; 0.02; 0.05; 0.1; 0.5; 1; 5; 10; 20; 30 and 40 mg/dm^3.
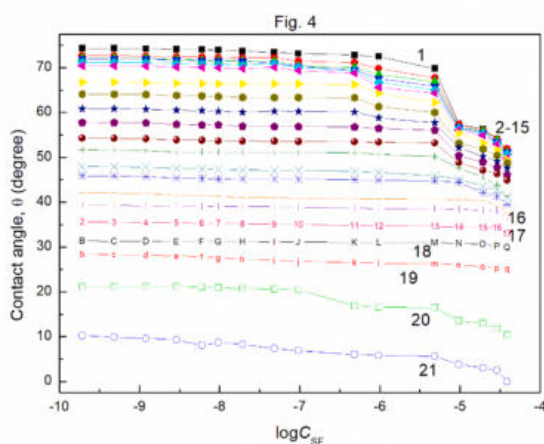
Fig. 4. A plot of the contact angle (θ) of the water/ethanol solution of SF vs. the logarithm of surfactin concentration (C_{SF}) for PMMA. Curves 1 – 21 correspond to the constant ET concentration equal to 0; 0.06692; 0.1338; 0.2677; 0.4015; 0.535; 1.0706; 1.6062; 2.1416; 2.677; 3.2124; 3.7478; 4.2832; 4.8185; 5.3538; 5.8893; 6.6925; 7.7245; 8.5664; 10.2797 and 11.968 M.

Fig. 6. A plot of the contact angle (θ) of the water/ethanol solution of SF vs. the logarithm of surfactin concentration (C_{SF}) for PMMA. Curves 1 – 24 correspond to the constant ET concentration equal to 0; 0.06692; 0.1338; 0.2677; 0.4015; 0.535; 1.0706; 1.6062; 2.1416; 2.677; 3.2124; 3.7478; 4.2832; 4.8185; 5.3538; 5.8893; 6.6925; 7.7245; 8.5664; 10.2797; 11.968; 12.145; 13.3794 and 14.5696 M.

parameter can be considered on the basis of Young (Eq. (1)) [46], Girifalco and Good (Eq. (2)) [47] as well as van Oss et al. (Eq. (3)) equations [48,49]. From these equations it is possible to obtain Eqs. (4)–(7) which were applied to calculate the ϕ parameter.

From Eqs. (4) and (7) it results that if the PTFE surface tension beyond the solution drop settled on its surface is constant independently of the composition and concentration of the SF and ET in the solution, then the ϕ values calculated from these both equations are the same and the dependence between $cos\theta$ and $\frac{\phi}{\sqrt{\gamma_{LV}}}$ according to Eq. (5) is linear. In the case of monopolar PMMA and bipolar quartz, if the surface layer of ET and SF mixture does not form beyond the solution drop settled on these solids, then the ϕ values calculated from Eqs. (4) and (6) should be the same and, as in the case of PTFE, $cos\theta$ should be changed linearly as a function of $\frac{\phi}{\sqrt{\gamma_{LV}}}$.

For these reasons the parameter ϕ was calculated not only from Eq. (4) but also from Eq. (7) for the PTFE-solution interface and from Eq. (6) for the PMMA-solution and quartz-solution interfaces based on the literature data [3,44] about the components and parameters of the solid

surface tension (Table 1).

It appeared that in the case of PTFE this dependence is linear and does not depend on the concentration and composition of ET and SF mixture (Fig. S2). This means that the changes of the contact angle as a function of ET concentration at the constant SF one and vice versa depend only on the solution surface tension and parameter of the intermolecular interactions across the PTFE-solution interface. This parameter depends on the composition, density and the orientation of the ET and SF molecules in the surface layer at the solid-solution interface.

In the case of PMMA and quartz, there is not one linear dependence between $cos\theta$ and $\frac{\phi}{\sqrt{\gamma_{LV}}}$ if parameter ϕ was calculated from Eq. (6) (Figs. S3 and S4). This indicates that in the case of PMMA and quartz beyond the solution drop settled on their surface, the mixed ET and SF layer is formed and it influences on the surface tension of PMMA and

quartz. The presence of ET in the layer results from the adsorption of - its molecules on these solid surfaces. On the other hand, the presence of SF in this layer results from the penetration of its molecules from the drop to the PMMA or quartz surfaces. Thus, the contact angle of the aqueous solution of SF and ET mixture is affected by not only the solid-air, solid-solution and solution-air interface tensions but also the pressure of the film (π) formed on the PMMA and quartz surface ($\pi = \gamma_{SW} - \gamma_{SVf}$).

4.2. Adsorption of the ET and SF at the solid-solution interface

The changes of the contact angle as a function of the ET and SF concentration and the composition of their mixtures depend on the adsorption of the ET and SF molecules at the solid-air, solid-solution and solution-air interfaces and the orientation of these molecules in the formed surface layer. The amount of ET and SF adsorption at the interfaces and their molecules orientation in the surface layers depend, among others, on the components and parameters of the surface tension of solid, water, ET as well as SF tail and head surface tension. The relative adsorption at the three interfaces (solid-solution, solid-air, and solution-air) in the solid-solution drop-air system can be established based on the Lucassen-Reynders equation (Eq. (8)) [59] if there is the linear dependence (Eq. (9)) between the adhesion and the surface tension of the solution or this dependence can be described by a proper equation from which it is possible to determine the differential from the adhesion tension to the surface tension.

From the Lucassen-Reynders equation (Eq. (8)), it results that the constant a in the linear function is equal to $\frac{\Gamma_{SV} - \Gamma_{SL}}{\Gamma_{LV}}$. Generally, the constant a can assume the value -1, between -1 and 0 as well as higher than 0. If Γ_{SV} is equal to zero and $a = -1$ then the Gibbs surface excess concentration at the solid-solution interface is equal to that at the solution-air one. For $a > -1$ but lower than 0, $\Gamma_{SV} - \Gamma_{SL} < \Gamma_{LV}$ or, if $\Gamma_{SV} = 0$, then $\Gamma_{SV} < \Gamma_{LV}$. In the case when $a > 0$, then $\Gamma_{SV} > \Gamma_{LV}$ or the adsorption at the solid-solution is negative.

According to the Young-Dupre equation (Eq. (15)) [46], if $a = -1$ then b is equal to the adhesion work of solution to solid surface and $b/2$ is equal to critical surface tension of solid wetting.

It is also possible to establish the Gibbs surface excess concentration of ET and SF at a given interface from the Gibbs isotherm equation (Eqs. (10)–(12)) [1,46] if the dependence between the interface tension and the concentration or activity can be expressed by the proper equation. In the case of apolar solid like PTFE, the relations between the adhesion tension and the concentration of one component at the constant other can be applied for determination of the Gibbs surface excess concentration at the solid-solution interface [3]. However, it should be stressed that the Gibbs surface excess concentration of ET at a given interface determined from its isotherm equation is close to the total concentration of ET at this interface only in the range of the low ET concentration. On the other hand, the values of the Gibbs surface excess concentration of ET in the range of its high concentration are uncertain which results from the Gibbs-Duhem equation for the surface region [46]. Thus, it seems that to obtain the real ET concentration, the Frumkin equation (Eqs. (13) and (14)) [1,3] is more useful in the case when we can establish the limiting adsorption basing on the Joos equation or we know the limiting area of ET molecule. In the case of SF, its Gibbs surface excess concentration is close to real concentration in the surface region at a given interface.

4.3. PTFE

For PTFE, the relationship between $\gamma_{LV}\cos\theta$ and γ_{LV} at both constant SF and ET concentration is linear but not in the whole ET concentration at the constant SF one and vice versa (Figs. S5 and S6). This relationship at the constant SF concentration is linear only in the range of ET concentration from zero to that at which the mole fraction of ET is equal to water one ($C_{ET} = 13.3794$ M). This indicates that there is one molecule

of alcohol for one molecule of water. It is worth noting that with such a ratio of water to alcohol molecules, the sum of the partial volumes of water and alcohol shows the smallest contraction [6]. In the other words, the volume of the aqueous solution of ET obtained by mixing the volume of water and ethanol including the same number of the moles is minimally lower than the sum of water and ET volume taken for solution preparation.

In the case of the aqueous solutions of ET and SF mixture at the constant ET concentration, there is a linear dependence between the adhesion and the surface tension in the whole range of SF concentration but only in the range of the ET constant concentration smaller than the value corresponding to the maximal Gibbs surface excess concentration of ET at the solution-air interface in the absence of SF ($C_{ET} = 3.7478$ M) [6]. On the other hand, in the range of ET concentration from this value to that close to CAC, the linear relationship between $\gamma_{LV}\cos\theta$ and γ_{LV} exists only in the range of SF concentration corresponding to the saturated monolayer at the solution-air interface in the absence of ET [42].

In all cases of the linear dependence between $\gamma_{LV}\cos\theta$ and γ_{LV}, the a constant is more or less close to -1 (Table 2).

Thus, according to the Lucassen-Reynders equation (Eq. (8)) [59], the adsorption of both ET and SF, in their above mentioned concentration range in the bulk phase at the PTFE-solution interface is similar to that at the solution-air one. Thus, it can take place if we assume that the adsorption of SF and/or ET on the PTFE surface does not change its surface tension. This assumption is based on the conclusion drawn from the parameter of the intermolecular interactions across the PTFE-solution interface as well as suggestions of the other investigators [49,63], who stated that in the case of the substrates having larger surface tension than PTFE their vapour does not change its surface tension. The surface tension of all substances present in the solution is higher than that of PTFE (Table 1), which means that our assumption is real. It raises a question: what is the relationship between the adsorption of ET and SF at the PTFE-solution interface to that at the solution-air one in the concentration range of ET and SF at which there is no linear relationship between the adhesion and surface tension. Unfortunately, on the basis of the dependence between $\gamma_{LV}\cos\theta$ and γ_{LV}, it is difficult to explain this problem. In the case of PTFE, the linear dependence between $\gamma_{LV}\cos\theta$ and γ_{LV} in a given range of SF and ET concentration can exist if the adhesion work of the solution to the PTFE surface (W_a) is constant in this concentration range. As the PTFE surface tension results only from the Lifshitz-van der Waals intermolecular interactions [51], this work can be calculated, among others, from the Eqs. (15) and (16b) [49].

The value of W_a for ET (41.62 mJ/m^2) calculated from Eq. (16b) is much lower than that of water (46.62 mJ/m^2) as well as that of SF tail and head. (Table 3). For this reason, the constant b in the linear dependence between $\gamma_{LV}\cos\theta$ and γ_{LV}, in the case when the ET concentration changes at the constant SF concentration, is lower than vice versa. Moreover, the W_a of the solution calculated from the Young-Dupre equation (Eq. (15)) [46] at the constant SF concentration above the ET mole fraction equal to 0.5 decreases up to the value of the ET adhesion work to the PTFE surface. In the case of solution at the low constant ET concentration, the Wa values of the solution are practically the same in the whole range of SF concentration. It should be emphasized that for the solution at the constant ET concentration the constant b values in all obtained linear dependences between $\gamma_{LV}\cos\theta$ and γ_{LV} are practically the same. However, for the solutions at the constant SF concentration, the b values are almost the same only at this concentration of SF corresponding to its unsaturated monolayer at the solution-air interface in the absence of ET. These b values are somewhat lower than W_a for water and those values obtained for the solution at the constant ET concentration but higher than W_a of ethanol to the PTFE surface.

Unfortunately, in the case of linear dependences between $\gamma_{LV}\cos\theta$ and γ_{LV} for PTFE, it is impossible to establish the conditions which can be fulfilled for complete wetting of PTFE surface because the values of $b/2$ are not real. From Eq. (16b) it results that complete wetting of PTFE

Table 2

The values of the constants a and b in the linear equation describing the relation between the adhesion and the surface tension as well as the average values of the solution adhesion work to the PTFE surface (W_a) calculated from Eq. (15).

Ethanol				Surfactin			
C_{SF} [mg/dm³]	b	a	W_aEq. (15)	C_{ET} [M]	b	a	W_aEq. (15)
0	43.99 ± 0.01	-0.999 ± 0.0021	43.99 ± 0.78	0	47.61 ± 0.40	-1.010 ± 0.0065	47.05 ± 0.65
0.01	42.96 ± 0.43	-0.971 ± 0.0093	44.18 ± 0.65	0.06692	48.40 ± 0.53	-1.031 ± 0.0115	47.02 ± 0.79
0.05	44.80 ± 0.38	-0.967 ± 0.0080	43.99 ± 0.55	1.0706	46.73 ± 0.80	-0.986 ± 0.0202	47.27 ± 0.83
0.1	44.81 ± 0.57	-0.955 ± 0.0138	44.81 ± 0.85	3.7478	47.42 ± 1.03	-1.012 ± 0.0308	47.00 ± 0.91
1	48.12 ± 0.49	-1.025 ± 0.0125	47.18 ± 0.78	4.8185	46.43 ± 0.99	-0.982 ± 0.0297	47.00 ± 1.01
5	46.68 ± 0.22	-0.995 ± 0.0064	46.85 ± 0.99	6.6925	46.71 ± 3.08	-0.997 ± 0.1020	46.81 ± 1.32
20	45.72 ± 0.17	-0.965 ± 0.0055	46.85 ± 0.55	8.5664	43.64 ± 3.76	-0.894 ± 0.1290	46.74 ± 1.25

Table 3

The values of adhesion work (W_a) calculated from Eq. (16a) and cohesion. (W_c) one equal to $2\gamma_{LV}$ as well as the difference between adhesion and cohesion work.

System	W_a [mJ/m²]	W_c [mJ/m²]	$W_a - W_c$ [mJ/m²]
Water-ET	79.58	145.60	-66.02
ET-water	79.58	46.40	33.18
Water-SF tail	51.51	145.60	-94.09
Water–SF head	133.85	145.60	-11.75
ET–SF tail	45.98	46.40	-0.42
E-SF head	62.01	46.40	15.61
PTFE-water	46.62	145.60	-98.98
PTFE-ethanol	41.62	46.40	-4.78
PTFE-SF tail	44.72	49.40	-4.68
PTFE-SF head	52.66	85.60	-32.94
PMMA-water	92.46	145.60	-53.14
PMMA–ethanol	61.06	46.40	14.66
PMMA–SF tail	63.86	49.40	14.46
PMMA–SF head	78.48	85.60	-7.12
Quartz–water	112.43	145.60	-33.17
Quartz–ethanol	66.97	46.40	20.57
Quartz–SF tail	61.33	49.40	11.93
Quartz–SF head SF	94.66	85.60	9.06

takes place if the surface tension of liquid and/or solution is equal to that of PTFE and results from the Lifshitz-van der Waals intermolecular interactions. The values of critical surface tension of PTFE wetting obtained from both $\gamma_{LV}cos\theta$ and γ_{LV} as well as cosine of contact angle and γ_{LV} dependences are different from the surface tension of PTFE (Table 1) [3].

For more detailed considerations of the SF and ET adsorption at the PTFE-solution interface and its relation to that at the solution-air one, the Gibbs [1,46] surface excess concentration as well as the Frumkin isotherm adsorption [1,46] were taken into account (Figs. S7–S10). For determination of the Frumkin isotherm adsorption, the contribution of ET and SF to the decrease of the PTFE-water interface tension due to their adsorption as well as the maximal adsorption of alcohol and surfactin must be known. For determination of ET and SF contribution to reduction of the PTFE-water interface tension affected by the SF and ET layer, it was assumed that this contribution is directly associated with the pressure of the single ET and SF. As the ET concentration in the studies was in the range from zero to single ET, therefore the maximal concentration (Γ_{ET}^{max}) at the both water-air and PTFE-water interfaces was assumed to be equal to 7.91×10^{-6} mol/m² [6]. However, the maximal concentration of SF (Γ_{SF}^{max}) at these interfaces was determined using the Joos equation [64].

The Gibbs and Frumkin isotherms of ET adsorption at the PTFE-water interface (PTFE-W) at the constant SF concentration corresponding to its unsaturated monolayer at the water-air interface (W-A) with the absence of ET (C_{SF}^{unsat}) [42] practically does not influence on the ET adsorption (Figs. S7 and S9). However, in the range of SF concentration corresponding to its saturated monolayer at the W-A interface (C_{SF}^{sat}), a decrease of ET adsorption takes place- in relation to the adsorption in the absence of SF. In the case of SF adsorption at the PTFE-W interface, the

presence of ET does not influence significantly on this adsorption if its concentration is in the range corresponding to the unsaturated monolayer at the W-A interface (C_{ET}^{unsat}) (Figs. S8 and S10) [6]. However, in the concentration range higher than CAC [6] (critical aggregation concentration of ET), a drastic decrease of SF adsorption occurs. In this concentration range, it was impossible to determine the Gibbs surface excess concentration because it was difficult to describe the PTFE-W interface tension as a function of SF concentration at the constant ET one higher than the CAC [6]. Thus, based on the determined Gibbs isotherm of SF adsorption, it seems that its adsorption at the PTFE-W interface is very small or does not occur at all. On the other hand, the Frumkin adsorption isotherm suggests that SF adsorbs at the PTFE-W interface in the whole ET concentration but the ET influences more on the SF adsorption than vice versa at its concentration higher than CAC [6].

The adsorption of the ET and SF at the PTFE-W interface depends on the interactions of water, ET and SF molecules with the PTFE surface as well as interactions between these molecules in the bulk phase (Table 3). As it is known, PTFE interacts with the adherent medium only by the Lifshitz-van der Waals forces [49]. If so, the largest interactions take place between the SF head and the PTFE surface and the smallest between PTFE and ET (Table 3). On the other hand, the largest interactions take place between the water molecules and the smallest between the ET and SF tail. In turn, the smallest difference is observed between the PTFE-ET and ET-ET interactions (Table 3). In the case of SF tail, these differences are smaller than for water. Probably, for this reason, the ET and SF molecules adsorbed on the PTFE surface can remove the water molecules from this surface. The mutual influence of ET and SF on their adsorption at the PTFE-W interface results not only from their interactions with the PTFE surface but also due to the interactions between each other. This interaction changes the hydration of both SF and ET. Dehydration of the SF head by the ET molecules can increase the SF tendency to adsorb at the PTFE-W interface but dehydration of SF tail decreases this tendency. The probabilities of the mutual dehydration of SF and ET molecules at the SF concentration equal to C_{SF}^{unsat} and ET to C_{ET}^{unsat} are smaller than at the concentration equal to C_{SF}^{sat} and C_{ET}^{sat} [6,42], respectively and therefore practically independent adsorption occurs. At the concentration of ET higher than CAC [6], the mixed ET and SF aggregates cannot be excluded. This process probably changes the solution Gibbs free energy to a larger extent than adsorption of SF at the PTFE-water interface. Besides this reason, the decrease of the dielectric constant of the solution causes that ET influences on the SF adsorption at the PTFE-water interface to a greater extent than vice versa.

From the comparison of the ET and SF adsorption at the PTFE-W and W-A interfaces it results that the adsorption of both substrates at the PTFE-W interface is smaller than that at W-A one (see for example Figs. S11–S20). The difference in the adsorption at these two interfaces increases for SF and ET with their increasing concentration in the bulk phase. This indicates that, at the constant SF concentration, the maximal adsorption of ET at the PTFE-W interface is smaller than at the W-A one and vice versa. For the changing concentration of ET at the constant concentration of SF, this relation between the ET adsorption at PTFE-W and PTFE-A takes place in the whole concentration range of ET in the

bulk phase. However, in the case of SF concentration changing, its adsorption at PTFE-W is smaller than at W-A only at a very small constant concentration of ET and this may result from the error in the calculations. The comparison of the Gibbs and Frumkin isotherms of the ET and SF adsorption at the both interfaces suggests that this adsorption at the solid-water interface is not exactly the same as that at the water-air interface despite the fact that there is the linear dependence between the adhesion and surface tension of the aqueous solution of the ET and SF mixture whose slope is close to unity. On the other hand, the lack of this dependence does not indicate that the adsorption at the two interfaces is different. - It can be also stated that the difference in the ET and SF maximal adsorption at the PTFE-W and W-A interfaces suggests that the orientation and packing of these substrates in the surface region at these interfaces is different.

4.4. PMMA

The mutual influence of ET and SF on their adsorption at the PMMA-water (PMMA-W) interface is more complicated than that at the PTFE-W interface. The aqueous solution of the ET and SF mixture spreads completely over the PMMA surface at the alcohol concentration $C_{ET} \geq 11.968$ M. This concentration does not depend on the SF concentration in the mixture. The surface tension of the solution of ET and SF mixture at which the solution begins to spread completely is insignificantly smaller than 27 mN/m [44] (Figs. 3 and 4) and also does not depend on the SF concentration. This tension can be treated as the critical surface tension of PMMA wetting by the studied solutions (γ_C). The γ_C value is considerably lower than that of the PMMA surface tension [3]. This fact and the values of the parameter of the intermolecular interactions across the PMMA-solution interface presented above suggest that the solution of ET and SF mixture drop settled on the PMMA surface spreads rather over the PMMA surface covered by the layer of ET and SF mixture than on pure PMMA. This is confirmed also by the fact that the adhesion interaction of ET and tail of SF is higher than the cohesion one (Table 3). Thus, the presence of ET in the layer beyond the solution drop settled on the PMMA surface results not only from its vapour adsorption but also from penetration of ET molecules from the drop on the PMMA surface. However, the presence of SF in this layer results rather only from the penetration of its molecule from the drop settled on PMMA on its surface beyond the drop. This suggestion confirms also the fact that, at the concentration of SF and ET corresponding to their C_{SF}^{sat} and C_{ET}^{sat} [6,42], the equilibrium state of the PMMA-solution drop-air system is achieved in longer time than that for the PTFE-solution drop-air one. From the mentioned facts, it probably results that the slope of the linear dependence between the adhesion and the surface tension is different from −1 and depends on the constant SF concentration (Fig. S21). According to the Lucassen-Reynders equation (Eq. (8)) [59], if the slope of the dependence between $\gamma_{LV}cos\theta$ and γ_{LV} is larger than −1 but smaller than 0, the adsorption of ET and SF cannot be excluded. It is possible that in such case the ET adsorption at the constant SF concentration beyond the drop settled on the PMMA surface is larger than zero but smaller than the adsorption of ET at the PMMA-W interface. To confirm this suggestion, the Gibbs and Frumkin isotherms [1,46] of ET adsorption at the PMMA-A and PMMA-W interfaces was calculated and compared to that at the W-A interface (Figs. S22–S29). Unfortunately, the Gibbs isotherm adsorption was possible to calculate only if the constant SF concentration was in the range from 0 to its CMC [42]. For determination of Gibbs and Frumkin isotherms of ET adsorption, the changes of PMMA-A and PMMA-solution interface tensions as a function of its concentration at a given constant SF concentration should be known. These changes were established based on the Young-Dupre (Eq. (15)) and van Oss et al. equations (Eq. (16a)) [46,48,49]. The procedure applied to determine the contribution of ET and SF adsorption to reduce of the PMMA-A and PMMA-W interface tension was the same as described for the systems including

PTFE. The Gibbs and Frumkin isotherms determined in such a way confirm the suggestion that the ET is present in the surface layer at the PMMA-A and PMMA-W interfaces and its amount at the PMMA-A interface is smaller than that at the PMMA-W one (see for example Figs. S26–S29). However, the adsorption of ET at these interfaces is smaller than that at the W-A one (Figs. S26–S29). In fact the Gibbs adsorption isotherm does not reflect the total ET concentration in the whole range of its concentration in the bulk phase.

The adsorption of a particular component of the solution depends to some extent on the adhesion and cohesion interactions of each component of this solution. In the studied PMMA-solution system, the water shows the largest adhesion interactions with the PMMA surface and ET the smallest (Table 3). The difference between the adhesion and cohesion interactions is negative for water and positive for ET. Thus, at the low ET and SF concentration, the water molecules can form the ordered film at the PMMA-W interface. It is known that ET and water are miscible in the bulk phase without limitation but they are not miscible in the surface layer [65]. Thus, it is possible that the ET molecules are adsorbed at the PMMA/water layer-solution but not at the PMMA-solution interface. This is confirmed by the fact that ET can completely spread over the water layer (Table 3). The adsorption of ET at its and SF low concentration at the PMMA-water interface can also be explained alternatively. Because the SF tendency to adsorb at the PMMA-W interface is considerably greater than ET, its molecules can remove water molecules and adsorb together with the ET molecules. Indeed, at high ET and SF concentration, the possibility to form a water layer in which its molecules are strongly ordered is less possible. In such case the adsorption of ET increases. The adsorption behaviour of SF at the PMMA-A and PMMA-W interfaces is different from that of ET. The relationship between $\gamma_{LV}cos\theta$ and γ_{LV} is impossible to describe by one function in the whole studied range of SF concentration at a given constant ET concentration (Fig. S30).

It is interesting that at the ET constant concentration, in the range from 0 to its concentration corresponding to the maximal Gibbs surface excess concentration at the W-A interface [6], dependence between $\gamma_{LV}cos\theta$ and γ_{LV} can be described by two linear functions (Fig. S30). One of them includes the SF concentration range from 0 to its CMC [42] and the other from CMC to the maximal concentration used. The slope of the first linear function is positive but of the second one negative. This indicates that probably at the SF concentration from 0 to CMC its adsorption is higher at the PMMA-A interface than that at the PMMA-W interface but at the concentration higher than CMC is vice versa.

This suggestion was confirmed by the Gibbs and Frumkin isotherms of SF adsorption (Figs. S31–S38). The comparison of these isotherms for three interfaces indicates that the SF adsorption at the PMMA-A and PMMA-W interface is smaller than that at the W-A one. This suggests that the SF molecules in the layer at the PMMA-A and PMMA-W interface are oriented parallel to the interface independently of the SF and ethanol concentration in the bulk phase, in the contrary to W-A one.

4.5. Quartz

For quartz, the dependence between $\gamma_{LV}cos\theta$ and γ_{LV} for ET at the constant SF concentration equal to C_{SF}^{unsat} [42] is linear with the exception for the small ET concentration and it can be described by the same linear function for each constant value of SF concentration (Fig. S39). According to the Lucassen-Reynders equation (Eq. (8)) [59], if the surface tension of quartz does not depend on the ET and SF concentration, then the ET adsorption at the quartz-water (Q-W) interface is negative. However, if the quartz surface tension is changed by the influence of ET and SF adsorption, then the ET adsorption at the quartz-A (Q-A) interface is higher than that at the quartz-water one. The above presented consideration suggests that formation of the mixed surface layer behind the solution drop settled on the quartz surface takes place. The ET as well as SF tail and head surface tensions are smaller than the surface

tension of quartz (Table 1) [3]. For this reason, the quartz surface tension decreases because it is affected by the mixed ET and SF layer. The adhesion forces of ET and tail and head of SF to quartz are larger than their cohesion forces (Table 3). This indicates that the ET and SF molecules can penetrate from the solution drop settled on the quartz surface beyond drop. Indeed, in the case of ET, its vapour can adsorb at the Q-A interface and be influenced on the quartz surface tension additionally.

Unfortunately, based on the dependence between $\gamma_{LV}cos\theta$ and γ_{LV} at the constant SF concentration equal to C_{SF}^{sat}, it is difficult to assess the adsorption of ET at the Q-A and Q-W interfaces.

The film of water can be formed on the quartz surface. In this film, the strong hydrogen bonds between the water molecules are saturated [66] and they can interact with adherent molecules only by weak hydrogen bonds and by the Lifshitz-van der Waals interactions. Such water film has ice-like properties [66]. Hence, depending on the ET and SF concentration, the adsorption of ET can take place at the quartz/-water layer-water and/or quartz-water interfaces.

More information on the ET adsorption at the interface of the considered phases can be provided by the Gibbs and Frumkin adsorption isotherms (Eqs. (10)–(14)). Therefore, applying the procedure mentioned above, these isotherms were determined (Figs. S40–S43). However, it was impossible to determine the Frumkin and Gibbs adsorption isotherms in the whole range of ET and SF concentrations. At the ET concentration equal or larger than 14.5696 M, the complete wetting of the quartz surface by the aqueous solution of ET and SF mixture is observed. The surface tension of this solution is close to 25 mN/m independently of the SF concentration. This value is considerably smaller than the quartz surface tension (Table 1) [3,45] and can be treated as γ_C for the quartz-aqueous solution of ET and SF mixture systems if the concentration of ET changes and concentration of SF is constant. At the ET concentration at which complete spreading of the solution takes place, the observed contact angle is equal to zero and it is impossible to establish the ET adsorption at the quartz-A and quartz-W interfaces. For this reason, it is difficult to determine the maximal ET adsorption at the constant SF concentration at the both considered interfaces. However, it can be stated, based on the comparison of the Gibbs and Frumkin isotherms [1,46] for W-A, Q-A and Q-W, that adsorption of ET at the Q-A and Q-W interfaces is smaller than at the W-A one and that adsorption at the Q-A interface is larger than at the Q-W one (see Figs. S44–S47). This confirms the suggestion resulting from the dependence between the adhesion and surface tension (Fig. S39). This should be also noted that the difference between the Frumkin adsorption isotherm (Eqs. (13) and (14)) at the Q-A and Q-W interface divided by the Frumkin isotherm of adsorption at the W-A interface is close to the value of the slope of the dependence between $\gamma_{LV}cos\theta$ and γ_{LV} obtained for ET at the constant SF concentration equal to C_{SF}^{unsat}. Knowing that the limiting adsorption of ET (Γ_{ET}^0), independently of its molecules perpendicular or parallel orientation, is equal to 7.91×10^{-6} mol/m^2 and it is possible to establish the ratio of the interface occupied by the ET molecules from the $\Gamma_{ET}/\Gamma_{ET}^0$. For example, the maximal coverage of the W-A, Q-A and Q-W interface by the ET molecules at the SF concentration equal to 0.1 mg (the beginning of the saturated monolayer at the W-A interface) is equal to 0.89, 0.64 and 0.26, respectively, However, at the SF concentration corresponding to its CMC, the coverage of these interfaces by ET is equal to 0.83, 0.53 and 0.23, respectively. It can be seen that ET adsorption decreases with the increasing of SF concentration. This is more evident at the quartz-water interface than at the water-air one. It should be emphasized that on the Frumkin isotherm for ET at the Q-A and Q-W interfaces the maximum is observed (Figs. S42 and S43). It is possible that at the ET concentration beginning with the concentration corresponding to the maximum on the Frumkin isotherm the water layer at the Q-W interface starts to destroy.

In the case of SF at the constant ET concentration, there is also the linear dependence between $\gamma_{LV}cos\theta$ and γ_{LV} whose slope, similarly to ET at the constant SF concentration, is positive (Fig. S48). This slope

depends on the ET concentration. As a matter of fact, not for all studied concentrations and composition of the ET and SF mixture the dependence between $\gamma_{LV}cos\theta$ and γ_{LV} is linear. However, the linear dependences at the positive slope indicate that adsorption of SF, similarly to ET at the Q-A interface, is larger than at the Q-W one. Such conclusion is confirmed by the comparison of the Gibbs and Frumkin isotherms at the three interfaces (Figs. S51–S55). Unfortunately, such comparison was possible to make only in the range of ET concentration from zero to the value corresponding to the maximum on the Gibbs isotherm of adsorption at the W-A interface. In this range of ET concentration, the difference between the Gibbs and Frumkin adsorption at the quartz-air and quartz-water interfaces divided by these adsorption isotherms at the W-A interface at the first approximation is close to the slope of the dependence between the adhesion and the surface tension (Fig. S48).

The determination of the coverage of the interfaces by SF molecules is more complicated than for ET. The limiting value of SF adsorption (Γ_{SF}^0) at the perpendicular orientation towards the interface is in the range from 1.38×10^{-6} mol/m^2 to 1.782×10^{-6} mol/m^2 depending on the configuration of SF head [42]. However, at the parallel orientation of SF molecules at the interface, Γ_{SF}^0 is equal to 1.06×10^{-6} mol/m^2 [6]. The adhesion interactions of SF oriented parallel to the quartz surface are considerably larger than that of perpendicular one [45]. On the other hand, the adhesion forces of SF tail and head to the quartz surface are higher than the cohesion ones (Table 3). Thus, as mentioned above the SF molecules can penetrate to the quartz surface from the solution drop and the replacement between the water and SF molecules at the quartz surface is more probable than in the case of ET. This may be a reason that there is the linear dependence between $\gamma_{LV}cos\theta$ and γ_{LV} only in a range of ET and SF concentrations.

Taking into account the above mentioned facts, it seems that the assumption that the SF molecules at the Q-A and Q-W interfaces are oriented rather parallel than perpendicular in the saturated layer is more probable. In such case, the maximal coverage of Q-A and Q-W interfaces in the absence of ET is equal to 0.78×10^{-6} and 0.41×10^{-6} mol/m^2, respectively. These values are smaller than the coverage of W-A interface by SF. Indeed, the coverage of the quartz-air and quartz-water interfaces as well as the water-air one by the SF molecules decreases with increasing ET concentration. Unfortunately, such type of comparison could be made in the low range of ET concentration (Figs. S49–S55). It should be stressed that some changes in the configuration of SF molecules as well as their orientation cannot be excluded.

4.6. Standard Gibbs free energy of ET and SF adsorption

During the adsorption of the ET and SF at the three interfaces in the solid-solution drop-air system, changes in the Gibbs free energy, enthalpy, and entropy of the system take place. If there is no chemical adsorption, then the changes of enthalpy during the adsorption process are associated only with the changes of the hydration of the solution components. In other words, the formation and breaking of hydrogen bonds determine the value of the adsorption enthalpy. In such case, the enthalpy achieves a small negative or positive value and the changes of entropy decide about the standard Gibbs free energy (ΔG_{ads}^0) changes during the adsorption process of the surface active agents at the interfaces. In the literature, it is possible to find many equations to calculate ΔG_{ads}^0. However, the Langmuir equation modified by de Boer is applied (Eq. (17)) [60] most often. In fact, the values of ΔG_{ads}^0 calculated for a low concentration of ET at the SF concentration smaller than C_{SF}^{sat} are real and for SF vice versa. The values of ET standard Gibbs free energy of adsorption at the PTFE-W interface are almost the same as the ΔG_{ads}^0 of ET adsorption at the W-A interface (Fig. S56) [6]. This indicates that in the range of SF concentration equal to C_{SF}^{unsat} [42] it does not influence on the ET adsorption. A similar conclusion as for ET can be drawn from the calculated ΔG_{ads}^0 values of SF adsorption (Fig. S57). This

fact suggests that in the range of SF concentration equal to C_{SF}^{unsat} and ET equal to C_{ET}^{unsat} [6,42] practically independent adsorption of ET and SF at the PTFE-W interface takes place.

In the case of PMMA and quartz, it was possible to calculate ΔG_{ads}^0 of ET and SF adsorption not only at PMMA-W and Q-W interfaces but also at the PMMA-A and Q-A ones (Figs. S58–S65). ΔG_{ads}^0 adsorption of ET at the PMMA-A and PMMA-W is almost the same and does not depend on the values of the constant SF concentration equal to C_{SF}^{unsat} (Figs. S58 and S59) [42]. However, the ET tendency to adsorb at the PMMA-A and PMMA-W is lower than at the W-A interface [6]. It results from the fact that the absolute values of ΔG_{ads}^0 for ET at the PMMA-A and PMMA-W interface (Figs. S58 and S59) are smaller than those of ET adsorption at the W-A interface [6]. This is probably connected with the increase of the enthalpy of adsorption due to the water surface layer destruction. This may be indicated by slight changes of ΔG_{ads}^0 for the ET adsorption at the PMMA-W interface as a function of SF concentration. ΔG_{ads}^0 of SF at the PMMA-A and PMMA-W (Figs. S60 and S61) is changed as a function of ET concentration to a greater extent than ET as a function of SF one. This can suggest that the SF molecules destroy the water layer at the interface to a larger extent than ET.

As mentioned above, the water layer on the quartz surface is ordered by the strong hydrogen bond between its molecules. This may be the reason that the absolute values of ΔG_{ads}^0 for ET adsorption at the quartz-water interface (Figs. S62 and S63) are considerably smaller than absolute values of ΔG_{ads}^0 for ET at the W-A interface [6]. However, the absolute values of ΔG_{ads}^0 for the ET adsorption at the Q-A interface are comparable to that at the W-A interface. It appeared that SF in the range of its concentration corresponding to C_{SF}^{unsat} practically does not influence on the ET adsorption at the both considered interfaces. However, the ET concentration influences on ΔG_{ads}^0 of SF adsorption insignificantly. Similar to ET the absolute values of ΔG_{ads}^0 for SF at the Q-W interface are slightly smaller than those at the W-A one (Figs. S64 and S65).

5. Conclusions

On the basis of the advancing contact angle measurements of the aqueous solution of ET and SF mixtures on the PTFE, PMMA and quartz surface as well as the thermodynamic analysis of the obtained results, the following conclusions can be drawn;.

In any case, the aqueous solution of ET and SF mixtures complete spread over the PTFE surface is not found. In the case of PMMA and quartz, the complete spreading of these solutions over their surface takes place at the ET concentration higher than its CAC in the absence of SF. The surface tension of the solution at the ET concentration ensuring complete wetting of these solids is considerably smaller than their surface tension.

The changes of the contact angle of studied solutions in the PMMA-solution drop-air and quartz-solution drop-air systems result not only from the changes of the solid-solution interface tension as a function of the ET and SF concentration but also arise from the changes of the surface tension of PMMA and/or quartz.

The dependence between the cosine of contact angle and interface interactions parameter divided by the root of the surface tension of the aqueous solution of ET and SF mixture suggests that the mixed layer of ET and SF formed on the PMMA and quartz surfaces beyond the solution drop in the PMMA(quartz)-solution drop-air system decreases their surface tension.

The concentration of ET and SF at the PTFE-solution interface differs only insignificantly from that at the solution-air interface. The lack of the linear dependence between the adhesion and the surface tension does not prove that there are significant differences between the adsorption of surface active agents at the solid-solution and solution-air interfaces. In turn, the positive slope of the linear dependence between the adhesion and surface tension does not indicate in each case that the

adsorption at the solid-solution interface is negative.

The adsorption of both ET and SF at the PMMA-solution and quartz-solution interfaces is lower than at the solution-air one. In the case of PMMA the adsorption of SF and ET at the PMMA-solution interface is higher than at the PMMA-air one but is vice versa for quartz.

The mechanism of SF and ET adsorption at the quartz-solution is more complicated than at the PTFE-solution and the PMMA-solution interfaces due to the strong ordered layer of water at the quartz-solution interface. This is reflected in the values of standard Gibbs free energy of adsorption. The absolute values of the standard Gibbs free energy of the ET and SF adsorption at the quartz-solution interface are lower not only than those for adsorption at the solution-air interface but also than the absolute values of this energy of adsorption at the PMMA-solution and PTFE-solution interfaces.

CRediT authorship contribution statement

Bronisław Jańczuk: Conceptualization, Formal analysis, Writing - review & editing. **Anna Zdziennicka:** Formal analysis, Supervision. **Edyta Rekiel:** Investigation, Methodology, Writing - original draft.

Declaration of Competing Interest

The authors declare that they have no known competing financial interests or personal relationships that could have appeared to influence the work reported in this paper.

Acknowledgments

Appendix A. Supporting information

Supplementary data associated with this article can be found in the online version at doi:10.1016/j.colsurfa.2021.127161.

References

[1] J.M. Rosen JM, Surfactants and Interfacial Phenomena, third ed., Wiley–Interscience, New York, 2004.

[2] R. Zana, Aqueous surfactant-alcohol systems: a review, Adv. Colloid Interface Sci. 57 (1995) 1–64, https://doi.org/10.1016/0001-8686(95)00235-I.

[3] A. Zdziennicka, B. Jańczuk, Modification of adsorption, aggregation and wetting properties of surfactants by short chain alcohols, Adv. Colloid Interface Sci. 284 (2020), 102249, https://doi.org/10.1016/j.cis.2020.102249.

[4] S. Shirzad, R. Sadeghi, Effects of addition of short-chain alcohol solvents on micellization and thermodynamic properties of anionic surfactants sodium dodecyl sulfate and sodium dodecyl sulfonate in aqueous solutions, J. Iran. Chem. Soc. 15 (2018) 1365–1375, https://doi.org/10.1007/s13738-018-1336-9.

[5] A.C. Ferreira, A. Sullo, S. Winston, I.T. Norton, A.B. Norton-Welch, Influence of Ethanol on Emulsions Stabilized by Low Molecular Weight Surfactants, J. Food Sci. 85 (2019) 28–35, https://doi.org/10.1111/1750-3841.14947.

[6] A. Chodzińska, A. Zdziennicka, B. Jańczuk, Volumetric and surface properties of short chain alcohols in aqueous solution-air systems at 293 K, J. Solut. Chem. 41 (2012) 2226–2245, https://doi.org/10.1007/s10953-012-9935-z.

[7] M. Bielawska, A. Zdziennicka, B. Jańczuk, Comparison between surface and volumetric properties of short-chain alcohols and some classical surfactants, ANNALES, SECTIO AA 71 (2016) 1–13, https://doi.org/10.17951/aa.2016.71.1.1.

[8] W.C. Pierce, D.P. MacMillan, X-ray studies on liquids: the inner peak for alcohols and acids, J. Am. Chem. Soc. 60 (1938) 779–783, https://doi.org/10.1021/ja01271a013.

[9] L. Pauling, The Nature of the Chemical Bond, Cornell University Press, Ithaca NY, 1960.

[10] M. Magini, G. Paschina, G. Piccaluga, On the structure of methyl alcohol at room temperature, J. Chem. Phys. 77 (1982) 2051–2056, https://doi.org/10.1063/1.444061.

[11] T. Weitkamp, J. Neuefeind, H.E. Fischer, M.D. Zeidler, Hydrogen bonding in liquid methanol at ambient conditions and at high pressure, Mol. Phys. 98 (2000) 125–134, https://doi.org/10.1080/00268970009483276.

[12] S. Sarkar, R.N. Joarder, Molecular clusters in liquid ethanol at room temperature, J. Chem. Phys. 100 (1994) 5118–5122, https://doi.org/10.1063/1.467177.

[13] K.S. Vahvaselkä, R. Serimaa, M.J. Torkkeli, Determination of liquid structures of the primary alcohols methanol, ethanol, 1-propanol, 1-butanol and 1-octanol by

Xray scattering, Appl. Crystallogr 28 (1995) 189–195, https://doi.org/10.1107/S0021888894010149.

[14] J.-H. Guo, Y. Luo, A. Augustsson, S. Kashtanov, J.E. Rubensson, D.K. Shuh, H. Ågren, J. Nordgren, Molecular structure of alcohol-water mixtures, Phys. Rev. Lett. 91 (2003), 157401, https://doi.org/10.1103/PhysRevLett.91.157401.

[15] C.J. Benmore, Y.L. Loh, The structure of liquid ethanol: a neutron diffraction and molecular dynamics study, J. Chem. Phys. 112 (2000) 5877–5883, https://doi.org/10.1063/1.481160.

[16] A. Zdziennicka, The wettability of polytetrafluoroethylene and polymethylmethacrylate by aqueous solutions of Triton X-100 and short chain alcohol mixtures, Appl. Surf. Sci. 255 (2009) 7369–7379, https://doi.org/10.1016/j.apsusc.2009.04.003.

[17] A. Zdziennicka, B. Jańczuk, Behavior of cationic surfactants and short chain alcohols in mixed surface layers at water-air and polymer-water interfaces with regard to polymer wettability. II Wettability of polymers, J. Colloid Interface Sci. 350 (2010) 568–576, https://doi.org/10.1016/j.jcis.2010.06.026.

[18] J.-B. Huang, M. Mao, B.-Y. Zhu, The surface physico-chemical properties of surfactants in ethanol–water mixtures, Colloids Surf. A 155 (1999) 339–348, https://doi.org/10.1016/S0927-7757(99)00003-5.

[19] K. Shirahama, T. Kashiwabara, The CMC-decreasing effects of some added alcohols on the aqueous sodium dodecyl sulfate solutions, J. Colloid Interface Sci. 36 (1971) 65–70, https://doi.org/10.1016/0021-9797(71)90240-2.

[20] S.S. Shah, M. Ali Awan, S.A. Idris, M. Ashraf, Effect of 1-alkanoles on the critical micelle concentration of cetyltrimethyl ammonium bromide, J. Chem. Soc. Pak. 19 (1997) 186–189.

[21] K. Shinoda, The effect of alcohols on the critical micelle concentrations of fatty acid soaps and the critical micelle concentration of soap mixtures, J. Phys. Chem. 58 (1954) 1136–1141, https://doi.org/10.1021/j150522a020.

[22] R. Zana, S. Yiv, C. Strazielle, P. Lianos, Effect of alcohol on the properties of micellar systems: I. Critical micellization concentration, micelle molecular weight and ionization degree, and solubility of alcohols in micellar solutions, J. Colloid Interface Sci. 80 (1981) 208–223, https://doi.org/10.1016/0021-9797(81)90177-6.

[23] S. Nishikawa, F. Matsuo, Dynamic study of aqueous solutions of 2-propanol and ethanol in the presence of anionic and cationic surfactants by ultrasonic methods, J. Phys. Chem. 95 (1991) 437–444, https://doi.org/10.1021/j100154a077.

[24] T. Parvin, M. Alauddin, M. Rokonuzzaman, Volumetric studies of alcohols in water and aqueous micelle solutions of cetyltrimethylammonium bromide, J. Bangladesh Chem. Soc. 24 (2011) 143–157, https://doi.org/10.3329/jbcs.v24i2.9703.

[25] M. Koshinuma, Studies of the dissolved state of sodium tetradecyl sulfate in ethanol–water mixtures by measurements of the activity, Bull. Chem. Soc. Jpn. 52 (1979) 1790–1795, https://doi.org/10.1246/bcsj.52.1790.

[26] N. Dharaiya, P. Bahadur, K. Singh, D.G. Marangoni, P. Bahadur, Light scattering and NMR studies of Triton X-100 micelles in the presence of short chain alcohols and ethoxylates, Colloids Surf. A 436 (2013) 252–259, https://doi.org/10.1016/j.colsurfa.2013.06.014.

[27] W. Li, Y.-C. Han, J.-L. Zhang, B.-G. Wang, Effect of ethanol on the aggregation properties of cetyltrimethylammonium bromide surfactant, Colloid J. 67 (2005) 159–163, https://doi.org/10.1007/s10595-005-0075-7.

[28] W. Li, Y.-C. Han, J.-L. Zhang, L.-X. Wang, J. Song, Thermodynamic modeling of CTAB aggregation in water-ethanol mixed solvents, Colloid J. 68 (2006) 304–310, https://doi.org/10.1134/S1061933×06030069.

[29] W. Li, M. Zhang, J. Zhang, Y. Han, Self-assembly of cetyltrimethylammonium bromide in ethanol-water mixtures, Front. Chem. China 4 (2006) 438–442, https://doi.org/10.1007/s11458-006-0069-y.

[30] A. Bhattarai, S.K. Shah, A.K. Yadav, Effect of solvent composition on the critical micelle concentration of cetylpyridinium chloride in ethanol-water mixed solvent media, Nepal J. Sci. Tech. 13 (2012) 89–93, https://doi.org/10.3126/NJST.V13I1.7446.

[31] J.D. Desai, I.M. Banat, Microbial production of surfactants and their commercial potential, Microbiol. Mol. Biol. Rev. 61 (1997) 47–64, https://doi.org/10.1128/.61.1.47-64.1997.

[32] R. Marchant, I.M. Banat, Biosurfactants: a sustainable replacement for chemical surfactants? Biotechnol. Lett. 34 (2012) 1597–1605, https://doi.org/10.1007/s10529-012-0956-x.

[33] D. Vollenbroich, M. Ozel, J. Vater, R.M. Kamp, G. Pauli, Mechanism of inactivation of enveloped viruses by the biosurfactant surfactin from *Bacillus subtilis*, Biologicals 25 (1997) 289–297, https://doi.org/10.1006/biol.1997.0099.

[34] A. Abalos, A. Pinazo, M.R. Casals, F. Garcia, A. Manresa, Physicochemical and antimicrobial properties of new rhamnolipids produced by *Pseudomonas aeruginosa* AT10 from soybean oil refinery wastes, Langmuir 17 (2001) 1367–1371, https://doi.org/10.1021/la0011735.

[35] M. Benincasa, A. Abalos, I. Oliveira, A. Manresa, Chemical structure, surface properties and biological activities of the biosurfactant Chemical structures and biological activities of rhamnolipids produced *by Pseudomonas aeruginosa* LBI from soap stock, Antonie Van. Leeuwenhoek 85 (2004) 1–8, https://doi.org/10.1023/B:ANTO.0000020148.45523.41.

[36] R. Makkar, S. Cameotra, An update on the use of unconventional substrates for biosurfactant production and their new applications, Appl. Microbiol. Biotechnol. 58 (2002) 428–434, https://doi.org/10.1007/s00253-001-0924-1.

[37] C.-C. Lai, Y.-C. Huang, Y.-H. Wei, J.-S. Chang, Biosurfactant-enhanced removal of total petroleum hydrocarbons from contaminated soil, J. Hazard. Mater. 167 (2009) 609–614, https://doi.org/10.1016/j.jhazmat.2009.01.017.

[38] C.N. Mulligan, Environmental applications for biosurfactants, Environ. Pollut. 133 (2005) 183–198, https://doi.org/10.1016/j.envpol.2004.06.009.

[39] G. Seydlová, J. Svobodová, Review of surfactin chemical properties and the potential biomedical applications (https://doi.org/), Cent. Eur. J. Med. 3 (2008) 123–133, https://doi.org/10.2478/s11536-008-0002-5.

[40] L. Rodrigues, I.M. Banat, J. Teixeira, R. Oliveira, Biosurfactants: potential applications in medicine, J. Antimicrob. Chemother. 57 (2006) 609–618, https://doi.org/10.1093/jac/dkl024.

[41] M. Nitschke, S.G.V.A.O. Costa, Biosurfactants in food industry, Trends Food Sci. Technol. 18 (2007) 252–259, https://doi.org/10.1016/j.tifs.2007.01.002.

[42] A. Zdziennicka, B. Jańczuk, Thermodynamic parameters of some biosurfactants and surfactants adsorption at water-air interface, J. Mol. Liq. 243 (2017) 236–244, https://doi.org/10.1016/j.molliq.2017.08.042.

[43] A. Zdziennicka, K. Szymczyk, J. Krawczyk, B. Jańczuk, Critical micelle concentration of some surfactants and thermodynamic parameters of their micellization, Fluid Ph. Equilib. 322–323 (2012) 126–134, https://doi.org/10.1016/j.fluid.2012.03.018.

[44] E. Rekiel, A. Zdziennicka, B. JańczuK, Adsorption of surfactin at water with ethanol mixture-air interface, J. Mol. Liq. (2019).

[45] A. Zdziennicka, B. Jańczuk, Wetting and adhesion properties of rhamnolipid and surfactin, Int. J. Adhes. Adhes. 84 (2018) 275–282, https://doi.org/10.1016/j.ijadhadh.2018.04.005.

[46] A.W. Adamson, A.P. Gast, Physical Chemistry of Surfaces, sixth ed., Wiley-Interscience, New York, 1997.

[47] L.A. Girifalco, R.J. Good, A theory for the estimation of surface and interfacial energies. I. Derivation and application to interfacial tension, J. Phys. Chem. 61 (1957) 904–909, https://doi.org/10.1021/j150553a013.

[48] C.J. van Oss, M.K. Chaudhury, R.J. Good, Monopolar surfaces, Adv. Colloid Interface Sci. 28 (1987) 35–64, https://doi.org/10.1016/0001-8686(87)80008-8.

[49] C.J. van Oss, Interfacial Forces in Aqueous Media, first ed., Marcel Dekker, New York, 1994.

[50] E. Bormashenko, Variational framework for defining contact angles: a general thermodynamic approach, J. Adhes. Sci. Technol. 24 (2) (2020) 219–230, https://doi.org/10.1080/01694243.2019.1663030.

[51] F.M. Fowkes, Attractive forces at interfaces, Ind. Eng. Chem. 56 (1964) 40–52, https://doi.org/10.1021/ie50660a008.

[52] D.H. Kaelble, K.C. Uy, A Reinterpretation of organic liquid-polytetrafluoroethylene surface interactions, J. Adhes. 2 (1970) 50–60, https://doi.org/10.1080/0021846708544579.

[53] D.K. Owens, R.C. Wendt, Estimation of the surface free energy of polymers, J. Appl. Polym. Sci. 13 (1969) 1741–1747, https://doi.org/10.1002/app.1969.070130815.

[54] S. Wu, Polar and nonpolar interactions in adhesion, J. Adhes. 5 (1973) 39–45, https://doi.org/10.1080/00218467308078437.

[55] S. Wu, Surface tension of solids: an equation of state analysis, J. Colloid Interface Sci. 71 (1979) 605–609, https://doi.org/10.1016/0021-9797(79)90332-1.

[56] D. Li, A.W. Neumann, Equation of state for interfacial tensions of solid-liquid systems, Adv. Colloid Interface Sci. 39 (1992) 299–345, https://doi.org/10.1016/0001-8686(92)80064-5.

[57] D.Y. Kwok, A.W. Neumann, Contact angle interpretation in terms of solid surface tension, Colloids Surf. A 161 (2000) 31–48, https://doi.org/10.1016/S0927-7757(99)00323-4.

[58] E. Chibowski, Surface free energy of a solid from contact angle hysteresis. Adv, Colloid Interface 103 (2003) 149–172, https://doi.org/10.1016/S0001-8686(02)00093-3.

[59] E.H. Lucassen-Reynders, Contact angles and adsorption on solids, J. Phys. Chem. 67 (1963) 969–972, https://doi.org/10.1021/j100799a005.

[60] J.H. de Boer, The Dynamical Character of Adsorption, first ed., Oxford University Press, London, 1953.

[61] A. Zdziennicka, K. Szymczyk, J. Krawczyk, B. Jańczuk, Activity and thermodynamic parameters of some surfactants adsorption at the water–air interface, Fluid Ph. Equilibr. 318 (2012) 25–33, https://doi.org/10.1016/j.fluid.2012.01.014.

[62] K. Szymczyk, A. Zdziennicka, J. Krawczyk, B. Jańczuk, Wettability, adhesion, adsorption and interface tension in the polymer/surfactant aqueous solution system. I. Critical surface tension of polymer wetting and its surface tension, Colloids Surf. A 402 (2012) 131–137, https://doi.org/10.1016/j.colsurfa.2012.02.054.

[63] P. Hu, A.W. Adamson, Adsorption contact angle studies. II. Water and organic substances on polished polytetrafluoroethylene, J. Colloid Interface Sci. 59 (1977) 605–614, https://doi.org/10.1016/0021-9797(77)90055-8.

[64] P. Joos, Thermodynamics of mixed monolayers, Bull. Soc. Chim. Belg. 76 (1967) 591–600, https://doi.org/10.1002/bscb.19670761105.

[65] D. Mukherji, C.M. Marques, K. Kremer, Polymer collapse in miscible good solventsis a generic phenomenon driven by preferential adsorption, Nat. Commun. 5 (2014) 4882, https://doi.org/10.1038/ncomms5882.

[66] F.M. Fowkes, Calculation of work of adhesion by pair potential summation, J. Colloid Interface Sci. 28 (1968) 493–505, https://doi.org/10.1016/0021-9797(68)90082-9.

MUTUAL INFLUENCE OF ETHANOL AND SURFACTIN ON THEIR WETTING AND ADHESION PROPERTIES

EDYTA REKIEL, ANNA ZDZIENNICKA* AND BRONISŁAW JAŃCZUK

Department of Interfacial Phenomena, Institute of Chemical Sciences, Faculty of Chemistry, Maria Curie-Skłodowska University in Lublin, Maria Curie-Skłodowska Sq. 3, 20-031 Lublin, Poland

Running title: mutual influence

*To whom correspondence should be addressed

  phone (48-81) 537-56-70   fax (48-81) 533-3348)

  e-mail aniaz@hektor.umcs.lublin.pl

Table S1 The comparison of the values of critical micelle concentration (CMC), the maximal Gibbs surface excess concentration at water-air interface (Γ^{max}) and the minimal surface tension of aqueous solution of SF and Triotns (γ^{min}) as well as the minimal contact angle (θ^{min}) of this solution on PTFE and PMMA surface to values of these magnitudes for some synthetic classical surfactants taken form literature [1 - 4].

Surfactant	CMC [mM]	Γ^{max}x 10^{-6} [mol/m^2]	γ^{min} [mN/m]	θ^{min}[degree]	
				PTFE	PMMA
SF	0.00966	1.38	32.37	62.00	51.90
TX-100	0.29	2.83	33.80	67.50	29.78
TX-165	0.541	2.12	39.50	78.15	49.40
TX-114	0.168	2.52	30.87	59.13	29.50

Surfactin (Fig. S1) is produced by *Bacillus subtilis* and belongs to lipopeptide. The surfactin molecule is built from seven amino acids bound with the carboxyl and hydroxyl groups of the 14-carbon acid. Surfactin is a heptapeptide with a b-hydroxy fatty acid within a lactone ring structure [5]. As stated by Ishigami this biosurfactant can fold into a b-sheet structure, which resembles a horse saddle in the aqueous solutions and at the air/water interface [6]. This is a very powerful biosurfactant which can reduce the surface tension of water to 32.37 mN/m at the concentration equal to 40 mg/dm^3 [7]. Surfactin forms rod-like micelles with an aggregation number of ~ 170 [8].
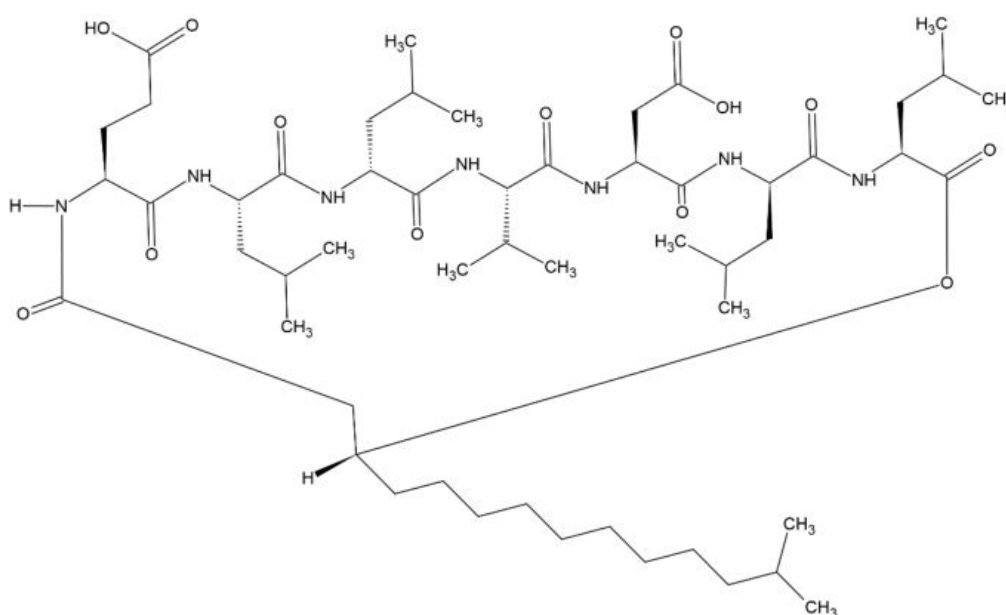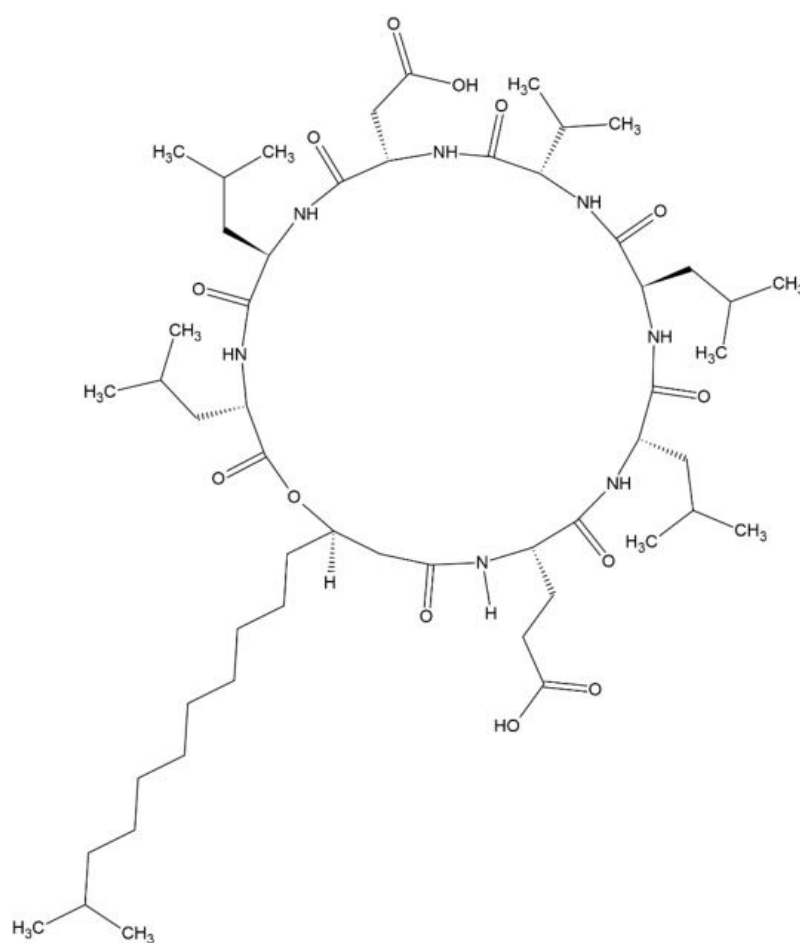
Fig. S1. Two forms of surfactin molecule

References

[1] A. Zdziennicka, B. Jańczuk, Thermodynamic parameters of some biosurfactants and surfactants adsorption at water-air interface, J. Mol. Liq. 243 (2017) 236–244. https://doi.org/10.1016/j.molliq.2017.08.042.

[2] A. Zdziennicka, K. Szymczyk, J. Krawczyk, B. Jańczuk, Critical micelle concentration of some surfactants and thermodynamic parameters of their micellization, Fluid Ph. Equilibria 322-323 (2012) 126-134.https://doi.org/10.1016/j.fluid.2012.03.018.

[3] A. Zdziennicka, B. Jańczuk, Wetting and adhesion properties of rhamnolipid and surfactin, Int. J. Adhes.Adhes.84 (2018) 275-282. https://doi.org/10.1016/j.ijadhadh.2018.04.005.

[4] A. Zdziennicka, K. Szymczyk, J. Krawczyk, B. Jańczuk, Activity and thermodynamic parameters of some surfactants adsorption at the water–air interface, Fluid Ph. Equilibria, 318 (2012) 25-33.https://doi.org/10.1016/j.fluid.2012.01.014.

[5] G. Seydlová, J. Svobodová, Review of surfactin chemical properties and the potential biomedical applications, Cent. Eur. J. Med. • 3(2) • 2008 • 123-133, DOI: 10.2478/s11536-008-0002-5

[6] Y. Ishigami, M. Osman, H. Nakahara, Y. Sano, R. Ishiguro, M. Matsumoto, Significance of β-sheet formation for micellization and surface adsorption of surfactin, Colloids Surfaces B, 4 (1995) 341-348. https://doi.org/10.1016/0927-7765(94)01183-6

[7] E. Rekiel, A. Zdziennicka, B. Jańczuk, Adsorption of surfactin at water with ethanol mixture-air interface, J. Mol. Liq. 300 (220) 11 https://doi.org/10.1016/j.molliq.2019.112240.
[8] (Heerklotz H., Seelig J., Detergent-like action of the antibiotic peptide surfactin on lipid membranes, Biophys. J., 2001, 81, 1547-1554). https://doi.org/10.1016/S0006-3495(01)75808-0
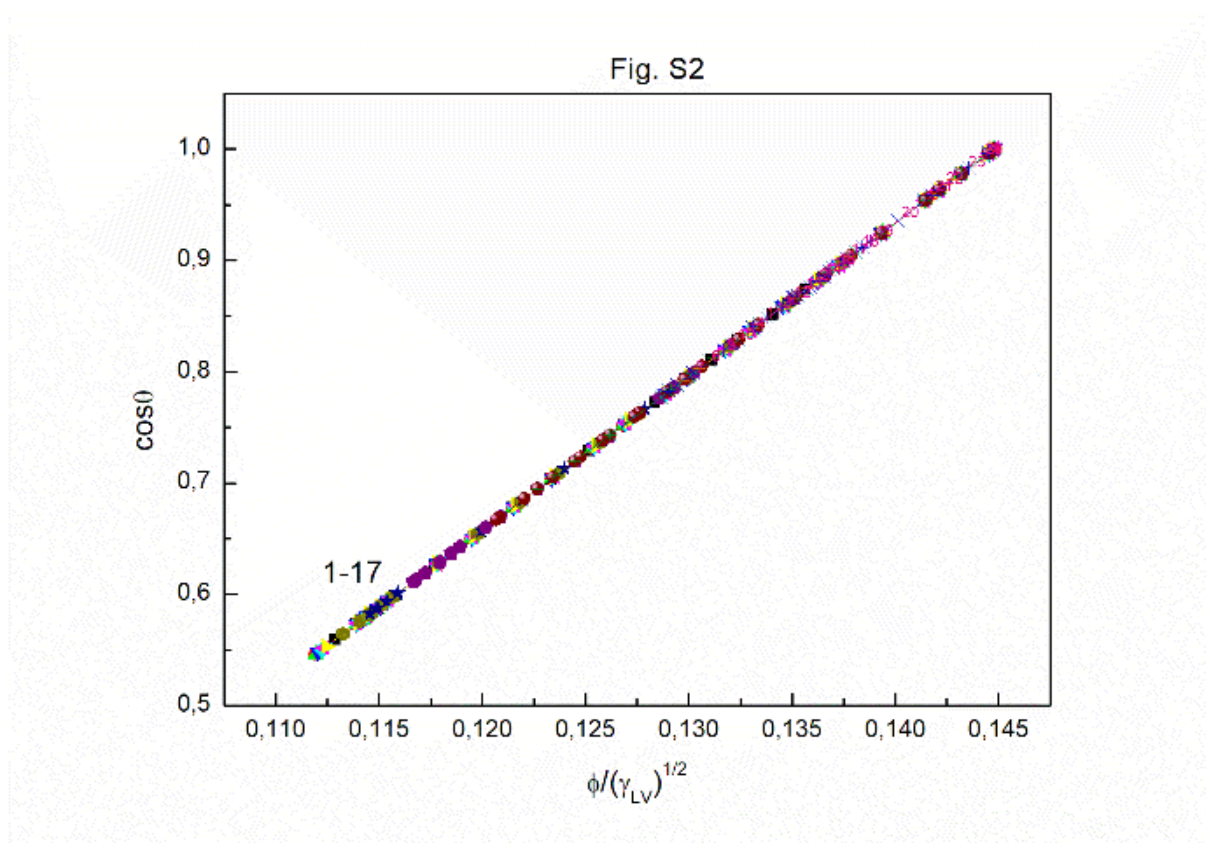
Figure S2. A plot of the cosine of the contact angle ($cos\theta$) for PTFE vs. the ratio of the parameter of intermolecular interactions to the root of the solution surface tension [7] $\left(\frac{\phi}{\sqrt{\gamma_{LV}}}\right)$. Curves 1 – 17 correspond to the constant SF concentration equal to 0; 0.0002; 0.0005; 0.00125; 0003; 0.00625; 0.01; 0.02; 0.05; 0.1; 0.5; 1; 5; 10; 20; 30 and 40 mg/dm^3.
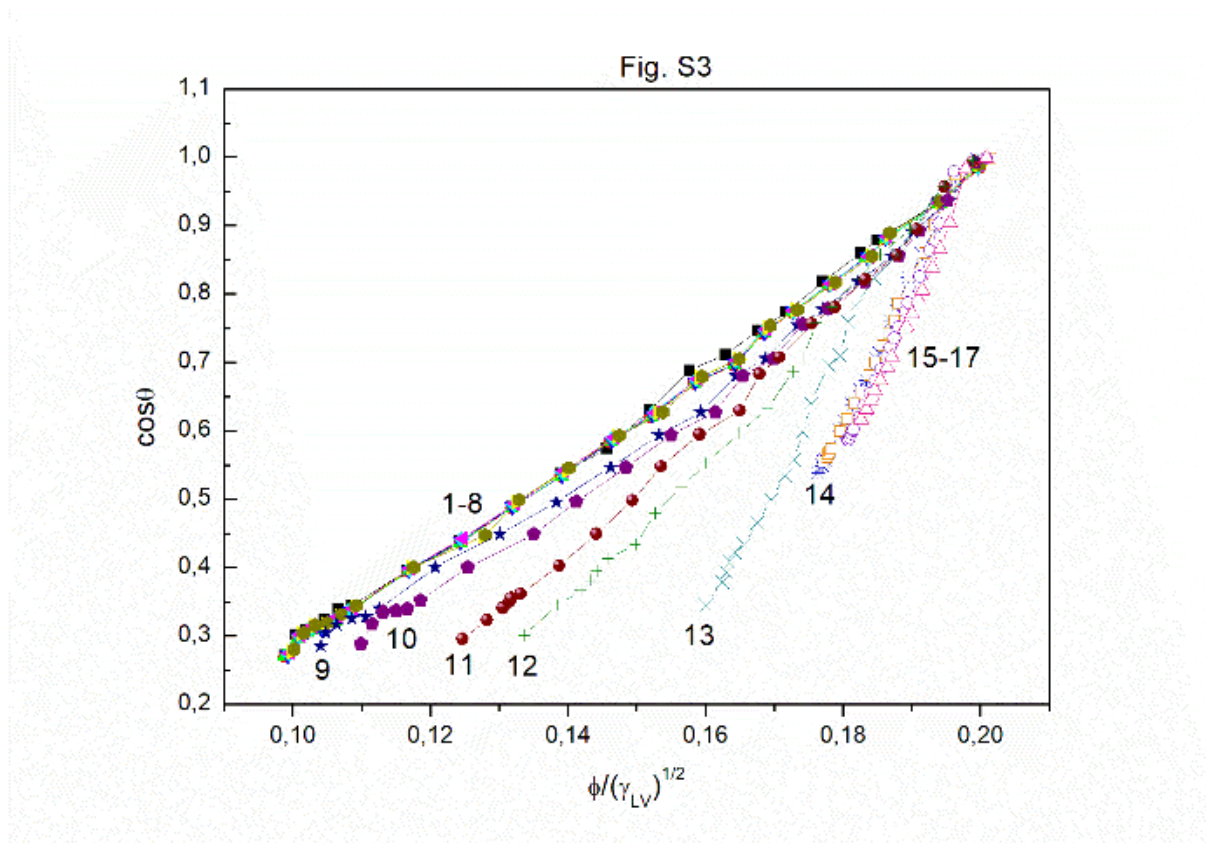
Figure S3. A plot of the cosine of the contact angle ($cos\theta$) for PMMA vs. the ratio of parameter of intermolecular interactions calculated from Eq. (6) to the root of solution surface tension [7] $\left(\frac{\phi}{\sqrt{\gamma_{LV}}}\right)$. Curves 1 – 17 correspond to the constant SF concentration equal to 0; 0.0002; 0.0005; 0.00125; 0003; 0.00625; 0.01; 0.02; 0.05; 0.1; 0.5; 1; 5; 10; 20; 30 and 40 mg/dm³.
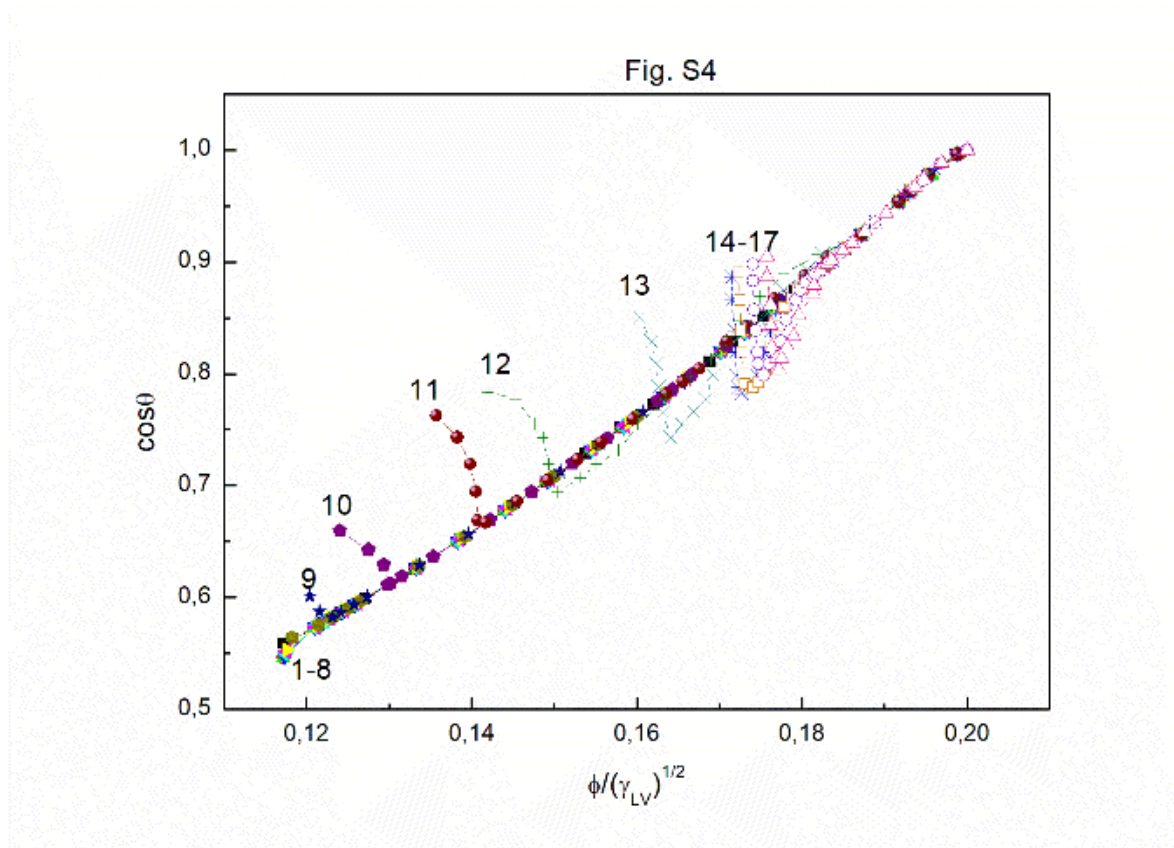
Figure S4. A plot of the cosine of the contact angle ($cos\theta$) for quartz vs. the ratio of parameter of intermolecular interactions calculated from Eq. (6) to the root of solution surface tension [7] $\left(\frac{\phi}{\sqrt{\gamma_{LV}}}\right)$. Curves 1 – 17 correspond to the constant SF concentration equal to 0; 0.0002; 0.0005; 0.00125; 0003; 0.00625; 0.01; 0.02; 0.05; 0.1; 0.5; 1; 5; 10; 20; 30 and 40 mg/dm^3.
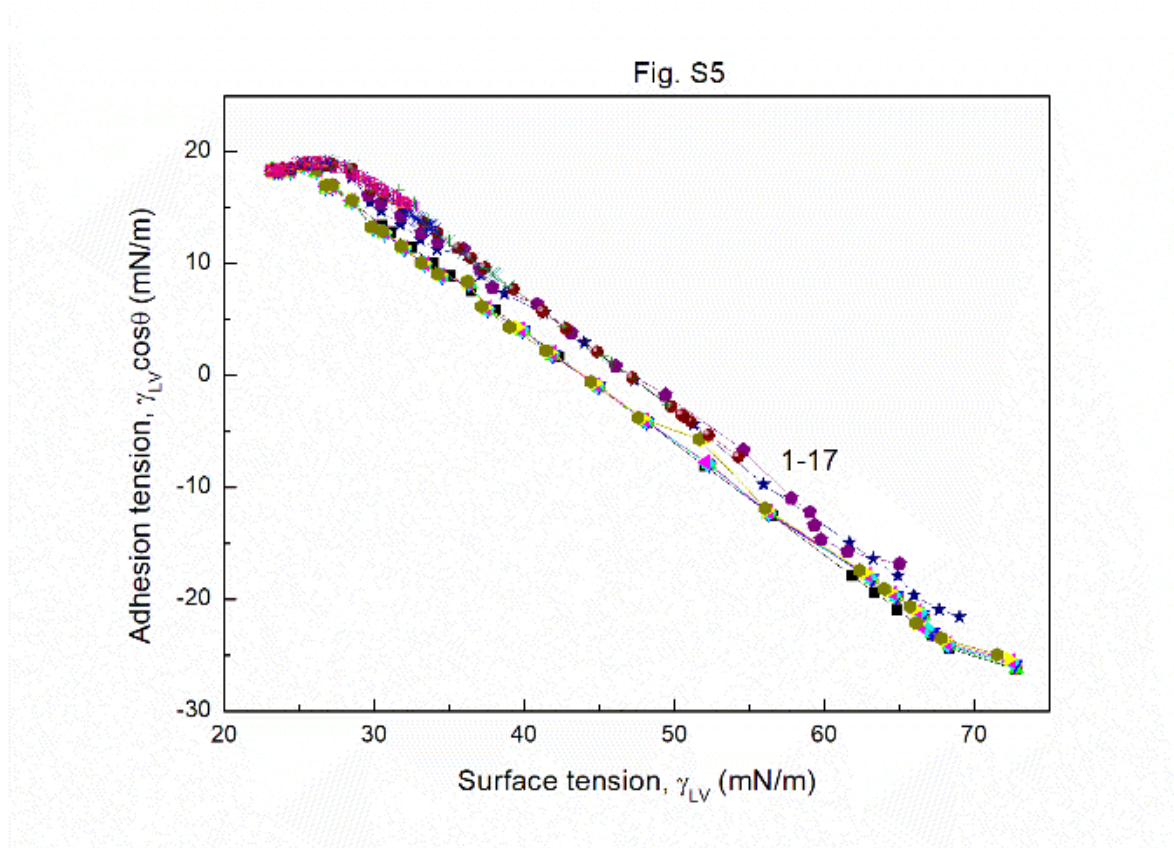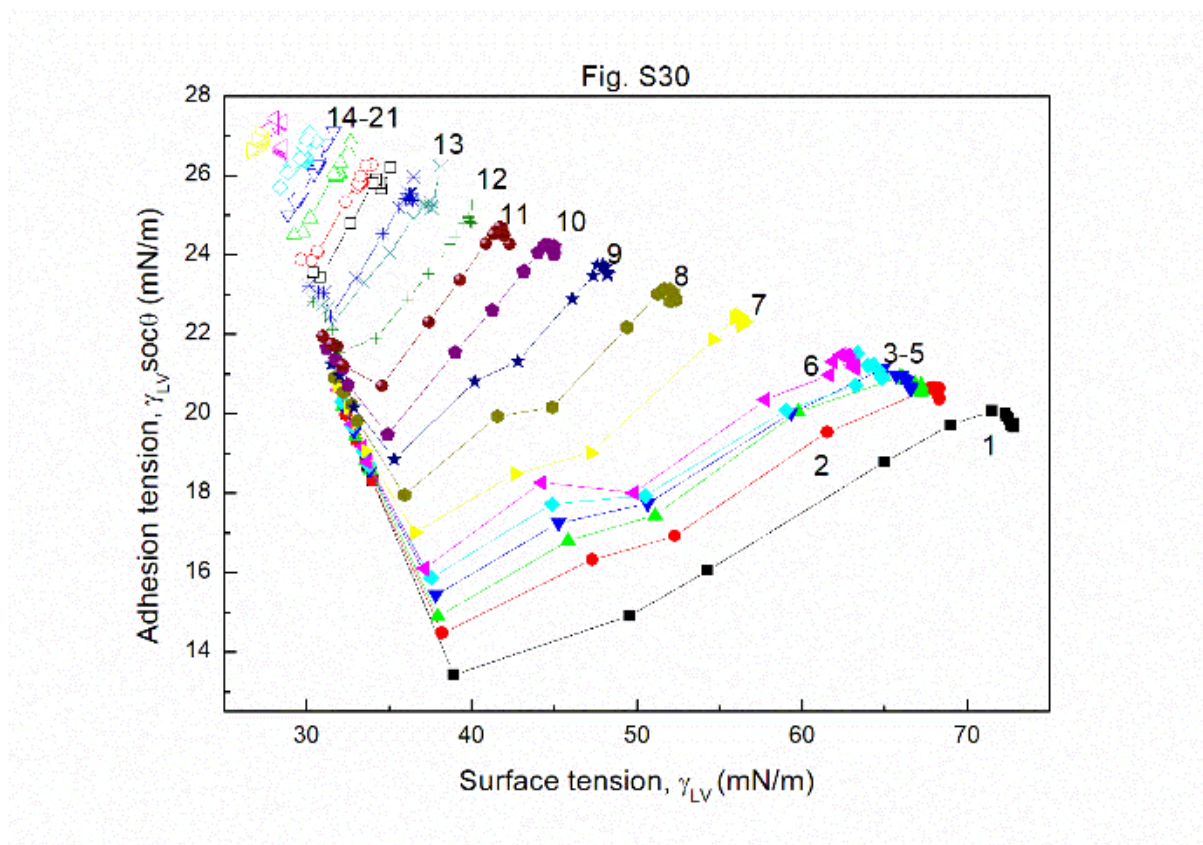
Figure S5. A plot of the adhesion tension ($\gamma_{LV}\cos\theta$) for PTFE vs. the solution surface tension (γ_{LV}) [7]. Curves 1 – 17 correspond to the constant SF concentration equal to 0; 0.0002; 0.0005; 0.00125; 0003; 0.00625; 0.01; 0.02; 0.05; 0.1; 0.5; 1; 5; 10; 20; 30 and 40 mg/dm^3.
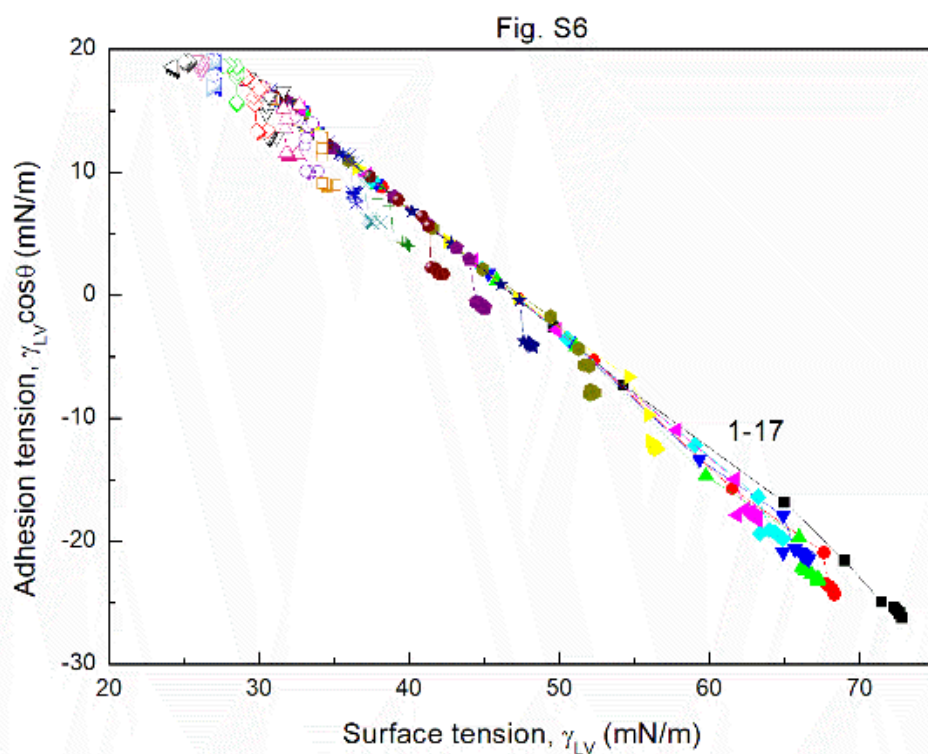
Figure S6. A plot of the adhesion tension ($\gamma_{LV}cos\theta$) for PTFE vs. the solution surface tension (γ_{LV}) [7]. Curves 1 – 25 correspond to the constant ET concentration equal to 0; 0.06692; 0.1338; 0.2677; 0.4015; 0.535; 1.0706; 1.6062; 2.1416; 2.677; 3.2124; 3.7478; 4.2832; 4.8185; 5.3538; 5.8893; 6.6925; 7.7245; 8.5664; 10.2797; 11.968; 12.145; 13.3794; 14.5696 and 15.4064 M.
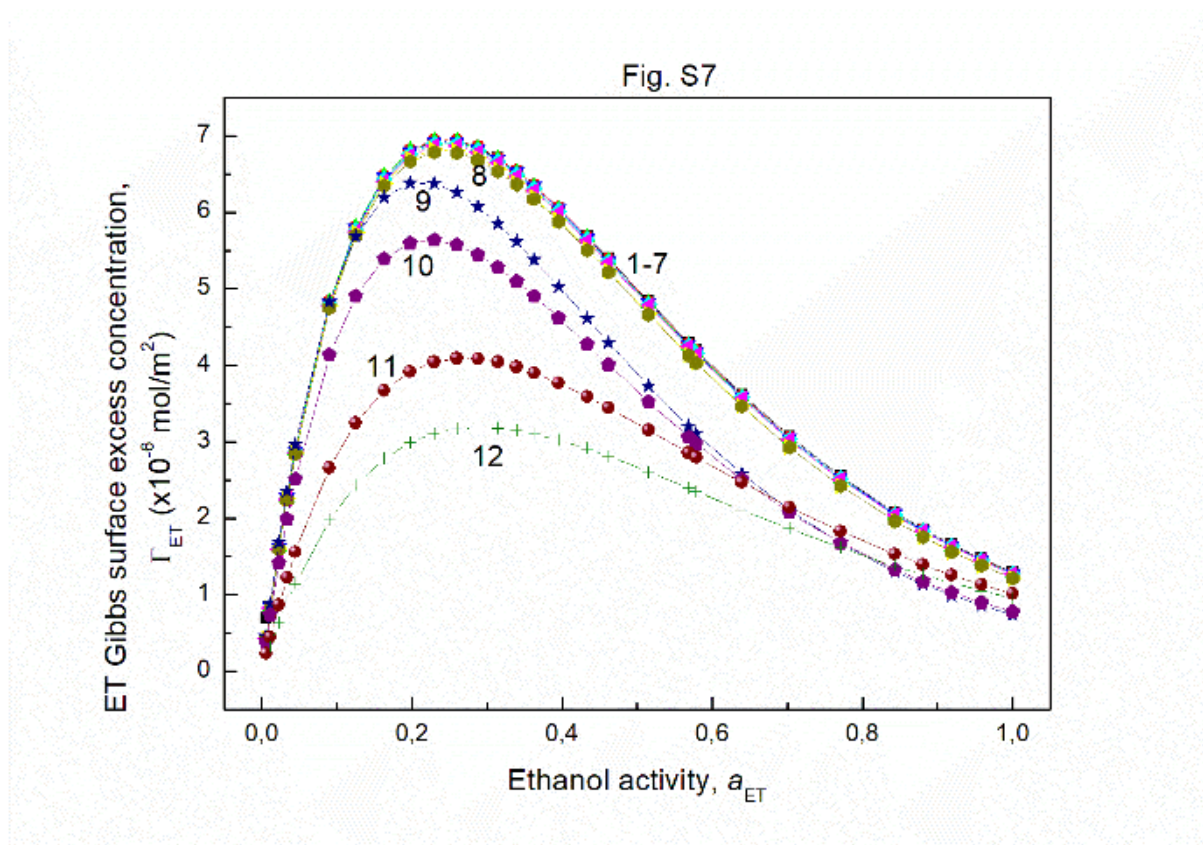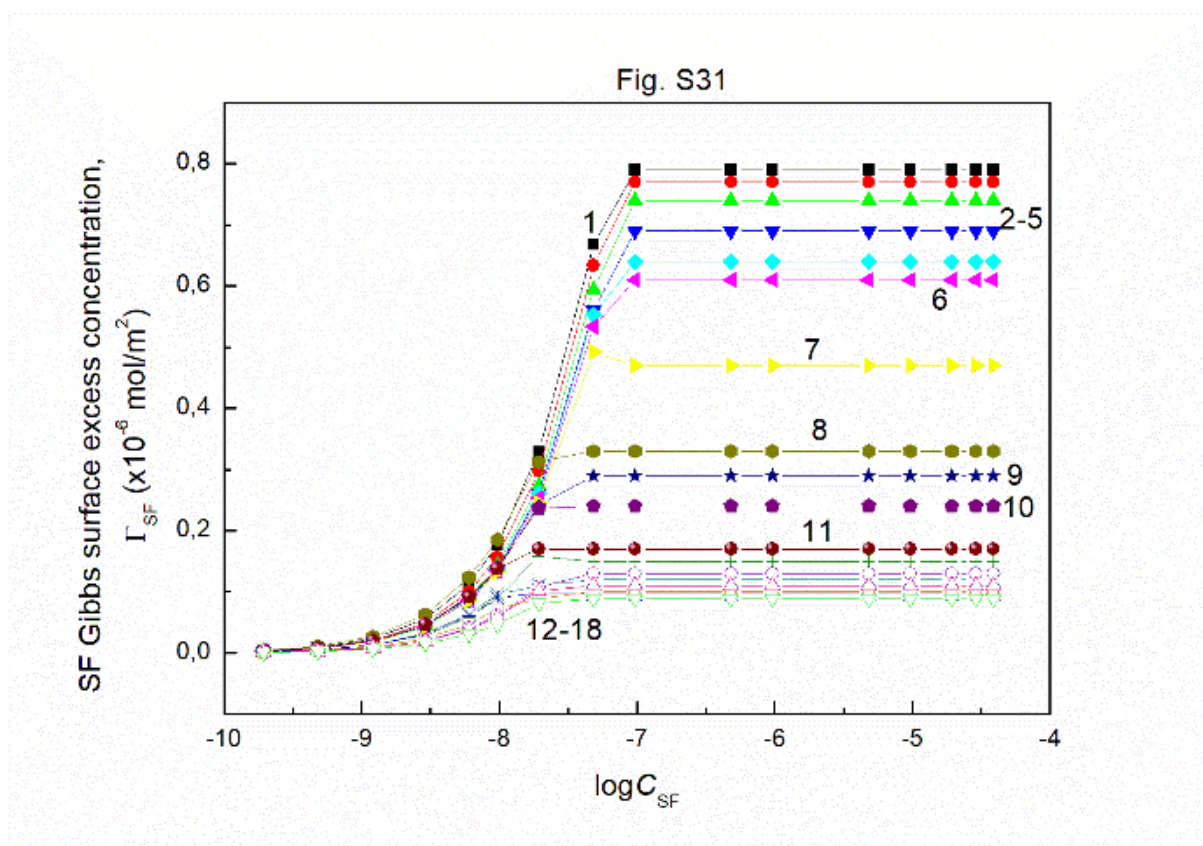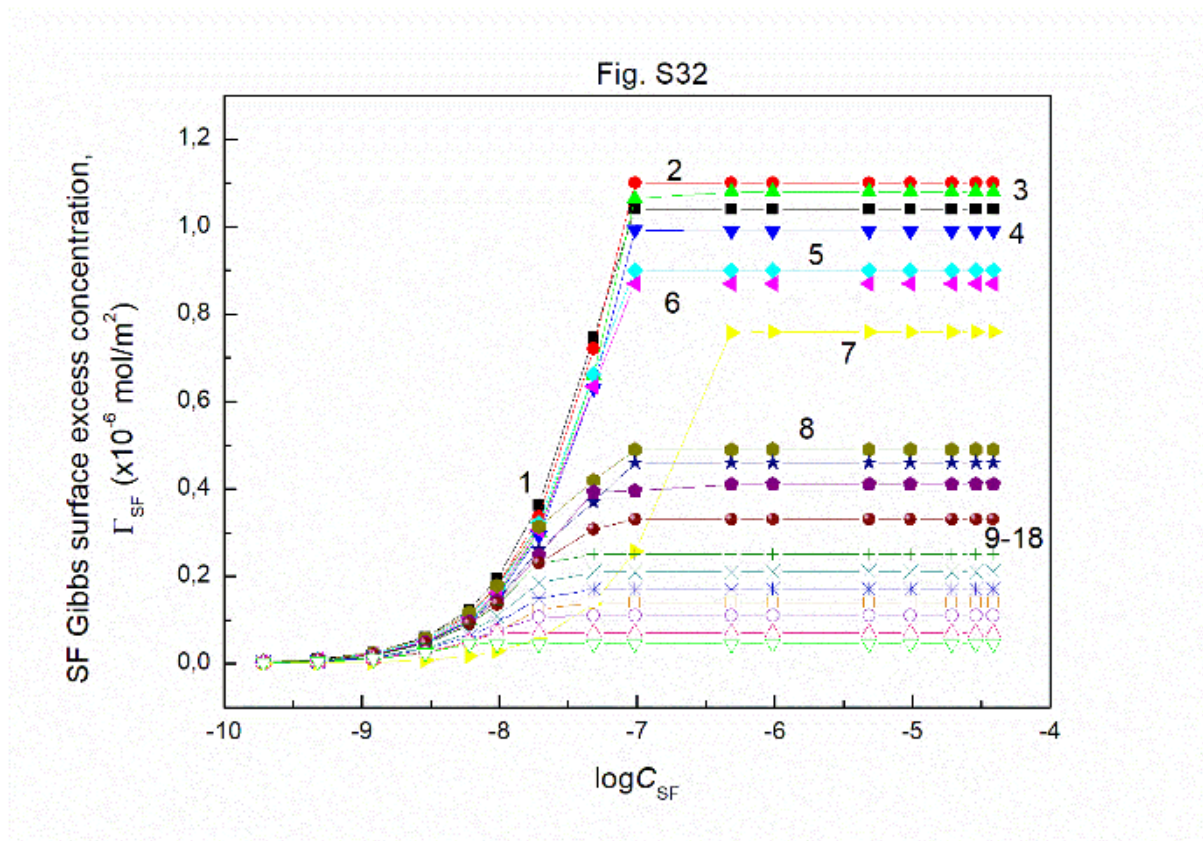
Figure S7. A plot of the ET Gibbs surface excess concentration at the PTFE–solution interface (Γ_{ET}) vs. the ethanol activity (a_{ET}). Curves $1 - 12$ correspond to the constant SF concentration equal to 0; 0.0002; 0.0005; 0.00125; 0003; 0.00625; 0.01; 0.02; 0.05; 0.1; 0.5 and 1 mg/dm³.
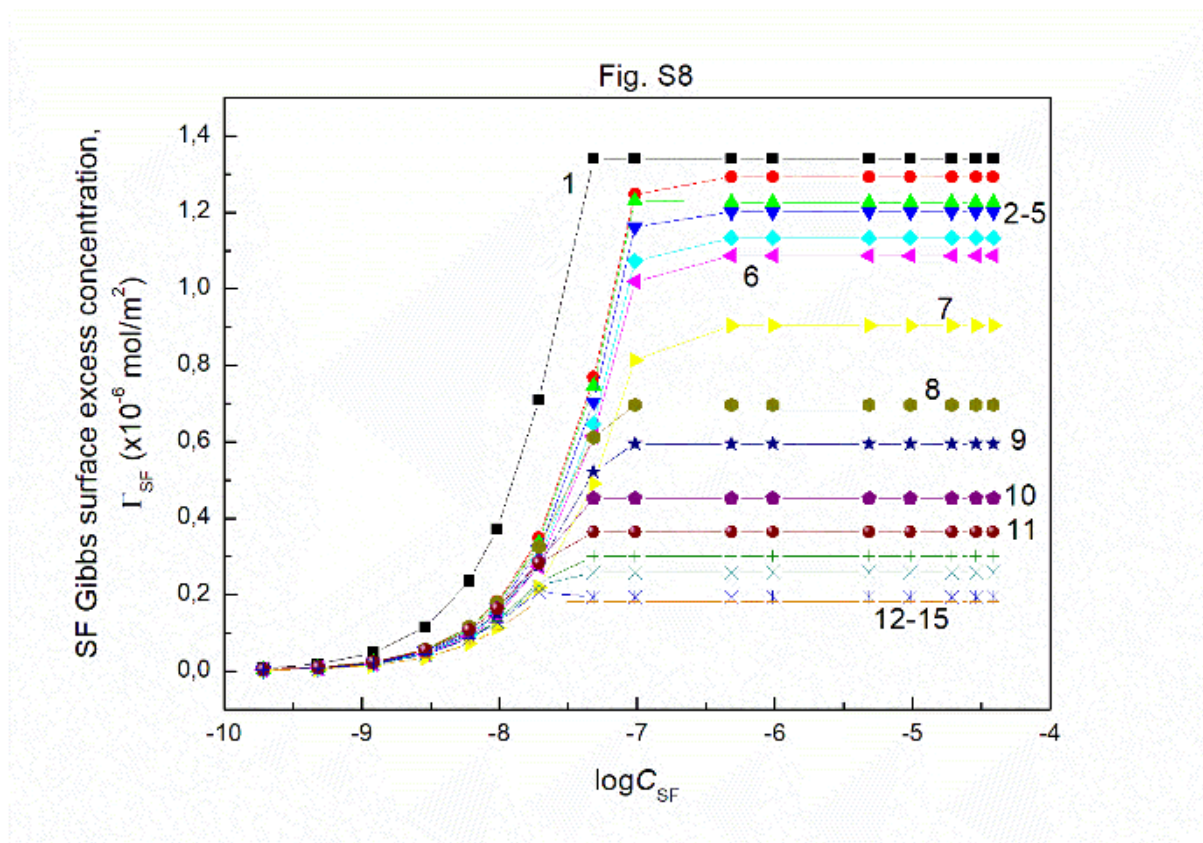
Figure S8. A plot of the SF Gibbs surface excess concentration at the PTFE–solution interface (Γ_{SF}) vs. the logarithm of surfactin concentration (C_{SF}). Curves 1 – 15 correspond to the constant ET concentration equal to 0; 0.06692; 0.1338; 0.2677; 0.4015; 0.535; 1.0706; 1.6062; 2.1416; 2.677; 3.2124; 3.7478; 4.2832; 4.8185; 5.3538 M.
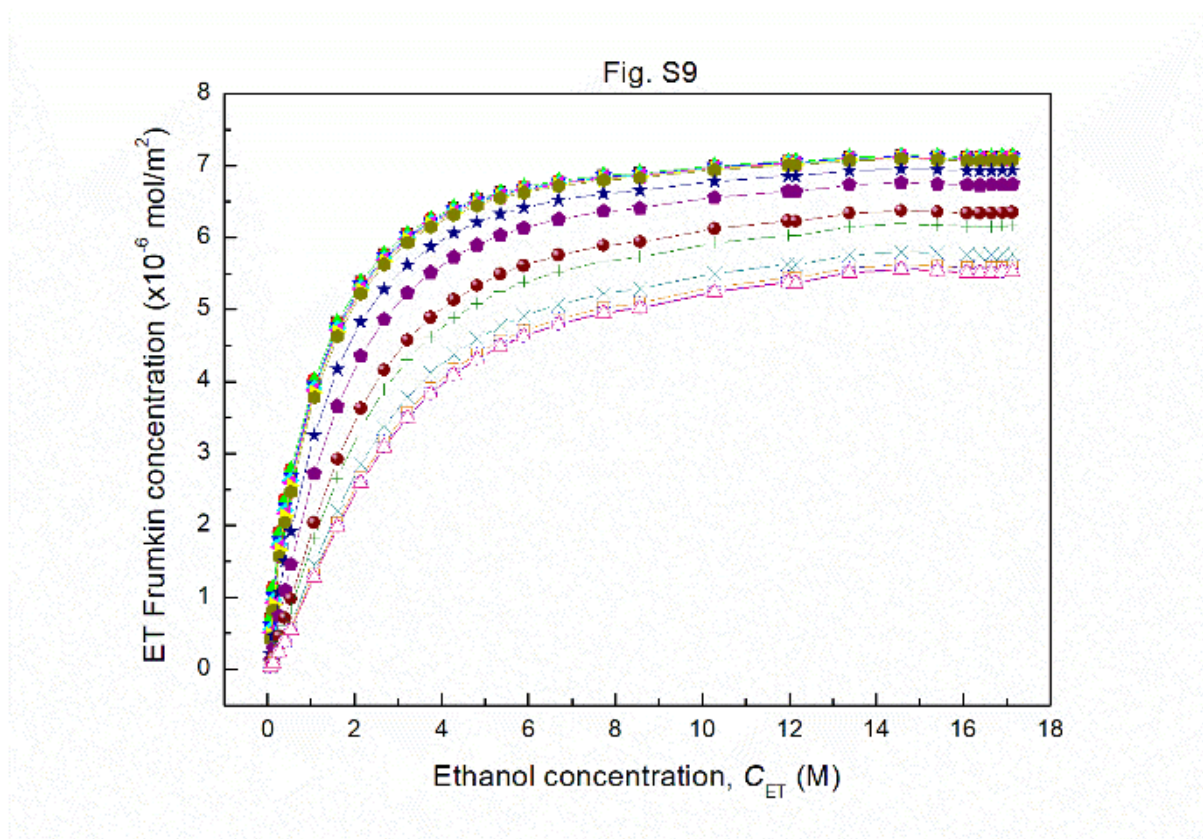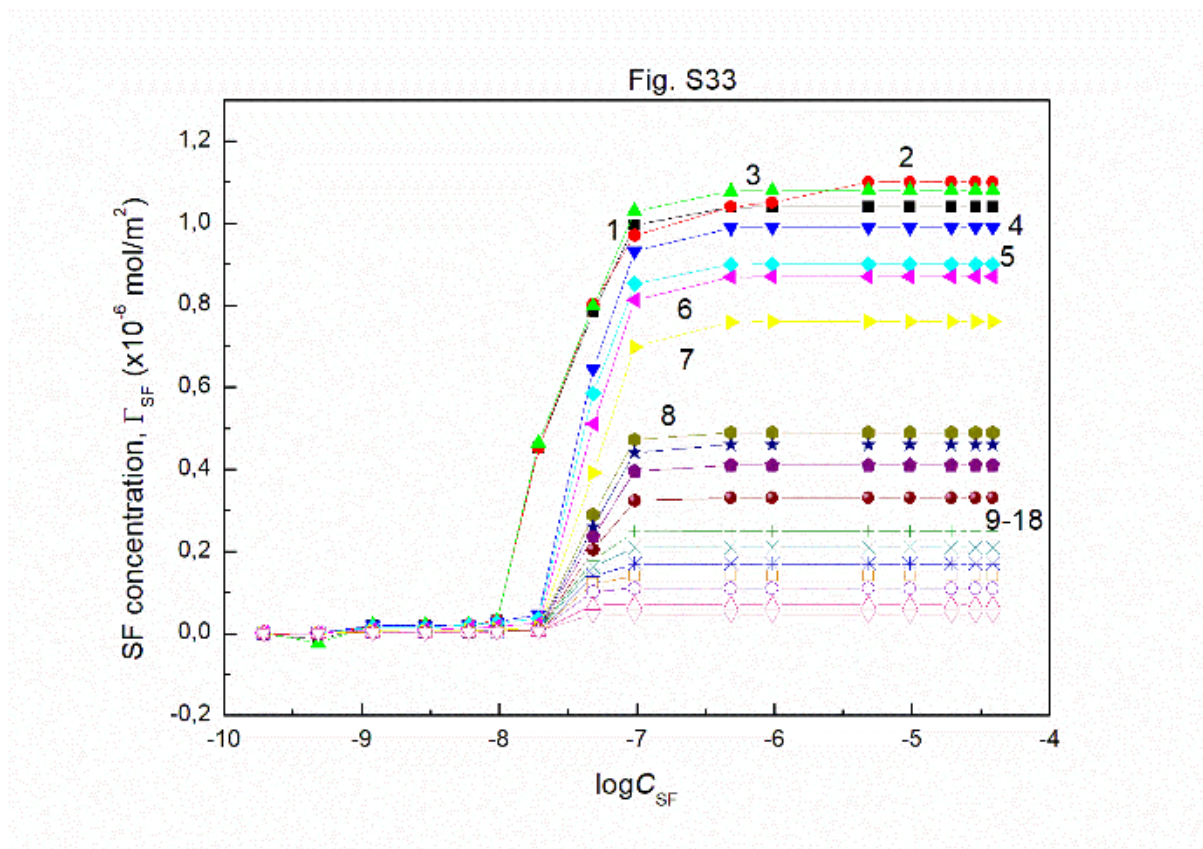
Figure S9. A plot of the ET Frumkin concentration at the PTFE-solution interface vs. the ethanol concentration (C_{ET}). Curves 1 – 17 correspond to the constant SF concentration equal to 0; 0.0002; 0.0005; 0.00125; 0003; 0.00625; 0.01; 0.02; 0.05; 0.1; 0.5; 1; 5; 10; 20; 30 and 40 mg/dm^3.
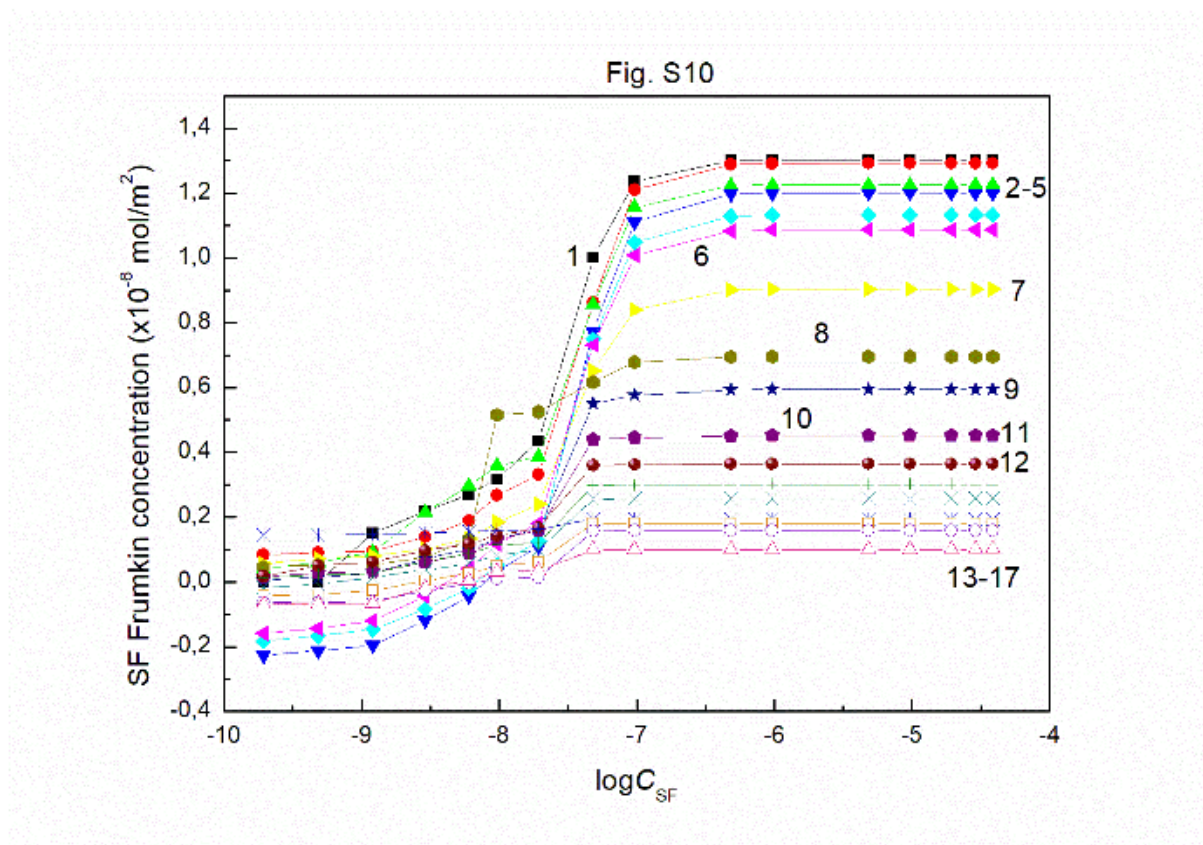
Figure S10. A plot of the Frumkin SF concentration at the PTFE-solution interface vs. the logarithm of surfactin concentration (C_{SF}). Curves 1 – 17 correspond to the constant ET concentration equal to 0; 0.06692; 0.1338; 0.2677; 0.4015; 0.535; 1.0706; 1.6062; 2.1416; 2.677; 3.2124; 3.7478; 4.2832; 4.8185; 5.3538; 5.8893 and 6.6925 M.
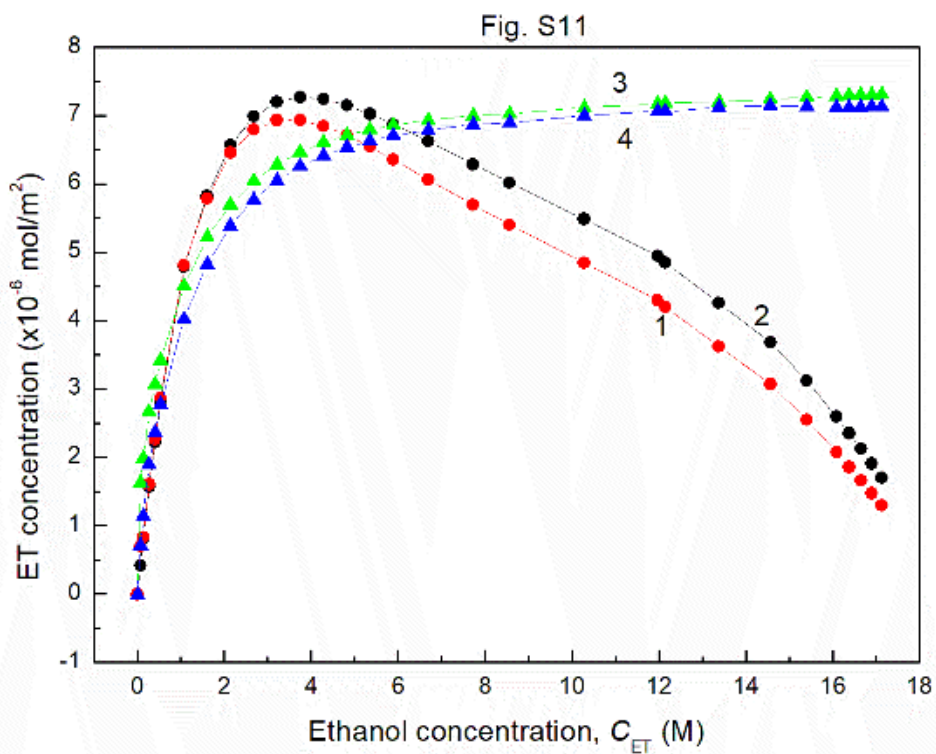
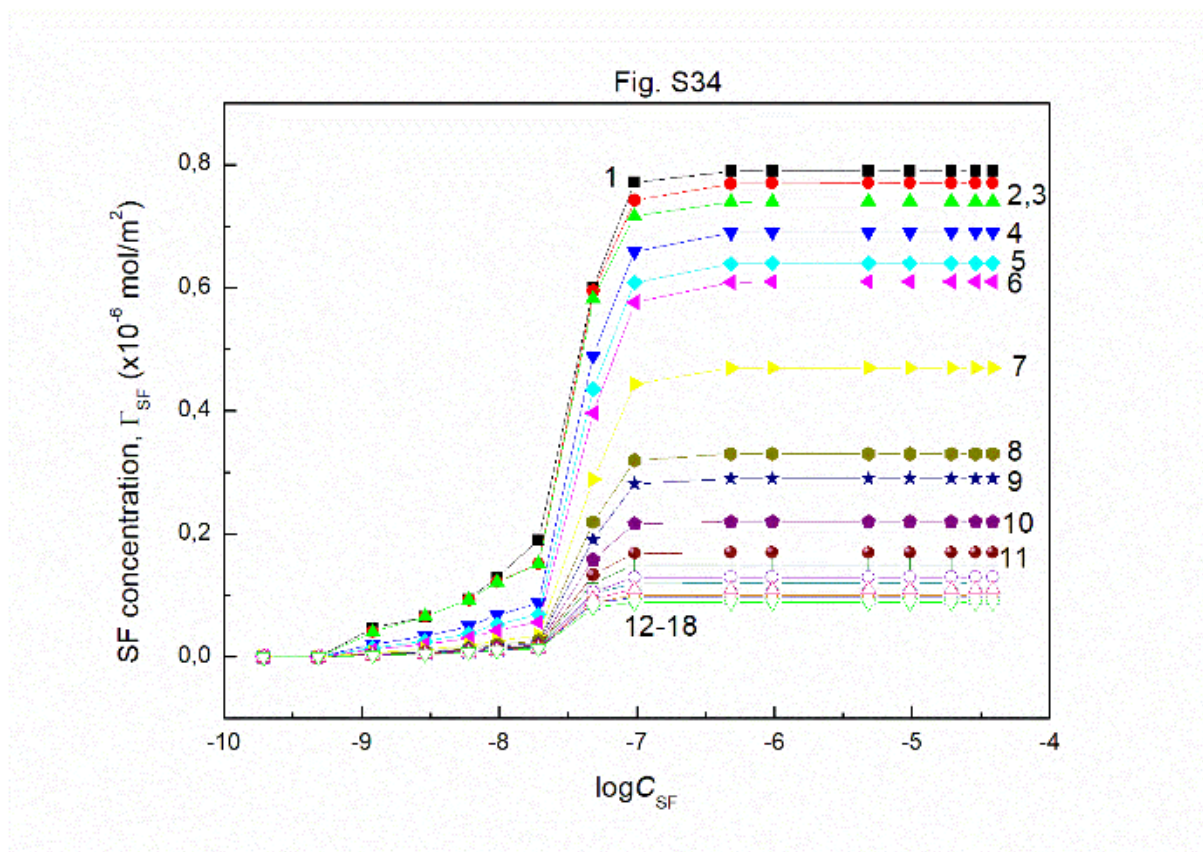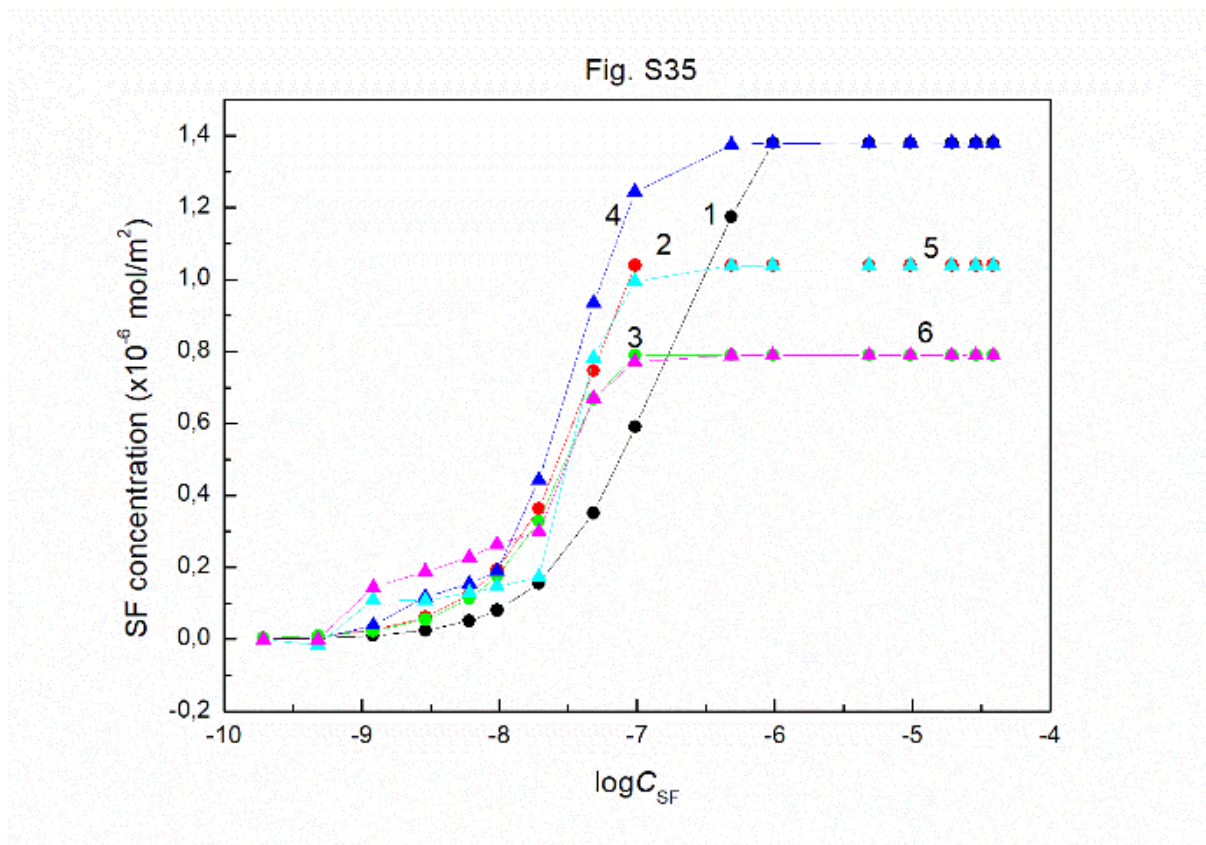Figure S11. A plot of the ET Gibbs surface excess concentration at the water-air (curve 1) and the PTFE-solution (curve 2) and ET Frumkin concentration at the water-air (curve 3) and PTFE-solution (curve 4) vs. the ethanol concentration (C_{ET}) at the constant SF concentration equal to 0.
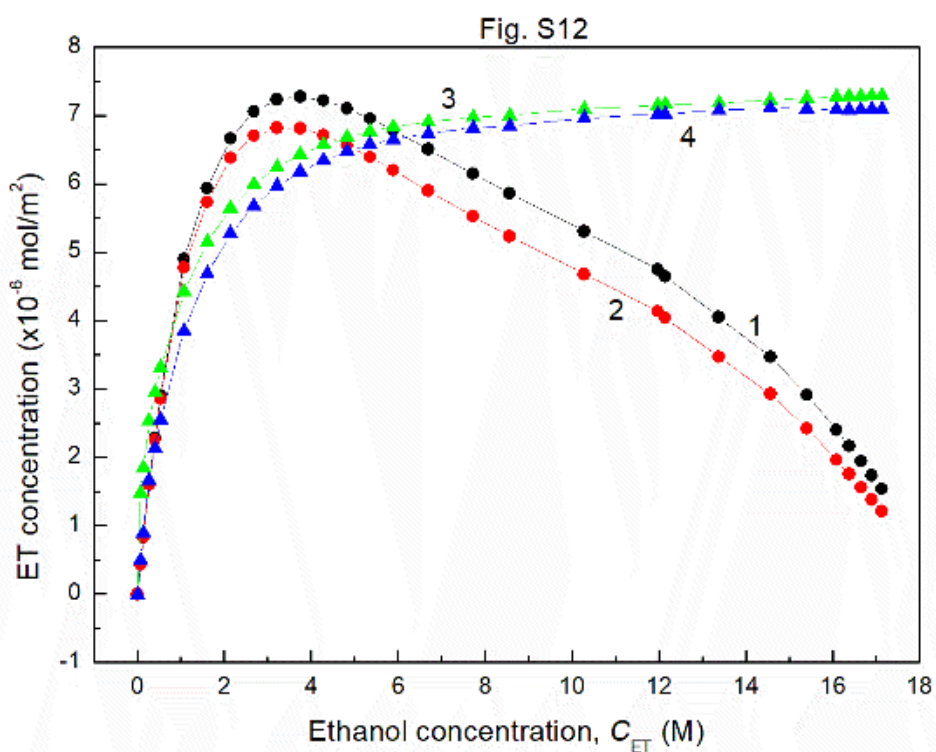
Figure S12. A plot of the ET Gibbs surface excess concentration at the water-air (curve 1) and PTFE-solution (curve 2) and ET Frumkin concentration at the water-air (curve 3) and PTFE-solution (curve 4) vs. the ethanol concentration (C_{ET}) at the constant SF concentration equal to 0.01 mg/dm^3.
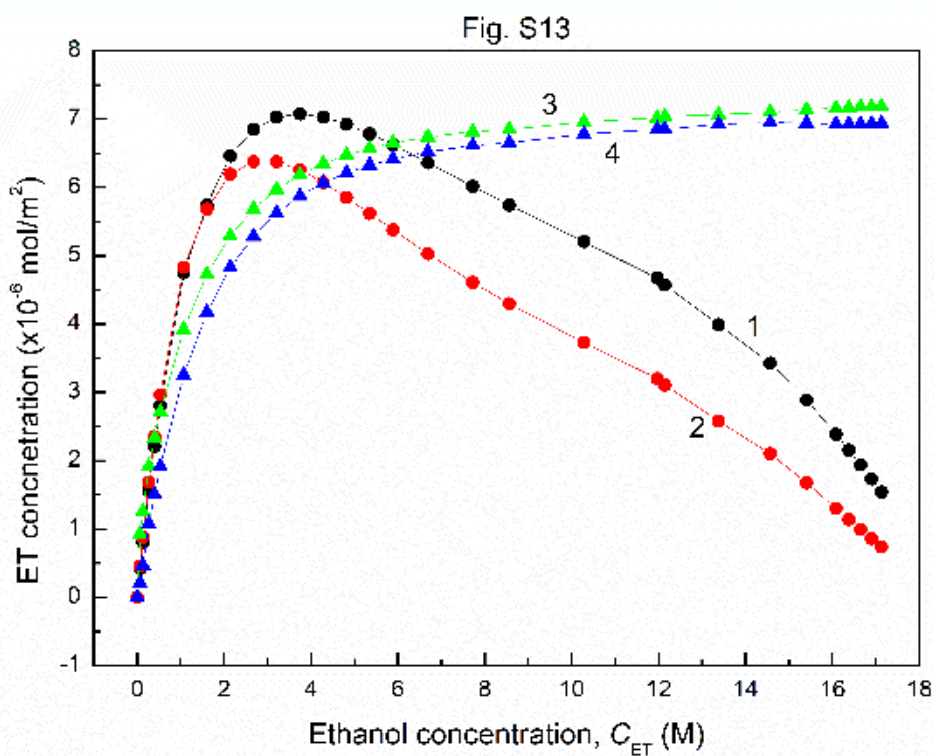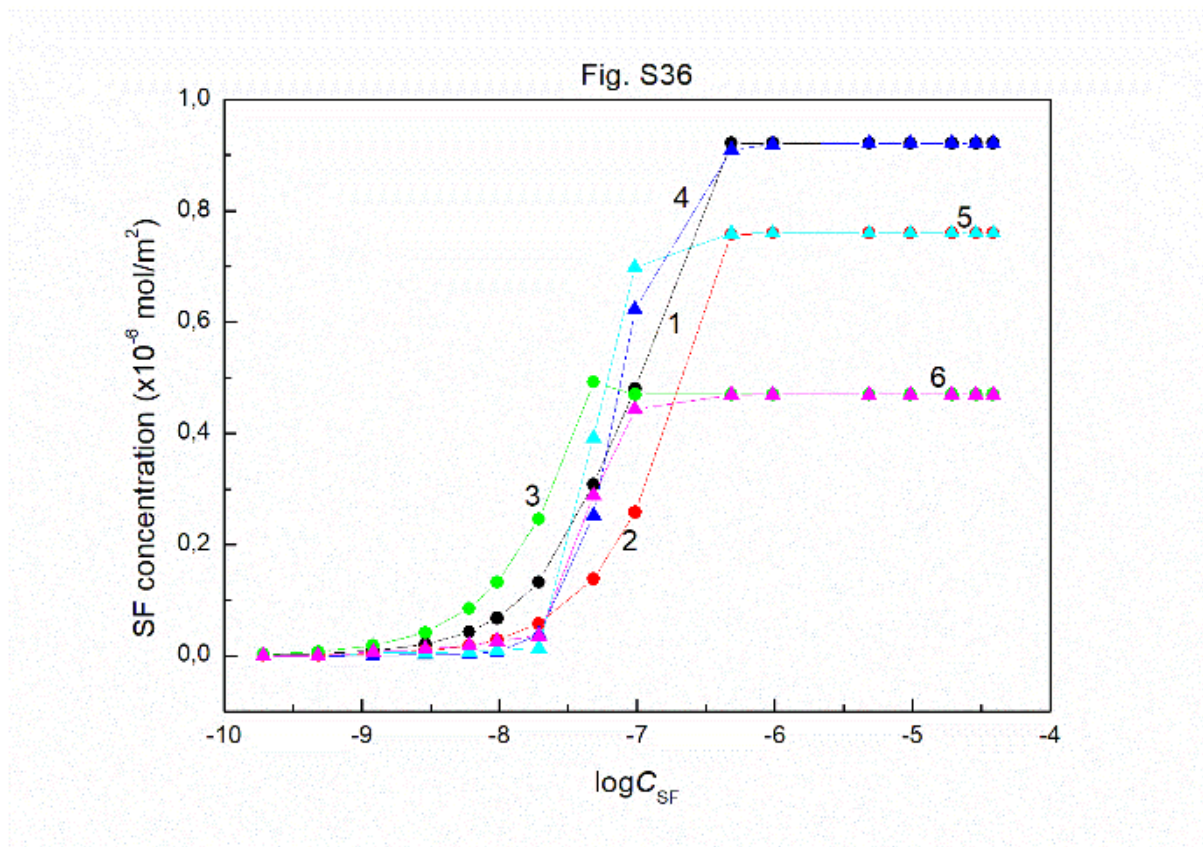
Figure S13. A plot of the ET Gibbs surface excess concentration at the water-air (curve 1) and PTFE-solution (curve 2) and ET Frumkin concentration at the water-air (curve 3) and PTFE-solution (curve 4) vs. the ethanol concentration (C_{ET}) at the constant SF concentration equal to 0.05 mg/dm^3.
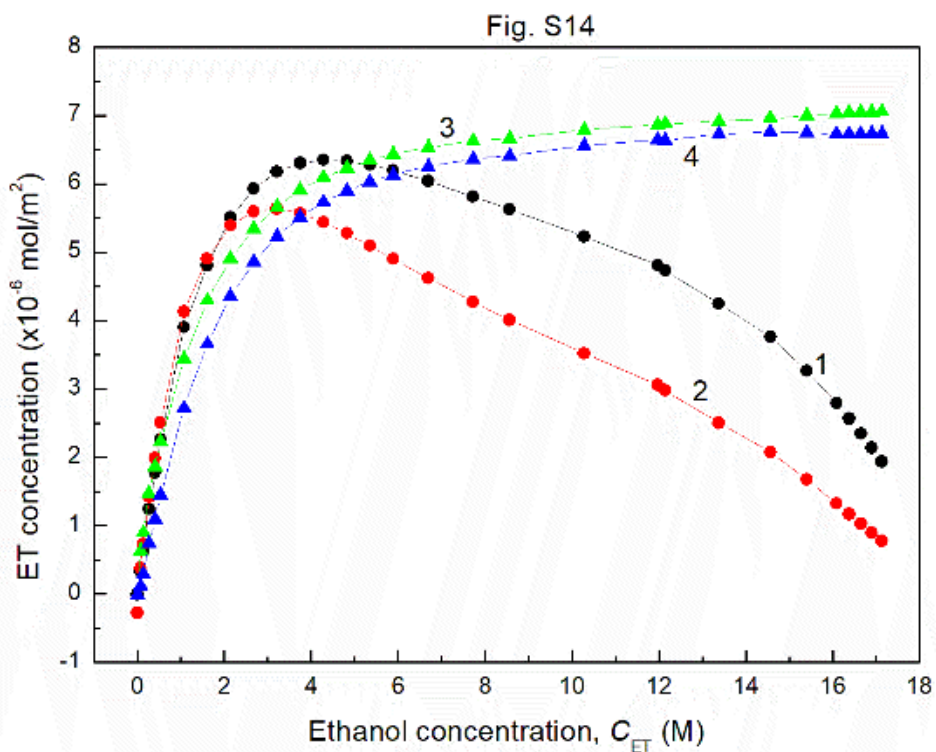
Figure S14. A plot of the ET Gibbs surface excess concentration at the water-air (curve 1) and PTFE-solution (curve 2) and ET Frumkin concentration at the water-air (curve 3) and PTFE-solution (curve 4) vs. the ethanol concentration (C_{ET}) at the constant SF concentration equal to 0.1 mg/dm^3.
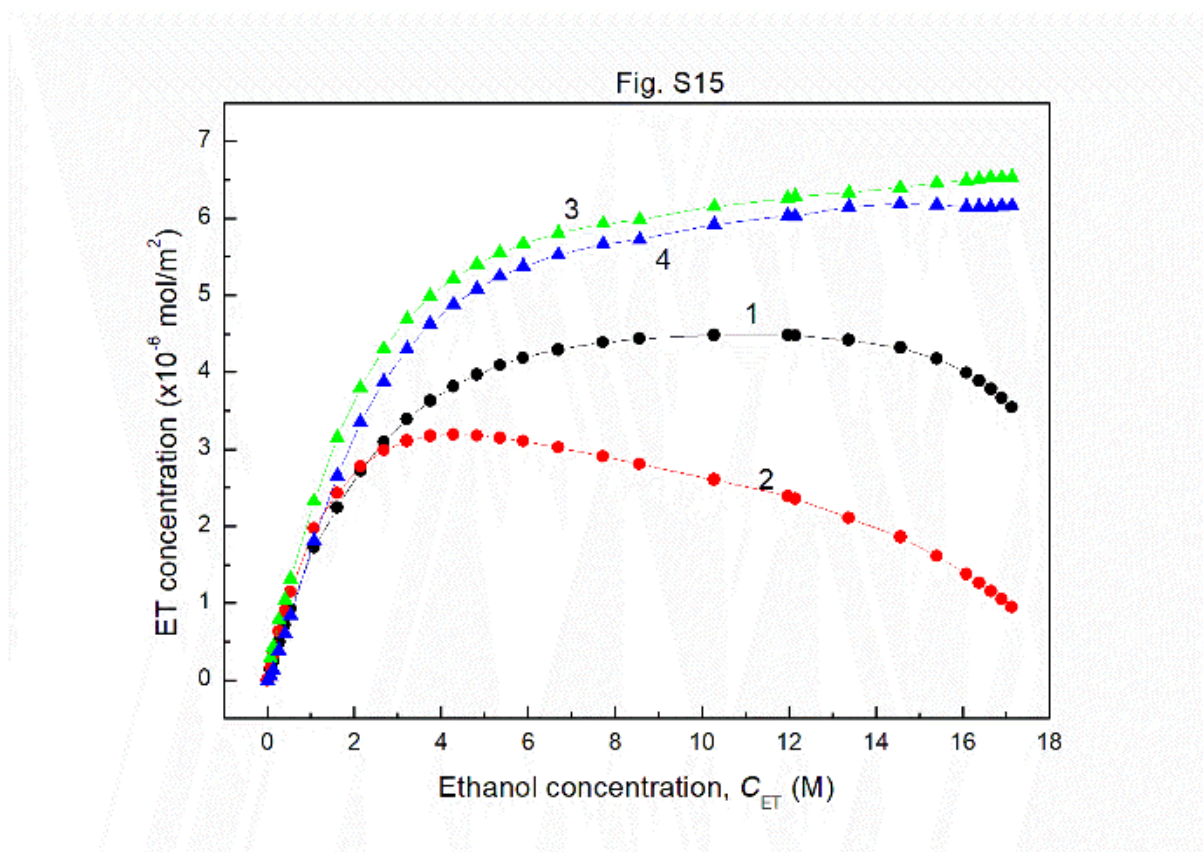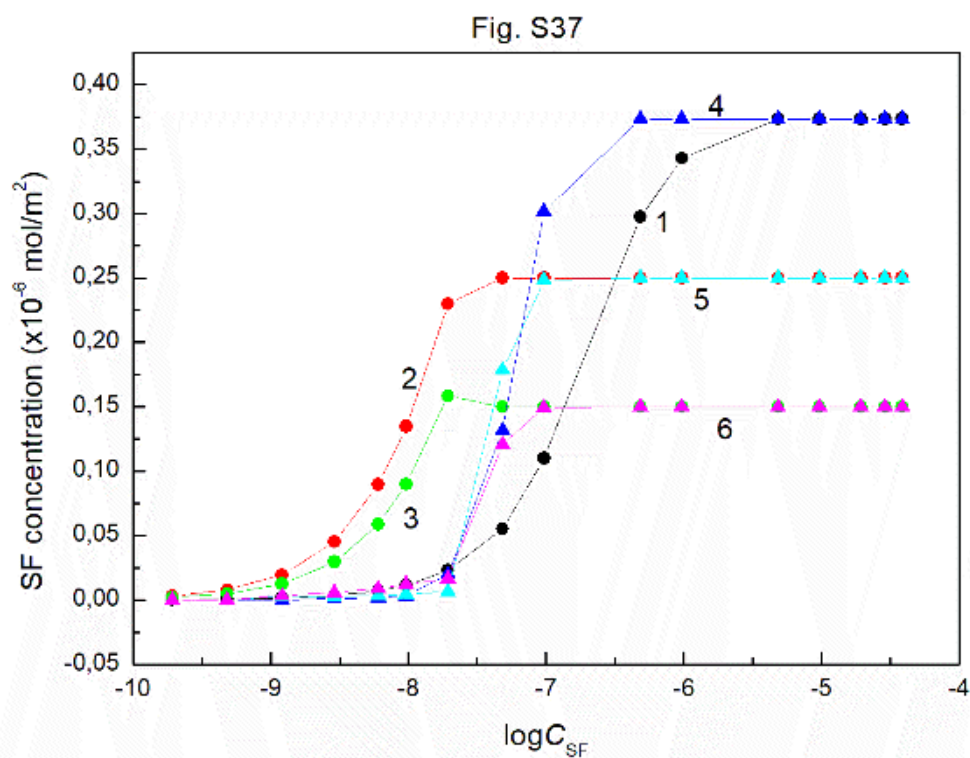
Figure S15. A plot of the ET Gibbs surface excess concentration at the water-air (curve 1) and PTFE-solution (curve 2) and ET Frumkin concentration at the water-air (curve 3) and PTFE-solution (curve 4) vs. the ethanol concentration (C_{ET}) at the constant SF concentration equal to 1 mg/dm^3.
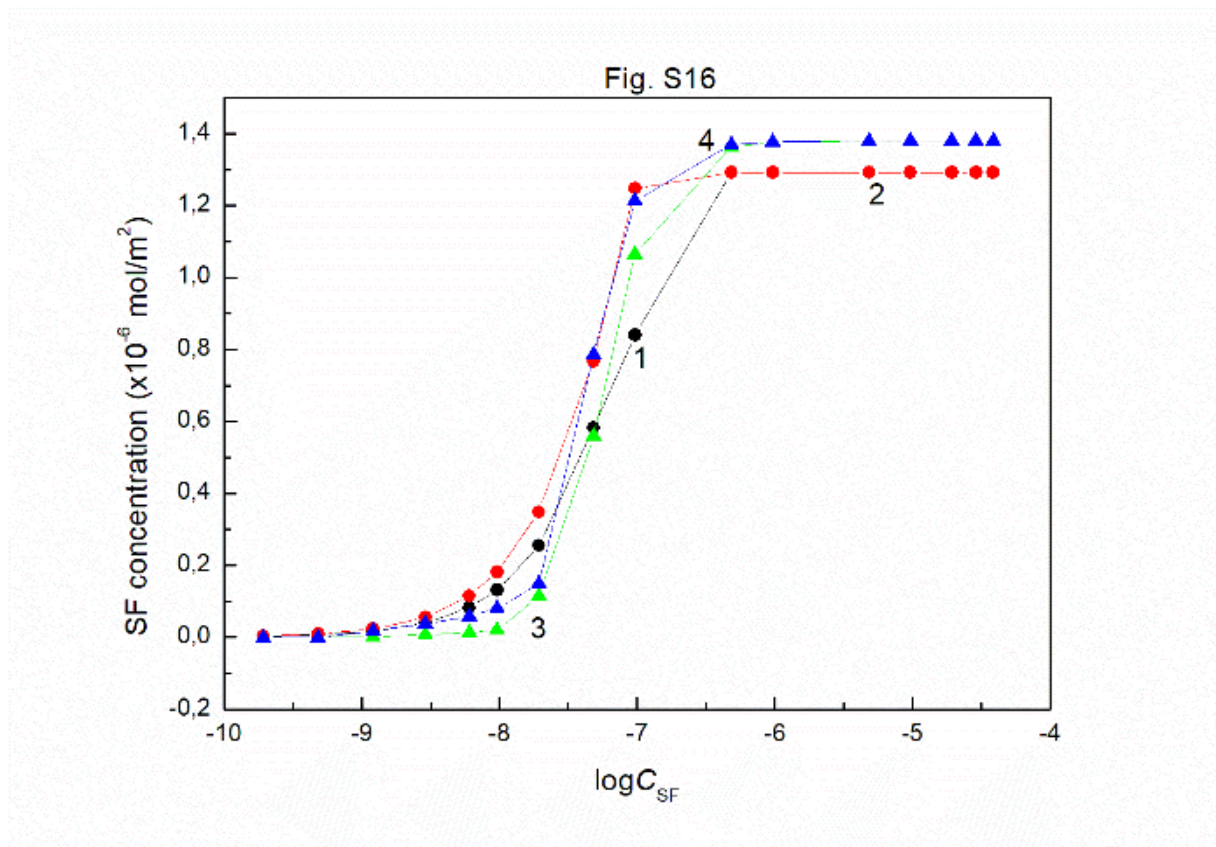
Figure S16. A plot of the SF Gibbs surface excess concentration at the water-air (curve 1) and PTFE-solution (curve 2) and SF Frumkin concentration at the water-air (curve 3) and PTFE-solution (curve 4) vs. the logarithm of surfactin concentration (C_{SF}) at the constant ethanol concentration equal to 0.
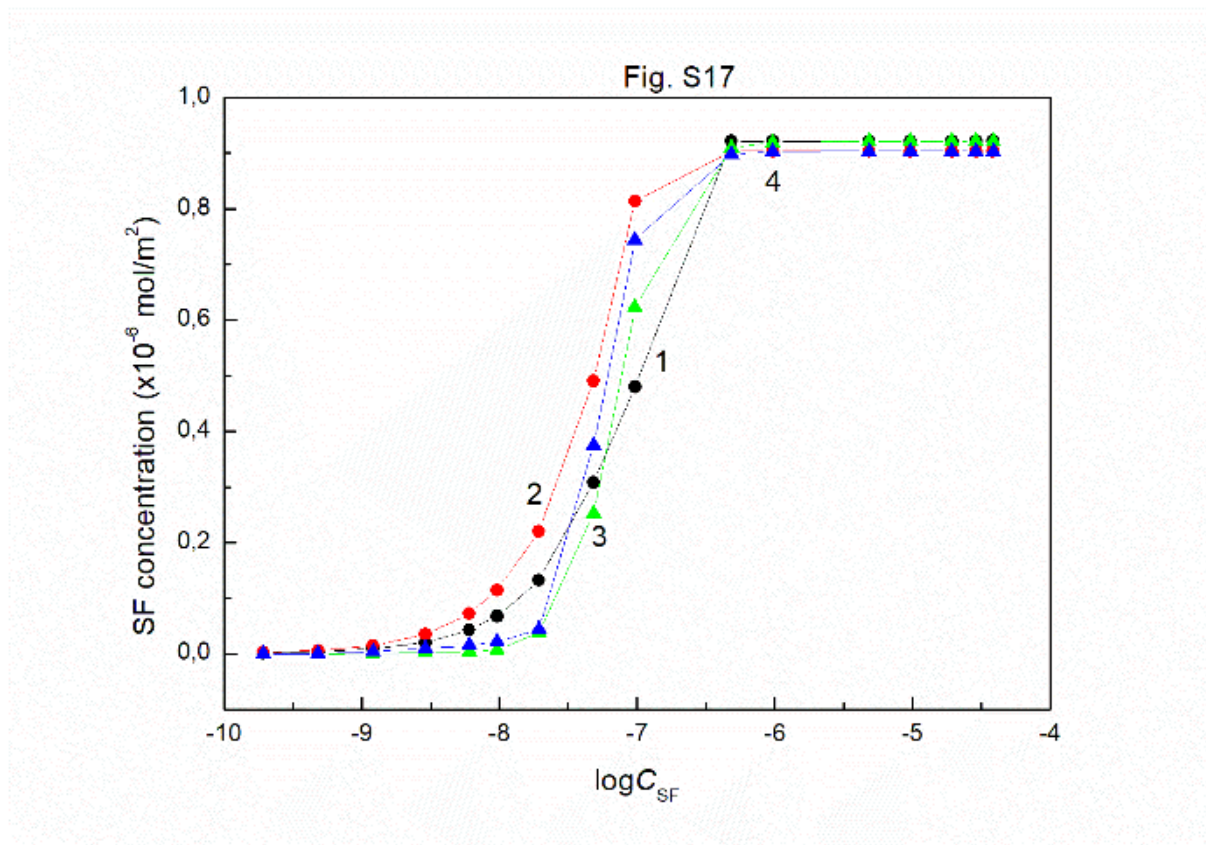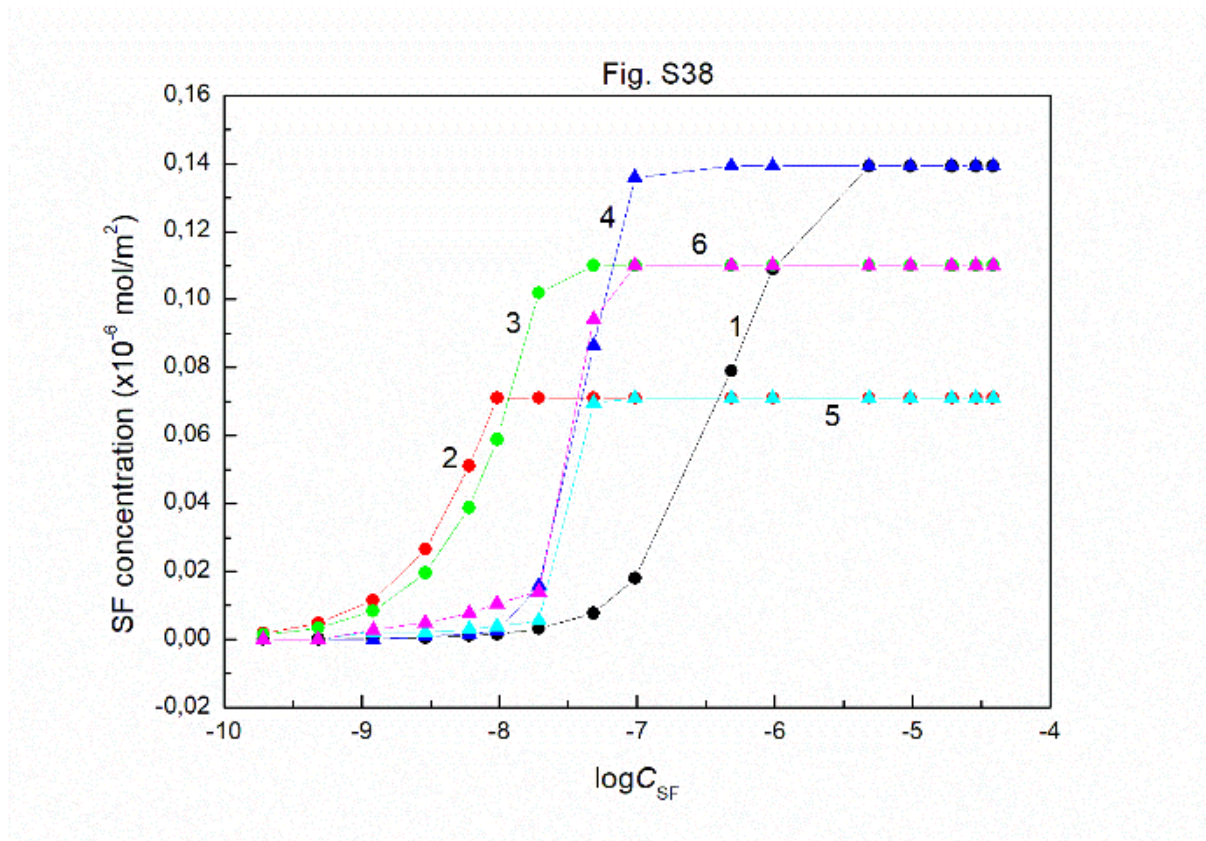
Figure S17. A plot of the SF Gibbs surface excess concentration at the water-air (curve 1) and PTFE-solution (curve 2) and SF Frumkin concentration at the water-air (curve 3) and PTFE-solution (curve 4) vs. the logarithm of surfactin concentration (C_{SF}) at the constant ethanol concentration equal to 0.06692 M.
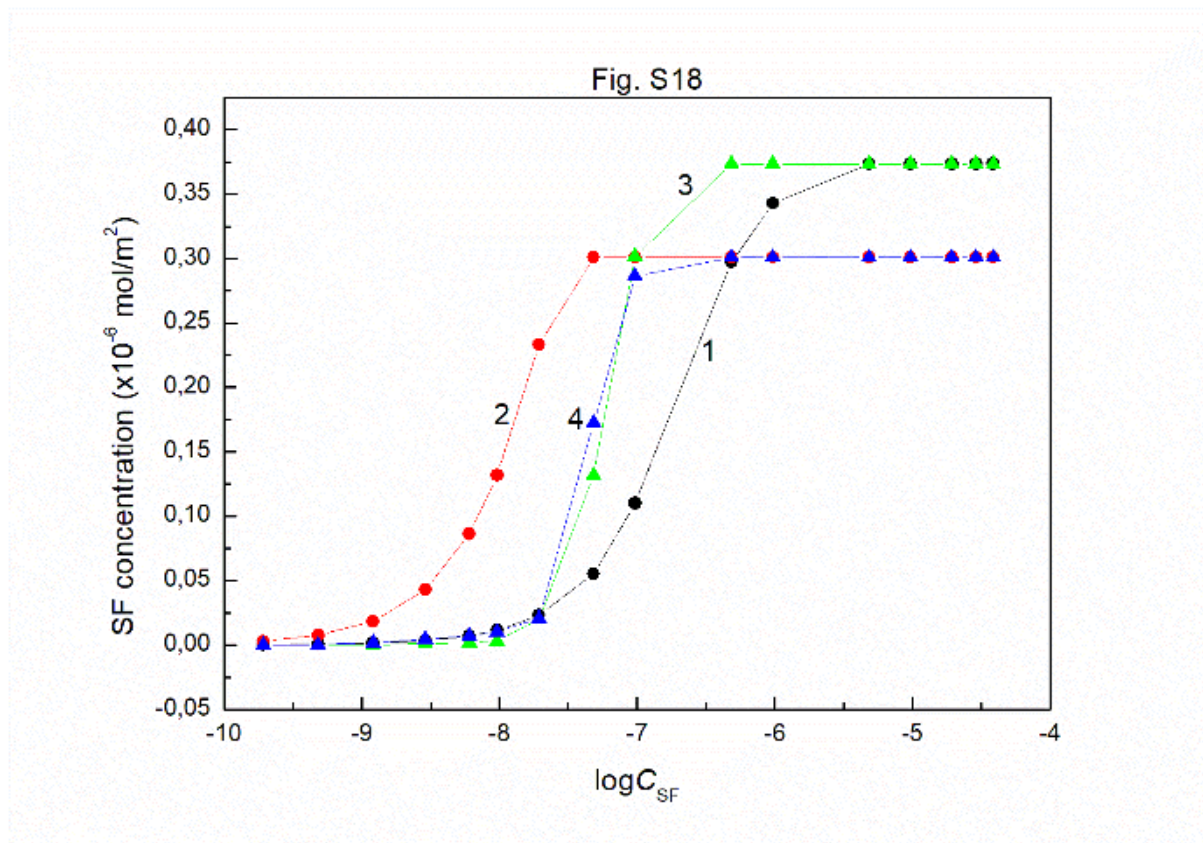
Figure S18. A plot of the SF Gibbs surface excess concentration at the water-air (curve 1) and PTFE-solution (curve 2) and SF Frumkin concentration at the water-air (curve 3) and PTFE-solution (curve 4) vs. the logarithm of surfactin concentration (C_{SF}) at the constant ethanol concentration equal to 3.7478 M.
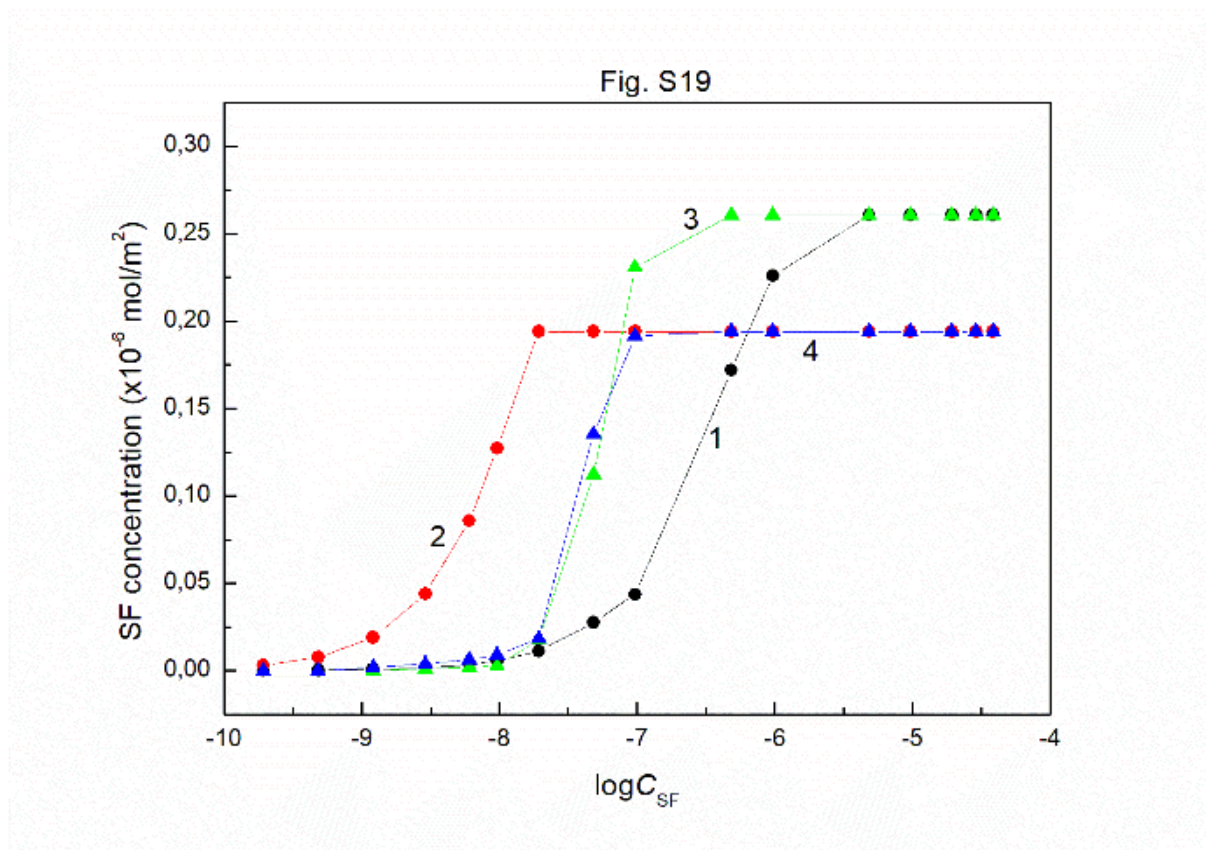
Figure S19. A plot of the SF Gibbs surface excess concentration at the water-air (curve 1) and PTFE-solution (curve 2) and SF Frumkin concentration at the water-air (curve 3) and PTFE-solution (curve 4) vs. the logarithm of surfactin concentration (C_{SF}) at the constant ethanol concentration equal to 4.8185 M.
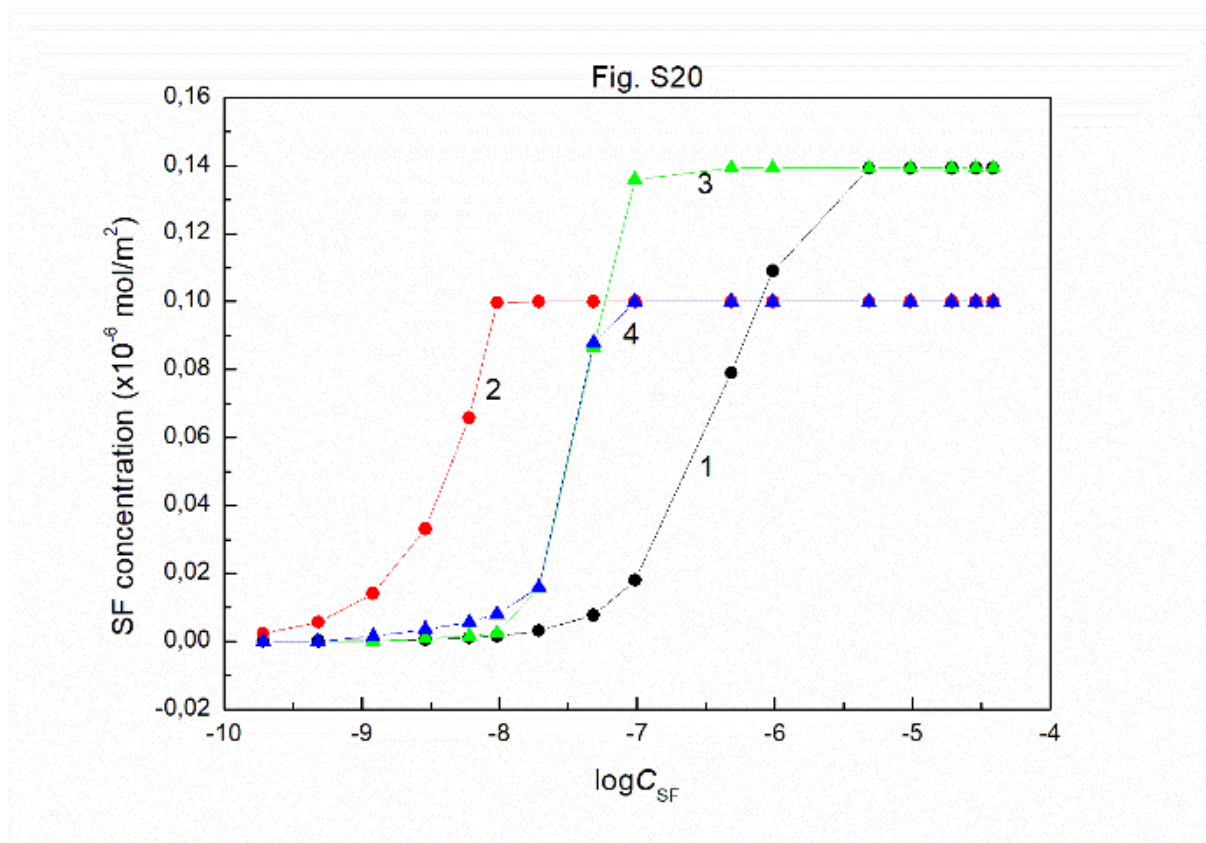
Figure S20. A plot of the SF Gibbs surface excess concentration at the water-air (curve 1) and PTFE-solution (curve 2) and SF Frumkin concentration at the water-air (curve 3) and PTFE-solution (curve 4) vs. the logarithm of surfactin concentration (C_{SF}) at the constant ethanol concentration equal to 6.6925 M.
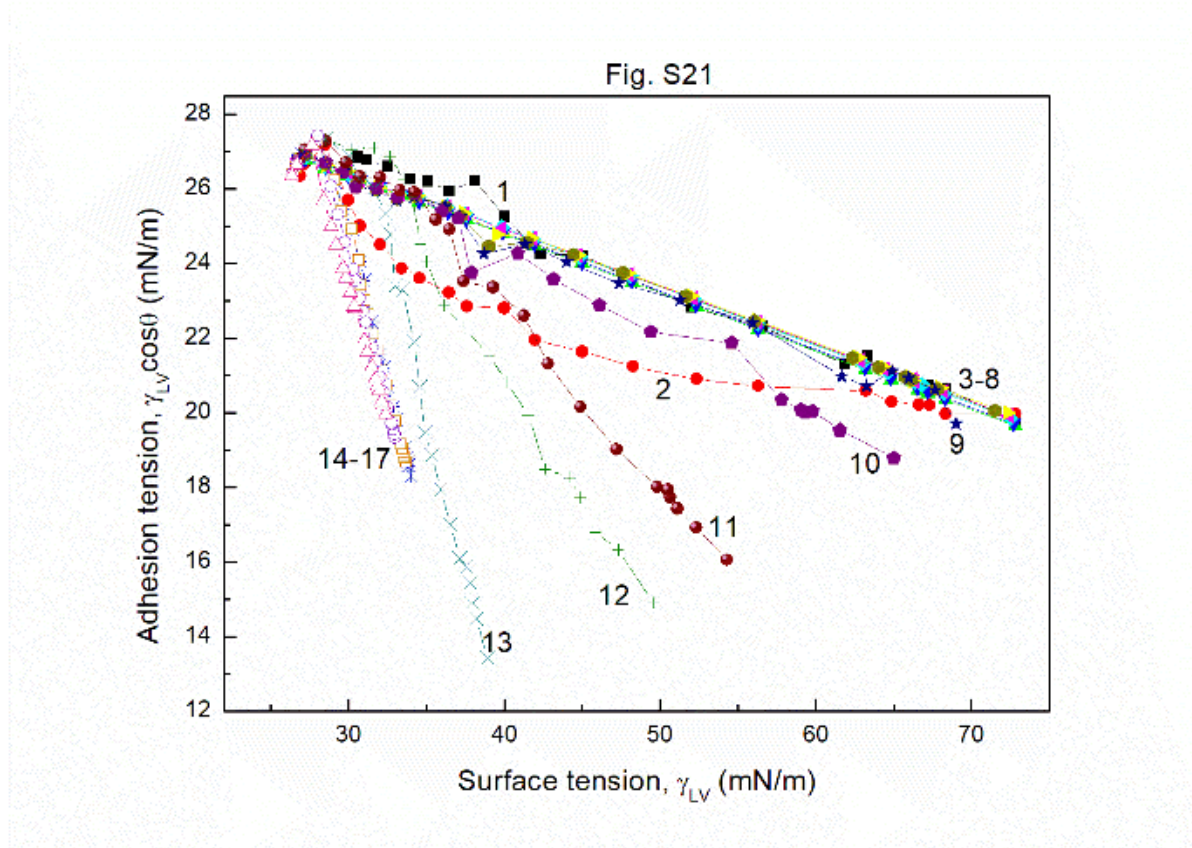
Figure S21. A plot of the adhesion tension ($\gamma_{LV}cos\theta$) for PMMA vs. the solution surface tension (γ_{LV}) [7]. Curves 1 – 17 correspond to the constant SF concentration equal to 0; 0.0002; 0.0005; 0.00125; 0003; 0.00625; 0.01; 0.02; 0.05; 0.1; 0.5; 1; 5; 10; 20; 30 and 40 mg/dm^3.
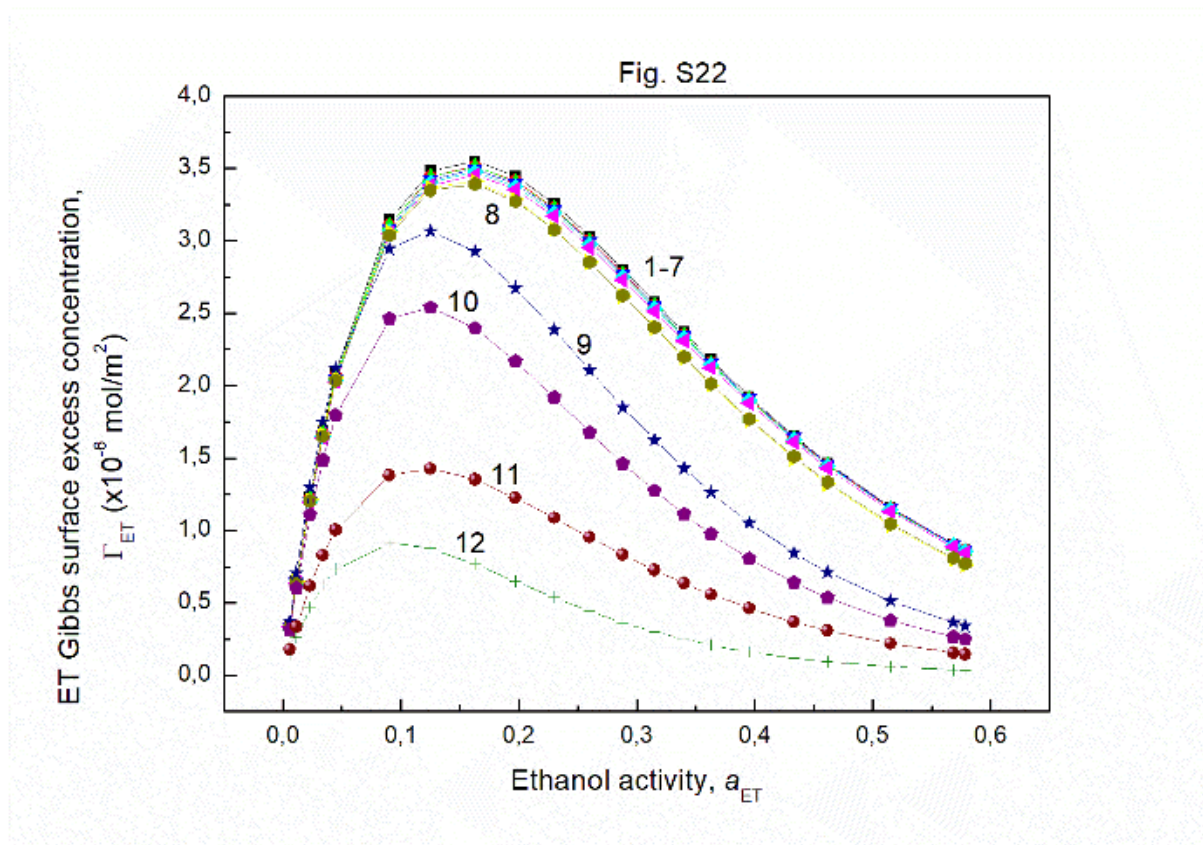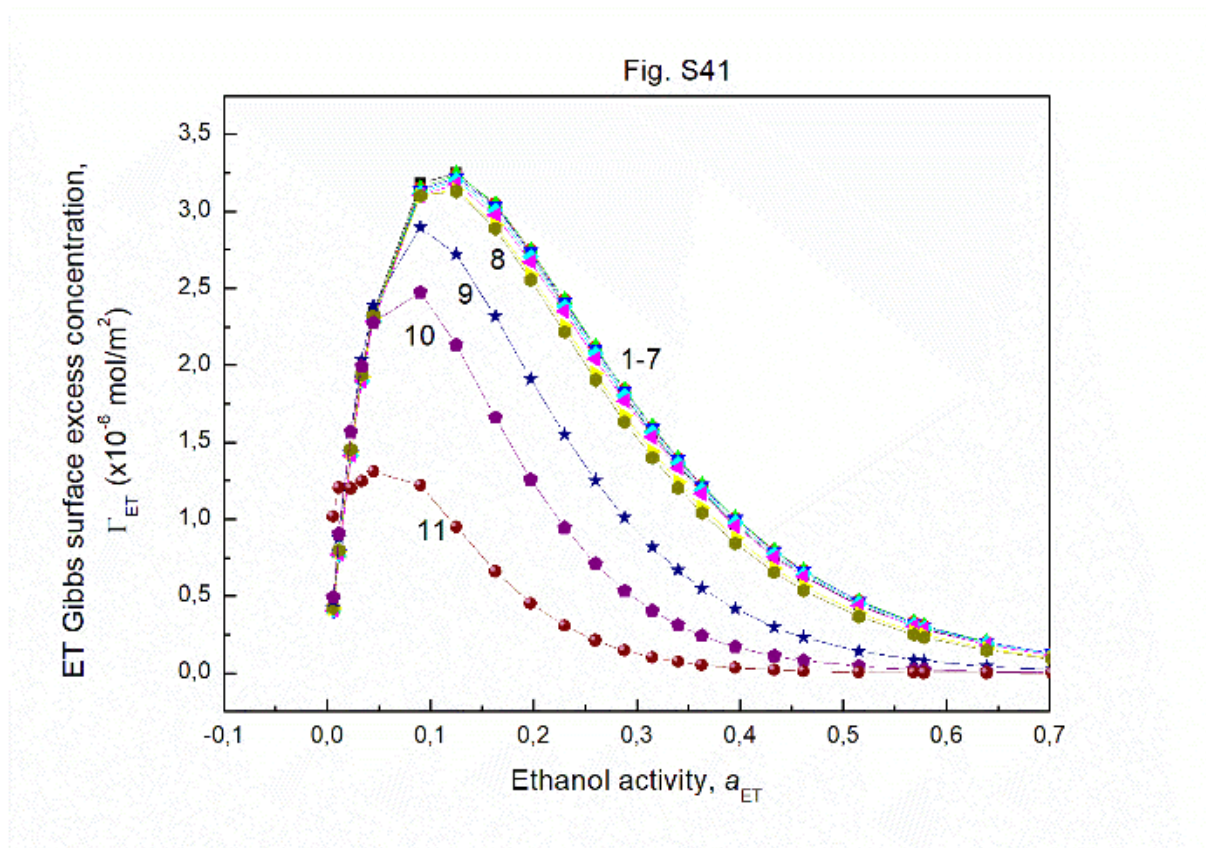
Figure S22. A plot of the ET Gibbs surface excess concentration at the PMMA–solution interface (Γ_{ET}) vs. the ethanol activity (a_{ET}). Curves 1 – 12 correspond to the constant SF concentration equal to 0; 0.0002; 0.0005; 0.00125; 0003; 0.00625; 0.01; 0.02; 0.05; 0.1; 0.5 and 1 mg/dm^3.
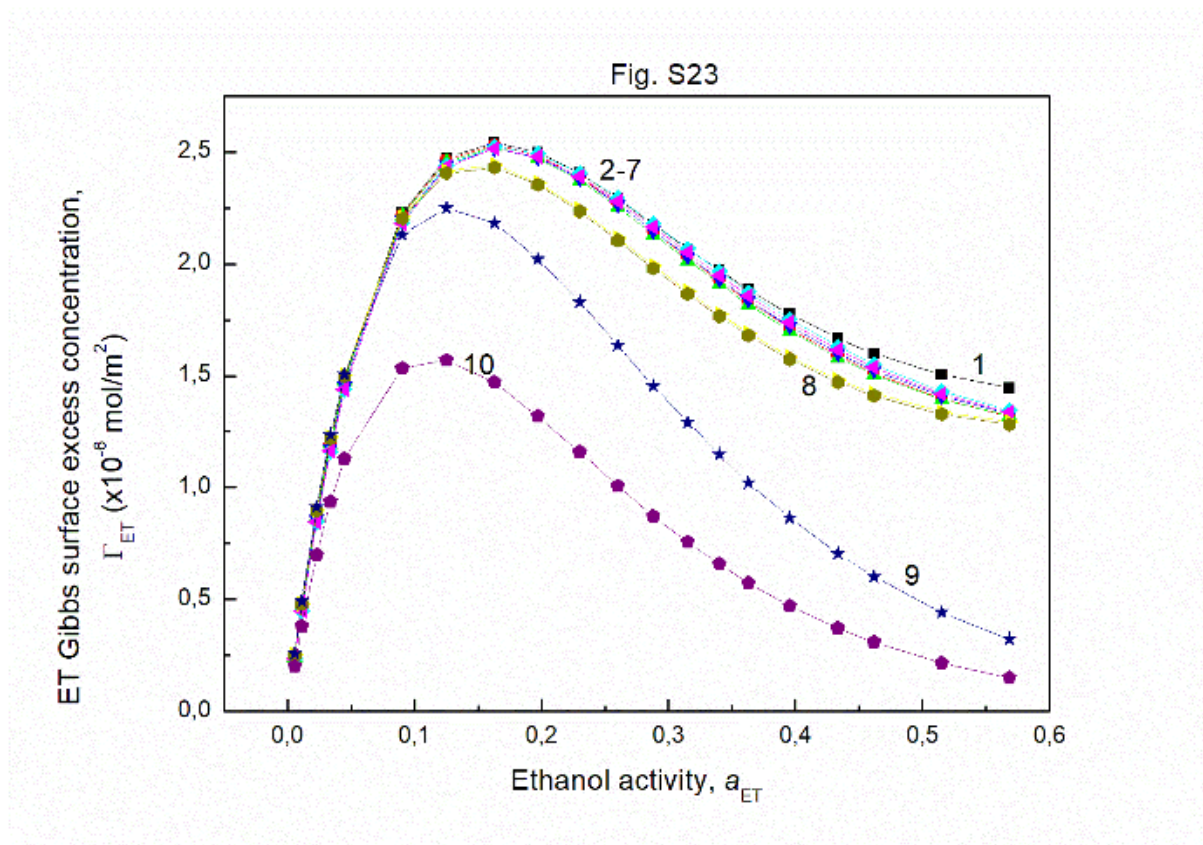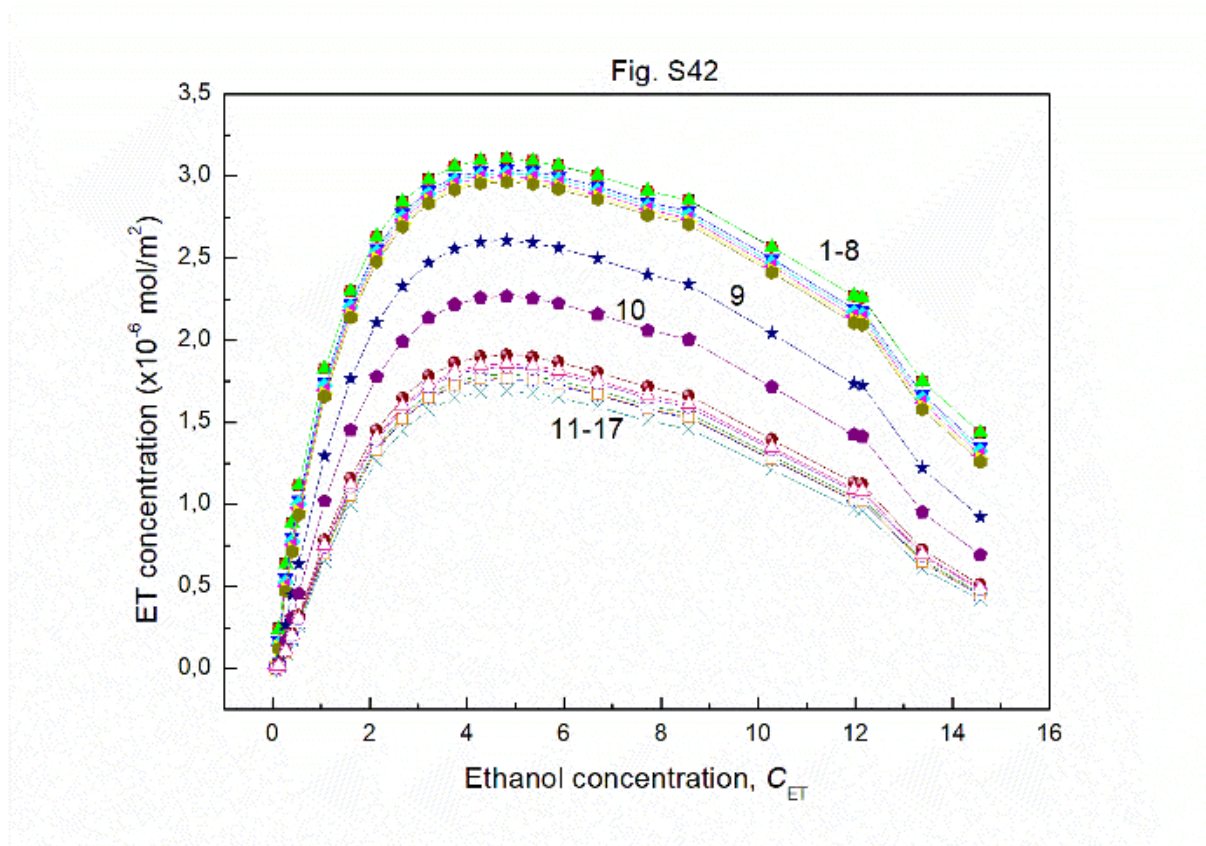
Figure S23. A plot of the ET Gibbs surface excess concentration at the PMMA–air interface (Γ_{ET}) vs. the ethanol activity (a_{ET}). Curves 1 – 10 correspond to the constant SF concentration equal to 0; 0.0002; 0.0005; 0.00125; 0003; 0.00625; 0.01; 0.02; 0.05 and 0.1 mg/dm^3.
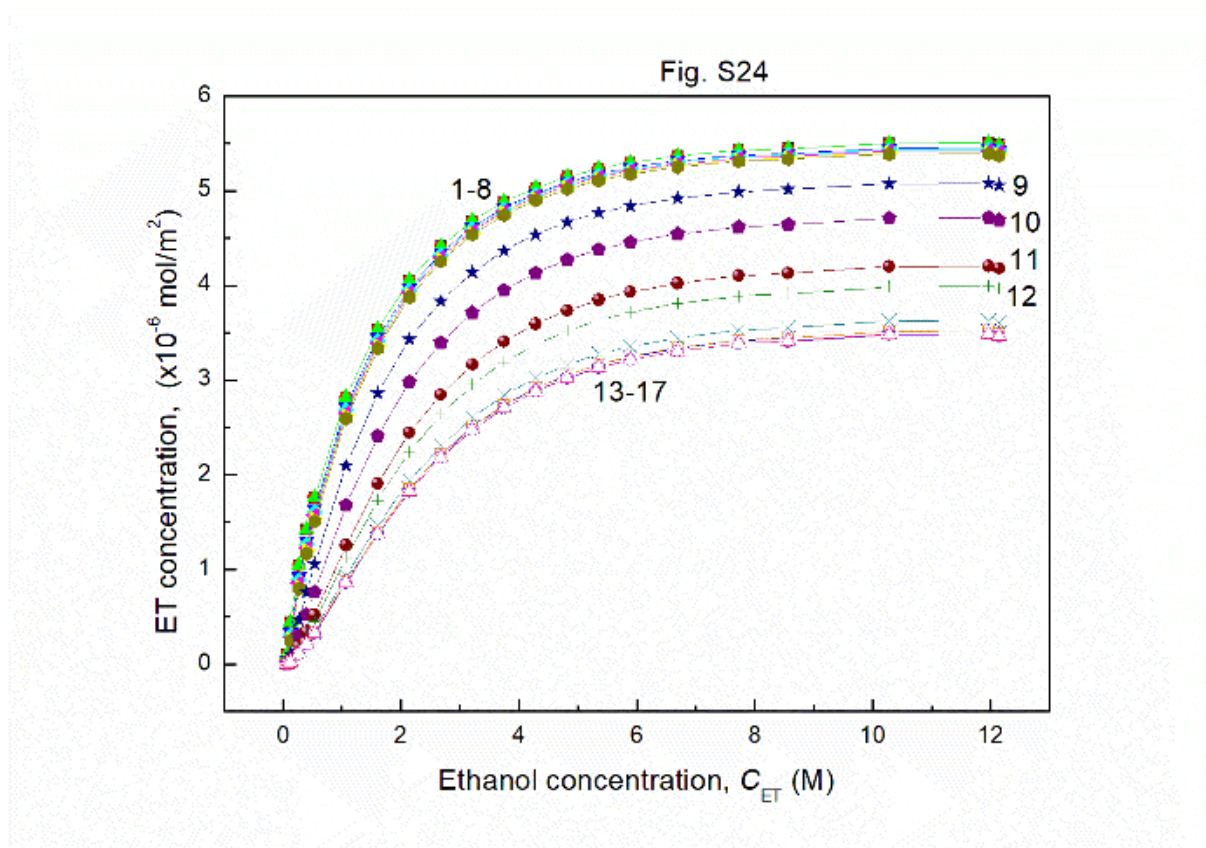
Figure S24. A plot of the ET Frumkin concentration at the PMMA-solution interface vs. ethanol concentration (C_{ET}). Curves 1 – 17 correspond to the constant SF concentration equal to 0; 0.0002; 0.0005; 0.00125; 0003; 0.00625; 0.01; 0.02; 0.05; 0.1; 0.5; 1; 5; 10; 20; 30 and 40 mg/dm^3.
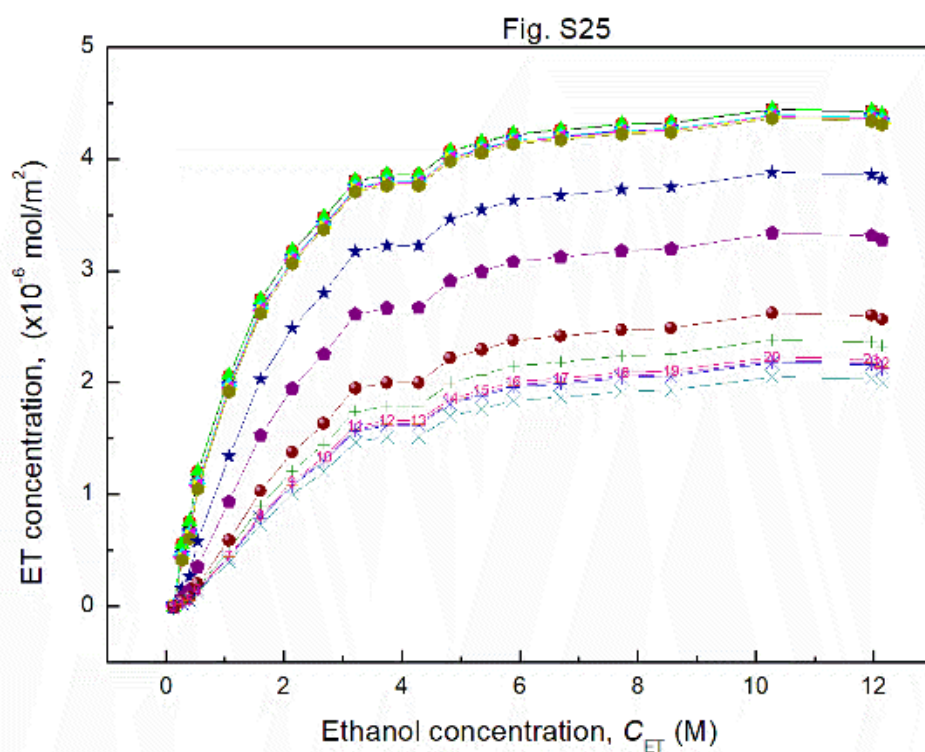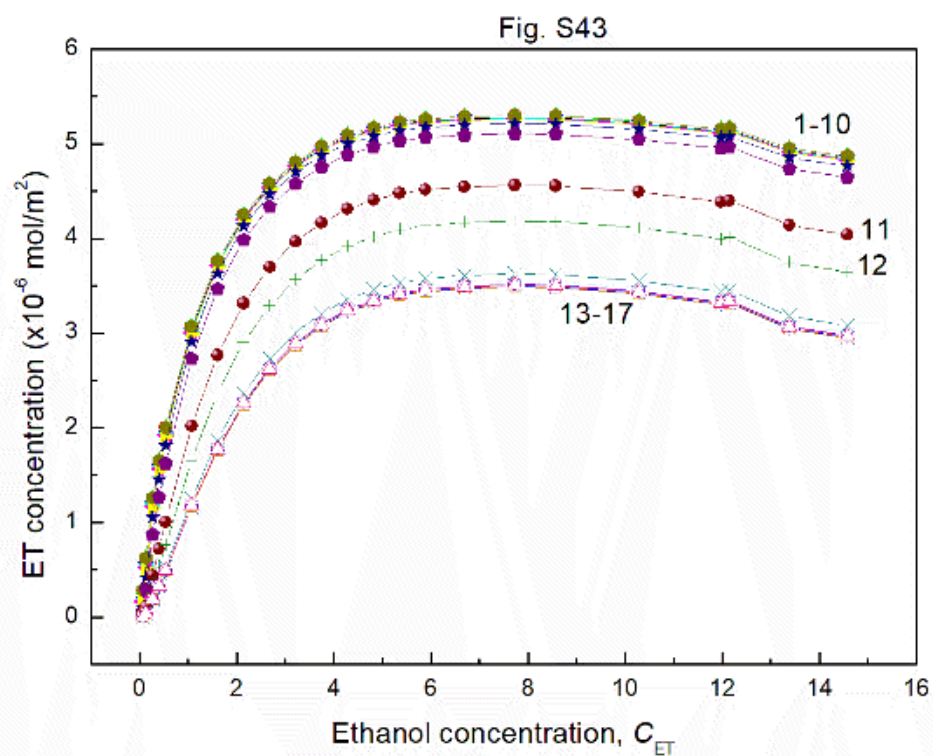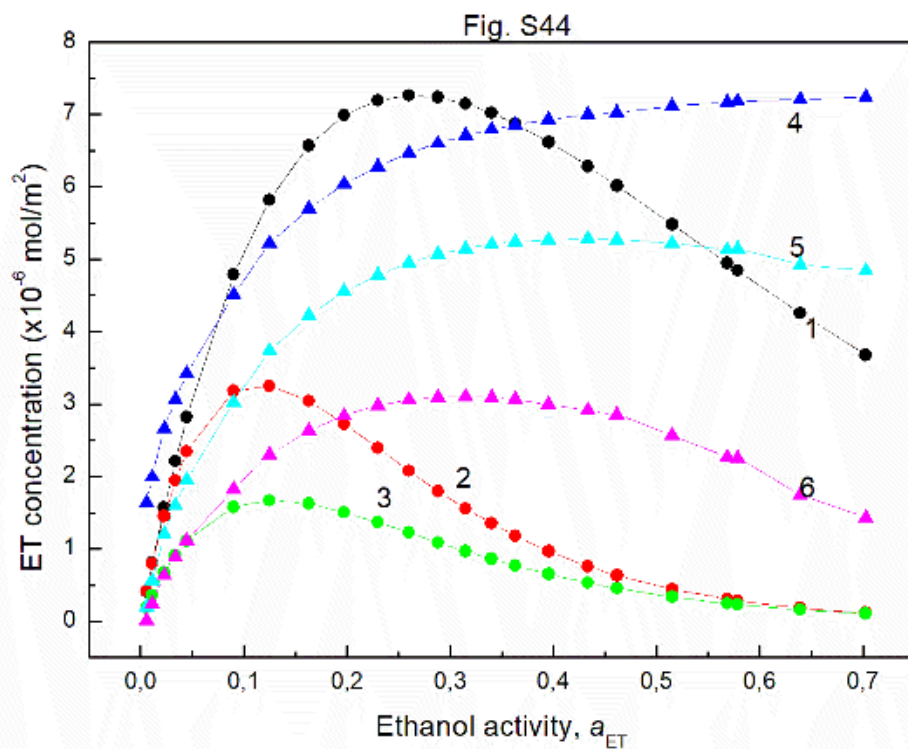
Figure S25. A plot of the ET Frumkin concentration at the PMMA-air interface vs. ethanol concentration (C_{ET}). Curves 1 – 17 correspond to the constant SF concentration equal to 0; 0.0002; 0.0005; 0.00125; 0003; 0.00625; 0.01; 0.02; 0.05; 0.1; 0.5; 1; 5; 10; 20; 30 and 40 mg/dm^3.
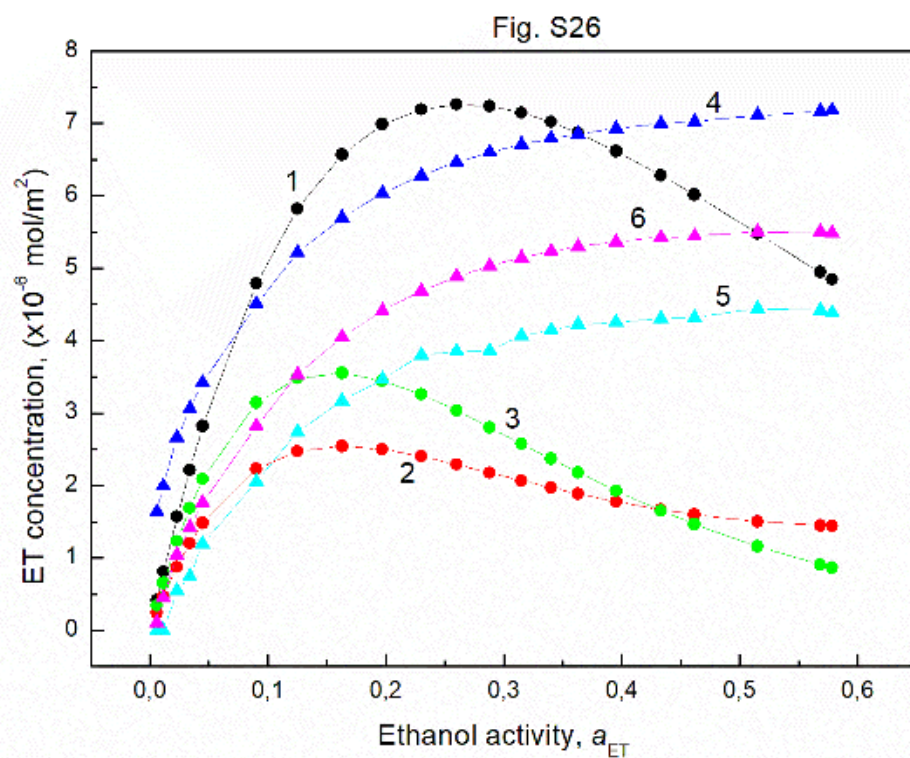
Figure S26. A plot of the ET Gibbs surface excess concentration at the water-air (curve 1), PMMA-air (curve 2) and PMMA-solution (curve 3) and ET Frumkin concentration at the water-air (curve 4), PMMA-air (curve 5) and PMMA-solution (curve 6) vs. the ethanol activity (a_{ET}) at the constant SF concentration equal to 0.
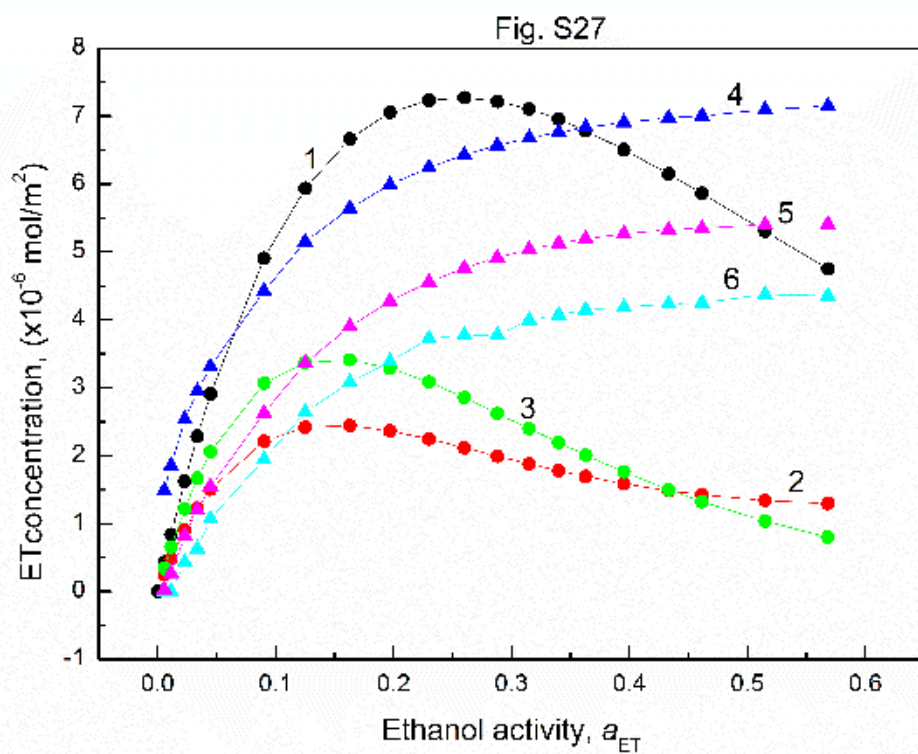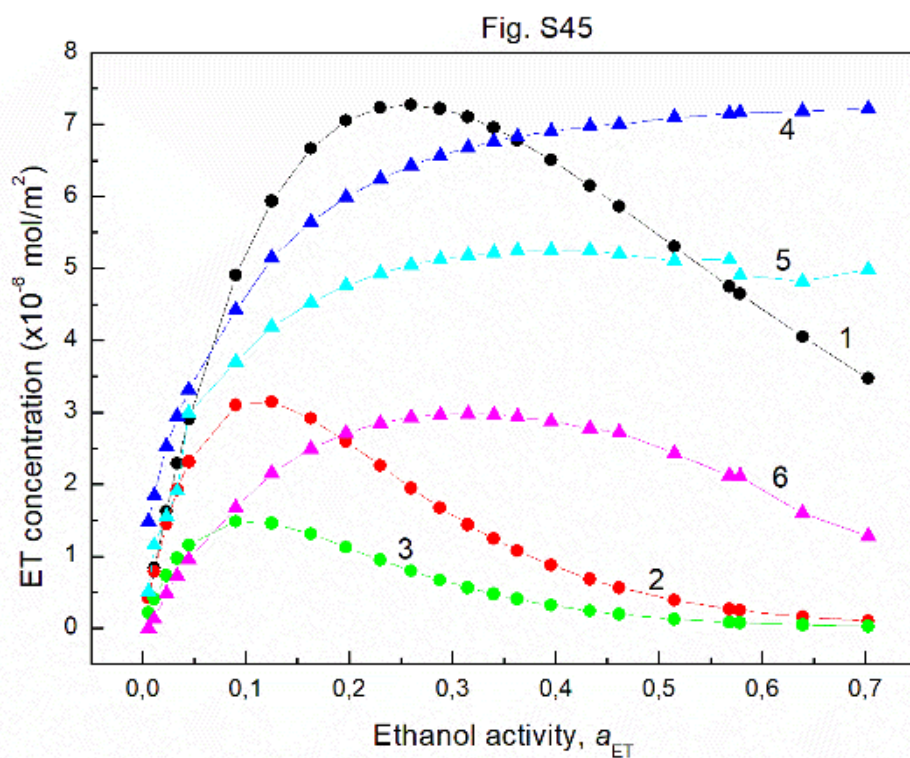
Figure S27. A plot of the ET Gibbs surface excess concentration at the water-air (curve 1), PMMA-air (curve 2) and PMMA-solution (curve 3) and ET Frumkin concentration at the water-air (curve 4), PMMA-air (curve 5) and PMMA-solution (curve 6) vs. the ethanol activity (a_{ET}) at the constant SF concentration equal to 0.01 mg/dm^3.
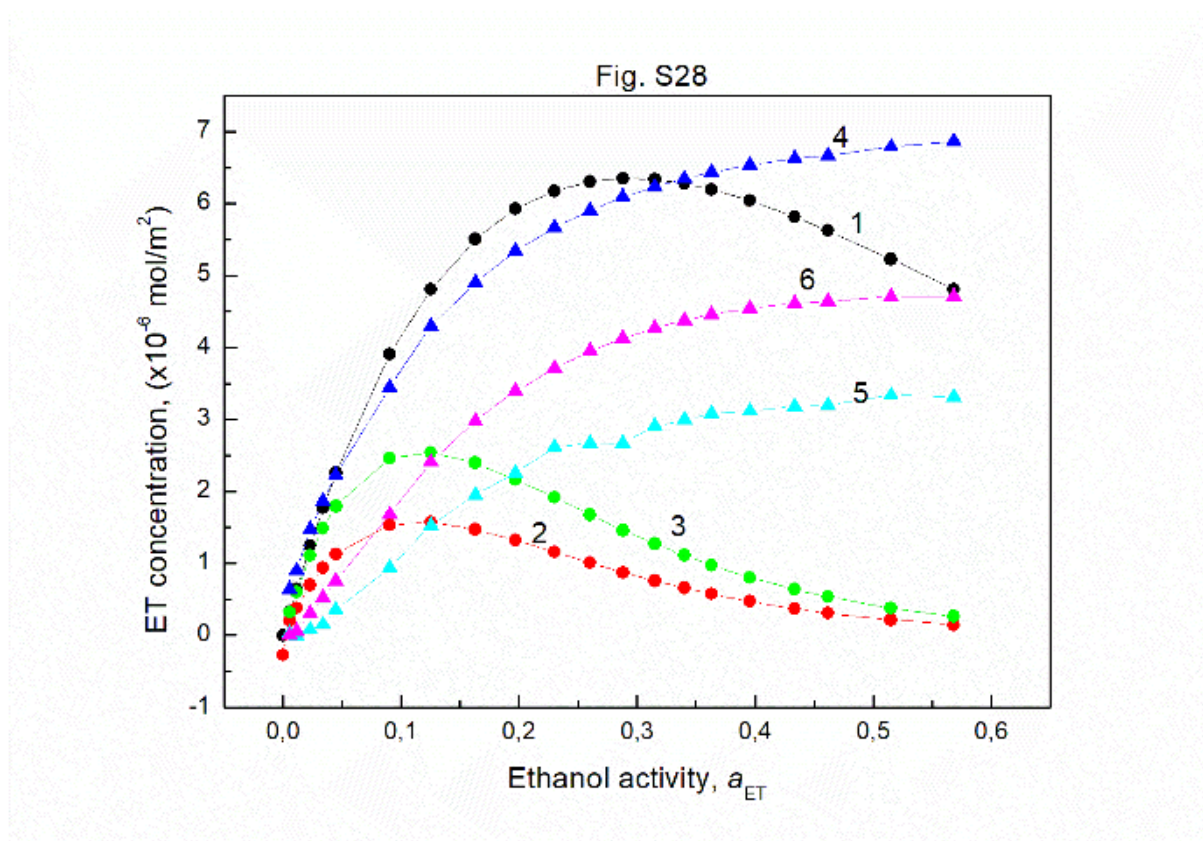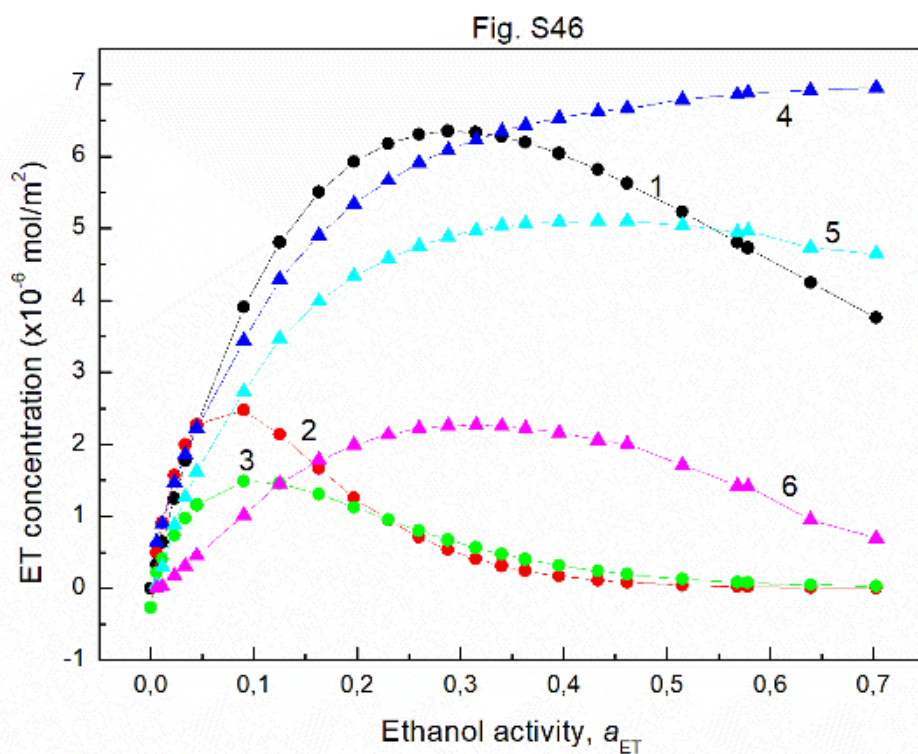
Figure S28. A plot of the ET Gibbs surface excess concentration at the water-air (curve 1), PMMA-air (curve 2) and PMMA-solution (curve 3) and ET Frumkin concentration at the water-air (curve 4), PMMA-air (curve 5) and PMMA-solution (curve 6) vs. the ethanol activity (a_{ET}) at the constant SF concentration equal to 0.1 mg/dm^3.
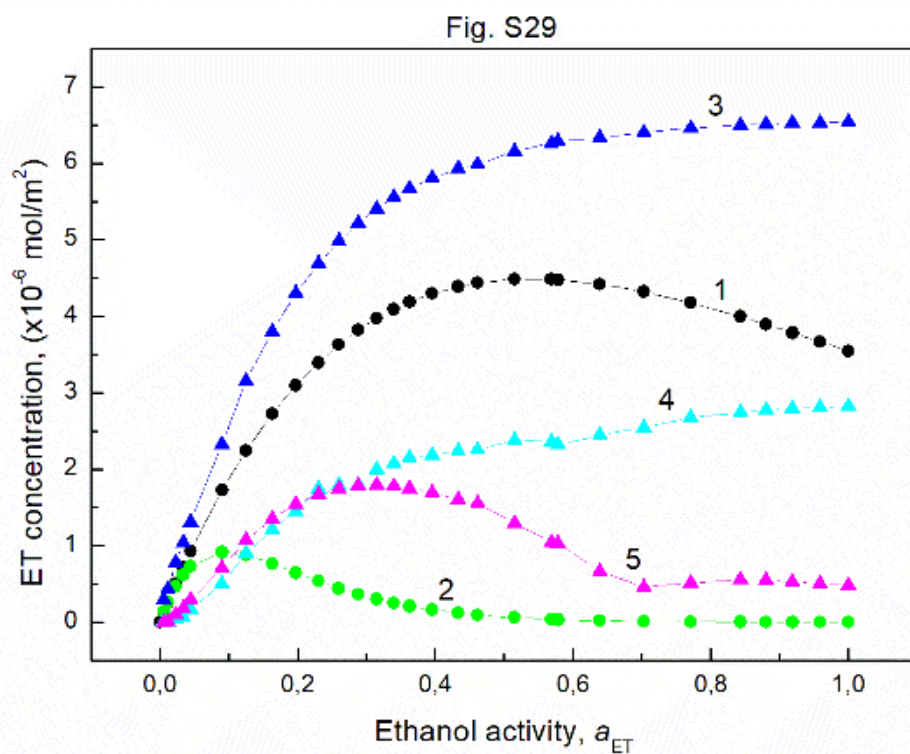
Figure S29. A plot of ET Gibbs surface excess concentration at the water-air (curve 1), PMMA-solution (curve 2) and ET Frumkin concentration at the water-air (curve 3), PMMA-air (curve 4) and PMMA-solution (curve 5) vs. the ethanol activity (a_{ET}) at the constant SF concentration equal to 1 mg/dm^3.
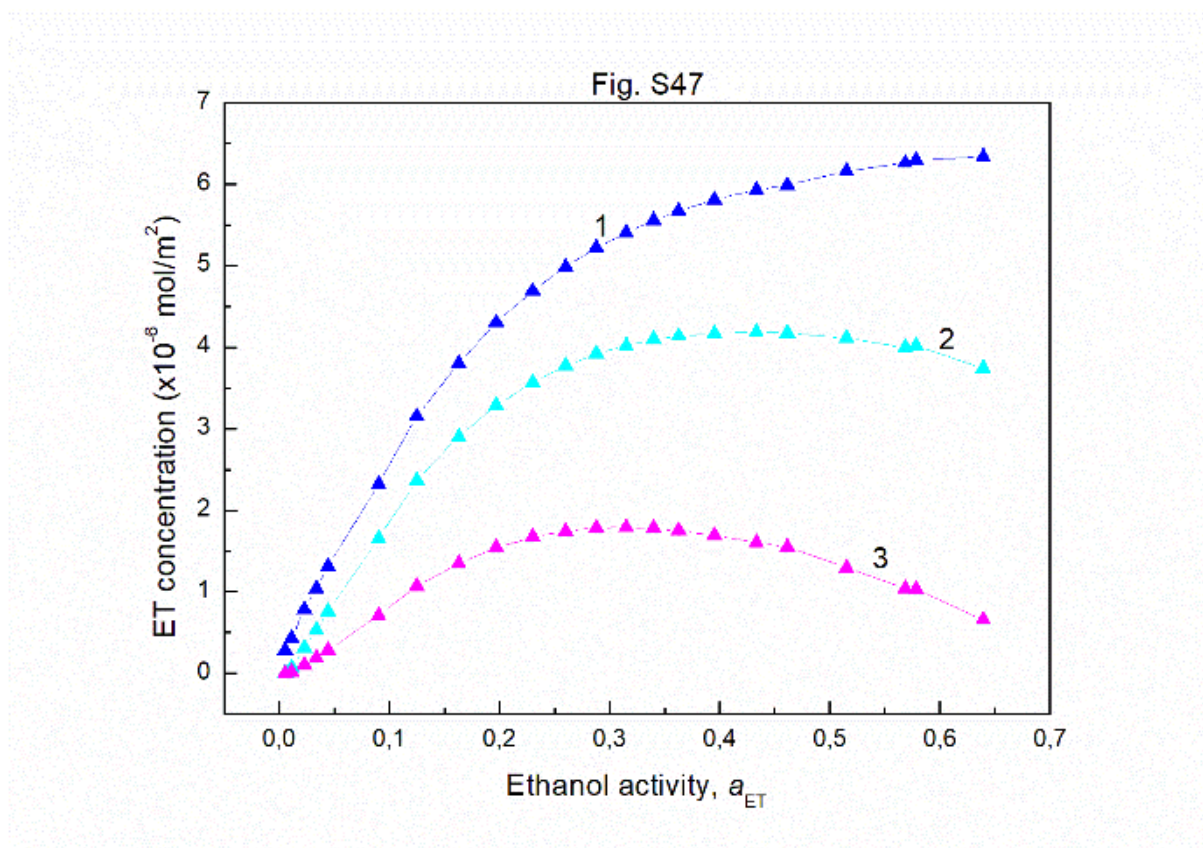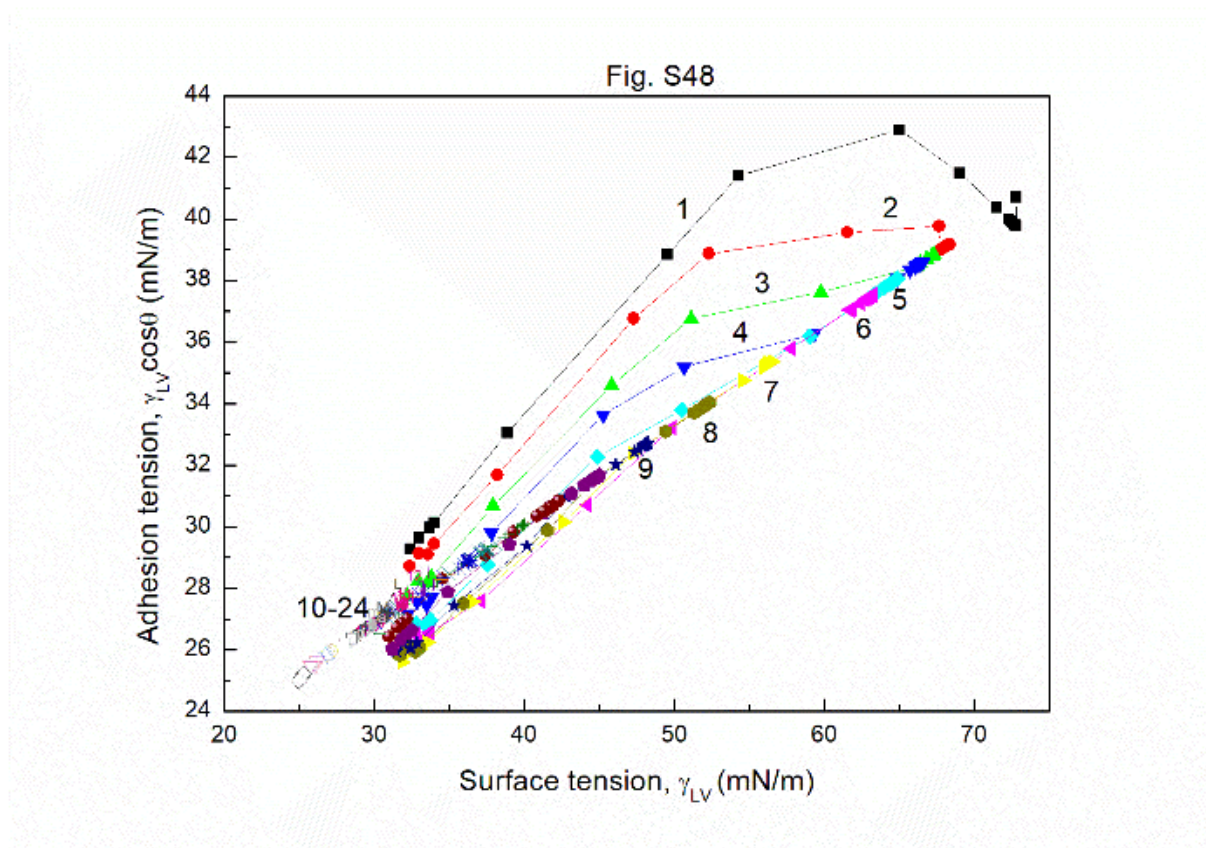
Figure S30. A plot of the adhesion tension ($\gamma_{LV} cos\theta$) for PMMA vs. the solution surface tension (γ_{LV}) [7]. Curves 1 – 21 correspond to the constant ET concentration equal to 0; 0.06692; 0.1338; 0.2677; 0.4015; 0.535; 1.0706; 1.6062; 2.1416; 2.677; 3.2124; 3.7478; 4.2832; 4.8185; 5.3538; 5.8893; 6.6925; 7.7245; 8.5664; 10.2797 and 11.968 M.

Figure S31. A plot of the SF Gibbs surface excess concentration at the PMMA–solution interface (Γ_{SF}) vs. the logarithm of surfactin concentration (C_{SF}). Curves 1 – 18 correspond to the constant ET concentration equal to 0; 0.06692; 0.1338; 0.2677; 0.4015; 0.535; 1.0706; 1.6062; 2.1416; 2.677; 3.2124; 3.7478; 4.2832; 4.8185; 5.3538; 5.8893; 6.6925 and 7.7245 M.
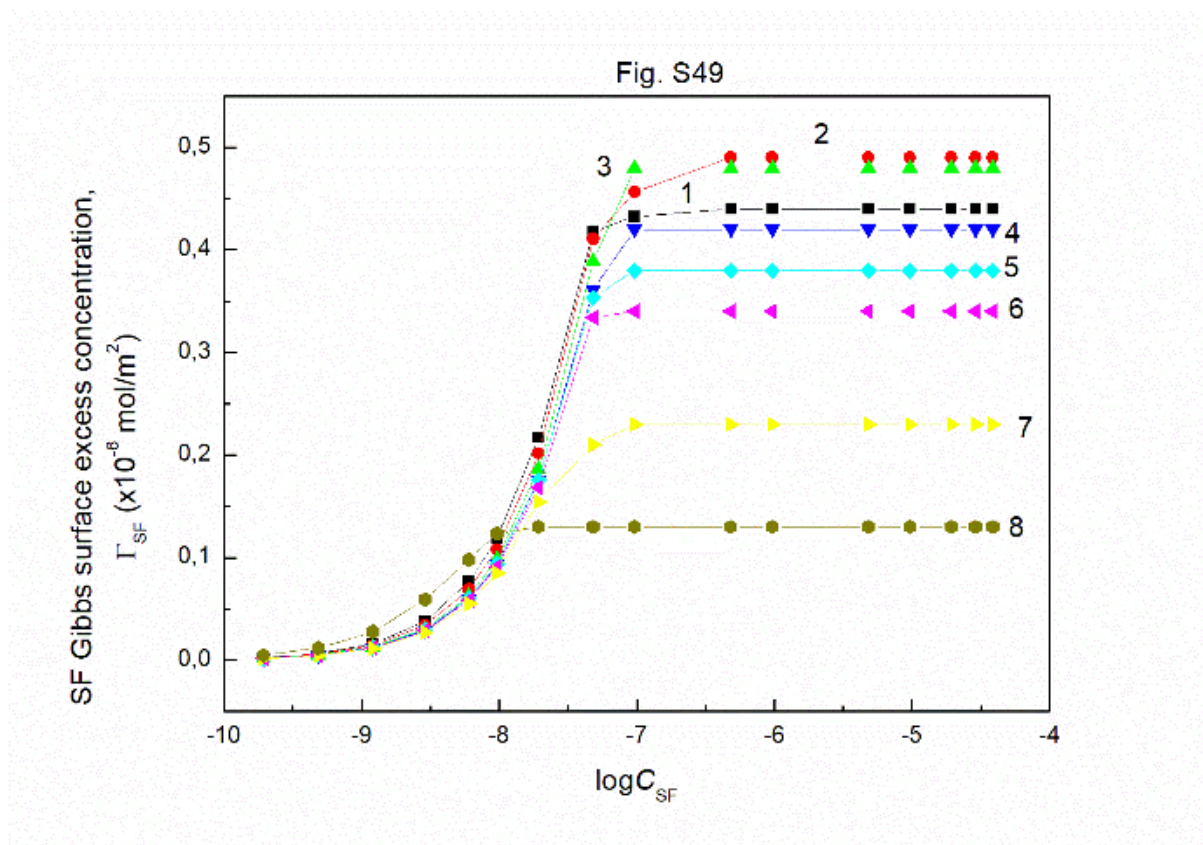
Figure S32. A plot of the SF Gibbs surface excess concentration at the PMMA–air interface (Γ_{SF}) vs. the logarithm of surfactin concentration (C_{SF}). Curves 1 – 18 correspond to the constant ET concentration equal to 0; 0.06692; 0.1338; 0.2677; 0.4015; 0.535; 1.0706; 1.6062; 2.1416; 2.677; 3.2124; 3.7478; 4.2832; 4.8185; 5.3538; 5.8893; 6.6925 and 7.7245 M.

Figure S33. A plot of the SF Frumkin concentration at the PMMA–air interface vs. the logarithm of surfactin concentration (C_{SF}). Curves 1 – 18 correspond to the constant ET concentration equal 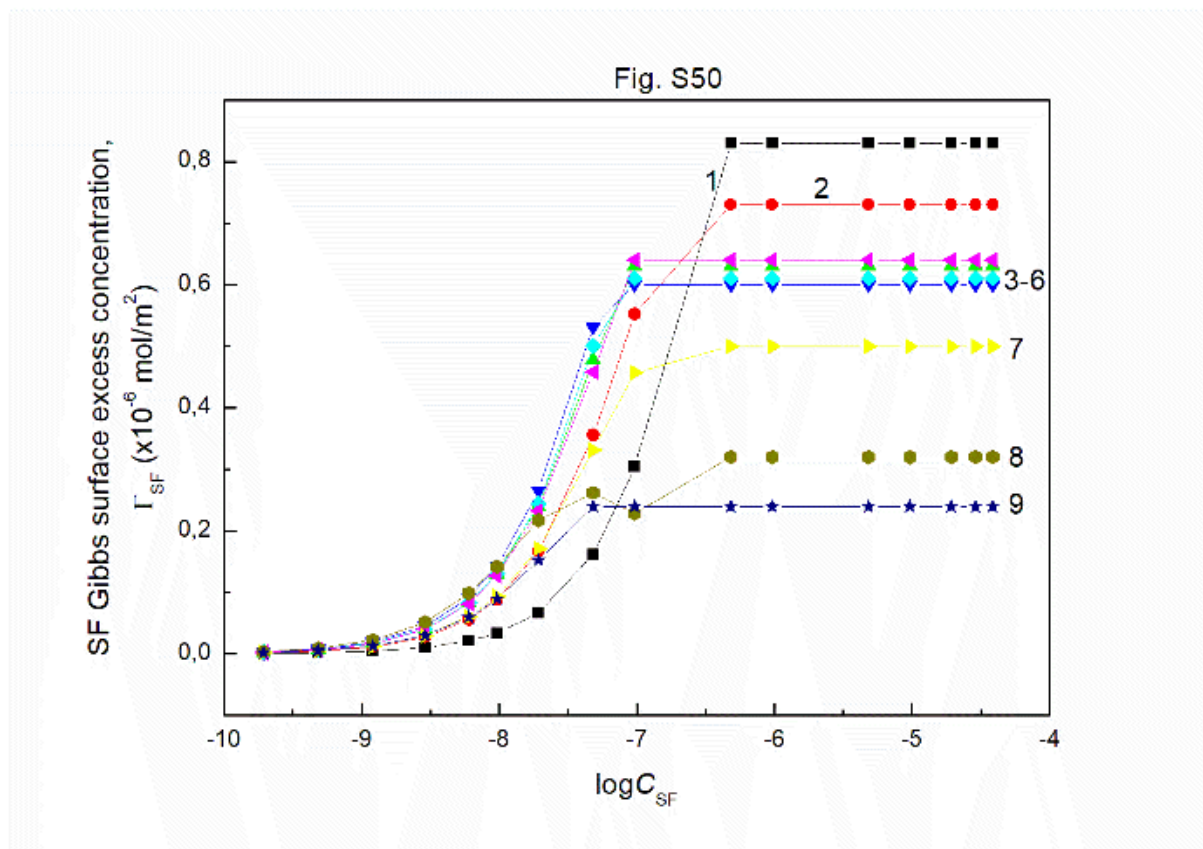to 0; 0.06692; 0.1338; 0.2677; 0.4015; 0.535; 1.0706; 1.6062; 2.1416; 2.677; 3.2124; 3.7478; 4.2832; 4.8185; 5.3538; 5.8893; 6.6925 and 7.7245 M.
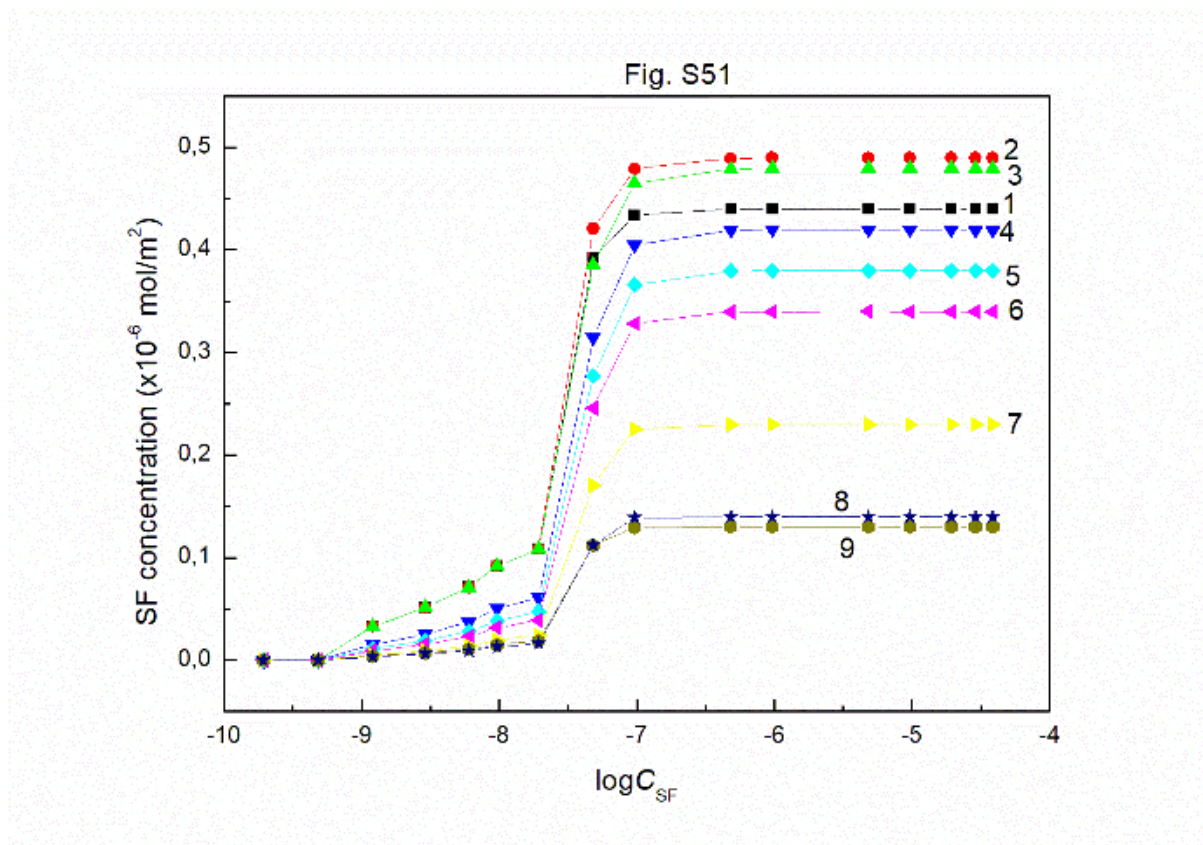
Figure S34. A plot of the SF Frumkin concentration at the PMMA–solution interface vs. the logarithm of surfactin concentration (C_{SF}). Curves 1 – 18 correspond to the constant ET concentration equal to 0; 0.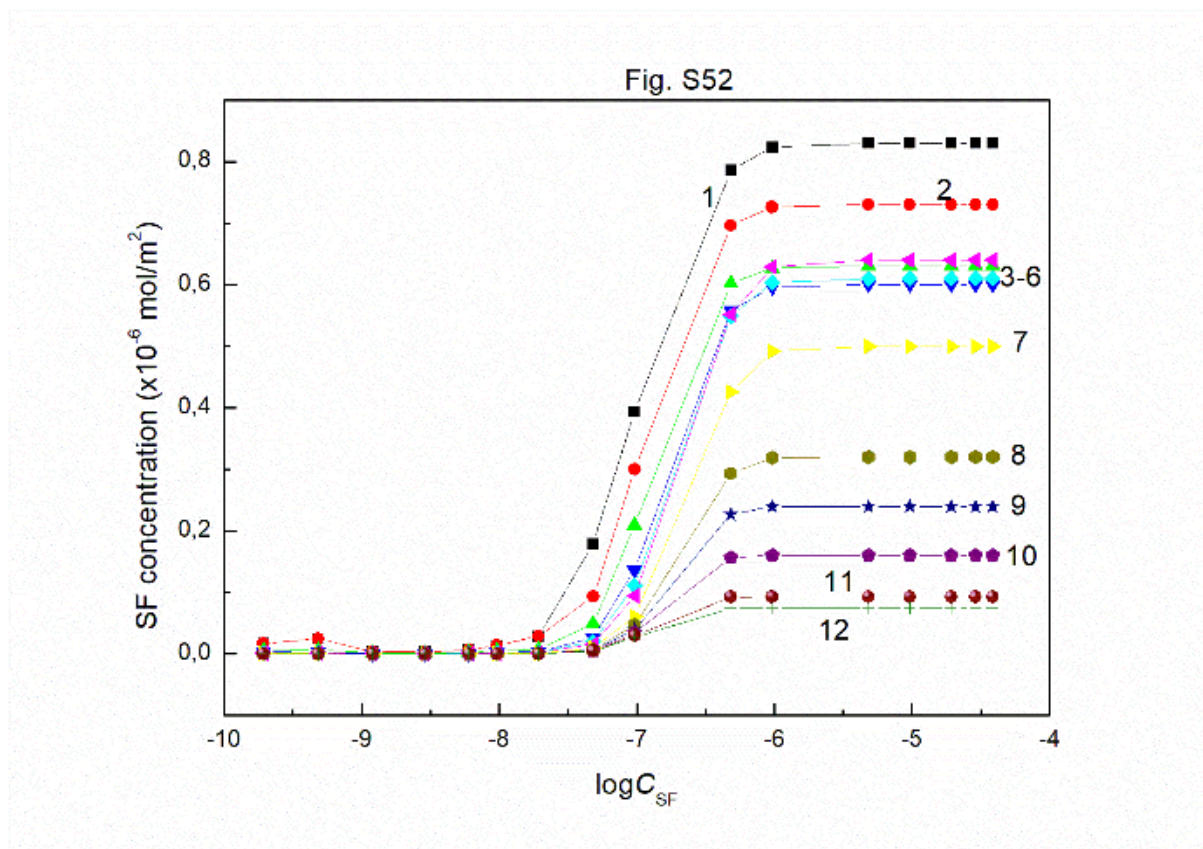06692; 0.1338; 0.2677; 0.4015; 0.535; 1.0706; 1.6062; 2.1416; 2.677; 3.2124; 3.7478; 4.2832; 4.8185; 5.3538; 5.8893; 6.6925 and 7.7245 M.

Figure S35. A plot of the SF Gibbs surface excess concentration at the water-air (curve 1), PMMA-air (curve 2) and PMMA-solution (curve 3) and SF Frumkin concentration at the water-air (curve 4), PMMA-air (curve 5) and PMMA-solution (curve 6) vs. the logarithm of surfactin concentration (C_{SF}) at the constant ET concentration equal to 0.

Figure S36. A plot of the SF Gibbs surface excess concentration at the water-air (curve 1), PMMA-air (curve 2) and PMMA-solution (curve 3) and SF Frumkin concentration at the water-air (curve 4), PMMA-air (curve 5) and PMMA-solution (curve 6) vs. the logarithm of surfactin concentration (C_{SF}) at the constant ET concentration equal to 1.0706 M.
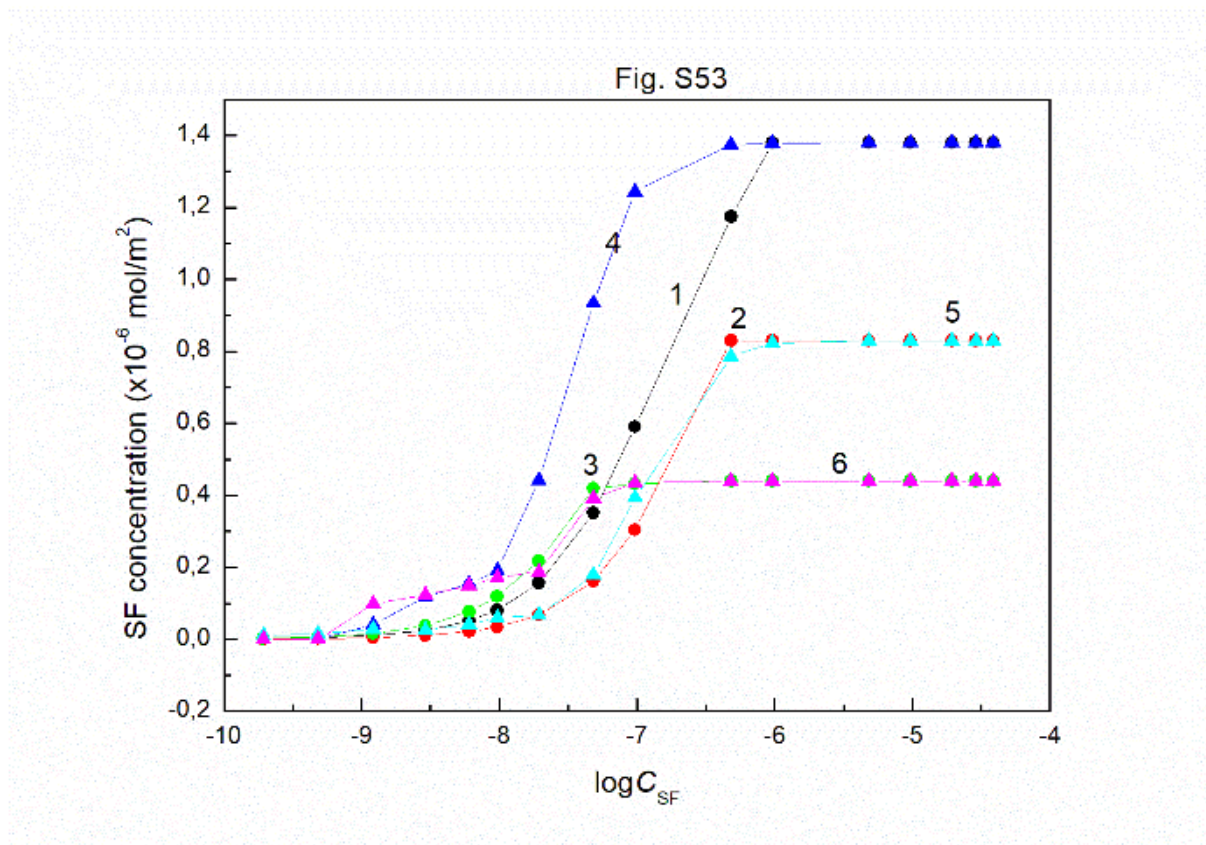
Figure S37. A plot of the SF Gibbs surface excess concentration at the water-air (curve 1), PMMA-air (curve 2) and PMMA-solution (curve 3) and SF Frumkin concentration at the water-air (curve 4), PMMA-air (curve 5) and PMMA-solution (curve 6) vs. the logarithm of surfactin concentration (C_{SF}) at the constant ET concentration equal to 3.7478 M.
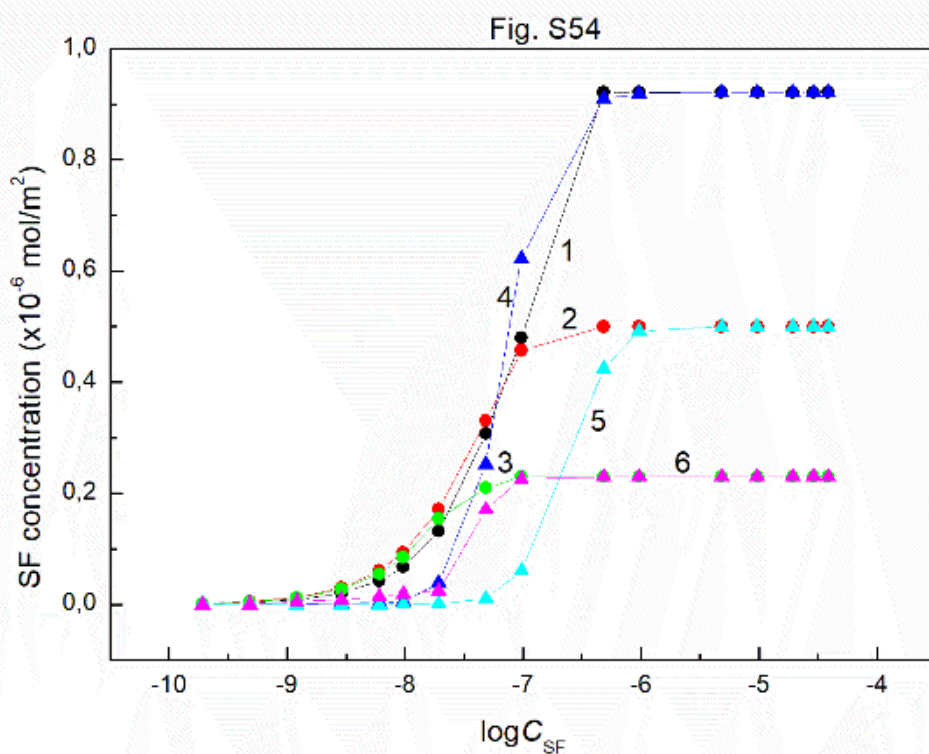
Figure S38. A plot of the SF Gibbs surface excess concentration at the water-air (curve 1), PMMA-air (curve 2) and PMMA-solution (curve 3) and SF Frumkin concentration at the water-air (curve 4), PMMA-air (curve 5) and PMMA-solution (curve 6) vs. the logarithm of surfactin concentration (C_{SF}) at the constant ET concentration equal to 6.6925 M.
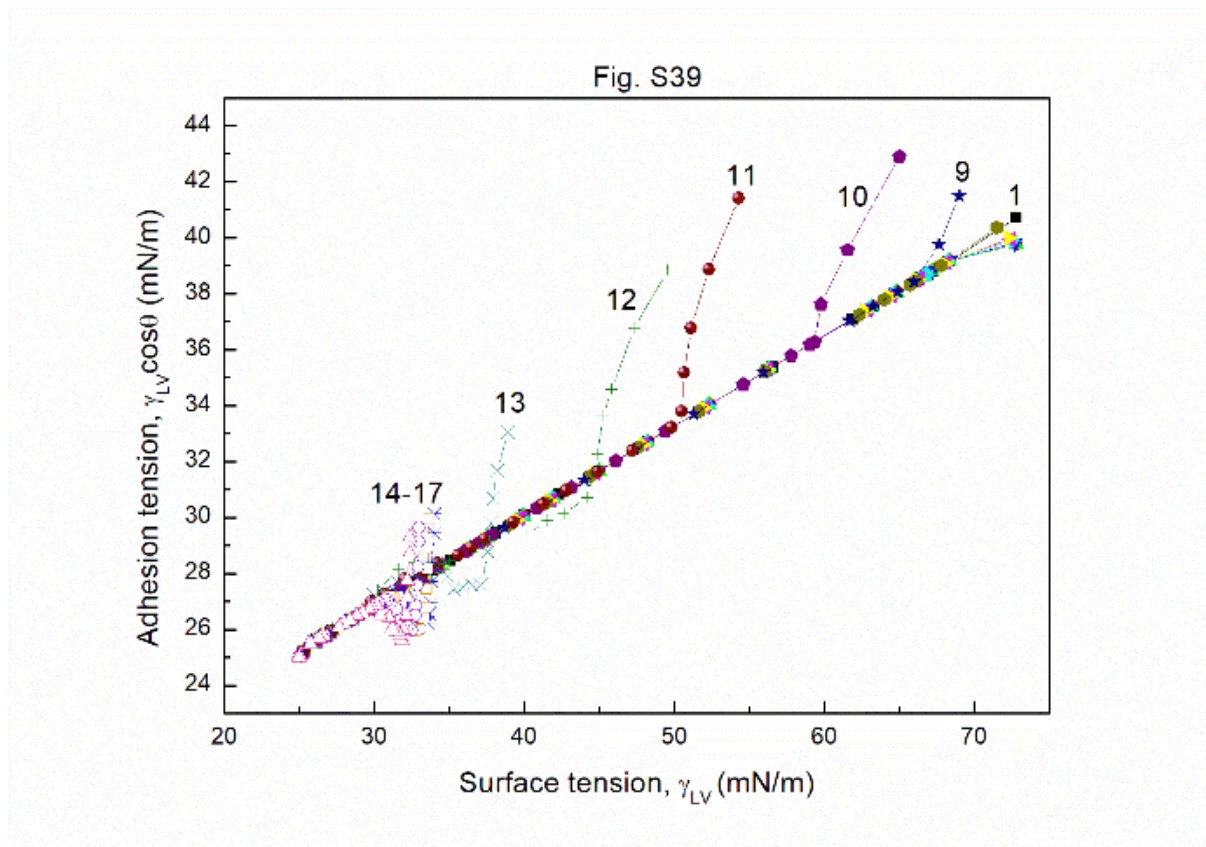
Figure S39. A plot of the adhesion tension ($\gamma_{LV}\cos\theta$) for quartz vs. the solution surface tension (γ_{LV}) [7]. Curves 1 – 17 correspond to the constant SF concentration equal to 0; 0.0002; 0.0005; 0.00125; 0003; 0.00625; 0.01; 0.02; 0.05; 0.1; 0.5; 1; 5; 10; 20; 30 and 40 mg/dm³.
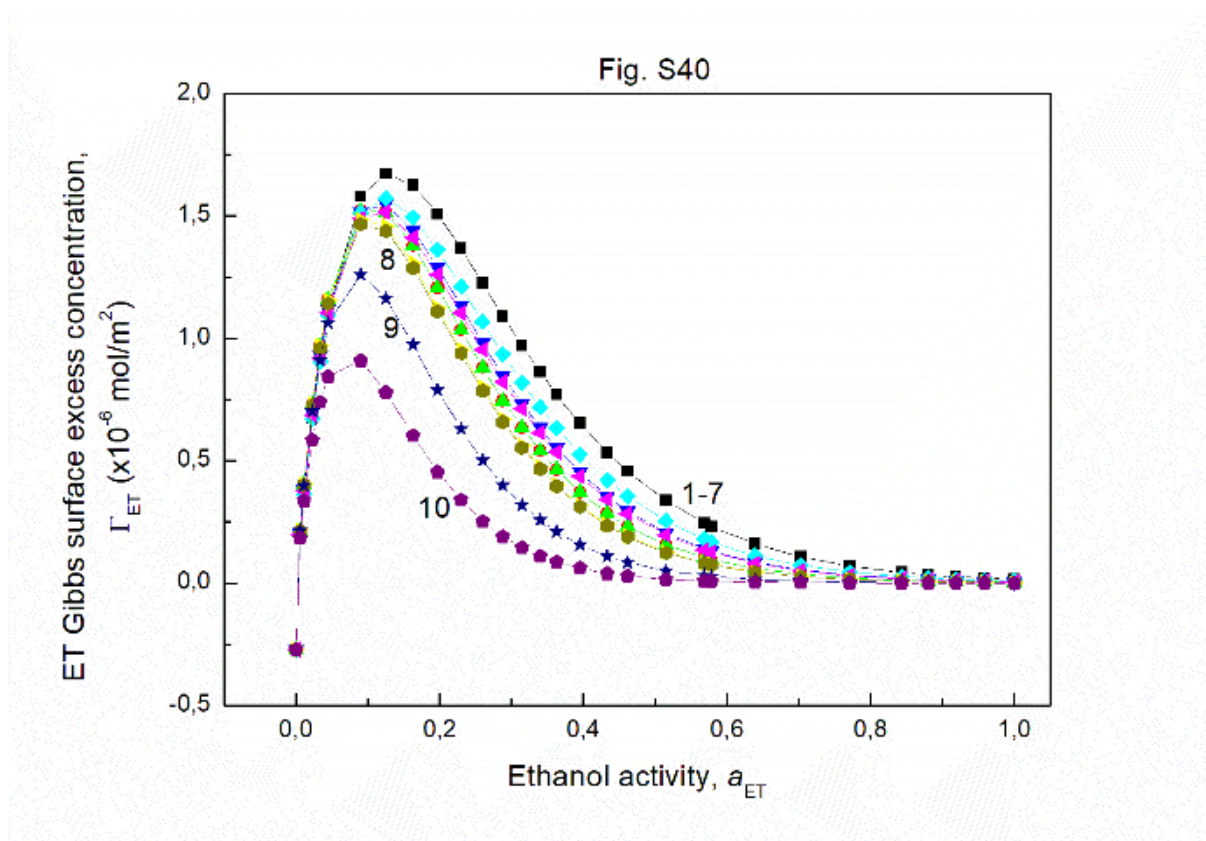
Figure S40. A plot of the ET Gibbs surface excess concentration at the quartz–solution interface (Γ_{ET}) vs. the ethanol activity (a_{ET}). Curves 1 – 10 correspond to the constant SF concentration equal to 0; 0.0002; 0.0005; 0.00125; 0003; 0.00625; 0.01; 0.02; 0.05 and 0.1 mg/dm^3.

Figure S41. A plot of the ET Gibbs surface excess concentration at the quartz–air interface (Γ_{ET}) vs. the ethanol activity (a_{ET}). Curves 1 – 11 correspond to the constant SF concentration equal to 0; 0.0002; 0.0005; 0.00125; 0003; 0.00625; 0.01; 0.02; 0.05, 0.1 and 0.5 mg/dm^3.

Figure S42. A plot of the ET Frumkin concentration at the quartz–solution interface vs. the ethanol concentration (C_{ET}). Curves 1 – 17 correspond to the constant SF concentration equal to 0; 0.0002; 0.0005; 0.00125; 0003; 0.00625; 0.01; 0.02; 0.05; 0.1; 0.5; 1; 5; 10; 20; 30 and 40 mg/dm^3.
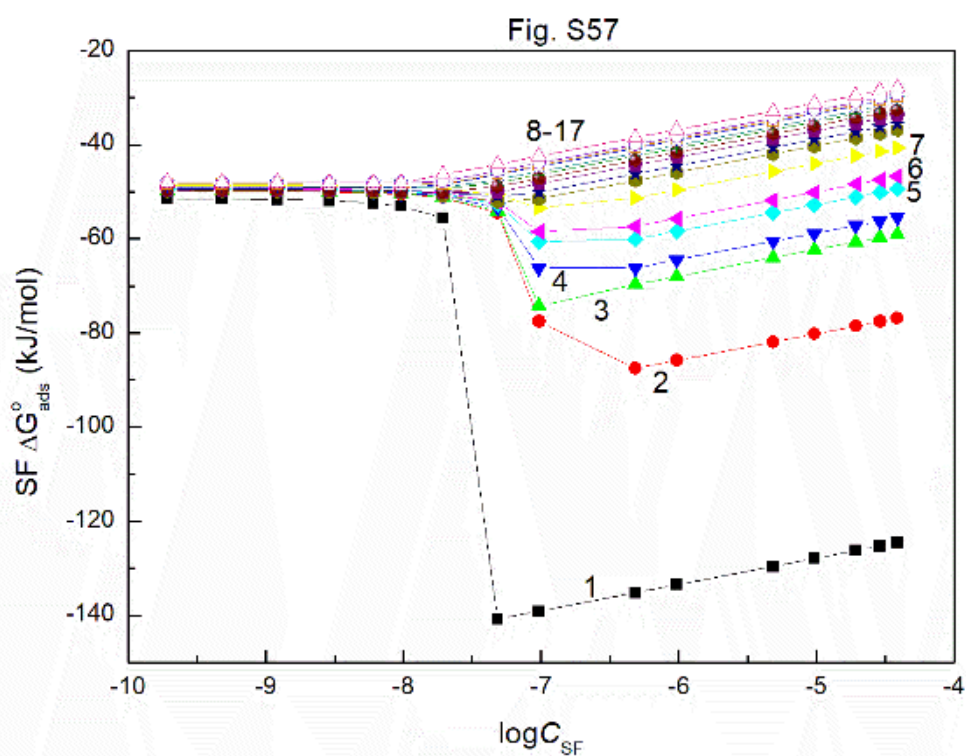
Figure S43. A plot of the ET Frumkin concentration at the quartz–air interface vs. the ethanol concentration (C_{ET}). Curves $1 - 17$ correspond to the constant SF concentration equal to 0; 0.0002; 0.0005; 0.00125; 0003; 0.00625; 0.01; 0.02; 0.05; 0.1; 0.5; 1; 5; 10; 20; 30 and 40 mg/dm³.

Figure S44. A plot of the ET Gibbs surface excess concentration at the water-air (curve 1), quartz-air (curve 2) and quartz-solution (curve 3) and ET Frumkin concentration at the water-air (curve 4), quartz-air (curve 5) and quartz-solution (curve 6) vs. the ethanol activity (a_{ET}) at the constant SF concentration equal to 0.

Figure S45. A plot of the ET Gibbs surface excess concentration at the water-air (curve 1), quartz-air (curve 2) and quartz-solution (curve 3) and ET Frumkin concentration at the water-air (curve 4), quartz-air (curve 5) and quartz-solution (curve 6) vs. the ethanol activity (a_{ET}) at the constant SF concentration equal to 0.01 mg/dm^3.

Figure S46. A plot of the ET Gibbs surface excess concentration at the water-air (curve 1), quartz-air (curve 2) and quartz-solution (curve 3) and ET Frumkin concentration at the water-air (curve 4), quartz-air (curve 5) and quartz-solution (curve 6) vs. the ethanol activity (a_{ET}) at the constant SF concentration equal to 0.1 mg/dm^3.

Figure S47. A plot of the ET Frumkin concentration at the water-air (curve 1), quartz-air (curve 2) and quartz-solution (curve 3) vs. the ethanol activity (a_{ET}) at the constant SF concentration equal to 0.5 mg/dm^3.

Figure S48. A plot of the adhesion tension ($\gamma_{LV}cos\theta$) for quartz vs. the solution surface tension (γ_{LV}) [7]. Curves 1 – 24 correspond to the constant ET concentration equal to 0; 0.06692; 0.1338; 0.2677; 0.4015; 0.535; 1.0706; 1.6062; 2.1416; 2.677; 3.2124; 3.7478; 4.2832; 4.8185; 5.3538; 5.8893; 6.6925; 7.7245; 8.5664; 10.2797; 11.968; 12.145; 13.3794 and 14.5696 M.
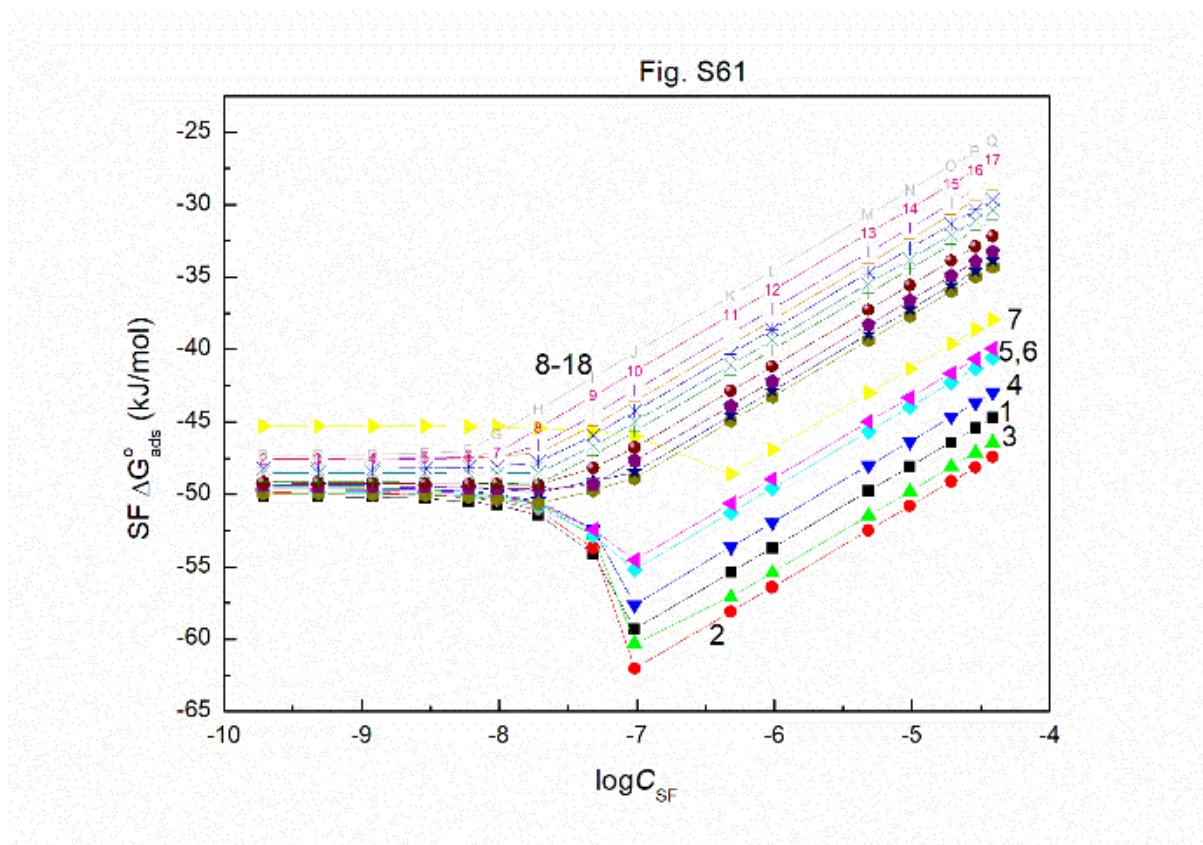
Figure S49. A plot of the SF Gibbs surface excess concentration at the quartz–solution interface (Γ_{SF}) vs. the logarithm of surfactin concentration (C_{SF}). Curves $1 - 8$ correspond to the constant ET concentration equal to 0; 0.06692; 0.1338; 0.2677; 0.4015; 0.535; 1.0706 and 1.6062 M.

Figure S50. A plot of the SF Gibbs surface excess concentration at the quartz–air interface (Γ_{SF}) vs. the logarithm of surfactin concentration (C_{SF}). Curves 1 – 9 correspond to the constant ET concentration equal to 0; 0.06692; 0.1338; 0.2677; 0.4015; 0.535; 1.0706, 1.6062 and 2.1416 M.

Figure S51. A plot of the SF Frumikn concentration at the quartz–solution interface vs. the logarithm of surfactin concentration (C_{SF}). Curves 1 – 9 correspond to the constant ET concentration equal to 0; 0.06692; 0.1338; 0.2677; 0.4015; 0.535; 1.0706, 1.6062 and 2.1416 M.

Figure S52. A plot of the SF Frumikn concentration at the quartz–air interface vs. the logarithm of surfactin concentration (C_{SF}). Curves 1 – 12 correspond to the constant ET concentration equal to 0; 0.06692; 0.1338; 0.2677; 0.4015; 0.535; 1.0706, 1.6062, 2.1416, 2.677, 3.2124 and 3.7478 M.

Figure S53. A plot of the SF Gibbs surface excess concentration at the water-air (curve 1), quartz-air (curve 2) and quartz-solution (curve 3) and SF Frumkin concentration at the water-air (curve 4), quartz-air (curve 5) and quartz-solution (curve 6) vs. the logarithm of surfactin concentration (C_{SF}) at the constant ET concentration equal to 0.

Figure S54. A plot of the SF Gibbs surface excess concentration at the water-air (curve 1), quartz-air (curve 2) and quartz-solution (curve 3) and SF Frumkin concentration at the water-air (curve 4), quartz-air (curve 5) and quartz-solution (curve 6) vs. the logarithm of surfactin concentration (C_{SF}) at the constant ET concentration equal to 1.0706 M.
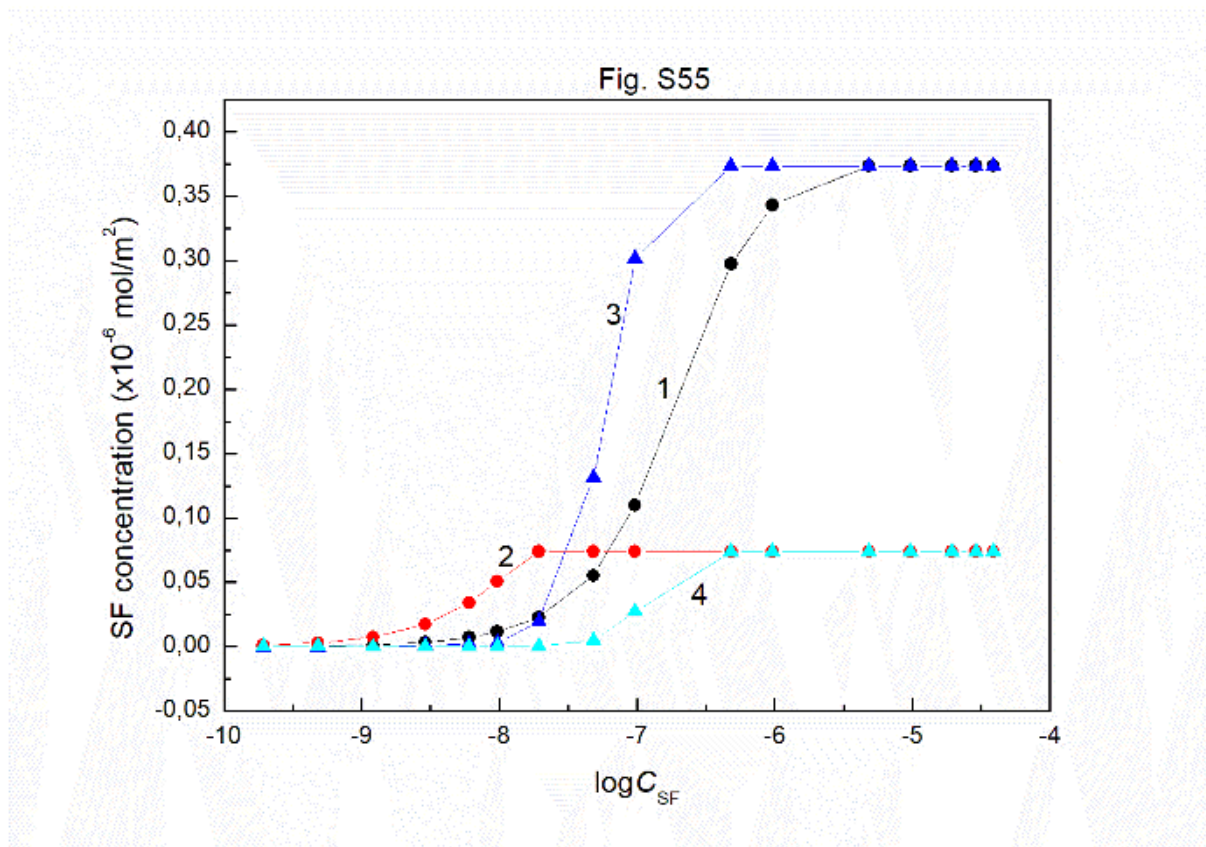
Figure S55. A plot of the SF Gibbs surface excess concentration at the water-air (curve 1), quartz-air (curve 2) and SF Frumkin concentration at the water-air (curve 3), quartz-air (curve 4) vs. the logarithm of surfactin concentration (C_{SF}) at the constant ET concentration equal to 3.7478 M.
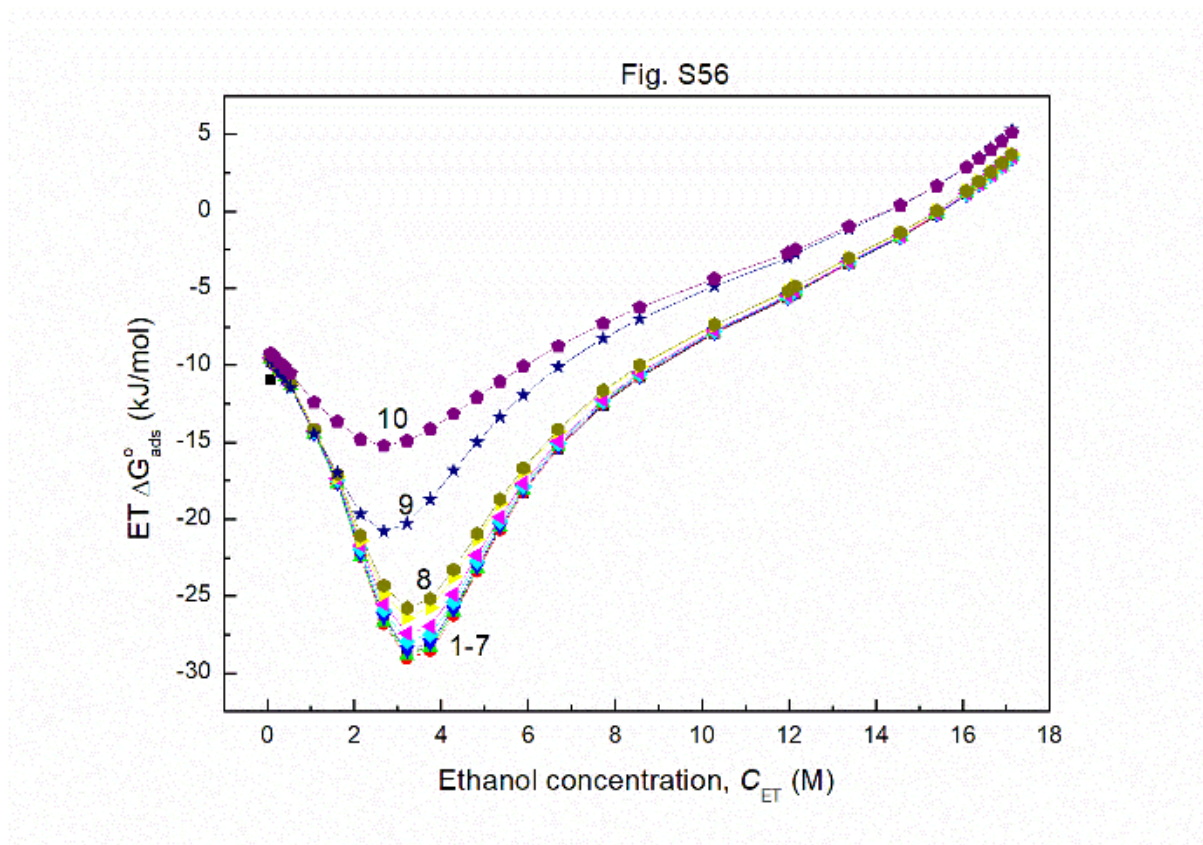
Figure S56. A plot of the standard Gibbs free energy of ET adsorption at the PTFE-solution interface (ΔG^0_{ads}) vs. alcohol concentration (C_{ET}). Curves 1 – 10 correspond to the constant SF concentration equal to 0; 0002; 0.0005; 0.00125; 0003; 0.00625; 0.01; 0.02; 0.05 and 0.1 mg/dm³.

Figure S57. A plot of the standard Gibbs free energy of SF adsorption at the PTFE-solution interface (ΔG_{ads}^0) vs. the logarithm of surfactin concentration (C_{SF}). Curves 1 – 17 correspond to the constant ET concentration equal to 0; 0.06692; 0.1338; 0.2677; 0.4015; 0.535; 1.0706; 1.6062; 2.1416; 2.677; 3.2124; 3.7478; 4.2832; 4.8185; 5.3538; 5.8893 and 6.6925 M.
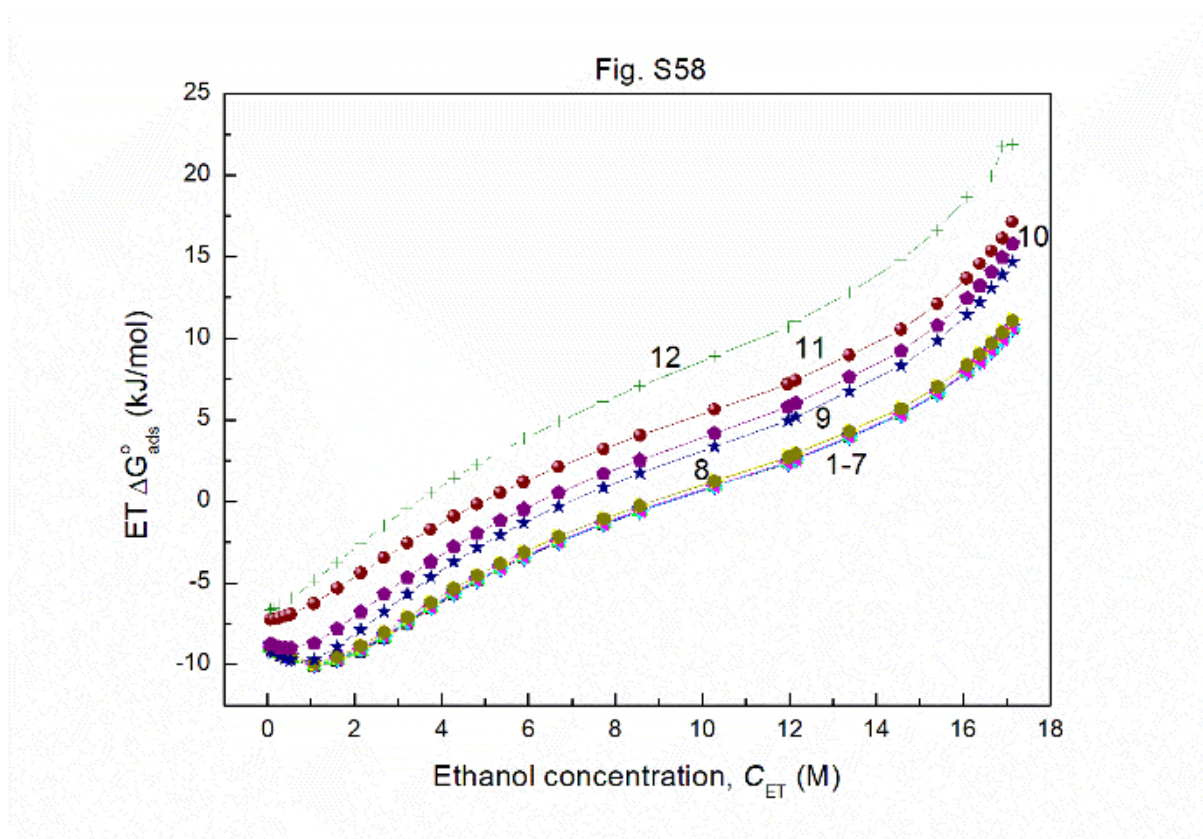
Figure S58. A plot of the standard Gibbs free energy of ET adsorption at the PMMA-solution interface (ΔG_{ads}^{0}) vs. alcohol concentration (C_{ET}). Curves 1 – 12 correspond to the constant SF concentration equal to 0; 0002; 0.0005; 0.00125; 0003; 0.00625; 0.01; 0.02; 0.05, 0.1, 0.5 and 1 mg/dm^3.
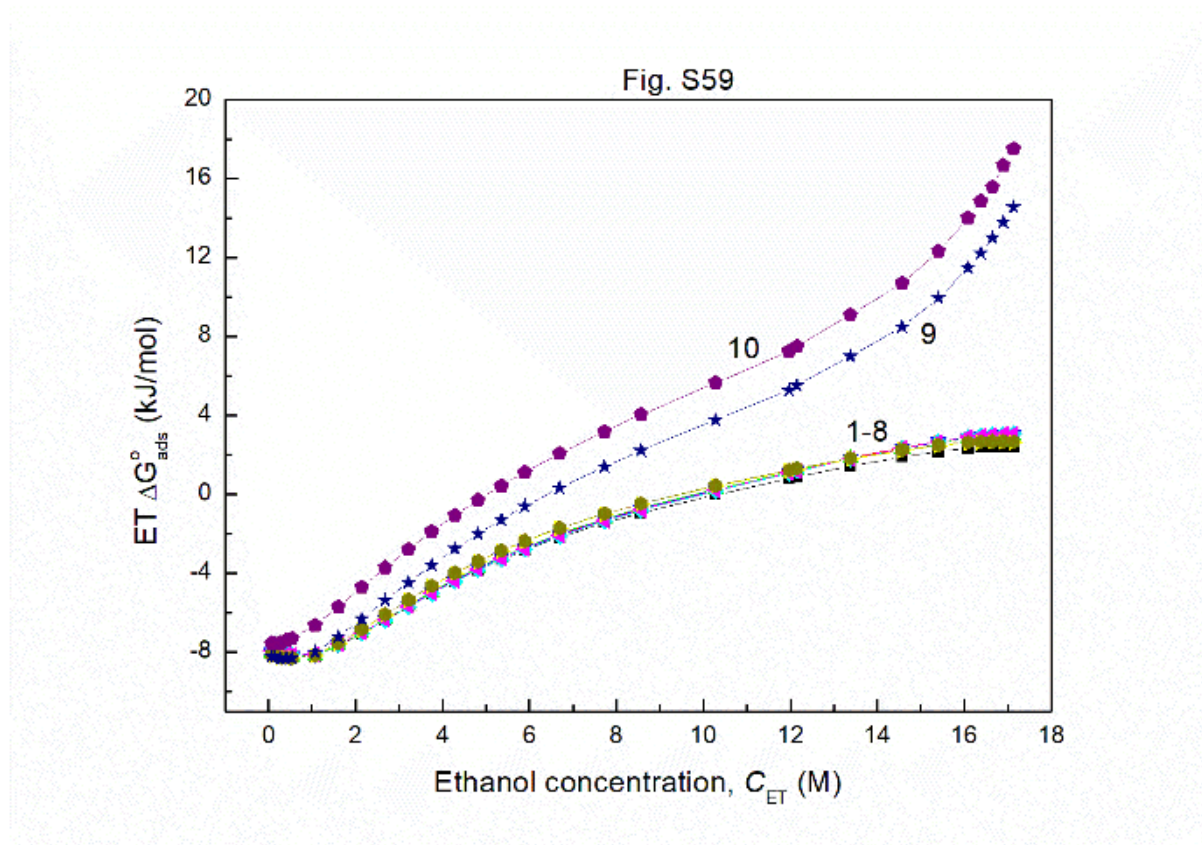
Figure S59. A plot of the standard Gibbs free energy of ET adsorption at the PMMA-air interface (ΔG^0_{ads}) vs. alcohol concentration (C_{ET}). Curves 1 – 10 correspond to the constant SF concentration equal to 0; 0002; 0.0005; 0.00125; 0003; 0.00625; 0.01; 0.02; 0.05 and mg/dm^3.
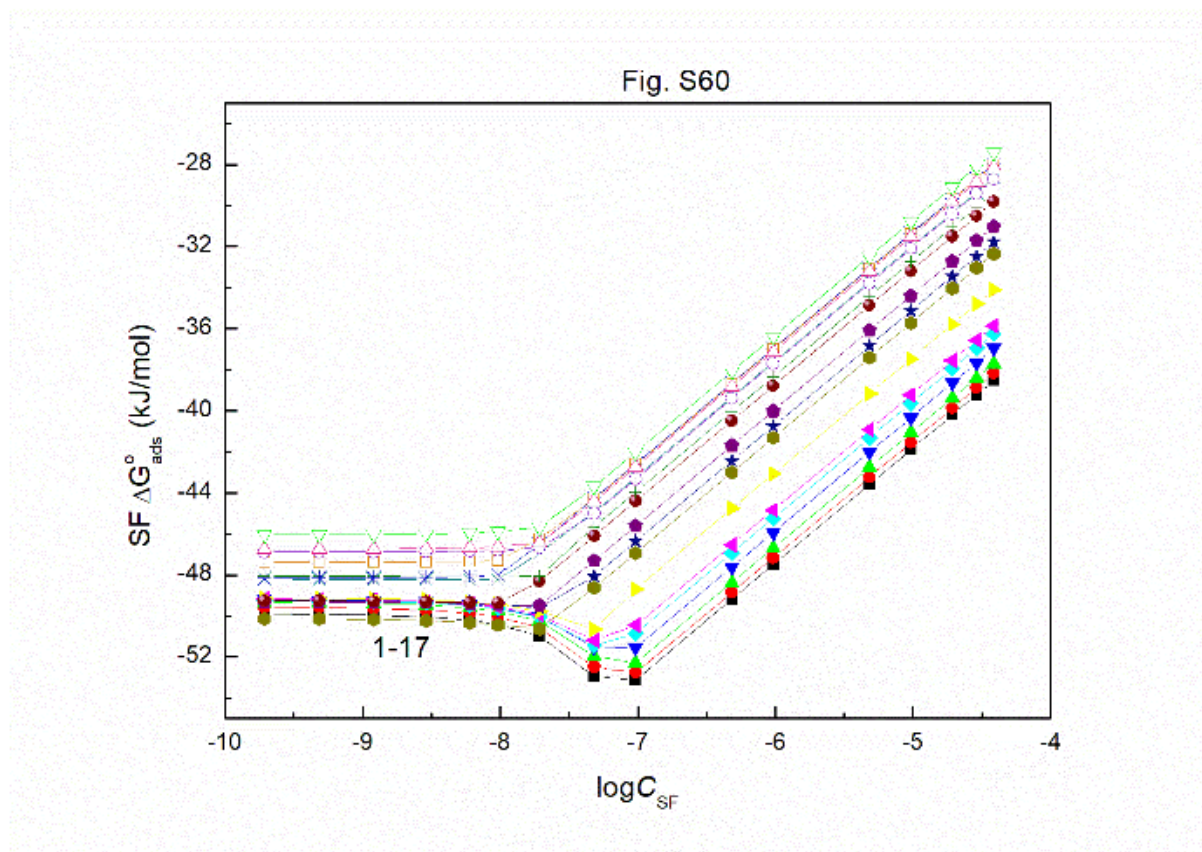
Figure S60. A plot of the standard Gibbs free energy of SF adsorption at the PMMA-solution interface (ΔG_{ads}^{0}) vs. the logarithm of surfactin concentration (C_{SF}). Curves 1 – 18 correspond to the constant ET concentration equal to 0; 0.06692; 0.1338; 0.2677; 0.4015; 0.535; 1.0706; 1.6062; 2.1416; 2.677; 3.2124; 3.7478; 4.2832; 4.8185; 5.3538; 5.8893, 6.6925 and 7.7245M.

Figure S61. A plot of the standard Gibbs free energy of SF adsorption at the PMMA-air interface (ΔG^0_{ads}) vs. the logarithm of surfactin concentration (C_{SF}). Curves 1 – 18 correspond to the constant ET concentration equal to 0; 0.06692; 0.1338; 0.2677; 0.4015; 0.535; 1.0706; 1.6062; 2.1416; 2.677; 3.2124; 3.7478; 4.2832; 4.8185; 5.3538; 5.8893, 6.6925 and 7.7245M.
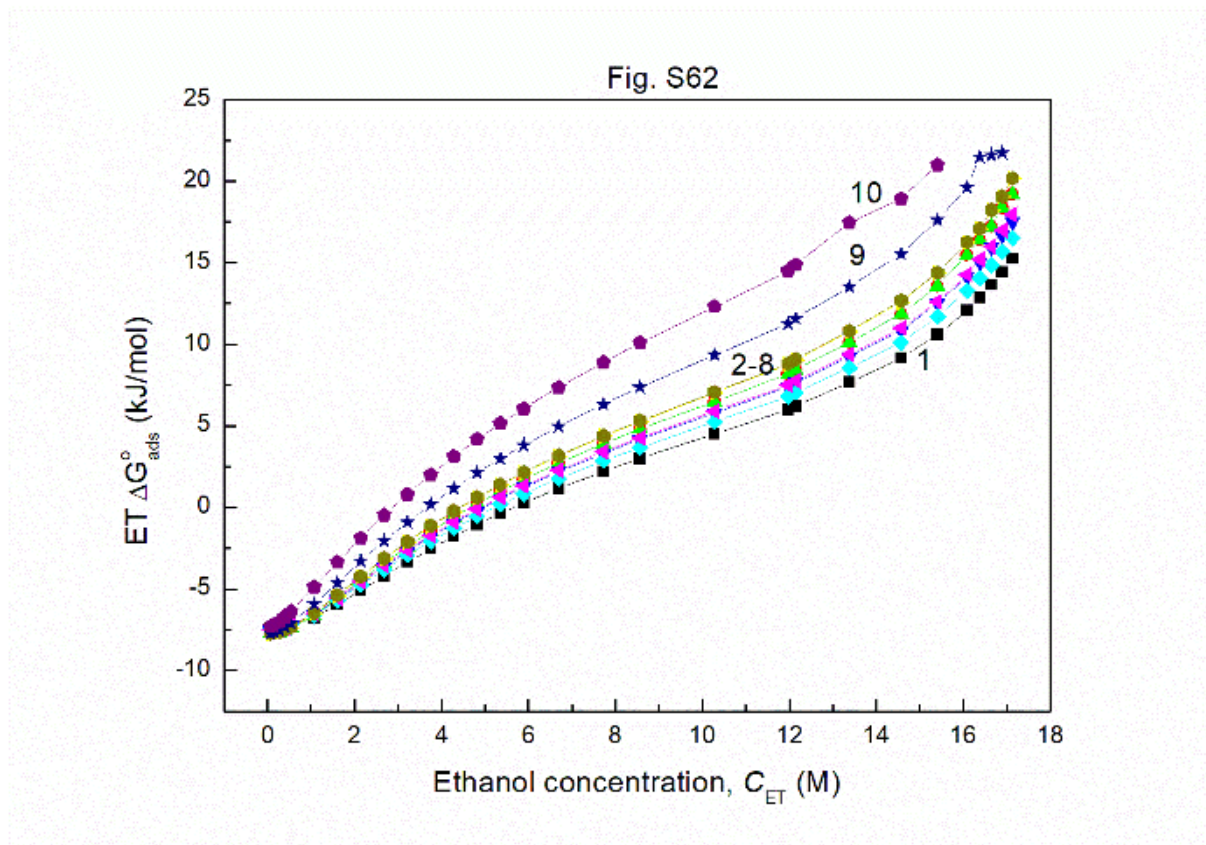
Figure S62. A plot of the standard Gibbs free energy of ET adsorption at the quartz-solution interface (ΔG_{ads}^0) vs. alcohol concentration (C_{ET}). Curves 1 – 10 correspond to the constant SF concentration equal to 0; 0002; 0.0005; 0.00125; 0003; 0.00625; 0.01; 0.02; 0.05 and mg/dm^3.
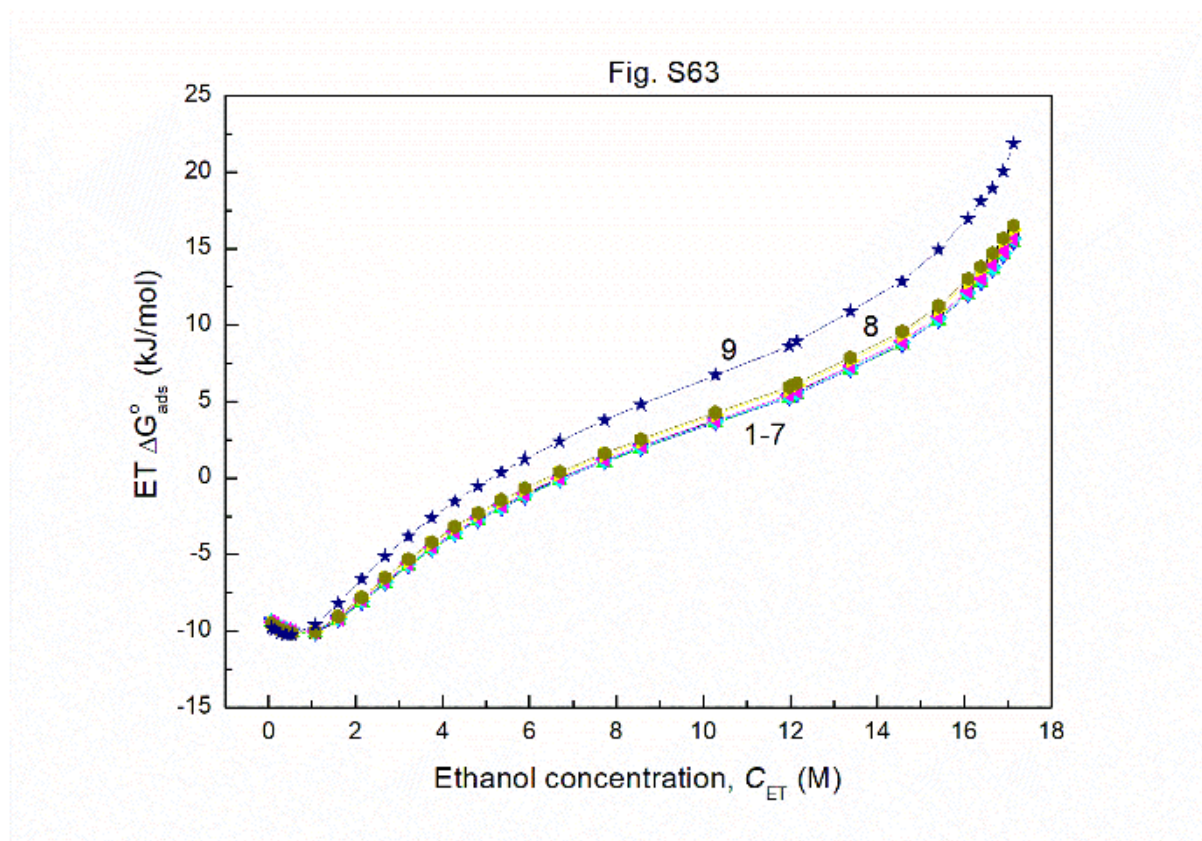
Figure S63. A plot of the standard Gibbs free energy of ET adsorption at the quartz-air interface (ΔG_{ads}^0) vs. alcohol concentration (C_{ET}). Curves $1 - 9$ correspond to the constant SF concentration equal to 0; 0002; 0.0005; 0.00125; 0003; 0.00625; 0.01; 0.02 and 0.05 mg/dm^3.
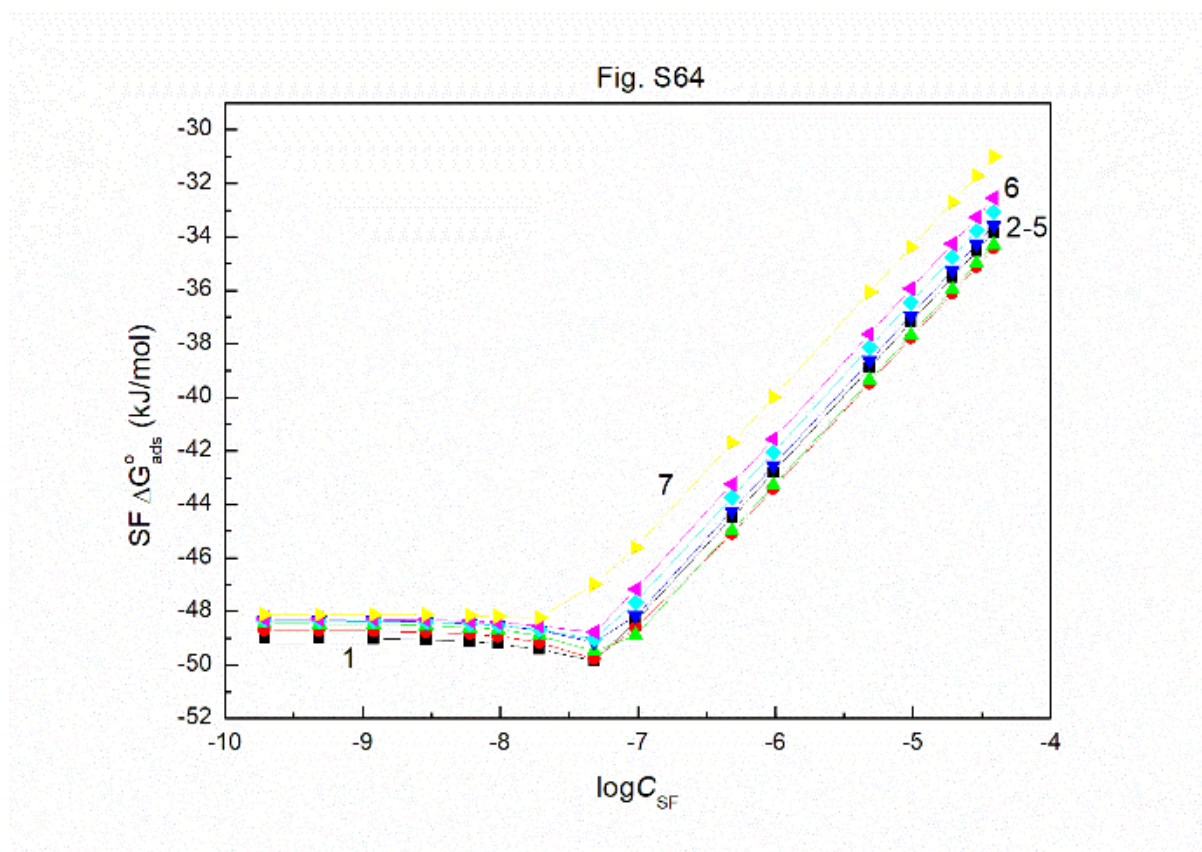
Figure S64. A plot of the standard Gibbs free energy of SF adsorption at the quartz-solution interface (ΔG_{ads}^{0}) vs. the logarithm of surfactin concentration (C_{SF}). Curves 1 – 7 correspond to the constant ET concentration equal to 0; 0.06692; 0.1338; 0.2677; 0.4015; 0.535 and 1.0706 M.
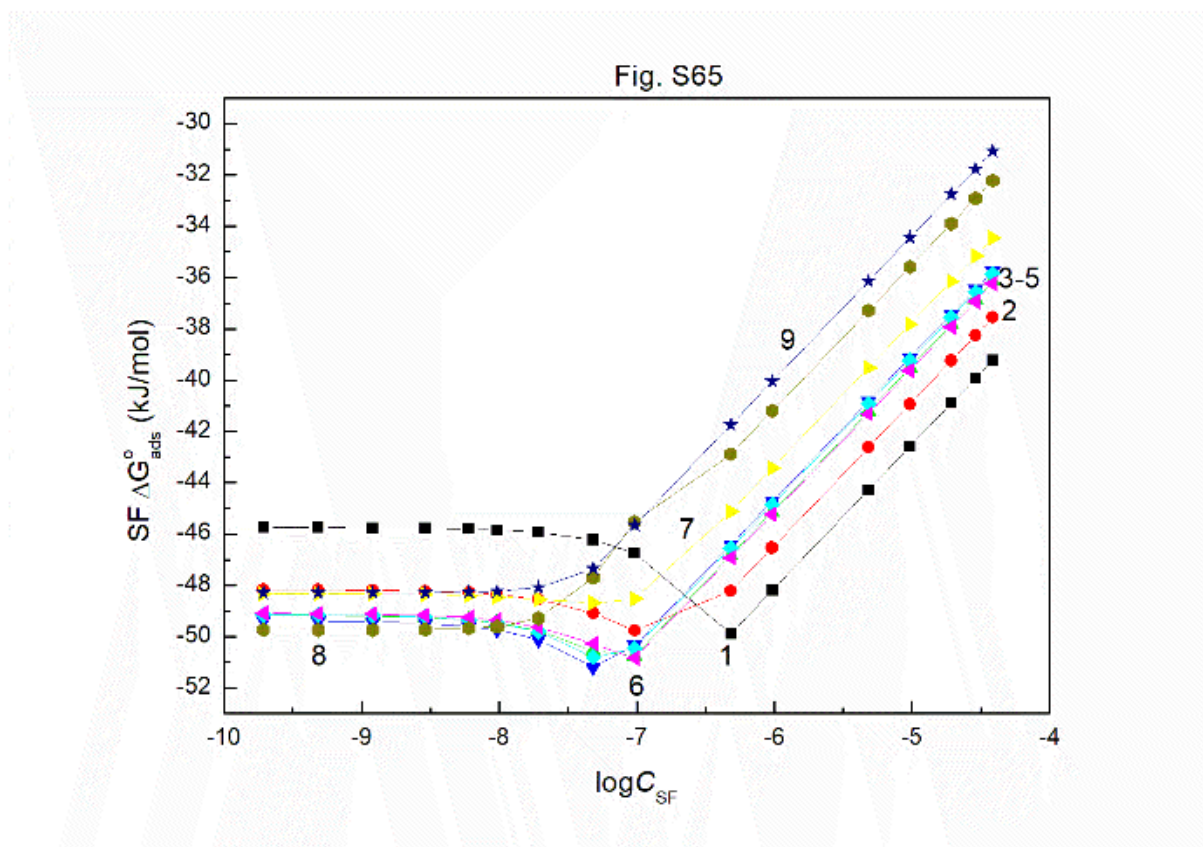
Figure S65. A plot of the standard Gibbs free energy of SF adsorption at the quartz-air interface (ΔG_{ads}^0) vs. the logarithm of surfactin concentration (C_{SF}). Curves $1-9$ correspond to the constant ET concentration equal to 0; 0.06692; 0.1338; 0.2677; 0.4015; 0.535, 1.0706 M, 1.6062 and 2.1416 M.

Prof. dr hab. Anna Zdziennicka
Katedra Zjawisk Międzyfazowych
Instytut Nauk Chemicznych
Wydział Chemii UMCS
Pl. M. Curie-Skłodowskiej 3
20-031 Lublin

Lublin, 17.01.2023

OŚWIADCZENIE

Oświadczam, że w pracy

E. Rekiel, **A. Zdziennicka***, B. Jańczuk, *Mutual influence of ethanol and surfactin on their wetting and adhesion properties*, Colloids and Surfaces A: Physicochemical and Engineering Aspects, 2021, 627, 127161;

mój udział wynosił **30%** i polegał na koordynowaniu merytorycznym badań, a także na analizie formalnej otrzymanych wyników, współredagowaniu odpowiedzi na recenzje pracy oraz na prowadzeniu korespondencji z czasopismem..

Anna Zdziennicka

Prof. dr hab. Bronisław Jańczuk
Katedra Zjawisk Międzyfazowych
Instytut Nauk Chemicznych
Wydział Chemii UMCS
Pl. M. Curie-Skłodowskiej 3
20-031 Lublin

Lublin, 17.01.2023

OŚWIADCZENIE

Oświadczam, że w pracy

E. Rekiel, A. Zdziennicka*, **B. Jańczuk**, *Mutual influence of ethanol and surfactin on their wetting and adhesion properties*, Colloids and Surfaces A: Physicochemical and Engineering Aspects, 2021, 627, 127161;

mój udział wynosił **10%** i polegał na opracowaniu koncepcji artykułu, analizie formalnej otrzymanych wyników, redagowaniu i edycji manuskryptu oraz współredagowaniu odpowiedzi na recenzje pracy.

Załącznik 6

[D6] E. Rekiel, A. Zdziennicka*, B. Jańczuk, *Effect of ethanol on wetting and adhesion properties of rhamnolipid*. **International Journal of Adhesion and Adhesives**, 2021, 110, 102955.

Effect of ethanol on wetting and adhesion properties of rhamnolipid

Edyta Rekiel, Anna Zdziennicka [*], Bronisław Jańczuk

Department of Interfacial Phenomena, Institute of Chemical Sciences, Faculty of Chemistry, Maria Curie-Skłodowska University in Lublin, Maria Curie-Skłodowska Sq. 3, 20-031, Lublin, Poland

ARTICLE INFO

ABSTRACT

The wetting and adhesion properties of the surfactants and biosurfactants play a very important role in the processes occurring in practice. These properties can be changed by the addition to the aqueous solution of the surfactants and biosurfactants different kinds of the substances influencing the structure of water and the hydration of the head and tail of the surfactants molecules. Therefore, we studied effect of the ethanol on the wetting and adhesion properties of rhamnolipid by the measurements of the contact angle of the aqueous solution of rhamnolipid in the presence of ethanol on the polytetrafluoroethylene (PTFE), polymethyl methacrylate (PMMA) and quartz surface. The obtained results of the contact angle were analyzed in the light of the surface tension components of the solids, water, ethanol as well as the head and tail of the rhamnolipid surface tension. Based on these analyses the adsorption of the ethanol and rhamnolipid at the solid-solution, the dependence between adhesion and surface tension, the dependence between the adhesion work of the solution to the solid surfaces and solution surface tension as well as the critical surface tension of solid wetting were considered. The critical surface tension was compared to the surface tension of the solid. From above mentioned consideration, it appeared, among other things, that on the basis of the PTFE-aqueous solution of ethanol (ET) and PTFE-aqueous solution of rhamnolipid (RL) interface tension, it is possible to predict the contribution of ET and RL adsorption at the PTFE-solution of RL and ET mixture. It also appeared that it is possible to determine the Gibbs standard free energy of ET and RL adsorption at the solid-air and solid-solution interfaces, by using the Gibbs excess concentration of ET and RL at these interfaces determined on the basis of contact angle in Langmuir equation modified by de Boer.

1. Introduction

Rhamnolipid has a wide practical application [1–3]. It is used, among others, to protect surgical instruments and implants. These rhamnolipid applications are based on the fact that it can form films on solid bodies it prevents the adhesion of bacteria to the solid surface [4]. The formation of the surfactant layer at the solid-solution interface depends on the components and parameters of the solid surface tension as well as on the contribution of the head and tail to the surfactants surface tension which depends on the orientation of their molecules towards the interface [5–8]. This layer formation can be modified, among others, by the addition of short chain alcohols to the aqueous solution of the surfactants. The alcohol affects the adsorption, aggregation, and adhesion properties of the surfactants [5–12].

In the literature it is possible to find many papers describing the effect of short chain alcohols including ethanol, on the surfactants properties [6,9–17]. Among others, some investigators suggest that at

their low concentration, the adsorption of the surfactants at the solution-air interface increases while at the high concentration it decreases in comparison to the solution without alcohols [6]. Many authors suggest [6,18,19] that short chain alcohols in the aqueous solutions at a given concentration form small aggregates. This concentration is called the critical concentration of alcohol aggregation (CAC) [6,19–21]. At the alcohols concentration higher than CAC, the adsorption of the surfactants at the solution-air interface is very small or does not occur at all [6]. According to many authors' opinion the surfactants critical micelle concentration (CMC) can decrease in the low concentration range of alcohols and increase at a high concentration [6,12]. At the concentration of alcohol higher than CAC, it is difficult to detect the surfactant micelles [6]. Such behaviour of the surfactants at the solution-air interface and in the bulk phase affected by the short chain alcohols results from the fact that alcohols change the water structure, hydration degree of the head and tail of the surfactant molecules as well as reduce the dielectric constant of the solution [6,22–24].

The influence of the short chain alcohols on the surfactants layer formation at the solid-solution interface is more complicated compared to the influence on individual surfactants adsorption at the solution-air interface and their aggregation.

It is possible to find the papers describing the effect of short chain alcohols on the adsorption at the solid-solution interface of some classical surfactants. According to these authors the formation of the layer of surfactants at the solid-solution interface depends not only on the type of alcohols and surfactants as well as alcohol concentration in contrast to their adsorption and aggregation but also on the values of the components and parameters of the surface tension of a given solid [6]. The effect of the short chain alcohols on the adsorption of surfactants at the solid-solution interface is different in the case of apolar solids in comparison to the mono- and bipolar ones. Adsorption on the monopolar solids is different from that on the bipolar ones. In the literature it is difficult to find papers discussing the influence of short chain alcohols on the biosurfactant layer formation at the solid-solution interface for the solids of great practical importance. Such solids, among others, include polytetrafluoroethylene (PTFE), polymethyl methacrylate (PMMA) and quartz. Among of them PTFE is apolar, PMMA monopolar and quartz bipolar.

The aim of our studies was to determine the influence of ethanol (ET) on the wetting and adhesion properties of the rhamnolipid by the measurements of contact angle of the aqueous solutions of rhamnolipid in the presence of ethanol on the PTFE, PMMA and quartz surface and the thermodynamic analysis of obtained results.

2. Experimental

2.1. Materials

R-95 Rhamnolipid (95%) was purchased from Sigma-Aldrich and used without further purification. Ethanol (96% pure) from POCH (Poland) was purified by the method described earlier [25]. For the preparation of the solution of RL and ET mixture, deionized water with the specific resistance of 18.2×10^6 and the surface tension at 293 K equal to 72.8 mN/m was used. For the measurements the series of aqueous solutions of RL with ethanol were prepared at the constant rhamnolipid concentrations equal to 0; 0.0002; 0.0005; 0.00125; 0003; 0.00625; 0.01; 0.02; 0.05; 0.1; 0.5; 1; 5; 10; 20; 30 and 40 mg/dm^{3}and changing the ethanol concentration from 0 to 17.13 mol/dm^3. The ET concentration was as follows: 0; 0.06692; 0.1338; 0.2677; 0.4015; 0.535; 1.0706; 1.6062; 2.1416; 2.677; 3.2124; 3.7478; 4.2832; 4.8185; 5.3538; 5.8893; 6.6925; 7.7245; 8.5664; 10.2797; 11.968; 12.145; 13.3794; 14.5696; 15.4064; 16.084; 16.3777; 16.648; 16.8988 and 17.13 M. These concentrations of ET were also used as the constant ones in the solution in which the concentration of RL was changed from 0 to 40 mg/dm^3. The plates of polytetrafluoroethylene (PTFE) (50 mm × 30 mm) and polymethyl methacrylate (PMMA) (50 mm × 30 mm) were cut from the planes obtained from Mega-Tech (Poland). The quartz plates (50 mm × 50 mm) were obtained from Conductance (Poland). Before measurements the PTFE plates were polished with a light pressure on a Buchler polishing wheel using a silk polishing cloth. PTFE as well as PMMA and quartz plates were washed with a gentle detergent and next with methanol, placed twice in an ultrasonic bath in the Milli-Q water for 15 min and then dried in the desiccator with a molecular sieve at room temperature. The quality of each plate surface was monitored by applying a polarizing microscope (Nikon, ECLIPSEE600POL). The plates with the best quality surfaces were additionally tested by measurements of the contact angle for water. If the contact angle for water on the PTFE surface was in the range from 111 to 112° and for PMMA from 74 to 75°, then such plates were taken into account for measurements of solution contact angle. In the case of quartz it was more complicated to choose the proper plates. As it is known there are three main types of the quartz surface in terms of its hydrophilic-hydrophobic properties. So, the quartz plates for each contact angle for water close to 56° were chosen

for the studies.

2.2. Methods

Measurements of the advancing contact angles for the aqueous solution of RL and ET mixture on the PTFE, PMMA and quartz surfaces (θ) were made using the sessile drop method using DSA30 measuring system (Krüss) in the thermostated chamber at 293 ± 0.1K. The chamber before the contact angle measurements was saturated with the solution at a given concentration by placing the cell filled with this solution. The volume of the drop used for contact angle measurements was deduced from the previous consideration dealing with the relationship between the interface pressure between liquid and gas phase and diameter of the drop [26]. From this consideration, it results that the volume of the solution drop equal to 6 μl is the most proper for the contact angle measurements for the solution of RL and ET mixture if its surface tension changed from 72.8 to 52.8 mN/m. However, below this surface tension the drop in the volume equal to 4 μl was better for the measurements of contact angle. For each concentration of the aqueous solution of RL and ET mixture the contact angle on the PTFE, PMMA and quartz surface was measured from right and left sides for 30 independent drops. If the difference between the contact angle measured from the left and right sides was different from than 2°, then the contact angle was measured for the additional drop. For each solid six plates were used and on each of them five or more drops were placed. Each drop of solution on the PTFE, PMMA and quartz surface was settled at the minimum distance possible from the surface. The contact angle was measured immediately after the drop was settled on the solid surface and then for 10 min at minute intervals. This procedure was used only for two droplets for each system to find the time interval in which the value of the angle was constant. It turned out that for the diluted solutions the time required to achieve a constant value of the contact angle was shorter than for the concentrated solutions. However, an equilibrium contact angle was established over a time interval of 0 to 3 min, and this angle was taken into account.

The contact angle for the solution was measured as a function of ET concentration at the constant RL one and vice versa. Hence the contact angle on each solid would be measured for 47 solutions of varying concentration. The standard deviation was calculated for each of 47 solutions. In this way the calculated value of the standard deviation depending on the concentration of solution was in the range from 1 to 2°. The more detail dealing with the conditions and procedure of the contact angle measurements were described in the previous papers [7]. On the basis of the obtained contact angle values of the aqueous solution of RL and ET mixture on the PTFE surface and its surface tension measured by us earlier [27] the relationships between the adhesion and surface tension as well as between the cosine of the contact angle and the surface tension were determined. These relationships were discussed with regard to the RL and ET adsorption at the PTFE-solution and solution-air interfaces and wetting properties of RL and ET mixture. Based on the value of the PTFE surface tension determined earlier [28], and the data mentioned above as well as the Young equation [29] the PTFE-solution interface tension and film pressure of RL and ET were determined. Taking into account the PTFE-solution interface tension the Gibbs surface excess concentration of ET and RL was determined applying the Gibbs isotherm equation [12,29]. In turn basing on the film pressure of RL and ET at this interface their total concentration was calculated from the Frumkin equation [6,12]. The obtained results from calculations were compared to those at the solution-air interface taken from the literature [6,27,30]. For better explanation of the adsorption behaviour of RL and ET at the PTFE-solution interface, the parameter of intermolecular interactions across the PTFE-solution interface using the Young and Girifalco and Good equations [29,31] as well as the standard Gibbs free energy of RL and ET adsorption from the Langmuir equation modified by de Boer [32] was calculated.

Similarly to the PTFE-solution-air system, the contact angle values

obtained in the PMMA-solution-air and quartz-solution-air systems were applied for determination of the relationship between the adhesion and surface tension, the cosine of contact angle and surface tension, PMMA-solution, quartz-solution interface tensions, the pressure of the ET and RL film at these interfaces, the parameter of interactions and the Gibbs surface excess concentration. The parameter of intermolecular interactions across the PMMA-solution and quartz-solution interfaces was determined in a different way from that for the PTFE-solution interface. For the calculation of this parameter the van Oss et al. [33] as well as the Girifalco and Good [31] equations were used. Additionally, for the PMMA-solution-air and the quartz-solution-air systems the pressure of the mixed RL and ET film at the PMMA-air and the quartz-air interfaces was determined by using the Neumann et al. equation [34–36]. Next using the film pressure at the PMMA-air and the quartz-air interfaces in the Young equation the pressure of the ET and RL mixed film at the PMMA-solution and the quartz-solution interfaces was calculated. Knowing the mixed film pressure at these interfaces the contribution of ET and RL to this pressure was found by application of the equation proposed by us. For all studied solids, the adhesion work of the aqueous solution to their surface was considered. The measured contact angle values are presented in the paper but all data determined based on these values are presented in SM. It should be noted that not all calculated values of different physicochemical magnitudes are presented in SM. Due to the large amount of data, we present only those corresponding to the specific properties of ET and RL. For the solutions of ET and RL mixture for which the ET concentration was changing all physicochemical magnitudes were presented at the constant RL concentration corresponding to that at which its unsaturated monolayer at the solution-air interface was formed and to the value at which the saturated monolayer begins to form as well as at the RL concentration close to its CMC [30] in absence of ET. In the case of the solutions of ET and RL mixture for which the RL concentration was changing all physicochemical properties were presented at the ET constant concentration corresponding to the value at which its unsaturated monolayer at the solution-air interface is formed and to the value at which the maximum on the isotherm of the Gibbs excess concentration of ET occurs as well as to that close to ET CAC [6,19] in absence of RL. Unfortunately, for not all studied solutions it was possible to calculate the data mentioned above.

3. Results and discussion

3.1. Contact angle

According to the Young equation [29]:

$$\gamma_{SV} - \gamma_{SL} = \gamma_{LV} cos\theta \tag{1}$$

the contact angle (θ) of the liquid or solution on the solid surface depends on the liquid (solution) (γ_{LV}) and solid (γ_{SV}) surface tension as well as the solid-liquid (solution) (γ_{SL}) interface tension. In the case of aqueous solution of surfactants and/or biosurfactants, the surface tension decreases as a function of their concentration (C) in the range from 0 to CMC [6,30]. After the CMC, the changes of γ_{LV} are small. The solid surface tension can be constant or decreases as a function of C. This depends on the properties of the layer formed by the surface active agents around the drop settled on the solid surface [6]. The changes of γ_{SL} as a function of C are more complicated than γ_{LV} and γ_{SV}. In the case of hydrophobic solids, the head of the surfactant molecules in the monolayer at the solid-solution interface are rather oriented towards the solution bulk phase while their tails are oriented parallel, at an angle or perpendicular to the interface. As the result of such surfactant molecules orientation in the monolayer, γ_{SL} decreases as a function of C. If the surfactant molecules in monolayer are oriented by head towards the solid surface, depending on the tail orientation (parallel or perpendicular) γ_{SL} can be constant or increases as a function of C. However, if at a given surfactant concentration the surfactant bilayer is formed, γ_{SL}

decreases [6,12]. For the mixtures of surfactants or biosurfactants with short chain alcohols, the changes of γ_{LV}, γ_{SV} and γ_{SL} as a function of their composition and concentration are more complicated than for individual surfactants.

It appeared that at the constant RL concentration, corresponding to the saturated monolayer at the solution-air interface in the absence of ET [30], the maxima on the isotherms showing the γ_{LV} changes as a function of ET concentration are observed. Probably for this reason the maxima on the curves presenting the changes of θ on PTFE as a function of ET concentration at the constant RL concentration corresponding to the saturated monolayer at the solution-air interface without ET were observed (Fig. 1a).

PTFE, being an apolar hydrophobic solid, has the surface tension resulting only from the Lifshitz-van der Waals intermolecular interactions. Its surface tension is determined from the contact angle for n-alkanes being equal to 20.24 mN/m [37] (Table 1).

The surface tensions of water, ethanol, as well as the head and the tail of rhamnolipid are higher than the surface tension of PTFE [28] (Table 1). Many authors suggest [33,38–40] that if the surface tension of a given substrate is higher than that of hydrophobic solid (PTFE) such substrate does not decrease the solid surface tension. Therefore, it can be assumed that the PTFE surface tension is constant independently of ET and RL concentration and the changes of contact angle depend only on those of solution-air and PTFE-solution interface tensions. In such a case, it is possible to determine the PTFE-solution interface tension directly from Eq. (1) (Figs. S1a–S2).

The calculations from Eq. (1) showed that there are maxima (Figs. S1a and S1b) on the curves presenting the changes of the PTFE-solution interface tension as a function of the ET concentration at the constant RL concentration corresponding to the saturated monolayer at the solution-air interface in the absence of ET [30], similarly to the changes of solution surface tension [27]. In the case of the solution surface tension, the maxima were explained by contribution of the ET and RL adsorption to the reduction of the water surface tension [27]. This indicates that if ET is added to the RL aqueous solution at the concentration at which the saturated monolayer at the solution-air is formed, the alcohol molecules remove part of RL molecules from the monolayer and the surface tension increases in comparison to that of single RL solution [30]. The isotherms of the PTFE-solution interface tension at the constant ET concentration are different from those at the constant RL concentration (Fig. S2). There are some small maxima on these isotherms at the ET concentration close to its CAC [19]. However, the PTFE-solution interface tension is practically constant up to CAC. In this case, only alcohol adsorption at the PTFE-solution interface decides about its value. As follows from this fact the maxima on the contact angle isotherm occurred due to RL molecules removal from the monolayer at the solution-air and PTFE-solution interfaces by ET molecules. In the other words the contribution of RL and ET adsorption to the reduction of the water-air and PTFE-water surface tensions decides about the contact angle changes as a function of composition and concentration of the ET and RL mixture.

The reduction of the PTFE-water interface tension (γ_{SW}) by the ET and RL mixed layer can be expressed by the equation [6,27]:

$$\gamma_{SL} = \gamma_{SW} - X_{RL}\pi_{RL} - X_{ET}\pi_{ET} \tag{2}$$

where X_{RL} and X_{ET} are the RL and ET fractions in the mixed layer at the PTFE-solution interface and π_{RL} and π_{ET} is the monolayer pressure of RL without ET and vice versa.

Introducing Eq. (2) to Eq. (1) we obtain:

$$cos\theta = \frac{\gamma_{SV} - \gamma_{SW} + X_{RL}\pi_{RL} + X_{ET}\pi_{ET}}{\gamma_{LV}} \tag{3}$$

From the calculations based on Eq. (3) it results that ET strongly decreases adsorption of RL in the concentration range in which (in the absence of alcohol) the saturated monolayer is formed at the solution-air
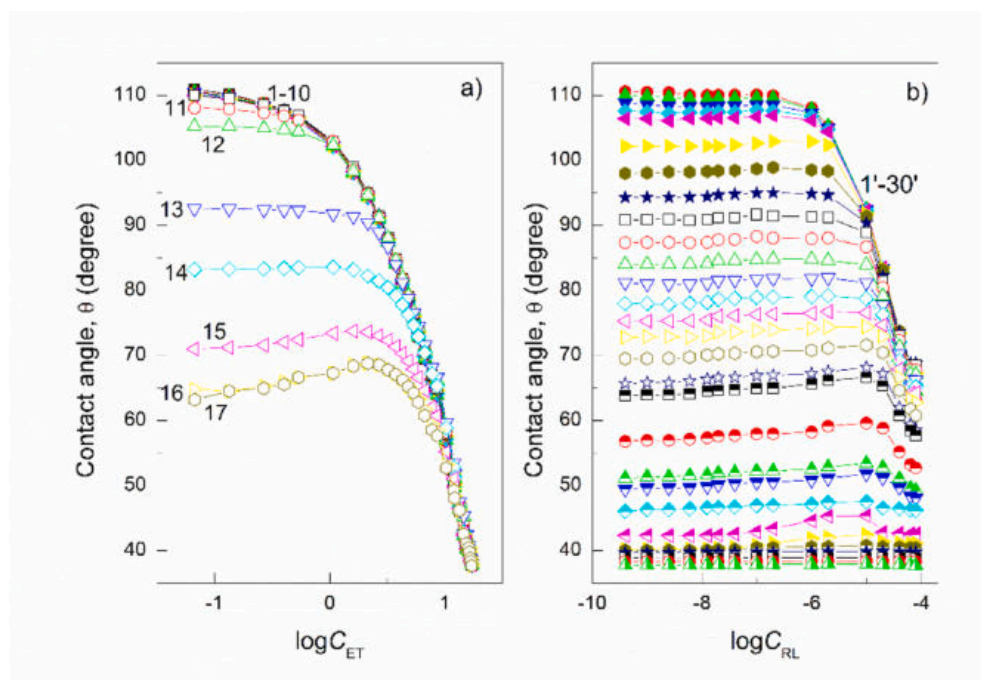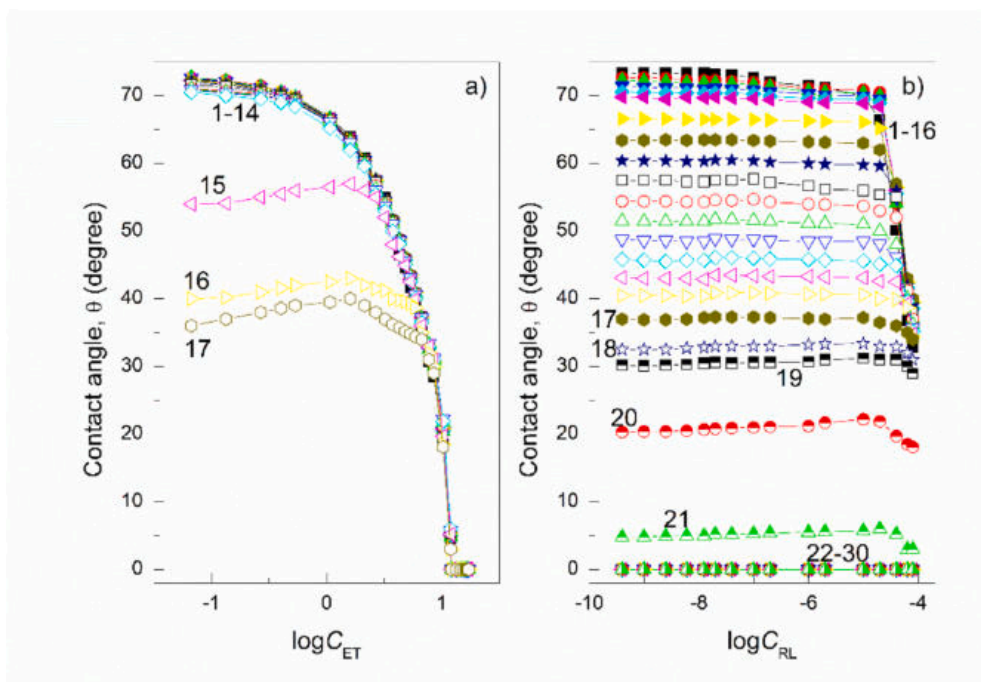
Fig. 1. A plot of contact angle (θ) of the water/ethanol solution of RL vs. the logarithm of ethanol ($\log C_{ET}$) (a) or RL concentration ($\log C_{RL}$) (b) for PTFE. Curves 1–17 correspond to the constant RL concentration equal to 0; 0.0002; 0.0005; 0.00125; 0003; 0.00625; 0.01; 0.02; 0.05; 0.1; 0.5; 1; 5; 10; 20; 30 and 40 mg/dm³. Curves 1′ – 30′ correspond to the constant ET concentration equal to 0; 0.06692; 0.1338; 0.2677; 0.4015; 0.535; 1.0706; 1.6062; 2.1416; 2.677; 3.2124; 3.7478; 4.2832; 4.8185; 5.3538; 5.8893; 6.6925; 7.7245; 8.5664; 10.2797; 11.968; 12.145; 13.3794; 14.5696; 15.4064; 16.084; 16.3777; 16.648; 16.8988 and 17.13 M.
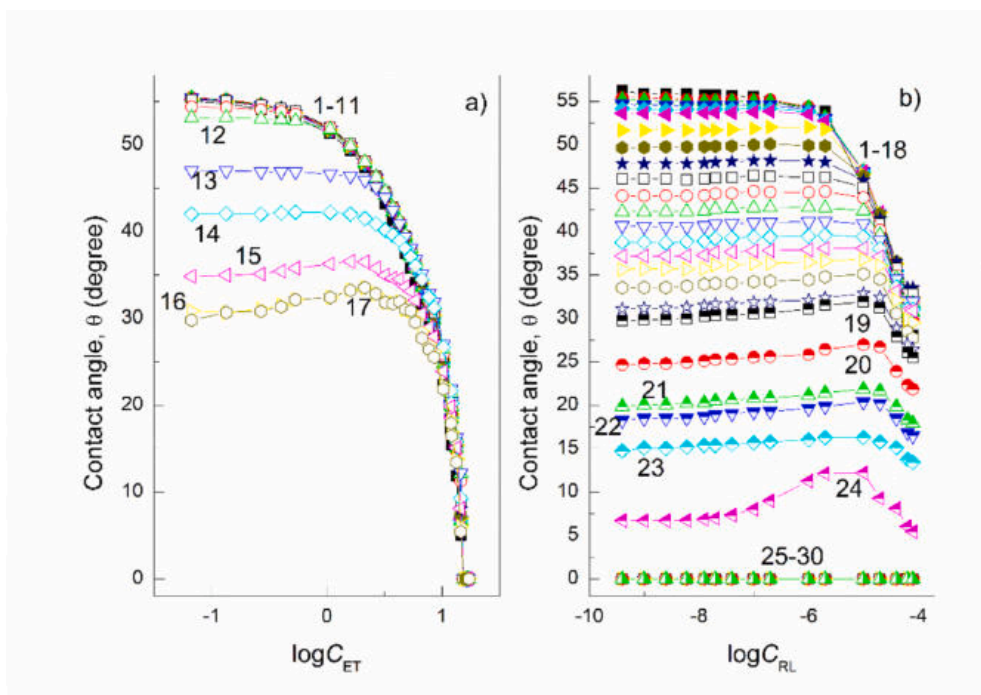
Table 1

The Lifshitz-van der Waals (γ^{LW}) and acid-base (γ^{AB}) components as well as the electron-acceptor (γ^+) and the electron-donor (γ^-) parameters of the water, ethanol, PTFE, PMMA and quartz surface tension (γ) as well the RL head and tail surface tension.

Substrate	Components and parameters				γ [mN/m]	Ref.
	γ^{LW} [mN/m]	γ^{AB} [mN/m]	γ^+ [mN/m]	γ^- [mN/m]		
PTFE	20.24	0.00	0.00	0.00	20.24	6
PMMA	41.28	0.00	0.00	7.28	41.28	6
Quartz	38.07	9,63	1.61	14.36	47.70	7
Water	26.85	45.95	22.975	22.975	72.80	7
Ethanol	21.40	1.80	0.09	9.00	23.20	6
RL head	35.38	3.01	0.04	56.74	38.39	7
tail	21.80	0.00	0.00	0.00	21.80	

and PTFE-solution interfaces (Figs. S3a and S3b) [6,30]. The replacement of RL molecules in the saturated monolayer at the solution-air and PTFE-solution interfaces by ET molecules causes the increase of solution-air and PTFE-solution interface tensions in comparison to the tensions at the same concentration of RL in the absence of ET in the solution. Due to the increase of γ_{LV} and γ_{SL} the increase of the contact angle of the aqueous solution of the ET and RL mixture up to a certain maximum at a given concentration of ET at the constant concentration of RL (Figs. S3a and S3b) takes place. In the other words, the changes of the contact angle as a function of the concentration and composition of the aqueous solution of ET and RL mixture depend on the contribution of the ET and RL adsorption to the reduction of the water-air and PTFE-water interface tensions. This ET contribution to the reduction of PTFE-water interface tension at the RL concentration, corresponding to the saturated monolayer at the solution-air and PTFE-solution interfaces in the absence of ET, is higher than it results from the independent adsorption of ET and RL. At the concentration of ET higher than its CAC [6,19], the RL contribution to the reduction of water-air and PTFE-water interface tensions is small and close to zero in the "pure" alcohol (Figs. S3a and S3b).

The considerations of the changes in the contact angle of the aqueous solutions of ET and RL mixture on the PMMA and quartz surfaces on the basis of the interfaces tension are more difficult than in the case of PTFE. The PMMA-air [7,37] and quartz-air [7,41] interface tensions are lower than that of water-air [30] but higher than ET-air [19], RL head-air as well as RL tail-air ones (Table 1) [41]. Thus, adsorption of the water vapour does not decrease the PMMA and quartz surface tensions but ET adsorption does. The pressure of RL vapour is practically equal to zero at 293 K and though its surface tension is lower than that of PMMA and quartz, it does not decrease by evaporation. On the other hand, the penetration of RL molecules from the drop settled on PMMA or quartz surfaces around the drop is not excluded. For this reason, it is difficult to explain the changes of the contact angle of the aqueous solution of ET and RL mixtures on the PMMA and quartz surfaces as a function of concentration and composition, based directly on Eq. (1). This results from the fact that the surface tension of these solids depends on the concentration of the ethanol and rhamnolipid mixtures. We can only conclude that the presence of maxima on the contact angle isotherms for PMMA and quartz (Figs. 2a–3b), similar to PTFE, depends on the competitive adsorption of ET and RL, not only at the solution-air, but also at the solid-solution interface.

However, the isotherms shape of the contact angle of solution on PMMA and quartz is somewhat different from that for PTFE. If the changes in the contact angles on these solids as a function of ET concentration at the constant RL concentration (Figs. 2a and 3a) are taken into account, it can be concluded that the maxima on the contact angle isotherms occur only at the RL concentration close to its CMC or higher than it [30]. In the case of the contact angle changes as a function of RL concentration, at the constant ET concentration, there is a plateau at the ET concentration lower than its CAC [19] (Figs. 2b and 3b). The difference in the shape of the contact angle isotherms between the apolar PTFE and monopolar PMMA and bipolar quartz results probably from the changes of not only γ_{LV} and γ_{SL} but also γ_{SV}.

In our earlier papers [6,42] it was suggested that the changes of γ_{SV} affected by the alcohol vapour and/or the migration of surfactant molecules from the settled solution drop on the solid to its surface around the drop can occur in two ways. One way is based on the Neumann et al. equation [34–36]. The other one consists in the difference between the water and solution surface tensions [42]. The Neumann et al. equation [34–36] can be expressed in the form:

Fig. 2. A plot of contact angle (θ) of the water/ethanol solution of RL vs. the logarithm of ethanol (logC_{ET}) (a) or RL concentration (logC_{RL}) (b) for PMMA. Curves 1–17 correspond to the constant RL concentration equal to 0; 0.0002; 0.0005; 0.00125; 0003; 0.00625; 0.01; 0.02; 0.05; 0.1; 0.5; 1; 5; 10; 20; 30 and 40 mg/dm³. Curves 1' – 30' correspond to the constant ET concentration equal to 0; 0.06692; 0.1338; 0.2677; 0.4015; 0.535; 1.0706; 1.6062; 2.1416; 2.677; 3.2124; 3.7478; 4.2832; 4.8185; 5.3538; 5.8893; 6.6925; 7.7245; 8.5664; 10.2797; 11.968; 12.145; 13.3794; 14.5696; 15.4064; 16.084; 16.3777; 16.648; 16.8988 and 17.13 M.

Fig. 3. A plot of contact angle (θ) of the water/ethanol solution of RL vs. the logarithm of ethanol (logC_{ET}) (a) or RL concentration (logC_{RL}) (b) for quartz. Curves 1–17 correspond to the constant RL concentration equal to 0; 0.0002; 0.0005; 0.00125; 0003; 0.00625; 0.01; 0.02; 0.05; 0.1; 0.5; 1; 5; 10; 20; 30 and 40 mg/dm³. Curves 1' – 30' correspond to the constant ET concentration equal to 0; 0.06692; 0.1338; 0.2677; 0.4015; 0.535; 1.0706; 1.6062; 2.1416; 2.677; 3.2124; 3.7478; 4.2832; 4.8185; 5.3538; 5.8893; 6.6925; 7.7245; 8.5664; 10.2797; 11.968; 12.145; 13.3794; 14.5696; 15.4064; 16.084; 16.3777; 16.648; 16.8988 and 17.13 M.

$$\frac{cos\theta + 1}{2} = \sqrt{\frac{\gamma_{SV}}{\gamma_{LV}}}exp\left[- \beta(\gamma_{LV} - \gamma_{SV})^2\right] \qquad (4)$$

where β is the constant which does not depend on the kind of solid and is assumed to be equal to 0.000115 (m²/mJ)².

As the surface tension of water is higher than that of PMMA and quartz, the adsorbed water molecules on their surface do not decrease their surface tension. Thus the values of PMMA and quartz surface tension calculated from Eq. (4) based on the water surface tension and contact angle can be treated as a real PMMA and quartz surface tension. However, the values γ_{SV} calculated form Eq. (4) using the contact angle

and surface tension of the solution of ET and RL mixture are different from those of the surface tension of PMMA and quartz and can be treated as a surface tension of these solids covered by the adsorption layer. In this way it is possible to establish the changes of the PMMA and quartz surface tension as a function of concentration and composition of ET and RL mixture. The difference between the γ_{SV} values of PMMA and quartz calculated from the contact angle and surface tension of the water as well as from the surface tension and contact angle of solution of the ET and RL mixture on these solids is equal to the film pressure.

On the other hand, the film pressure (π) around the drop settled on the mono- and bipolar solids, at the first approximation, can be obtained

from the simple equation [6,42]:

$$\pi = \frac{\gamma_W - \gamma_{LV}}{2} \tag{5}$$

The calculated values of γ_{SV} for PMMA and quartz indicate that indeed their surface tension depends on the composition and concentration of ET and RL mixture. Moreover, the π values calculated from (4) are close to those determined from Eq. (5), not only in the range of the RL concentration corresponding to the unsaturated monolayer at the solution-air interface and ET concentration lower than its CAC [19,30] (Figs. S4a - S4c and S5a – S5c as example). This suggests that not only the vapour of ET but also RL molecules can influence on the PMMA and quartz surface tensions as a result of their penetration from a solution drop settled on the PMMA or quartz surface.

3.2. Adhesion work and critical surface tension of solid wetting

The complete spreading of the liquid and solution over the given solid occurs if the adhesion work of liquid (solution) to the solid surface (W_a) is equal or higher than the cohesion work of liquid (solution) (W_c). If $W_a = W_c$ then $\frac{W_a}{2} = \gamma_c$, where γ_c was called the critical surface tension of solid wetting by Zisman [43].

The adhesion work of the liquid (solution) to the solid surface fulfills the equation [38]:

$$W_a = \gamma_{SV} + \gamma_{LV} - \gamma_{SL} \tag{6}$$

When the liquid (solution) drop on the solid surface does not spread completely over the solid surface, W_a can be expressed by the Young-Dupre equation [38]:

$$W_a = \gamma_{LV}(cos\theta + 1) \tag{7}$$

Girifalco and Good [31] proposed the equation expressing the dependence between W_a and surface tension of liquid and solid. It has the form [31]:

$$W_a = 2\varphi\sqrt{\gamma_{SV}\gamma_{LV}} \tag{8}$$

where φ is the parameter of the interfacial interactions.

In turn, van Oss et al. [33,40,44] proposed the dependence between the adhesion work of the liquids or solution to the solid surface as well as components and parameters of the liquid and solid surface tension, which has the form [33,40,44]:

$$W_a = 2\sqrt{\gamma_{SV}^{LW}\gamma_{LV}^{LW}} + 2\sqrt{\gamma_{SV}^{+}\gamma_{LV}^{-}} + 2\sqrt{\gamma_{SV}^{-}\gamma_{LV}^{+}} \tag{9}$$

where the indices LW, + and – refer to the Lifshitz-van der Waals component of solid and liquid surface tension, and to the electron-acceptor and electron-donor parameters of the acid-base component of the solid and liquid surface tensions, respectively.

For the hydrophobic solids whose surface tension results from only the Lifshitz-van der Waals intermolecular interactions Eq. (9) assumes the simpler form [33]:

$$W_a = 2\sqrt{\gamma_{SV}^{LW}\gamma_{LV}^{LW}} \tag{10}$$

The comparison of Eqs. (7) and (8) gives [33]:

$$\varphi = \frac{\gamma_{LV}(cos\theta + 1)}{2\sqrt{\gamma_{SV}\gamma_{LV}}} \tag{11}$$

It results from Eq. (11) that if φ is equal to 1 for the contact angle equal zero $\gamma_{SV} = \gamma_c$. Unfortunately, in the case of the PTFE-solution drop-air system, the parameter φ for each concentration and composition of the ET and RL mixture is lower than 1 (Figs. S6 and S7). It is interesting that in contrast to Neumann et al. [34–36], there is no linear dependence between the parameter φ and the PTFE-solution interface tension (Fig. S6). The linear dependence is found between φ and the logarithm of

the sum of PTFE-solution and solution-air interface tensions (Fig. S7).

To establish the relationship between the φ parameter for the PTFE-solution interface and the PTFE surface tension (γ_{SV}) and the critical surface tension of PTFE wetting (γ_c) as well as between γ_{SV}, and γ_{LV}, the values of γ_c were determined from the dependence between the adhesion and surface tensions as well as between the cosine of contact angle and surface tension (Figs. S8a–S9b). It appears that there is a linear dependence between the adhesion and surface tension but not in the whole range of ET concentration (Figs. S8a and S8b). However, the relation between the cosine of contact angle and the surface tension can be described by the exponential function of the first order (Figs. S9a and S9b). The values of γ_c calculated from the dependence between the adhesion and the surface tensions for the solutions at the constant ET or RL concentration are practically the same (22.76 and 22.7 mN/m) (Table 2). The values are higher than the PTFE surface tension (20.24 mN/m) [37]. However, the γ_c values calculated from the dependence between the cosine of contact angle and the surface tension (21.56 and 20.07 mN/m) (Table 2) are closer to the PTFE surface tension [37] than those determined from the dependence between the adhesion and surface tensions. By introducing these values into Eq. (11), the parameter φ was calculated. These values appear to be different from 1.

In the case of PTFE, Eq. (8) can be compared to Eq. (10) from which it results that:

$$\varphi = \sqrt{\frac{\gamma_{LV}^{LW}}{\gamma_{LV}}} \tag{12}$$

The values of φ calculated from Eq. (12) are the same as those obtained from Eq. (11). It results from Eq. (12) that the γ_c values determined from only the contact angle of the liquids whose surface tension originates from the Lifshitz-van der Waals intermolecular interactions can be equal to that of PTFE also resulting from these interactions. Thus, the question arises as to what is the significance of the value of the critical surface tension of PTFE determined by the above mentioned methods.

The linear dependence between the adhesion and the surface tensions for the aqueous solution of ET and RL mixture is described by the linear function but only in a range of ET concentrations. This function has the form (Figs. S8a and S8b):

$$\gamma_{LV}cos\theta = a\gamma_{LV} + b \tag{13}$$

For PTFE the constant a is close to -1. Then the constant b is equal to the adhesion work of the aqueous solution of ET and RL mixture to PTFE, and $\gamma_c = \frac{b}{2}$. This indicates that complete spreading of the solution over the PTFE surface can occur when in the whole concentration range of ET and RL the adhesion work of solution to PTFE is constant and Eq. (10) must be fulfilled. On the other hand, the Lifshitz-van der Waals component (LW) of the aqueous solution of ET and RL mixture, regardless of its composition and concentration, should be the same and close to the LW component of water surface tension. Unfortunately, the dependence between W_a and γ_{LV} shows that the adhesion work is

Table 2
The values of critical surface tension of PTFE, PMMA and quartz wetting (γ_C) calculated from the dependence between the adhesion and surface tension as well as between the cosine of contact angle and the surface tension of the aqueous solution of ethanol and rhamnolipid mixture.

γ_c [mN/m]					
PTFE		PMMA		Quartz	
$cos\theta = f(\gamma_{LV})$	$\gamma_{LV}cos\theta = f(\gamma_{LV})$	$cos\theta = (\gamma_{LV})$	$\gamma_{LV}cos\theta = f(\gamma_{LV})$	$cos\theta = (\gamma_{LV})$	$\gamma_{LV}cos\theta = f(\gamma_{LV})$
21.56[a]	22.76[a]	27.64[a]	27.95[a]	25.06[a]	24.73[a]
20.07[b]	22.70[b]	–	–	25.11[b]	25.39[b]

[a] - constant RL.
[b] - constant ET.

constant only in a range of ET concentrations (Figs. S10a and S10b). From this reason, the γ_c determined from the dependence between $\gamma_{LV}cos\theta$ and γ_{LV} has not practical significance. Therefore the γ_c values determined from the dependence between $cos\theta$ and γ_{LV} seems to be more reasonable.

The determination of the φ parameter for the PMMA-solution and quartz-solution interface in the same way as for the PTFE-solution interface is unreliable. For the systems including PMMA and quartz, the relation between the surface tension of PMMA and/or quartz and the critical surface tension of their wetting with regard to φ is more complicated than for PTFE.

As mentioned above, around the drop of the aqueous solution of ET and RL mixture settled on these solids the vapour film of ET can be formed decreasing their surface tension. Thus the values of W_a calculated from Eq. (7) should be different from those obtained based on Eq. (8). Eq. (8) was proposed by Girifalco and Good [31] for the systems in which the film around the liquid drop settled on the solid surface is not formed. On the other hand, Eq. (9) was derived by van Oss et al. [33,40, 44] based on the Girifalco and Good equation [31]. Thus, taking into account Eqs. (8) and (9) the expression for calculating φ parameter can be obtained:

$$\varphi = \frac{\sqrt{\gamma_{SV}^{LW}\gamma_{LV}^{LW}} + \sqrt{\gamma_{SV}^{+}\gamma_{LV}^{-}} + \sqrt{\gamma_{SV}^{-}\gamma_{LV}^{+}}}{\sqrt{\gamma_{SV}\gamma_{LV}}} \quad (14)$$

Knowing the components and parameters of the PMMA and quartz surface tension, it is possible to determine φ from Eq. (14) (Fig. S11a – S14b). It seems that this parameter has quite reasonable values. Similar to PTFE, there is not a linear dependence between φ and PMMA (quartz)-solution surface tension (Figs. S11a and S11b). However, there is a linear dependence between this parameter and the logarithm from the sum of surface tension of solution and PMMA-solution interface tension (Figs. S12a and S12b) in the whole range of solution concentrations and compositions. However, in the case of quartz the linear dependence between the φ parameter and the logarithm from the sum of quartz-solution and solution-air interface tensions takes place only in a range of ET and RL concentration (Figs. S14a and S14b). In contrast to PTFE, the φ parameter is close to 1 in the range of ethanol concentration up to CAC [19]. Taken into account the φ values it was possible to determine the PMMA(quartz)-solution interface tension as well as that of PMMA and quartz covered by the adsorption layer. For calculation of γ_{SL} there was used the following equation [31]:

$$\gamma_{SL} = \gamma_{SV} + \gamma_{LV} - 2\varphi\sqrt{\gamma_{SV}\gamma_{LV}} \quad (15)$$

Introducing the γ_{SL} values calculated from Eq. (15) to Eq. (1), the surface tension of PMMA and quartz covered by the adsorption layer was determined. It appears that the values of PMMA and quartz surface tension determined in such a way are close to those calculated from the Neumann et al. equation [34–36] in many cases. Moreover, the pressure of the adsorption layer on the solids calculated on the basis of the Neumann et al. equation [34–36] is close to the difference in the values of the adhesion work calculated from Eqs. (7) and (8) (Figs. S4a–S5c) in the range of ET concentrations from 0 to CAC [19] and with the RL concentration corresponding to the unsaturated monolayer at the solution-air interface in the absence of ET [30].

It is interesting that there is a linear dependence between the adhesion work of the solution to the surface and the surface tension of the solution for PMMA and quartz (Figs. S15 and S16). For both solids, the adhesion work cannot be determined from the dependence between the adhesion and surface tensions. However, it is linear and the critical surface tension of wetting of PMMA and quartz (Fig. S17a) determined from this dependence is close to that determined from the dependence between the cosine of contact angle and the surface tension (Table 2) (Figs. S18a–S19b). The values of γ_c correspond to the φ parameter being close to 1. However, the γ_c values are considerably lower than those of the surface tension of PMMA and quartz without the adsorption layer

[37,41] but close to the surface tension calculated on the basis of the φ parameter. It should be mentioned that for the aqueous solution of ET and RL mixture at the high constant concentration it was impossible to establish the real changes of the adhesion work, adhesion tension, and cosine of contact angle against the ET concentration. In the case of PMMA for the solution of ET and RL mixture it is impossible to describe the above mentioned dependences by one function in the whole range of ET constant concentrations.

3.3. Adsorption of ethanol and rhamnolipid at the solid-solution interface

The mechanism of ET and RL adsorption at the solid-solution interface is more complicated than that at the solution-air one. It depends largely on the kind of the solid. The adsorption of ET and RL at the PTFE (PMMA, quartz)-solution interface, among others, depends on the difference between the adhesion work of a given component of the solution and its cohesion work (Table 3). Thus, the possibility of ET and RL adsorption at the PTFE-solution interface is similar in the case of diluted solutions. For the ET and RL tails there is a small difference between W_a and W_c. Indirectly, the magnitude of the ET and RL adsorption at the PTFE-solution interface can be estimated from the Lucassen-Reynders equation [45]. According to this equation, if the linear dependence between the adhesion and surface tension of the solution has a slope equal to −1, the adsorption of the surface active agent at the solid-solution is similar to that at the solution-air interface. Such dependence is fulfilled for the aqueous solution of the ET and RL mixture for both the constant ET and RL concentration (Figs. S8a and S8b). However, if the ET concentration changes and the RL concentration is constant, it is impossible to describe the dependence between the adhesion and surface tension by one linear function (Fig. S8a). Therefore, the adsorption of ET and RL at the PTFE-solution interface probably is not the same as at that at the solution-air one.

Because the PTFE surface tension can be assumed to be constant independently of the composition and concentration of the solution, it is possible to calculate the Gibbs surface excess concentration of ET and RL (Γ_{SL}) at the PTFE-solution interface directly from the Gibbs isotherm equation based on the adhesion tension. For such a case, the Gibbs isotherm equation can be written in the form [6]:

$$\Gamma_{SL} = -\frac{a}{nRT}\frac{\partial(-\gamma_{LV}cos\theta)}{\partial a} \quad (16)$$

where a is the activity of surface active agent, R is the gas constant and T is the temperature. The constant n is equal to 2 for RL and 1 for ET.

It appears that Γ_{SL} isotherm for RL (Fig. S20) is the same as the Gibbs surface excess concentration isotherm at the solution-air interface (Γ_{LV}) (Figs. S21a–S21c). However, it was possible to determine Γ_{SL} for RL only at the constant ET concentration lower than its CAC (Fig. S20). As mentioned above, the contact angle values of the solution at the ET concentration higher than CAC are similar to those without RL. Unfortunately, it was possible to determine the Γ_{SL} values for ET at the constant RL concentration only in the range corresponding to the unsaturated monolayer of RL at the solution-air interface in the absence of ET (Fig. S22) [30]. It appears that the Γ_{SL} isotherms are different from those of Γ_{LV} (Figs. S23a–S23c) [27]. The difference between Γ_{SL} and Γ_{LV}

Table 3

The values of the water, ethanol and rhamnolipid adhesion work to the PTFE, PMMA and quartz surface (W_a) as well as their cohesion work (W_c).

Substrate	W_a [mJ/m^2]			W_c [mJ/m^2]
	PTFE	PMMA	Quartz	
Water	46.62	92.45	112.43	145.60
Ethanol	43.34	61.06	66.97	46.40
RL head tail	53.52	77.51	94.03	76.78
	42.01	60.00	57.62	43.60

increases as a function of RL concentration. It can indicate that the adsorption of ET at the PTFE-solution interface is different from that at the solution-air one. On the other hand, in the case of ET, the values of Γ_{SL} are close to the total concentration of ET at the PTFE-solution interface only a low concentration, in contrast to RL.

To find out whether there are differences in the adsorption of ET and/or RL at the PTFE-solution interface in comparison to that at the solution-air one in contrast to the results obtained on the basis of the linear relationship between the adhesion and surface tension, the adsorption of ET and RL was determined based on the Frumkin isotherm. This isotherm of surface active agents at the solid-solution interface can be expressed in the form [6,12]:

$$\gamma_{SL(0)} - \gamma_{SL} = -RT\Gamma_{SL}^{max} ln\left(1 + \frac{\Gamma_{SL}^{Tot}}{\Gamma_{SL}^{max}}\right) \tag{17}$$

where $\gamma_{SL(0)}$ is the solid-water and/or solid-solution interface tension in the absence of the component whose adsorption is calculated, Γ_{SL}^{max} is the maximal amount of a given adsorbed component and Γ_{SL}^{Tot} is the amount of a given adsorbed component of the solution.

It appears that in contrast to the Gibbs surface excess concentration of ET isotherm there is no difference between the Frumkin isotherm of ET adsorption at the PTFE-solution interface (Figs. S24, S25a - S25c) and its adsorption at the solution-air interface at the constant RL concentration corresponding to the unsaturated monolayer of RL at the solution-air interface in the absence of ET [30] (Figs. S25a and S25b). At the RL concentration corresponding to the saturated monolayer in the absence of ET at this interface, the adsorption of ET at its concentration higher than CAC [19] is lower at the PTFE-solution interface than that at the solution-air one (Fig. S25c) [27]. In the case of RL adsorption at the constant ET concentration, it was possible to establish the amount of this adsorption only in the range of ET concentration lower than its CAC (Fig. S26). The adsorption of RL at the PTFE-solution interface in this range of alcohol concentration is higher than at the solution-air one (Figs. S27a–S27c). This is not consistent with the conclusion drawn from the Lucassen-Reynders equation [45]. Based on the isotherm of ET and RL adsorption determined in a different way, it can be stated that the adsorption of RL at the PTFE-solution interface at the ET concentration lower than its CAC [19] is higher than expected, due to its adsorption at this interface without ET. As it was stated earlier [41] there are strong hydrophobic interactions between the RL molecules and the PTFE surface through the water phase. It is possible that at the low concentration of alcohol its molecules remove the water molecules surrounding the head of the RL molecules but still do not have a significant effect on tail hydration. In such a case, the hydrophilic properties of RL head decrease and the hydrophobic interactions of RL molecules with PTFE through the water phase increase. The increase of ET concentration caused not only the decrease of hydrophobic properties of RL tail but also that of the solution dielectric constant [6,22–24] and, in consequence, the decrease of RL adsorption at the PTFE-solution interface. This is confirmed by the contribution fraction of ET to the reduction of the PTFE-water interface tension close to 1 (Figs. S3a and S3b). Moreover, the contribution of RL approaches zero simultaneously.

In the case of the PMMA, there is not a linear dependence between the adhesion and the surface tension at the constant ET concentration. Thus, it is impossible to compare the RL adsorption at the PMMA-solution interface to that at the solution-air one. On the other hand, the dependence between $\gamma_{LV}cos\theta$ and γ_{LV} at the constant RL concentration is linear but its slope is higher than -1 (-0.168). This indicates that the ET adsorption at the PMMA-solution interface is lower than at the solution-air one and the adsorption of ET on the PMMA surface around the solution drop settled on this surface cannot be excluded. As mentioned above, the surface tension of ET is lower than that of PMMA (Table 1) and the vapour of ET can decrease the PMMA surface tension. Therefore, the surface tension of PMMA changes as a function of ET concentration. In such a case, for the calculation of ET adsorption at the

PMMA-solution interface Eq. (6) cannot be applied, but only the following one [6]:

$$\Gamma_{SL} = -\frac{1}{nRT}\frac{\partial\gamma_{SL}}{\partial a} \tag{18}$$

To establish the γ_{SL} values, $\gamma_{SV} - \pi$ should be known (π is the ET film pressure). The values of π were determined from the difference between the adhesion work of the solution to the PMMA surface calculated from Eqs. (7) and (8). Next, γ_{SL} values were calculated from the following equation [6,29]:

$$\gamma_{SL} = \gamma_{SV} - \pi - \gamma_{LV}cos\theta \tag{19}$$

It proves that in the range of the RL constant concentration lower than its CMC [30] in the absence of ET, the dependence between γ_{SL} and a can be described by the exponential function of the first or second order. Unfortunately, in the range of RL concentration close and/or higher than its CMC, it was impossible to describe this dependence by a mathematical function. Therefore, it was impossible to determine the Gibbs surface excess concentration of ET at the PMMA-solution interface in the whole range of RL concentration. The calculated values of Γ_{SL} (Fig. S28) are considerably lower than those of Γ_{LV} (Figs. S29a–S29c). This may result from the fact that the adhesion work of water to PMMA is considerably higher than that of ET (Table 3) and the hydrophobic interactions of ET through the water phase are a few times lower than RL. As mentioned above the ET can also adsorb at the PMMA-air interface. The Gibbs surface excess concentration can be determined from the Gibbs isotherm equation in the form of:

$$\Gamma_{SV} = -\frac{1}{nRT}\frac{\partial(\gamma_{SV} - \pi)}{\partial a} \tag{20}$$

The Γ_{SV} values calculated from Eq. (20) (Fig. S30) are lower than those of Γ_{SL} and Γ_{LV} (Figs. S28, S29a - S29c). It is interesting that $\frac{\Gamma_{SV} - \Gamma_{SL}}{\Gamma_{LV}}$ does not depend on the ET and RL concentration in the range of RL concentration lower than its CMC [30] in the absence of ET. The average value is equal to -0.16 being close to the slope of the dependence between $\gamma_{LV}cos\theta$ and γ_{LV} (-0.168). The RL adsorption at the PMMA-solution interface (Fig. S31) is also lower than that at the solution-air one (Figs. S32a–S32c). Similarly to ET, the adhesion work of RL is lower than that of water but the hydrophobic interactions through the water phase are larger than for ET [41]. This suggests that the adsorption of RL at the PMMA-solution interface from the dilute solution is more favourable than for ET. It is interesting that the ratio of maximal adsorption of RL at the PMMA-solution interface to that at the solution-air one at the constant ET concentration is similar to that of the area occupied by the RL molecule at the perpendicular orientation towards that at parallel orientation to the interface [41]. This indicates that the RL molecules have parallel orientation towards the PMMA-solution interface independently on its concentration. However, the head of RL molecules can be directed towards the bulk phase rather than the PMMA surface. This suggestion is based on the fact that PMMA is a monopolar solid whose electron-acceptor parameter of acid-base component is equal to zero and the electron-donor component is significantly larger than zero [37] but the parameter of the RL head surface tension is small [41].

The mechanism of ET and RL adsorption on the quartz surface is the most complicated of the studied solids. For quartz the slope of the linear dependence between $\gamma_{LV}cos\theta$ and γ_{LV} is positive at both the constant RL and ET concentrations (Figs. S18a and S19a). It should be mentioned that the linear dependences are present only at the constant RL concentration corresponding to its unsaturated monolayer at the solution-air interface and the constant ET concentration lower than its CAC [19]. The positive slope of the linear dependence between $\gamma_{LV}cos\theta$ and γ_{LV} indicates that the RL and ET adsorption is negative or that adsorption at the quartz-air interface is larger than at the quartz-solution one. To confirm this conclusion Γ_{SV} and Γ_{SL} were calculated from Eqs. (2) and (18). The values of γ_{SL} and $\gamma_{SV} - \pi$ used for the calculation were obtained in the same way as for PMMA. It proved that the Γ_{SV} values of ET at the

constant RL concentration (Fig. S33) are higher than those of Γ_{SL} (Fig. S34) and lower than Γ_{LV} (Figs. 35a–c). This fact explains why there is a positive slope of the linear dependence between $\gamma_{LV}cos\theta$ and γ_{LV} at the constant RL concentration. Similarly to PMMA, the average values of $\frac{\Gamma_{SV}-\Gamma_{SL}}{\Gamma_{LV}}$ are close to the slope of the line describing the dependence between the adhesion and the surface tensions.

It was possible to determine the values of Γ_{SV} and Γ_{SL} for RL at the constant ET concentration but only in the range of low ET concentration corresponding to the unsaturated monolayer at the solution-air interface in the absence of RL [19] (Figs. S36 and S37). The values of Γ_{SV} indicate that the RL molecules migrate from the solution drop to the quartz surface, changing its surface tension. Similarly to ET, the values of Γ_{SV} are higher than those of Γ_{SL}, and $\frac{\Gamma_{SV}-\Gamma_{SL}}{\Gamma_{LV}}$ (Figs. S38a–S38c) assumes a positive value which is close to the slope of the dependence between $\gamma_{LV}cos\theta$ and γ_{LV}. Unfortunately, when the ET concentration increases, it is difficult to describe the changes of γ_{SV} and γ_{SL} as a function of RL concentration. The question arises why? The water layer with the molecules properly packed and oriented [46–48] can be formed on the quartz surface. The water molecules can form a strong hydrogen bond with the –O- and –OH group present on the quartz surface as well as between each other. Since the possibility of strong hydrogen binding by water molecules is limited, the quartz surface covered with a layer of water becomes less hydrophilic [46–48]. It is possible that the ET and RL molecules are adsorbed from the solution in the range of low ET concentration on the quartz surface covered by the water layer. In such a case, it is possible that the ET molecules are connected with water by hydrogen bonds. The increase of ET concentration causes that the water layer is less ordered and RL molecules can penetrate to the quartz surface. At the ET concentration higher than its CAC, the RL adsorption decreases. Thus, the quartz surface tension under the solution drop and around the drop can change as a function of solution components and concentration not only by the ET and RL adsorption on its surface but also as a result of the changes of the water layer structure on the quartz surface. This is confirmed by the changes of φ parameter as well as γ_{SV} and γ_{SL} as a function of ET concentration which is difficult to describe by a given mathematical function at the ET concentration approaching its CAC as well as higher than CAC [6,19].

3.4. Standard Gibbs free energy of ET and RL adsorption

The standard Gibbs free energy of adsorption (ΔG^0_{ads}) is an important thermodynamic function in the studies of adsorption properties of the surface active agents at a given interface. The literature reports many different equations used for the ΔG^0_{ads} determination. One of the most common is the Langmuir equation modified by de Boer which has the form [12,32]:

$$\frac{A_0}{A-A_0}exp\frac{A_0}{A-A_0}=\frac{C}{w}exp\left(\frac{-\Delta G^0_{ads}}{RT}\right) \tag{21}$$

where: A is the area occupied per the adsorbing molecule at a given interface, A_0 is the limited are for a given molecule and w is the number of solvent moles in 1 dm^3.

The values of ΔG^0_{ads} calculated from Eq. (21) at the ET and RL concentration corresponding to their unsaturated monolayer at a given interface are considered. In the range of RL concentration corresponding to its unsaturated layer at the solution-air interface, the ET values of ΔG^0_{ads} at the PTFE-solution interface are almost constant and close to those at the PTFE-water [6] as well as at the solution-air interface (Fig. S39). This is consistent with the Frumkin isotherm of adsorption at the PTFE-solution and solution-air interfaces (Fig. S27a – S27c). In contrast to ET, the ΔG^0_{ads} values of RL adsorption at the PTFE-solution interface increase as a function of ET concentration (Fig. S40). This indicates that the RL tendency to adsorb at this interface decreases as a function of the ET concentration. From the comparison of the changes of

ΔG^0_{ads} values of ET as a function of RL and RL as a function of ET concentration results that ET has stronger influence on the RL adsorption at the PTFE-solution interface than vice versa.

The values of ΔG^0_{ads} adsorption of ET at the PMMA-air and PMMA-solution interfaces were calculated from Eq. (21). These values are similar to those of PTFE and practically they do not depend on the RL concentration in the range of its unsaturated layer in the absence of ET (Figs. S41 and S42). The values of ET ΔG^0_{ads} adsorption at the PMMA-air and PMMA-solution interfaces are similar to the ΔG^0_{ads} value for ET at the PMMA-water interface (in the absence of RL) [6] but they are insignificantly larger than the ΔG^0_{ads} values of ET adsorption at the water-air interface [6]. The ΔG^0_{ads} values of RL adsorption increase as a function of ET concentration similarly to the case of PTFE (Fig. S43). The ΔG^0_{ads} values of RL adsorption at the PMMA-solution interface are higher than those at the solution-air one [6]. From comparison of the influence of ET on the RL adsorption and vice versa, it can be concluded that ET influences on the RL adsorption at the PMMA-solution interface in larger extent than RL on ET.

The values of ΔG^0_{ads} adsorption of ET and RL at the quartz-air interface (Figs. S44 and S45) are close to those at the solution-air interface [6]. Similarly, to PMMA, RL influences on ΔG^0_{ads} to a smaller extent than vice versa. In the case of the quartz-solution interface, the ΔG^0_{ads} values of ET and RL adsorption (Figs. S46 and S47) are higher than those at the solution-air interface and ET influences on ΔG^0_{ads} adsorption of RL in the smaller extent than at other interfaces. This confirms the suggestion that in the range of low ET concentration the surface tension of quartz under the solution drop is different from that around the drop.

4. Conclusions

Based on the measurements of the contact angle of the aqueous solution of ethanol and rhamnolipid mixtures on the PTFE, PMMA and quartz surface and their thermodynamic analysis it can be stated that:

The replacement of the RL molecules by the ET ones in the mixed interface layer can cause the contact angle increase.

Above the ethanol CAC, the contact angle depends practically on the ET adsorption at the PTFE-solution and solution-air interfaces.

For PTFE the contact angle and the parameter of interface interactions change linearly as a function of the logarithm from the sum of the aqueous solution of ET and RL mixture surface tension and PTFE-solution interface tension.

For PTFE there is a linear dependence between the adhesion and the surface tensions of the solution for ET and RL mixture at the constant ET concentration and vice versa. However, at the constant RL concentration, the linear dependence between the adhesion and the surface tension takes place only in the range of ET concentration in which the adhesion work of the solution to PTFF surface is constant and close to that of the water one.

The critical surface tension of PTFE wetting is higher than its surface tension while it is lower for PMMA and quartz.

The adsorption of ET and RL at the PTFE-solution and solution-air interfaces is insignificantly different at the RL concentration close and higher than its CMC in the absence of ET.

The aqueous solution of ET and RL mixture spreads completely over the PMMA and quartz surfaces at the ET concentration higher than its CAC in the absence of RL.

Similarly to PTFE, the maxima of the contact angle of its isotherm are observed for PMMA and quartz, being the result of RL molecules replacement by the ET ones in the mixed layer at the interfaces.

For PMMA the linear dependence between the adhesion and the surface tension takes place only for the solution at the constant RL concentration but at both the constant ET and RL concentrations for quartz. The slope of that dependence for PMMA is negative but higher than −1 and for quartz the slope is positive and lower than 1.

The surface tension of PMMA and quartz around the settled drop on the surface changes with the changes of the composition and concentration of the solution.

The parameter of interface interactions for PMMA behaves similarly to that for PTFE. It cannot be described by one function for quartz in the whole range of solution concentrations and composition.

The adsorption of both ET and RL at the PMMA-solution and quartz-solution interfaces is lower than that at the solution-air one. In the case of quartz, the ET and RL adsorption on its surface is higher than at the quartz-solution one which accounts for the positive slope of the dependence between the adhesion and surface tensions.

The difference between the adsorption of ET and/or RL on the solid surface and at the solid-solution interface divided by the adsorption at the solution-air interface is close to the slope of dependence between the adhesion and surface tension.

For PMMA and quartz there is a linear dependence between the adhesion work of solution to their surface and surface tension of solution.

The Gibbs standard free energy of ET and RL adsorption from the dilute solutions at the PTFE (PMMA)-solution interface differs only slightly from that of the adsorption at the solution-air interface. However the ΔG^0_{ads} values of ET and RL adsorption at the quartz-solution interface is higher than that at the solution-air one. In the PTFE-solution and PMMA-solution systems, ET influences on the RL adsorption to a larger extent than vice versa.

Appendix A. Supplementary data

Supplementary data to this article can be found online at https://doi.org/10.1016/j.ijadhadh.2021.102955.

References

[1] Tiso T, et al. Rhamnolipids: production, performance, and application. In: Lee S, editor. Consequences of microbial interactions with hydrocarbons, oils, and lipids: production of fuels and chemicals. Handbook of hydrocarbon and lipid microbiology. Cham: Springer; 2017. p. 587–622. https://doi.org/10.1007/978-3-319-50436-0_388.

[2] Sinumvayo JP, Ishimwe N. Agriculture and food applications of rhamnolipids and its production by *Pseudomonas aeruginosa*. J Chem Eng Process 2015;6(2). https://doi.org/10.4172/2157-7048.1000223.

[3] Kamaljeet K, Pattanathu R. Rhamnolipid biosurfactants – past, present, and future scenario of global market. Front Microbiol 2014;5:454. https://doi.org/10.3389/fmicb.2014.00454.

[4] Ł Chrzanowski, Ławniczak Ł, Czaczyk K. Why do microorganisms produce rhamnolipids? World J Microbiol Biotechnol 2012;28(2):401–19. https://doi.org/10.1007/s11274-011-0854-8.

[5] Zana R. Aqueous surfactant-alcohol systems: a review. Adv Colloid Interface Sci 1995;57:1–64. https://doi.org/10.1016/0001-8686(95)00235-I.

[6] Zdziennicka A, Jańczuk B. Modification of adsorption, aggregation and wetting properties of surfactants by short chain alcohols. Adv Colloid Interface Sci 2020; 284:102249. https://doi.org/10.1016/j.cis.2020.102249.

[7] Zdziennicka A, Jańczuk B. Wetting and adhesion properties of rhamnolipid and surfactin. Int J AdhesAdhes 2018;84:275–82. https://doi.org/10.1016/j.ijadhadh.2018.04.005.

[8] van Oss CJ, Constanzo PM. Adhesion of anionic surfactants to polymer surfaces and low-energy materials. J Adhes Sci Technol 1992;4:477–87. https://doi.org/10.1163/156856192X00809.

[9] Tåg CM, Toiviainen M, Juuti M, et al. The effect of isopropyl alcohol and non-ionic surfactant mixtures on the wetting of porous coated paper. Transport Porous Media 2012;94:225–42. https://doi.org/10.1007/s11242-012-0001-5.

[10] Shirzad S, Sadeghi R. Effects of addition of short-chain alcohol solvents on micellization and thermodynamic properties of anionic surfactants sodium dodecyl sulfate and sodium dodecyl sulfonate in aqueous solutions. J Iran Chem Soc 2018; 15:1365–75. https://doi.org/10.1007/s13738-018-1336-9.

[11] Wang T, et al. Effects of short-chain alcohol on the micellization of gemini surfactant C16-6-16 · 2Br in aqueous solution. Dispers Sci Technol 2007;28(8): 1169–72. https://doi.org/10.1080/01932690701526880.

[12] Rosen JM. Surfactants and interfacial Phenomena. 3rded. New York: Wiley–Interscience; 2004.

[13] Shah SK, Chatterjee SK, Bhattarai A. Micellization of cationic surfactants in alcohol — water mixed solvent media. J Mol Liq 2016;222:906–14. https://doi.org/10.1016/j.molliq.2016.07.098.

[14] Kovtun AI, Khil'ko SL, Zholob SA, et al. Effect of lower alcohols on adsorption characteristics of sodium dodecyl sulfate solutions at liquid-gas interfaces. Colloid J 2010;72:389–95. https://doi.org/10.1134/S1061933X10030129.

[15] Ferreira A, Sullo A, Winston S, et al. Influence of ethanol on emulsions stabilized by low molecular weight surfactants. J Food Sci 2019;85:28–35. https://doi.org/10.1111/1750-3841.14947.

[16] Huang J-B, Mao M, Zhu B-Y. The surface physico-chemical properties of surfactants in ethanol–water mixtures. Colloids Surf A Physicochem Eng Asp 1999;155(2–3): 339–48. https://doi.org/10.1016/S0927-7757(99)00003-5.

[17] Bracko S, span J. Anionic dye–cationic surfactant interactions in water–ethanol mixed solvent. Dyes Pigments 2001;50(1):77–84. https://doi.org/10.1016/S0143-7208(01)00025-0.

[18] Zana R, Eljebari MJ. Fluorescence probing of self-association of alcohols in aqueous solution. J Phys Chem 1993;97:11134–6. https://doi.org/10.1021/j100144a039.

[19] Chodzińska A, Zdziennicka A, Jańczuk B. Volumetric and surface properties of short chain alcohols in aqueous solution-air systems at 293 K. J Solut Chem 2012; 41(12):2226–45. https://doi.org/10.1007/s10953-012-9935-z.

[20] Bourrier O, Butlin J, Hourani R, et al. Aggregation of 3,5-dihydroxybenzyl alcohol-based dendrimers and hyperbranched polymers, and encapsulation of DR1 in such dendritic aggregates. Inorg Chim Acta 2004;357(13):3836–46. https://doi.org/10.1016/j.ica.2004.02.016.

[21] Pal A, Yadav A. Modulating the aggregation behavior of 1-methyl-3-octylimidazolium chloride by alcohols in aqueous media. J SurfactDeterg 2016;19:1053–62. https://doi.org/10.1007/s11743-016-1859-y.

[22] Anderson MT, Martin JE, Odinek JG, et al. Effect of methanol concentration on CTAB micellization and on the formation of surfactant-templated silica (STS). Chem Mater 1998;10:1490–500. https://doi.org/10.1021/cm970240m.

[23] Emerson MF, Holtzer A. Hydrophobic bond in micellar systems. Effects of various additives on the stability of micelles of sodium dodecyl sulfate and of n-dodecyltrimethylammonium bromide. J Phys Chem 1967;71:3320–30. https://doi.org/10.1021/j100869a031.

[24] Niraula TP, Bhattarai A, Chatterjee SK. Conductometric studies on the effect of NaBr on the micellization of sodium dodecyl sulphate (SDS) in pure water and methanol-water mixed solvent media at different temperatures. Modern Trends Sci Tech 2013:62–74.

[25] Bielawska M, Chodzińska A, Jańczuk B, Zdziennicka A. Determination of CTAB CMC in mixed water+short-chain alcohol solvent by surface tension, conductivity, density and viscosity measurements. Colloids Surf, A 2013;424:81–8. https://doi.org/10.1016/j.colsurfa.2013.02.017.

[26] Zdziennicka A, Szymczyk K, Jańczuk B, Longwic R, Sander P. Adhesion of canola and diesel oils to some parts of diesel engine in the light of surface tension components and parameters of these substrates. Int J Adhesion Adhes 2015;60: 23–30. https://doi.org/10.1016/j.ijadhadh.2015.03.001.

[27] Rekiel E, Zdziennicka A, Jańczuk B. Adsorption properties of rhamnolipid and ethanol at water/ethanol solution-air interface. J Mol Liq 2020;309:113080. https://doi.org/10.1016/j.molliq.2020.113080.

[28] Jańczuk B, Zdziennicka A, Wójcik W. Relationship between wetting of Teflon by cetyltrimethylammonium bromide solution and adsorption. Eur Polym J 1997;33: 1093–8.

[29] Adamson W, Gast AP. Physical Chemistry of surfaces. sixth ed. New York: Wiley Interscience; 1997.

[30] Mańko D, Zdziennicka A, Jańczuk B. Thermodynamic properties of rhamnolipid micellization and adsorption. Coll Biol 2014;119:22–9. https://doi.org/10.1016/j.colsurfb.2014.04.020.

[31] Girifalco LA, Good RJ. A theory for the estimation of surface and interfacial energies. I. Derivation and application to interfacial tension. J Phys Chem 1957;61 (7):904–9. https://doi.org/10.1021/j150553a013.

[32] de Boer JH. The dynamic character of adsorption. Oxford: Oxford University; 1953.

[33] van Oss CJ. Interfacial forces in aqueous media. New York: Marcel Dekker; 1994.

[34] Li D, Neumann AW. Equation of state for interfacial tensions of solid-liquid systems. Adv Colloid Interface Sci 1992;39:299–345. https://doi.org/10.1016/0001-8686(92)80064-5.

[35] Spelt JK, Li D, Neumann AW. The equation of state approach to interfacial tensions. In: Schrader ME, Loeb GL, editors. Modern approaches to wettability. New York: Plenum Press; 1992.

[36] Kwok DY, Neumann AW. Contact angle measurement and contact angle interpretation. Adv Colloid Interface Sci 1999;81:167–249. https://doi.org/10.1016/S0001-8686(98)00087-6.

[37] Zdziennicka A, Krawczyk J, Szymczyk K, Jańczuk B. Components and parameters of liquids and some polymers surface tension at different temperature. Colloids Surf, A 2017;529:864–75. https://doi.org/10.1016/j.colsurfa.2017.07.002.

[38] Hu P, Adamson AW. Adsorption contact angle studies. II. Water and organic substances on polished polytetrafluoroethylene. J Colloid Interface Sci 1977;59: 605–14. https://doi.org/10.1016/0021-9797(77)90055-8.

[39] Fowkes FM. Attractive forces at interfaces. Ind Eng Chem 1964;56:40–52. https://doi.org/10.1021/ie50660a008.

[40] van Oss CJ, Chaudhury MK, Good RJ. Monopolar surfaces. Adv Colloid Interface Sci 1987;28:35–64. https://doi.org/10.1016/0001-8686(87)80008-8.

[41] Zdziennicka A, Krawczyk J, Szymczyk K, Jańczuk B. Macroscopic and microscopic properties of some surfactants and biosurfactants. Int J Mol Sci 2018;19(7):1934. https://doi.org/10.3390/ijms19071934.

[42] Zdziennicka A, Krawczyk J, Jańczuk B. Wettability and adhesion work prediction in the polymer-aqueous solution of surface active agent systems. Colloids Interfaces 2018;2(2):21. https://doi.org/10.3390/colloids2020021.

[43] Zisman WA. Relation of the equilibrium contact angle to liquid and solid constitution43. Washington DC: Am Chem; 1964. p. 1–51. Contact Angle Wettability and Adhesion. In: Advances in chemistry series.

[44] van Oss CJ, Good RJ. Surface tension and the solubility of polymers and biopolymers: the role of polar and apolar interfacial free energies. J Macromol Sci, Chem 1989;26:1183–203. https://doi.org/10.1080/00222338908052041.

[45] Lucassen-Reynders EH. Contact angles and adsorption on solids. J Phys Chem 1963;67:969–72. https://doi.org/10.1021/j100799a005.

[46] Mc Cafferly E, Pravdic V, Zettlemoyer AC. Dielectric behaviour of adsorbed water films on the α-Fe$_2$O$_3$surface. Trans Faraday Soc 1970;66:1720–40. https://doi.org/10.1039/TF9706601720.

[47] Mc Cafferly E, Zettlemoyer AC. Entropy of adsorption and the mobility of water vapor on α-Fe$_2$O. J Colloid Interface Sci 1970;34:452–60. https://doi.org/10.1016/0021-9797(70)90205-5.

[48] Fowkes FM. Calculation of work of adhesion by pair potential summation. J Colloid Interface Sci 1968;28:493–505. https://doi.org/10.1016/0021-9797(68)90082-9.

EFFECT OF ETHANOL ON WETTING AND ADHESION PROPERTIES OF RHAMNOLIPID

EDYTA REKIEL, ANNA ZDZIENNICKA* AND BRONISŁAW JAŃCZUK

Department of Interfacial Phenomena, Institute of Chemical Sciences, Faculty of Chemistry, Maria Curie-Skłodowska University in Lublin, Maria Curie-Skłodowska Sq. 3, 20-031 Lublin, Poland

Running title: Effect of ethanol

*To whom correspondence should be addressed

  phone (48-81) 537-56-70   fax (48-81) 533-3348

e-mail aniaz@hektor.umcs.lublin.pl
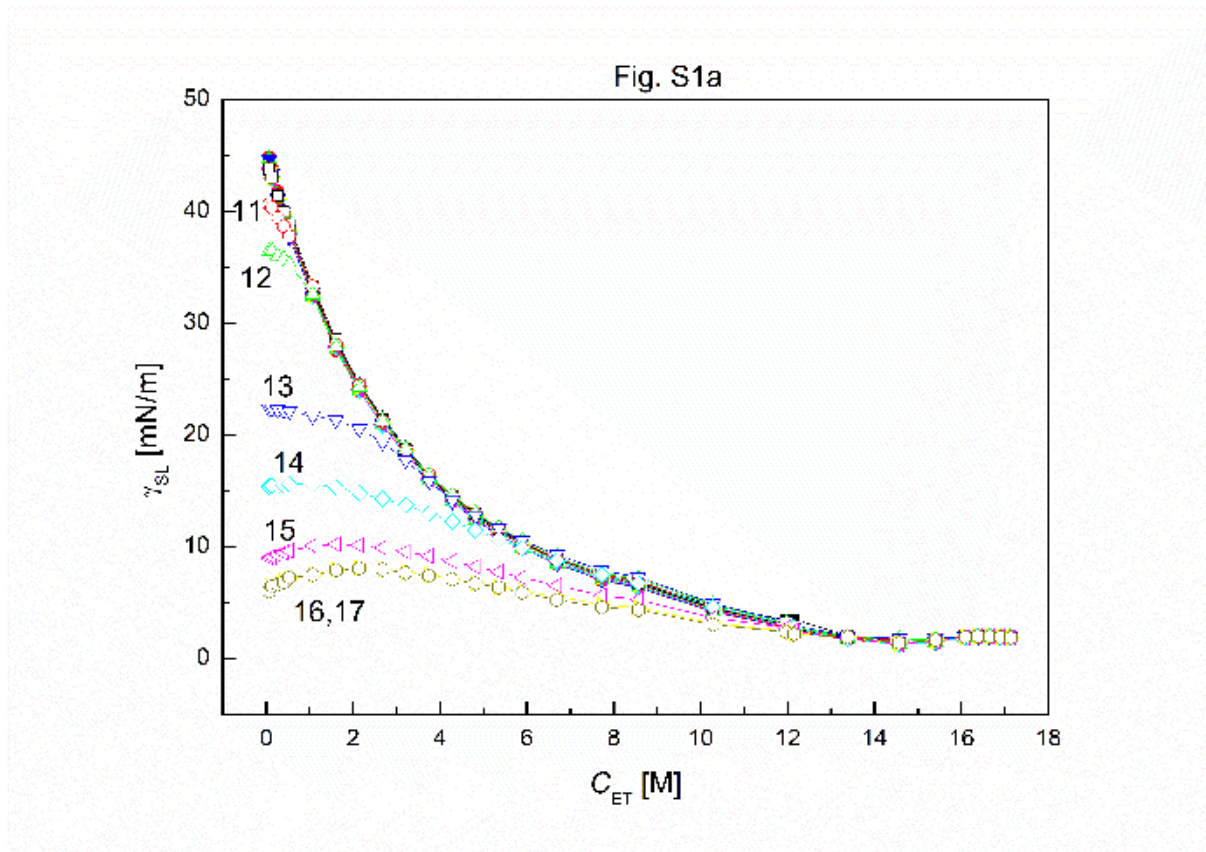
Fig. S1a. A plot of PTFE-solution interface tension (γ_{SL}) vs. the ethanol concentration (C_{ET}) Curves 1 – 17 correspond to the constant RL concentration equal to 0; 0.0002; 0.0005; 0.00125; 0003; 0.00625; 0.01; 0.02; 0.05; 0.1; 0.5; 1; 5; 10; 20; 30 and 40 mg/dm^3.
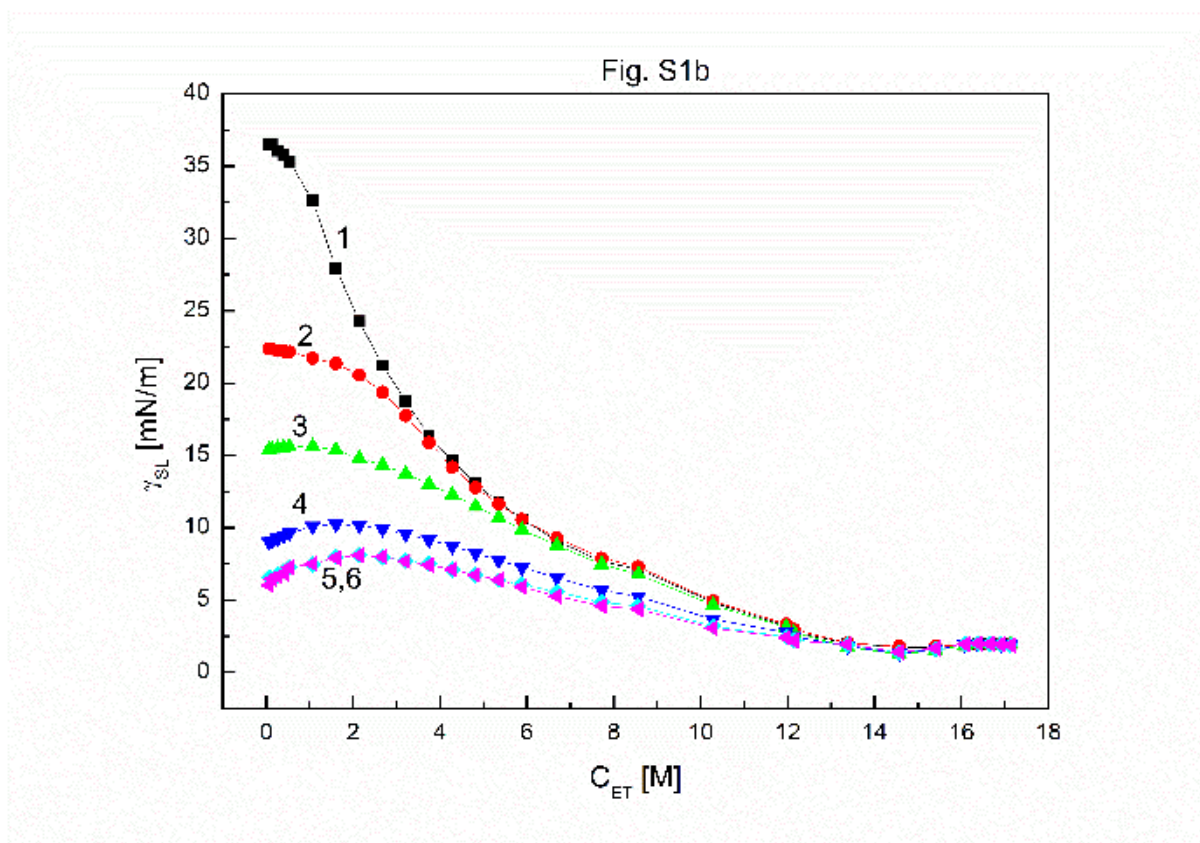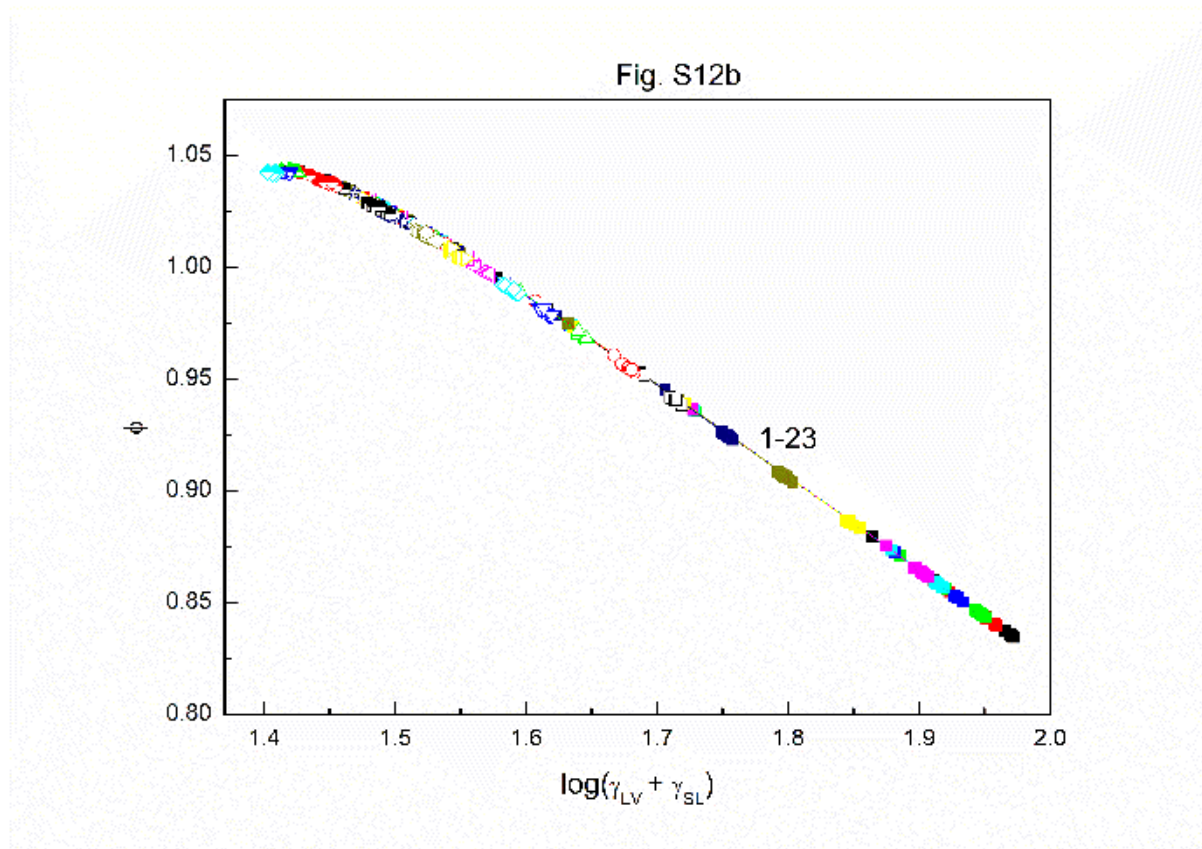
Fig. S1b. A plot of PTFE-solution interface tension (γ_{SL}) vs. of ethanol concentration (C_{ET})
Curves 1 – 6 correspond to the constant RL concentration equal to 1; 5; 10; 20; 30 and
40 mg/dm^3.
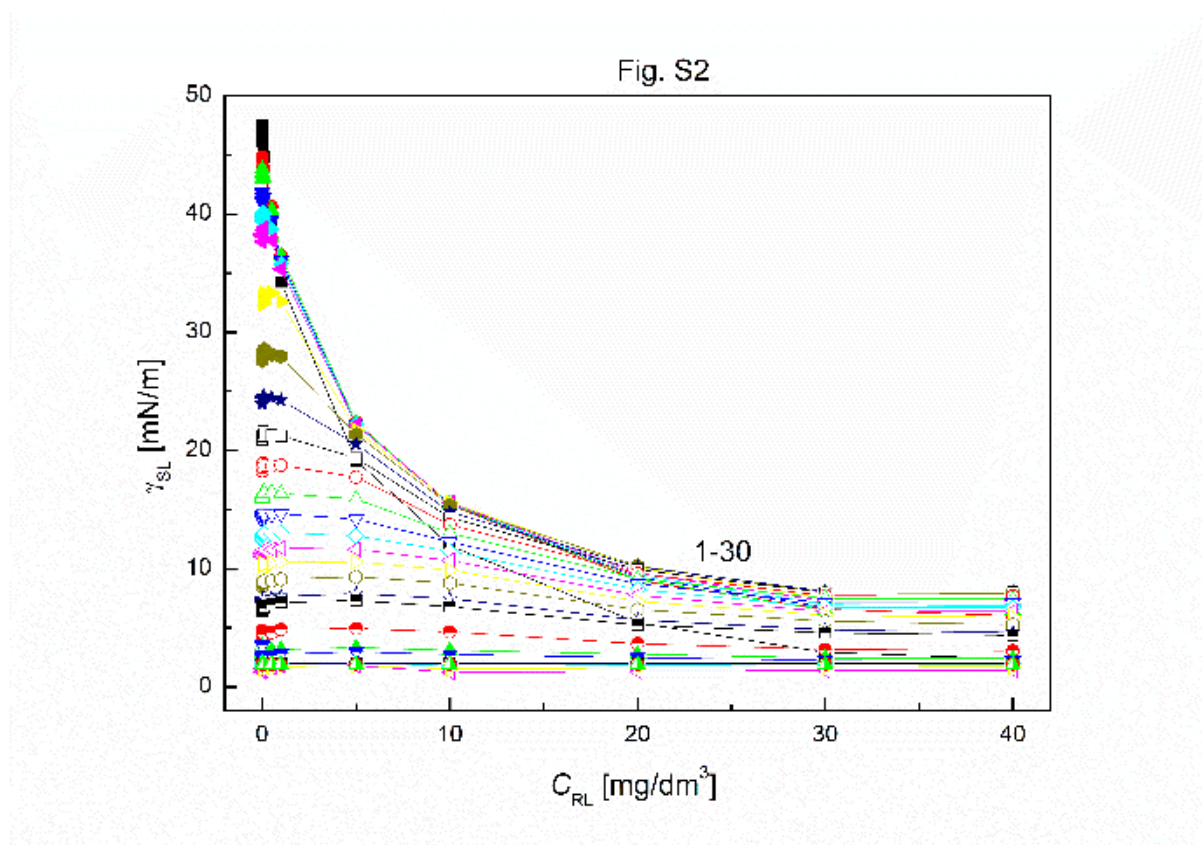
Fig. S2. A plot of PTFE-solution interface tension (γ_{SL}) vs. the RL concentration (C_{RL}).
Curves 1 – 30 correspond to the constant ET concentration equal to 0; 0.06692;
0.1338; 0.2677; 0.4015; 0.535; 1.0706; 1.6062; 2.1416; 2.677; 3.2124; 3.7478; 4.2832;
4.8185; 5.3538; 5.8893; 6.6925; 7.7245; 8.5664; 10.2797; 11.968; 12.145; 13.3794;
14.5696; 15.4064; 16.084; 16.3777; 16.648; 16.8988 and 17.13 M.
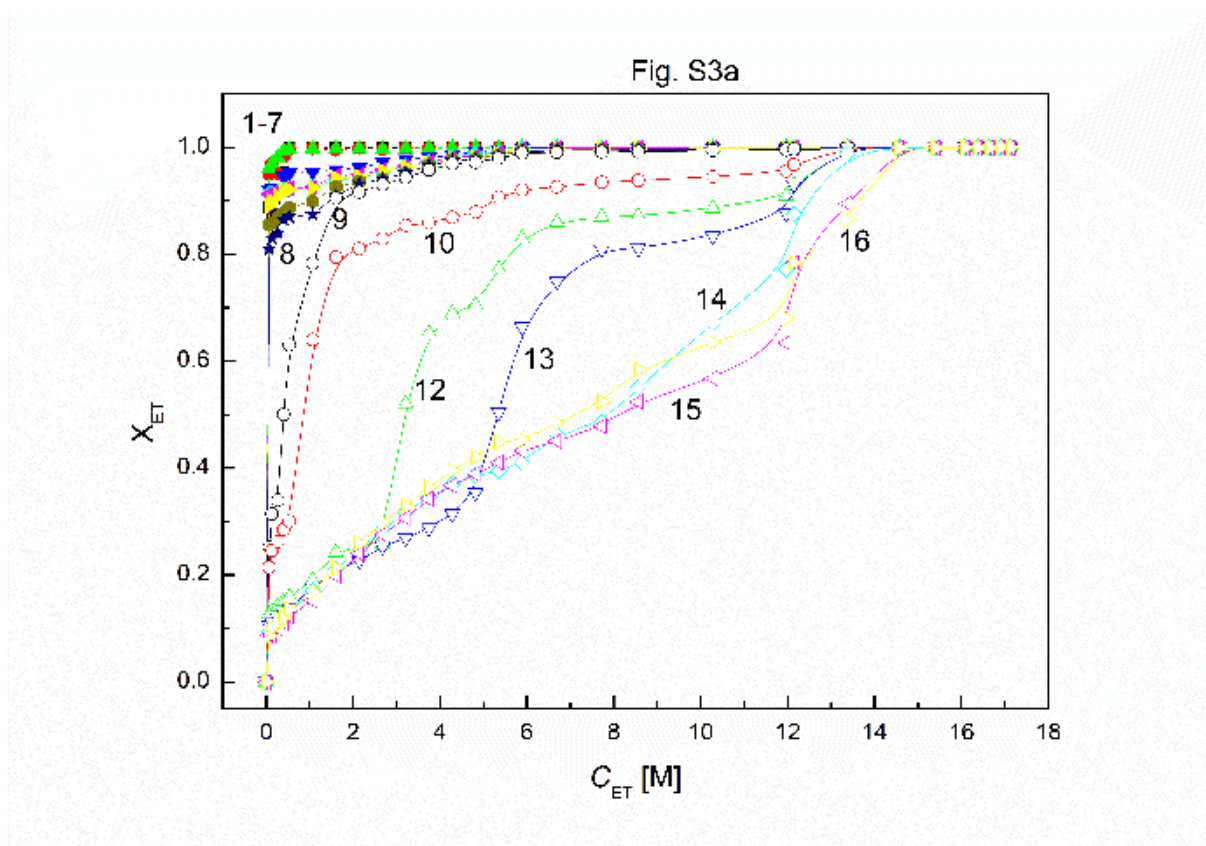
Fig. S3a. A plot of ethanol mole fraction (X_{ET}) calculated from Eq. (2) vs. its concentration (C_{ET}). Curves 1 – 16 correspond to the constant RL concentration equal to 0.0002; 0.0005; 0.00125; 0003; 0.00625; 0.01; 0.02; 0.05; 0.1; 0.5; 1; 5; 10; 20; 30 and 40 mg/dm^3.
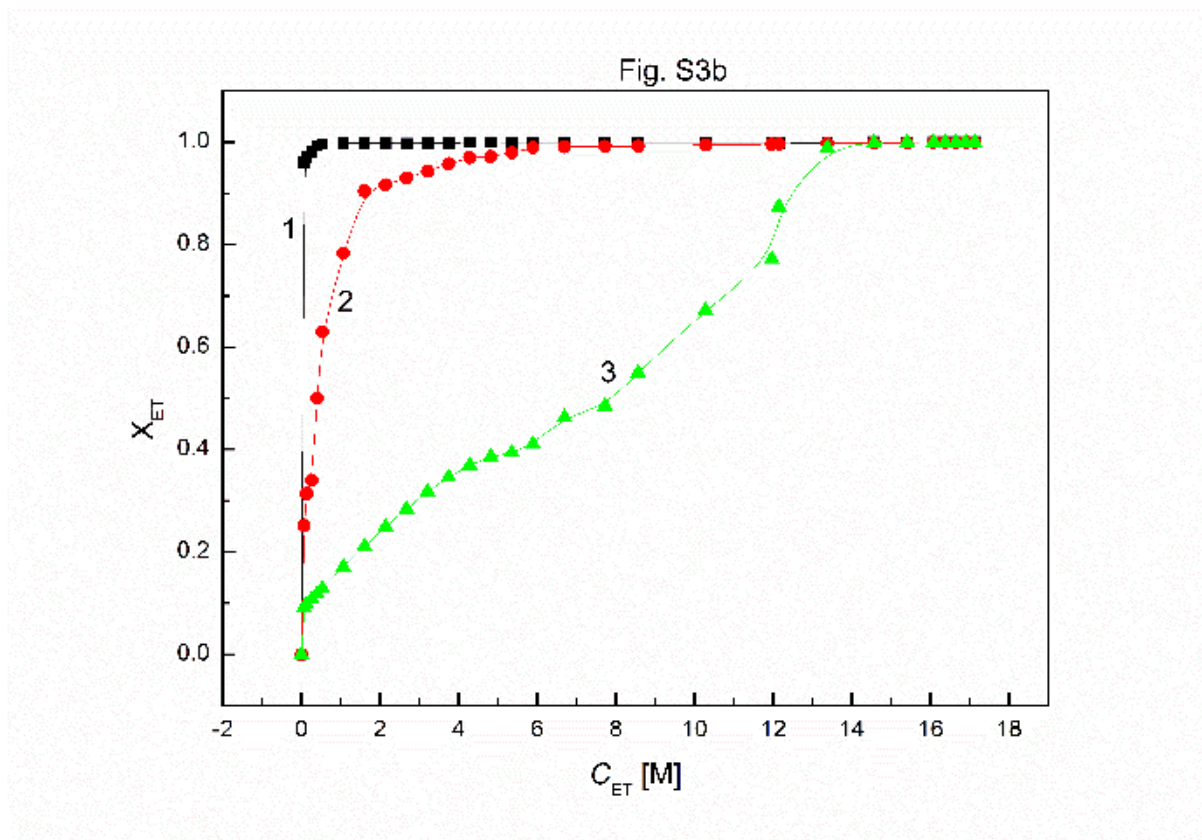
Fig. S3b. A plot of ethanol mole fraction (X_{ET}) calculated from Eq. (2) vs. its concentration (C_{ET}). Curves 1 – 3 correspond to the constant RL concentration equal to 0.00125; 0.5 and 20 mg/dm^3.
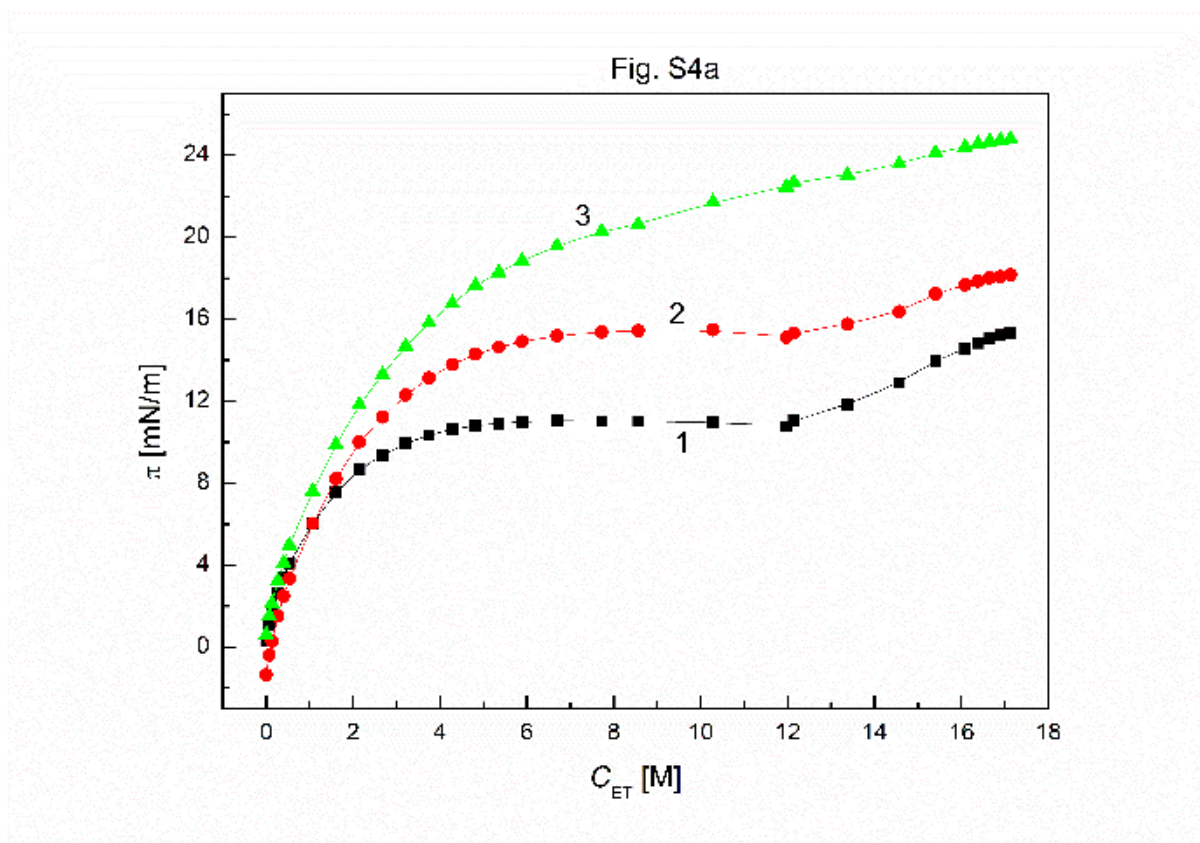
Fig. S4a. A plot of pressure of surface film (π) for PMMA vs. the ethanol concentration (C_{ET}) at the constant RL concentration equal to 0.00125 mg/dm^3. Curves 1 – 3 correspond to the values calculated based on Eqs. (4), (7) and (9) and from Eq. (5), respectively.
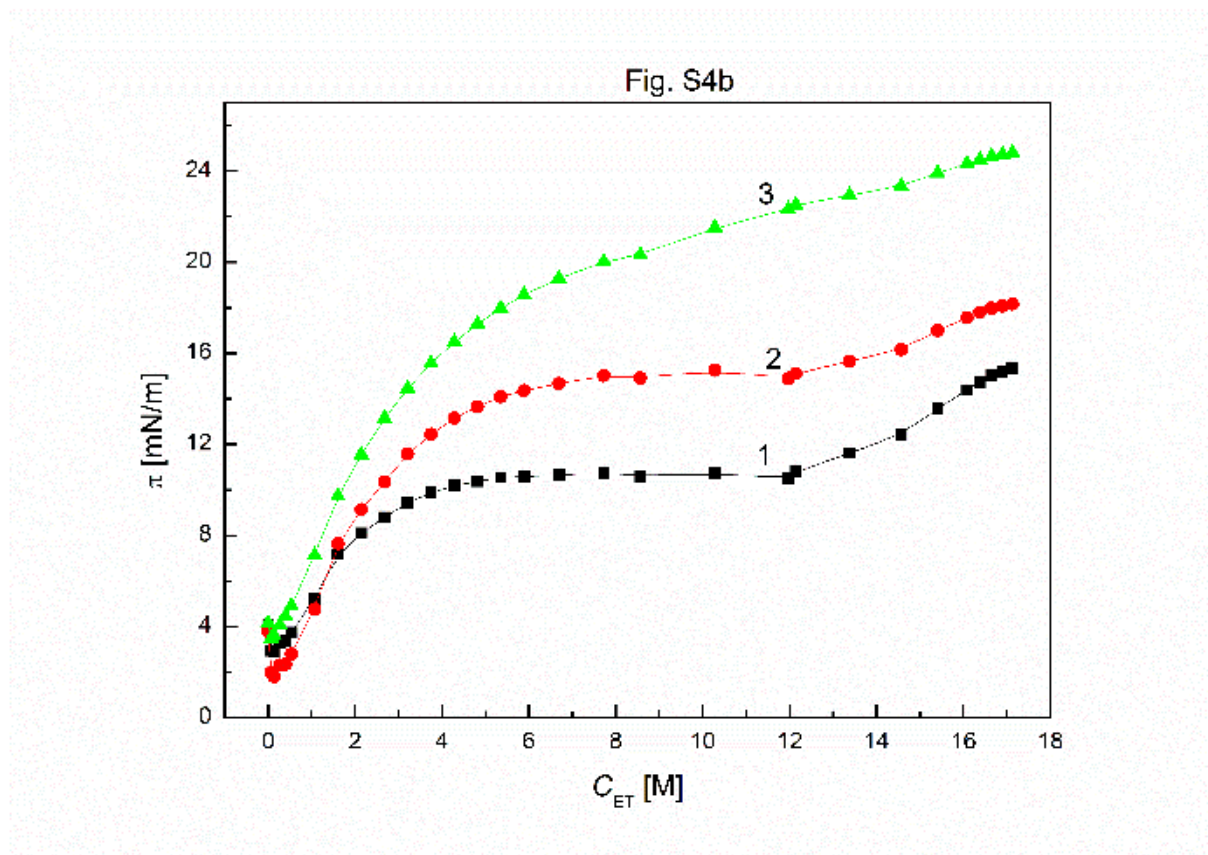
Fig. S4b. A plot of pressure of surface film (π) for PMMA vs. the ethanol concentration (C_{ET}) at the constant RL concentration equal to 0.5 mg/dm^3. Curves 1 – 3 correspond to the values calculated based on Eqs.(4), (7) and (9) and from Eq. (5) and from Eq. (5), respectively.
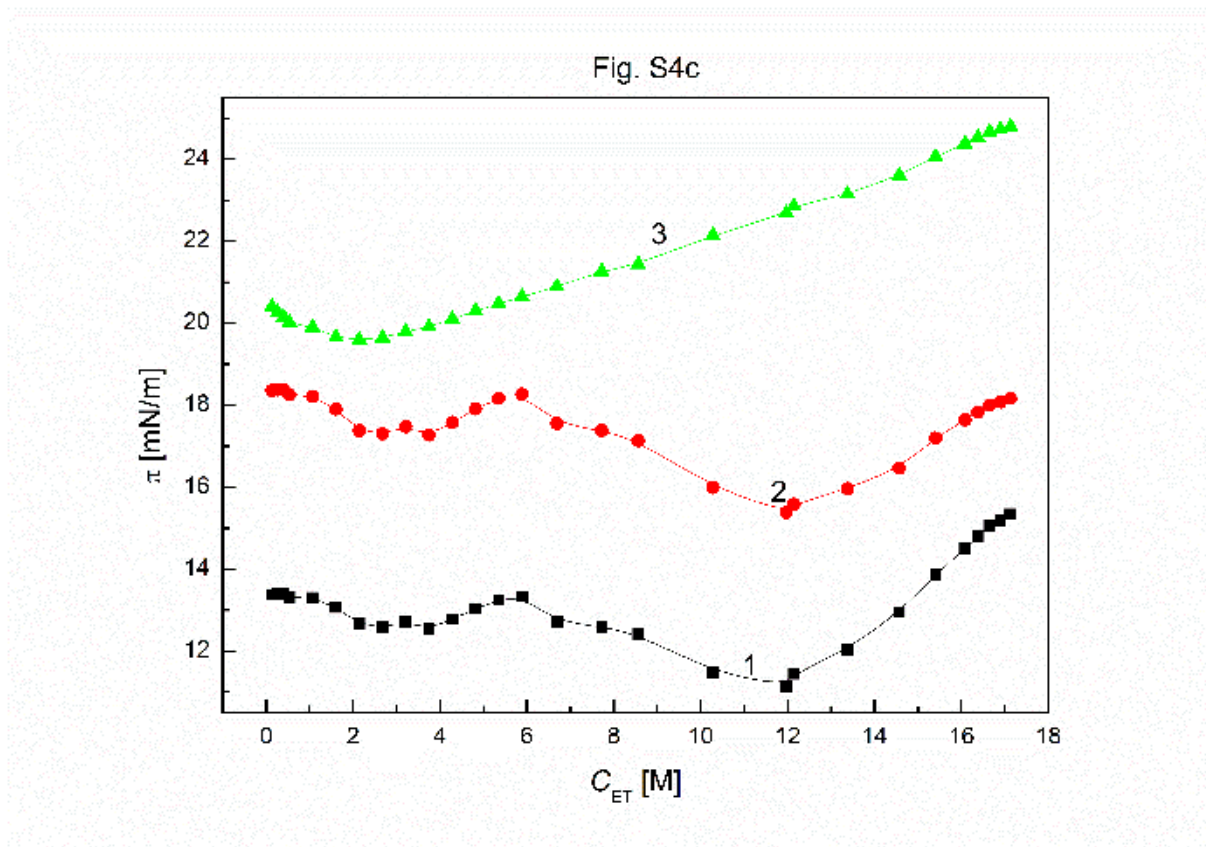
Fig. S4c.. A plot of pressure of surface film (π) for PMMA vs. the ethanol concentration (C_{ET}) at the constant RL concentration equal to 20 mg/dm^3. Curves 1 – 3 correspond to the values calculated based on Eqs. (4), (7) and (9) and from Eq. (5) and from Eq. (5), respectively.
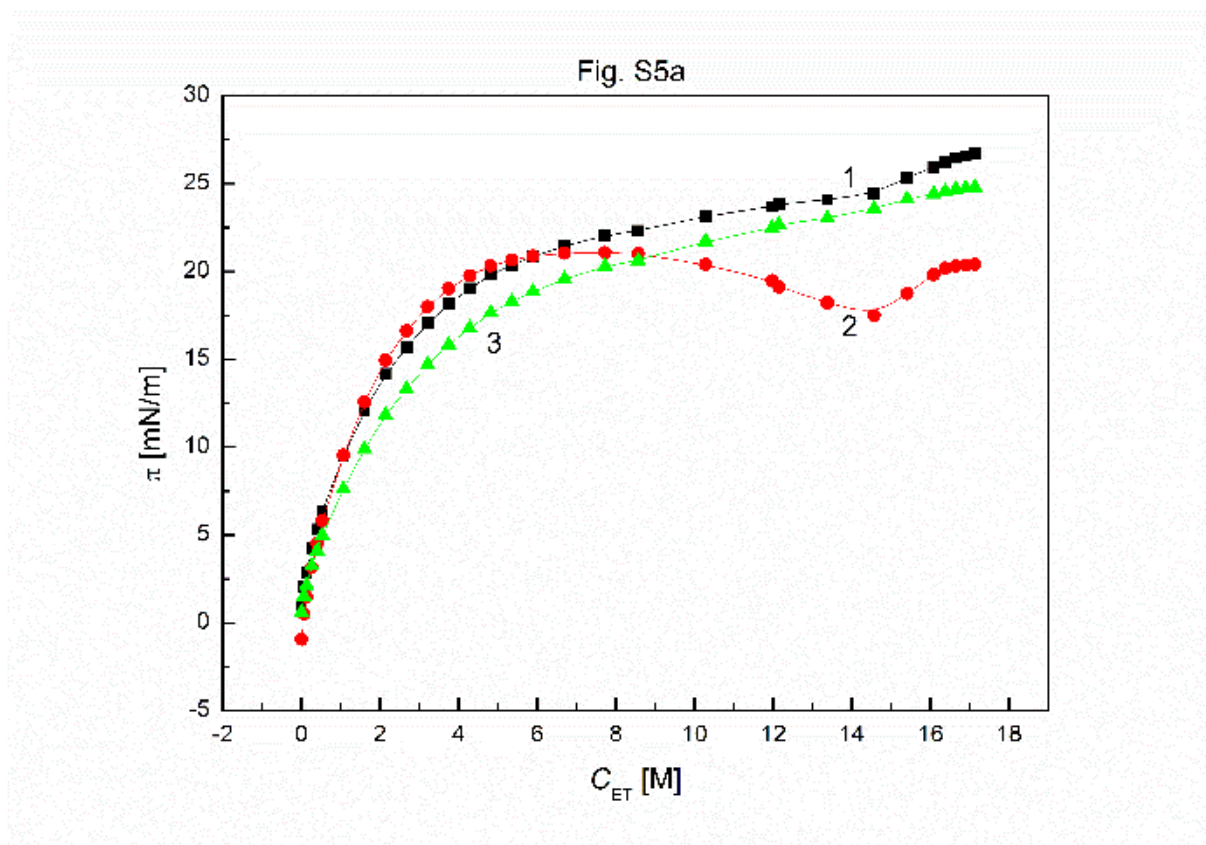
Fig. S5a.. A plot of pressure of surface film (π) for quartz vs. the ethanol concentration (C_{ET}) at the constant RL concentration equal to 0.00125 mg/dm^3. Curves 1 – 3 correspond to the values calculated based on Eqs. (4), (7) and (9) and from Eq. (5) and from Eq. (5), respectively.
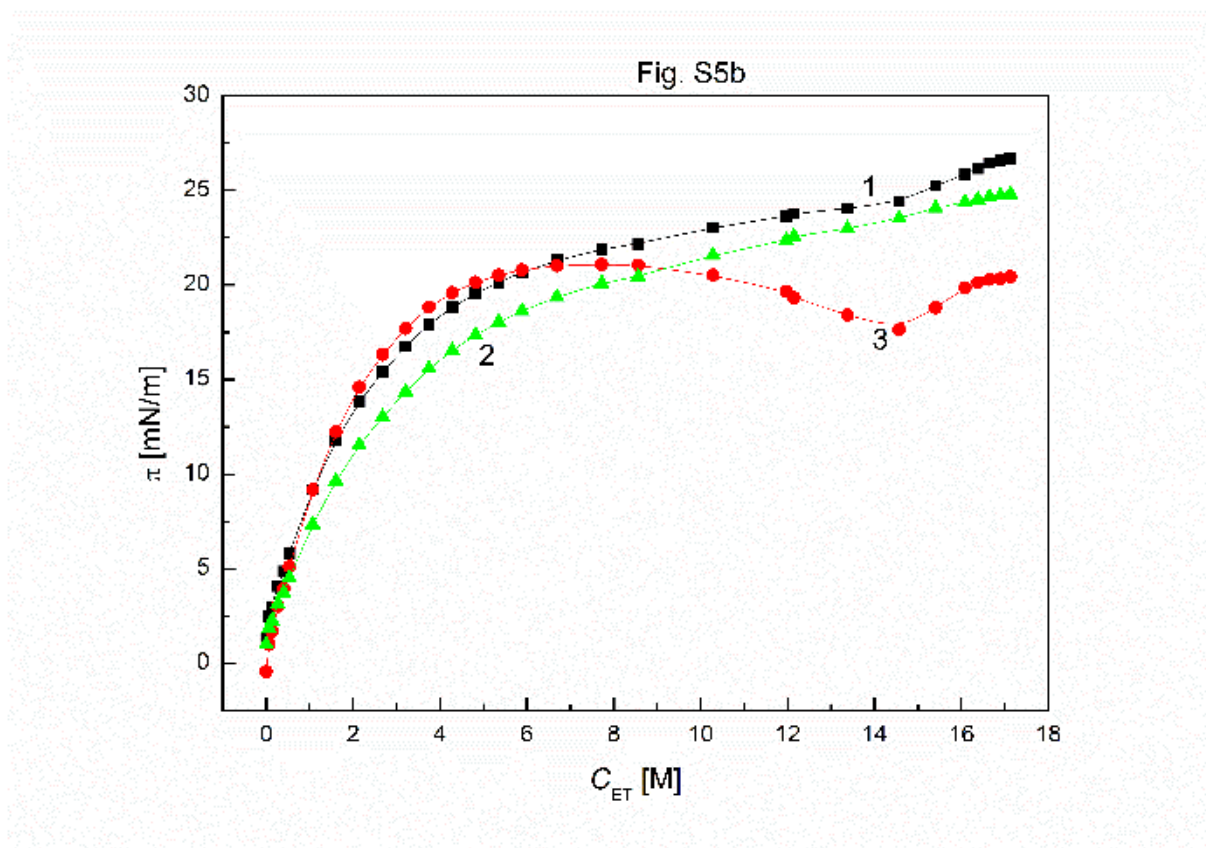
Fig. S5b.. A plot of pressure of surface film (π) for quartz vs. the ethanol concentration (C_{ET}) at the constant RL concentration equal to 0.5 mg/dm^3. Curves 1 – 3 correspond to the values calculated based on Eqs. (4), (7) and (9) and from Eq. (5) and from Eq. (5), respectively.
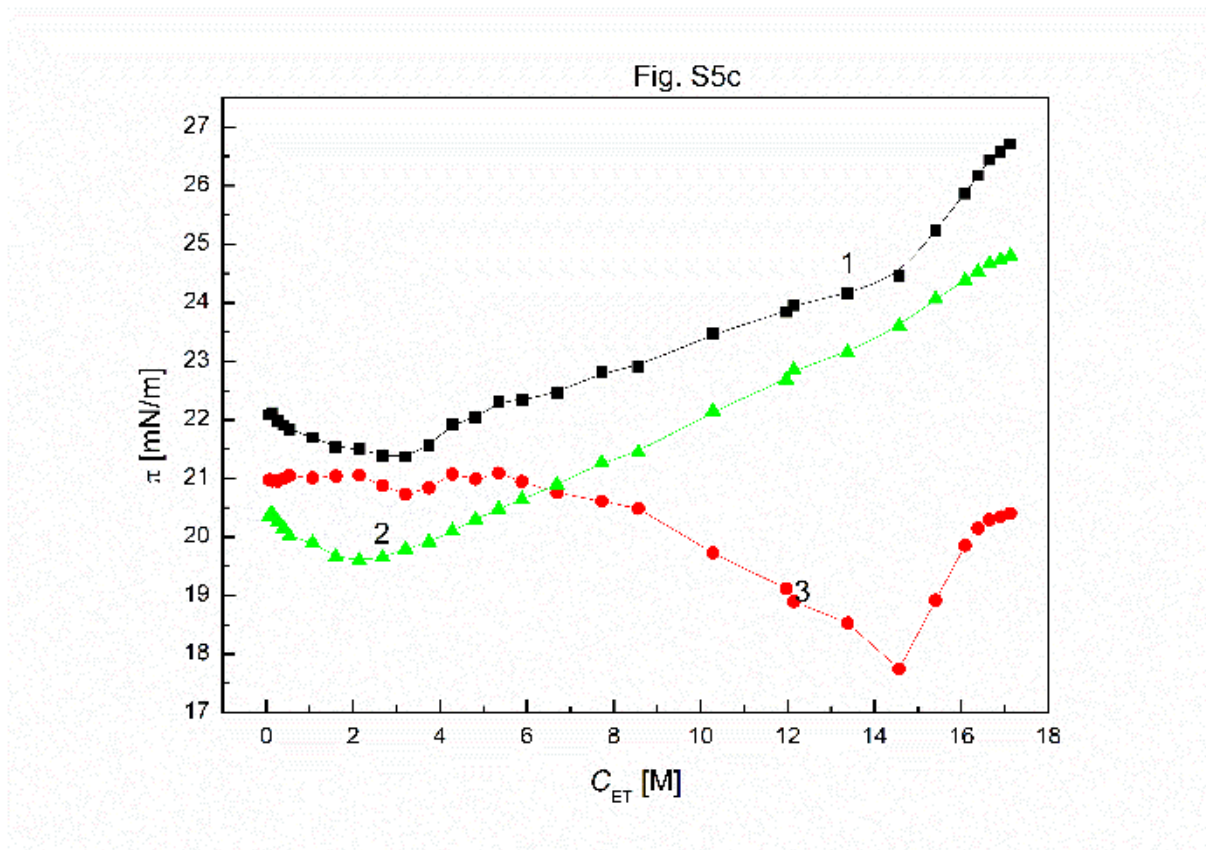
Fig. S5c.. A plot of pressure of surface film (π) for quartz vs. the ethanol concentration (C_{ET}) at the constant RL concentration equal to 20 mg/dm^3. Curves 1 – 3 correspond to the values calculated based on Eqs. (4), (7) and (9) and from Eq. (5) and from Eq. (5), respectively.
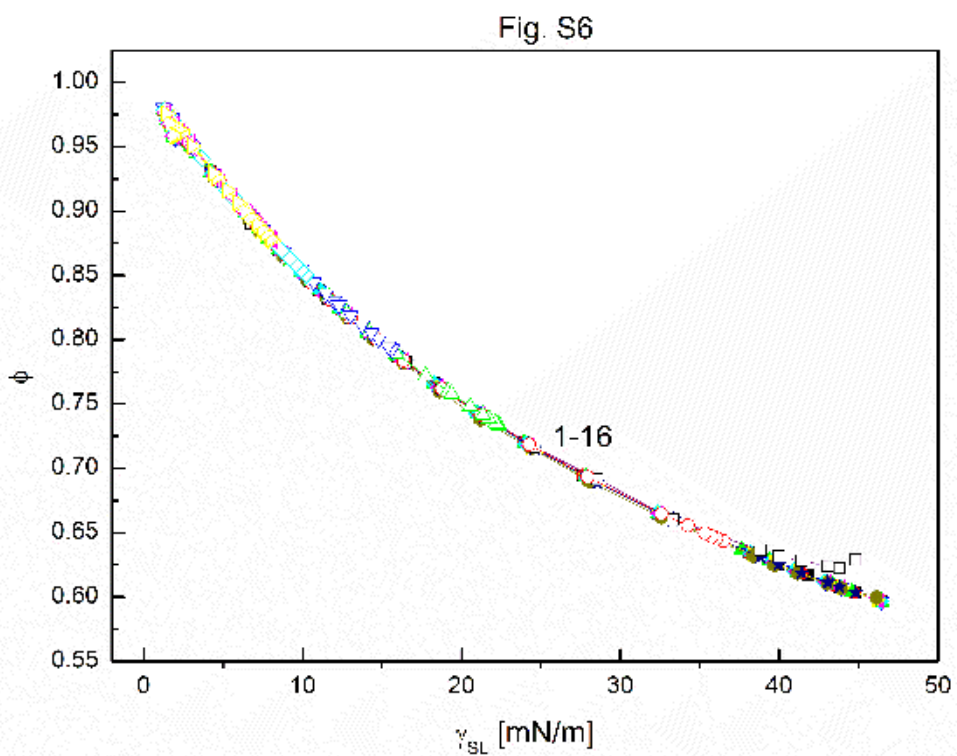
Fig. S6. A plot of parameter ϕ calculated on the basis of Eq. (11) for PTFE vs. the PTFE-solution interface tension (γ_{SL}). Curves 1 – 16 correspond to the constant RL concentration equal to 0.0002; 0.0005; 0.00125; 0003; 0.00625; 0.01; 0.02; 0.05; 0.1; 0.5; 1; 5; 10; 20; 30 and 40 mg/dm^3.
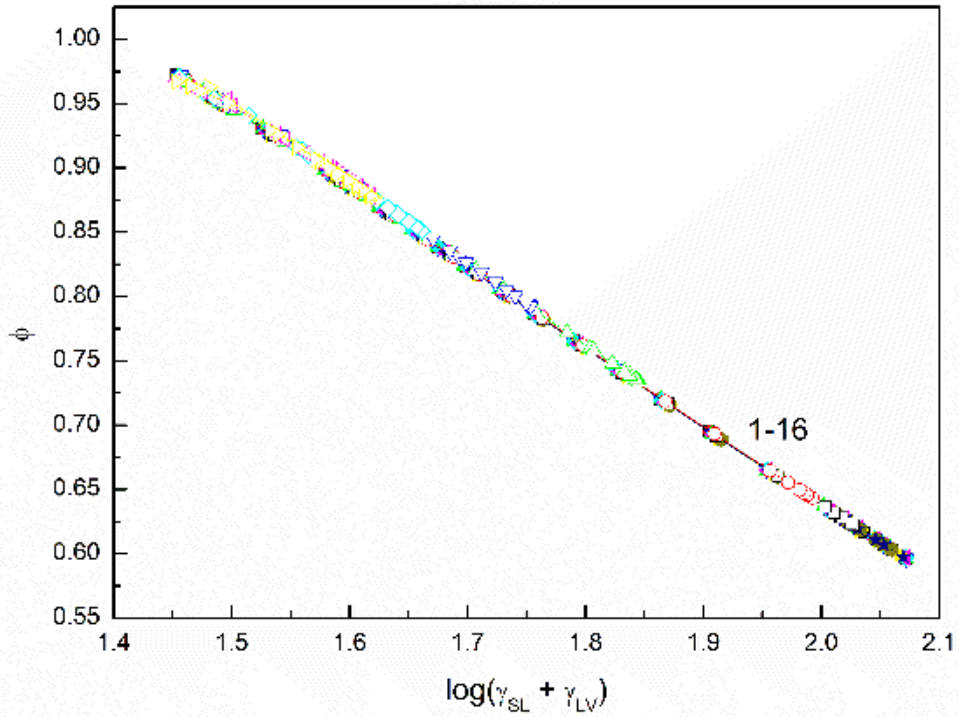
Fig. S7. A plot of parameter ϕ calculated from Eq. (11) for PTFE vs. the logarithm of the sum of solution surface tension and PTFE-solution interface tension $(\log(\gamma_{LV} + \gamma_{SL}))$. Curves 1 – 16 correspond to the constant RL concentration equal to 0.0002; 0.0005; 0.00125; 0003; 0.00625; 0.01; 0.02; 0.05; 0.1; 0.5; 1; 5; 10; 20; 30 and 40 mg/dm³.
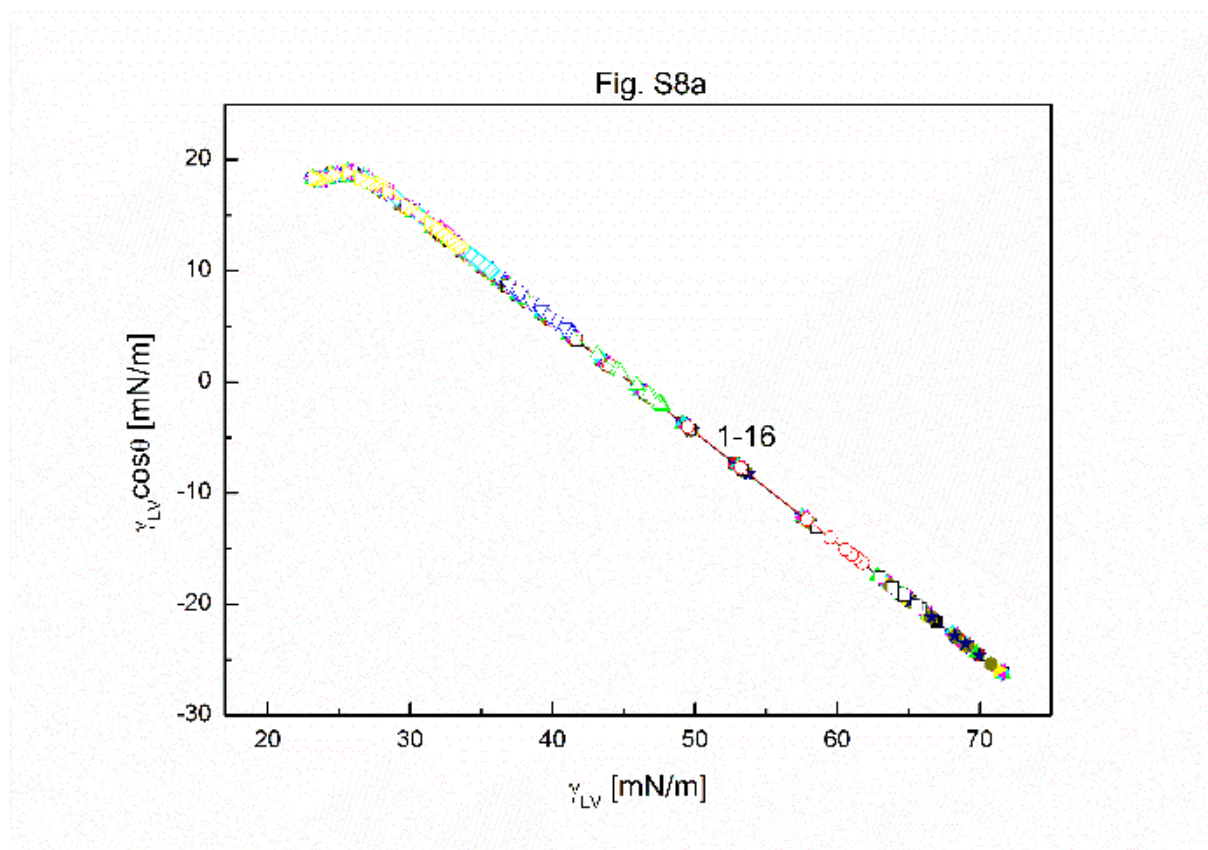
Fig. S8a. A plot of adhesion tension ($\gamma_{LV}cos\theta$) for PTFE vs. the solution surface tension (γ_{LV}). Curves 1 – 16 correspond to the constant RL concentration equal to 0.0002; 0.0005; 0.00125; 0003; 0.00625; 0.01; 0.02; 0.05; 0.1; 0.5; 1; 5; 10; 20; 30 and 40 mg/dm^3.
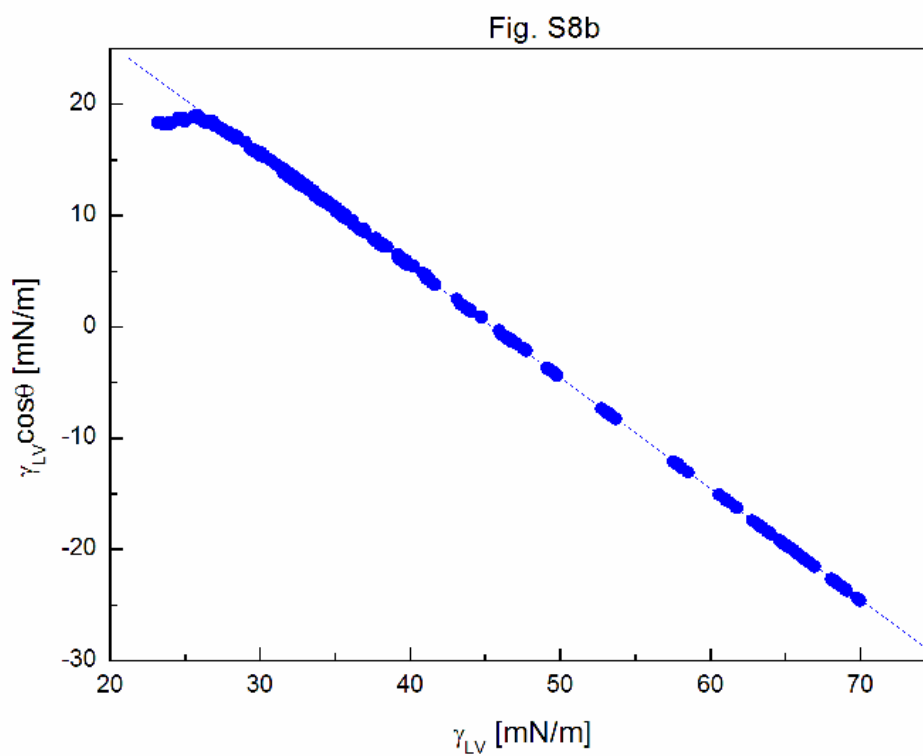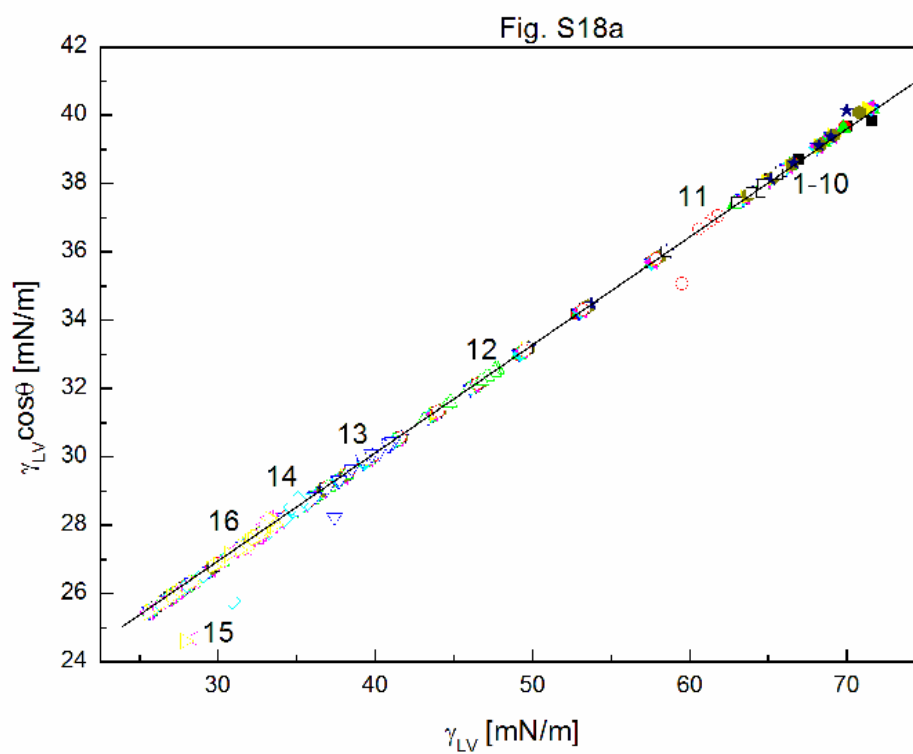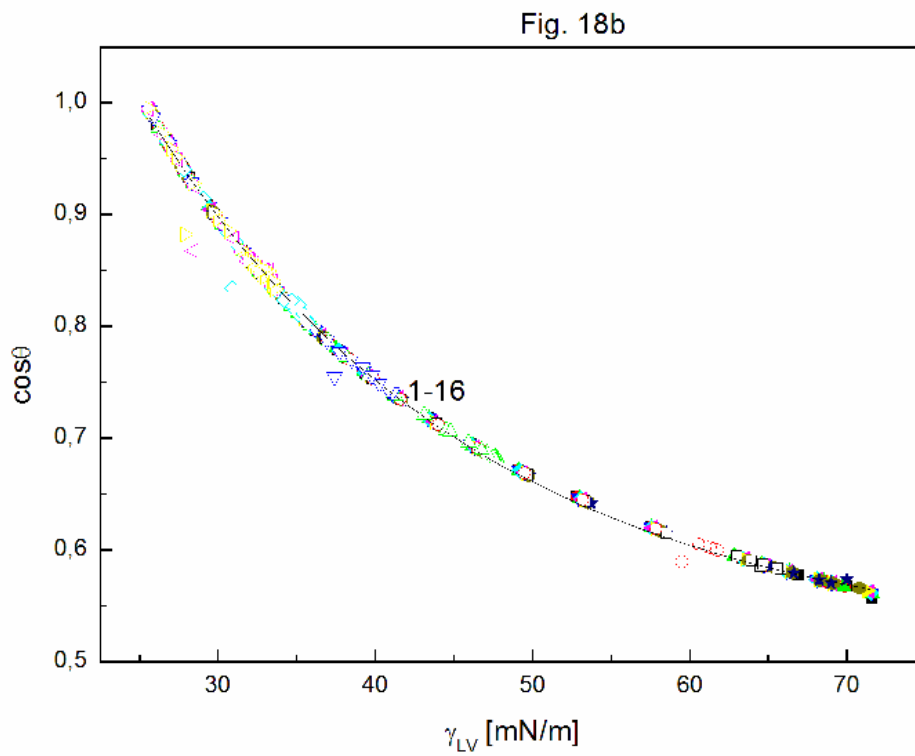
Fig. S8b. A plot of adhesion tension ($\gamma_{LV}\cos\theta$) for PTFE vs. the solution surface tension (γ_{LV}) at the constant ET concentration. The points correspond to the RL concentration form 0 to 40 mg/dm^3 and constant ET concentration from 0 to 17.13 M.
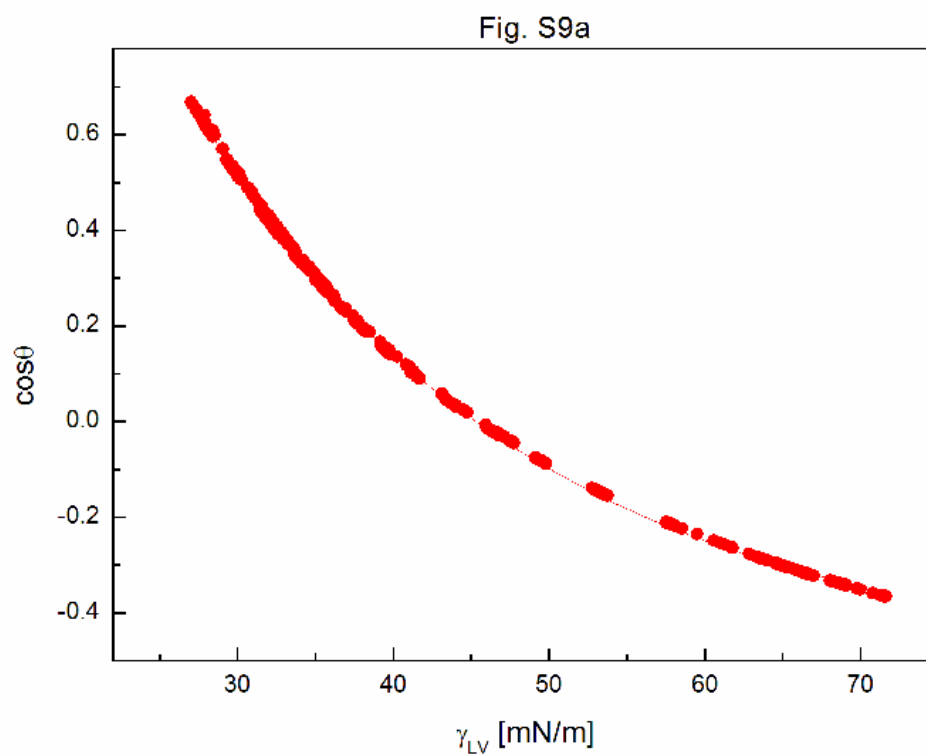
Fig. S9a. A plot of the cosine of the contact angle (cosθ) for PTFE vs. the solution surface tension (γ_{LV}) at the constant RL concentration. The points correspond to the ET concentration from 0 to 17.13 M at the constant RL concentration form 0 to 40 mg/dm^3.
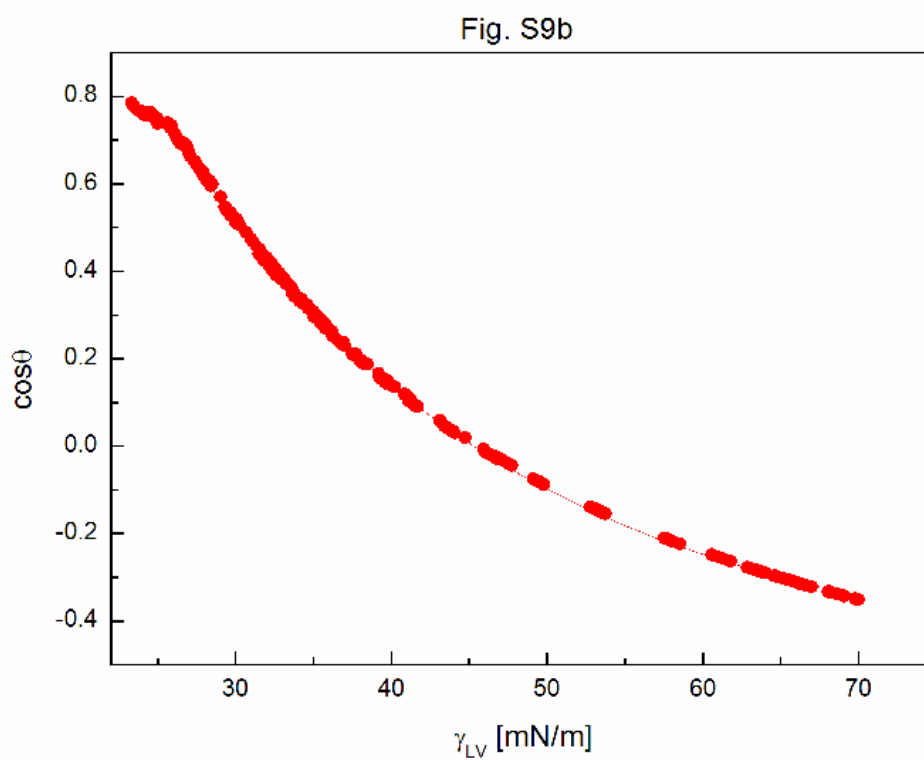
Fig. S9b. A plot of cosine of the contact angle (cosθ) for PTFE vs. the solution surface tension (γ_{LV}) at the constant ethanol concentration. The points correspond to the RL concentration form 0 to 40 mg/dm^3 and constant ET concentration from 0 to 17.13 M.
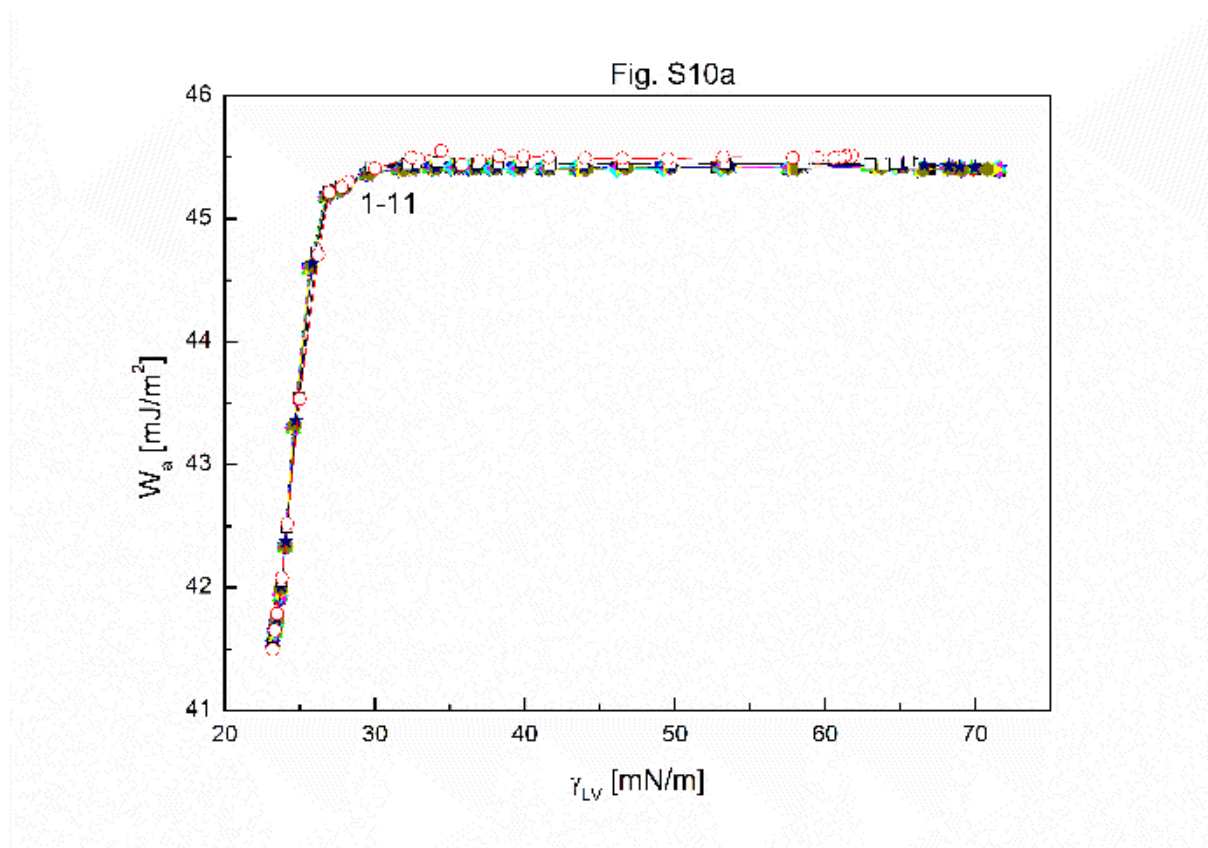
Fig. S10a. A plot of adhesion work of solution to PTFE (w_a) vs. the solution surface tension (γ_{LV}). Curves 1 – 11 correspond to the constant RL concentration equal to 0.0002; 0.0005; 0.00125; 0003; 0.00625; 0.01; 0.02; 0.05; 0.1; 0.5 and 1 mg/dm^3.
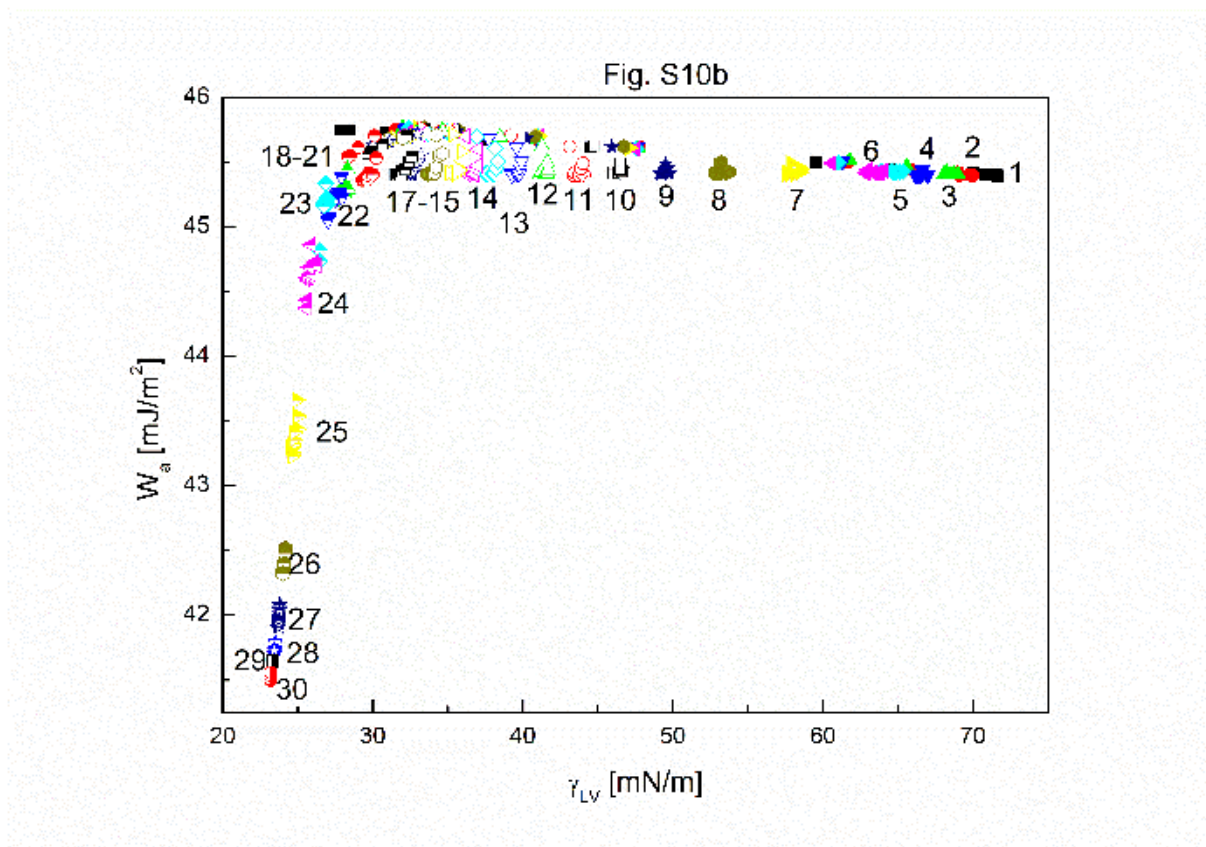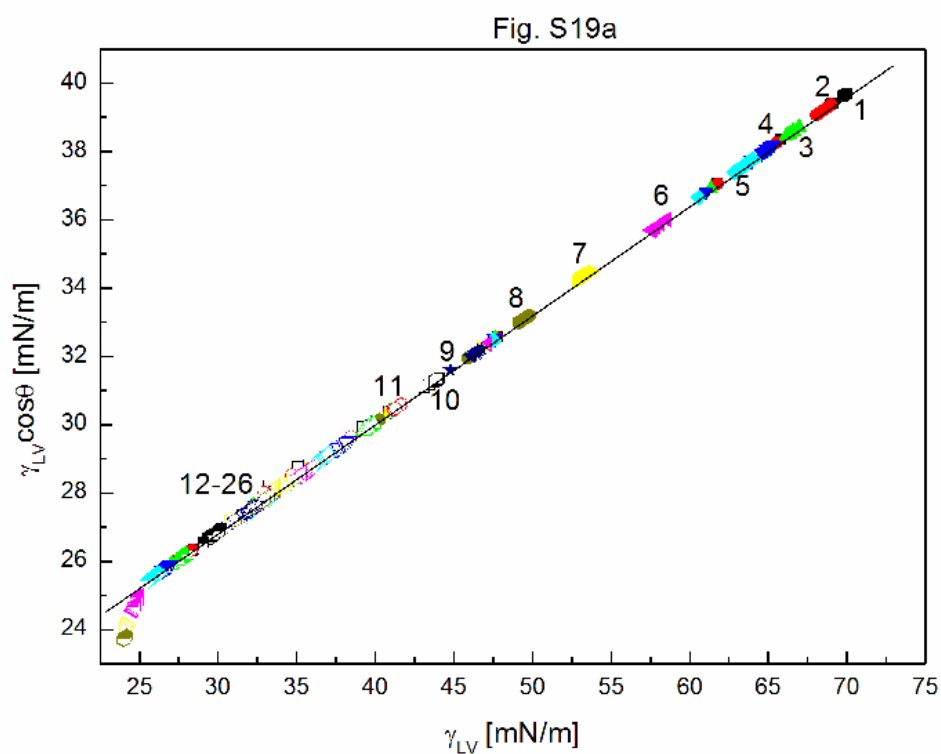
Fig. S10b. A plot of adhesion work of solution to PTFE (w_a) vs. the solution surface tension (γ_{LV}). Curves 1 – 30 correspond to the constant ET concentration equal to 0; 0.06692; 0.1338; 0.2677; 0.4015; 0.535; 1.0706; 1.6062; 2.1416; 2.677; 3.2124; 3.7478; 4.2832; 4.8185; 5.3538; 5.8893; 6.6925; 7.7245; 8.5664; 10.2797; 11.968; 12.145; 13.3794; 14.5696; 15.4064; 16.084; 16.3777; 16.648; 16.8988 and 17.13 M.
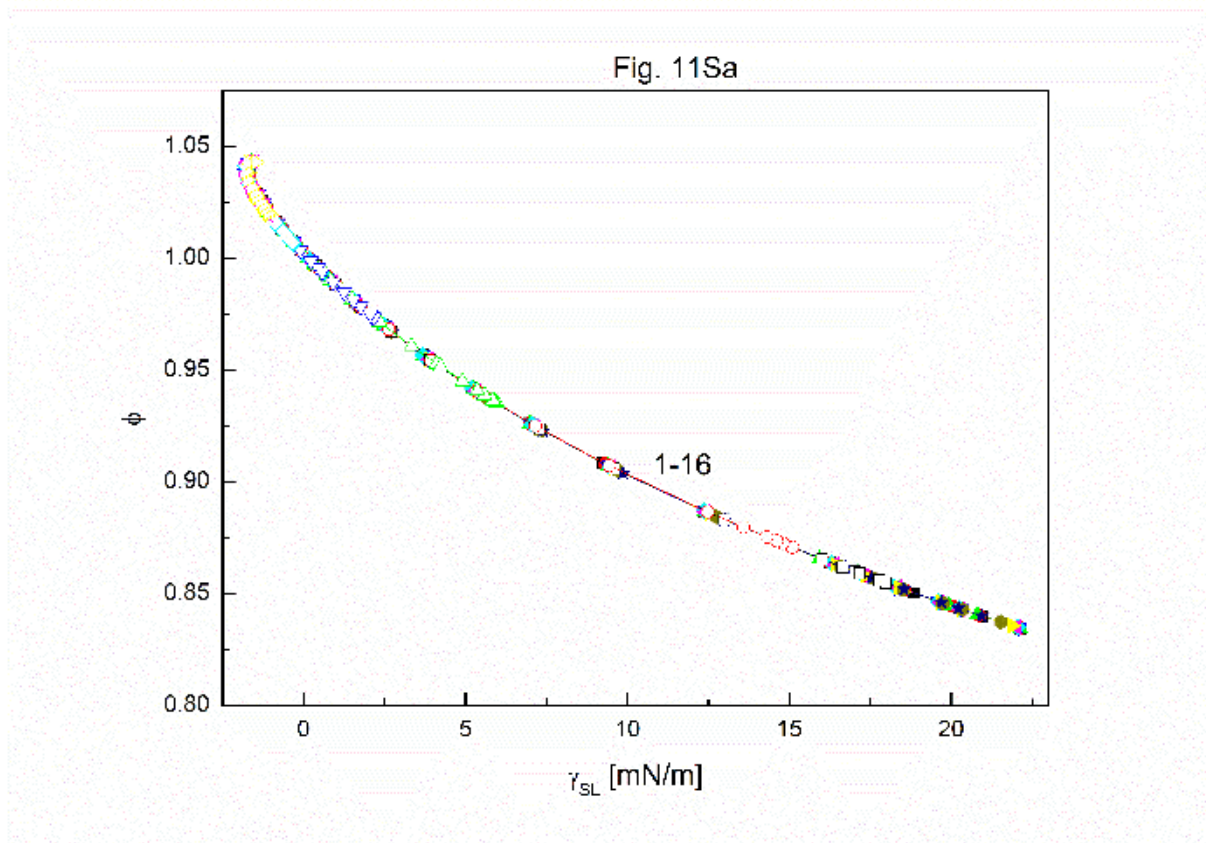
Fig. S11a. A plot of parameter ϕ calculated from Eq. (14) for PMMA vs. the PMMA-solution interface tension (γ_{SL}). Curves 1 – 16 correspond to the constant RL concentration equal to 0.0002; 0.0005; 0.00125; 0003; 0.00625; 0.01; 0.02; 0.05; 0.1; 0.5; 1; 5; 10; 20; 30 and 40 mg/dm^3.
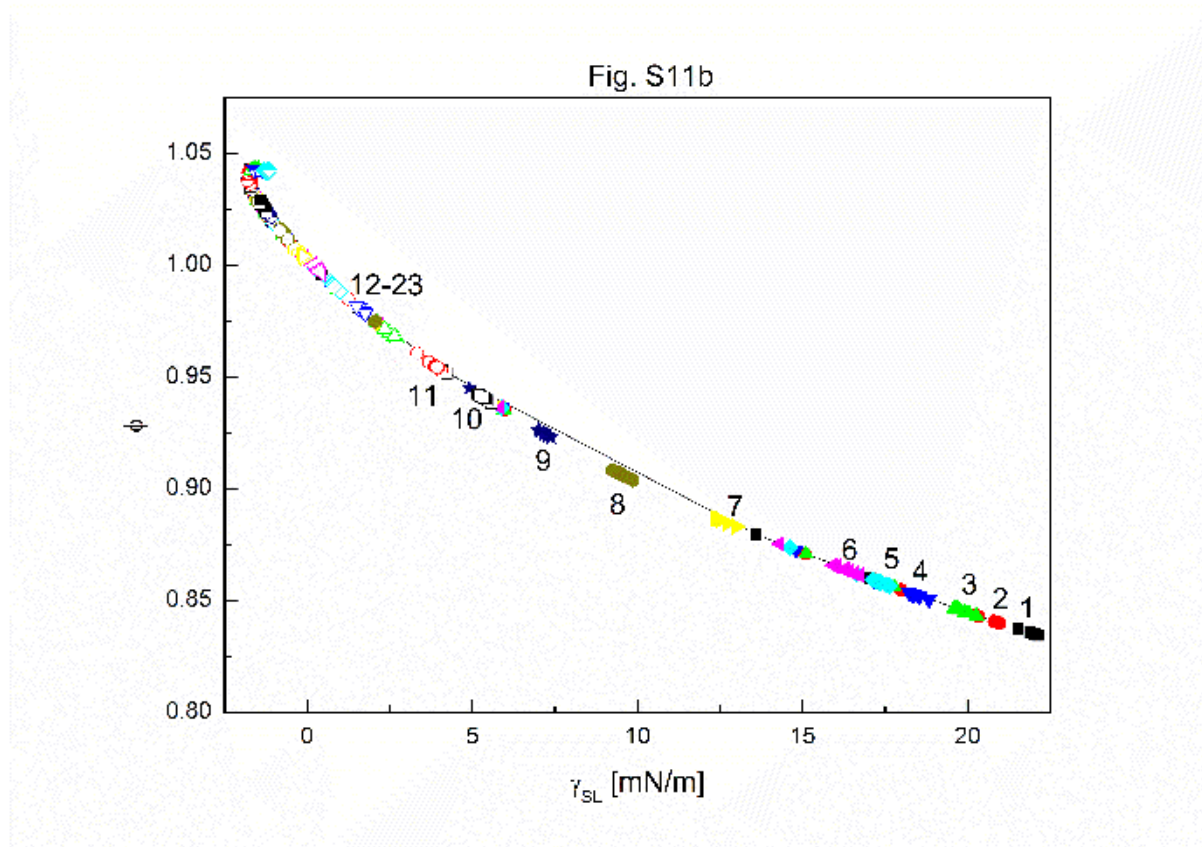
Fig. S11b. A plot of parameter ϕ calculated from Eq. (14) for PMMA vs. PMMA-solution interface tension (γ_{SL}). Curves 1 – 23 correspond to the constant ET concentration equal to 0; 0.06692; 0.1338; 0.2677; 0.4015; 0.535; 1.0706; 1.6062; 2.1416; 2.677; 3.2124; 3.7478; 4.2832; 4.8185; 5.3538; 5.8893; 6.6925; 7.7245; 8.5664; 10.2797; 11.968; 12.145 and 13.3794 M
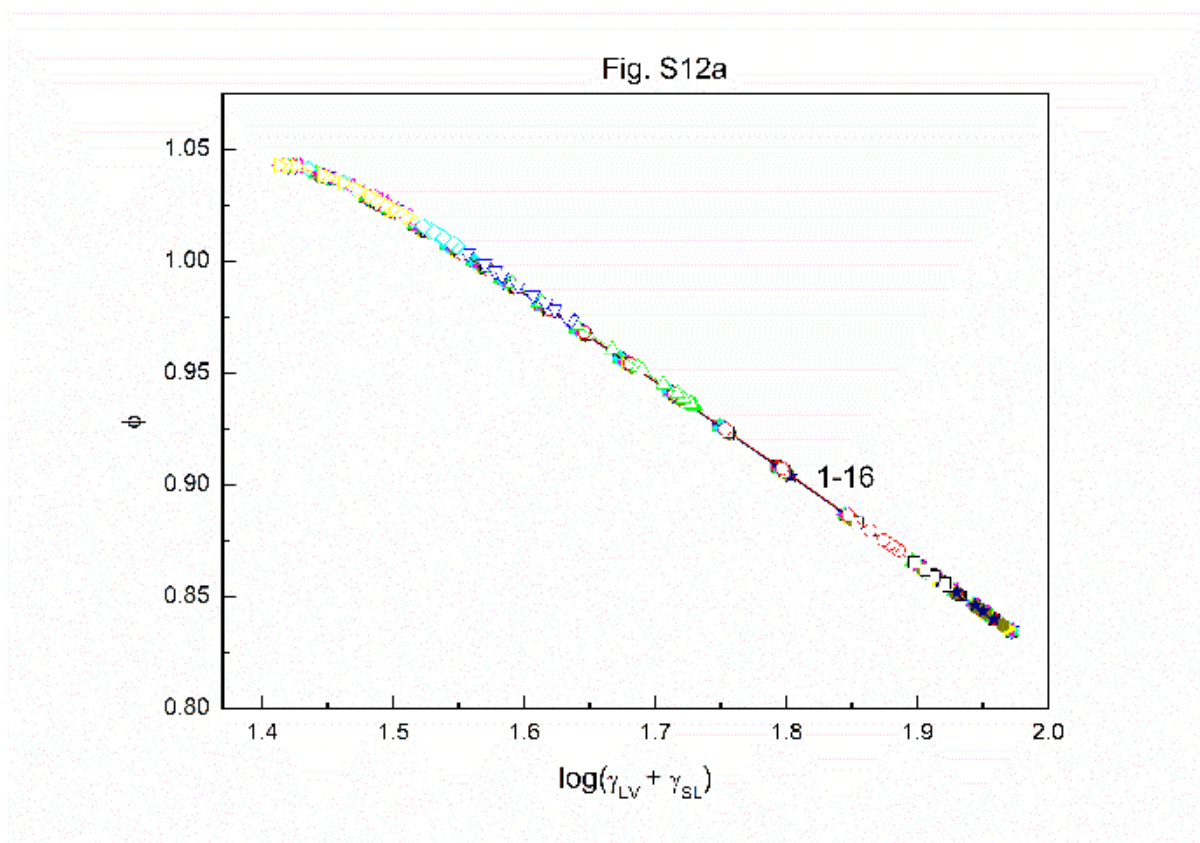
Fig. S12a. A plot of parameter φ calculated from Eq. (14) for PMMA vs. the logarithm of the sum of solution surface tension and PMMA-solution interface tension ($\log(\gamma_{LV} + \gamma_{SL})$). Curves 1 – 16 correspond to the constant RL concentration equal to 0.0002; 0.0005; 0.00125; 0003; 0.00625; 0.01; 0.02; 0.05; 0.1; 0.5; 1; 5; 10; 20; 30 and 40 mg/dm^3.

Fig. S12b. A plot of parameter ϕ calculated from Eq. (14) for PMMA vs. the logarithm of the sum of solution surface tension and PMMA-solution interface tension ($\log(\gamma_{LV} + \gamma_{SL})$). Curves 1 – 23 correspond to the constant ET concentration equal to 0; 0.06692; 0.1338; 0.2677; 0.4015; 0.535; 1.0706; 1.6062; 2.1416; 2.677; 3.2124; 3.7478; 4.2832; 4.8185; 5.3538; 5.8893; 6.6925; 7.7245; 8.5664; 10.2797; 11.968; 12.145 and 13.3794 M.
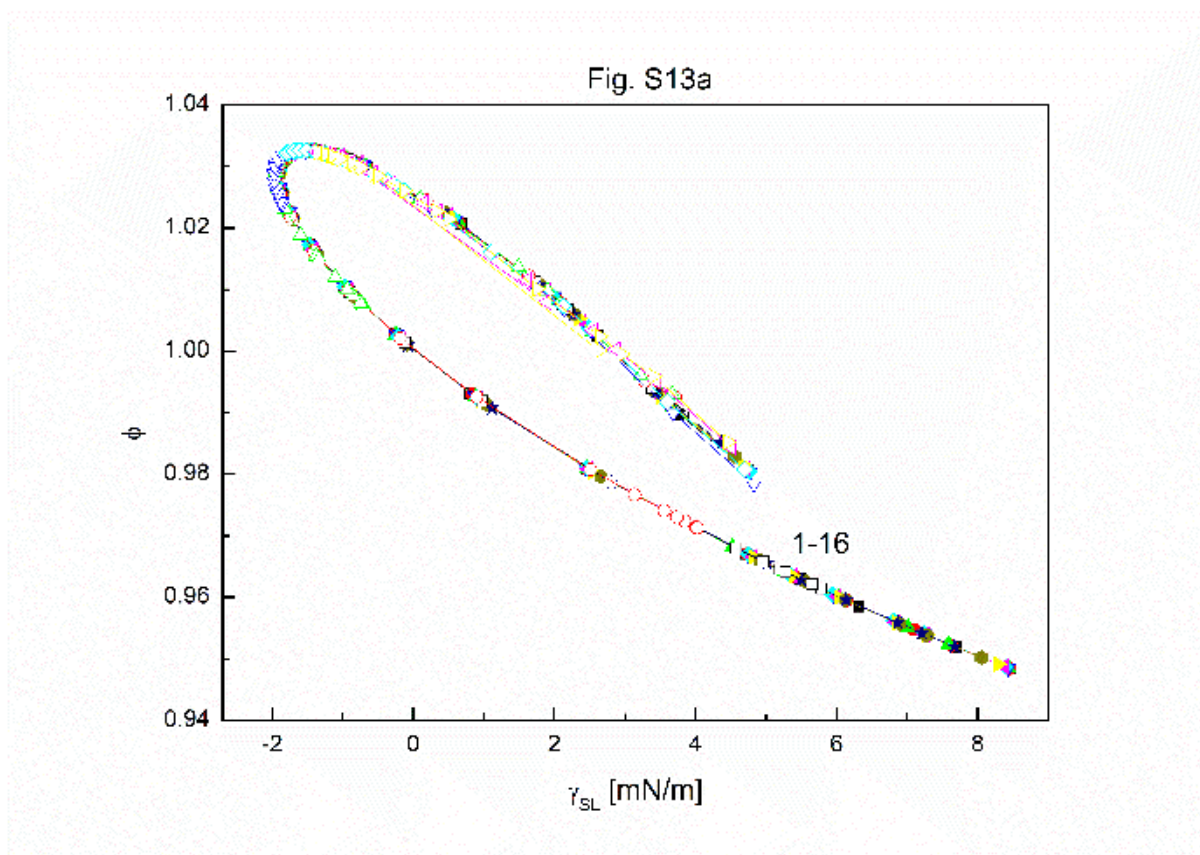
Fig. S13a. A plot of parameter ϕ calculated from Eq. (14) for quartz vs. the quartz-solution interface tension (γ_{SL}). Curves 1 – 16 correspond to the constant RL concentration equal to 0.0002; 0.0005; 0.00125; 0003; 0.00625; 0.01; 0.02; 0.05; 0.1; 0.5; 1; 5; 10; 20; 30 and 40 mg/dm^3.
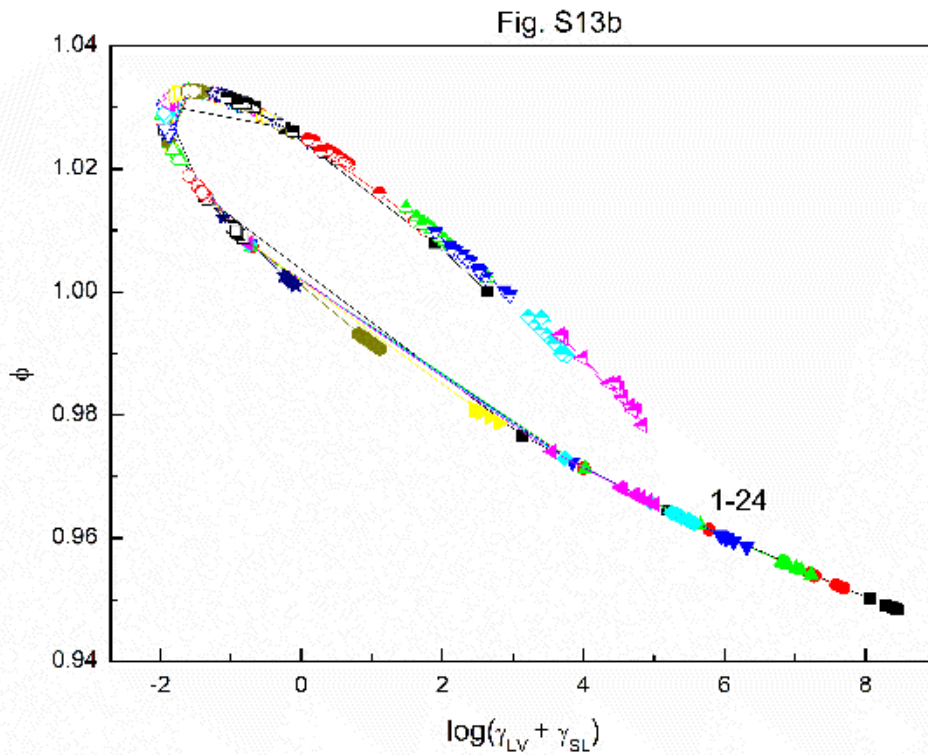
Fig. S13b. A plot of parameter ϕ calculated from Eq. (14) for quartz vs. quartz-solution interface tension (γ_{SL}). Curves 1 – 24 correspond to the constant ET concentration equal to 0; 0.06692; 0.1338; 0.2677; 0.4015; 0.535; 1.0706; 1.6062; 2.1416; 2.677; 3.2124; 3.7478; 4.2832; 4.8185; 5.3538; 5.8893; 6.6925; 7.7245; 8.5664; 10.2797; 11.968; 12.145, 13.3794 and 14.5696M.
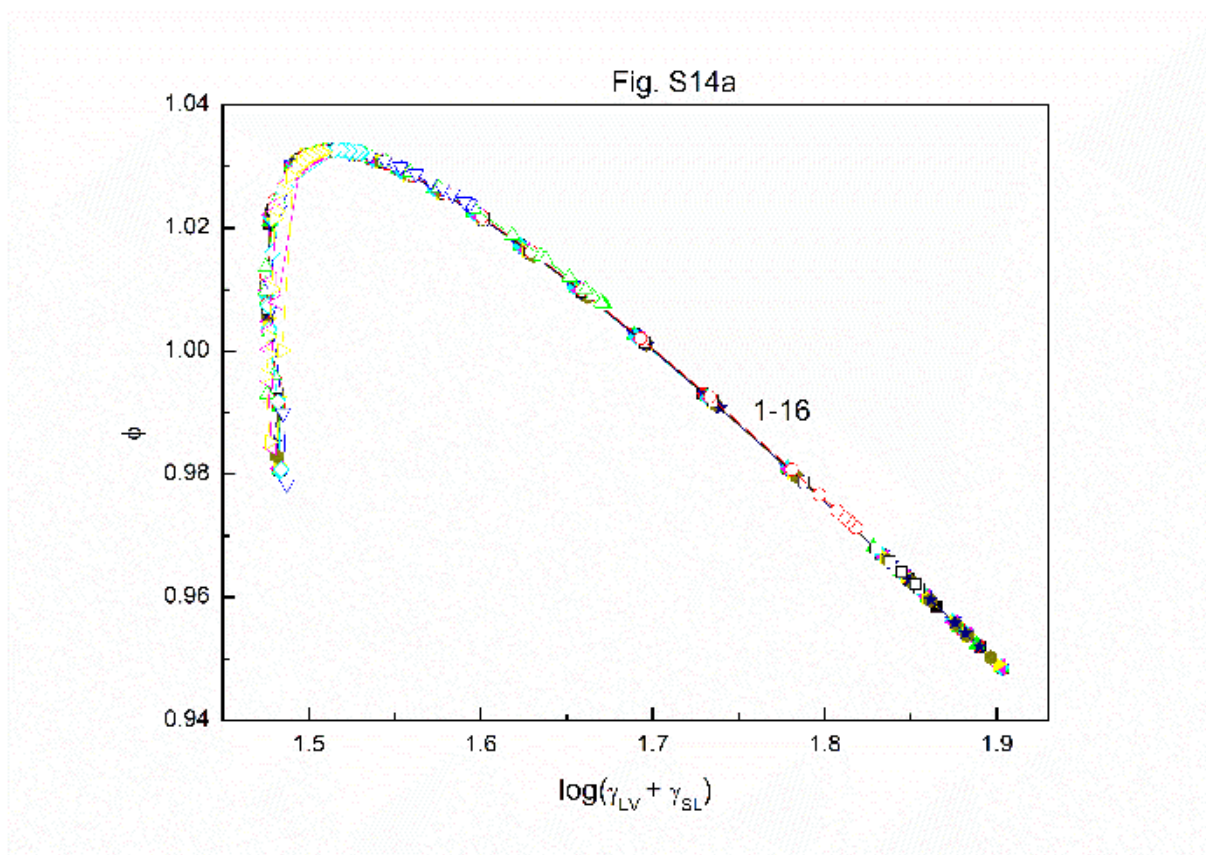
Fig. S14a. A plot of parameter ϕ calculated from Eq. (14) for quartz vs. the logarithm of the sum of solution surface tension and quartz-solution interface tension ($\log(\gamma_{LV} + \gamma_{SL})$). Curves 1 – 16 correspond to the constant RL concentration equal to 0.0002; 0.0005; 0.00125; 0003; 0.00625; 0.01; 0.02; 0.05; 0.1; 0.5; 1; 5; 10; 20; 30 and 40 mg/dm³.
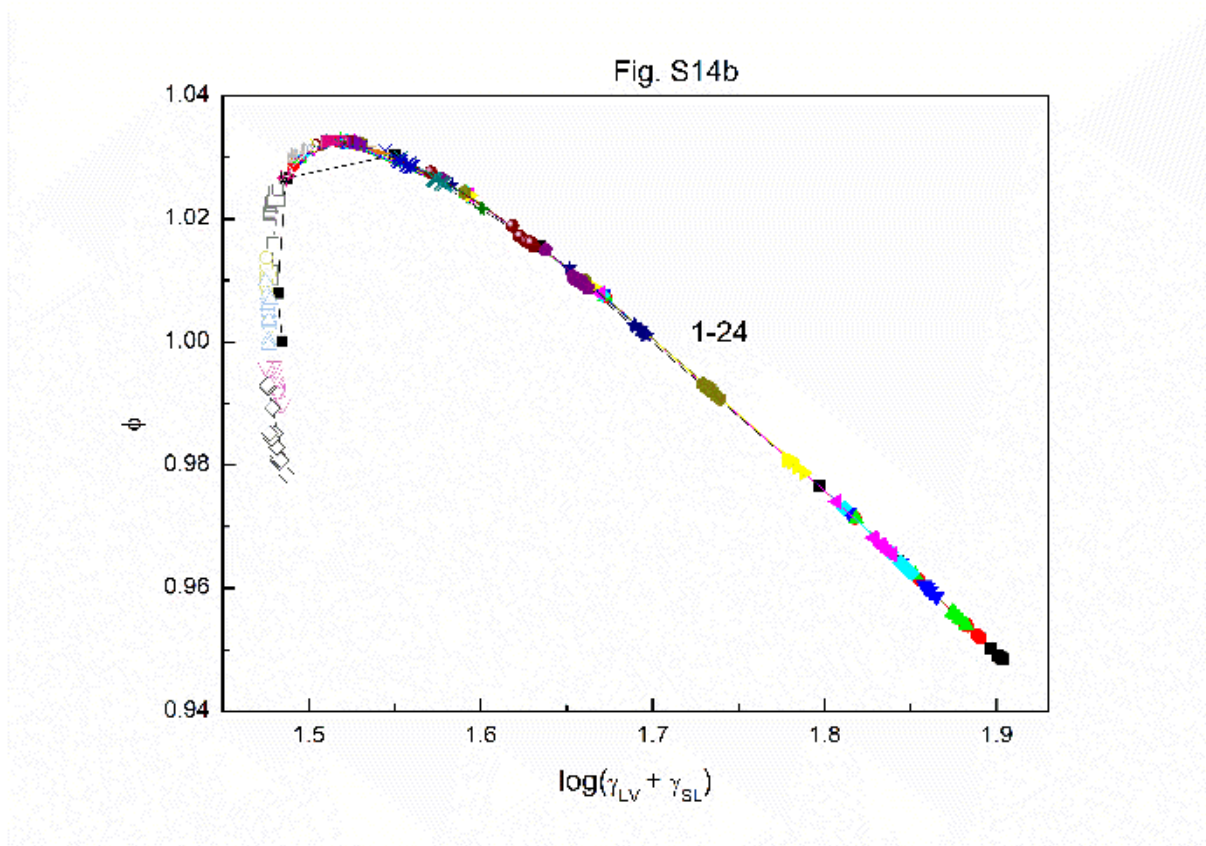
Fig. S14b. A plot of parameter ϕ calculated from Eq. (14) for quartz vs. the logarithm of the sum of solution surface tension and quartz-solution interface tension ($\log(\gamma_{LV} + \gamma_{SL})$). Curves 1 – 24 correspond to the constant ET concentration equal to 0; 0.06692; 0.1338; 0.2677; 0.4015; 0.535; 1.0706; 1.6062; 2.1416; 2.677; 3.2124; 3.7478; 4.2832; 4.8185; 5.3538; 5.8893; 6.6925; 7.7245; 8.5664; 10.2797; 11.968; 12.145, 13.3794 and 14.5696M.
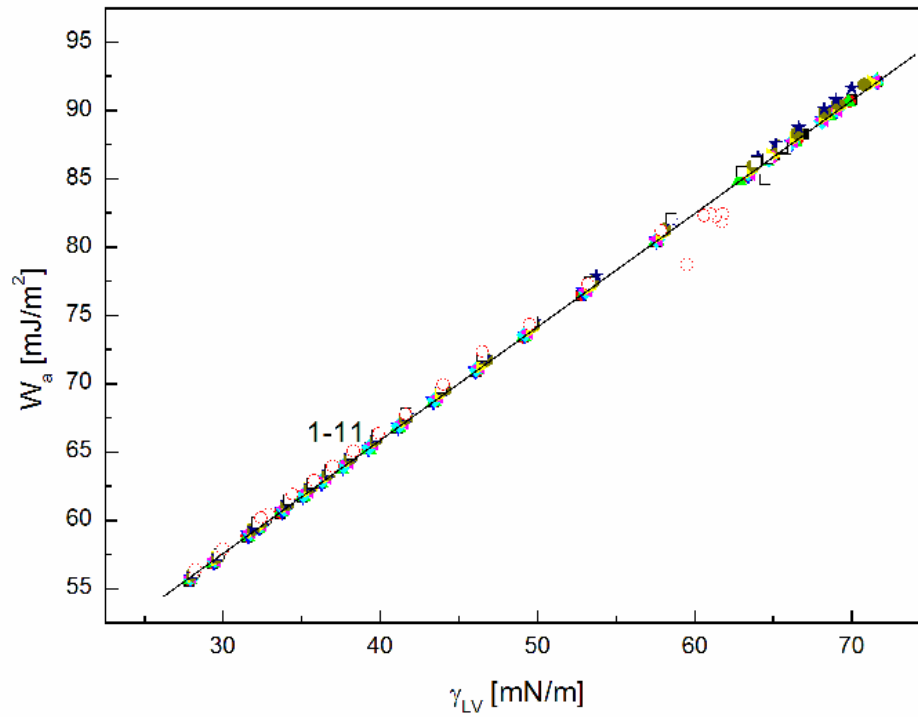
Fig. S15. A plot of adhesion work of solution to PMMA (w_a) calculated from Eq. (7) vs. the solution surface tension (γ_{LV}). Curves 1 – 11 correspond to the constant RL concentration equal to 0.0002; 0.0005; 0.00125; 0003; 0.00625; 0.01; 0.02; 0.05; 0.1; 0.5 and 1 mg/dm^3.
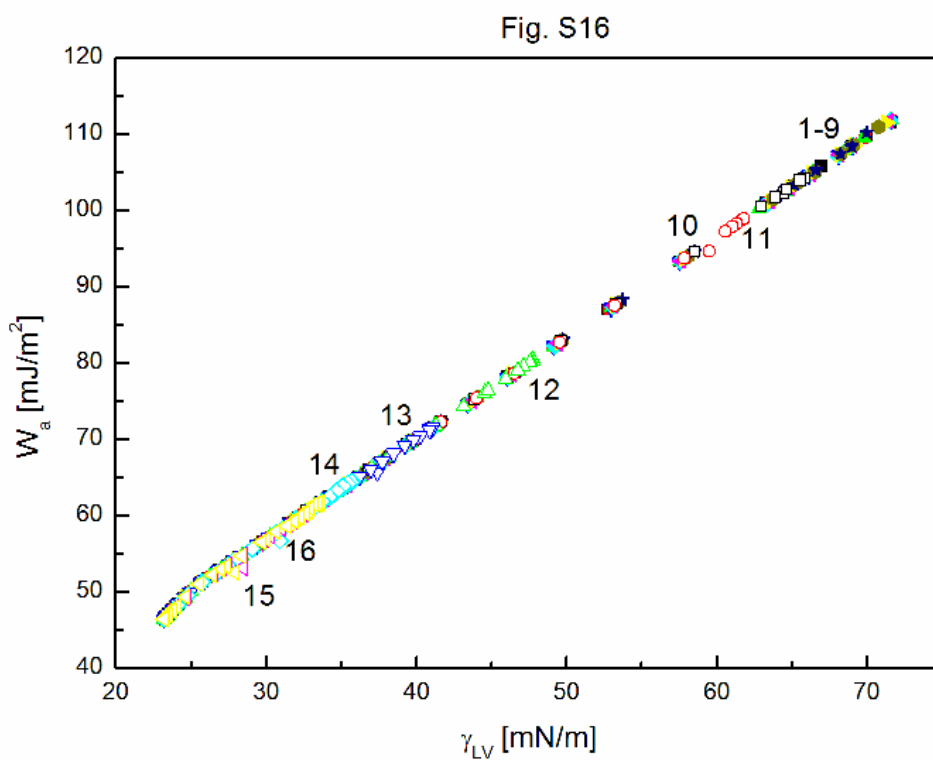
Fig. S16. A plot of adhesion work of solution to quartz (w_a) calculated from Eq. (7) vs. the solution surface tension (γ_{LV}). Curves 1 – 16 correspond to the constant RL concentration equal to 0.0002; 0.0005; 0.00125; 0003; 0.00625; 0.01; 0.02; 0.05; 0.1; 0.5; 1; 5; 10; 20; 30 and 40 mg/dm^3.
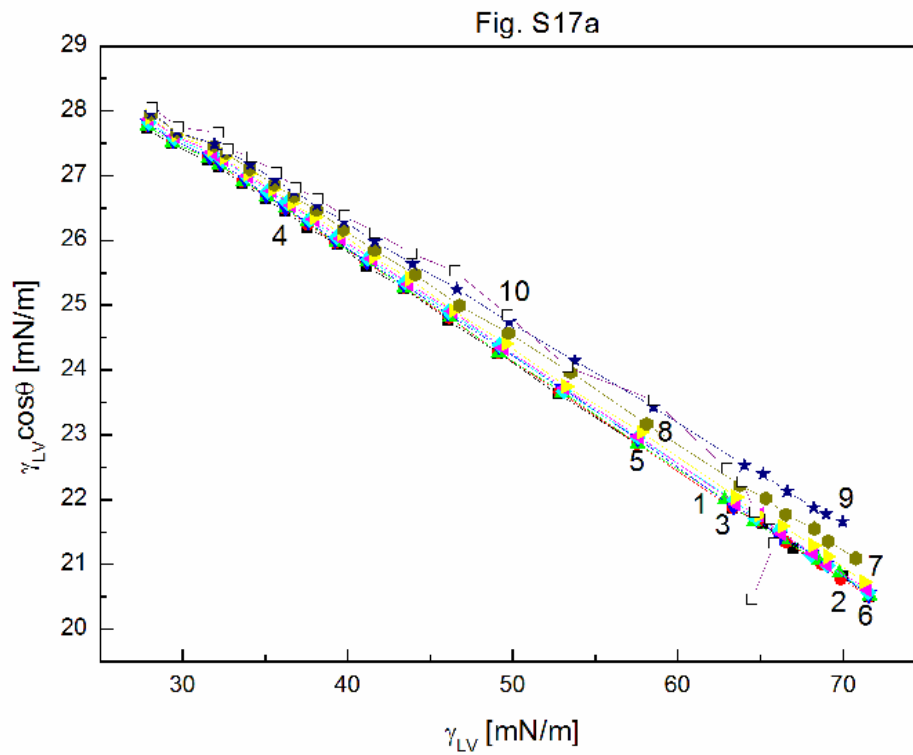
Fig. S17a. A plot of adhesion tension ($\gamma_{LV}\cos\theta$) for PMMA vs. the solution surface tension (γ_{LV}). Curves 1 – 10 correspond to the constant RL concentration equal to 0.0002; 0.0005; 0.00125; 0003; 0.00625; 0.01; 0.02; 0.05; 0.1 and 0.5 mg/dm^3.
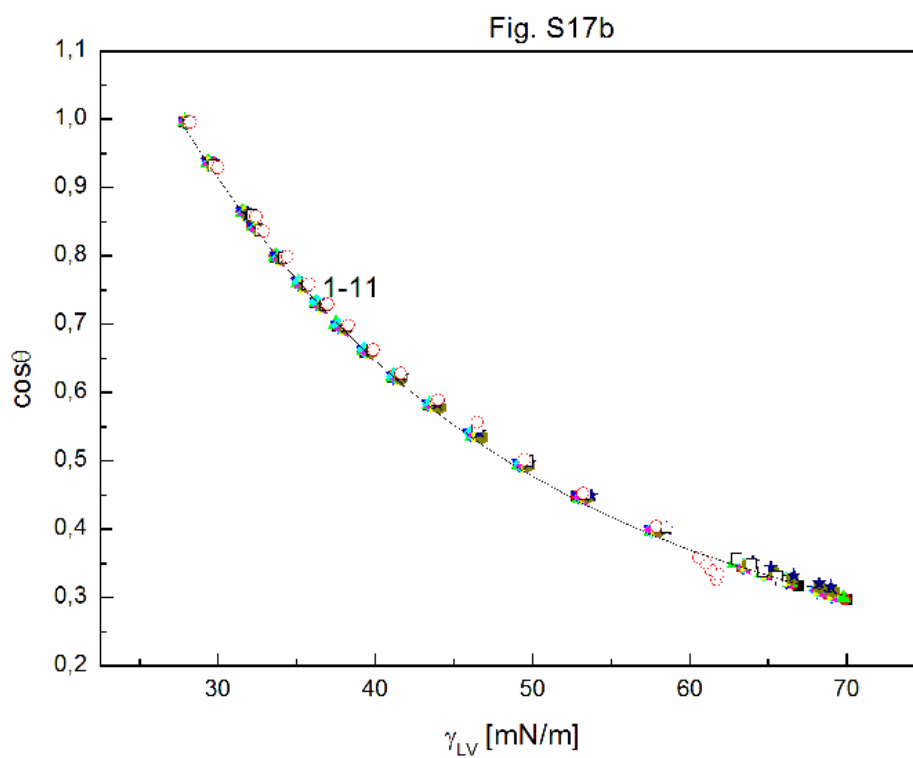
Fig. S17b. A plot of cosinus of contact angle (cosθ) for PMMA vs. the solution surface tension (γ_{LV}). Curves 1 – 11 correspond to the constant RL concentration equal to 0.0002; 0.0005; 0.00125; 0003; 0.00625; 0.01; 0.02; 0.05; 0.1; 0.5 and 1 mg/dm^3.

Fig. S18a. A plot of adhesion tension ($\gamma_{LV}\cos\theta$) for quartz vs. the solution surface tension (γ_{SL}). Curves 1 – 16 correspond to the constant RL concentration equal to 0.0002; 0.0005; 0.00125; 0003; 0.00625; 0.01; 0.02; 0.05; 0.1; 0.5; 1; 5; 10; 20; 30 and 40 mg/dm^3.

Fig. S18b. A plot of cosinus of contact angle (cosθ) for quartz vs. the solution surface tension (γ_{LV}). Curves 1 – 16 correspond to the constant RL concentration equal to 0.0002; 0.0005; 0.00125; 0003; 0.00625; 0.01; 0.02; 0.05; 0.1; 0.5; 1; 5; 10; 20; 30 and 40 mg/dm^3.

Fig. S19a. A plot of adhesion tension ($\gamma_{LV}\cos\theta$) for quartz vs. the solution surface tension (γ_{LV}). Curves 1 – 26 correspond to the constant ET concentration equal to 0.06692; 0.1338; 0.2677; 0.4015; 0.535; 1.0706; 1.6062; 2.1416; 2.677; 3.2124; 3.7478; 4.2832; 4.8185; 5.3538; 5.8893; 6.6925; 7.7245; 8.5664; 10.2797; 11.968; 12.145; 13.3794; 14.5696; 15.4064; 16.084 nad 16.3777 13 M.
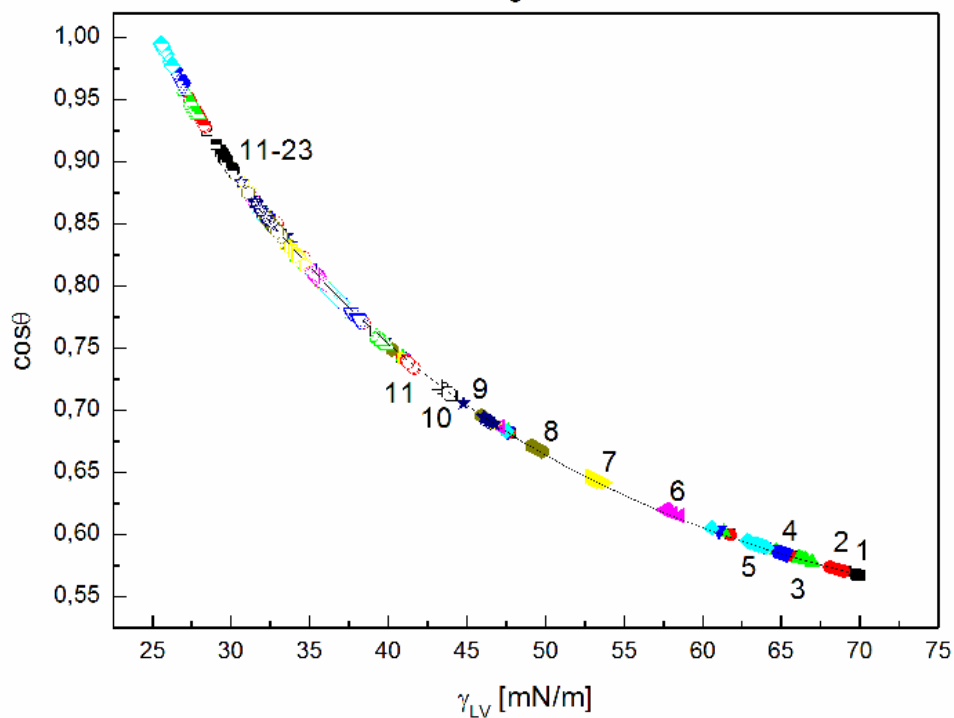
Fig. S19b. A plot of cosinus of contact angle (cosθ) for quartz vs. the solution surface tension (γ_{LV}). Curves 1 – 23 correspond to the constant ET concentration equal to 0.06692; 0.1338; 0.2677; 0.4015; 0.535; 1.0706; 1.6062; 2.1416; 2.677; 3.2124; 3.7478; 4.2832; 4.8185; 5.3538; 5.8893; 6.6925; 7.7245; 8.5664; 10.2797; 11.968; 12.145; 13.3794 and 14.5696 M.
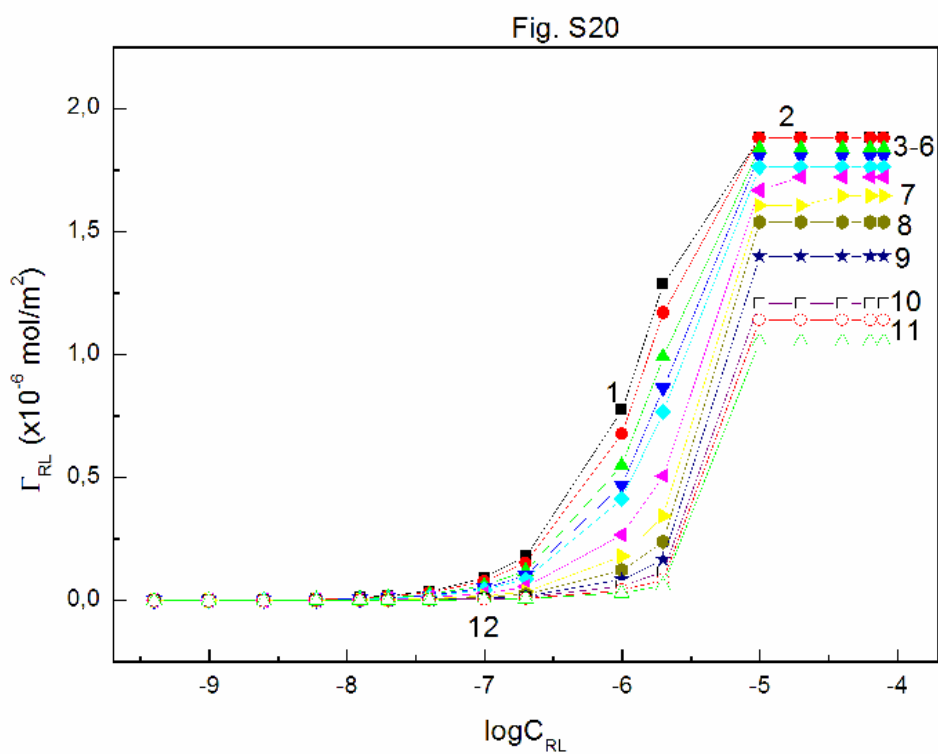
Fig. S20. A plot of RL Gibbs surface excess concentration at PTFE –solution interface (Γ_{RL}) calculated from Eq. (16) vs. the logarithm of RL concentration ($\log C_{RL}$). Curves 1 – 12 correspond to the constant ET concentration equal to 0.06692; 0.1338; 0.2677; 0.4015; 0.535; 1.0706; 1.6062; 2.1416; 2.677; 3.2124; 3.7478 and 4.2832 M.
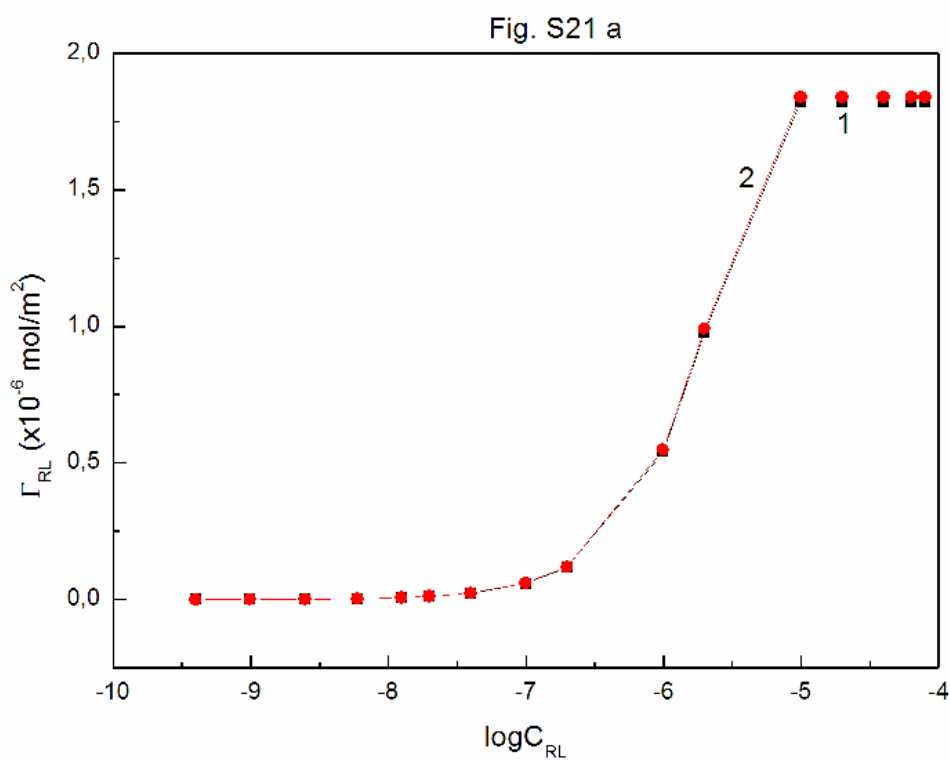
Fig. S21a. A plot of RL Gibbs surface excess concentration at (Γ_{RL}) at the solution air interface (curve 1) and at the PTFE-solution interface (curve 2) vs. the logarithm of RL concentration ($\log C_{RL}$) at the constant ET concentration equal to 0.2677 M.
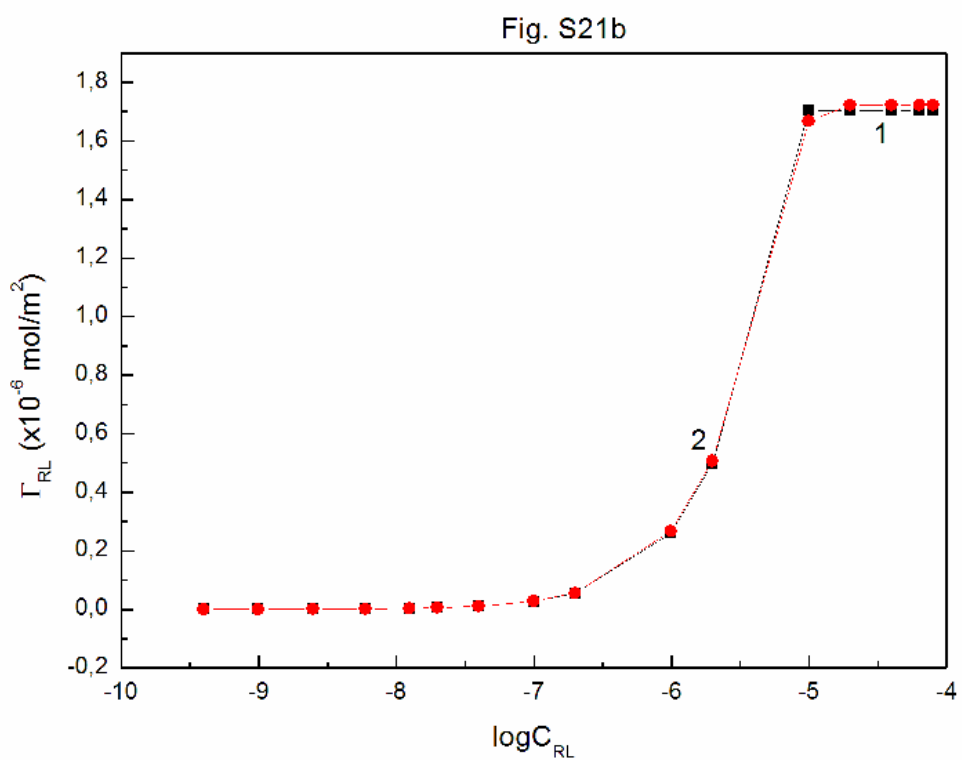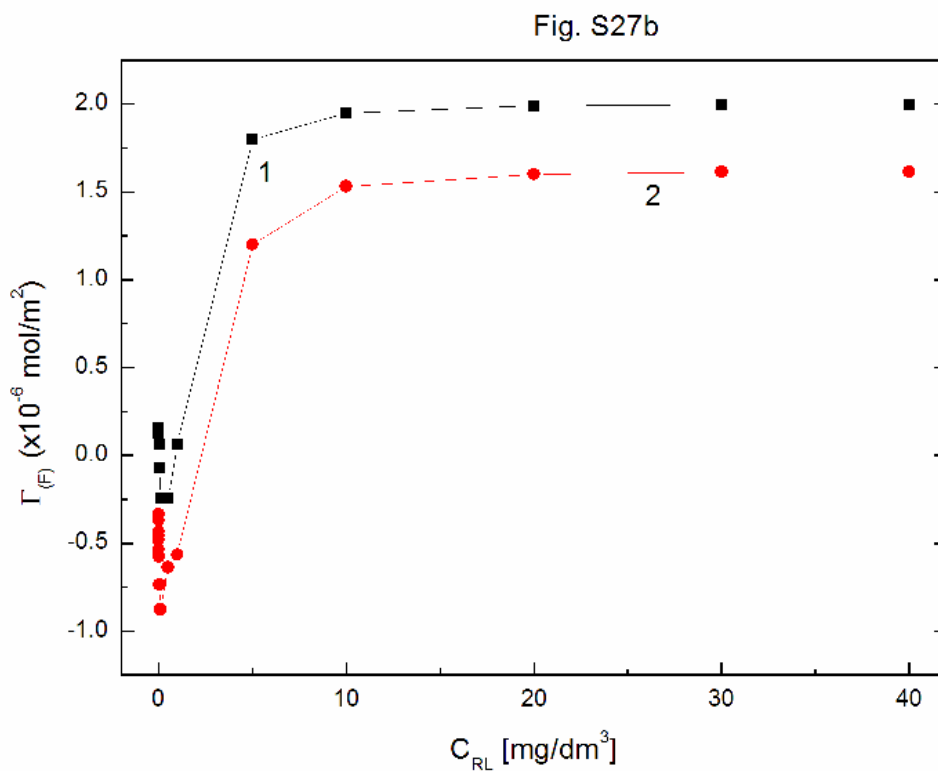
Fig. S21b. A plot of RL Gibbs surface excess concentration at (Γ_{RL}) at the solution air interface (curve 1) and at the PTFE-solution interface (curve 2) vs. the logarithm of RL concentration ($\log C_{RL}$) at the constant ET concentration equal to 1.0706 M.
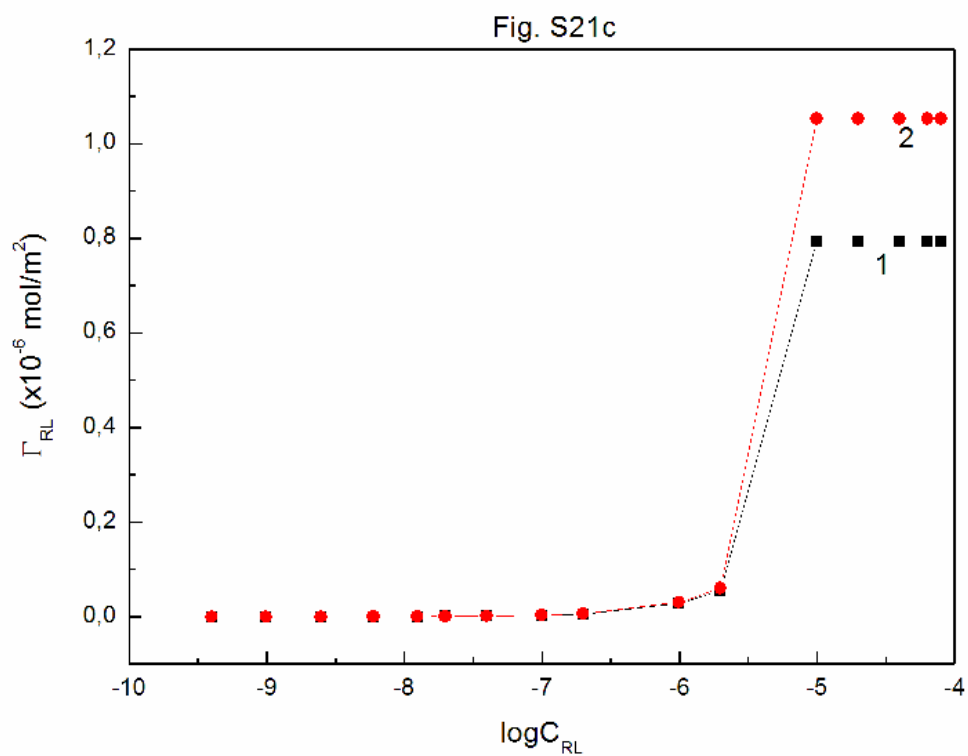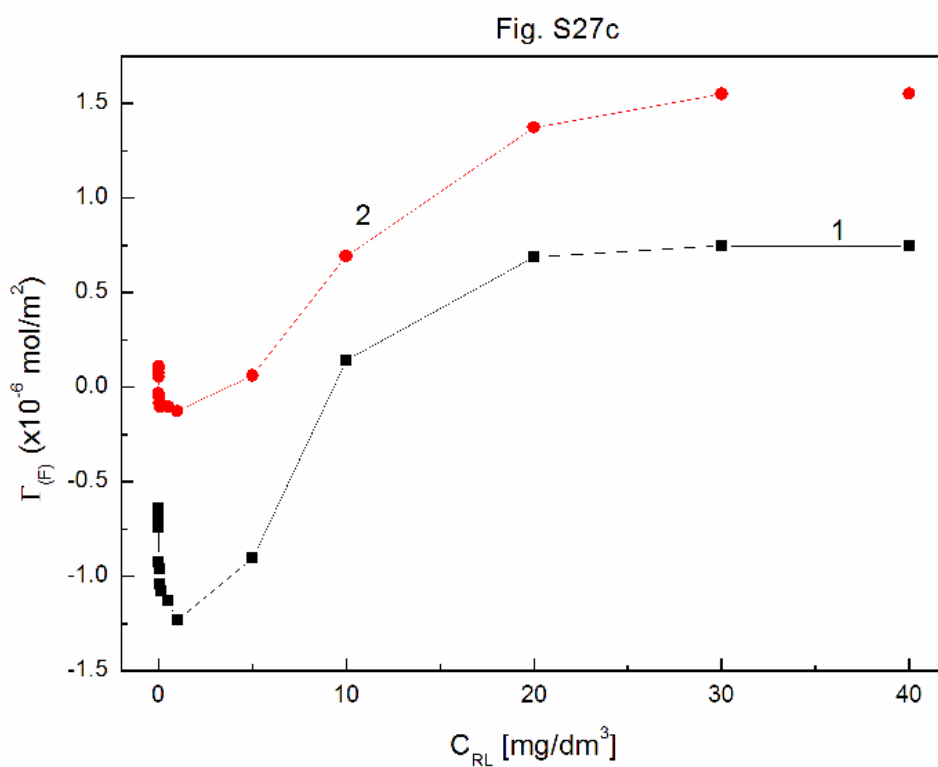
Fig. S21c. A plot of RL Gibbs surface excess concentration at (Γ_{RL}) at the solution air interface (curve 1) and at the PTFE-solution interface (curve 2) vs. the logarithm of RL concentration ($\log C_{RL}$) at the constant ET concentration equal to 4.2832 M.
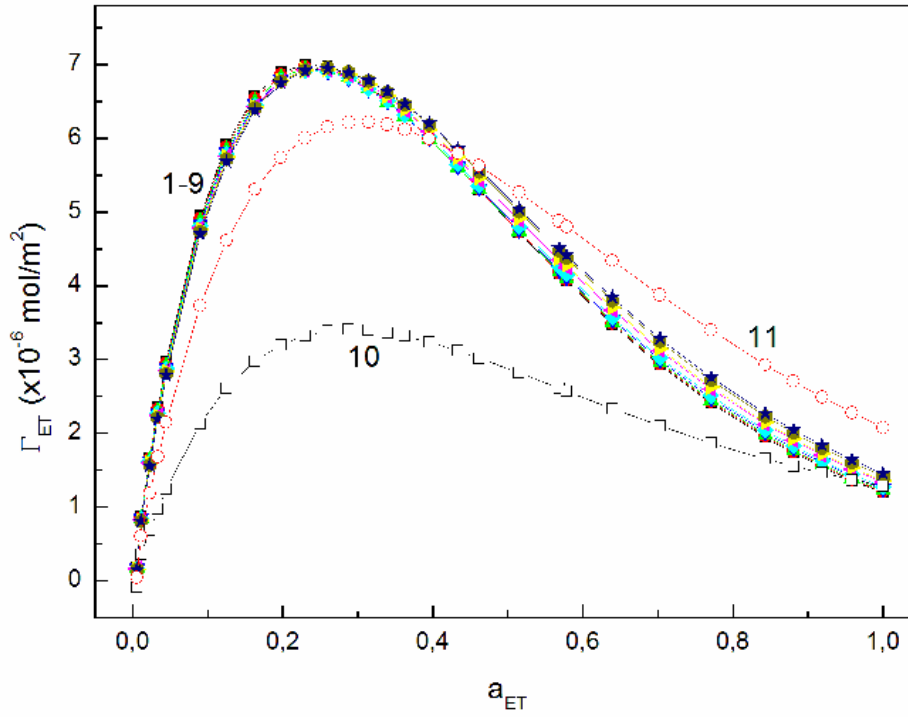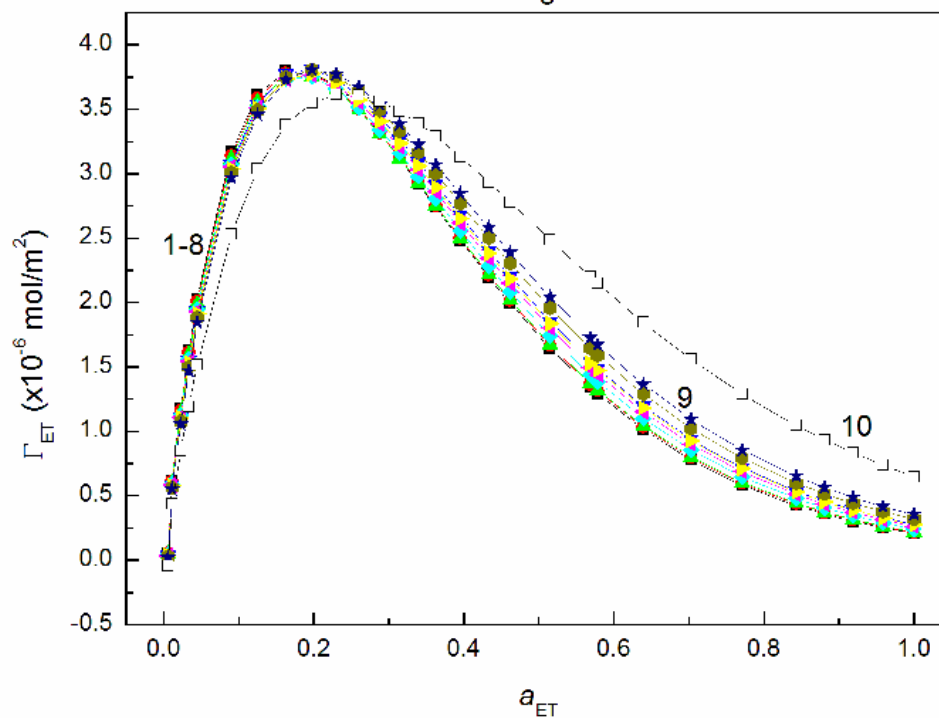
Fig. S22. A plot of ET Gibbs surface excess concentration at the PTFE-solution interface (Γ_{ET})) calculated from Eq. (16) vs. the alcohol activity (a_{ET}). Curves 1 – 11 correspond to the constant RL concentration equal to 0.0002; 0.0005; 0.00125; 0003; 0.00625; 0.01; 0.02; 0.05; 0.1; 0.5 and 1 mg/dm^3.
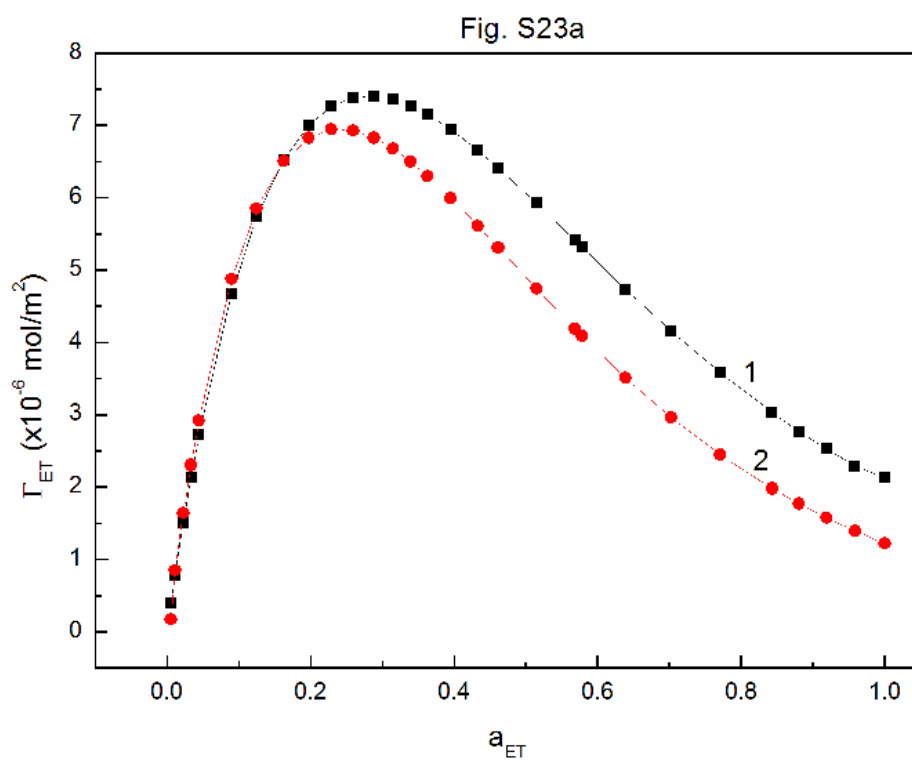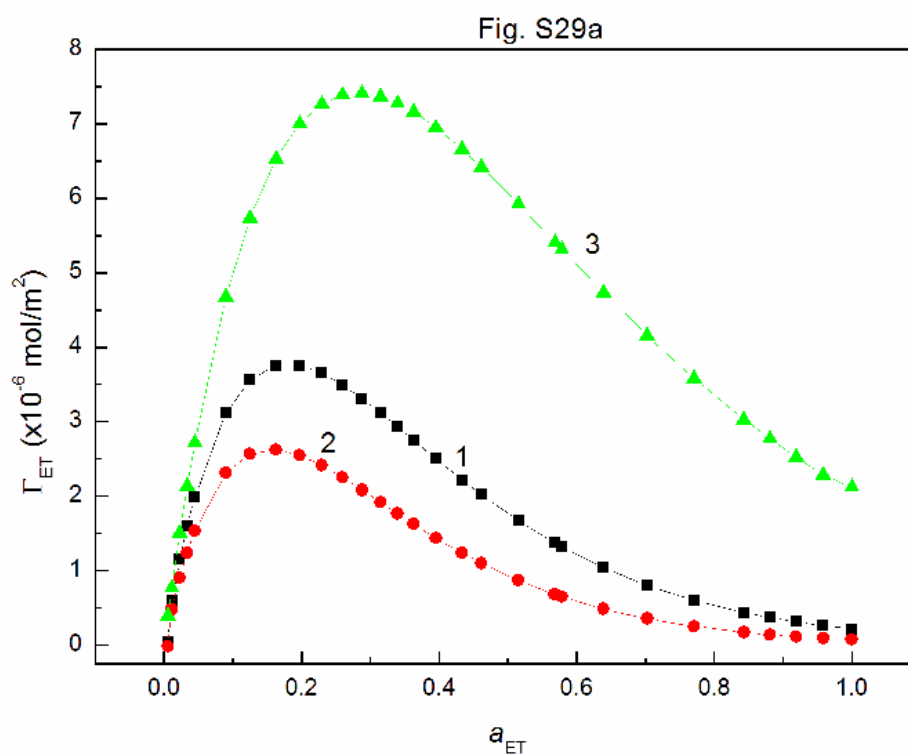
Fig. S23a. A plot of ET Gibbs surface excess concentration (Γ_{ET}) at the solution-air interface (curve 1) and at PTFE-solution interface (curve 2) vs. alcohol activity (a_{ET}) at the constant RL concentration equal to 0.00125 mg/dm^3.
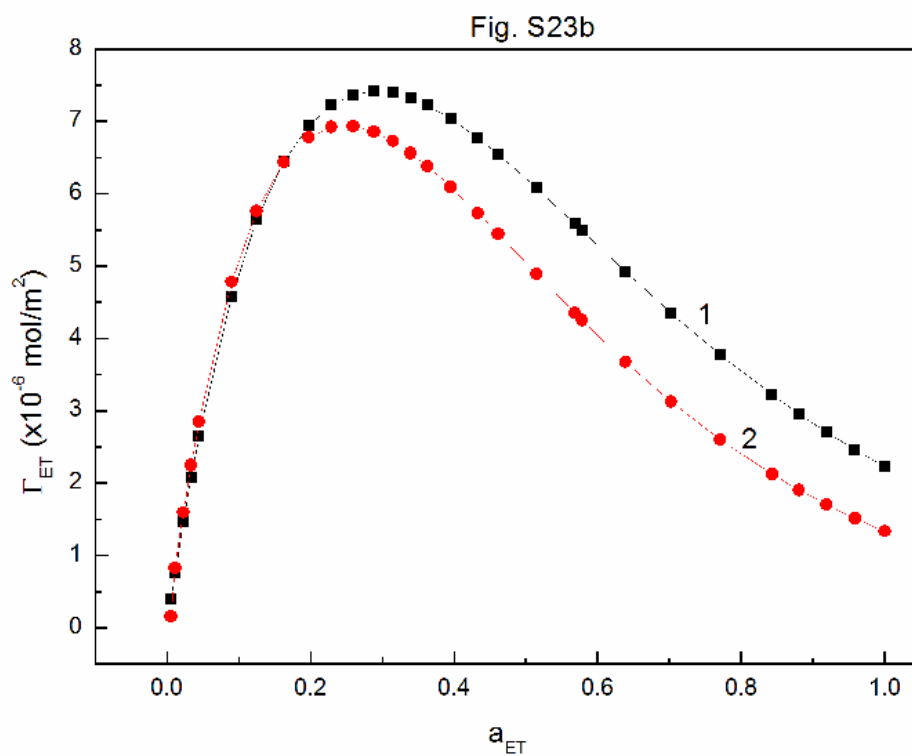
Fig. S23b. A plot of ET Gibbs surface excess concentration (Γ_{ET}) at the solution-air interface (curve 1) and at the PTFE-solution interface (curve 2) vs. the alcohol activity (a_{ET}) at the constant RL concentration equal to 0.01 mg/dm^3.
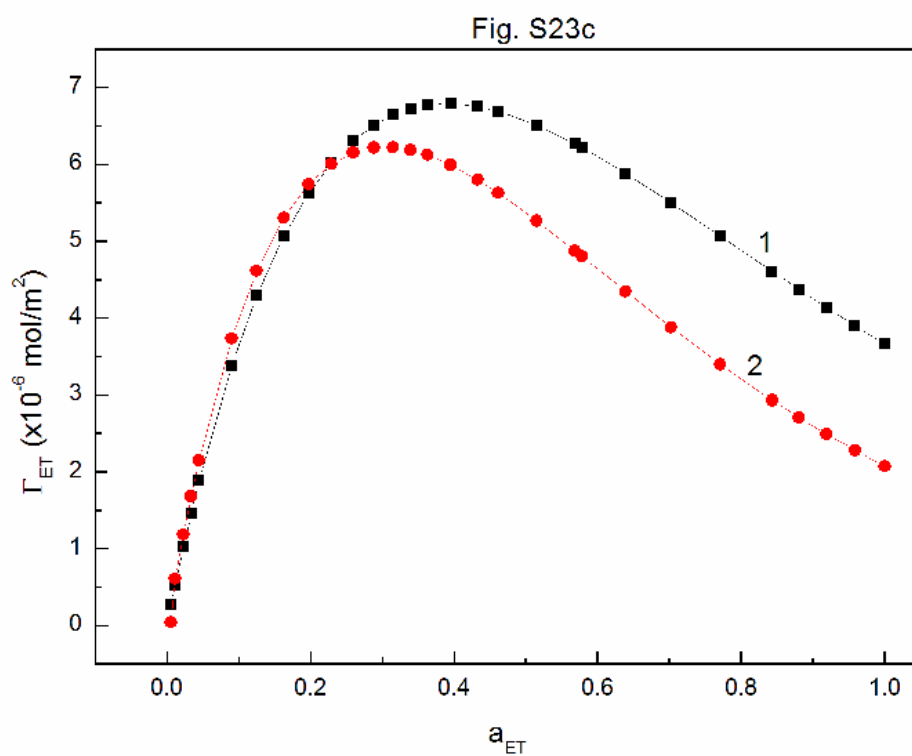
Fig. S23c. A plot of ET Gibbs surface excess concentration (Γ_{ET}) at the solution-air interface (curve 1) and at the PTFE-solution interface (curve 2) vs. the alcohol activity (a_{ET}) at the constant RL concentration equal to 1 mg/dm^3.
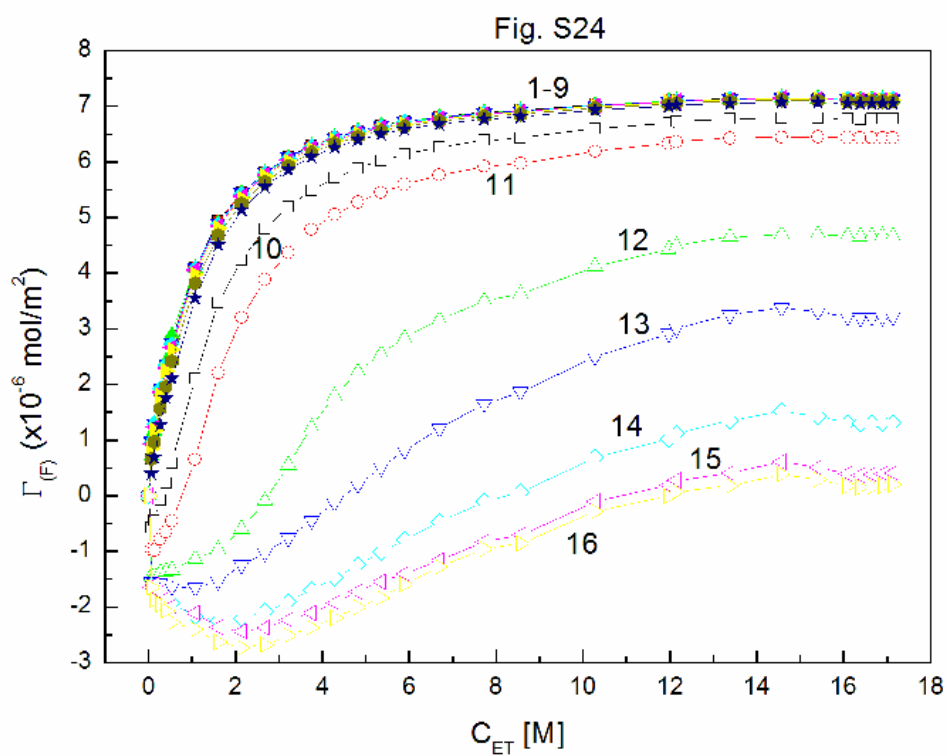
Fig. S24. A plot of Frumkin ET concentration at the PTFE-solution interface calculated from Eq. (17) vs. the ethanol concentration (C_{ET}) Curves 1 – 16 correspond to the constant RL concentration equal to 0.0002; 0.0005; 0.00125; 0003; 0.00625; 0.01; 0.02; 0.05; 0.1; 0.5; 1; 5; 10; 20; 30 and 40 mg/dm^3.
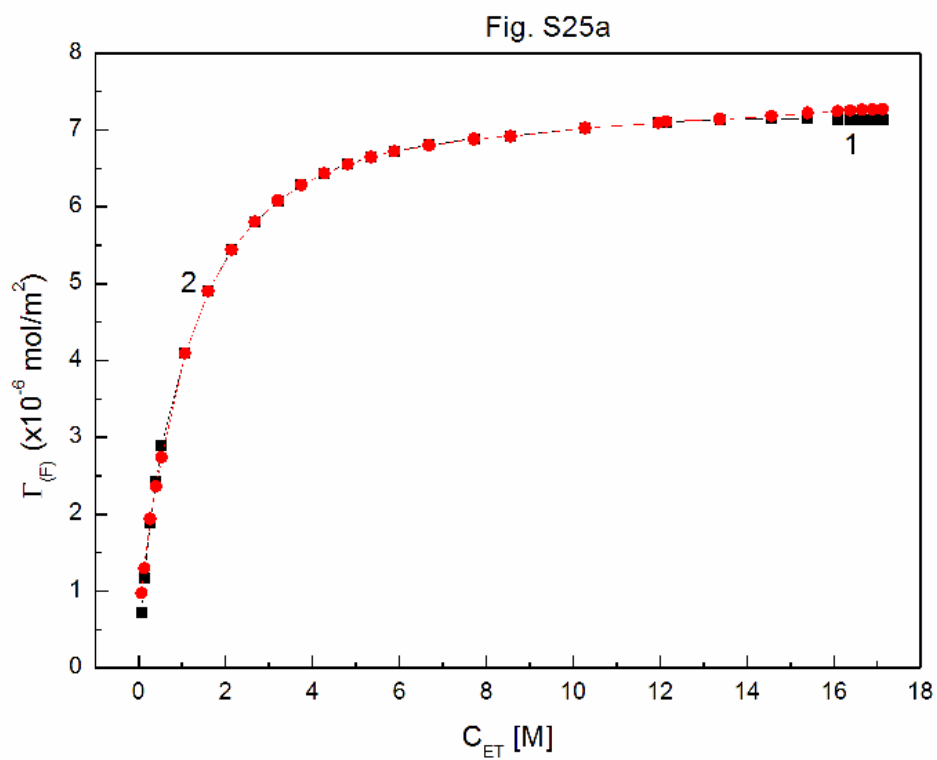
Fig. S25a. A plot of Frumkin ET concentration (Γ_{ET}) at the solution air interface (curve 1) and at the PTFE-solution interface (curve 2) vs. the alcohol concentration (C_{ET}) at the constant RL concentration equal to 0.00125 mg/dm^3.
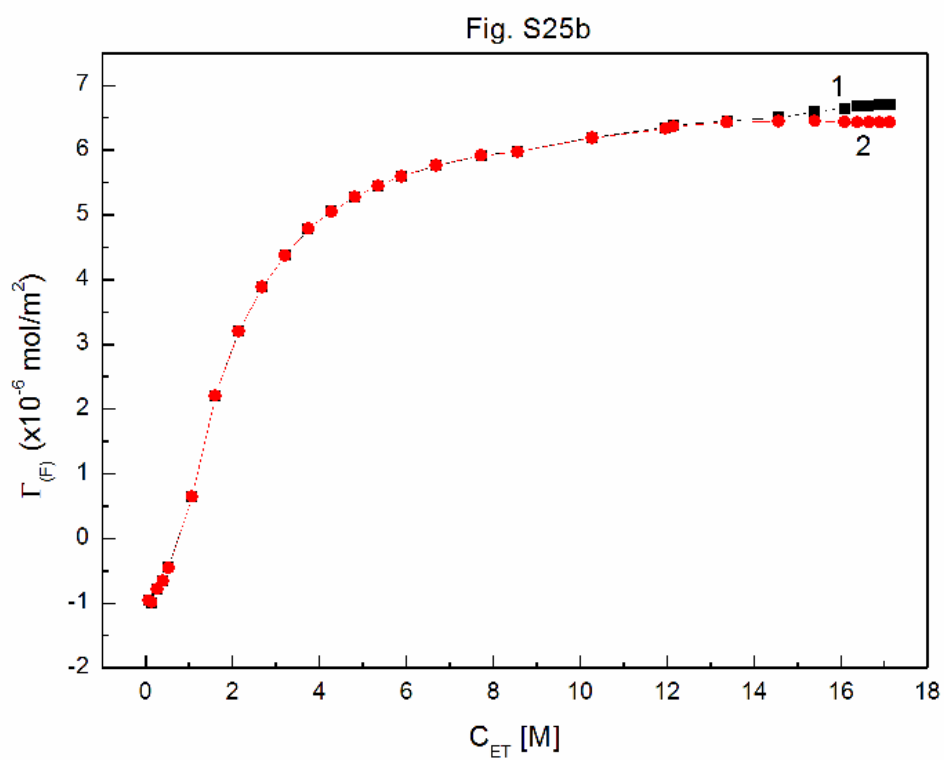
Fig. S25b. A plot of Frumkin ET concentration (Γ_{ET}) at the solution air interface (curve 1) and at the PTFE-solution interface (curve 2) vs. the alcohol concentration (C_{ET}) at the constant RL concentration equal to 1 mg/dm^3.
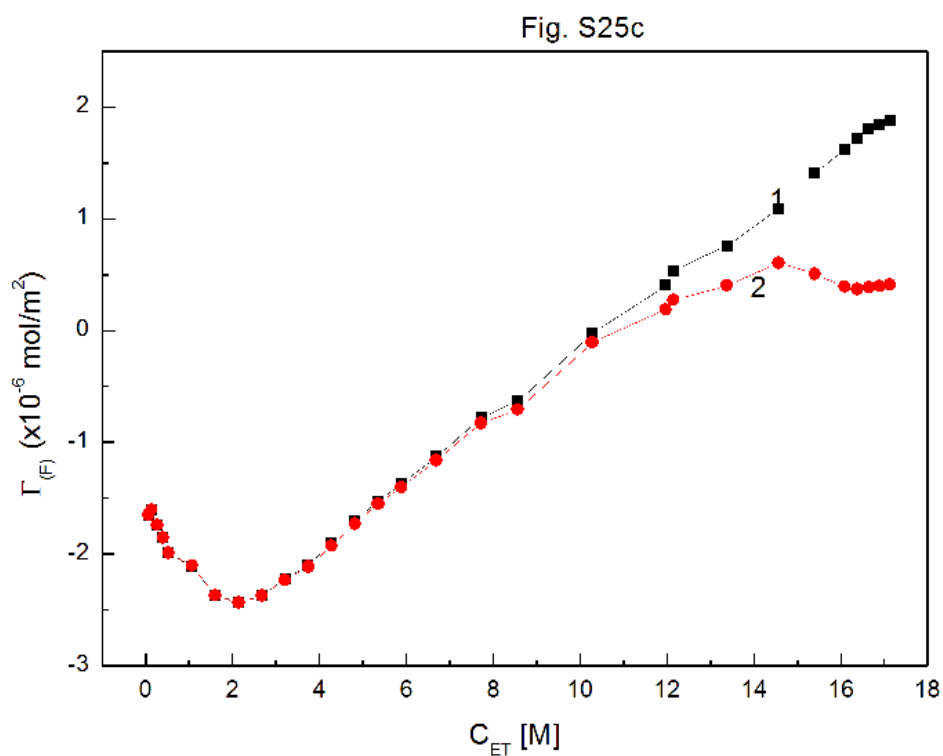
Fig. S25c. A plot of Frumkin ET concentration (Γ_{ET}) at the solution air interface (curve 1) and at the PTFE-solution interface (curve 2) vs. the alcohol concentration (C_{ET}) at the constant RL concentration equal to 30 mg/dm^3.
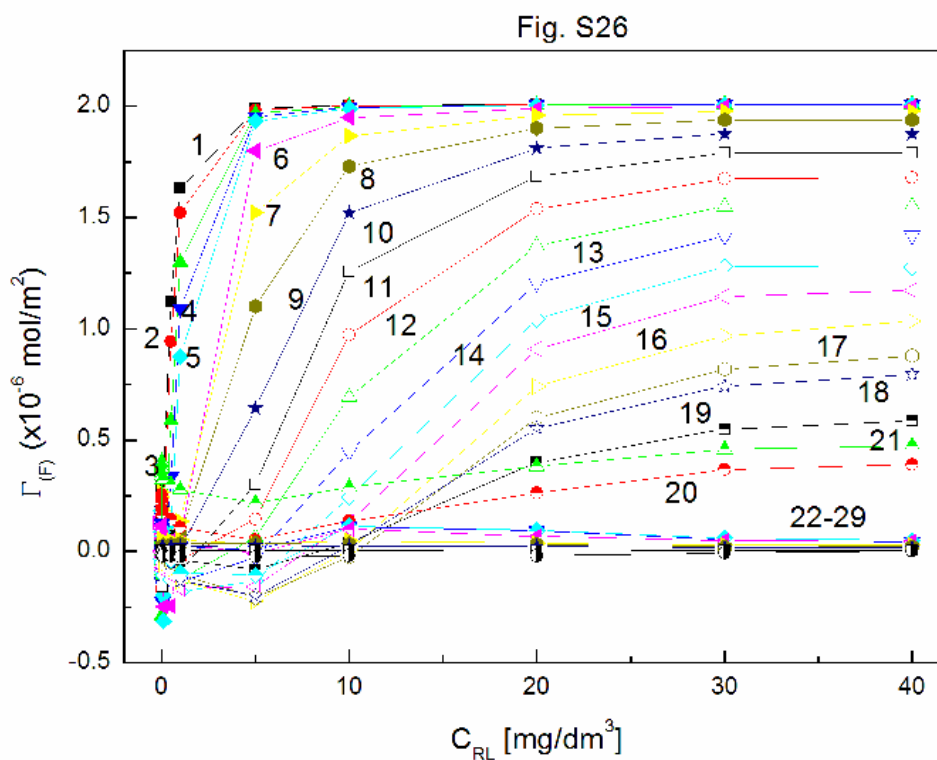
Fig. S26. A plot of Frumkin RL concentration (Γ_{RL}) at the PTFE-solution interface vs. RL concentration (C_{RL}) at the constant ET concentration. Curves 1 – 29 correspond to the constant ET concentration equal to 0.06692; 0.1338; 0.2677; 0.4015; 0.535; 1.0706; 1.6062; 2.1416; 2.677; 3.2124; 3.7478; 4.2832; 4.8185; 5.3538; 5.8893; 6.6925; 7.7245; 8.5664; 10.2797; 11.968; 12.145; 13.3794; 14.5696; 15.4064; 16.084; 16.3777; 16.648; 16.8988 and 17.13 M.
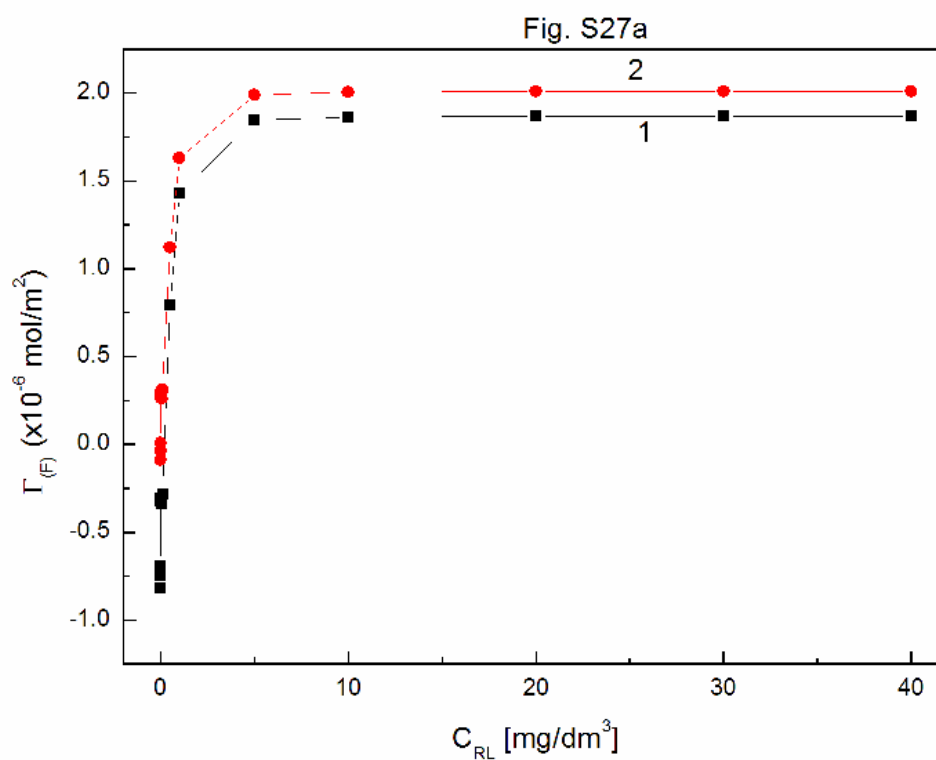
Fig. S27a. A plot of Frumkin RL concentration (Γ_{RL}) at the solution-air interface (curve 1) and at the PTFE-solution interface (curve 2) vs. the RL concentration (C_{RL}) at the constant ET concentration equal to 0.06692 M.

Fig. S27b. A plot of Frumkin RL concentration (Γ_{RL}) at the solution- air interface (curve 1) and at the PTFE-solution interface (curve 2) vs. the RL concentration (C_{RL}) at the constant ET concentration equal to 1.07096 M.

Fig. S27c. A plot of Frumkin RL concentration (Γ_{RL}) at the solution- air interface (curve 1) and at the PTFE-solution interface (curve 2) vs. the RL concentration (C_{RL}) at the constant ET concentration equal to 4.2832 M.

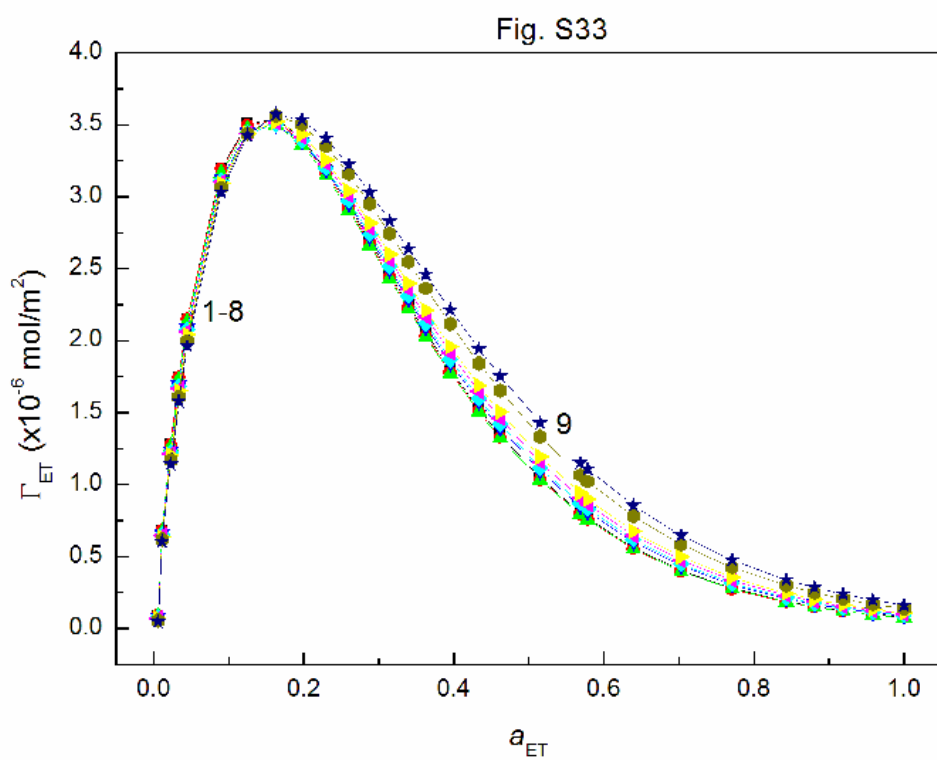Fig. S28. A plot of ET Gibbs surface excess concentration at the PMMA-solution interface (Γ_{ET}) calculated from Eq. (18) vs. the alcohol activity (a_{ET}). Curves 1 – 10 correspond to the constant RL concentration equal to 0.0002; 0.0005; 0.00125; 0003; 0.00625; 0.01; 0.02; 0.05; 0.1 and 0.5 mg/dm^3.

Fig. S29a. A plot of ET Gibbs surface excess concentration at the PMMA-solution, PMMA-air and solution-air interfaces (Γ_{ET}) vs. the alcohol activity (a_{ET}) at the constant RL concentration equal to 0.00125 mg/dm^3. Curves 1 – 3 correspond to Γ_{ET} at the PMMA-solution, PMMA-air and solution-air interface, respectively.
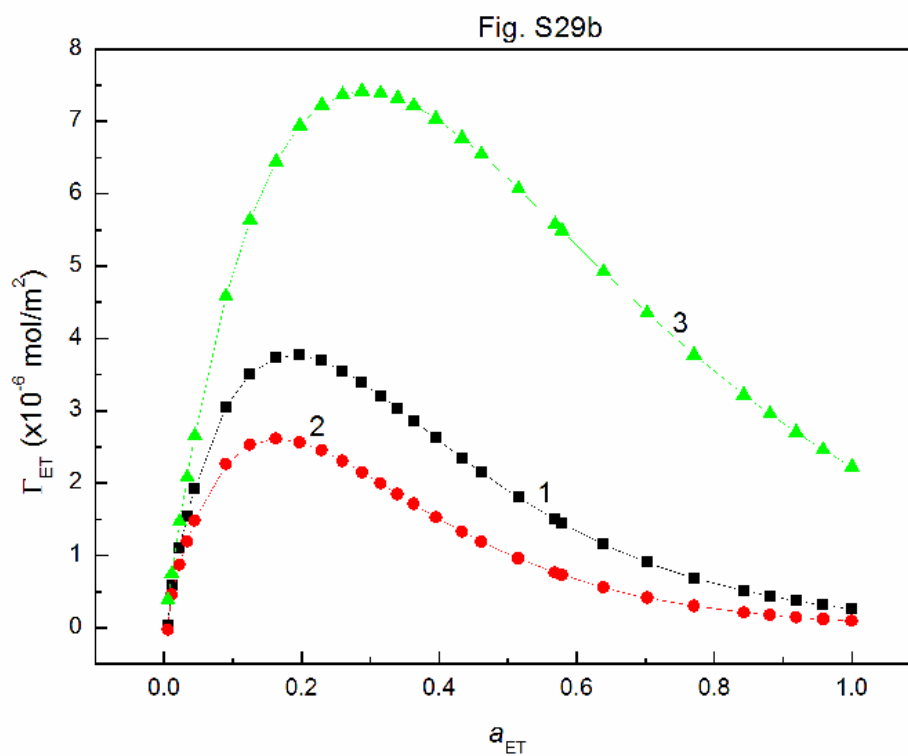
Fig. S29b. A plot of ET Gibbs surface excess concentration at the PMMA-solution, PMMA-air and solution-air interfaces (Γ_{ET}) vs. the alcohol activity (a_{ET}) at the constant RL concentration equal to 0.01 mg/dm^3. Curves 1 – 3 correspond to Γ_{ET} at the PMMA-solution, PMMA-air and solution-air interface, respectively.
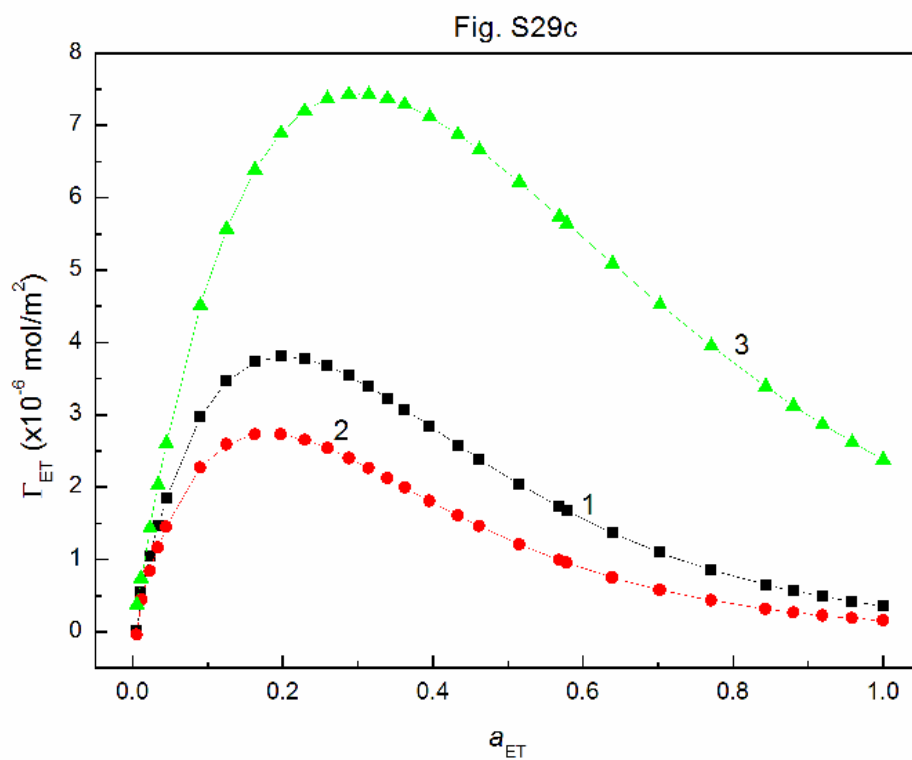
Fig. S29c. A plot of ET Gibbs surface excess concentration at the PMMA-solution, PMMA-air and solution-air interfaces (Γ_{ET}) vs. the alcohol activity (a_{ET}) at the constant RL concentration equal to 0.1 mg/dm^3. Curves 1 – 3 correspond to Γ_{ET} at the PMMA-solution, PMMA-air and solution-air interface, respectively.
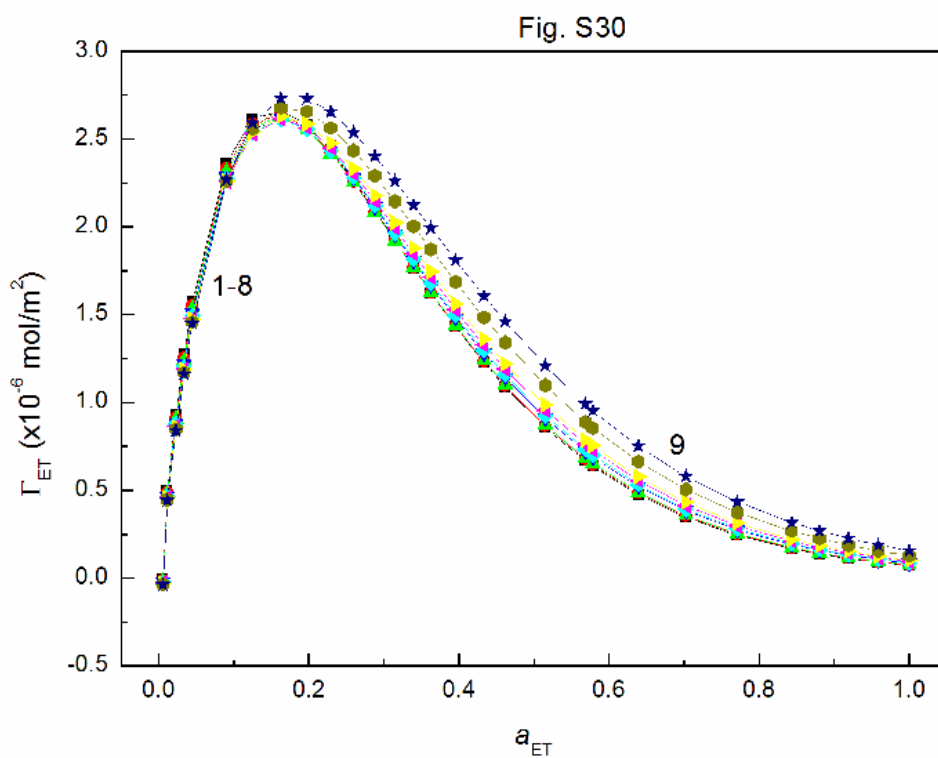
Fig. S30. A plot of ET Gibbs surface excess concentration at the PMMA-air interface calculated from Eq. (20) (Γ_{ET}) vs. the alcohol activity (a_{ET}). Curves 1 – 9 correspond to the constant RL concentration equal to 0.0002; 0.0005; 0.00125; 0003; 0.00625; 0.01; 0.02; 0.05 and 0.1 mg/dm^3.
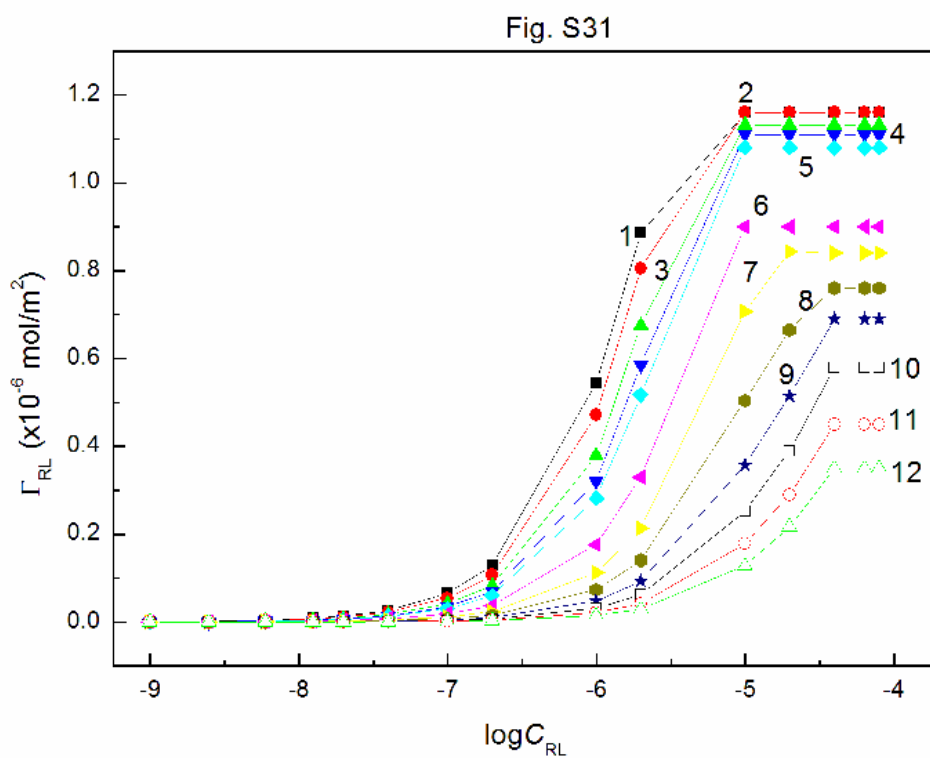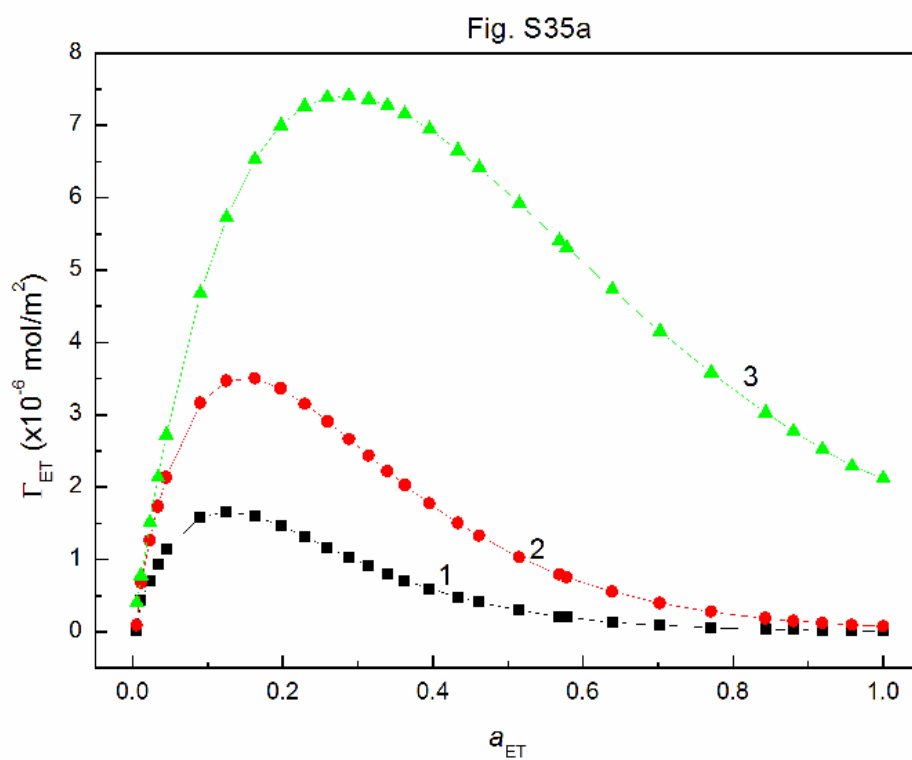
Fig. S31. A plot of RL Gibbs surface excess concentration at the PMMA-solution interface (Γ_{RL}) vs. the logarithm of RL concentration (logC_{RL}). Curves 1 – 12 correspond to the constant ET concentration equal to 0.06692; 0.1338; 0.2677; 0.4015; 0.535; 1.0706; 1.6062; 2.1416; 2.677; 3.2124; 3.7478 and 4.2832 M.
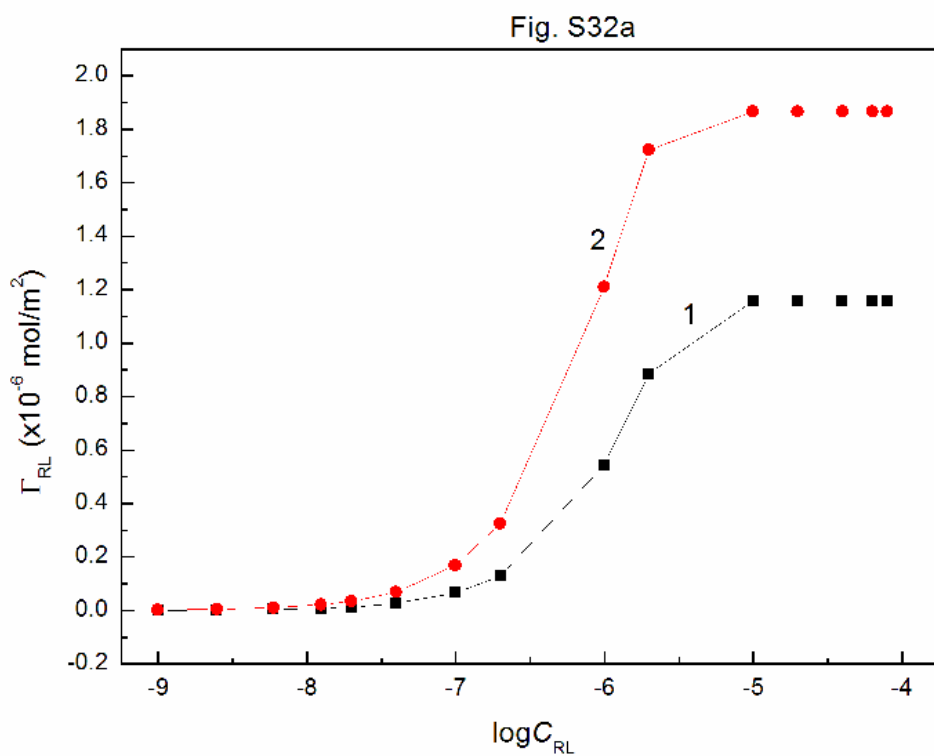
Fig. S32a. A plot of RL Gibbs surface excess concentration (Γ_{RL}) at the PMMA-solution (curve 1) and solution-air interfaces (curve 2) vs. the logarithm of RL concentration ($\log C_{RL}$) at the constant ET concentration equal to 0.09962 M.
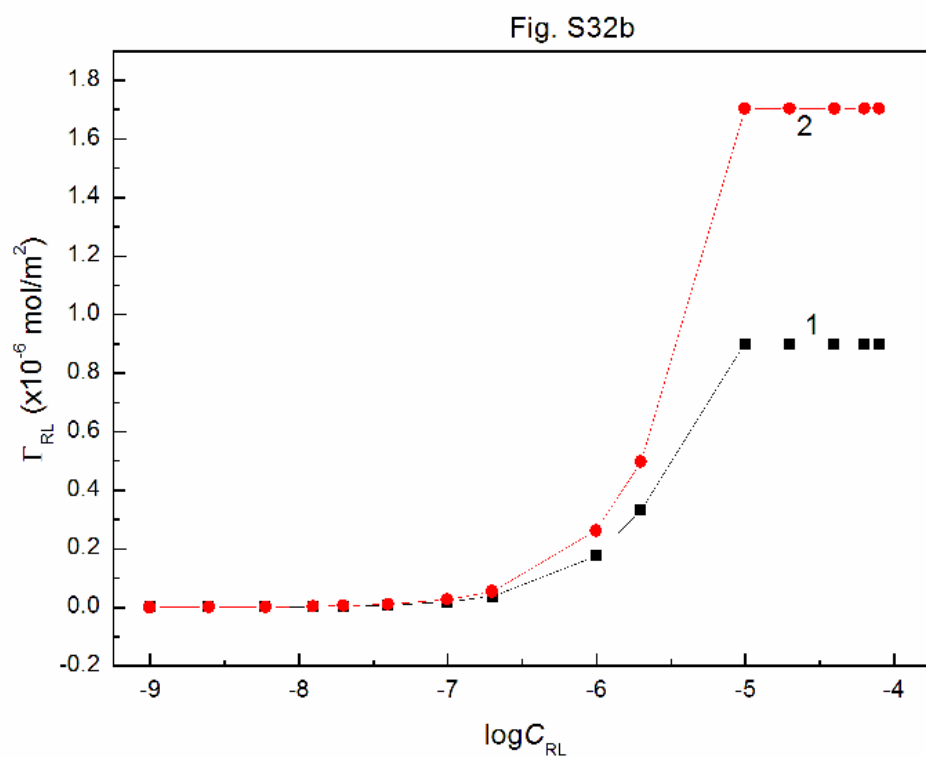
Fig. S32b. A plot of RL Gibbs surface excess concentration (Γ_{RL}) at the PMMA-solution (curve 1) and solution-air interfaces (curve 2) vs. the logarithm of RL concentration ($\log C_{RL}$) at the constant ET concentration equal to 1.0706 M.
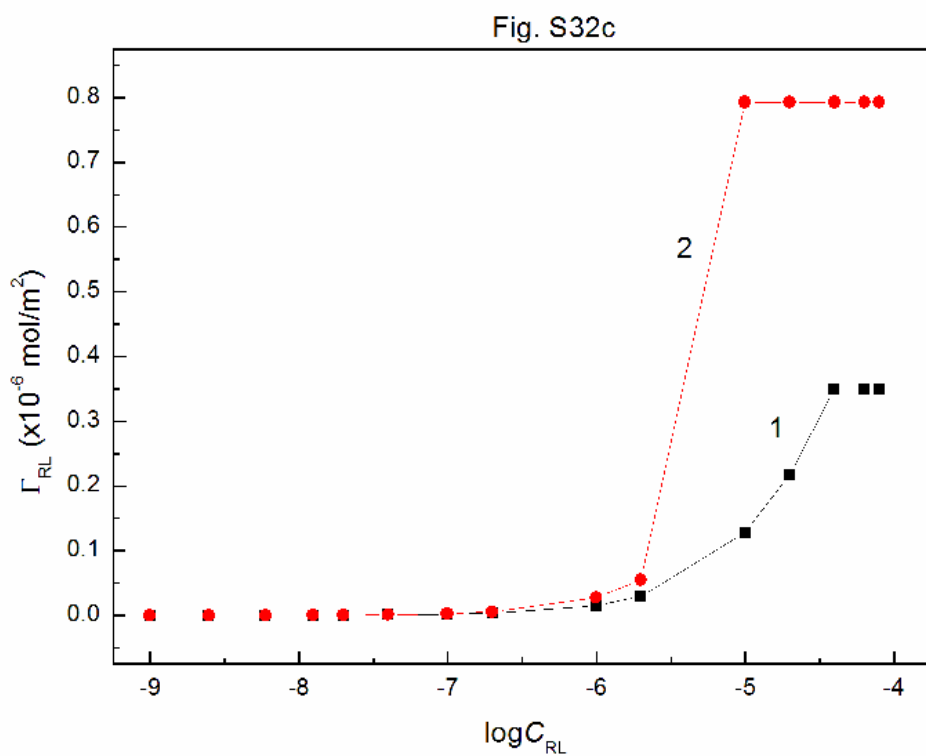
Fig. S32c. A plot of RL Gibbs surface excess concentration (Γ_{RL}) at the PMMA-solution (curve 1) and solution-air interfaces (curve 2) vs. the logarithm of RL concentration ($\log C_{RL}$) at the constant ET concentration equal to 4.2832 M.

Fig. S33. A plot of ET Gibbs surface excess concentration at the quartz-air interface (Γ_{ET}) calculated from Eq. (20) vs. the alcohol activity (a_{ET}). Curves 1 – 9 correspond to the constant RL concentration equal to 0.0002; 0.0005; 0.00125; 0003; 0.00625; 0.01; 0.02; 0.05 and 0.1 mg/dm^3.
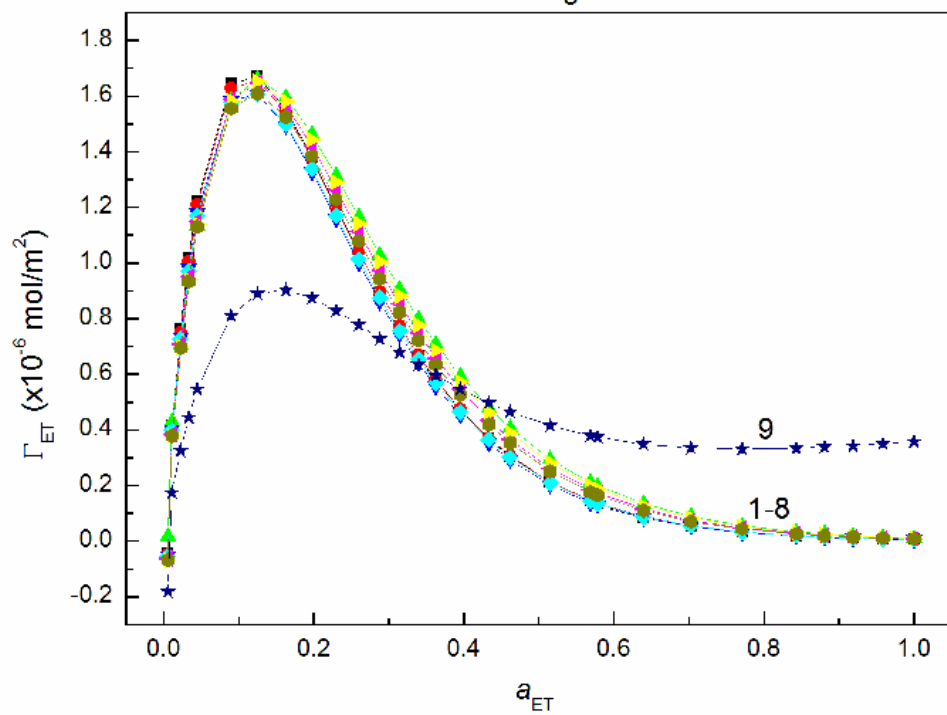
Fig. S34. A plot of ET Gibbs surface excess concentration at the quartz-solution interface (Γ_{ET}) calculated from Eq. (18) vs. the alcohol activity (a_{ET}). Curves 1 – 9 correspond to the constant RL concentration equal to 0.0002; 0.0005; 0.00125; 0003; 0.00625; 0.01; 0.02; 0.05 and 0.1 mg/dm^3.

Fig. S35a. A plot of ET Gibbs surface excess concentration (Γ_{ET}) vs. the alcohol activity (a_{ET}) at the constant RL concentration equal to 0.00125 mg/dm^3. Curves 1 – 3 correspond to Γ_{ET} at the quartz-air, quartz-solution and solution-air interfaces, respectively.
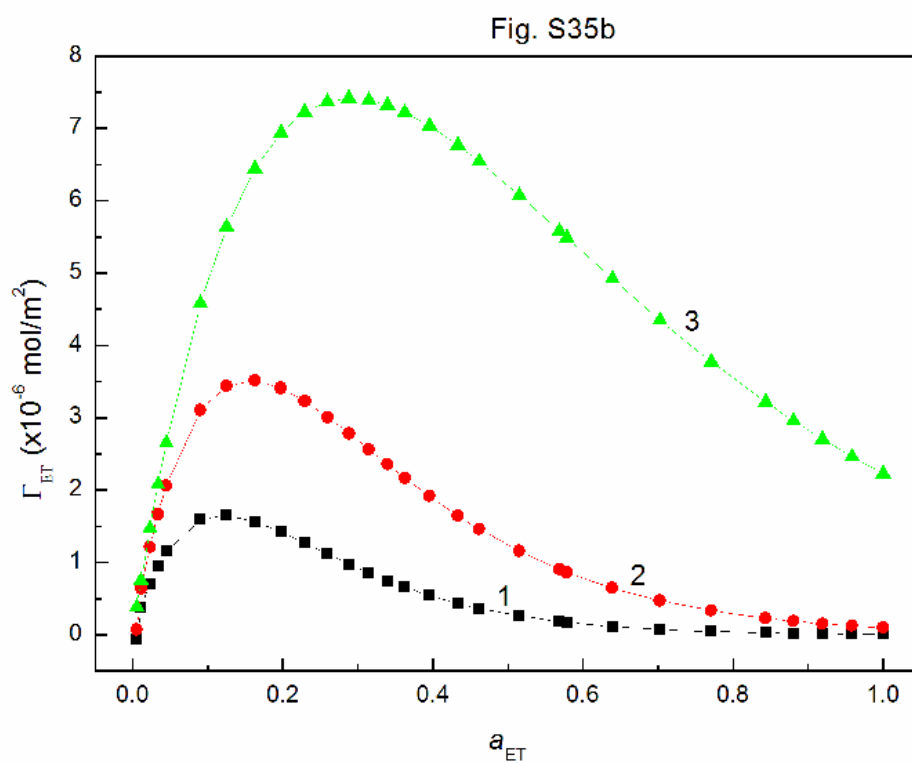
Fig. S35b. A plot of ET Gibbs surface excess concentration (Γ_{ET}) vs. the alcohol activity (a_{ET}) at the constant RL concentration equal to 0.01 mg/dm^3. Curves 1 – 3 correspond to Γ_{ET} at the quartz-air, quartz-solution and solution-air interfaces, respectively.
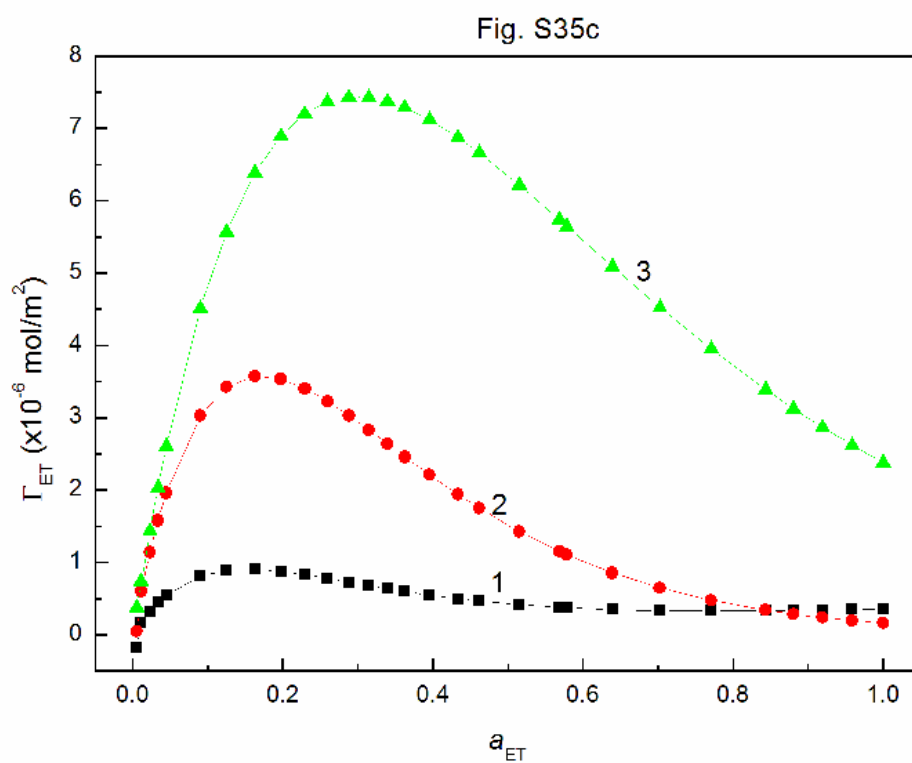
Fig. S35c. A plot of ET Gibbs surface excess concentration (Γ_{ET}) vs. the alcohol activity (a_{ET}) at the constant RL concentration equal to 0.1 mg/dm^3. Curves 1 – 3 correspond to Γ_{ET} at the quartz-air, quartz-solution and solution-air interfaces, respectively.
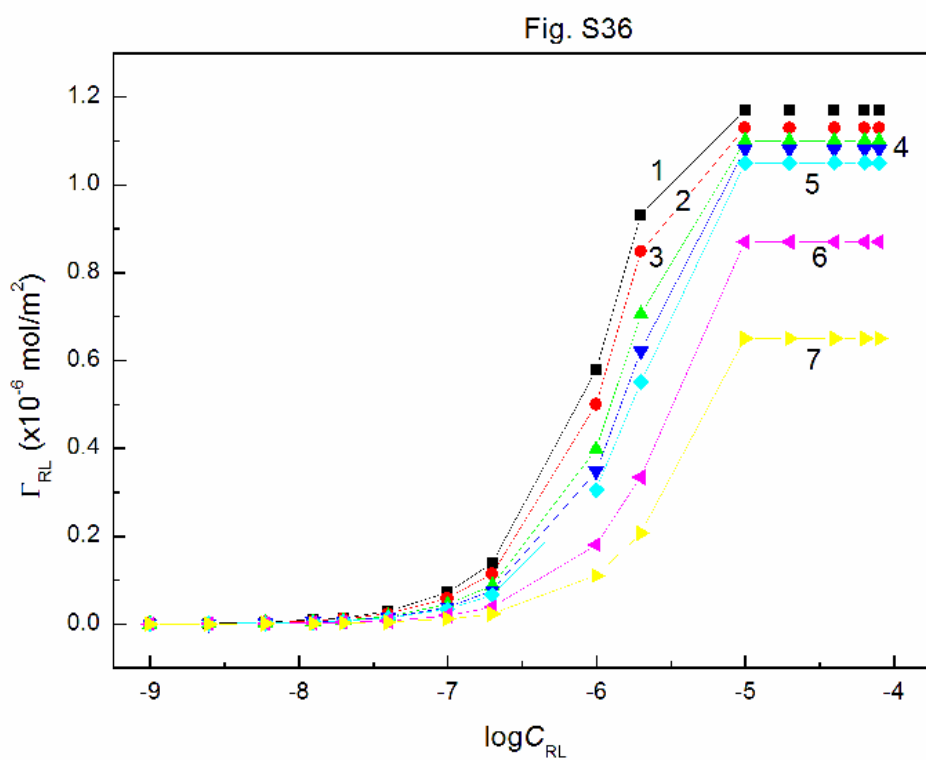
Fig. S36. A plot of RL Gibbs surface excess concentration at (Γ_{RL}) at the quartz-air interface calculated from Eq. (20) vs. the logarithm of RL concentration (logC_{RL}). Curves 1 – 7 correspond to the constant ET concentration equal to 0.06692; 0.1338; 0.2677; 0.4015; 0.535; 1.0706 and 1.6062 M.
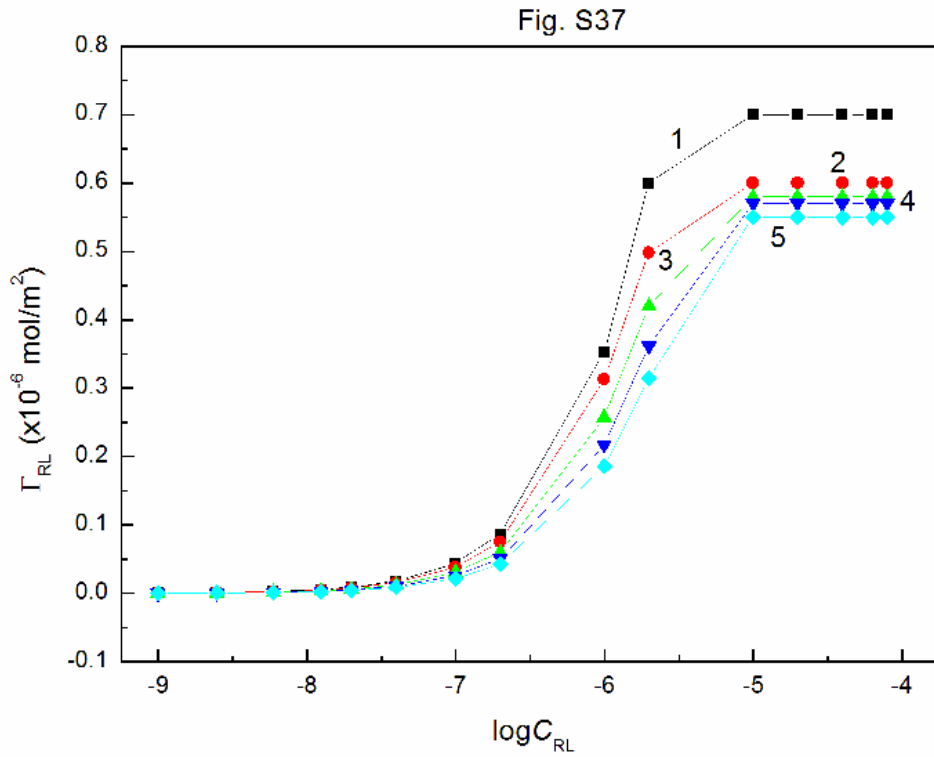
Fig. S37. A plot of RL Gibbs surface excess concentration at (Γ_{RL}) at the quartz-solution interface calculated from Rq. (18) vs. the logarithm of RL concentration ($\log C_{RL}$). Curves 1 – 5 correspond to the constant ET concentration equal to 0.06692; 0.1338; 0.2677; 0.4015 and 0.535 M.
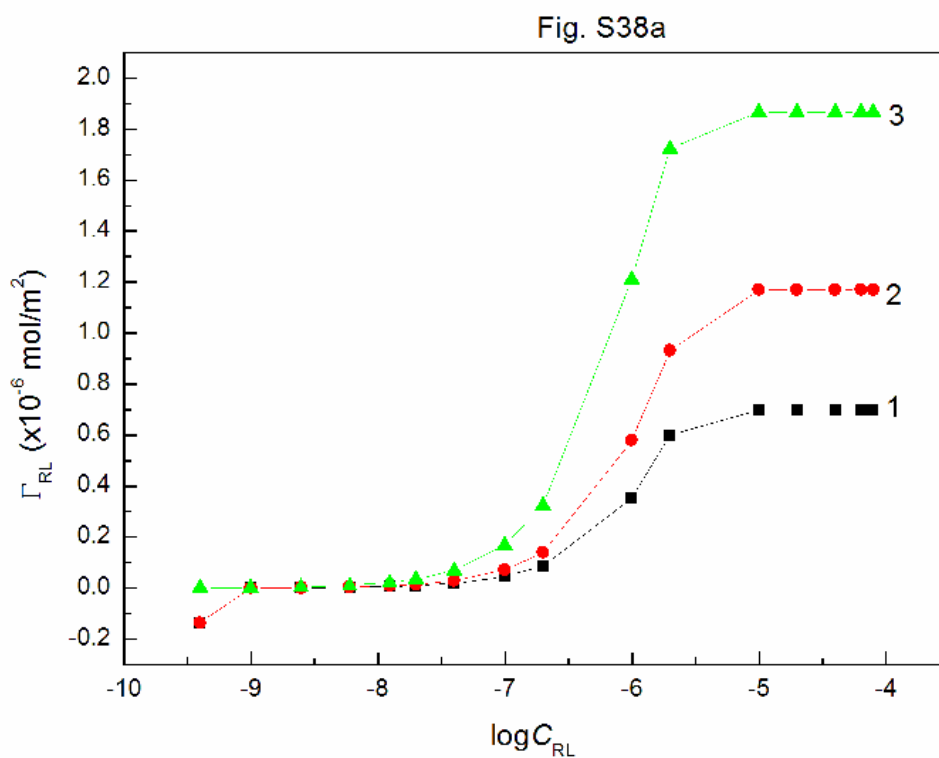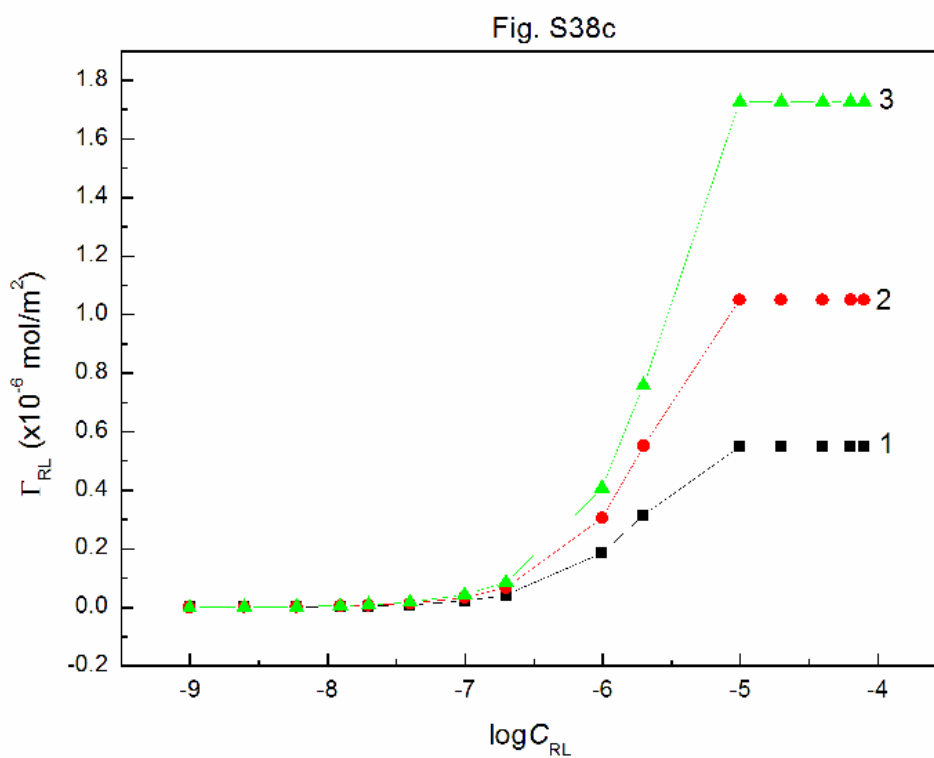
Fig. S38a. A plot of RL Gibbs surface excess concentration (Γ_{RL}) vs the RL concentration (C_{ET}) at the constant ET concentration equal to 0.06692 M. Curves 1 – 3 correspond to Γ_{RL} at the quartz-solution, quartz-air and solution-air interfaces, respectively.
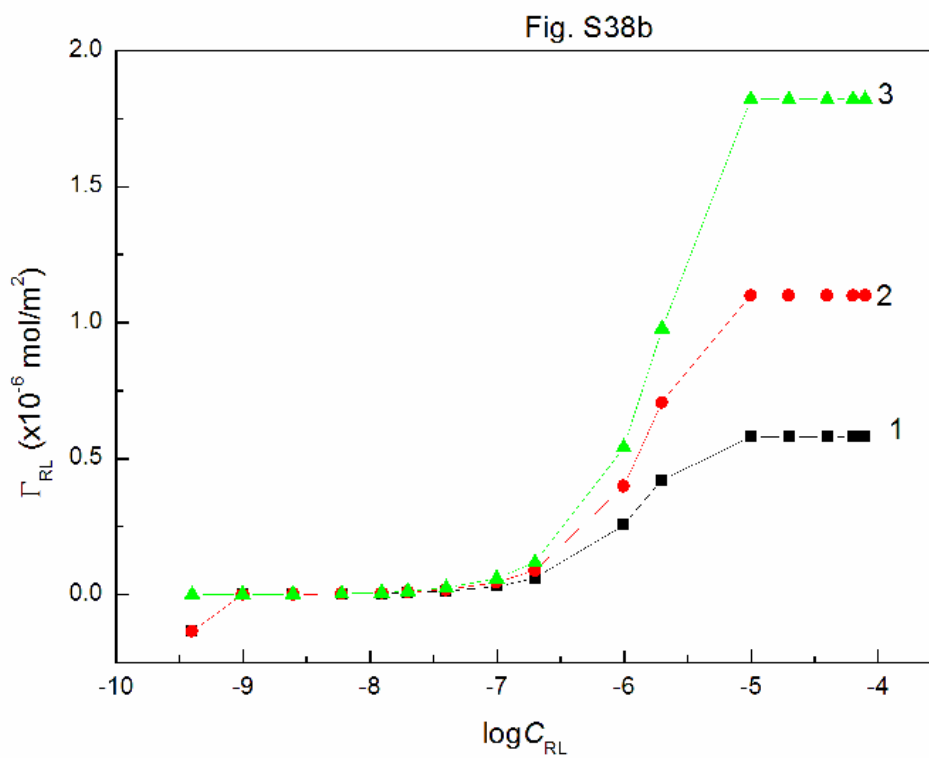
Fig. S38b. A plot of RL Gibbs surface excess concentration (Γ_{RL}) vs the RL concentration (C_{ET}) at the constant ET concentration equal to 0.2677. Curves 1 – 3 correspond to Γ_{RL} at the quartz-solution, quartz-air and solution-air interfaces, respectively.

Fig. S38c. A plot of RL Gibbs surface excess concentration (Γ_{RL}) vs RL concentration (C_{ET}) at the constant ET concentration equal to 0.535 M. Curves 1 – 3 correspond to Γ_{RL} at the quartz-solution, quartz-air and solution-air interfaces, respectively.
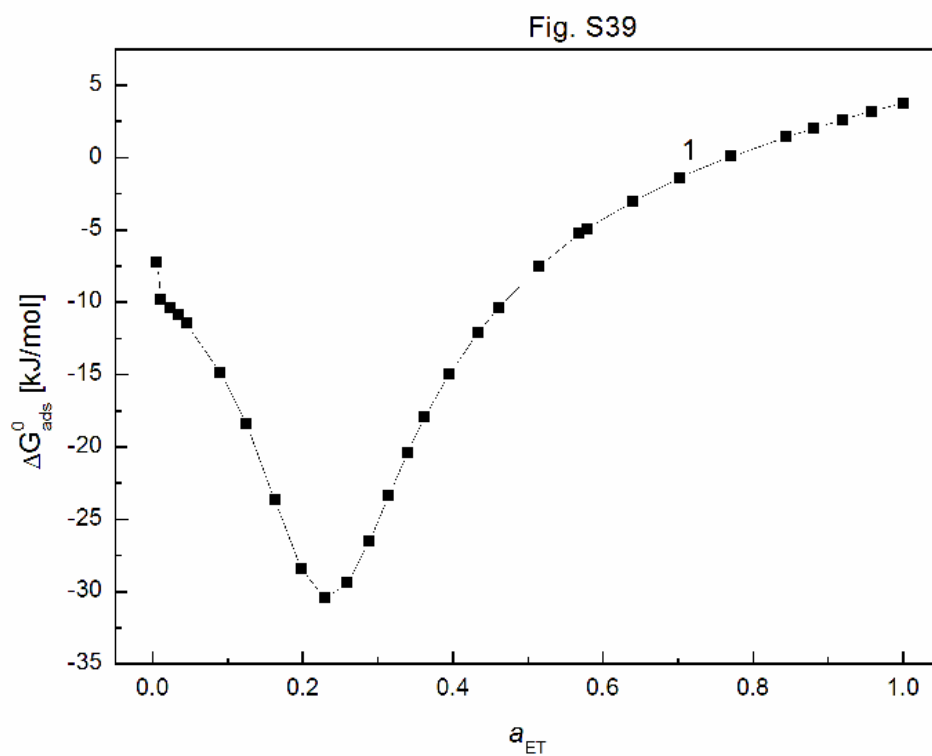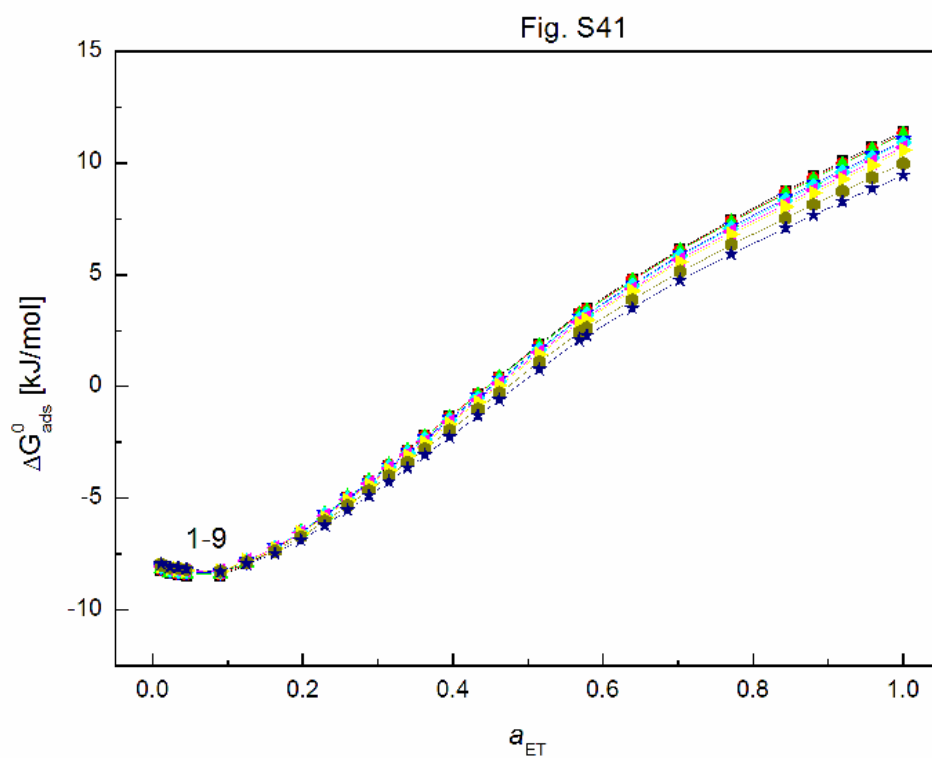
Fig. S39. A plot of standard Gibbs free energy of ET adsorption at the PTFE-solution interface calculated from Eq. (21) (ΔG_{ads}^{0}) alcohol activity (a_{ET}). Curves 1 – 6 correspond to the RL concentration equal to 0.0002; 0.0005; 0.00125; 0003; 0.00625 and 0.01 mg/dm^3.
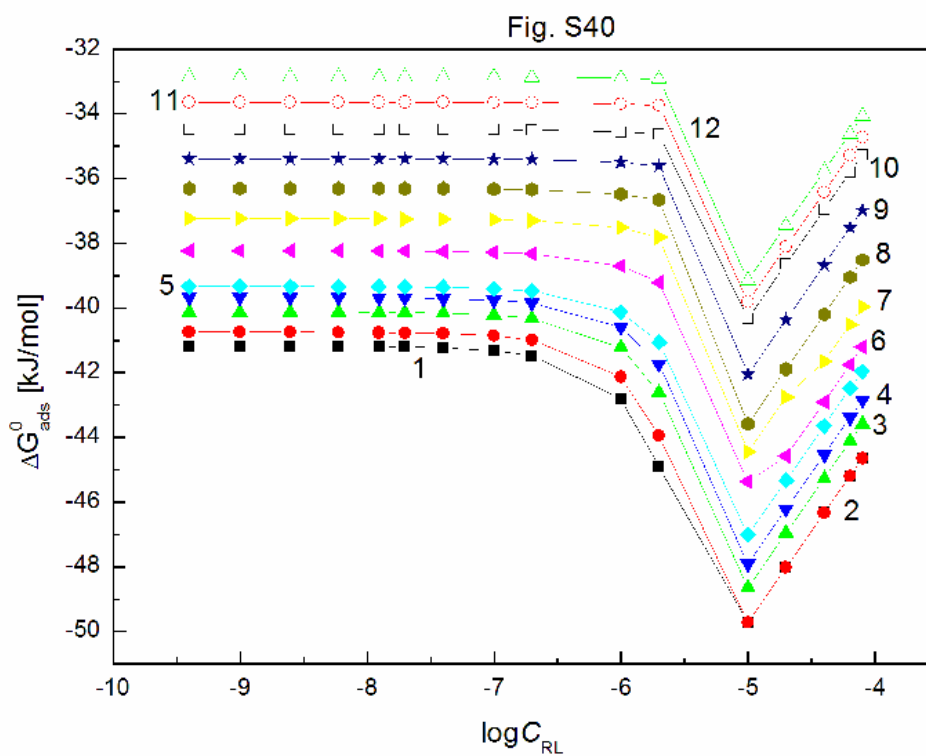
Fig. S40. A plot of standard Gibbs free energy of RL adsorption at the PTFE-solution interface (ΔG_{ads}^{0}) vs. the logarithm RL concentration ($\log C_{RL}$). Curves 1 – 12 correspond to the constant ET concentration equal to 0.06692; 0.1338; 0.2677; 0.4015; 0.535; 1.0706; 1.6062; 2.1416; 2.677; 3.2124; 3.7478 and 4.2832 M.

Fig. S41. A plot of standard Gibbs free energy of ET adsorption at the PMMA-air interface calculated from Eq. (21) (ΔG_{ads}^{0}) vs. the alcohol activity (a_{ET}). Curves 1 – 9 correspond to the constant RL concentration equal to 0.0002; 0.0005; 0.00125; 0003; 0.00625; 0.01; 0.02; 0.05 and 0.1 mg/dm^3.
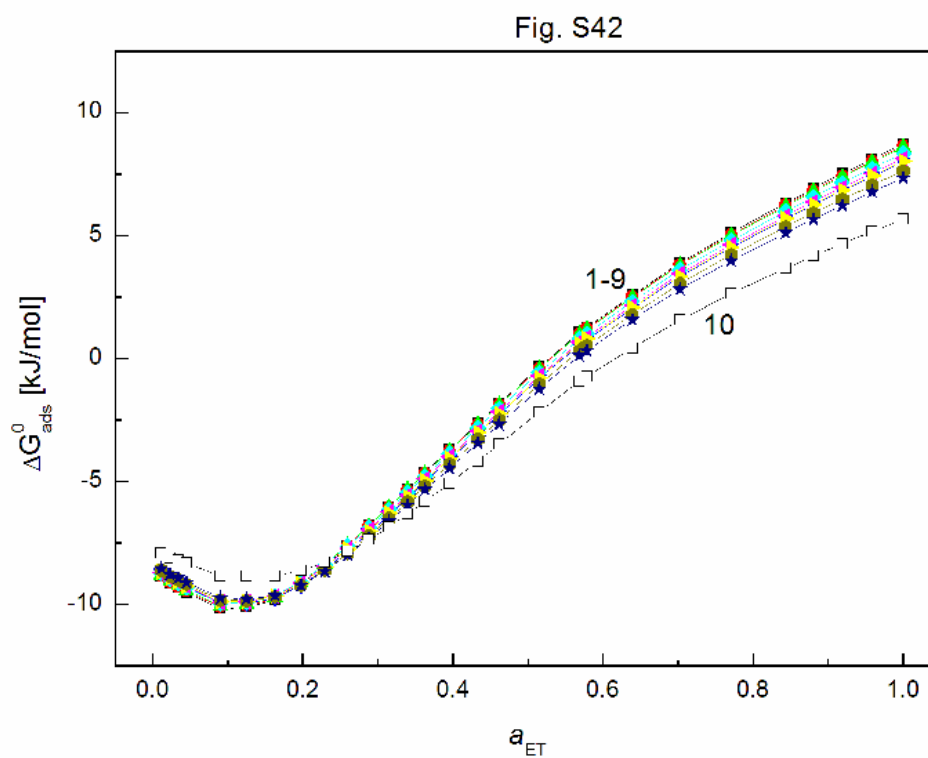
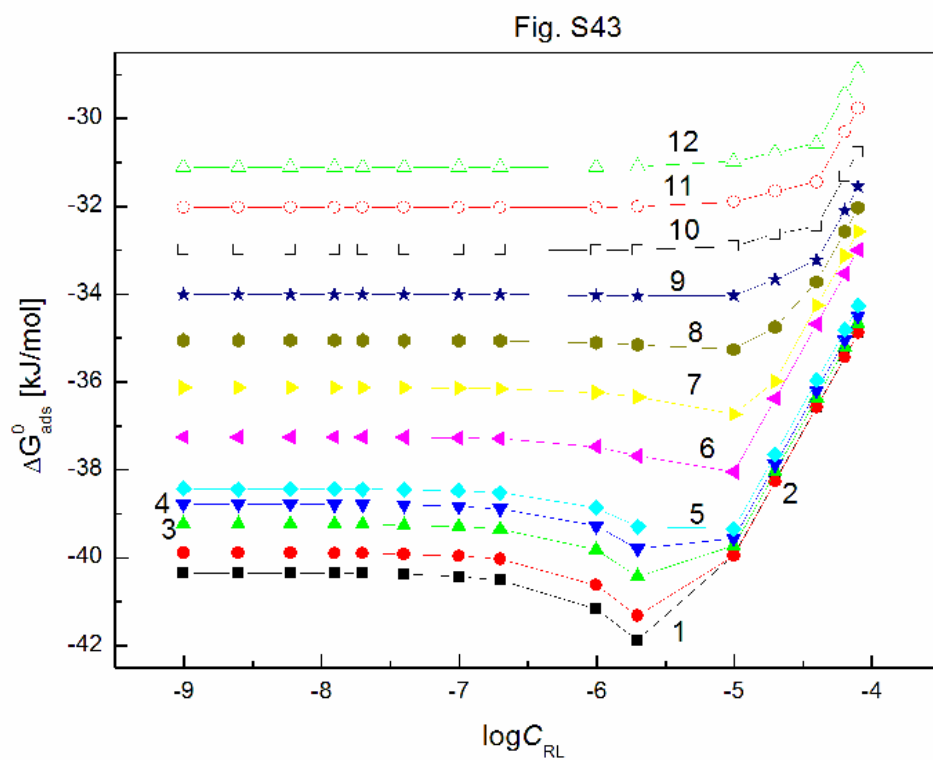Fig. S42. A plot of standard Gibbs free energy of ET adsorption at the PMMA-solution interface calculated from Eq. (21) (ΔG_{ads}^{0}) vs. the alcohol activity (a_{ET}). Curves $1 - 10$ correspond to the constant RL concentration equal to 0.0002; 0.0005; 0.00125; 0003; 0.00625; 0.01; 0.02; 0.05, 0.1 and 0.5 mg/dm^3.

Fig. S43. A plot of standard Gibbs free energy of RL adsorption at the PMMA-solution interface calculated from Eq. (21) (ΔG^0_{ads}) vs. the logarithm of RL concentration ($\log C_{RL}$). Curves 1 – 12 correspond to the constant ET concentration equal to 0.06692; 0.1338; 0.2677; 0.4015; 0.535; 1.0706; 1.6062; 2.1416; 2.677; 3.2124; 3.7478 and 4.2832 M.
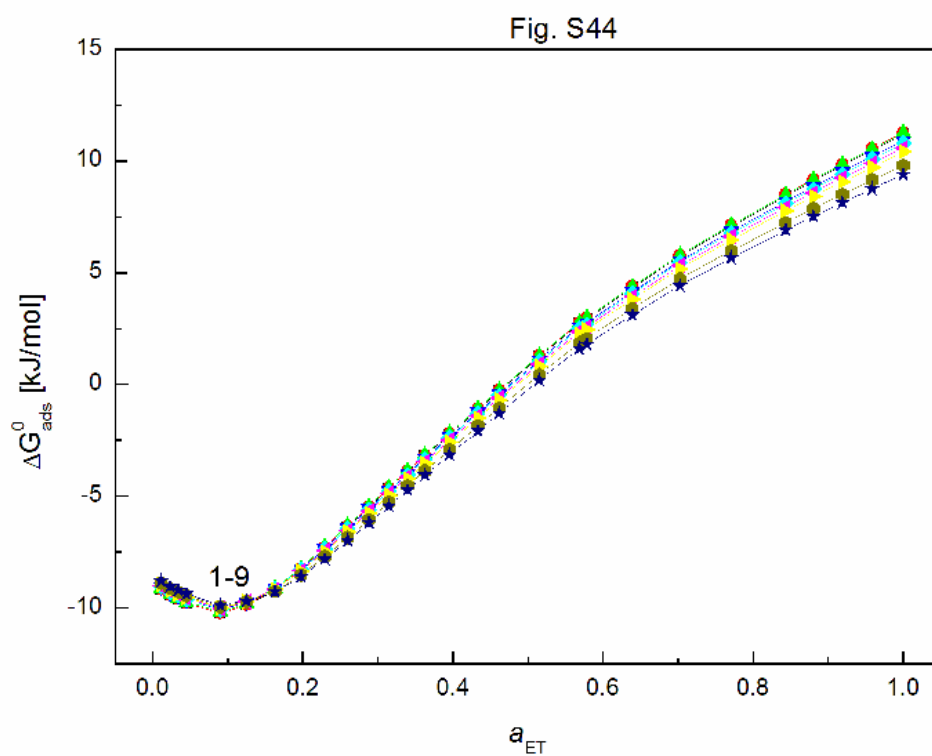
Fig. S44. A plot of standard Gibbs free energy of ET adsorption at the quartz-air interface (ΔG_{ads}^{0}) calculated from Eq. (21) vs. the alcohol activity (a_{ET}). Curves 1 – 9 correspond to the constant RL concentration equal 0002; 0.0005; 0.00125; 0003; 0.00625; 0.01; 0.02; 0.05 and 0.1 mg/dm³.
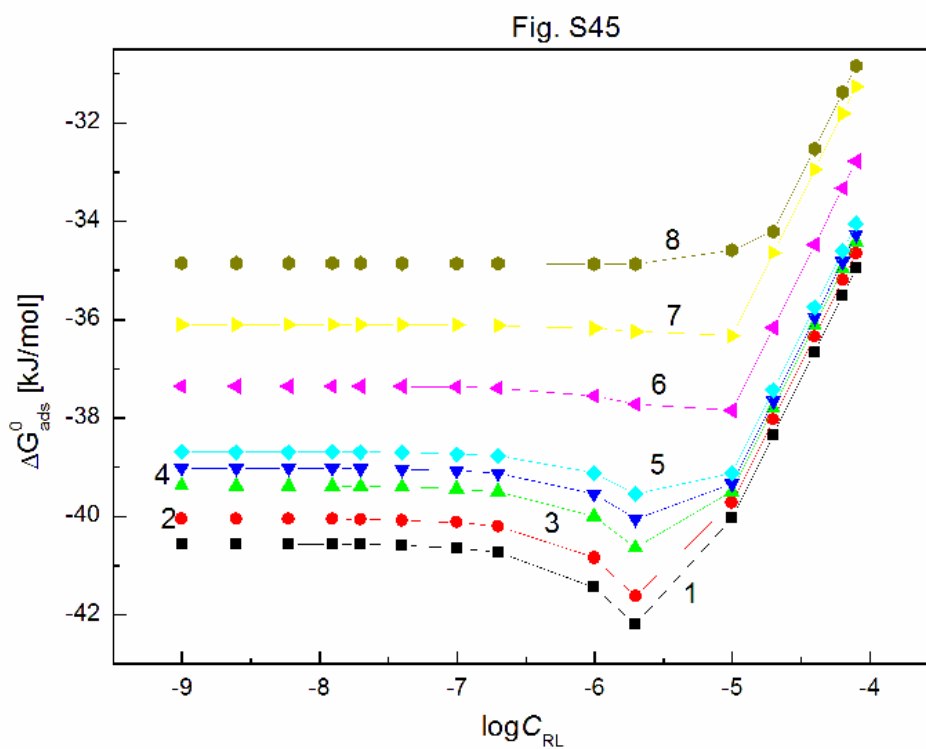
Fig. S45. A plot of standard Gibbs free energy of RL adsorption at the quartz-air interface calculated from Eq. (21) (ΔG_{ads}^{0}) vs. the logarithm of RL concentration ($\log C_{RL}$). Curves 1 – 8 correspond to the constant ET concentration equal to 0.06692; 0.1338; 0.2677; 0.4015; 0.535; 1.0706; 1.6062 and 2.1416 M.
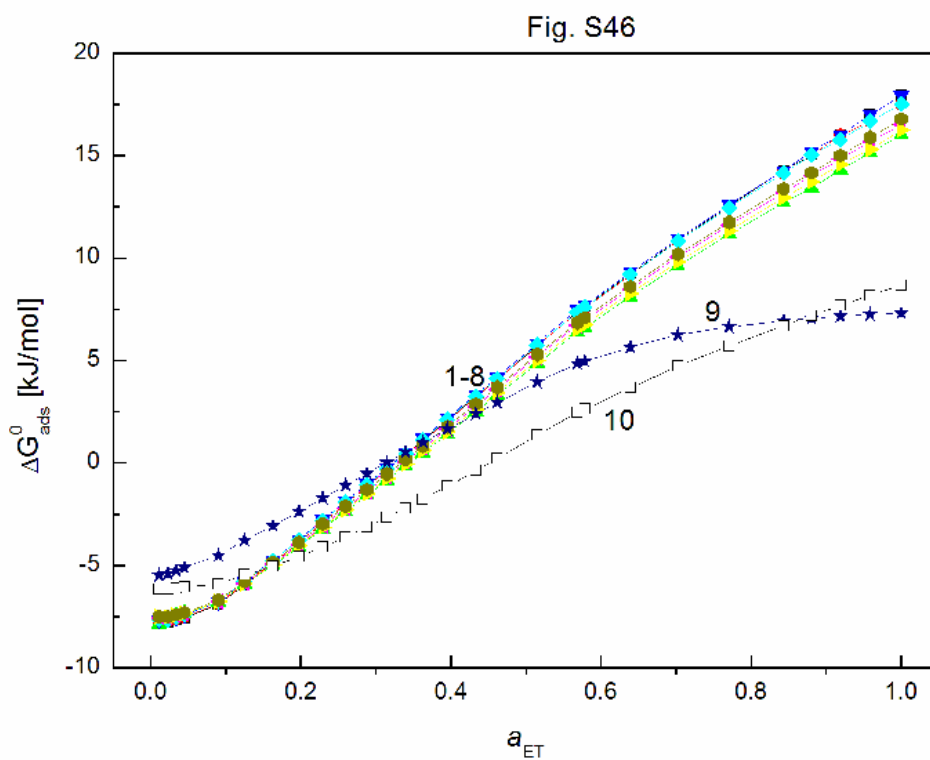
Fig. S46. A plot of standard Gibbs free energy of ET adsorption at the quartz-solution interface (ΔG_{ads}^{0}) calculated from Eq. (21) vs. the alcohol activity (a_{ET}). Curves 1 – 10 correspond to the constant RL concentration equal to 0002; 0.0005; 0.00125; 0003; 0.00625; 0.01; 0.02; 0.05, 0.1 and 0.5 mg/dm^3.
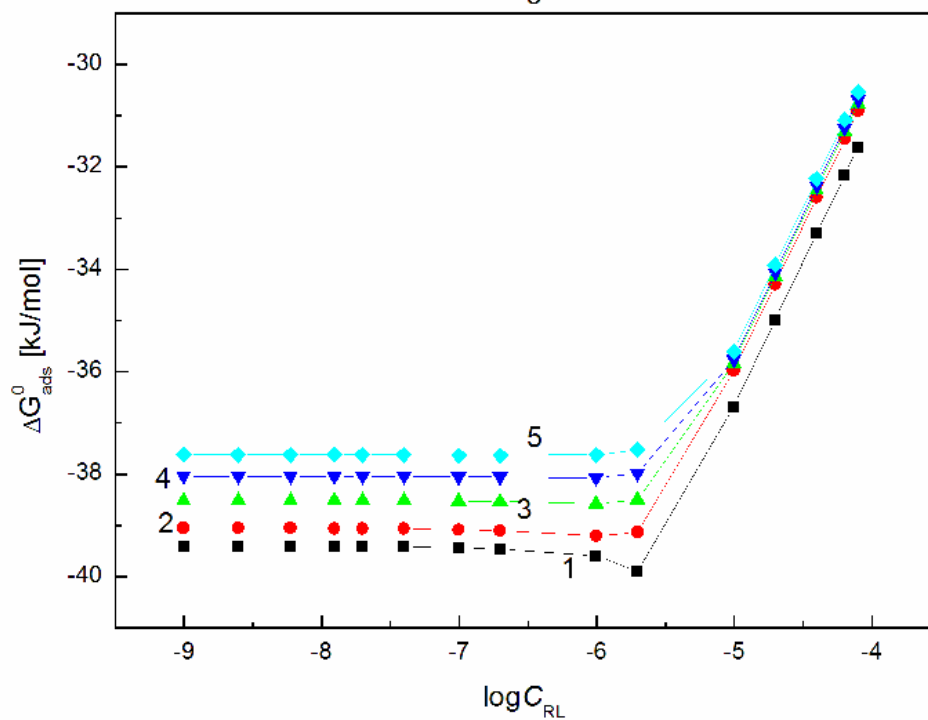
Fig. S47. A plot of standard Gibbs free energy of RL adsorption at the quartz-solution interface calculated from Eq. (21) (ΔG_{ads}^{0}) vs. the logarithm of RL concentration ($\log C_{RL}$). Curves 1 – 5 correspond to the constant ET concentration equal to 0.06692; 0.1338; 0.2677; 0.4015 and 0.535 M.

Prof. dr hab. Anna Zdziennicka   Lublin, 17.01.2023
Katedra Zjawisk Międzyfazowych
Instytut Nauk Chemicznych
Wydział Chemii UMCS
Pl. M. Curie-Skłodowskiej 3
20-031 Lublin

OŚWIADCZENIE

Oświadczam, że w pracy

E. Rekiel, **A. Zdziennicka***, B. Jańczuk, *Effect of ethanol on wetting and adhesion properties of rhamnolipid*. International Journal of Adhesion and Adhesives, 2021, 110, 102955;

mój udział wynosił **30%** i polegał na opracowaniu koncepcji artykułu i dobraniu metodologii, weryfikacji procesu pisania pracy, interpretacji oraz wizualizacji otrzymanych wyników, pisaniu oryginalnej wersji manuskryptu, redagowaniu i edycji manuskryptu, współredagowaniu odpowiedzi na recenzje pracy oraz prowadzeniu korespondencji z czasopismem.

Prof. dr hab. Bronisław Jańczuk
Katedra Zjawisk Międzyfazowych
Instytut Nauk Chemicznych
Wydział Chemii UMCS
Pl. M. Curie-Skłodowskiej 3
20-031 Lublin

Lublin, 17.01.2023

OŚWIADCZENIE

Oświadczam, że w pracy

E. Rekiel, A. Zdziennicka*, **B. Jańczuk**, *Effect of ethanol on wetting and adhesion properties of rhamnolipid*. International Journal of Adhesion and Adhesives, 2021, 110, 102955;

mój udział wynosił **10%** i polegał na opracowaniu koncepcji artykułu i dobraniu metodologii, weryfikacji procesu pisania pracy, pisaniu oryginalnej wersji manuskryptu, redagowaniu i edycji manuskryptu oraz współredagowaniu odpowiedzi na recenzje pracy.